

THESIS

HYDRAULIC AND CHEMICAL PROPERTIES OF GEOSYNETHETIC CLAY LINERS IN MINING
APPLICATIONS

Submitted by

Joel Conzelmann

Department of Civil and Environmental Engineering

In partial fulfillment of the requirements

For the Degree of Master of Science

Colorado State University

Fort Collins, Colorado

Fall 2017

Master's Committee:

Advisor: Joseph Scalia

Charles Shackelford
Sally Sutton

Copyright by Joel Thomas Conzelmann 2017

All Rights Reserved

ABSTRACT

HYDRAULIC AND CHEMICAL PROPERTIES OF GEOSYNTHETIC CLAY LINERS IN MINING APPLICATIONS

Geosynthetic clay liners (GCLs) are thin (< 10 mm) factory manufactured hydraulic barriers used in environmental containment systems because of the propensity of bentonite to swell and immobilize water which results in low hydraulic conductivity, $k (\leq 2-3 \times 10^{-11} \text{ m/s})$. GCLs consist of bentonite (clay) bonded or sandwiched between layer(s) of geotextile and/or geomembrane. The effectiveness of GCLs in containment applications has been demonstrated for systems with low ionic strength solutions and leachates, such as municipal solid waste leachates. Increasingly, GCLs are being used in mining applications; these applications require further research and laboratory testing to demonstrate barrier effectiveness.

Existing standard test methods are not well suited for testing of mine-waste-leachates; simple procedures to collect effluent for analysis are lacking, commercially available testing equipment is typically incompatible with extreme pH solutions often encountered, and the use of backpressure is recommended requiring testing at elevated pressures. To overcome these limitations, an alternative gravity method without backpressure, paired with a permeameter constructed from non-reactive materials and intended to minimize clogging was used. Validation of the gravity method is demonstrated through k and hydration testing with synthetic mine waste leachates and comparative tests performed by a standard method. Tests results support that GCLs attain saturation, and that the gravity method does not exhibit uncharacteristically low k due to unsaturated conditions. However, the gravity method revealed the possibility of preferential flow through fiber bundles for GCLs with higher degrees of needle punching which was not observed in standard method tests. The cause of the discrepancy between the two methods is

hypothesized to be associated with applying backpressure in the standard method, indicating that the standard method may provide an un-conservative estimate of k for higher peel strength GCLs. Regardless, bentonite saturation is shown to occur without backpressure under conditions typical of k testing, illustrating that saturated (maximum k) tests can be achieved without backpressure.

The k of GCLs to synthetic mine leachate solutions was tested using the gravity method with the chemical-resistant permeameter. Three different mine waste leachates are investigated, a neutral pH synthetic gold mining process solution, a high pH synthetic bauxite mining process solution, and a low pH synthetic copper mining process solution. Three different GCL products were also investigated, two higher peel strength GCLs (2170 N/m and 3500 N/m), and a standard peel strength GCL (700 N/m). The preliminary results of k testing are reported.

ACKNOWLEDGEMENTS

I would first like to thank my committee members for their time and effort in assisting in the completion of this thesis, and their contribution to my engineering education. To Joe Scalia for serving as my advisor, his enthusiasm and dedication to the geoenvironmental profession has been an inspiration to me and I cannot thank him enough for his mentorship throughout the entire process of master's coursework, this thesis, and choosing a career path. To Dr. Shackelford for his passion for geoenvironmental topics and constant standard of excellence. In addition, to Dr. Sutton for serving on my committee and flexibility throughout my changing plans.

I also would like to thank all of the members of the CSU geo-group for creating such a fantastic community. Specifically, to Professor Bareither for convincing me to come to CSU, to Shahin Ghazi Zadeh for his enthusiasm in studying GCLs and the many hours of working together in the laboratory, to Monika Popang for her assistance in helping complete experiments, to Justin Thompson for his assistance in the laboratory and his construction of the burette frames necessary for much of the data presented in this thesis, and to Morgan for her assistance in collecting much of the GCL index properties data.

I would also like to thank my friends and family for their constants support. To my parents, Janet and Jeff, for always supporting me throughout my education. To my roommate Andrew for his friendship, encouragement throughout the writing process, and for all of our adventures in the Colorado mountains. To the members of the Christian Grads Fellowship for their constant prayers and fellowship. In addition, to my sister Kate for her perseverance and joy through difficult times; thank you for teaching me to never give up and to live life here and now.

Lastly, above all else I thank my Lord and Savior, Jesus Christ, for making me all that I am and allowing me to grow in discovery of knowledge and truth.

“Show me your ways, LORD, teach me your paths. Guide me in your truth and teach me, for you are God my Savior, and my hope is in you all day long.” Psalm 25:4-5.

TABLE OF CONTENTS

ABSTRACT	ii
ACKNOWLEDGEMENTS	iv
LIST OF TABLES	x
LIST OF FIGURES	xi
CHAPTER 1. Introduction	1
1.1 Background	1
1.1.1 <i>Geosynthetic Clay Liners</i>	1
1.1.2 <i>Hydraulic Behavior</i>	2
1.1.3 <i>Factors Effecting Hydraulic Behavior</i>	2
1.1.3.1 <i>Hydrating and Permeating Liquid Chemistry</i>	2
1.1.3.2 <i>Bentonite Quality and Additives</i>	4
1.1.3.3 <i>Effective Stress</i>	5
1.1.4 <i>Hydraulic Compatibility Testing</i>	5
1.1.4.1 <i>Hydraulic conductivity testing by the standard ASTM method</i>	6
1.1.4.2 <i>Backpressure Saturation</i>	6
1.1.4.3 <i>Alternative Testing Method</i>	7
1.2 Research Objectives	8
CHAPTER 2. Effect of backpressure on the hydraulic conductivity of GCLs	9
2.1 Introduction	10
2.2 Materials and Methods	10
2.2.1 <i>Liquids</i>	10

2.2.2 GCLs	12
2.2.3 Granular Bentonite	14
2.2.4 Hydraulic Conductivity Testing by ASTM method	15
2.2.5 Hydraulic Conductivity Testing by the Gravity Method	21
2.2.6 Verification of Degree of Saturation	24
2.2.7 Hydraulic Conductivity Testing by Alternative Standard Methods	25
2.2.7.1 Backpressure Time Interval Changed From 1 min to 1 hr	25
2.2.7.2 Backpressure Time Interval Changed From 1 min to 4 hr	25
2.2.7.3 Changing Both the Backpressure Time Interval to 4 hr and Stress Increment to 35 kPa	25
2.2.7.4 Backpressure Stress Increment Changed From 10 psi to 5 psi	25
2.2.7.5 Changing Both the Backpressure Time Interval to 1 d and Stress Increment to 35 kPa	26
2.2.7.6 Backpressure Without Time Intervals and Stress Increments	26
2.2.7.7 Gravity Method Followed by Standard Method on the Same Specimen	26
2.2.8 Hydration Testing in Oedometers	26
2.2.9 Hydration Testing in Permeameters	27
2.2.10 Flow Path Dying	27
2.2.11 Hydraulic Conductivity Test Disassembly	27
2.2.12 Thickness Measurement and Weight-Volume Relationships	28
2.2.13 Index properties	29
2.3 Results	29
2.3.1 Degree of Saturation	29
2.3.1.1 Degree of Saturation from Hydraulic Conductivity Tests	29
2.3.1.2 Degree of Saturation from Oedometer Hydration Tests	30

2.3.1.3 Degree of Saturation from Permeameter Hydration Tests	30
2.3.2 Water Content	31
2.3.2.1 Water Contents of Hydraulic Conductivity Tests	31
2.3.2.2 Water Contents of Oedometer Hydration Tests	31
2.3.2.3 Water Contents of Permeameter Hydration Tests	32
2.3.3 Hydraulic Conductivity	32
2.3.3.1 Comparison of S-Method to G-Method	32
2.3.3.2 Preferential Flow Through Fiber Bundles	33
2.3.3.3 Comparison of S-Method and G-Method to Modified Standard Methods	33
2.4 Discussion	35
2.4.1 Verification of the Degree of Saturation	34
2.4.1.1 Verification of the Degree of Saturation for Hydraulic Conductivity Tests	34
2.4.1.2 Verification of the Degree of Saturation for Oedometer Hydration Tests	34
2.4.1.3 Verification of the Degree of Saturation for Permeameter Hydration Tests	36
2.4.1.4 Effect of Backpressure on Degree of Saturation	37
2.4.2 Water Content	38
2.4.2.1 Effect of Permeant Liquid	38
2.4.2.2 Effect of GCL	38
2.4.2.3 Effect of S-Method versus G-Method	38
2.4.3 Hydraulic Conductivity	39
2.4.3.1 Effect of S-Method Versus G-Method	40
2.4.3.2 Effect of Preferential Flow	40

2.4.3.3 <i>Effect of Changing Time and Stress of Backpressure Increments</i>	40
2.4.3.4 <i>Effect of S-Method</i>	41
2.4.3.5 <i>Effect of G-Method</i>	42
2.4.3.6 <i>Effect of Removing Backpressure Steps</i>	43
2.4.3.7 <i>Effect of Applying Backpressure During Permeation</i>	46
2.5 Conclusion	47
CHAPTER 3. Hydraulic conductivity measurement of GCLs with mine waste leachates	84
3.1 Introduction	85
3.2 Materials and Methods	85
3.2.1 <i>Liquids</i>	87
3.2.2 <i>GCLs</i>	88
3.2.3 <i>Granular Bentonite</i>	88
3.2.4 <i>Hydraulic Conductivity Testing by the G-Method</i>	88
3.2.5 <i>Chemical Resistant Permeameter</i>	90
3.2.6 <i>Flowrates Through Empty Permeameters</i>	91
3.3 Results	91
3.3.1 <i>Hydraulic Conductivity</i>	93
3.3.2 <i>Degree of Saturation</i>	93
3.4 Discussion	93
3.4.1 <i>Comparison of k Between GCL Products</i>	93
3.4.2 <i>Chemical Equilibrium Termination Criteria</i>	94
3.4.3 <i>Effect of Effective Stress</i>	95
3.5 Conclusion	95
REFERENCES	113
APPENDIX A. Hydrating and Permeating Liquid Chemistries	118

APPENDIX B. GCL Properties	126
APPENDIX C. Burette Stand Calibration	193
APPENDIX D. Hydraulic Conductivity Data Tables	202
APPENDIX E. Additional Plots	207
APPENDIX F. Additional Photographs	247
APPENDIX G. Test Summary Sheets	320
APPENDIX H. Procedural Analysis Between the Standard Method and the Gravity Method	371

LIST OF TABLES

Table 2.1. Hydrating and permeating liquid chemistries	49
Table 2.2. Properties of GCLs	50
Table 2.3. Characteristics of needle-punched fibers for the three GCLs used in this study	51
Table 2.4. Index properties of GCLs	52
Table 2.5. Comparison of the stress conditions between the standard method (S-Method) and the gravity method (G-Method)	60
Table 2.6. Testing program for hydraulic conductivity tests	61
Table 2.7. Testing program for oedometer hydration tests	62
Table 2.8. Testing program for permeameter hydration tests	63
Table 2.10. Results of hydraulic conductivity tests	64
Table 2.11. Results of oedometer hydration tests	65
Table 2.12. Results of permeameter hydration tests	66
Table 3.1. Hydrating and permeating liquid chemistries	97
Table 3.2. Testing program hydraulic conductivity tests	98
Table 3.3. Testing program and results for empty permeameter flowrates	103
Table 3.4. Results of hydraulic conductivity tests	106

LIST OF FIGURES

Figure 2.1. Cross-section of dry GCL specimens. (a) GCL-3 (b) GCL-1 (c) GCL-2. Scale in mm	53
Figure 2.2. Zoomed out cross-section of dry GCL specimens. (a) GCL-3 (b) GCL-1 (c) GCL-2. Scale in mm.	54
Figure 2.3. Zoomed in cross-section of dry GCL specimens. (a) GCL-3 (b) GCL-1 (c) GCL-2. Scale in mm.	55
Figure 2.4. Exemplary photograph for (a) measuring fiber bundle thickness and (b) counting the number of monofilament fibers per fiber bundle using a digital stereoscopic microscope.	56
Figure 2.5. (a) Schematic of test setup using the standard method. (b) Schematic of test setup using the gravity method.	57
Figure 2.6. Picture of experimental setup following the standard method.	58
Figure 2.7. Picture of experimental setup using the gravity method. (a) Elevated inflow burette. (b) Permeameter.	59
Figure 2.8. Comparison between the standard method and the gravity method of the determined degree of saturation for GCL-1 and GCL-2 permeated with conservative water (CW) and synthetic gold mining process solution (Au-PS).	67
Figure 2.9. Degrees of saturation for tests permeated by the standard method, gravity method, and modified standard methods for GCL-1, GCL-2, and granular bentonite (GB) permeated with conservative water (CW), synthetic gold mining process solution (Au-PS), and deionized water (DW).	67

Figure 2.10. Void ratio for tests permeated by the standard method, gravity method, and modified standard methods for GCL-1, GCL-2, and granular bentonite (GB) permeated with conservative water (CW), synthetic gold mining process solution (Au-PS), and deionized water (DW).68

Figure 2.11. Dry density (Mg/m³) for tests permeated by the standard method, gravity method, and modified standard methods for GCL-1, GCL-2, and granular bentonite (GB) permeated with conservative water (CW), synthetic gold mining process solution (Au-PS), and deionized water (DW).68

Figure 2.12. Comparison of the determined degree of saturation with the textile correction method to the determined degree of saturation without the textile correction method.69

Figure 2.13. Average degree of saturation for GCL-1 and granular bentonite (GB) hydrated in oedometers with deionized water (DW), conservative water (CW), and synthetic gold mining process solution (Au-PS).69

Figure 2.14. Degree of saturation for GCL-1 and granular bentonite (GB) hydrated in oedometers with deionized water (DW), conservative water (CW), and synthetic gold mining process solution (Au-PS).70

Figure 2.15. Void ratio of saturation for GCL-1 and granular bentonite (GB) hydrated in oedometers with deionized water (DW), conservative water (CW), and synthetic gold mining process solution (Au-PS).70

Figure 2.16. Dry density (Mg/m³) of saturation for GCL-1 and granular bentonite (GB) hydrated in oedometers with deionized water (DW), conservative water (CW), and synthetic gold mining process solution (Au-PS).71

Figure 2.17. Comparison of the degree of saturation with the textile correction method to the degree of saturation without the textile correction method for GCL-1 hydrated in oedometers with deionized water (DW), conservative water (CW), and synthetic gold mining process solution (Au-PS).71

Figure 2.18. Average degrees of saturation for GCL-1 and hydrated in permeameters using the standard method and gravity method with conservative water (CW).72

Figure 2.19. Degrees of saturation for GCL-1 and hydrated in permeameters using the standard method and gravity method with conservative water (CW).72

Figure 2.20. Void ratio for GCL-1 and hydrated in permeameters using the standard method and gravity method with conservative water (CW).73

Figure 2.21. Dry density (Mg/m³) for GCL-1 and hydrated in permeameters using the standard method and gravity method with conservative water (CW).73

Figure 2.22. Comparison of the degree of saturation with the textile correction method to the degree of saturation without the textile correction method for GCL-1 hydrated in permeameters with conservative water using the standard method and gravity method. 74

Figure 2.23. Average measured bentonite water contents for GCL-1 and GCL-2 permeated with conservative water (CW) and synthetic gold mining process solution (Au-PS).74

Figure 2.24. Average measured bentonite water contents for GCL-1 and granular bentonite (GB) hydrated in oedometers with deionized water (DW), conservative water (CW), and synthetic gold mining process solution (Au-PS).75

Figure 2.25. Average measured water content for GCL-1 and hydrated in permeameters using the stand method and gravity method procedures with conservative water (CW).75

Figure 2.26. Hydraulic conductivity, k , for tests permeated by the standard method and gravity method for GCL-1, GCL-2, and granular bentonite (GB) permeated with conservative water (CW), synthetic gold mining process solution (Au-PS), and deionized water (DW).76

Figure 2.27. Fiber bundles and surrounding bentonite stained with rhodamine-WT dye at termination of permeation for tests conducted by gravity method.77

Figure 2.28. (a) View of dyed carrier (black) textile during dyed disassembly. (b) Fiber bundles and surrounding bentonite stained with rhodamine-WT dye after termination.78

Figure 2.29. Hydraulic conductivity, k , for tests permeated by the standard method, gravity method, and modified standard methods for GCL-1 permeated with conservative water (CW), synthetic gold mining process solution (Au-PS), and deionized water (DW).79

Figure 2.30. Hydraulic conductivity, k , for tests permeated by the standard method, gravity method, and modified standard methods for GCL-2 permeated with conservative water (CW).79

Figure 2.31. Hydraulic conductivity, k , versus pore volumes of flow (PVF) for Test Series 10, GCL-2 permeated with conservative water using the standard method. Pore volume of Test 10a calculated using avg. pore volume from Tests 10b and 10c.80

Figure 2.32. Hydraulic conductivity, k , versus pore volumes of flow (PVF) for Test Series 11, GCL-2 permeated with conservative water using the gravity method. Pore volume of Test 11a calculated using avg. pore volume from Tests 11b and 11c.80

Figure 2.33. Hydraulic conductivity, k , versus pore volumes of flow (PVF) for Test Series 2. GCL-1 permeated with conservative water using the gravity method. Pore volume of Test 2d calculated using avg. pore volume from Tests 2a, 2b, and 2c.81

Figure 2.34. Determined hydraulic conductivity, k , versus pore volumes of flow (PVF) for Test Series 4. GCL-1 permeated with synthetic gold mining process solution using the gravity method.81

Figure 2.35. Hydraulic conductivity, k , versus pore volumes of flow (PVF) for Test Series 12, GCL-2 permeated with conservative water using modified standard method 6.82

Figure 2.36. Hydraulic conductivity, k , versus pore volumes of flow (PVF) for Test Series 13, GCL-2 permeated with conservative water using modified standard method 7.82

Figure 2.37. Hydraulic conductivity, k , versus cumulative inflow for test series 16 (standard method) and 17 (gravity method), GCL-3 permeated with conservative water.83

Figure 3.1. Schematic of test setup using the gravity method.99

Figure 3.2. Schematic of mine-waste-leachate resistant flexible wall permeameter setup.	100
Figure 3.3. Cross-section schematic comparison of 3.18-mm (1/8-in) and 6.35-mm (1/4-in) tubing sizes.	101
Figure 3.4. Photograph of external acetal tubing clamps used on flexible polypropylene tubing in lieu of metal valves. Scale in mm.	101
Figure 3.5. Photographs of (a) assembled mine-waste-leachate resistant permeameter assembly using gravity head method and (b) permeameter close up.	102
Figure 3.6. Equivalent k (m/s) through empty permeameters. MW permeameter = mine-waste-resistant permeameter.	104
Figure 3.7. Determined hydraulic conductivity, k , for GCL-1, GCL-2, and GCL-3, permeated with deionized water (DW), tap water (TW), conservative water (CW), synthetic gold mining process solution (Au-PS), synthetic bauxite mining process solution (BX-PS), and synthetic copper mining process solution Cu-PS.	105
Figure 3.8. Hydraulic conductivity, k , by chemical termination criteria (hydraulic and chemical equilibrium), versus k by hydraulic termination criteria (hydraulic equilibrium) for GCL-1, GCL-2, and GCL-3 permeated with conservative water (CW), synthetic gold mining process solution (Au-PS), synthetic bauxite mining process solution (BX-PS), and synthetic copper mining process solution (Cu-PS).	107
Figure 3.9. (a) Dyed specimen permeated with conservative water. (b) Dyed specimen permeated with synthetic gold mining process solution. (c) Dyed specimen permeated with synthetic bauxite mining process solution.	108
Figure 3.10. (a) Bentonite removed from GCL-2 permeated with synthetic copper mining process solution (Cu-PS). (b) GCL-2 cross-section permeated with Cu-PS.	109
Figure 3.11. (a), (b) Dyed cross-section of GCL-2 permeated with synthetic copper mining process solution.	110

Figure 3.12. Hydraulic conductivity, k , versus cumulative inflow for specimens permeated with conservative water.111

Figure 3.13. Hydraulic conductivity, k , versus pore volumes of flow (PVF) for specimens permeated with synthetic gold mining process solution.111

Figure 3.14. Hydraulic conductivity, k , versus pore volumes of flow (PVF) for specimens permeated with synthetic bauxite mining process solution.112

Figure 3.15. Determined hydraulic conductivity, k , versus pore volumes of flow (PVF) for specimens hydrated with synthetic copper mining process solution.112

CHAPTER 1

Introduction

1.1 Background

1.1.1 Geosynthetic Clay Liners

Geosynthetic clay liners (GCLs) are thin (< 10 mm) factory manufactured hydraulic barriers used in environmental containment systems. GCLs consist of bentonite (clay) bonded or sandwiched between layer(s) of geotextile and/or geomembrane. Layers may be connected by needle-punched fibers that provide shear strength and maintain bentonite distribution during transportation and installation. GCLs are effective barriers because of the propensity of bentonite to swell and immobilize water which results in low hydraulic conductivity. When hydrated and permeated with a dilute solution (e.g. tap water), the layer of bentonite within the GCL forms a low hydraulic conductivity ($\leq 2\text{-}3 \times 10^{-11}$ m/s), k , layer that acts as a barrier for fluid flow and contaminant transport (Shackelford et al. 2000). However, the same factors that result in low k are sensitive to chemical interactions that may reduce swelling and thus increase k .

GCLs have been used as barriers in waste containment (e.g., liners and covers for municipal and hazardous waste landfills as well as liners for evaporation ponds, wastewater ponds, manure lagoons, and secondary containment in tank farms) for the past three decades. The effectiveness of GCLs in containment applications has been demonstrated for systems with low ionic strength solutions and leachates (Shackelford et al. 2000, Jo et al. 2004), such as municipal solid waste leachates (Bradshaw and Benson 2014). However, GCLs are being increasingly used in wider ranging applications that stretch the limits of GCL performance, such as to contain brines generated in energy production and leaching solutions generated during mineral extraction, such that further research and laboratory testing is necessary to demonstrate the limits of GCL effectiveness.

1.1.2 Hydraulic Behavior

The hydraulic behavior of GCLs is governed by the swelling of montmorillonite, the dominant mineral of the bentonite component of the GCL (Bergaya and Lagaly 2013, Shackelford et al. 2000). Bentonite in GCLs is in the form of dry granules of the sand or silt-sized range that are assemblages of montmorillonite platelets as well as accessory minerals (Shackelford et al. 2000, Scalia et al. 2011). When hydrated, the low k of bentonite results from the osmotic adsorption of water around montmorillonite platelets (McBride 1994), which is manifested as swelling of an immobile phase of water and results in the sealing of inter-granular pores (Mersi & Olson 1971, Mitchell & Soga 2005). Thus, mobile phase water is relegated to narrow and tortuous intra-granular flow-paths (Jo et al. 2006), which results in low k , typically $< 3 \times 10^{-11}$ m/s at low effective stresses, < 35 kPa. However, for osmotic swelling to occur, monovalent cations (e.g. Na^+) must dominate the montmorillonite exchange complex, and the permeant solutions must have a low ionic strength (Norrish and Quirk 1954); the definition of low depends of the specific combination of bentonite (mineralogy, bound cation composition, granule size, ect.), liquid chemistry, and effective stress.

1.1.3 Factors Affecting Hydraulic Behavior

Unfortunately, many liquids, such as brines generated in energy production and mining applications, may result in high k of GCLs, particularly at low effective stress, σ' . Three factors that must be considered when evaluating the hydraulic performance of GCLs in these applications: the hydrating and permeating liquid chemistry; the bentonite quality and any additives to the bentonite; and the effective stress. These factors are described subsequently.

1.1.3.1 Hydrating and Permeating Liquid Chemistry

The chemistry of the hydrating and permeating liquid plays a critical role in the hydraulic performance of GCLs. Three chemical mechanisms exist which can substantially reduce swelling

in bentonite, resulting (at low effective stresses) in a substantial increase in k ; cation exchange plus wet-dry cycles, high concentrations, and extreme pH ($\text{pH} < 3$ and $\text{pH} > 12$).

Exchange of multivalent cations replacing monovalent cations can reduce bentonite swell and increase k , an effect that is exponentially magnified if bentonite experiences wet-dry cycles (Benson and Meer 2009). For high swell to occur, monovalent cations (such as sodium, Na^+) must satisfy the exchange complex of montmorillonite; Na^+ is the dominant cation in bentonite used in GCLs. However, monovalent cations are thermodynamically unfavorable in environments where multivalent cations are present (Sposito 1989), including most naturally occurring pore waters and most leachates (Kolstad et al. 2004, Bradshaw and Benson 2014). When present, multivalent cations replace monovalent cations, resulting in partial removal of immobile water (Benson & Meer 2009), more conductive pore spaces, and up to a 10-times increase in k (Jo et al. 2005, Lee & Shackelford 2005). If the exchanged clay is then desiccated and rehydrated, high swelling will not occur, and up to a 100,000-times increase in k will result (Benson and Meer 2009). Pre-hydration also influences the impact of cation exchange in GCLs; a prehydrated GCL is initially hydrated with deionized water (DW), distilled water, tap water (TW), or other dilute solution, whereas a non-prehydrated GCL is first wetted with the same solution used during permeation. Prehydrated GCLs have been shown to initially exhibit lower k compared to the non-prehydrated GCLs (Shackelford et al. 2000). More rapid changes in k have been shown to occur for a given divalent cation concentration permeant solution for the non-prehydrated case relative to the prehydrated case with the same solution (Jo et al. 2004). All GCL specimens presented in this study are non-prehydrated to represent worst-case scenario field hydration conditions, and to increase the rapidity at which chemical equilibrium is attained. As discussed, increasing the bound cation valence from +1 to +2 increases the k for GCLs. However, increasing the cation valence from +2 to +3 results in negligible increases in k , demonstrating that the specific polyvalent cation is unimportant. (Jo et al. 2001).

The magnitude of bentonite swell is also a function of the concentration of dissolved ions in the pore water, with more swell occurring when pore water is more dilute (Norrish & Quirk 1954). Sufficiently strong hydrating or permeant solutions will reduce or eliminate high swell (Norrish & Quirk 1954, McBride 1994), and result in up to a 100,000-times increase in k relative to dilute conditions (Guyonnet et al. 2009, Scalia & Benson 2011). For single species salt solutions, at low concentrations (< 0.01 M) increases in k are often negligible. However, k can increase to the order of 10^{-7} m/s (the k with DW is $\sim 10^{-11}$ m/s) as concentrations increase above 0.1 M for monovalent cations and above 0.025 M for divalent and trivalent cations (Jo et al. 2001). For multi-species salt solutions, Kolstad et al. (2004) related the effects of concentration with cation exchange by presenting plots of the ratio of monovalent-to-divalent cations (RMD, defined in greater detail in Chapter 2) versus ionic strength that included contours for predicting k . Kolstad et al. (2004) found k to be inversely related to RMD and directly related to ionic strength with the most extreme solution (ionic strength = 0.5 M and RMD = 0.00) exhibiting a k of 1.0×10^{-7} m/s.

Bentonite is also unstable at $\text{pH} < 3$ and $\text{pH} > 12$, these solutions can result in bentonite dissolution and increase k (e.g. Jozefaciuk and Matyka-Sarzynska 2006, Gates and Bouazza 2010, Jo et al. 2001). In addition, extreme pH solutions have high concentrations of dissolved protons and hydroxyls, as well as other dissolved elements, which will reduce or eliminate high swell (Shackelford et al. 2010), resulting in high k .

1.1.3.2 Bentonite Quality and Additives

The quality of the bentonite primarily depends on the montmorillonite content, but also the surface area of the bentonite, and the surface charge density of the bentonite (Lee and Shackelford 2005b). A higher quality bentonite with greater montmorillonite content can have up to $\sim 3\times$ lower k compared to a lower quality bentonite (Lee and Shackelford 2005b). The quality of the bentonite can also affect the time and pore volumes of flow (PVF) necessary to achieve chemical equilibrium, with higher quality bentonite generally requiring greater PVF (Lee and

Shackelford 2005b). Additionally, natural Na-bentonite has been shown to exhibit lower k compared to sodium-activated bentonite (Guyonnet et al. 2005) (sodium-activated bentonite is naturally occurring calcium bentonite that has been artificially converted to Na-bentonite prior to hydration). Additives, such as polymers, may also be added to bentonite to enhance k to aggressive permeant solutions (Katsumi et al. 2008, Scalia et al. 2014).

1.1.3.3 Effective Stress

Potentially counteracting the described mechanisms that reduce bentonite swell yielding more open and connected pores and higher k , greater effective stress results in lower void ratio (greater dry density) and lower k (Mersi and Olson 1971, Petrov et al. 1997, Shackelford et al. 2000). Petrov and Rowe (1997) demonstrated this affect in GCLs. For a given permeant liquid, increases in the confining stress resulted in decreases in k with the lower and higher k ranging by one and a half orders of magnitude over σ' ranging from 3.5 kPa to 115 kPa. The decreases in k were attributed to decreases in the volume of voids that resulted from increases in confining stress. (Petrov and Rowe 1997).

1.1.4 Hydraulic Compatibility Testing

Often, project specific hydraulic compatibility tests are necessary to identify specific combinations of permeant liquid, bentonite, and effective stress that may result in high k . If the specific combination of project specific permeant, bentonite, and effective stress, results in an unacceptably high k (e.g., $\gg 3 \times 10^{-11}$ m/s), then the GCL may be deemed incompatible, and an alternative technology may be required. To demonstrate low k and the suitability of a GCL to be used as a containment barrier in a specific application, hydraulic compatibility testing is performed through laboratory k testing to chemical equilibrium.

1.1.4.1 Hydraulic Conductivity Testing by the Standard ASTM Method

ASTM D6766-12 (*Standard Test Method for Evaluation of Hydraulic Properties of Geosynthetic Clay Liners Permeated with Potentially Incompatible Solutions*) provides a method for measuring k of a GCL with potentially incompatible solutions. The default procedure described in ASTM D6766-12 will henceforth be referred to as the standard method (S-Method). The S-Method employs a flexible wall permeameter [typically with 10.2 cm (4-in) diameter] with an average effective stress of 27.6 kPa (4 psi) and an average head loss across the specimen of 1.41 m (2 psi). However, this method, and the equipment (i.e., permeameters and bladder accumulators) typically employed, are not designed for the high concentration and extreme pH solutions (pH < 3 or pH > 12) encountered in some applications, such as in mine waste leachates. Additionally, the S-Method recommends that backpressure be used to attain saturation.

1.1.4.2 Backpressure Saturation

Backpressure saturation involves applying elevated fluid pressure to both the inflow and outflow ends of a k test; elevated fluid pressure is intended to dissolve small air bubbles that remain in the pore space of the specimen after the specimen has been inundated in the permeant liquid. The S-Method employs default backpressures of approximately 550 kPa (80 psi).

Implementation of backpressure saturation in the S-Method is intended to ensure a saturated specimen. A given soil in an unsaturated state will have lower k than when in a saturated state (Lu and Likos 2004). Ensuring that a soil specimen is saturated ensures that a maximum k is being measured for a given combination of permeant liquid, bentonite, and effective stress. In containment applications, measuring a maximum k is necessary to provide a conservative estimate for leakage rate calculations. Unintentionally measuring the k of an unsaturated specimen will result in an uncharacteristically low k and provide an un-conservative estimate of leakage rates in containment applications

In this study, bentonite is hypothesized to be a self-saturating material, in that bentonite will reach 100% saturation without backpressure saturation. GCLs are homogenous and high swelling and that high swelling will induce swelling pressures on a confined GCL which are hypothesized to dissolve any air bubbles remaining in the pores. Thus, the hypothesis tested is that backpressure saturation is not necessary for GCLs to attain saturation.

The implementation of backpressure saturation to a hydraulic compatibility test leads to a more complex test, such as the additional need for permeant interface devices, safety concerns of elevating potentially hazardous permeant liquids to high pressures, and the requirement on a constant supply of compressed air for long-duration tests. These concerns have led to the implementation of an alternative method for hydraulic compatibility testing.

1.1.4.3 Alternative Testing Method

A simpler gravity-head based method has been used in research (e.g., Jo et al. 2004, Kolstad et al. 2004, Lee and Shackelford 2005, Meer and Benson 2007, Bradshaw and Benson 2014, Scalia et al. 2014, Tian et al. 2016). This simplified method is like the falling headwater-constant tailwater method in ASTM D6766-12 (*Method B*), except backpressure saturation and permeant interface devices are not included, and an elevation head is used to produced flow. This method has been employed to facilitate long-term k testing of GCLs, with some tests lasting up to 7 yr (Katsumi et al. 2008, Bradshaw & Benson 2014). Gravity heads are used to apply the hydraulic gradient and (at low stresses) cell pressure to minimize potential problems associated with implementing backpressure saturation. This alternative method will be referred to herein at the gravity method (G-Method). The use of the G-Method in this study employs a flexible wall permeameter with an average effective stress of 27.6 kPa (4 psi) and average head loss across the specimen of 1.41 m (2 psi), and introduces the use of a mine-waste-resistant permeameter (MW permeameter) made of materials that are resistant to solution with high ionic strength and extreme pH. The MW permeameter is discussed in further detail in Chapter 2.

1.2 Research Objectives

The goal of this study is to verify that the S-Method and G-Method yield the same results for k and show that backpressure saturation is not necessary to achieve complete saturation in GCL specimens, and to begin testing GCLs with mine-waste leachates using the G-Method. Results are compared to assess the accuracy of the G-Method used with the MW permeameter to the S-Method described by ASTM 6766-12 and a commercially available permeameter. This comparative study is necessary to show that the G-Method and MW permeameter can be used in ongoing and future k testing of GCLs with mine-waste leachates.

CHAPTER 2

Effect of backpressure saturation on the hydraulic conductivity of GCLs

2.1 Introduction

Often project specific hydraulic compatibility tests are necessary to identify specific combinations of permeant liquid, bentonite, and effective stress that may result in high k . If the specific combination of interest results in an unacceptably high k (e.g., $\gg 3 \times 10^{-11}$ m/s), then the GCL may be deemed incompatible, and an alternative barrier technology may be required. To demonstrate low k and the suitability of a GCL for use as a containment barrier in each application, hydraulic compatibility testing is performed through laboratory k testing to chemical equilibrium.

D6766-12 (*Standard Test Method for Evaluation of Hydraulic Properties of Geosynthetic Clay Liners Permeated with Potentially Incompatible Solutions*) provides a method for measuring k of a GCL with potentially incompatible solutions. The default procedure described in D6766-12 will henceforth be referred to as the “standard method” (S-Method). However, this method, and the equipment (i.e., permeameters and bladder accumulators) typically employed, are not designed for the high concentration and extreme pH solutions ($\text{pH} < 3$ or $\text{pH} > 12$) encountered in some applications, such as in mine waste leachates. Additionally, the S-Method requires that backpressure saturation be used. Backpressure saturation involves applying elevated fluid pressure to both the inflow and outflow ends of a k test; elevated fluid pressure is intended to dissolve small air bubbles that remain in the pore space of the specimen after the specimen has been inundated in the permeant liquid. Implementation of backpressure saturation is intended to ensure a saturated specimen. A given soil in an unsaturated state will have lower k than when in a saturated state (Lu and Likos 2004). Ensuring that a soil specimen is saturated ensures that a maximum k is measured for a given combination of permeant liquid, bentonite, and effective stress. In containment applications, measuring a maximum k is necessary to provide a conservative estimate of anticipated leakage rates. Unintentionally measuring the k of an

unsaturated specimen will result in an uncharacteristically low k and provide an un-conservative estimate of leakage rates in a containment application. The implementation of backpressure saturation to a hydraulic compatibility test leads to a more complex test, such as the additional need for permeant interface devices, safety concerns of elevating potentially hazardous permeant liquids to high pressures, and the requirement of a constant supply of compressed air for long-duration tests. These concerns have led to the implementation of an alternative method for k testing. Additionally, bentonite is hypothesized to be a self-saturating material, in that bentonite will reach 100% saturation without backpressure saturation; this hypothesis is tested in this study.

A simpler gravity-head based method has been used in research (e.g., Jo et al. 2004, Kolstad et al. 2004, Lee & Shackelford 2005, Meer & Benson 2007, Bradshaw & Benson 2014, Scalia et al. 2014, Tian et al. 2016). This simplified method is like the falling headwater-constant tailwater method in D6766-12 (*Method B*), except backpressure saturation and permeant interface devices are not included, and an elevation (gravity) head is used to produce flow. This alternative method will be referred to herein as the gravity method (G-Method). The goal of this study is to verify that the S-Method and G-Method yield the same results for k and show that backpressure saturation is not necessary to achieve 100% saturation in GCL specimens during hydraulic compatibility tests.

2.2 Materials and Methods

2.2.1 Liquids

Three liquids were used in this study: deionized water (DW), a synthetic conservative soil porewater (CW), and a synthetic gold mining process solution (Au-PS). The chemical properties of each liquid are summarized in Table 2.1. Target anion and cation concentrations can be found in Appendix A. The DW (electrical conductivity, EC, = 4.2×10^{-4} S/m, pH = 7.0) is classified as Type II reagent water (ASTM D1193-06). The CW (EC, = 5.1×10^{-2} S/m, pH = 5.7) is a synthetic solution intended to represent a worst-case chemistry for natural subgrade hydration and

percolation that could be encountered in a cover system (Scalia and Benson 2010a), and is recommended for use in ASTM D5084-16a. The CW is described in detail in Scalia and Benson 2010a. The Au-PS (EC, = 0.34 S/m, pH 5.1) represents an average leachate encountered in gold heap leach mining operations (Ghazi Zadeh et al. 2017). All liquids were used in k and hydration testing, the methods of which are described in subsequent sub-sections. The CW and Au-PS were prepared by adding reagent grade salts (Fisher Scientific, Waltham, MA) to DW. The CW was prepared by dissolving 15.5 mg of NaCl and 214.6 mg of CaCl₂ in 1 L of DW. The Au-PS was prepared by combining 415.34 mg CaCl₂, 121.44 mg MgCl₂, 1464.6 mg Na₂SO₄, 19.57 mg KNO₃, 141.19 mg NaCl, and 17.99 mg KCl in 1 L of DW. After preparation, solutions were stored in collapsible carboys.

The ionic strength (I) of each liquid was calculated based on the target concentrations as follows:

$$I = \frac{1}{2} * \sum_{i=1}^n c_i z_i^2 \quad (2.1)$$

where I is the ionic strength, i is the constituent number, n is the number of constituents, c_i is the molar concentration of the i^{th} constituent, and z_i is the ion valence of the i^{th} constituent.

The ration of monovalent-to-divalent cations (RMD) was calculated based on target concentrations using the following equation:

$$RMD = \frac{M_M}{\sqrt{M_D}} \quad (2.2)$$

where M_M is the total molarity of the monovalent cations in solution, and M_D is the total molarity of the divalent cations in solution (Kolstad et al. 2004).

Electrical conductivity and pH were measured using a benchtop pH/EC meter (Orion Versa Star, Thermo Scientific, Waltham, MA). The values reported in Table 2.1 are averages taken from multiple measurements (number of measurements, $n > 30$) from May 2016 to July 2017, i.e., during testing. All measurements are reported in Appendix A. Electrical conductivity and pH were used to verify solution concentrations as recommended by Ghazi Zadeh et al. (2017), using EC and pH values from Scalia and Benson (2010a) and Ghazi Zedah et al. (2017).

These liquids (DW, CW, Au-PS) were selected to provide a range of relatively low concentrations and near-neutral pH liquids for verification of the k test methods before additional tests with high concentration and extreme pH mining liquids were tested. The DW represents a base case for GCL k . The CW provides a low concentration solution ($I = 6$ mM), but with a low RMD ($0.19 \text{ mM}^{1/2}$) that will exchange Na^+ for Ca^{2+} and potentially increase k . The Au-PS provides a higher concentration solution ($I = 49$ mM), but also a higher RMD ($10 \text{ mM}^{1/2}$) that is less likely to yield increases in k from cation exchange.

2.2.2 GCLs

In this study three different commercially available needle-punched GCLs were tested, GCL-1, GCL-2, and GCL-3. The initial properties of the GCLs are listed in Table 2.2. GCL-1 consisted of a layer of natural sodium bentonite (mass-per-area = 5.62 kg/m^2) sandwiched between a non-woven carrier geotextile (mass-per-area = 0.28 kg/m^2) and a non-woven cover geotextile (mass-per-area = 0.24 kg/m^2). GCL-2 consisted of a layer of natural sodium bentonite (mass-per-area = 5.04 kg/m^2) sandwiched between a non-woven carrier geotextile (mass-per-area = 0.28 kg/m^2) and a non-woven cover geotextile (mass-per-area = 0.31 kg/m^2). GCL-3 consisted of a layer of natural sodium bentonite (mass-per-area = 5.22 kg/m^2) sandwiched between a woven carrier geotextile (mass-per-area = 0.13 kg/m^2) and a non-woven cover geotextile (mass-per-area = 0.11 kg/m^2). All three products contained coarse sand-sized (ASTM D6913) granules of sodium bentonite from Wyoming, USA. A summary of the mineralogical

composition of the bentonite is included in Table 2.2. The bentonite has a swell index (ASTM D5890), *Si*, of 25.2 mL/2 g in DW and a fluid loss (ASTM D5891) of 13.1 mL/20 min in DW. The bentonite also had Atterberg limits (ASTM D4318; reported in Table 2.2) typical of sodium bentonite used in GCLs (ASTM D4318; Shackelford et al. 2000). As-received water contents were between 5.7 to 10. All textiles were made of polypropylene.

The three products tested represent a range in peel strength, and thus degrees of needle-punching fibers. The characteristics of the needle punching of GCLs 1, 2, and 3 are listed in Table 2.3. GCL-1 (manufacturer reported peel strength, MRPS = 2170 N/m) has an average bundle size of 0.91 mm, and average number of bundles per area of 80,900 bundles/m², an average number of monofilament fibers per bundle of 44, and an estimated percent area covered by fiber bundles of 5.3%. GCL-2 (MRPS = 3500 N/M) has an average bundle size of 1.05 mm, an average number of bundles per area of 105,000 bundles/m², an average number of monofilament fibers per bundle of 41, and an estimated percent area covered by fiber bundles of 9.0%. GCL-3 (MRPS = 700 N/m) has an average bundle size of 0.76 mm, an average number of bundles per area of 21,200 bundles/m², an average number of monofilament fibers per bundle of 20, and an estimated percent area covered by fiber bundles of 1.0%. Figs. 2.1-2.3 includes cross-sectional photographs of the virgin GCLs for visual comparison of needle-punching. GCL-3 has noticeably smaller bundles and fewer numbers of bundles per area than GCL-1 and GCL-2. GCL-1 and GCL-2 have similar bundles sizes and number of monofilament fibers per bundle, though GCL-2 has more fiber bundles per area and a noticeably thicker cover geotextile (Fig. 2.3b,c).

Fiber bundle analysis was conducted on ten 76.2 mm by 76.2 mm (3 in by 3 in) specimens cut from each GCL roll (a total of 30 specimens were analyzed). To determine the number of fiber bundles per area, first the number of fiber bundle per unit length in both the machine direction and cross machine direction were determined by counting the number of fiber bundles visible on two specimen edges along an area extending 5 mm (3/16 in) into the specimen. For each specimen, the average number of fiber bundles per m in the machine direction was multiplied by

the average number of fiber bundles per m in the cross-machine direction to obtain the estimated number of fiber bundles per m². Rowe et al. 2017 described a similar technique along with light table technique (the light table technique would be considered a more accurate method as it is a direct measurement rather than an estimate made by multiplying the number of fiber bundles per unit length in the two dimensions of a given specimen) and concluded that the two techniques do not give statistically different results. The light table technique was not used in this study because all the carrier geotextiles were black and thus light would not penetrate through them to a sufficient degree to give an accurate result (Rowe et al. 2017). The fiber bundle size and number of monofilament fibers per fiber bundle were determined manually using a digital stereoscopic microscope (Fig. 2.4). Two fiber bundles were selected randomly from each specimen for a total of 20 measurements per GCL. Bundle widths were recorded (Fig. 2.4a) and averaged, as were the number of monofilaments per bundle (Fig. 2.4b). Lastly, the percent area of the GCL initially occupied by fiber bundles was estimated assuming circular fiber bundles. Rowe et al. 2017 conducted similar analyses and described similar techniques.

2.2.3 Granular Bentonite

A simulated non-reinforced granular bentonite (GB) GCL was also tested. The GB GCL (mass-per-area = 4.6 kg/m², liquid limit = 420, plastic index = 39, *SI* = 31.4 mL/2 g in DW, fluid loss = 9.0 mL/20 min in DW) consisted of coarse-sand sized granular sodium bentonite. The mineralogical composition of GB, determined by X-ray diffraction (XRD), is 85-95% montmorillonite, 0-5% augite, 2-4% quartz, and <3% cristobalite, plagioclase feldspar-andesine, calcite, illite/mica, heulandite, gypsum, ferroan dolomite, and K-feldspar-microcline (Scalia et al. 2014). The in-permeameter assembly method was used to assemble GCL specimens, this method is described in detail by Scalia et al. (2014).

2.2.4 Hydraulic Conductivity Testing by ASTM Method

Standard method tests were conducted in accordance with the default method described in ASTM D6766-12, *Standard Test Method for Evaluation of Hydraulic Properties of Geosynthetic Clay Liners Permeated with Potentially Incompatible Aqueous Solutions*, using 102-mm (4-in) diameter commercially available flexible wall permeameters. The water or other aqueous solution permeated through the GCL will be referred to herein as the “test liquid.” A testing program of all k tests is provided in Table 2.6.

D6766-12 describes two scenarios where the test methods can be applied; scenario 1 and scenario 2. In scenario 1 the GCL is hydrated with water (DW or tap water, TW) prior to contact with the test liquid. Tests following scenario 1 are referred to as prehydrated. In scenario 2 the GCL is both hydrated and permeated with the test liquid. Tests following scenario 2 are referred to as non-prehydrated and represent a worst-case scenario where the hydraulic and chemical properties of the GCL are governed by the interaction with the test liquid only (refer to Section 1.1.3.1). All tests described in this thesis are non-prehydrated, i.e., following Scenario 2 – Hydrated/Saturated with Test Liquid (Worst Case).

ASTM D6766-12 provides four test methods: Method A, constant headwater – tailwater elevations; Method B, falling headwater elevation – constant tailwater elevation; Method C, falling headwater elevation – rising tailwater elevation, and; Method D, constant rate of flow using a flow pump and measurement of head loss across the specimen with an electronic pressure transducer. All S-method GCLs in this study were permeated using a falling head – rising tail system (Method C).

ASTM D6766-12 specifies use of a permeant interface device when a hazardous/corrosive liquid is tested. These devices commonly are used for all GCL compatibility tests to isolate corrodible and hard-to-clean panel boards from permeant solutions. Thus, permeant interface devices were used for all tests. Often the permeant interface devices used are bladder accumulators which allow direct fluid measuring on the panel board. However, for simplicity

external liquid reservoirs with applied air pressure (i.e., external column reservoirs) were used in this study. Refer to Fig. 2.5a for a schematic of the test set up and Fig. 2.6 for a picture of the test set up in the laboratory.

The ASTM D6766-12 default backpressure saturation/hydration and consolidation procedure (i.e., for tests not specified otherwise by the requester) was followed, as described subsequently. This procedure is described in detail to compare to the gravity method in the next section. A schematic of the test set up, with labeled components discussed in this section, is provided in Fig. 2.5a.

After permeameters were assembled, specimens were hydrated and saturated following ASTM D6766-12 section 8.2 *Backpressure/Hydration and Consolidation*. Section 8.2.4 states “Increase the cell pressure to 105 kPa (15 psi) and then backpressure to 70 kPa (10 psi) on both ends of the specimen.” This is the only text that describes the procedures for introducing the test liquid to the GCL which at this stage is still completely dry granules (with exception on a small portion of the edges that were hydrated with the test liquid to prevent any bentonite loss from the specimen during specimen preparation and handling). For the GCL to saturate, the test liquid must be introduced to the dry granules. However, this cannot be done while maintaining both the inflow and outflow at the same pressure; a gradient must be applied to the specimen in this step to introduce the test liquid to the GCL’s dry granules, and to remove air from permeameter tubing. Initial specimen hydration was accomplished by raising the cell pressure to 105 kPa (15 psi) and inflow pressure to 70 kPa (10 psi) while venting the outflow pressure (viz. maintain atmospheric conditions) for between 30 seconds to 2 minutes. In this step the void space between dry bentonite granules (water content of 5.6-10%) is replaced by water, and the bentonite granules begin to hydrate, swell, and saturate. Implementation of *Section 8.2.4* is described sequentially below, permeameter components are labeled in Fig. 2.5a:

1. Valves A, B, C, D, and E are closed.

2. The headwater reservoir is filled with the test liquid.
3. Regulator Z is set to 105 kPa (15 psi), while regulators X and Y are bridged (the pressure panels allow for adjacent regulators to be connected to output identical pressures) and set to 70 kPa (10 psi).
4. Regulator Y is unbridged and vented.
5. Valves I and J are opened to apply the pressure from the regulators to the headwater and tailwater reservoirs respectively. This is all the while valves A and B remain closed keeping the liquid out of contact with the test specimen.
6. Valve E is opened to apply 105 kPa (15 psi) to the cell water.
7. Valve B is opened applying the inflow pressure of 70 kPa (10 psi).
8. Valve C is opened to the atmosphere allowing the test liquid to flush all of the air out of the inflow lines. Valve C is closed when all visible air bubbles have been removed. This takes 15 s to 1 min.
9. Valve D is opened to the atmosphere. This creates at 70 kPa (10 psi) head loss across the specimen, permeating the specimen and introducing the test liquid to the previously dry porous stones, filter paper and bentonite granules. Valve D is closed when all visible air bubbles have been removed. This takes 15 s to 1 min.
10. Valve A is opened. With regulator Y vented to the atmosphere this creates the same scenario as when valve D was opened to the atmosphere permeating the dry granules that have now begun to hydrate. Valve A is closed when all visible air bubbles have been removed and the tailwater reservoir has been filled to a measurable level. Filling the tailwater reservoir to a measurable level ensures that the effluent line has been completely filled with the test liquid.
11. Valve B and also valves I and J are closed.
12. Regulator Y is bridged to regulator X.

13. Valves I and J are then reopened, followed by valves A and B being opened simultaneously. If valves A and B are not able to be opened simultaneously then valve B (influent line) should be opened first to keep the head losses across specimen consistent with the rest of the testing procedure, even for short times. With the cell pressure now at 105 kPa (15 psi) and backpressure now at 70 kPa (10 psi) this concludes *Section 8.2.4* of D6766-12.

The next phase in the procedure is applying the increased backpressure. Backpressure is increased in steps starting from the initial 105 kPa (15 psi) cell pressure, 70 kPa (10 psi) backpressure state. *Section 8.2.5* of ASTM 6766-12 states “Increase the cell pressure and backpressure simultaneously in increments of 70 kPa (10 psi) in 1-min intervals until a final cell pressure of 550 kPa (80 psi) and a final backpressure of 515 kPa (75 psi) are obtained.” 1 min is allowed to pass after the conclusion of *Section 8.2.4* before starting this section. Implementation of *Section 8.2.5* is described sequentially below.

1. Valves I, J, and K are closed. For consistency valve J is closed first followed by valve I and then valve K.
2. Regulator Z is increased to 25 psi and regulator X is increased to 20 psi (regulator Y is still bridged to regulator X, thus also carries 20 psi). Valves I, J, and K are closed so pressure increases are not applied to the specimen.
3. *Section 8.2.5* of ASTM D6766-12 states that the cell pressure and backpressure be increased “simultaneously.” Based on this description, valves I, J, and K should be opened simultaneously. However, they are three separate valves and a single operator can in practice, having only two hands, only open two valves simultaneously. In this study, each valve is opened individually in rapid succession. Valve K (cell pressure) is opened first (opening the cell pressure valve first, and thus increasing the cell pressure before increasing the backpressure, ensuring that the effective stress on the specimen never falls

below zero which would cause a loss of contact between the specimen to the membrane), immediately followed by valve I (inflow backpressure), and valve J (outflow backpressure). Generally, there is about 1-3 s between opening each valve. This creates a pulse of increased effective stress of ~ 105 kPa (15 psi) for ~ 2-5 s, when the cell pressure is increased before the backpressure has been increased, when, in theory, the effective stress should never exceed 35 kPa (5 psi). The consequence of this brief stress increase, and detailed analysis of the stress conditions during the standard method procedure, is discussed in Section 2.5.

4. After 1 minute, valves I, J, and K are again closed. Valves are closed in the reverse order; valve J is closed first, followed by valve I, then valve K.
5. Regulators Z and X are again increased by 70 kPa (10 psi), and the same pattern is followed until a final cell pressure and backpressure of 550 kPa (80 psi), and 515 kPa (75 psi), respectively, are reached. The final step follows the same pattern, but with regulators Z and X only increased by 35 kPa (5 psi) [as oppose to 70 kPa (10 psi)]. After the final pressure step has been applied, valves I, J, and K are left open concluding *Section 8.2.5* of ASTM D6766-12.

Finally, specimens are allowed to saturate for 48 hr under backpressure prior to permeation. *Section 8.2.6* of ASTM 6766 states “Maintain the cell pressure of 550 kPa (80 psi) and backpressure of 515 kPa (75 psi) for a period of 48 h to allow saturation, hydration, swell, and consolidation to occur.” After 48 hr, permeation is initiated:

1. Valves I, J, and K are closed in the order of J, I, K.
2. Regulator K is left at 550 kPa (80 psi), regulator Y is un-bridged from regulator X and increased to 515 kPa (75 psi), and regulator X is increased to 530 kPa (77 psi).
3. To begin permeation, valves I, J, and K are opened in the order of K, I, J.

Measurements are taken at regular intervals (dependent on the k of the specimen) until the termination criteria outlined in *Section 8.4* of ASTM D6766-12 have been met. Measurements were continued until the hydraulic termination criteria listed in ASTM D6766-12 were met, i.e., three consecutive measurements of hydraulic conductivity and volumetric flowrate ratio (the ratio of outflow to inflow volumes over a given measurement interval) within 25% of the average of the three measurements.

Hydraulic conductivity (m/s) is calculated using the following equation:

$$k = \frac{aL}{2At} \ln\left(\frac{h_1}{h_2}\right) \quad (2.3)$$

where a is the cross-sectional area of the reservoir containing the influent and effluent liquid in m^2 , L is the length of the specimen in m, A is the cross-sectional area of the specimen in m^2 , t is the elapsed time between the determination of h_1 and h_2 in seconds ($t_2 - t_1$), h_1 is the head loss across the specimen at time t_1 , and h_2 is the head loss across the specimen at time t_2 . Equation 2.3 is a special case of the falling-headwater rising-tailwater equation provided in *Section 9.3.2* of ASTM D6766-12 where the cross-sectional areas of the influent and effluent reservoirs are equivalent and a single value for a is used. L is assumed to be 7.5 mm for calculations performed to monitor test status (7.5 mm is a typical value for hydrated GCL thickness (Shackelford et al. 2000)). The final determination of L is completed after the test has been terminated and the specimen is removed from the permeameter. A is measured prior to permeation, and is assumed to not change during the test. h_1 and h_2 are determined by calculating the hydraulic head from both the applied air pressure and the elevations of the test liquid in the headwater and tailwater reservoirs.

The volumetric flowrate ratio is calculated by the following equation:

$$\text{Volumetric Flow Ratio} = \frac{q_{out}}{q_{in}} \quad (2.4)$$

where q_{out} is the total effluent volume collected for a given measurement time period, and q_{in} is the total influent volume measured for a given measurement time period.

2.2.5 Hydraulic Conductivity Testing by the Gravity Method

Hydraulic conductivity of GCLs with chemical solutions was also measured by a simplified gravity head based method (G-Method). A testing program of all k tests is provided in Table 2.6. This method is similar to the default method prescribed in ASTM D6766-12 except backpressure saturation and permeant interface devices are not included. A volumetrically graded burette is used as the falling headwater reservoir, in conjunction with constant (atmospheric) outflow for convenient collection for chemical analysis, and to preclude changes in effluent chemistry with changes in pressure. In the G-Method the inflow pressure is supplied with the burette. The burette is elevated in a stand such that the average water level in the burette during the permeation phase is 1.41 m (2 psi) above the effluent orifice. Calibration of the frames used in this study can be found in Appendix C. An average head loss of 1.41 m (2 psi) is maintained across the specimen during testing, identical to the average head loss across the specimen in the standard method. Refer to Table 2.5 for the stress conditions of the gravity method compared to the standard method. A schematic of the test set up, with labeled components is provided in Figure 2.5b.

The gravity method procedure is described subsequently:

Set-up and saturation:

1. The test is assembled and the cell water is filled with TW and valve F is closed.

2. Regulator Z is set to 34.5 kPa (5 psi) and valve E is opened applying 5 psi cell pressure to dry (pre-hydration) specimen. A gravity head of 3.52 m can also be used to apply the 34.5 kPa (5 psi) cell pressure.
3. Valve B is opened (if present).
4. The test liquid is poured into the burette until the burette reaches a water level equivalent to 1.41 m of head.
5. Valve C is opened to the atmosphere, allowing saturation of the influent lines. Valve C is closed when all visible air bubbles have been removed. While saturating the influent lines, the water level in the influent burette should be refilled as necessary to maintain a height of water in the burette of $1.41 \text{ m} \pm 0.125 \text{ m}$.
6. Valve D is opened to the atmosphere, creating an approximately 13.8 kPa (2 psi) head loss across the specimen, permeating the dry granules and introducing the test liquid into the inter-granular bentonite pores. Valve D is closed when all visible air bubbles have been removed. The water level in the influent burette should be refilled as necessary so that the height of water in the burette maintains a head loss across the specimen of $1.41 \text{ m} \pm 0.125 \text{ m}$.
7. Valve A is opened until all visible air bubbles have been removed. This takes 15s to 1 min. The water level in the burette should be refilled as necessary so that the burette maintains a head loss across the specimen of $1.41 \text{ m} \pm 0.125 \text{ m}$. Note steps 2 through 7 replaces *Section 8.2.4* of D6766-12 for the G-Method.
8. *Section 8.2.6* is followed, and 48 h is allowed for bentonite hydration with the effluent line (i.e., valve A) closed. Throughout the 48-h period, the water level in the burette should be monitored to ensure the water level remains between $1.41 \text{ m} \pm 0.125 \text{ m}$. After 48 h, permeation is initiated (described subsequently).

Permeation:

9. The water level in the burette is filled to yield a head loss of 1.41 + 0.125 m.
10. The weight of the effluent collection container is recorded.
11. Valve A is opened to initiate permeation.
12. The water level in the burette lowers as the test liquid is permeated through the specimen. Readings (described in steps 13 – 16) are taken at a regular interval. If necessary, valve A should be closed during a reading to prevent loss of effluent. Once the water level in the burette lowers to a height corresponding to a head loss of approximately 1.41 m – 0.125 m, the inflow burette is refilled to approximately 1.41 + 0.125 m.
13. The water level in the burette is recorded (the water level in the burette corresponds to a head loss across the specimen based on the calibration provided in Appendix C.
14. The weight of the effluent collection container is recorded again
15. The EC and pH of the effluent is measured for tests running to chemical equilibrium. Generally, a minimum effluent volume of 10 mL is required for these analyses.
16. The effluent collection container is emptied, acid washed, re-weighed, and returned to the effluent orifice. Flow is then reinitiated (as necessary) by opening valve A.
17. Steps 12-15 are repeated until the required termination criterion described previously for the standard method (i.e. the same termination criteria are used for the gravity and standard method) have been met.

Hydraulic conductivity for the gravity method can be calculated using the following equation:

$$k = \frac{aL}{At} \ln\left(\frac{h_1}{h_2}\right) \quad (2.5)$$

Table 2.5 provides a comparison of the stress conditions between the standard and gravity methods used in this study. The stress conditions associated with the G-Method were chosen

to mirror the head loss [14 kPa (2 psi) pressure difference] and average effective stress [28 kPa (4 psi)] of the S-Method to facilitate comparison of measured saturation, water content, and k .

2.2.6 Verification of Degree of Saturation

Verification of the degree of saturation was completed by calculation based on weight-volume relationships at the end of permeation. Although D6766-12 provides no requirement for verifying the degree of saturation, ASTM D5084-16a (section 9.3.4) recommends using one of two specific methods to verify saturation (i.e. saturation within 95%-105%). The first method is to verify saturation using the B coefficient (ASTM D4767) after the backpressure saturation phase (measurement of a B value requires backpressure saturation). The second method is calculating the degree of saturation at the end of the test using weight-volume relationships. The advantage of using a B value is that confirmation of saturation is completed prior to permeation rather than waiting until the termination of the test, however, the B value was not used in this study for either the S-Method or the G-Method. The reason for the omission of the B value and the verification of saturation by weight-volume measurements after termination only is that direct comparison with the G-Method, which does not include any backpressure saturation, is desired. Additionally, calculation of the final degree of saturation using weight-volume relationships has been shown to be a more accurate method for verifying the degree of saturation (Chapuis 2017).

Although common practice, and often necessary to achieve saturation for many cohesive soils, backpressure saturation is not required by either ASTM D5084-16a or D6766-12. Both ASTM D5084-16a (section 5.1.7) and ASTM D6766-12 (section 5.2.5) state “The hydraulic system shall have the capability to apply back pressure to the specimen to facilitate saturation”. D5084-16a also states in section 9.3 that “to saturate the specimen, back pressuring is usually necessary.” The purpose of this study is to test whether or not facilitation of saturation by back pressuring is necessary for GCLs.

2.2.7 Hydraulic Conductivity Testing by Alternative Standard Methods

As discussed in Section 2.3.3.1 the S-Method and G-Method did not universally result in similar measured k . To test hypotheses for the discrepancy between the two methods, modified S-Method tests were conducted. The methods of these modified standard method tests are described in the subsequent sections. A testing program of all k tests is provided in Table 2.6.

2.2.7.1 Backpressure Time Interval Changed From 1 min to 1 hr

The first variation to the S-Method is to change the time between stress increments in the backpressure saturation stage described in D6766-12. The time was changed from 1-min to 1-hr. This variation of the S-Method is referred to herein as S-M1.

2.2.7.2 Backpressure Time Interval Changed From 1 min to 4 hr

The second variation to the S-Method is to change the time between stress increments in the backpressure saturation stage described in D6766-12. The time was changed from 1-min to 4-hr, similar to the method described in the previous section, but using 4-hr instead of 1-hr. This variation of the S-Method will be referred to herein as S-M2.

2.2.7.3 Changing Both the Backpressure Time Interval to 4 hr and Stress Increment to 35 kPa

The third variation to the S-Method is to change the stress increments from 70 kPa (10 psi) to 35 kPa (5 psi) and to change the time between steps from 1-min to 4-hr. This variation of the S-Method will be referred to herein as S-M3.

2.2.7.4 Backpressure Stress Increment Changed From 10 psi to 5 psi

The fourth variation to the S-Method is to change the stress increments in the backpressure stage from 70 kPa (10 psi) to 35 kPa (5 psi). This variation of the S-Method will be referred to herein as S-M4.

2.2.7.5 Changing Both the Backpressure Time Interval to 1 d and Stress Increment to 35 kPa

The fifth variation to the S-Method is to change the stress increments from 70 kPa (10 psi) to 35 kPa (5 psi) and to change the time between steps from 1-min to 1-d. This variation of the S-Method will be referred to herein as S-M5.

2.2.7.6 Backpressure Without Time Intervals and Stress Increments

The sixth variation to the standard method is to conduct the test at the elevated backpressures of D6766-12, but do so in a way that there are no stress increments to reach the elevated backpressure and thus, there are no pulses of effective stress during the backpressure stage. This is done in two steps. The first step is to follow the backpressure procedure in ASTM D6766-12 before the test liquid is introduced to the specimen. At the end of this step, the GCL specimen is under the same elevated cell pressure and porewater pressure, but is still in dry granules. Next the permeameter lines are flushed in the same manner as the S-Method while always keeping the cell and porewater pressures elevated. This variation of the S-Method method will be referred to herein as S-M6.

2.2.7.7 Gravity Method Followed by Standard Method on the Same Specimen

The seventh variation to the standard method is to conduct a test mirroring the G-Method (identical cell pressures and pore pressures) to hydraulic equilibrium and then follow the backpressure procedure of the S-Method. This variation of the S-Method will be referred to herein as S-M7.

2.2.8 Hydration Testing in Oedometers

Hydration tests were completed in Oedometer cells on GB and GCL-1 specimens hydrated with DIW, CW, and Au-PLS. Specimens had the same vertical effective stress as the average effective stress of the S-Method and G-Method, 27.6 kPa (4 psi). After allowing 48-hr,

the same hydration period as the S-Method and G-Method, the measured water content and determined weight-volume relationships were used to calculate the degree of saturation, void ratio, and dry density. A testing program of all oedometer hydration tests is provided in Table 2.7.

2.2.9 Hydration Testing in Permeameters

Hydration tests were completed in Oedometer cells on GCL-1 specimens hydrated with CW using both the S-Method and the G-Method hydration procedures described in Section 2.2.5 and Section 2.2.6 respectively. After allowing 48-hr the measured water content and determined weight-volume relationships were used to calculate the degree of saturation, void ratio, and dry density. A testing program of all permeameter hydration tests is provided in Table 2.8.

2.2.10 Flow Path Dying

For hydraulic conductivity specimens that exhibited high k ($> 10^{-10}$ m/s), and after the specified termination criteria had been achieved, rhodamine WT dye (5mg/L) was added to the influent to determine if preferential flow was occurring. Tests were permeated with rhodamine WT dye bearing influent solution until dye became visible in the effluent. Tests then were immediately terminated and disassembled, as described in Section 2.2.12. No indication of sidewall leakage was found in any tests. However, dye testing did reveal preferential flow paths along fiber bundles as described in Section 2.3.3.2.

2.2.11 Hydraulic Conductivity Test Disassembly

Tests were depressurized in the reverse order of the method used for pressurization. For tests conducted by the S-Method, at 1-min intervals, influent and effluent pressures were reduced by 70 kPa (10 psi), followed within 1-5 s by a 70 kPa (10 psi) reduction in cell pressure. Pressures were reduced until only hydrostatic pressure from the panel board and interface device water columns were applied to the specimen. The specimen then was disconnected from the panel

board, and inflow and outflow pressures were vented, followed within 1-5 s by a venting of the cell pressure. For tests conducted by the G-Method, both cell water and influent heads were simultaneously removed from the permeameter. Cells then were disassembled, and GCL specimens were carefully removed and massed.

2.2.12 Thickness Measurement and Weight-Volume Relationships

The final step in k and hydration testing is establishing the final dimensions of the specimen. The final height and diameter of the clay portion of the specimen are estimated to establish a final specimen thickness, L , and volume. The volume and measured water content are used to establish the weight-volume relationships for a specimen, including degree of saturation, S . Section 8.5.2 of ASTM D6766-12 states “The final height and diameter of the specimen (clay portion) shall be measured to the tolerances specified in 5.12.” This was done by measuring at 6 equidistant locations around the perimeter of the specimen using digital calipers, with care taken to compress the carrier geotextile fibers without squeezing the bentonite. The total weight of the GCL was also recorded. Then the textiles are carefully separated from the clay using a scalpel and the compressed thicknesses of each of the top and bottom textiles are measured with calipers. The measured textile thicknesses are subtracted from the total thickness measurement to obtain the thickness of the bentonite layer. The textiles are thin, ~0.1-0.7 mm, and the thickness varies based the pressure applied of the calipers. As there was potential for variability the compression of the textiles by the calipers, care was taken to fully compress the textile to the extent possible. The water content of the bentonite, top textile, and bottom textile are then determined independently. Bentonite water content was measured on extracted bentonite (i.e., collected with minimal geotextile fibers) by ASTM D2216 (*Standard Test Methods for Laboratory Determination of Water (Moisture) Content of Soil and Rock by Mass*) Method B. The water content of each textile was also measured. The water content of the textiles along with the mass per area of the textiles (Table 2.2) allows the full weight of the wet textiles to be subtracted

from the measured total GCL weight for a more accurate determination of *S*. Determination and subtraction of water associated with the textiles is a deviation from ASTM D6766-12 as the method only requires subtraction of the textile (dry) mass-area based on measurements or manufacturer reported values.

2.2.13 Index Properties

Indicator parameters for the granular bentonite and bentonite component of GCLs (e.g., swell index and fluid loss), are used to screen bentonite quality when performed with DW as the hydrating solution and/or the potential for hydraulic incompatibility (i.e., the potential for high *k*) when performed with the permeant liquid. Swell index tests were performed in general accordance with ASTM D5890 (*Standard Method for Swell Index of Clay Mineral Component of Geosynthetic Clay Liners*). Fluid loss tests were performed in general accordance with ASTM D5891 (*Standard Test Method for Fluid Loss of Clay Component of Geosynthetic Clay Liners*). The results of the swell index and fluid loss tests are presented in Table 2.4. Bentonite removed from GCL-1 had an average SI (n=10) of 28.3 mL/2 g in CW and 27.2 mL/2 g in Au-PLS, and an average fluid loss (n=2) of 13.8 mL/20 min in CW and 17.9 mL/20 min in Au-PLS. GCL-1 exhibited index parameters in the range typical for low-*k* GCLs conductivity ($< 3 \times 10^{-10}$ m/s), viz. SI > 20 mL/2 g, and fluid loss < 18 mL/2 g. The determination of the index parameters for GCL-2 and GCL-3 is part of ongoing research.

2.3 Results

2.3.1 Degree of Saturation

2.3.1.1 Degree of Saturation from Hydraulic Conductivity Tests

The final average degrees of saturation at the termination of permeation are shown in Figure 2.8 for test series where $n > 1$ (Test Series 1, 2, 3, 4, 5, 6, 7, 8, 9, 10, 11, and 12). For GCL-1 permeated with CW using the S-Method (both S-Method and modified S-Method tests, i.e.

all tests where backpressure saturation was used) the average degree of saturation is 96% (n = 8, SD = 4.2%) whereas using the G-Method (all tests where backpressure saturation was not used) is 94% (n = 3, SD = 8.9%). For GCL-1 permeated with Au-PS using the S-Method the average degree of saturation is 90% (n = 3, SD = 5.5%) whereas using the G-Method is 91% (n = 3, SD = 7.5%). For GCL-2 permeated with CW the using S-Method (both S-Method and modified S-Method tests) the average degree of saturation is 105% (n = 6, SD = 5.8%) whereas using the G-Method is 101% (n = 2, SD = 3.3%). For all test series analyzed, both the S-Method and G-Method yielded similar final degrees of saturation demonstrating the test method had no effect on the final degree of saturation.

2.3.1.2 Degree of Saturation from Oedometer Hydration Tests

The final average degrees of saturation calculated at the termination of oedometer hydration tests are shown in Figure 2.13. For GCL-1 the average degree of saturation when hydrated with DW is 96% (n = 3, SD = 2.1%), with CW is 97% (n = 3, SD = 3.9%), and with Au-PS is 100% (n = 3, SD = 1.7%). For GB, the average degree of saturation when hydrated with DW is 103% (n = 3, SD = 1.8%), with CW is 107% (n = 3, SD = 3.2%), and with Au-PS is 104% (n = 3, SD = 1.7%). Only one test series GB hydrated with CW resulted in an average degree of saturation outside the range specified in D6766-12 (i.e., 95-105%) demonstrating that saturation of GCLs is achieved without backpressure and before commencement of permeation.

2.3.1.3 Degree of Saturation from Permeameter Hydration Tests

The final average degrees of saturation calculated at the termination of in-permeameter hydration tests are shown in in Figure 2.18 for GCL-1 hydrated with CW. For GCL-1 the average degree of saturation using the S-Method is 105% (n = 3, SD = 5.7%), whereas using the G-Method is 109% (n = 3, SD = 1.5%). Both the S-Method and G-Method yielded similar final degrees of

saturation demonstrating the test method had none to minimal effect on the degree of saturation after the hydration period.

2.3.2 Water Content

2.3.2.1 Water Contents of Hydraulic Conductivity Tests

Water content measurements conducted at the termination of S-Method and G-Method hydraulic conductivity tests are shown in Figure 2.23 as average values for test series where $n > 1$ (Test Series 1, 2, 3, 4, 5, 6, 7, 8, 9, 10, 11, and 12) and summarized in Table 2.10 for all data. For GCL-1 permeated with CW, the average water content using the S-Method (both S-Method and modified S-Method tests, i.e. all tests where backpressure saturation was used) is 109% ($n = 6$, $SD = 6.4\%$), whereas using the G-Method is 108% ($n = 3$, $SD = 3.6\%$). For GCL-1 permeated with Au-PS, the average water content using the S-Method is 89% ($n = 2$, $SD = 2.5\%$), whereas using the G-Method is 91% ($n = 3$, $SD = 2.2\%$). For GCL-2 permeated with CW, the average water content using the S-Method (both S-Method and modified S-Method tests) is 133% ($n = 6$, $SD = 9.7\%$), whereas using the G-Method is 133% ($n = 2$, $SD = 1.6\%$). For all test series where $n > 1$, both the S-Method and G-Method yielded similar final water contents demonstrating the test method had no effect on the final water content of the GCL.

2.3.2.2 Water Contents of Oedometer Hydration Tests

Water content measurements conducted at the termination of oedometer hydration tests are shown in Figure 2.24. For GCL-1 the average water content when hydrated with DW is 117% ($n = 3$, $SD = 12\%$), with CW is 114% ($n = 3$, $SD = 9\%$), and with Au-PS is 108% ($n = 3$, $SD = 11\%$). For GB the average water content when hydrated with DW is 135% ($n = 3$, $SD = 12\%$), with CW is 137% ($n = 3$, $SD = 9\%$), and with Au-PS is 117% ($n = 3$, $SD = 8\%$).

2.3.2.3 Water Contents of Permeameter Hydration Tests

Water content measurements conducted at the termination of permeameter hydration tests are shown in Figure 2.25. For GCL-1 hydrated with CW, the average water content using the S-Method is 94% ($n = 3$, $SD = 2.0\%$), whereas using the G-Method is 116% ($n = 3$, $SD = 3.7\%$). These results demonstrate that the S-Method procedures result in a lower water content at the end of the hydration period.

2.3.3 Hydraulic Conductivity

2.3.3.1 Comparison of S-Method to G-Method

The ranges in k measured by the S-Method and the G-Method are compared in Figure 2.26 for GCL-1, GCL-2, GCL-3, and GB permeated with DW, CW, or Au-PS. For GCL-1 permeated with CW the S-Method (Test Series 1, 14) resulted in low k ranging from 2.5×10^{-11} m/s to 6.7×10^{-11} m/s ($n = 4$), whereas the G-Method (Test Series 2, 15) resulted in low k for two of five tests, 1.8×10^{-11} m/s and 4.4×10^{-11} m/s, and higher k for three of five tests, 1.0×10^{-9} m/s, 5.3×10^{-9} m/s, and 6.1×10^{-9} m/s. For GCL-1 permeated with Au-PS the S-Method (Test Series 3) resulted in low k ranging from 1.5×10^{-11} m/s to 4.4×10^{-11} m/s ($n = 3$), whereas the G-Method (Test Series 4) resulted in higher k ranging from 4.9×10^{-10} m/s to 2.6×10^{-8} m/s ($n = 3$). For GCL-1 permeated with DW the S-Method (Test Series 20) and the G-Method (Test Series 21) both resulted in similar low k values ($n = 1$) of 3.0×10^{-11} m/s and 2.3×10^{-11} m/s respectively. For GCL-2 permeated with CW the S-Method (Test Series 10) resulted in low k ranging from 2.0×10^{-11} m/s to 3.0×10^{-11} m/s ($n = 3$), whereas the G-Method (Test Series 11) resulted in low k for one of three tests, 2.5×10^{-11} m/s, and higher k for two of three tests, 1.3×10^{-9} m/s and 8.7×10^{-9} m/s. For GCL-3 permeated with CW the S-Method (Test Series 16) and the G-Method (Test Series 17) both resulted in similar low k values ($n = 1$) of 2.0×10^{-11} m/s and 2.3×10^{-11} m/s respectively. For GB permeated with CW the S-Method (Test Series 18) and G-Method (Test Series 19) both resulted in similar low k values

($n = 1$) of 1.4×10^{-11} m/s and 1.7×10^{-11} m/s respectively, values that are slightly lower than the low k observed by specimens in GCL-1, GCL-2, and GCL-3.

2.3.3.2 Preferential Flow Through Fiber Bundles

Rhodamine-WT dye was added to the influent liquid, and permeated through GCL-1 and GCL-2 specimens tested by the G-Method that exhibited high k (i.e., specimens that exhibited $k > 10^{-10}$ m/s). The dyed specimens revealed preferential flow along some, but not all needle punching fiber bundles. Photographs of the stained fiber bundles for tests with GCL-1 are shown in Figure 2.27 whereas for tests with GCL-2 are shown in Figures 2.28. No preferential flow was observed in any specimens of GCL-3.

2.3.3.3 Comparison of S-Method and G-Method to Modified Standard Methods

The ranges in k measured by the S-Method, G-Method, and modified S-Methods (M1-M5) are compared in Figure 2.29 for GCL-1 permeated with CW, or Au-PS. For GCL-1 permeated with CW the modified S-Method (M1-M5) tests (Test Series 5-9) all resulted in low k ranging from 2.3×10^{-11} m/s to 3.8×10^{-11} m/s. These modified S-Method tests changed the time and stress intervals in the backpressure application procedure demonstrating that decreasing the stress interval or increasing time between stress intervals still resulted in the prevention of fiber bundles acting as preferential flow paths, and thus similar k values to the S-Method.

The ranges in k measured by the S-Method, G-Method, and modified SMs (M6, M7) are compared in Figure 2.30 for GCL-2 permeated with CW. The S-M6 (Test Series 12) tests all resulted in low k at termination ranging from 2.6×10^{-11} m/s to 3.7×10^{-11} m/s ($n = 3$), but exhibited different temporal behavior than the tests conducted using the S-Method. The S-M7 (Test Series 13) tests were conducted in two phases. Phase 1 (simulated G-Method) resulted in low k for one of three tests, 2.7×10^{-11} m/s, and higher k for two of three tests, 1.9×10^{-9} m/s and 1.8×10^{-10} m/s matching the results of the G-Method, but exhibiting different temporal behavior. Phase 2 (S-

Method backpressure) was conducted on the two tests exhibiting higher k after phase 1 which resulted in an immediate decrease to low k and hydraulic termination at low k (5.9×10^{-11} m/s) for one test, and a slight decrease in k (to 9.6×10^{-11} m/s) for the other test that has not yet reached hydraulic termination criteria. Further comparisons between the S-Method, G-Method, and modified standard methods, including the temporal behavior of k versus PVF, are provided in the discussion section.

2.4 Discussion

2.4.1 Verification of the Degree of Saturation

2.4.1.1 Verification of the Degree of Saturation For Hydraulic Conductivity Tests

For all k test series analyzed, both the S-Method and G-Method yielded similar final degrees of saturation demonstrating the test method had no effect on the final degree of saturation. The final degrees of saturation calculated at the termination of k testing are shown in Figure 2.9 and summarized in Table 2.10 for all tests conducted by the S-Method, G-Method, and modified standard methods. Viewing the plot of each data point in addition to the averages shows some degrees of saturation falling outside the range specified by D6766-12 (i.e., 95-105%), either above or below. There was no indication that specific data points that fall outside the range are erroneous or that tests that fall below the range are unsaturated, rather these tests illustrate the difficulty in determining the degree of saturation by weight-volume calculations. This difficulty is evidenced by the standard that allows for up to a 10% (95-105% range) error in the degree of saturation determination, and for degrees of saturation above 100% (i.e. 100-105%) that are theoretically not possible.

Both the S-Method and G-Method also yielded similar final void ratios demonstrating that the test method had no effect on the final void ratio. The final void ratios at the termination of k testing are shown in Figure 2.10 and summarized in Table 2.10 for all tests conducted by the S-Method, G-Method, and modified standard methods. Values range from 2.47 to 3.60.

Both the S-Method and G-Method also yielded similar final dry densities demonstrating that the test method had no effect on the final dry density. The final dry densities at the termination of *k* testing are shown in Figure 2.11 and summarized in Table 2.10 for all tests conducted by the S-Method, G-Method, and modified standard methods. Values ranged from 0.58 Mg/m³ to 0.77 Mg/m³.

The difficulty in accurate determination of the degree of saturation may be the result of a variety of factors, however the primary factor in this study is believed to be the difficulty in determining the bentonite weight and thickness (the measured thickness along with the measured diameter is necessary to determine the bentonite volume). Textile correction procedures (referred to herein as Textile Correction) must be completed (outlined in Section 2.2.13) to account for the weight and thicknesses of the textiles and provide an estimate of only the specimen's bentonite weight and thickness. ASTM D6766-12 (section 5.12) addresses the thickness measurement stating: "Devices used to measure the dimensions of the specimen shall be capable of measuring to the nearest 0.3 mm (0.01 in.) or better..." However, this can provide additional evidence in the difficulty in determining the degree of saturation. For example, Test 4c has a determined bentonite thickness of 6.9 mm and a degree of saturation of 98%. A +0.3 mm error in measurement of bentonite thickness will result in a degree of saturation of 92% whereas a -0.3 mm error will result in a degree of saturation of 104%. Thus, up to a ~12% error in the degree of saturation determination may be possible simply due to the accuracy of the measurement tool.

A comparison of the degree of saturation using the Textile Correction to the degree of saturation without the Textile Correction is shown in Figure 2.12. Although many tests fall on or near the 1:1 line, showing no to minimal difference in using the Textile Correction, many tests fall below the 1:1 line demonstrating that many tests had a higher degree of saturation using the Textile Correction compared to without using the Textile Correction. Additionally, using the Textile Correction was more likely to result in the degree of saturation falling within the range specified

by D6766-12 (i.e., 95-105%). These results suggest that the Textile Correction is necessary for a more accurate determination of the degree of saturation by weight-volume calculations.

For tests where the Textile Correction had no effect on the degree of saturation, the additional thickness of the textiles (greater determined specimen volume), and the additional textile weight (a greater measured specimen weight) had canceling effect that resulted in a calculation of the degree of saturation with the Textile Correction to be equivalent to the calculation without using the Textile Correction.

2.4.1.2 Verification of the Degree of Saturation for Oedometer Hydration Tests

The final degrees of saturation calculated at the termination of hydration tests are shown for all tests in Figure 2.14 and summarized in Table 2.11. Viewing the plot of each data point in addition to the averages shows that some tests fall outside the range specified by D6766-12 (i.e., 95-105%), either above or below the range. There was no indication that specific data points that fall outside the range are erroneous or that tests that fall below the range are unsaturated, rather these tests illustrate the difficulty in determining the degree of saturation by weight-volume calculations as discussed in the previous section.

All tests yielded similar final void ratios and dry densities as the *k* tests. The final void ratios calculated at the termination of oedometer hydration tests are shown for all tests in Figure 2.15 and summarized in Table 2.11. Values ranged from 2.69 to 3.71. The final dry densities calculated at the termination of oedometer hydration tests are shown for all tests in Figure 2.16 and summarized in Table 2.11. Values ranges from 0.57 Mg/m³ to 0.72 Mg/m³.

A comparison of the degree of saturation using the Textile Correction to the degree of saturation without the textile correction is shown in Figure 2.17. Although minor variability can be seen, there is no systematic difference in the determined degree of saturation using the Textile Correction compared to results without using the Textile Correction. For tests where the Textile Correction had no effect on the degree of saturation, the additional thickness of the textiles

(greater determined specimen volume), and the additional textile weight (a greater measured specimen weight) had canceling effect that resulted in a calculation of the degree of saturation with the Textile Correction to be equivalent to the calculation without using the Textile Correction. For example, Test 1a had a degree of saturation using the Textile Correction of 96%, without using the Textile Correction of 96%, with only using the thickness correction of 112%, and with only using the weight correction of 83%.

2.4.1.3 Verification of the Degree of Saturation for Permeameter Hydration Tests

The final degrees of saturation calculated at the termination of hydration tests are shown in Figure 2.19 and summarized in Table 2.12 for all tests. Viewing the plot of each data point in addition to the averages shows that some data falls outside the range specified by D6766-12 (i.e., 95-105%), either above or below the range. There is no indication that specific data points that fall outside the range are erroneous or that tests that fall below the range are unsaturated, rather these tests illustrate the difficulty in determining the degree of saturation by weight-volume calculations as discussed in the Section 2.4.1.1

All tests yielded similar final void ratios and dry densities as the *k* tests. The final void ratios calculated at the termination of permeameter hydration tests are shown for all tests in Figure 2.15 and summarized in Table 2.11. Values ranged from 2.25 to 2.92. The final dry densities calculated at the termination of permeameter hydration tests are shown for all tests in Figure 2.16 and summarized in Table 2.11. Values ranges from 0.68 Mg/m³ to 0.82 Mg/m³.

A comparison of the determined degree of saturation using the Textile Correction to the determined degree of saturation without the textile correction is shown in Figure 2.22. All data points fall below the 1:1 line demonstrating that using the Textile Correction results in a greater degree of saturation determination than without using the Textile Correction. However using the Textile Correction method did not lead to more data points falling within the range specified by

D6766-12 (i.e., 95-105%), further illustrating the difficulty in accurately determining the degree of saturation.

2.4.1.4 Effect of Backpressure on Degree Of Saturation

The results of all k , oedometer hydration, and in-permeameter hydration test series verify degrees of saturation within the range specified by D6766-12 (i.e., 95-105%), and resulted in similar final void ratios and dry densities regardless of whether or not backpressure was applied. These results demonstrate that backpressure saturation is not necessary to achieve saturated GCL specimens. The hypotheses that bentonite is a self-saturating material and that G-Method tests saturated k without backpressure are shown to be valid.

2.4.2 Water Content

2.4.2.1 Effect of Permeant Liquid

For k tests, comparing the permeant liquids used with GCL-1 shows that a lower water content results when permeating with the Au-PS compared to the CW (Au-PS: S-Method = 89%, G-Method = 91%, CW: S-Method = 109% G-Method = 108%). For oedometer hydration tests, comparing the water contents to the permeant liquid used shows that the DW and CW result in similar final water contents (GCL-1: DW = 117%, CW = 114%, GB: DW = 135%, CW = 137%) while the Au-PS results in a lower final water content (GCL-1 = 108%, GB = 117%). The lower resultant water content using the Au-PLS is likely due to the higher ionic strength of the Au-PLS compared to the CW (49 mM versus 6.0 mM). This higher ionic strength is likely to have reduced swelling, i.e. adsorption of water, and thus resulted in a lower measured water content.

2.4.2.2 Effect of GCL

For k tests, comparing the material used when permeating with CW, shows that a higher water content results when using GCL-2 compared to GCL-1 (GCL-2: S-Method, G-Method =

133%, GCL-1: S-Method = 109% G-Method= 108%). One possible reason for this difference is the greater percent area covered by fiber bundles of GCL-2 (9.0%) compared to GCL-1 (5.3%). As the fiber bundles in both of these GCLs have been shown to be large enough to potentially lead to preferential flow (Section 2.3.3.2) a hypothesis is that more larger fiber bundles could create more “cavities” where additional water could collect. This would result in a higher weight of water and thus a higher measurement of water content. Another possible reason is that although the bentonite from each GCL is from the same manufacturer and source material, they are from different rolls and thus the bentonite may have a slightly different mineralogical composition that has yet to be determined (Table 2.2). A greater montmorillonite content in GCL-2 may lead to increased swelling and thus a higher water content (Lee & Shackelford 2005b).

For oedometer hydration tests, comparing the final water contents to the material used shows that GCL-1 achieved a lower water content than the GB (DW: 117% versus 135%, CW: 114% versus 137%, Au-PS: 108% versus 117%). This lower water content in GCL-1 compared to GB is hypothesized to be due to the greater confinement associated with the fiber bundles and textiles that surround the bentonite and hold the GCL together. The GB has no fiber bundles or textiles allowing the bentonite to more freely swell (both materials had the same applied vertical effective stress) (Lake and Rowe 2000).

2.4.2.3 Effect of S-Method versus G-Method

Comparing the water contents of the in-permeameter hydration tests to the hydraulic conductivity tests shows that for GCL-1 using CW, the S-Method water content is greater at the termination of permeation than at the termination of the hydration period (108% versus 94%). In contrast, the G-Method water content is similar (slightly less) at the termination of permeation than at the termination of the hydration period (109% versus 116%). The hydration test using the G-Method also results in a similar water content to the oedometer hydration tests (116% versus 114%). This comparison demonstrates the potential for the water content to change during

permeation, increasing for the S-Method, and decreasing slightly for the G-Method, although more data is necessary to confirm these results. These results also demonstrate that the S-Method procedures result in a lower water content than the G-Method at the end of the hydration period (94% versus 116%), indicating the possibility of compression from the S-Method procedures.

2.4.3 Hydraulic Conductivity

2.4.3.1 Effect of S-Method Versus G-Method

The resultant higher k in some of the G-Method tests compared to the S-Method is the opposite of what would have been expected if the G-Method had resulted in unsaturated specimens. Unsaturated soils have been shown to have a lower k than saturated specimens of the same soil (Lu and Likos 2004). The G-Method did not result in uncharacteristically low k due to unsaturated condition, but resulted in higher k for some specimens of GCL-1 and GCL-2, and no difference in k for specimens of GCL-3.

2.4.3.2 Effect of Preferential Flow

The larger fiber average bundle size of GCL-1 (0.91 mm) and GCL-2 (1.05 mm) compared to GCL-3 (0.76 mm), and the increased percent area covered by fiber bundles of GCL-1 (5.3%) and GCL-2 (9.0%) compared to GCL-3 (1.0 %) likely explains why preferential flow was observed in GCL-1 and GCL-2, but not in GCL-3. Similar preferential flow is reported by Scalia and Benson (2010b) and Rowe et al. (2017) for GCLs hydrated on natural subgrades in composite final covers. These results demonstrate that the S-Method and G-Method may not yield the same k for GCLs with higher degrees of needle punching (fiber bundle size and percent area covered by fiber bundles) and that the S-Method may be an un-conservative measurement of k as it can mask the presence of preferential flow through fiber bundles. Modified S-Method tests were conducted in order to hypothesize why the G-Method may demonstrate preferential flow through fiber bundles, while the S-Method does not.

For GCL-3 permeated with CW the S-Method (Test Series 16) and the G-Method (Test Series 17) both resulted in similar low k values ($n = 1$) of 2.0×10^{-11} m/s and 2.3×10^{-11} m/s respectively as discussed in Section 2.3.3.2. The temporal behavior of each test is reported in Figure 2.37 showing initial low k that persisted until termination for both methods. Test Series 16 and 17 demonstrate that the S-Method and G-Method exhibit the same k and same temporal behavior for GCL-3, and that higher k associated with preferential flow is not observed during any period of the test in either the S-Method or the G-Method for GCL-3, though more data is necessary to support this conclusion.

2.4.3.3 Effect of Changing Time and Stress of Backpressure Increments

Test series 5-9 changed the time and/or the stress increment of the backpressure procedure (Section 2.2.8) One hypothesis is that due to the low hydraulic conductivity of the bentonite material (when hydrated) there is not time for excess pore pressures to dissipate in 1-min, but there is time in 1-hr, 4-hr, or 1-d. Not allowing the excess pore pressures to dissipate could build up higher pore pressures throughout the backpressure procedure and when they eventually dissipate will result in an over consolidated specimen. This greater degree of consolidation is more likely to lead to the bentonite fully saturating around the fiber bundles and squeezing them tight in complete contact with the bentonite. The counter to this hypothesis is that during the backpressure pressure increment the bentonite has not completely saturated and may not be in a low conductivity state. The conductivity of the bentonite could still be high enough for the excess pore pressures to dissipate during the 1-min between stress increments.

A second hypothesis is that the pulse of effective stress during the backpressure procedure consolidated the specimen under higher effective stresses (Section 2.2.5, the backpressure procedure creates a pulse of increased effective stress of about 15 psi for about 2-5 s when the cell pressure increased before the backpressure has been increased on both the influent and effluent end of the specimen, when in theory based on the standard the effective

stress should never exceed 5 psi). Higher effective stresses are more likely to lead to the bentonite fully hydrating around the fiber bundles and squeezing them tight in complete contact with the bentonite (having the bentonite saturate completely around the fiber bundles is necessary to prevent the fiber bundles from acting as preferential flow paths). Changing the stress increment from 10 psi (kPa) to 5 psi (kPa) would reduce the magnitude in the pulse of effective stress during each backpressure step from 15 psi (kPa) to 7.5 psi (kPa), and thus reduce the likelihood of consolidating the bentonite more tightly around the fiber bundles.

A third hypothesis is that both the elevated effective stresses and lack of dissipation of pore pressures play a mutual role in having the bentonite in tighter contact with the fiber bundles. Test series 3 and 5 changed both variables.

All combinations of changing the time increment and stress interval resulted in no difference in the measured k compared to the S-Method. These results indicate that additional hypotheses are necessary to resolve the differences in the measured k between the S-Method and G-Method.

2.4.3.4 Effect of S-Method

Test Series 10, GCL-2 permeated with CW using the S-Method, resulted in low k as described in Section 2.3.3.2. The temporal behavior of the three tests in the test series are plotted in Figure 2.31 as a plot of k versus PVF. All three tests exhibited initial high k (7×10^{-10} m/s – 2×10^{-9} m/s) for ~1.5-3.5 PVF. The tests then exhibited an immediate drop to low k where hydraulic equilibrium was reached. Test Series 10 illustrates that the S-Method does not reveal preferential flow and results in low k for GCL-2, but that up to 3.5 PVF may be required before low k is observed for GCL-2.

2.4.3.5 Effect of G-Method

Test Series 11, GCL-2 permeated with CW using the G-Method, resulted in one test with low k and two tests with higher k as described in Section 2.3.3.2. The temporal behavior of the GCLs is shown in Figure 2.32 as a plot of k versus PVF. All tests exhibited initial high k (1×10^{-9} m/s – 1×10^{-8} m/s) that persisted for 3-7 PVF. Test 11a reached the reported k of 8.7×10^{-9} m/s based on hydraulic termination criteria at ~3.4 PVF (400 mL cumulative inflow, PVF estimated using average terminated pore volumes of tests 11b and 11c). Test 11a is continuing to run to chemical termination criteria, and at ~6.7 PVF (800 mL cumulative inflow) exhibited a sudden decrease in k to 5.9×10^{-11} m/s. Test 11a is currently at hydraulic equilibrium with a k of 2.0×10^{-11} m/s and an EC Ratio of 1.94. Test 11b exhibited inconsistent preferential flow ($k = 1.4 \times 10^{-9}$ m/s – 6.9×10^{-9} m/s) for 2.8 PVF of flowed by a sudden decrease in k to 2.5×10^{-11} m/s before reaching the reported k of 2.5×10^{-11} m/s based on hydraulic termination criteria at 3.9 PVF. Test 11c reached the reported k of 1.3×10^{-9} m/s based on hydraulic termination criteria at 2.9 PVF. Rhodamine-WT dye was also added to Test 11c which revealed preferential flow along some, but not all needle punching fiber bundles, observed in Figure 2.28. Test Series 11 illustrates that for GCL-2 the G-Method can result in high k ($>1 \times 10^{-9}$ m/s) due to preferential flow through fiber bundles, but that permeating to greater PVF may result in the sudden closure of preferential flow paths and thus low k .

Test Series 2, GCL-1 permeated with CW using the G-Method, resulted in low k for two of five tests and a higher k due to preferential flow for three out of five tests as described in Section 2.3.3.2. The temporal behavior of the GCLs in Test Series 2 is shown in Figure 2.33 as a plot of k versus PVF. Tests 2a ($k = 4.5 \times 10^{-9}$ m/s, PVF =4.2), 2b ($k = 5.3 \times 10^{-9}$ m/s, PVF =2.6), and 2c ($k = 9.2 \times 10^{-10}$ m/s, PVF =6.0) all exhibited higher k due to preferential flow at termination by hydraulic termination criteria. Rhodamine-WT dye was added to Tests 2a, 2b, and 2c which revealed preferential flow along some, but not all needle punching fiber bundles, observed in Figure 2.27a,b. Test 2d exhibited initial high k ($>1 \times 10^{-10}$ m/s) for ~1-2 PVF before rapidly decreasing to

lower k , behavior consistent with Test Series 10. Test 2d reached the reported k of 1.8×10^{-11} m/s based on ASTM D5084-16a termination criteria at ~ 3.9 PVF (390 mL cumulative inflow, PVF estimated using average terminated pore volumes of tests 2a, 2b, and 2c). Test 2d is currently at hydraulic equilibrium with a k of 3.5×10^{-11} m/s and an EC Ratio of 2.43. Test series 2 demonstrates that the G-Method may reveal preferential flow through fiber bundles at termination by hydraulic termination criteria for GCL-1, and also demonstrates the variability of the needle punching fibers in GCL-1 that led to persistent preferential flow in three out of four tests.

Test Series 4, GCL-1 permeated with Au-PLS using the G-Method, resulted in a higher k due to preferential flow for all three tests as described in Section 2.3.3.2 The temporal behavior of the GCLs in Test Series 4 is shown in Figure 2.34 as a plot of k versus PVF. Tests 4a ($k = 4.8 \times 10^{-9}$ m/s, PVF = 10.7), 4b ($k = 2.3 \times 10^{-8}$ m/s, PVF = 4.2), and 4c ($k = 4.3 \times 10^{-10}$ m/s, PVF = 2.4) all exhibited higher k due to preferential flow at termination by hydraulic termination criteria. Rhodamine-WT dye was also added to Tests 4a, 4b, and 4c which revealed preferential flow along some, but not all needle punching fiber bundles, observed in Figure 2.27c,d. Test Series 4 demonstrates that the G-Method may reveal preferential flow through fiber bundles at termination by hydraulic termination criteria for GCL-1, and also demonstrates the variability in the magnitude of k when preferential flow is present with Test 4b exhibiting ~ 50 times the k of test 4c.

2.4.3.6 Effect of Removing Backpressure Steps

Test Series 12, GCL-2 permeated with CW using the S-M6, resulted in low k ranging from 2.1×10^{-11} m/s to 3.1×10^{-11} m/s ($n = 3$) shown in Figure 2.30. S-M6 involved hydrating the GCL after elevated pressures were applied allowing high backpressure to be used without any backpressure steps or sudden increases in pressure after the specimen had been exposed to liquid. Following this procedure there are no pulses of effective stress and thus the specimen should hydrate under a more representative equivalent effective stress condition as the G-Method.

The temporal behavior of Test Series 12 is shown in Figure 2.35 as a plot of k versus PVF. Test 12b exhibited initial higher k ($\sim 4 \times 10^{-10}$ m/s) before suddenly decreasing to low k at ~ 2.3 PVF and then reaching termination by hydraulic termination criteria at $k = 2.5 \times 10^{-11}$ m/s. This result is similar to the behavior of the GCLs permeated by the S-Method (Test Series 10). Test 12a exhibited initial variable higher k (5.9×10^{-10} m/s – 4.5×10^{-9} m/s) before suddenly decreasing to low k at ~ 7.0 PVF and then reached termination by hydraulic termination criteria at $k = 2.1 \times 10^{-11}$ m/s and 8.9 PVF. Test 12c exhibited initial variable higher k (1.3×10^{-10} m/s – 9.9×10^{-9} m/s) before suddenly decreasing to low k at ~ 19.5 PVF and then reached termination by hydraulic termination criteria at $k = 3.1 \times 10^{-11}$ m/s and 20.2 PVF. During the period of Tests 12a and 12c that exhibited higher k , the k was observed to steadily decrease during continuous permeation with sudden increases in k when the experiment was paused or when the experiment was paused and the influent reservoir was refilled. Test Series 12 demonstrates that the S-M6 can closely mirror the G-Method (Test Series 11, 2, 4), and that the use of backpressure steps in the S-Method may be the reason for the closure of preferential flow paths and prevention of higher k being observed due to preferential flow. However, Test Series 12 also indicates backpressure may be more likely to lead to a sudden closure in preferential flow paths and thus low k as all three tests were terminated at low k .

The primary difference between Test Series 12 and Test Series 11, 2, and 4 is the steady decrease in k with continuous permeation while exhibiting preferential flow. There are two possible explanations for this difference: 1. The G-Method (Test Series 11, 2, 4) does not allow for continuous permeation, every data point represents a pause in the experiment and refilling of the inflow burette, thus no effects resulting from continuous permeation can be observed in the G-Method, and 2. Both the G-Method and S-M6 are falling head methods that have variable head losses across the specimen and thus variable effective stresses. The S-Method and all variations of the S-Method (including S-M6) have a larger range in the head loss across the specimen. The head loss across the specimen in the G-Method varies by ~ 25 cm of water (2.45 kPa), whereas

the head loss the specimen in the S-Method and variations of the S-Method varies by ~50 cm of water (4.9 kPa). A second difference between Test Series 12 and Test Series 11, 2, and 4 is that all three tests in Test Series 12 were terminated at low k indicating that simply the presence of backpressure may be more likely to lead to closure of preferential flow paths.

2.4.3.7 Effect of Applying Backpressure During Permeation

The hydraulic conductivity results for Test Series 13, GCL-2 permeated with CW, are reported for each of the two phases of the S-M7. The final k after both phase 1 and phase 2 (if applicable) is reported in Figure 2.30. S-M7 involved two phases, a first phase of a simulated G-Method followed by a second phase of a normal S-Method. The hypothesis in conducting this method is that preferential flow associated with the G-Method will be observed by first permeating the specimen under the same cell pressure and pore pressures and then any changes to that preferential flow or any changes in hydraulic behavior can be recorded after the backpressure procedure has taken place.

The temporal behavior of each of the three tests in the series is reported in Figures 2.36 as a plot of k versus PVF. Test 13a resulted in low k (3.2×10^{-11} m/s) during phase one with temporal behavior similar to the S-Method (Test Series 10). Thus, 13a did not have persistent preferential flow and was terminated at the end of phase 1 without proceeding to phase 2. Test 13b exhibited variable high k (2.1×10^{-10} m/s – 5.4×10^{-9} m/s) for ~35 PVF and then reached termination of phase 1 by hydraulic termination criteria at $k = 1.9 \times 10^{-9}$ m/s and 36.9 PVF (2040 mL cumulative inflow, pore volume estimated using average pore volume of test series 10), indicating likely preferential flow. The backpressure procedure was then conducted on Test 13b (phase 2) which resulted in an immediate decrease in k to 6.3×10^{-11} m/s and termination of phase 2 by hydraulic termination criteria at low k of 5.9×10^{-11} m/s and 38.6 PVF (2130 mL cumulative inflow). Test 13c exhibited higher variable k (3.1×10^{-10} m/s – 5.6×10^{-9} m/s) for ~27 PVF before steadily decreasing to a low k of 2.7×10^{-11} m/s. The k then increased steadily and reached

termination of phase 1 by hydraulic termination criteria at $k = 1.8 \times 10^{-10}$ m/s and 36.5 PVF (2020 mL cumulative inflow, pore volume estimated using average pore volume of test series 10), indicating possible preferential flow. The backpressure procedure was then conducted on Test 13b (phase 2) which resulted in a slight decrease in k to 9.6×10^{-11} m/s, indicating that possible preferential flow paths may not have been affected by the backpressure procedure. Test 13b has not yet reached hydraulic termination criteria. Similar temporal behavior observed during the preferential flow period of Tests 12a and 12c was observed in 13b and 13c. Test Series 13 demonstrates that preferential flow can be observed under G-Method conditions for many (> 20) PVF, and that conducting the backpressure procedure on a GCL exhibiting preferential flow under G-Method conditions can immediately result in the closure of preferential flow paths and a decrease in k to $\sim 2-3 \times 10^{-11}$ m/s.

2.5 Conclusion

The degree of saturation has been shown to be a difficult property to determine accurately using weight-volume relationships for GCLs, the results of all k , oedometer hydration, and in-permeameter hydration test series indicate degrees of saturation within the range specified by D6766-12 (i.e., 95-105%) and demonstrate that backpressure saturation is not necessary to achieve saturated GCL specimens. Additionally, the G-Method did not yield an uncharacteristically low k due to unsaturated conditions; the S-Method and the G-Method gave near identical results when preferential flow was not observed. The hypotheses that bentonite is a self-saturating material and that the G-Method tests saturated k without backpressure are shown to be valid.

The S-Method and G-Method may not result in the same k value for GCLs with higher degrees of needle punching. The G-Method, a method more representative of field conditions where backpressure is not present, revealed the possibility of preferential flow through fiber

bundles. In contrast, the S-Method masks the possibility of preferential flow and thus provides an un-conservative estimate of k for GCLs with higher degrees of needle punching.

The cause of the discrepancy between the methods is likely the test procedures associated with applying backpressure in the S-Method. Test Series 12 indicates that removing the steps of the backpressure procedure while still applying backpressure results in preferential flow for many PVF (~7-20) while Test Series 13 indicates that conducting the backpressure procedure can immediately close off preferential flow paths. The procedures of backpressure saturation result in pulses of effective stress. Based on the results of this study, the hypothesis is that these pulses of effective stress result in compression of the specimen, closer contact of the bentonite to the needle punching fibers, and thus closure of preferential flow paths. Compression of the specimen is evidenced by the lower water content measured in in-permeameter hydration specimens by the S-Method versus the G-Method. This study indicates that the magnitude and timing of stress application are likely important factors in predicting whether GCLs with higher degrees of needle punching will exhibit preferential flow through fiber bundles.

All test series reveal that preferential flow is likely present, at least initially, for GCL-1 and GCL-2, but not for GCL-3 under low effective stresses (< 35 kPa). This suggests that the presence of preferential flow must be evaluated for GCLs with higher degrees of needle punching.

Table 2.1. Hydrating and permeating liquid chemistries

Parameter	Liquids		
	DW	CW	Au-PS
Ionic Strength, I (mM)	-	6.0	49
RMD (mM ^{1/2}) ^(a)	-	0.19	10
Electrical Conductivity, EC (S/m) ^(b)	4.2×10^{-4}	5.1×10^{-2}	0.34
pH ^(b)	7.0	5.7	5.1

^(a) RMD = ratio of monovalent-to-divalent cations; refer to Kolstad et al. (2004) for additional details

^(b) Measured using Orion Versa Star pH/Conductivity meter, Thermo Scientific, Waltham, MA

DW = Deionized water

CW = Conservative water

Au-PS = Synthetic gold mining process solution

Table 2.2. Properties of GCLs

		GCL-1	GCL-2	GCL-3
As-delivered form		Coarse granular		
Mineralogy	Montmorillonite (%)	tbd		
	Feldspar (%)	tbd		
	Quartz (%)	tbd		
	Mica (%)	tbd		
	Cristobalite (%)	tbd		
Atterberg Limits (ASTM D4318)	Liquid Limit, LL	396-405		
	Plastic Limit, PL	29-31		
Avg. dry bentonite mass/area, M_b , (kg/m^2) (ASTM D5993)	Measured	5.62 (SD=0.02, n=3)	5.04 (SD=0.15, n=10)	5.22 (SD=0.13, n=5)
	MARV ^(a)	3.6	3.6	3.6
Carrier GTX ^(b) (ASTM D5291)	Type	NW	NW	W
	Mass (kg/m^2)	0.28 (SD=0.015, n=10)	0.28 (SD=0.020, n=10)	0.13 (SD=0.002, n=10)
Cover GTX ^(b) (ASTM D5291)	Type	NW	NW	NW
	Mass (kg/m^2)	0.24 (SD=0.015, n=10)	0.31 (SD=0.020, n=10)	0.11 (SD=0.004, n=10)
Structure	Needle-punched	Yes	Yes	Yes
	Thermally treated	No	No	No
Initial (off roll) thickness (mm)		7.63 (SD=0.56 n=40)	8.54 (SD=0.28, n=40)	6.17 (SD=0.35, n=40)
Initial (off roll) water content (%)		5.7-10		

Values given are average with SD = standard deviation and n = number of samples when multiple tests were performed All tests conducted according to ASTM standards

^(a) Manufacturer published minimum average roll value

^(b) NW = nonwoven, W = woven

tbd = to be determined

Table 2.3. Characteristics of needle-punched fibers for the three GCLs used in this study

GCL	Bundle size (mm) ^(a)	No. of bundles/area (bundles/m ²)	No. of fibers/bundle ^(a)	% area covered by bundles ^(b)	MRPS ^(c) (N/m)	Avg. bonding peel strength (N/m)	Avg. peak peel strength (N)
GCL-1	0.91 (SD=0.27, n=20)	80,900 (SD=18,500, n=10)	44 (SD=15, n=20)	5.3	2170	tbd	tbd
GCL-2	1.05 (SD=0.25, n=20)	105,000 (SD=13,000, n=10)	41 (SD=14, n=20)	9.0	3500	tbd	tbd
GCL-3	0.76 (SD=0.22, n=20)	21,200 (SD=3,950, n=10)	20 (SD=9, n=20)	1.0	700	tbd	tbd

Values given are average with SD = standard deviation and n = number of samples when multiple tests were performed

^(a) Based on manual measurement using stereoscopic microscope

^(b) Assuming average values for fiber bundle size and assuming cylindrical fiber bundles

^(c) Manufacturer reported peel strength

tbd = to be determined

Table 2.4. Index properties of GCLs

Parameter	GCL-1	GCL-2	GCL-3
Swell index ^(a) (mL/2 g)	25.2	tbd	tbd
Fluid loss ^(b) (mL/20 min)	13.1	tbd	tbd

^(a) ASTM D5890. Tests conducted in deionized water

^(b) ASTM D5891. Tests conducted in deionized water

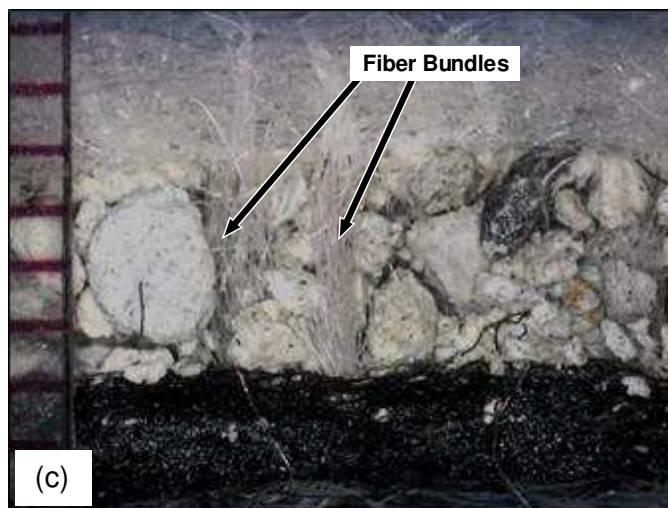
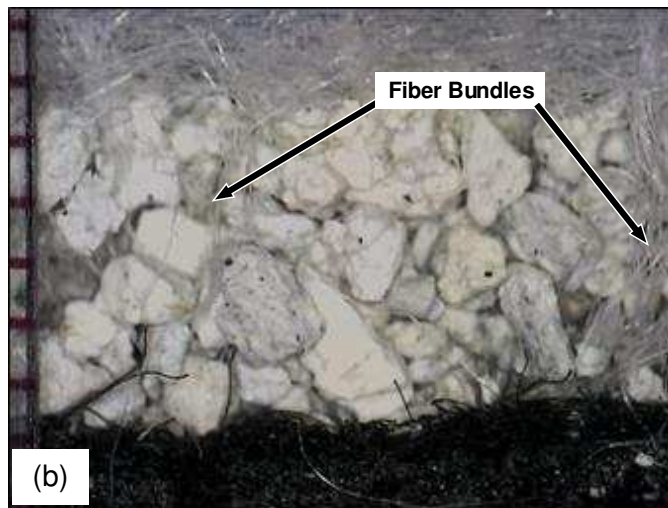
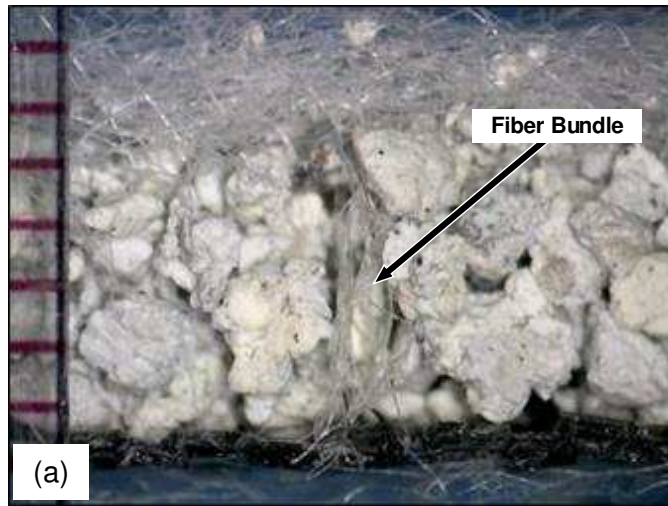


Figure 2.1. Cross-section of dry GCL specimens. (a) GCL-3 (b) GCL-1 (c) GCL-2. Scale in mm.

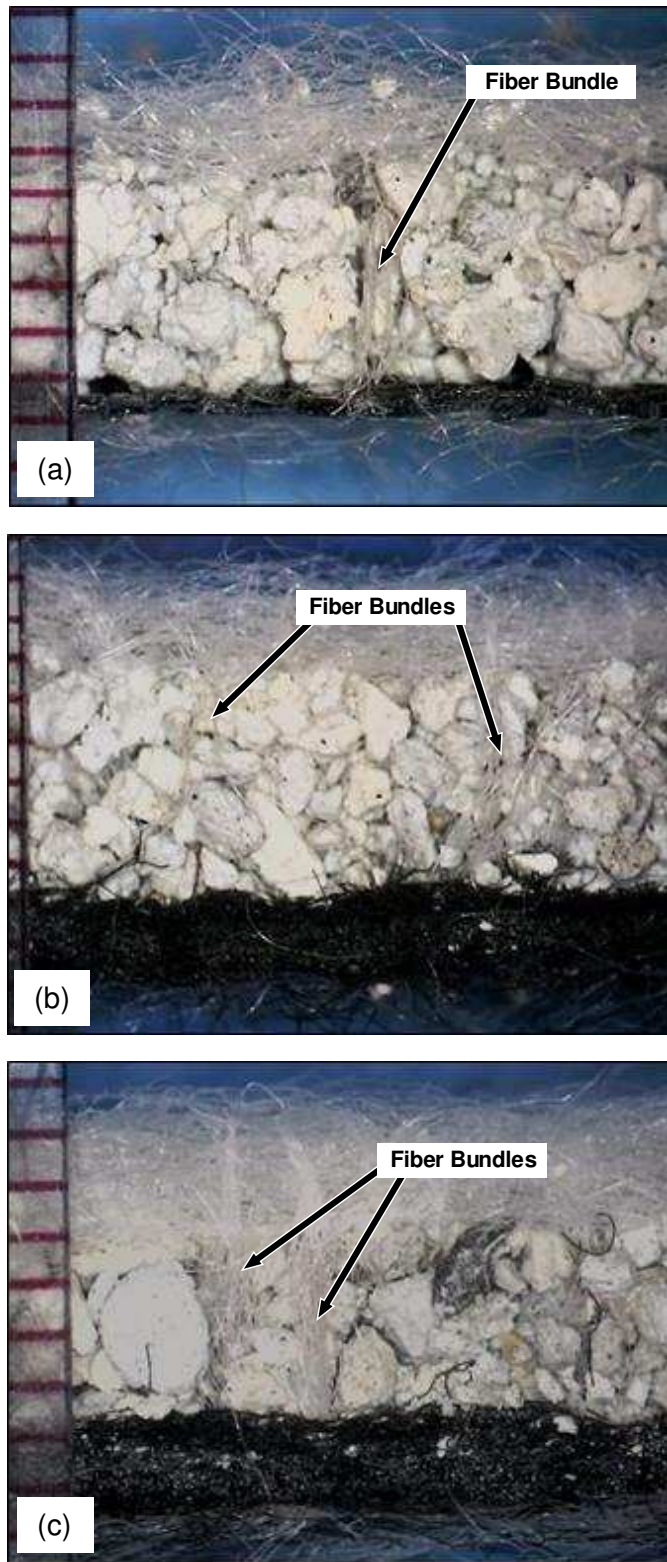


Figure 2.2. Zoomed out cross-section of dry GCL specimens. (a) GCL-3 (b) GCL-1 (c) GCL-2. Scale in mm.

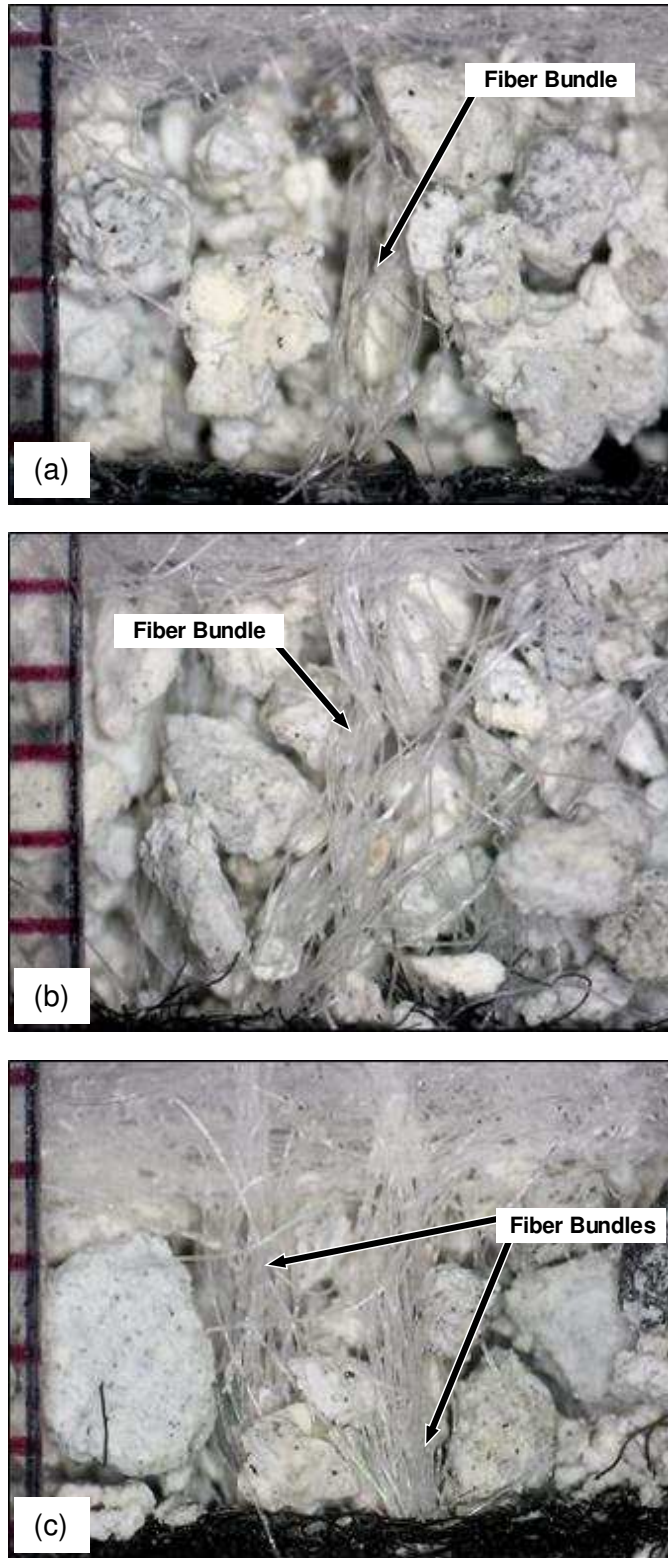


Figure 2.3. Zoomed in cross-section of dry GCL specimens. (a) GCL-3 (b) GCL-1 (c) GCL-2. Scale in mm.



Figure 2.4. Exemplary photograph for (a) measuring fiber bundle thickness and (b) counting the number of monofilament fibers per fiber bundle using a digital stereoscopic microscope.

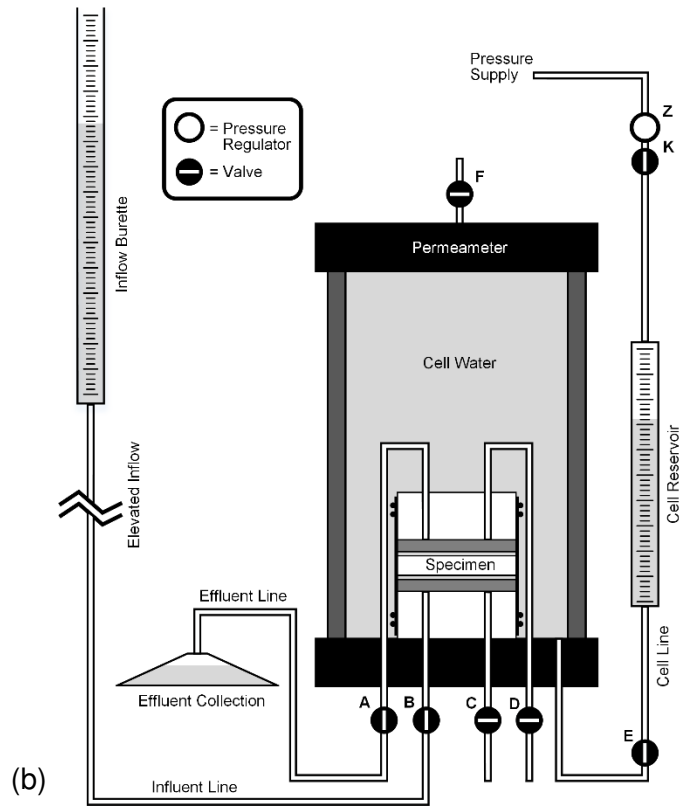
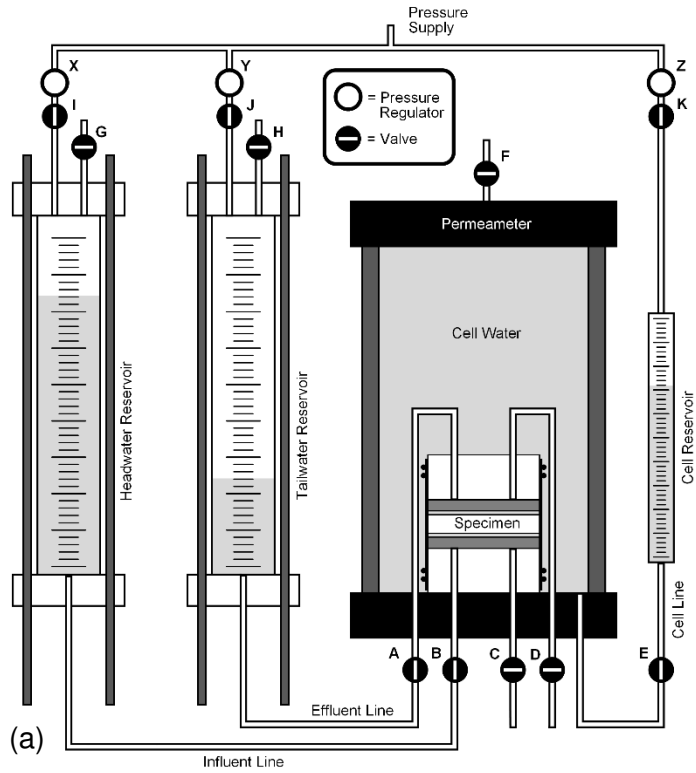


Figure 2.5. (a) Schematic of test setup using the S-Method. (b) Schematic of test setup using the G-Method.

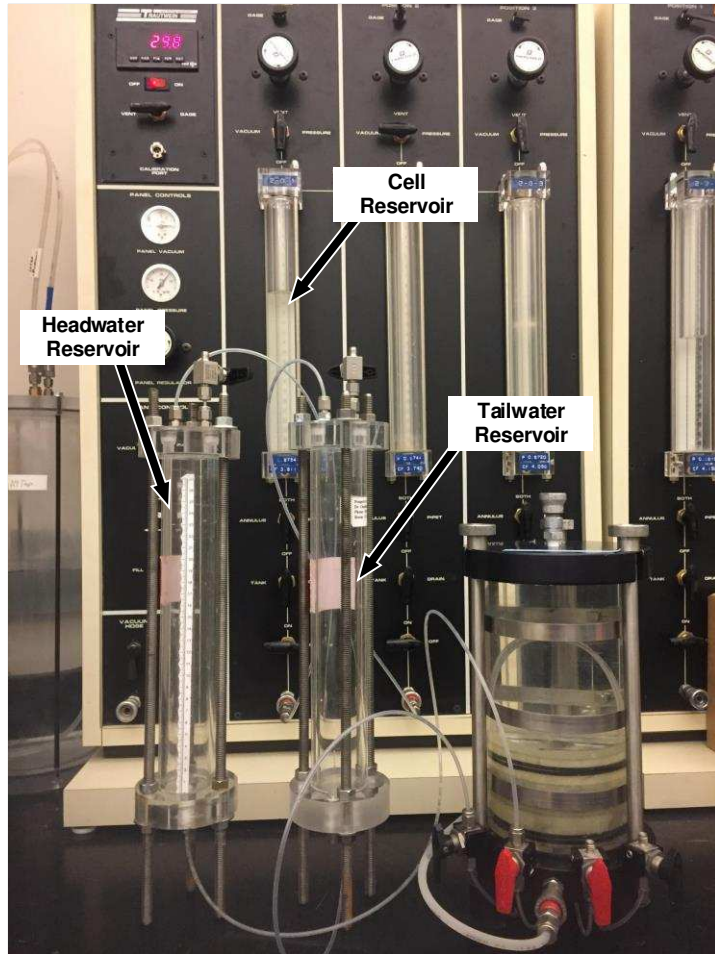


Figure 2.6. Picture of experimental setup following the standard method (S-Method).

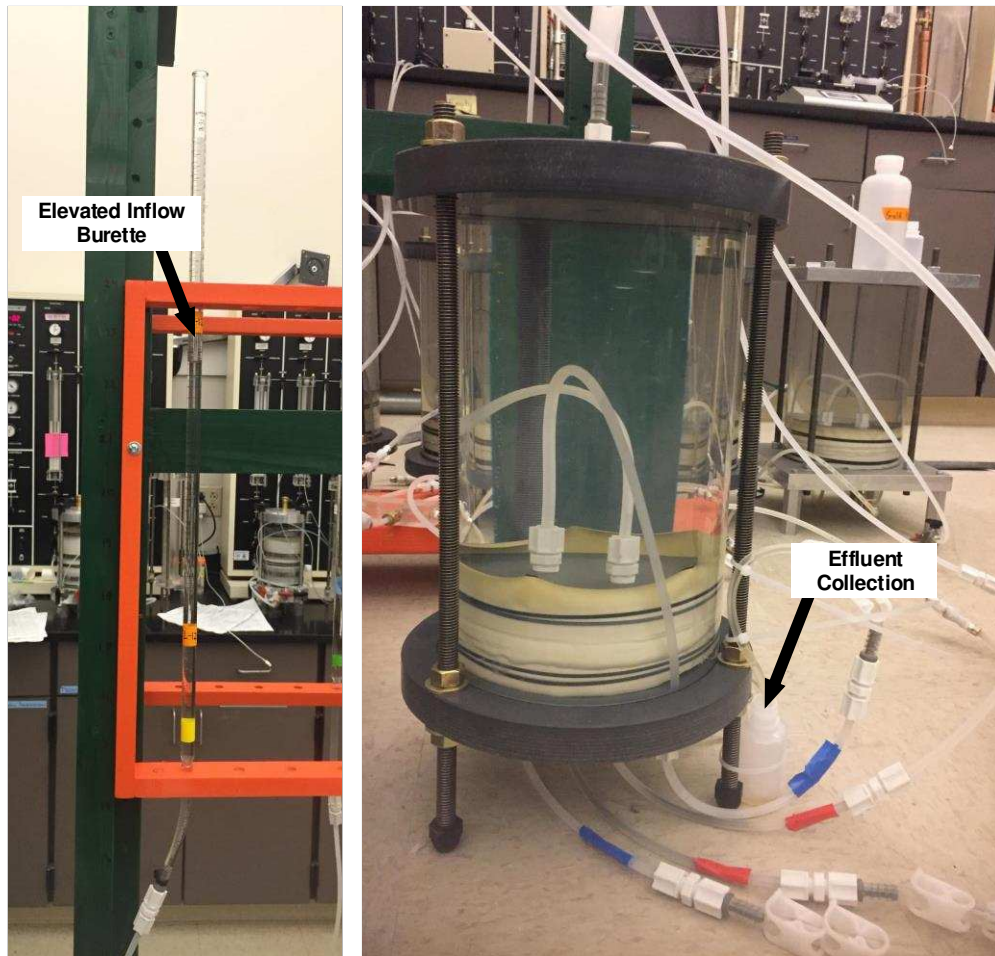


Figure 2.7. Picture of experimental setup using the G-Method. (a) Elevated inflow burette. (b) Permeameter.

Table 2.5. Comparison of the stress conditions between the standard method (S-Method) and the gravity method (G-Method)

Parameter	Method of Testing	
	S-Method	G-Method
Cell pressure (kPa)	550	34.5 (3.52 m head)
Inflow pressure (kPa)	530	13.8 (1.41 m head)
Outflow pressure (kPa)	515	0
Average backpressure, u_{avg} (kPa)	523	6.9
Average effective stress, σ'_{avg} (kPa)	27.6 (4 psi)	27.6 (4 psi)
Average head loss across specimen (kPa)	13.8 (2 psi)	13.8 (2 psi)

Table 2.6. Testing program for hydraulic conductivity tests

Test Series	Material	Method	Permeant	Comment
1	GCL-1	S-Method	CW	Base case
2	GCL-1	G-Method	CW	Effect of G-Method
3	GCL-1	S-Method	Au-PS	Effect of Au-PS
4	GCL-1	G-Method	Au-PS	Effect of G-Method, Au-PS
5	GCL-1	S-M1	CW	Modified S-Method
6	GCL-1	S-M2	CW	Modified S-Method
7	GCL-1	S-M3	CW	Modified S-Method
8	GCL-1	S-M4	CW	Modified S-Method
9	GCL-1	S-M5	CW	Modified S-Method
10	GCL-2	S-Method	CW	Higher peel strength GCL
11	GCL-2	G-Method	CW	Higher peel strength GCL, Effect of G-Method
12	GCL-2	S-M6	CW	Higher peel strength GCL, Modified S-Method
13	GCL-2	S-M7	CW	Higher peel strength GCL, Modified S-Method
16	GCL-3	S-Method	CW	Lower peel strength GCL
17	GCL-3	G-Method	CW	Lower peel strength GCL, Effect of G-Method
18	GB	S-Method	CW	Comparison to GB
19	GB	G-Method	CW	Comparison to GB, Effect of G-Method
20	GCL-1	S-Method	DW	Comparison to DIW
21	GCL-1	G-Method	DW	Comparison to DIW, Effect of G-Method

GB = Granular Bentonite

S-Method = Standard method

G-Method = Gravity method

CW = Conservative water

Au-PS = Synthetic mining process solution

DW = Deionized water

S-M1 = Modified S-Method with 1 hr between backpressure increments

S-M2 = Modified S-Method with 4 hr between backpressure increments

S-M3 = Modified S-Method with 4 hr between 35 kPa (5 psi) backpressure increments

S-M4 = Modified S-Method with 5 psi backpressure increments

S-M5 = Modified S-Method with 1 day between 35 kPa (5 psi) backpressure increments

S-M6 = Modified S-Method where hydration is completed under elevated pressure, i.e. no backpressure steps are used.

S-M7 = Modified S-Method where phase one is equivalent G-Method and phase two is S-Method.

Table 2.7. Testing program for oedometer hydration tests

Test Series	Material	Hydrating Liquid	Comment
1	GB	DW	Base case for GB
2	GB	CW	Effect of CW
3	GB	Au-PS	Effect of Au-PS
4	GCL-1	DW	Base case for GCL-1
5	GCL-1	CW	Effect of CW
6	GCL-1	Au-PS	Effect of Au-PS

GB = Granular bentonite

DW = Deionized water

CW = Conservative water

Au-PS = Synthetic gold mining process solution

Table 2.8. Testing program for permeameter hydration tests

Test Series	Material	Hydrating Liquid	Method
1	GCL-1	CW	S-Method
2	GCL-1	CW	G-Method

CW = Conservative water

S-Method = Standard method

G-Method = Gravity method

Table 2.10. Results of hydraulic conductivity tests

Test Series	Test Number	Material	Method	Permeant	Water Content (%)	Final Degree of Saturation (%)	Final Degree of Saturation (%) ^(a)	Void Ratio	Dry Density (Mg/m ³)	Pore Volumes of Flow, PVF	Hydraulic Conductivity, <i>k</i> (m/s) ^(b)
1	1a	GCL-1	S-Method	CW	103%	89%	88%	3.09	0.65	15.4	5.9×10 ⁻¹¹
	1b	GCL-1	S-Method	CW	113%	95%	94%	3.18	0.64	5.4	2.2×10 ⁻¹¹
	1c ^(c)	GCL-1	S-Method	CW	tdb	tdb	tdb	tdb	tdb	tdb	3.4×10 ⁻¹¹
2	2a	GCL-1	G-Method	CW	103%	91%	90%	3.03	0.66	4.2	4.5×10 ⁻⁹
	2b	GCL-1	G-Method	CW	110%	87%	87%	3.38	0.61	2.6	5.3×10 ⁻⁹
	2c	GCL-1	G-Method	CW	109%	104%	105%	2.79	0.70	6.0	9.2×10 ⁻¹⁰
	2d ^(c)	GCL-1	G-Method	CW	tdb	tdb	tdb	tdb	tdb	tdb	1.8×10 ⁻¹¹
	3	3a	GCL-1	S-Method	Au-PS	87%	85%	83%	2.74	0.71	1.9
4	3b	GCL-1	S-Method	Au-PS	91%	96%	89%	2.53	0.76	10.5	2.9×10 ⁻¹¹
	3c ^(d)	GCL-1	S-Method	Au-PS	nr	89%	87%	2.68	0.72	8.6	3.8×10 ⁻¹¹
	4a	GCL-1	G-Method	Au-PS	88%	93%	91%	2.53	0.76	10.7	4.8×10 ⁻⁹
	4b	GCL-1	G-Method	Au-PS	93%	83%	83%	2.97	0.67	4.2	2.3×10 ⁻⁸
5	4c	GCL-1	G-Method	Au-PS	90%	98%	92%	2.47	0.77	2.4	4.3×10 ⁻¹⁰
	5a ^(d)	GCL-1	S-M1	CW	nr	95%	92%	3.07	0.66	6.1	3.1×10 ⁻¹¹
6	6a ^(d)	GCL-1	S-M2	CW	nr	92%	90%	3.18	0.64	4.8	2.5×10 ⁻¹¹
7	7a	GCL-1	S-M3	CW	119%	103%	102%	3.10	0.65	5.9	3.4×10 ⁻¹¹
8	8a	GCL-1	S-M4	CW	104%	96%	98%	2.87	0.69	4.9	2.2×10 ⁻¹¹
	8a	GCL-1	S-M4	CW	110%	98%	99%	3.02	0.66	4.0	2.3×10 ⁻¹¹
9	9a	GCL-1	S-M5	CW	106%	97%	95%	2.93	0.68	3.7	1.9×10 ⁻¹¹
	10a ^(c)	GCL-2	S-Method	CW	tdb	tdb	tdb	tdb	tdb	tdb	2.0×10 ⁻¹¹
10	10b	GCL-2	S-Method	CW	143%	109%	108%	3.52	0.59	5.1	2.9×10 ⁻¹¹
	10c	GCL-2	S-Method	CW	146%	111%	112%	3.51	0.59	6.9	3.0×10 ⁻¹¹
	11a ^(c)	GCL-2	G-Method	CW	tdb	tdb	tdb	tdb	tdb	tdb	8.7×10 ⁻⁹
	11b	GCL-2	G-Method	CW	135%	104%	99%	3.45	0.60	3.9	2.5×10 ⁻¹¹
11	11c	GCL-2	G-Method	CW	131%	97%	91%	3.60	0.58	2.9	1.3×10 ⁻⁹
	12a	GCL-2	S-M6	CW	115%	101%	91%	3.04	0.66	8.9	2.1×10 ⁻¹¹
	12b	GCL-2	S-M6	CW	130%	106%	104%	3.27	0.63	3.6	2.5×10 ⁻¹¹
12	12c	GCL-2	S-M6	CW	138%	107%	104%	3.44	0.60	20.2	3.1×10 ⁻¹¹
	13a	GCL-2	S-M7	CW	124%	95%	91%	3.48	0.60	3.4	2.7×10 ⁻¹¹
	13b	GCL-2	S-M7	CW	tdb	tdb	tdb	tdb	tdb	tdb	6.0×10 ⁻¹¹
13	13c	GCL-2	S-M7	CW	tdb	tdb	tdb	tdb	tdb	tdb	9.6×10 ⁻¹¹
	16a ^(c)	GCL-3	S-Method	CW	tdb	tdb	tdb	tdb	tdb	Tbd	2.0×10 ⁻¹¹
17	17a ^(c)	GCL-3	G-Method	CW	tdb	tdb	tdb	tdb	tdb	Tbd	2.3×10 ⁻¹¹
18	18a	GB	S-Method	CW	114%	106%	-	2.86	0.69	6.7	1.7×10 ⁻¹¹
19	19a	GB	G-Method	CW	100%	96%	-	2.76	0.71	7.1	1.4×10 ⁻¹¹
20	20a	GCL-1	S-Method	DW	116%	102%	103%	3.02	0.66	6.4	2.6×10 ⁻¹¹
21	21a	GCL-1	G-Method	DW	108%	91%	93%	3.16	0.64	1.5	2.0×10 ⁻¹¹

GB = Granular Bentonite
 S-Method = Standard method
 G-Method = Gravity method
 CW = Conservative water
 Au-PS = Synthetic mining process solution
 DW = Deionized water
 S-M1 = Modified S-Method with 1 hr between backpressure increments
 S-M2 = Modified S-Method with 4 hr between backpressure increments
 S-M3 = Modified S-Method with 4 hr between 35 kPa (5 psi) backpressure increments
 S-M4 = Modified S-Method with 5 psi backpressure increments
 S-M5 = Modified S-Method with 1 day between 35 kPa (5 psi) backpressure increments
 S-M6 = Modified S-Method where hydration is completed under elevated pressure, i.e. no backpressure steps are used.
 S-M7 = Modified S-Method where phase one is equivalent G-Method and phase two is S-Method.
^(a)Degree of saturation determined without the Textile Correction
^(b)Based on hydraulic termination criteria of ASTM D6766-12
^(c)Ongoing tests. PVF estimated using average pore volume of test series.
^(d)Water content not reported.
 tdb = To be determined
 nr = Not reported. Averages of similar test series used for determination of specimen properties

Table 2.11. Results of oedometer hydration tests

Test Series	Test Number	Material	Hydration Liquid	Water Content (%)	Final Degree of Saturation (%) ^(a)	Final Degree of Saturation (%)	Void Ratio	Dry Density (Mg/m ³)
1	1a	GB	DW	145	104	-	3.71	0.57
	1b	GB	DW	139	101	-	3.66	0.57
	1c	GB	DW	121	104	-	3.11	0.65
2	2a	GB	CW	139	110	-	3.37	0.61
	2b	GB	CW	143	104	-	3.68	0.57
	2c	GB	CW	130	106	-	3.27	0.63
3	3a	GB	Au-PS	110	100	-	2.93	0.68
	3b	GB	Au-PS	125	109	-	3.07	0.66
	3c	GB	Au-PS	116	102	-	3.04	0.66
4	4a	GCL-1	DW	114	96	96	3.18	0.64
	4b	GCL-1	DW	118	97	101	3.22	0.63
	4c	GCL-1	DW	120	93	96	3.43	0.60
5	5a	GCL-1	CW	124	100	99	3.31	0.62
	5b	GCL-1	CW	111	93	96	3.20	0.64
	5c	GCL-1	CW	107	100	97	2.86	0.69
6	6a	GCL-1	Au-PS	101	99	97	2.70	0.72
	6b	GCL-1	Au-PS	121	99	101	3.24	0.63
	6c	GCL-1	Au-PS	103	102	103	2.69	0.72

^(a)Degree of saturation determined the textile correction method

GB = Granular bentonite

DW = Deionized water

CW = Conservative water

Au-PS = Synthetic gold mining process solution

Table 2.12. Results of permeameter hydration tests

Test Series	Test Number	Material	Hydration Liquid	Water Content (%)	Final Degree of Saturation (%)	Final Degree of Saturation (%) ^(a)	Void Ratio	Dry Density (Mg/m ³)
1	1a	GCL-1	CW	97	100	95	2.57	0.75
	1b	GCL-1	CW	93	103	94	2.41	0.78
	1c	GCL-1	CW	94	111	101	2.25	0.82
2	2a	GCL-1	CW	112	110	97	2.71	0.72
	2b	GCL-1	CW	119	109	106	2.89	0.69
	2c	GCL-1	CW	117	107	101	2.92	0.68

^(a)Degree of saturation determined without the Textile Correction
 CW = Conservative water

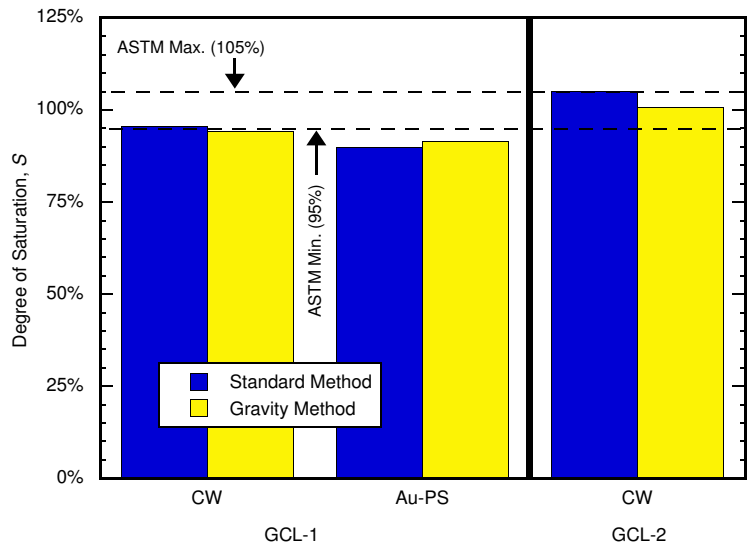


Figure 2.8. Comparison between the standard method and the gravity method of the determined degree of saturation for GCL-1 and GCL-2 permeated with conservative water (CW) and synthetic gold mining process solution (Au-PS).

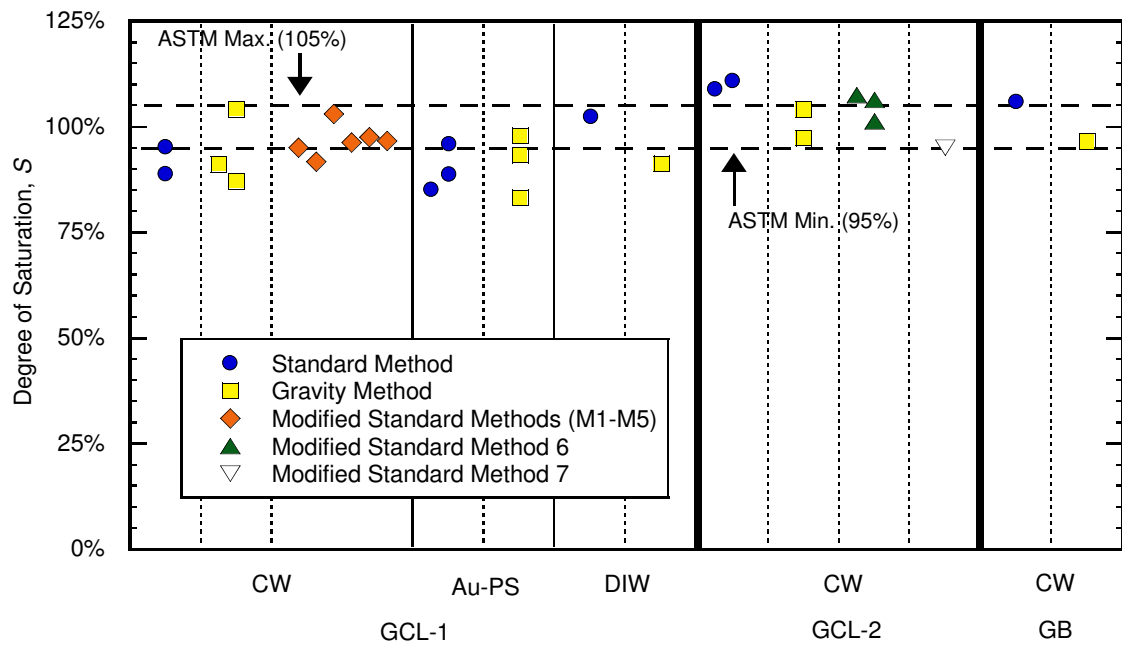


Figure 2.9. Degrees of saturation for tests permeated by the standard method, gravity method, and modified standard methods for GCL-1, GCL-2, and granular bentonite (GB) permeated with conservative water (CW), synthetic gold mining process solution (Au-PS), and deionized water (DW).

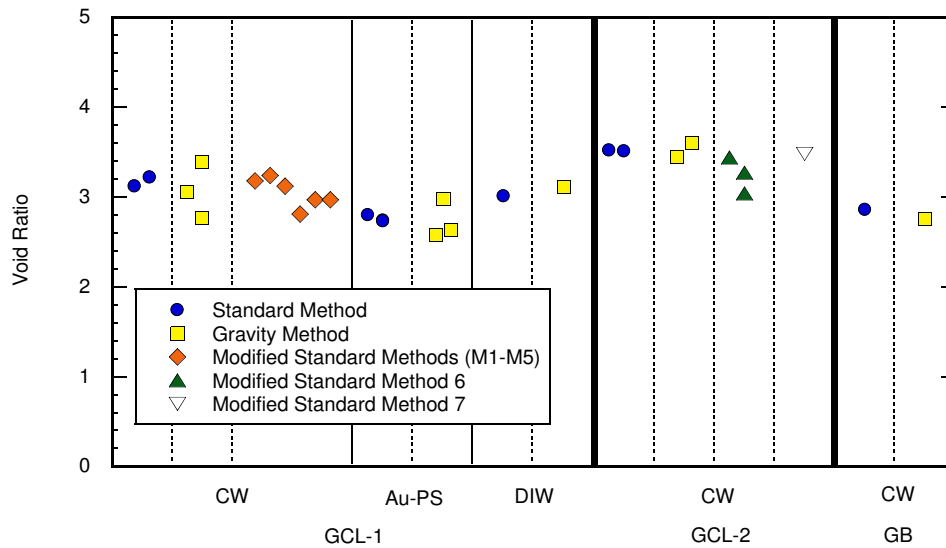


Figure 2.10. Void ratio for tests permeated by the standard method, gravity method, and modified standard methods for GCL-1, GCL-2, and granular bentonite (GB) permeated with conservative water (CW), synthetic gold mining process solution (Au-PS), and deionized water (DW).

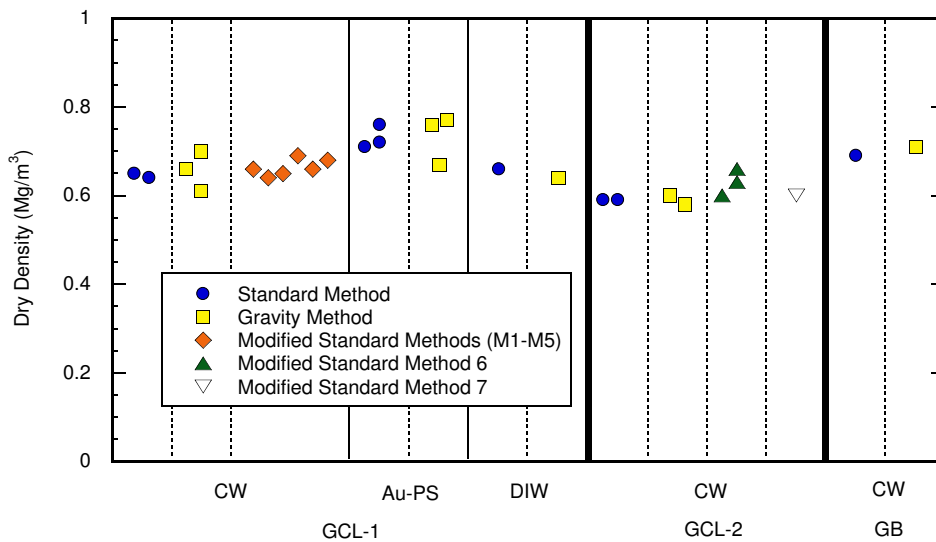


Figure 2.11. Dry density (Mg/m^3) for tests permeated by the standard method, gravity method, and modified standard methods for GCL-1, GCL-2, and granular bentonite (GB) permeated with conservative water (CW), synthetic gold mining process solution (Au-PS), and deionized water (DW).

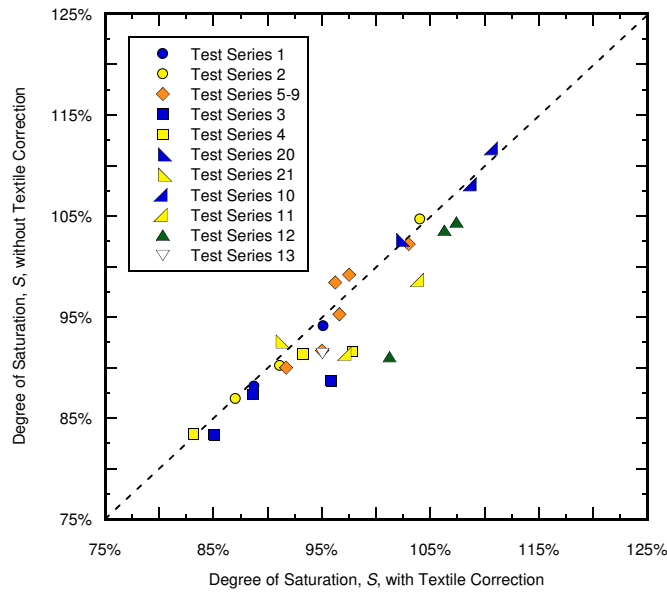


Figure 2.12. Comparison of the determined degree of saturation with the textile correction method to the determined degree of saturation without the textile correction method.

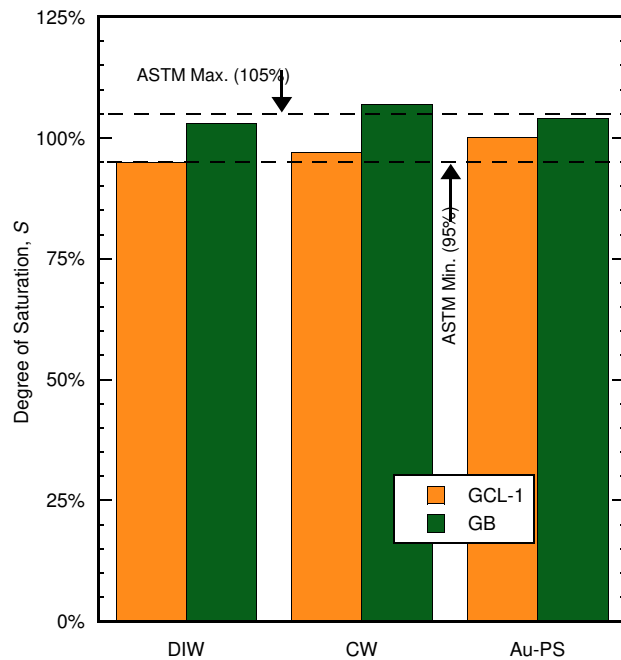


Figure 2.13. Average degree of saturation for GCL-1 and granular bentonite (GB) hydrated in oedometers with deionized water (DW), conservative water (CW), and synthetic gold mining process solution (Au-PS).

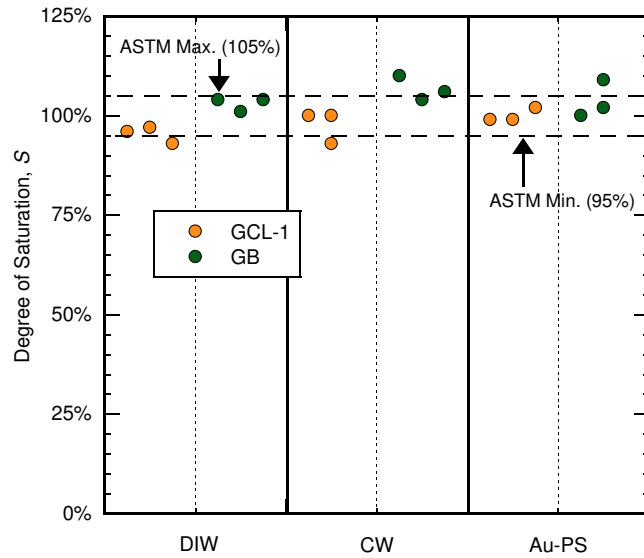


Figure 2.14. Degree of saturation for GCL-1 and granular bentonite (GB) hydrated in oedometers with deionized water (DW), conservative water (CW), and synthetic gold mining process solution (Au-PS).

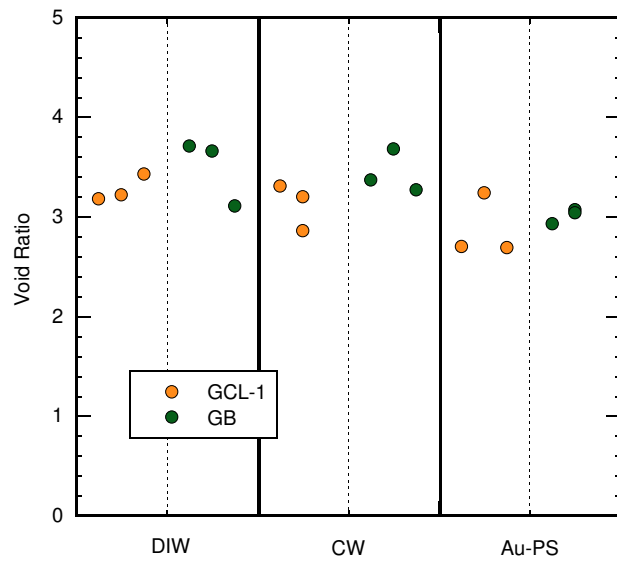


Figure 2.15. Void ratio of saturation for GCL-1 and granular bentonite (GB) hydrated in oedometers with deionized water (DW), conservative water (CW), and synthetic gold mining process solution (Au-PS).

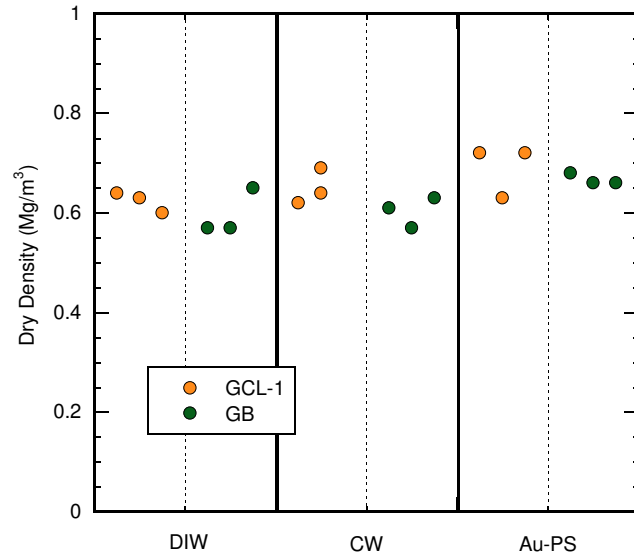


Figure 2.16. Dry density (Mg/m^3) of saturation for GCL-1 and granular bentonite (GB) hydrated in oedometers with deionized water (DW), conservative water (CW), and synthetic gold mining process solution (Au-PS).

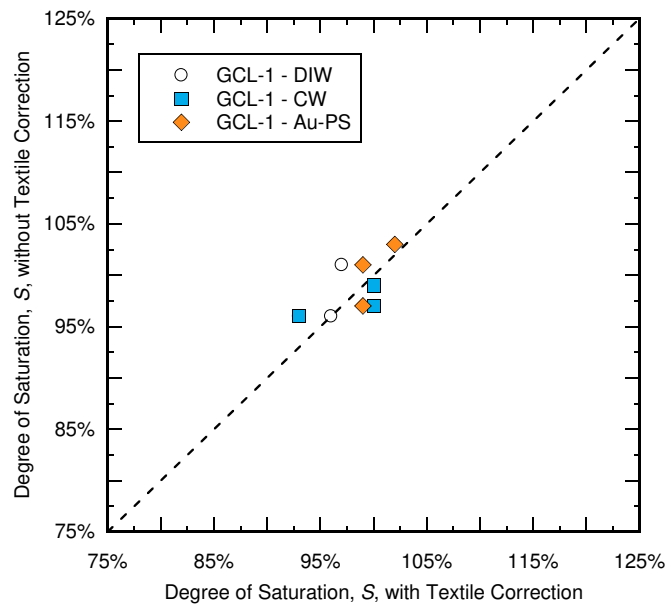


Figure 2.17. Comparison of the degree of saturation with the textile correction method to the degree of saturation without the textile correction method for GCL-1 hydrated in oedometers with deionized water (DW), conservative water (CW), and synthetic gold mining process solution (Au-PS).

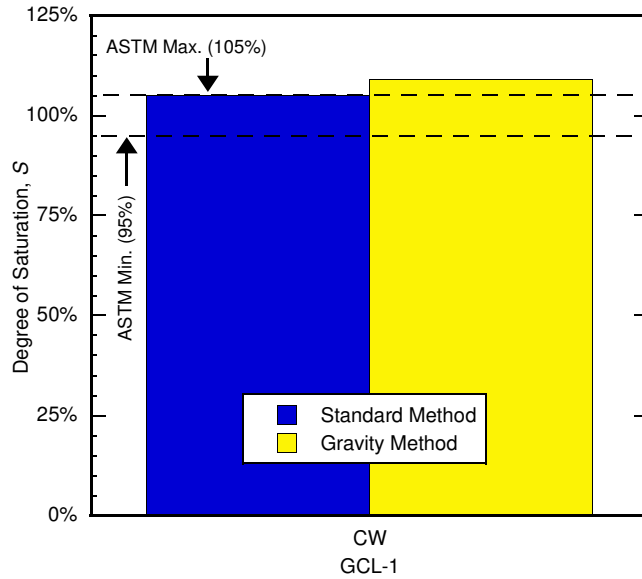


Figure 2.18. Average degrees of saturation for GCL-1 and hydrated in permeameters using the standard method and gravity method with conservative water (CW).

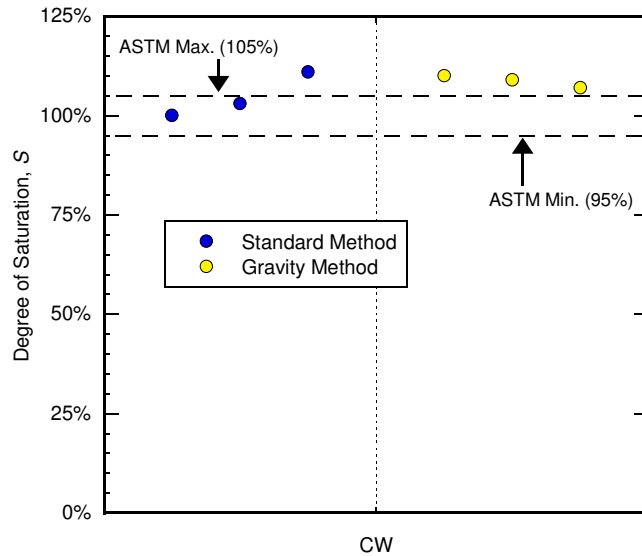


Figure 2.19. Degrees of saturation for GCL-1 and hydrated in permeameters using the standard method and gravity method with conservative water (CW).

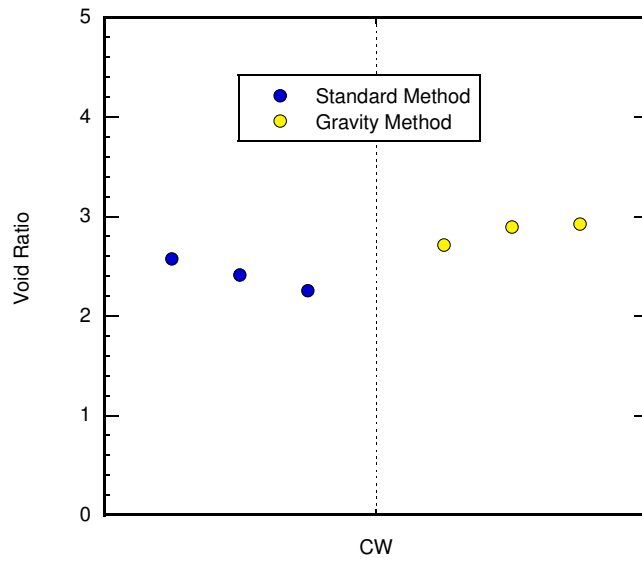


Figure 2.20. Void ratio for GCL-1 and hydrated in permeameters using the standard method and gravity method with conservative water (CW).

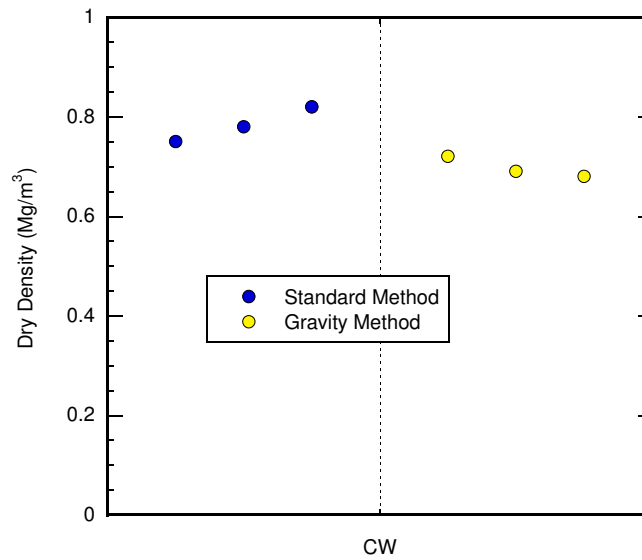


Figure 2.21. Dry density (Mg/m³) for GCL-1 and hydrated in permeameters using the standard method and gravity method with conservative water (CW).

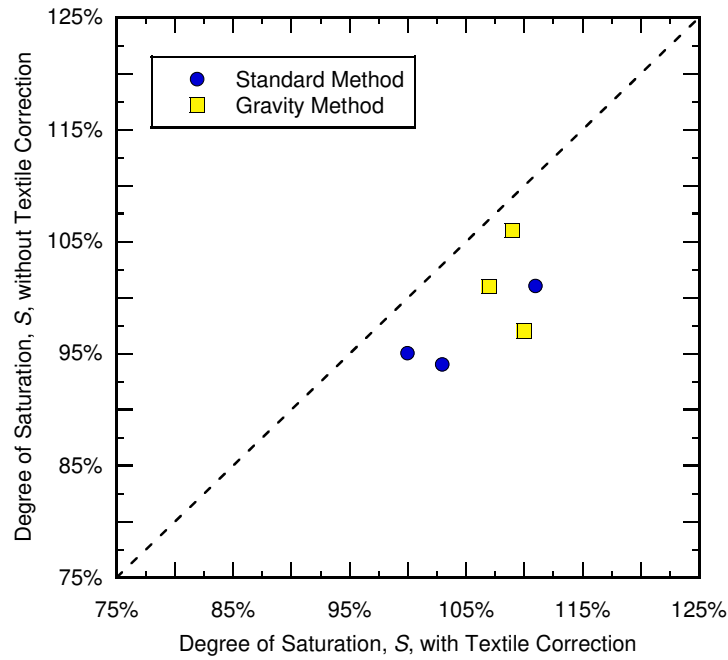


Figure 2.22. Comparison of the degree of saturation with the textile correction method to the degree of saturation without the textile correction method for GCL-1 hydrated in permeameters with conservative water using the standard method and gravity method.

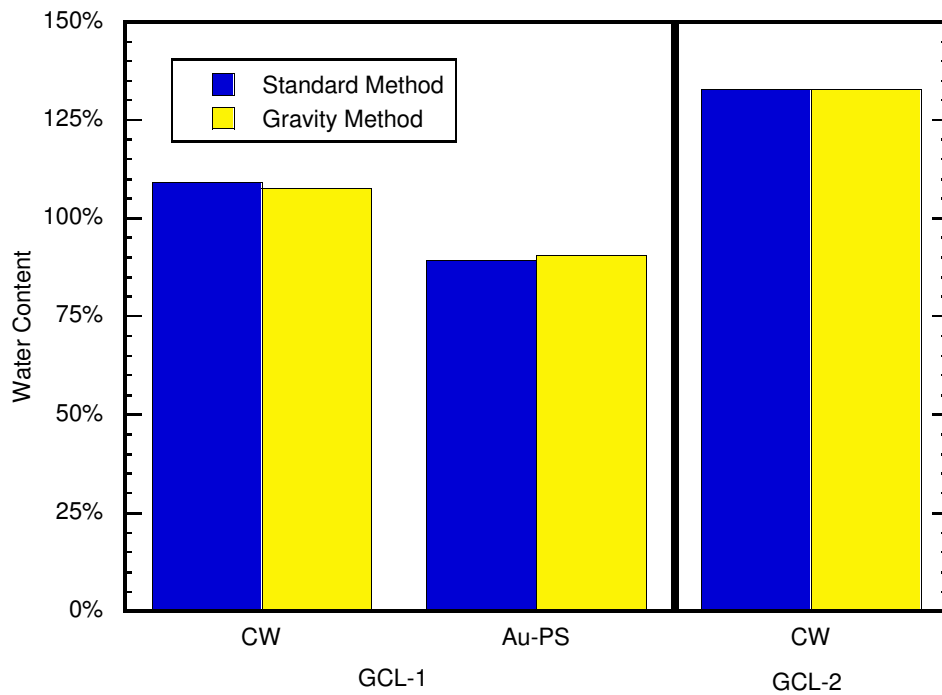


Figure 2.23. Average measured bentonite water contents for GCL-1 and GCL-2 permeated with conservative water (CW) and synthetic gold mining process solution (Au-PS).

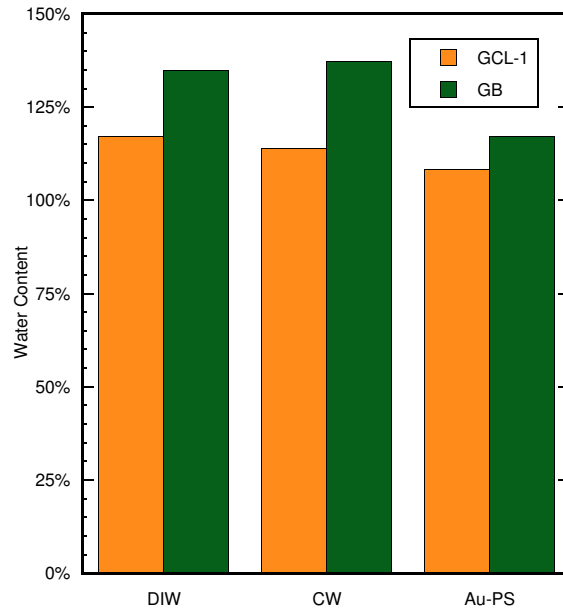


Figure 2.24. Average measured bentonite water contents for GCL-1 and granular bentonite (GB) hydrated in oedometers with deionized water (DIW), conservative water (CW), and synthetic gold mining process solution (Au-PS).

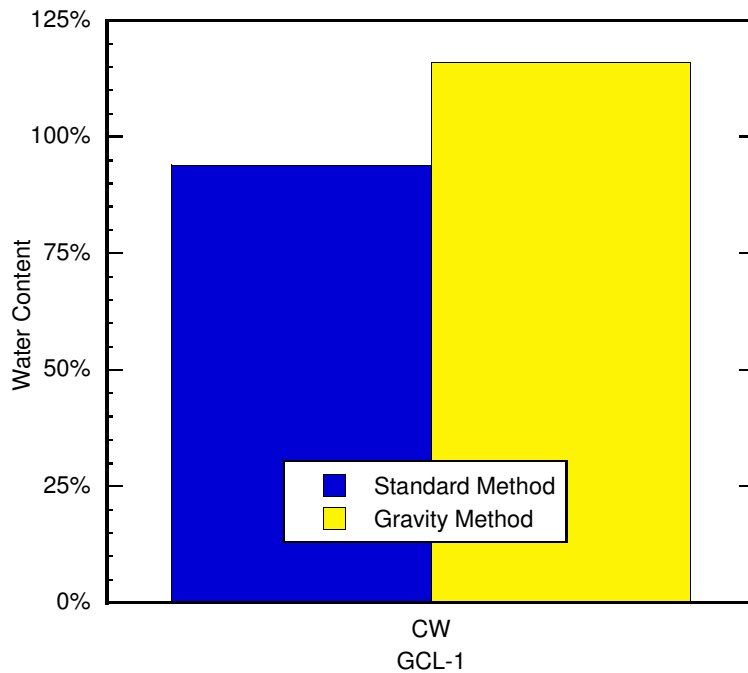


Figure 2.25. Average measured water content for GCL-1 and hydrated in permeameters using the stand method and gravity method procedures with conservative water (CW).

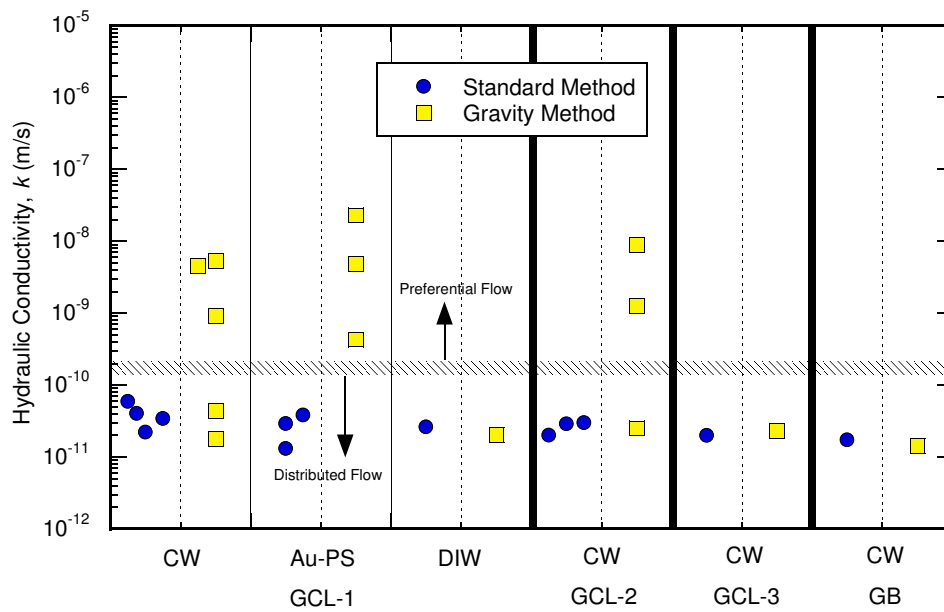


Figure 2.26. Hydraulic conductivity, k , for tests permeated by the standard method and gravity method for GCL-1, GCL-2, and granular bentonite (GB) permeated with conservative water (CW), synthetic gold mining process solution (Au-PS), and deionized water (DW).

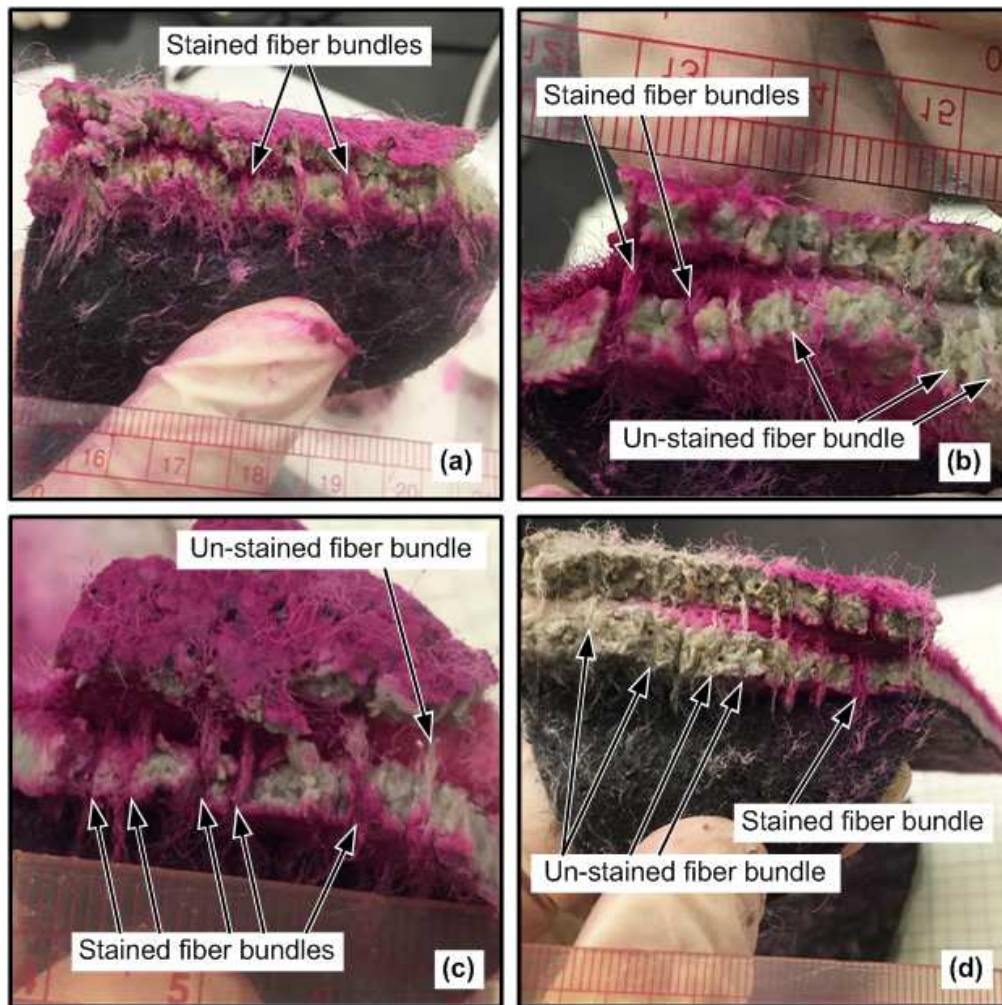


Figure 2.27. Fiber bundles and surrounding bentonite stained with rhodamine-WT dye at termination of permeation for tests conducted by gravity method.

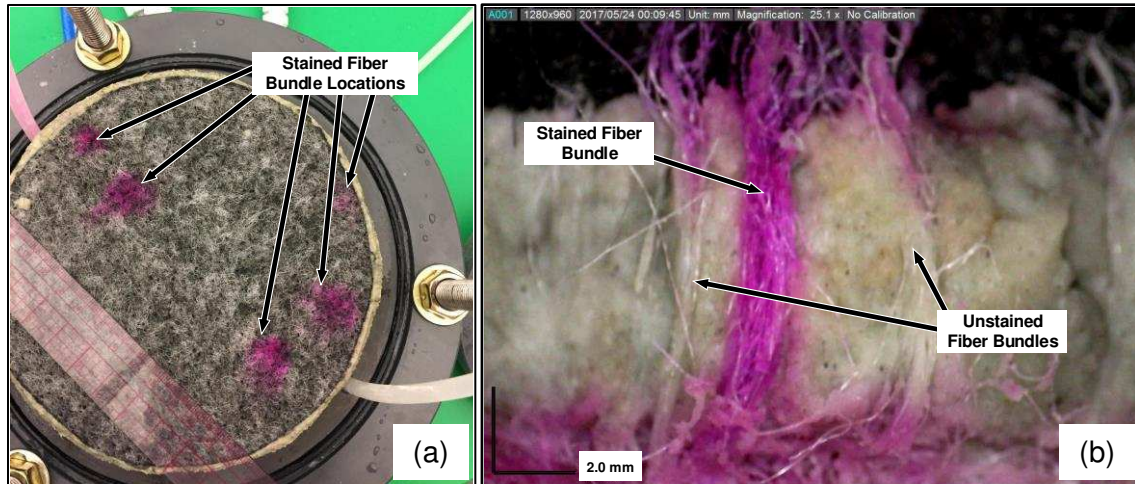


Figure 2.28. (a) View of dyed carrier (black) textile during dyed disassembly. (b) Fiber bundles and surrounding bentonite stained with rhodamine-WT dye after termination.

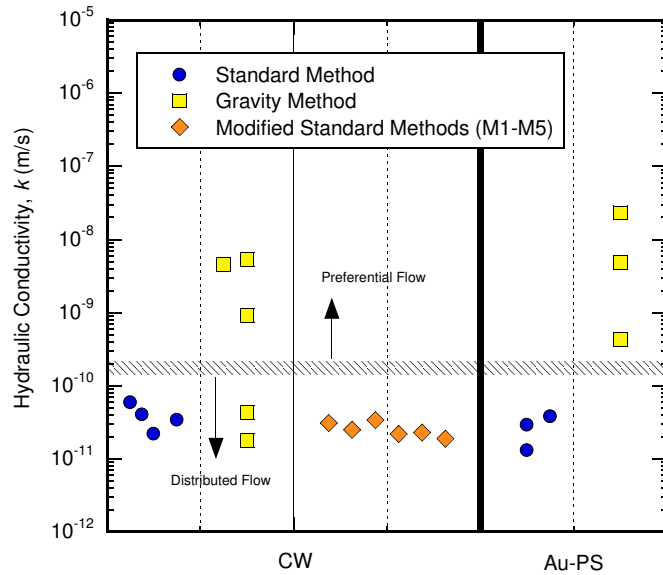


Figure 2.29. Hydraulic conductivity, k , for tests permeated by the standard method, gravity method, and modified standard methods for GCL-1 permeated with conservative water (CW), synthetic gold mining process solution (Au-PS), and deionized water (DW).

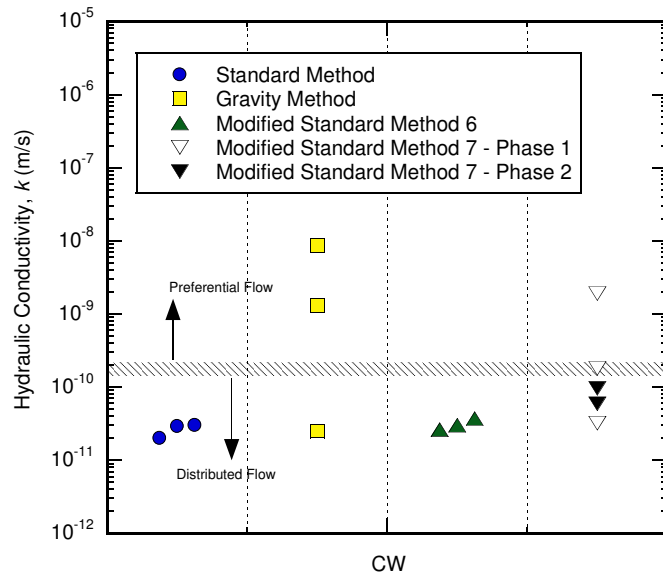


Figure 2.30. Hydraulic conductivity, k , for tests permeated by the standard method, gravity method, and modified standard methods for GCL-2 permeated with conservative water (CW).

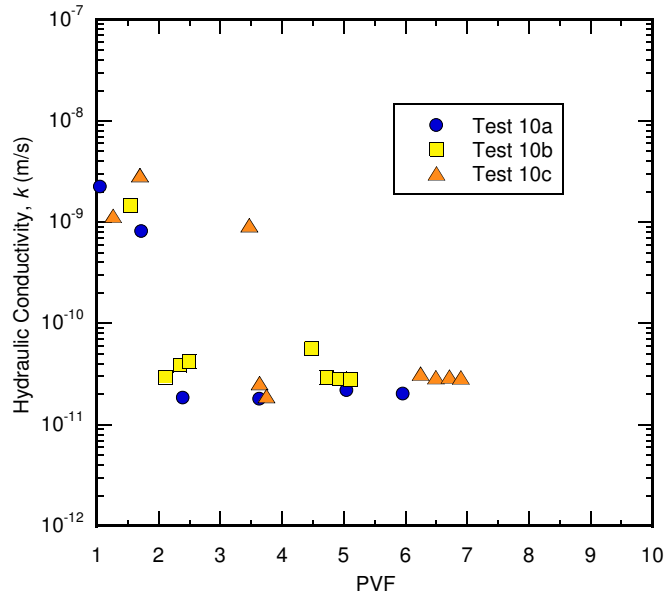


Figure 2.31. Hydraulic conductivity, k , versus pore volumes of flow (PVF) for Test Series 10, GCL-2 permeated with conservative water using the standard method. Pore volume of Test 10a calculated using avg. pore volume from Tests 10b and 10c

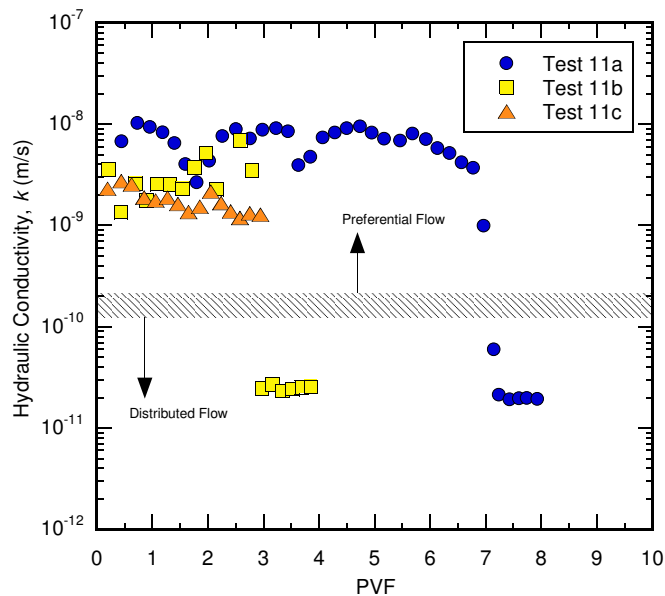


Figure 2.32. Hydraulic conductivity, k , versus pore volumes of flow (PVF) for Test Series 11, GCL-2 permeated with conservative water using the gravity method. Pore volume of Test 11a calculated using avg. pore volume from Tests 11b and 11c

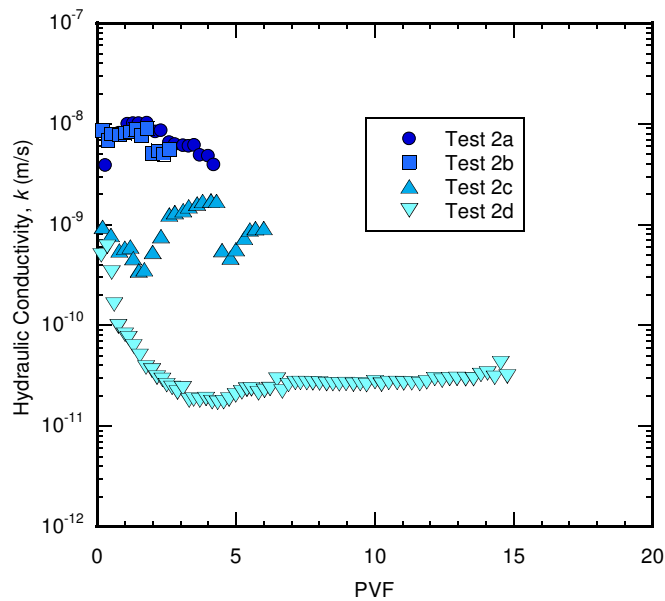


Figure 2.33. Hydraulic conductivity, k , versus pore volumes of flow (PVF) for Test Series 2. GCL-1 permeated with conservative water using the gravity method. Pore volume of Test 2d calculated using avg. pore volume from Tests 2a, 2b, and 2c

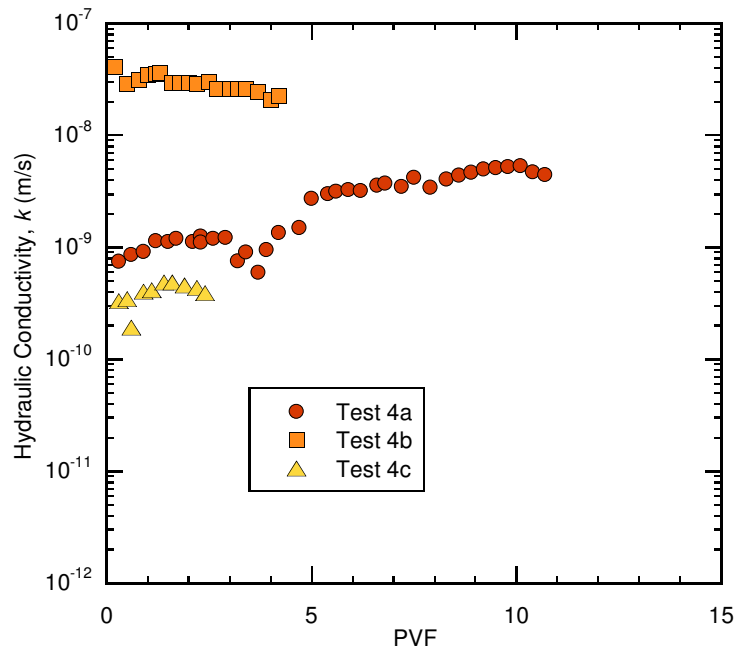


Figure 2.34. Determined hydraulic conductivity, k , versus pore volumes of flow (PVF) for Test Series 4. GCL-1 permeated with synthetic gold mining process solution using the gravity method.

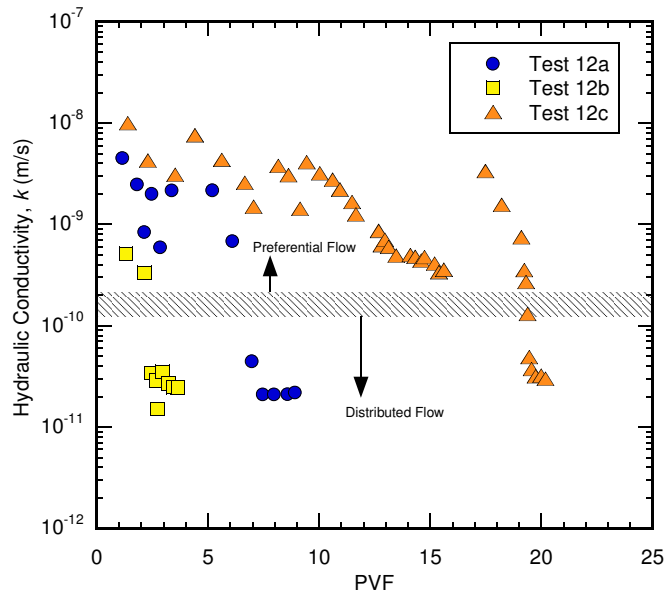


Figure 2.35. Hydraulic conductivity, k , versus pore volumes of flow (PVF) for Test Series 12, GCL-2 permeated with conservative water using modified standard method 6.

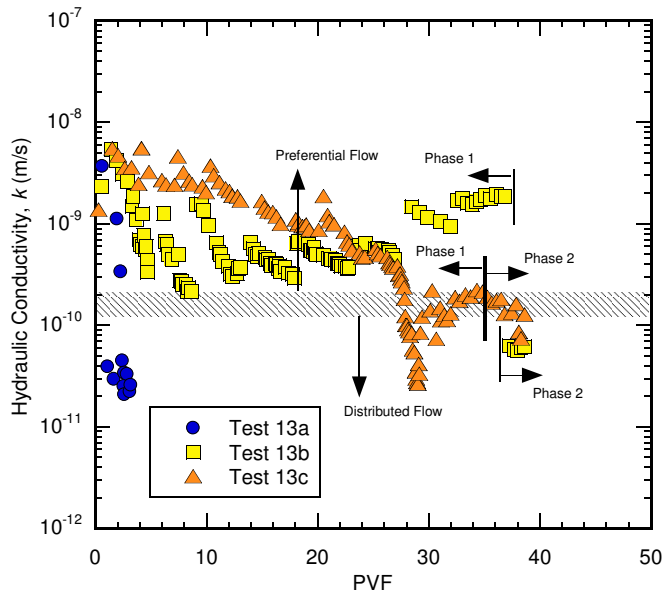


Figure 2.36. Hydraulic conductivity, k , versus pore volumes of flow (PVF) for Test Series 13, GCL-2 permeated with conservative water using modified standard method 7.

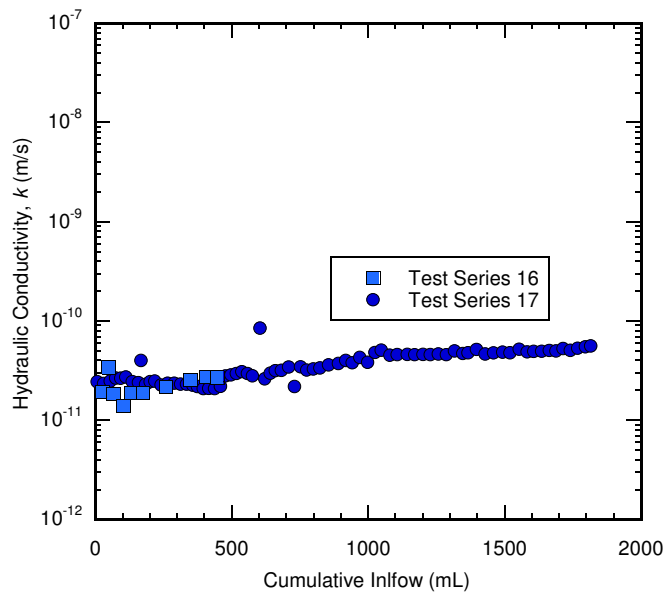


Figure 2.37. Hydraulic conductivity, k , versus cumulative inflow for test series 16 (standard method) and 17 (gravity method), GCL-3 permeated with conservative water.

CHAPTER 3

Hydraulic conductivity measurement of GCLs with mine waste leachates

3.1 Introduction

Increasingly, GCLs are being used in mining applications, including as liners for uranium mill facility tailings, brine evaporation ponds, waste rock dumps, and secondary liners for heap leach pads (Bouazza 2010). These applications often involve containing leachates with higher dissolved salt concentrations and potentially extreme pHs ($\text{pH} < 3$ and $\text{pH} > 12$) which exceed thresholds typically encountered in other environmental containment applications (Bouazza 2010). Thus, site-specific hydraulic compatibility tests are often necessary in mining applications to identify specific combinations of permeant liquid, bentonite, and effective stress that may result in high k . If the permeant liquid of interest results in an unacceptably large increase in k (e.g., $>> 3 \times 10^{-11}$ m/s), then the GCL typically is deemed incompatible with the permeant liquid, often necessitating the use of an alternative technology.

As discussed in Chapter 1, the standard method (S-Method) described by ASTM D6766-12 is not well suited for mine waste leachates. This method, and the equipment (i.e., permeameters and bladder accumulators) typically employed, are not designed for the high concentration and extreme pH solutions ($\text{pH} < 3$ or $\text{pH} > 12$) encountered in mine waste leachates. These solutions can clog permeameter tubing (e.g., by precipitation of salts or amorphous phase minerals), and corrode equipment, resulting in inaccurate k measurements as well as damage to testing equipment. The S-Method also lacks simple procedures for collecting effluent for analysis and requires additional safety procedures as the result of placing potentially hazardous mine waste leachates under elevated fluid pressures for backpressure saturation.

Chapter 2 demonstrated that an alternative method, the gravity method (G-method), results in GCL saturation without backpressure (i.e. saturation within 95%-105%), provides accurate results for k compared to the S-Method when preferential flow is not exhibited, and

reveals possible preferential flow that can be masked by the S-Method. Thus, the G-Method can be used in conjunction with a mine-waste-resistant permeameter (MW permeameter) to measure the k of GCLs to mine waste leachates.

The purpose of this study is to investigate the use of the MW permeameter in conjunction with the simplified G-Method for future hydraulic compatibility testing of GCLs with mine waste leachates. Three different mine waste leachates are investigated, a neutral pH synthetic gold mining process solution (Au-PS), a high pH synthetic bauxite mining process solution (BX-PS), and a low pH synthetic copper mining process solution (Cu-PS).

3.2 Materials and Methods

3.2.1 Liquids

Six liquids were used in this study: de-ionized water (DW), tap water (TW), a synthetic conservative soil porewater (CW), Au-PS, BX-PS, and Cu-PS. The chemical properties of each liquid are summarized in Table 3.1. Target anion and cation concentrations can be found in Appendix A. The DW (electrical conductivity, EC, = 4.2×10^{-4} S/m, pH = 7.0) is classified as Type II reagent water (ASTM D1193-06). The TW (EC = 1.3×10^{-2} S/m, pH = 6.7) was taken from the geoenvironmental laboratory at CSU. The CW (EC, = 5.1×10^{-2} S/m, pH = 5.7) is a synthetic solution intended to represent a worst-case chemistry for natural subgrade hydration and percolation that could be encountered in a cover system (Scalia and Benson 2010a), and is recommended for use in ASTM D5084-16; CW is described in detail in Scalia and Benson 2010a. The Au-PS (EC, = 0.34 S/m, pH 5.1) represents an average leachate encountered in gold heap leach mining operations (Ghazi Zadeh et al. 2017); Au-PS is described in detail in Ghazi Zadeh et al. 2017. The BX-PS (EC = 0.70 S/m, pH = 12.0) represents an average leachate encountered in bauxite mining operations (Ghazi Zadeh et al. 2017); BX-PS is described in detail in Ghazi Zadeh et al. 2017. The Cu-PS (EC = 5.7 S/m, pH = 1.2) represents a possible worst-case scenario leachate encountered in copper heap leach mining operations (Ghazi Zadeh et al. 2017); Cu-PS

is described in detail in Ghazi Zadeh et al. 2017. All six liquids were used in k testing, the methods of which are described in a subsequent sub-section. The CW, Au-PS, BX-PS, and Cu-PS were prepared by adding reagent grade salts (Fisher Scientific, Waltham, MA) to DW. The CW was prepared by dissolving 15.5 mg of NaCl and 214.6 mg of CaCl₂ in 1 L of DW. The Au-PS was prepared by combining 415.34 mg CaCl₂, 121.44 mg MgCl₂, 1464.6 mg Na₂SO₄, 19.57 mg KNO₃, 141.19 mg NaCl, and 17.99 mg KCl in 1 L of DIW. The BX-LS was prepared by combining 321.5 mg CaSO₄, 60 mg MgSO₄, 800 mg NaOH, and 1,715 mg Na₂SO₄ in 1 L of DW. The Cu-PLS was prepared by combining 16,990 mg Al₂(SO₄)₃ 14-18 H₂O, 1,628 mg CaCl₂, 2750.5 mg CuCl₂, 418 mg MgCl₂ 6H₂O, 25,010 mg MgSO₄, 5,992 mg MnSO₄ H₂O, 1,504 mg KCl, 9,196 mg Na₃PO₄ 12H₂O, 1,890 mg NaCl, 54.5 mg Na₂SO₄, and 25 mL HCl (37%) in 1 L of DW. After preparation, solutions were stored in collapsible carboys to minimize interaction with the atmosphere.

The ionic strength (I) and ratio of monovalent-to-divalent cations (RMD) were calculated based on target concentrations using the equations described in Section 2.2.1.

Electrical conductivity and pH were measured using a benchtop pH/EC meter (Orion Versa Star, Thermo Scientific, Waltham, MA). The values reported in Table 2.1 are averages taken from multiple measurements (number of measurements, $n > 30$) from May 2016 to July 2017, i.e., during testing. All measurements are reported in Appendix A. Electrical conductivity and pH were used to verify solution concentrations as recommended by Ghazi Zadeh et al. (2017), using EC and pH values from Scalia and Benson (2010a) and Ghazi Zadeh et al. (2017) as indices.

These liquids (DW, TW, CW, Au-PS, BX-PS, Cu-PS) were selected to assess how mining leachates affect the k of GCLs. The DW and TW represent a base case for GCL k . The CW provides a low concentration solution ($I = 6$ mM), but with a low RMD (0.19 mM^{1/2}) that will exchange Na⁺ for Ca²⁺ and potentially increase k . The Au-PS provides a near neutral mining leachate. The BX-LS (pH = 12.0) provides an alkaline mining leachate. Lastly, the Cu-PLS (pH = 1.2) provides an acidic mining leachate.

Select tests were also permeated to chemical equilibrium (i.e. meeting chemical termination criteria of ASTM D6766-12). Chemical equilibrium is defined as having been met when the EC ratio is 1 ± 0.1 ; EC ratio is calculated using the following equation:

$$EC \text{ Ratio} = \frac{EC_{out}}{EC_0} \quad (3.1)$$

where EC_{out} is the measured EC of the outflow in S/m, and EC_0 is the measured EC of the bulk solution used as influent the test liquid in S/m.

In addition, although not used as a termination criteria, a pH ratio was also recorded for all tests where an EC ratio was recorded. The pH ratio is calculated using the following equation:

$$pH \text{ Ratio} = \frac{pH_{out}}{pH_0} \quad (3.2)$$

where pH_{out} is the measured pH of the outflow, and pH_0 is the measured pH of the bulk solution used as the influent test liquid.

3.2.2 GCLs

In this study, three different commercially available needle-punched GCL products were tested, GCL-1, GCL-2, and GCL-3. The properties of these GCLs are listed in Tables 2.2 and 2.3, and described in detail in Section 2.2.2. GCL-1 (manufacturer reported peel strength, MRPS = 2170 N/m) and GCL-2 (MRPS = 3500 N/M) represent GCLs with higher degrees of needle punching that are designed for potential use in mining applications, whereas GCL-3 (MRPS = 700 N/m) represents a typical needle-punched GCL.

3.2.3 Granular Bentonite

A simulated non-reinforced granular bentonite (GB) GCL was also tested. The GB GCL is described in detail in Section 2.2.3. The in-permeameter assembly method was used to assemble GB-GCL specimens, this method is described in detail by Scalia et al. (2014).

3.2.4 Hydraulic Conductivity Testing by the G-Method

Hydraulic conductivity of GCLs with chemical solutions was measured the simplified G-Method. A testing program of all k tests is provided in Table 3.2. This method is similar to the default method prescribed in ASTM D6766-12 except backpressure saturation and permeant interface devices are not included. Section 2.2.6 provides a detailed description of the G-Method. A schematic of the test set up, with labeled components is provided in Figure 3.1. All tests were permeated until the hydraulic termination criteria of ASTM D6766-12 was met while select test were permeated until chemical termination criteria of ASTM D6766-12 was met. The volumetric flow ratio is calculated using Equation 2.4 while the k for the G-Method is calculated using Equation 2.5. Verification of the degree of saturation was completed by calculation based on weight-volume relationships at the end of permeation as described in Sections 2.2.7 and 2.2.13. For k specimens that exhibited high k ($> 10^{-10}$ m/s), and after the specified termination criteria had been achieved, rhodamine WT dye (5mg/L) was added to the influent to determine if preferential flow was occurring, as described in Section 2.2.11. Tests were depressurized in the reverse order of the method used for pressurization, as describe in Section 2.2.12.

3.2.5 Chemical Resistant Permeameter

A flexible-wall permeameter, the MW permeameter, was developed to facilitate the following experimental conditions:

- Resist corrosion from high ionic strength acidic and alkaline solutions;

- Minimize possible constrictions (locations for precipitation and clogging) in influent and effluent tubing to prevent tube- or fitting-clogging precipitates; constructions associated with bladder accumulators, such as outflow ports, are eliminated with the gravity head method described above;
- Increase the volume of effluent generated for analysis of outflow chemistry (required to document chemical equilibrium) without increasing hydraulic gradient.

A cross-section schematic of the flexible-wall permeameter developed is shown in Figure 3.2. The permeameter incorporates six main modifications from commercially available flexible-wall permeameters:

- The permeameter top plate, bottom plate, top pedestal, and bottom pedestal are machined from gray PVC Type I, and polypropylene fittings were used for all hydraulic connections, these materials were chosen because they are resistant to high ionic strength acidic and alkaline solutions (of note, these components will not perform well with organic contaminants);
- Effluent is collected in a flexible fluorinated ethylene propylene (FEP) bag (Jensen Inert Products, Coral Springs, FL) placed flat on a level surface, or in a polyethylene narrow-mouth bottle, to facilitate convenient collection and analysis of effluent;
- A 0.75 kg/m² nonwoven needle-punched geotextile is used in lieu of porous stones; traditional porous stones made of bronze or aluminum oxide may corrode in extreme pH solutions;
- 6.35-mm (1/4-in) outside diameter (OD) tubing is used to reduce the potential for tube clogging relative to more typical 3.18-mm (1/8-in) OD tubing; a comparison of 6.35-mm and 3.18-mm OD tubing is shown schematically in Figure 3.3; 6.35-mm OD tubing has an inside area greater than 5-times that of 3.18-mm OD tubing (14.64 mm² vs. 2.77 mm²);

- External acetal tubing clamps (Bel-Art SP Scienceware Tubing Clamps, Wayne, NJ) are used instead of metal valves; Scalia et al. (2014) reports clogging of metal valves by mobile polymer from a polymerized bentonite; Figure 3.4 shows a photograph of the tubing closure system used.
- 152-mm (6-in) diameter base plates are used instead of the more common 102-mm (4-in) (or smaller) diameter base plates to allow testing of specimens with a larger cross-sectional area to increase the volumetric flow rate of effluent for a given hydraulic gradient (e.g., a 152-mm diameter specimen will generate 2.25-times more effluent than a 102-mm diameter specimen).

Photographs of the assembled MW permeameter using the gravity head method is shown in Figure 3.5.

3.2.6 Flowrates Through Empty Permeameters

Flowrates through empty permeameters were recorded for the two types of permeameters used (4-in commercially available and 6-in MW permeameter). Knowing the maximum possible flowrates through each permeameter is necessary to establish the maximum k that can be recorded for a given material and applied gradient. Procedures similar to the G-Method were used for all flowrate tests with both permeameter types.

Three different textiles for distribution of flow were used, viz. a porous stone, a commercially available 30 oz/yd² nonwoven geotextile, and a commercially available fiberglass sheeting.

The testing program and results for the empty permeameter flowrates tests are presented in Table 3.3 and shown in Figures 3.6. The maximum flow rate through the empty MW permeameter was 7.9 cm³/s, while the maximum flow rate through the empty standard permeameter was 1.0 cm³/s (Table 3.3). These flow rates correspond to a maximum measurable

k of 2.1×10^{-6} m/s for the MW permeameter, and 6.1×10^{-7} m/s for the standard permeameter for a 0.7-mm thick (typical) GCL (accounting for different cross-sectional areas). These flow rates also illustrate the potential viability of using geotextiles and fiberglass sheeting in lieu of porous stones, however, additional testing is required at higher effective stresses.

The lower recorded maximum flowrate for the standard permeameter versus the MW permeameter ($1.0 \text{ cm}^3/\text{s}$ versus $7.9 \text{ cm}^3/\text{s}$) is likely due to the smaller tubing diameter in the standard permeameter versus the MW permeameter (3.18 mm outside diameter versus 6.35 mm outside diameter, Figure 3.3). A smaller tubing diameter will have a smaller maximum flowrate for a given hydraulic pressure based on Poiseuille's Law which governs the flowrate of laminar flow of liquid through a long cylindrical pipe of constant cross section.

3.3 Results

3.3.1 Hydraulic Conductivity

Hydraulic conductivity test results are summarized in Table 3.2 and shown in Figure 3.7 for GCL-1, GCL-2, and GCL-3, permeated with DW, TW, CW, Au-PS, BX-PS, or Cu-PS. The results in Table 3.2 include the measured k values based on both hydraulic and chemical (chemical termination criteria meet both hydraulic and chemical equilibrium) termination criteria, the elapsed time, the pore volumes of flow (PVF) corresponding to the elapsed time, and the final degree of saturation at the end of the test. Note that ASTM D6766-12 does not require an indication of PVF, which represents the cumulative volume of outflow normalized with respect to the void or pore volume of the specimen, so the values of PVF have been provided only to provide insight into how much of each specimen was exposed to the permeant water during the test. The k based on hydraulic termination criteria is reported for all tests as well as the k based on chemical termination criteria for some tests to provide insight into how the k of each specimen had changed once hydraulic equilibrium was reached. The k at termination, either by hydraulic or chemical termination criteria, if applicable, is shown in Figure 3.7 and a comparison of the reported k based

on hydraulic termination criteria versus chemical termination criteria is shown in Figure 3.8 for tests where both values are reported. As recommended by ASTM D6766-12 both plots of k versus elapsed time and PVF are presented in Appendix E.

Specimens of GCL-1 were permeated with DW, TW, and CW. All the k for DW (Test Series 21) and TW (Test Series 22) were low, ranging from 8.3×10^{-12} m/s to 2.6×10^{-11} m/s (DW: $n = 1$, TW: $n = 3$, $SD = 8.9 \times 10^{-12}$ m/s). Tests with CW (Test Series 2) resulted in low k for one of four tests, 3.5×10^{-11} m/s (this test has not yet reached chemical termination criteria and is ongoing at the time of writing this thesis), and higher k for three of four tests, 9.2×10^{-10} m/s, 5.3×10^{-9} m/s, and 4.5×10^{-9} m/s. Tests with Au-PLS (Test Series 4) resulted in higher k for all three tests ranging from 4.9×10^{-10} m/s to 2.6×10^{-8} m/s.

Specimens of GCL-2 were permeated with CW, Au-PS, BX-PS, and Cu-PS. Tests with CW (Test Series 11) resulted in low k for two of three tests, 1.9×10^{-11} m/s and 2.5×10^{-11} m/s, and higher k for one of three tests, 1.3×10^{-9} m. The test with the Au-PLS (Test Series 26) resulted in a higher k of 1.1×10^{-8} m/s. The test with the BX-LS (Test Series 27) resulted in a higher k of 2.3×10^{-10} m/s. Rhodamine-WT dye was added to the influent liquid, and permeated through specimens that exhibited high k (i.e., specimens that exhibited $k > 10^{-10}$ m/s). The dyed specimens revealed preferential flow along some, but not all needle punching fiber bundles. Photographs of the stained fiber bundles for tests with CW are shown in Figure 3.9a, with Au-PLS in Figures 3.9b, and with BX-LS in Figure 3.9c. The test with Cu-PLS (Test Series 28) resulted in a higher k of 6.7×10^{-7} m/s. The higher k was attributed to limited swelling of the bentonite granules as observed in Figure 3.10.

Specimens of GCL-3 were permeated with CW, Au-PS, BX-PS, and Cu-PS. The test with CW (Test Series 17) resulted in a low k of 5.4×10^{-11} m/s (this test has not yet reached chemical termination criteria and is ongoing at the time of writing this thesis). The test with the Au-PLS (Test Series 23) resulted in a low k of 3.2×10^{-11} m/s. The test with the BX-PS (Test Series 24) resulted in a low k of 2.7×10^{-11} m/s. The test with the Cu-PLS (Test Series 25) resulted in a higher

k of 1.8×10^{-7} m/s. To investigate the cause of the higher k in the Cu-PLS test, Rhodamine-WT dye was added to the influent liquid and permeated through the specimen. The dyed specimen did not reveal preferential flow through fiber bundles, but revealed limited bentonite swelling, similar to that of Test Series 12 and Rhodamine-WT sorbed to the bentonite granule surface as observed in Figures 3.11

3.3.2 Degree of Saturation

The final degrees of saturation are reported in Table 3.2. All tests with DW, TW, CW, Au-PS, and BX-PS exhibit behavior consistent with the findings reported in Chapter 2, i.e., saturation within the range specified by ASTM D6766-12 (i.e. 95%-105%). Tests with Cu-PS exhibited lower degrees of saturation, potentially indicating unsaturated specimens. However, limited swelling (Figures 3.10, 3.11) resulted in the bentonite behaving more like a coarse-grained soil than a fine-grained soil and that some of the permeant liquid in the pore spaces between the granules may have drained during test disassembly and water content sampling. Thus, all specimens are believed to have saturation during permeation, but saturation was not able to be accurately determined due to the nature of the material.

3.4 Discussion

3.4.1 Comparison of k Between GCL Products

A plot of the temporal trends for specimens permeated with CW is shown in Figure 3.12 as k versus cumulative inflow. Cumulative inflow is used in place of PVF as tests 2d, 17a, and 11a have not yet been terminated, and thus pore volumes have not yet been determined. All specimens of GCL-1 and GCL-2 exhibited initial higher k ($> 10^{-10}$ m/s) indicative of preferential flow. Tests 2a, 2b, and 2c (GCL-1) were terminated at higher k while Test 2d immediately decreased to low k , reaching hydraulic termination criteria at $k = 1.8 \times 10^{-11}$ m/s, and currently exhibits steady k at 3.5×10^{-11} m/s, as permeation is continuing until chemical termination criteria

is met. Test 11c was terminated at higher k while Test 11a and 11c exhibited steady higher k before suddenly decreasing to low k . Test 17a (GCL-3) exhibited an initial low k that reached hydraulic termination criteria at $k = 2.3 \times 10^{-11}$ m/s, and at the time of writing this thesis, exhibits steady k at 5.4×10^{-11} m/s. These results demonstrate that GCLs with higher degrees of needle punching may result in high k that can be attributed to preferential flow through fiber bundles, while tests with low k steadily increase in k (up to 2-3 times) as chemical equilibrium is established.

A plot of the temporal trends for specimens permeated with the Au-PS is shown in Figure 3.13 as a plot of k versus PVF. All tests on specimens of GCL-1 and GCL-2 exhibited higher k ranging from 2.3×10^{-8} m/s – 4.3×10^{-10} m/s that persisted until termination. Test 10a (GCL-2) had k within the range of Tests 4a, 4b, and 4c (GCL-1) suggesting that GCL-1 and GCL-2 exhibited similar preferential flow when permeated with Au-PS. Test 23a (GCL-3) exhibited initial low k that persisted until termination within minimal change in k once chemical equilibrium was established.

A plot of the temporal trends for specimens permeated with the BX-PS is shown in Figure 3.14 as a plot of k versus PVF. GCL-2 (Test 11a) exhibited preferential flow that persisted until termination. However the k dropped ~ 30 times to 2.3×10^{-10} m/s before reaching chemical equilibrium. In contrast, GCL-3 (Test Series 7) exhibited low k that reached chemical equilibrium at 2.7×10^{-11} m/s.

A plot of the temporal trends for specimens permeated with the Cu-PS is shown in Figure 3.15 as a plot of k versus PVF. Both GCL-2 (Test Series 28) and GCL-3 (Test Series 25) exhibited high k of 6.7×10^{-7} m/s and 1.8×10^{-7} m/s respectively. This high k was attributed in both tests to limited swelling resulting in maintenance of a granular structure (Figure 3.10, 3.11).

3.1.4 Chemical Equilibrium Termination Criteria

Hydraulic compatibility testing has been shown to be necessary for GCLs permeated with potentially incompatible liquids as described by ASTM D6766 (Shackelford et al. 2000, ASTM D6766-12). A plot comparing the k based on the chemical termination criteria versus k when

initially meeting the hydraulic termination criteria of ASTM D6766-12 is shown in Figure 3.8; two observations are apparent in Figure 3.8. First, tests permeated with CW show an increase in k after permeating beyond hydraulic termination criteria to chemical termination criteria. This demonstrates that chemical equilibrium is necessary to obtain the true long term k . Second, that permeating for greater PVF may result in the sudden closure of preferential flow paths that may be initially present. Note that no tests that exhibited low k at equilibrium by hydraulic termination criteria exhibited high k at equilibrium by chemical termination criteria. This demonstrates that once preferential flow paths are closed these pathways are unlikely to reopen.

3.1.5 Effect of Effective Stress

All results presented thus far in have been for low effective stress conditions, 27.6 kPa (4 psi), consistent with the default method in ASTM D6766-12, however, increased effective stress has been shown to reduce k for GCLs (Mersi & Olson 1971, Petrov et al. 1997, Shackelford et al. 2000). Test 30a involved permeation of GCL-1 under a higher effective stress of 93.2 kPa (13.5 psi) with CW. Although this test has not yet been terminated, at the time of writing this thesis, k indicative of preferential flow ($k = 6.8 \times 10^{-9}$ m/s) has been observed at high PVF (4400 mL cumulative inflow, ~45 PVF) possibly showing that preferential flow can exist even with increased effective stresses. Collecting more data on GCLs permeated with CW, Au-PLS, BX-LS, and Cu-LS under higher effective stress conditions is the subject of ongoing research.

3.5 Conclusion

These results demonstrate that GCLs with higher degrees of needle punching may result in high k that can be attributed to preferential flow through fiber bundles. GCL-1 (2170 N/m peel strength) and GCL-2 (3500 N/m peel strength) can exhibit preferential flow through fiber bundles when low k is otherwise expected for non-standard liquids (CW, Au-PS, and BX-PS) under low effective stress, 27.6 kPa (4 psi), whereas GCL-3 (700 N/m peel strength) does not exhibit

preferential flow. DW, TW, CW, Au-PS, and BX-PS are all compatible with GCLs if preferential flow is not present. Ongoing research of testing GCL-1, GCL-2, and GCL-3 with CW and mining liquids (Au-PS, BX-PS) will provide insight if preferential flow is still observed at higher effective stresses.

GCL specimens permeated with Cu-PS exhibit much higher k ($> 10^{-7}$ m/s) due to limited swelling of bentonite granules under low effective stress, 27.6 kPa (4 psi). Ongoing research of testing GCL-1, GCL-2, and GCL-3 with Cu-PS will provide insight if limited swelling of the bentonite granules still leads to much higher k under higher effective stresses.

Table 3.1. Hydrating and permeating liquid chemistries

Parameter	Liquids					
	DW	TW	CW	Au-PS	BX-PS	Cu-PS
Ionic Strength, I (mM)	-	-	6.0	49	67	2200
RMD (mM ^{1/2}) ^(a)	-	-	0.19	10	26	32
Electrical Conductivity, EC (S/m) ^(b)	4.2×10^{-4}	1.3×10^{-2}	5.1×10^{-2}	0.34	0.70	5.7
pH ^(b)	7.0	6.7	5.7	5.1	12.0	1.2

^(a) RMD = ratio of monovalent-to-divalent cations; refer to Kolstad et al. (2004) for additional details

^(b) Measured using Orion Versa Star pH/Conductivity meter, Thermo Scientific, Waltham, MA

DW = Deionized water

TW = Tap water

CW = Synthetic conservative water (recommended in ASTM D5084)

Au-PS = Synthetic gold mining process solution

BX-PS = Synthetic bauxite mining process solution

Cu-PS = Synthetic copper mining process solution

Table 3.2. Testing program hydraulic conductivity tests

Test Series	Material	Permeant	Comment
2	GCL-1	CW	Base case
4	GCL-1	Au-PS	Effect of Au-PLS
21	GCL-1	DW	Effect of DIW
22	GCL-1	TW	Effect of TW
17	GCL-3	CW	Lower peel strength GCL
23	GCL-3	Au-PS	Lower peel strength GCL, Effect of Au-PS
24	GCL-3	BX-PS	Lower peel strength GCL, Effect of BX-PS
25	GCL-3	Cu-PS	Lower peel strength GCL, Effect of Cu-PS
11	GCL-2	CW	Higher peel strength GCL
26	GCL-2	Au-PS	Higher peel strength GCL, Effect of Au-PS
27	GCL-2	BX-PS	Higher peel strength GCL, Effect of BX-PS
28	GCL-2	Cu-PS	Higher peel strength GCL, Effect of Cu-PS
30 ^(a)	GCL-1	CW	Effect of increased σ'

All test permeated using the gravity method

^(a)Higher effective stress test. 93.2 kPa versus 27.6 kPa.

DW = Deionized water

TW = Tap water

CW = Synthetic conservative water

Au-PS = Synthetic gold mining process solution

BX-PS = Synthetic bauxite mining process solution

Cu-PS = Synthetic copper mining process solution

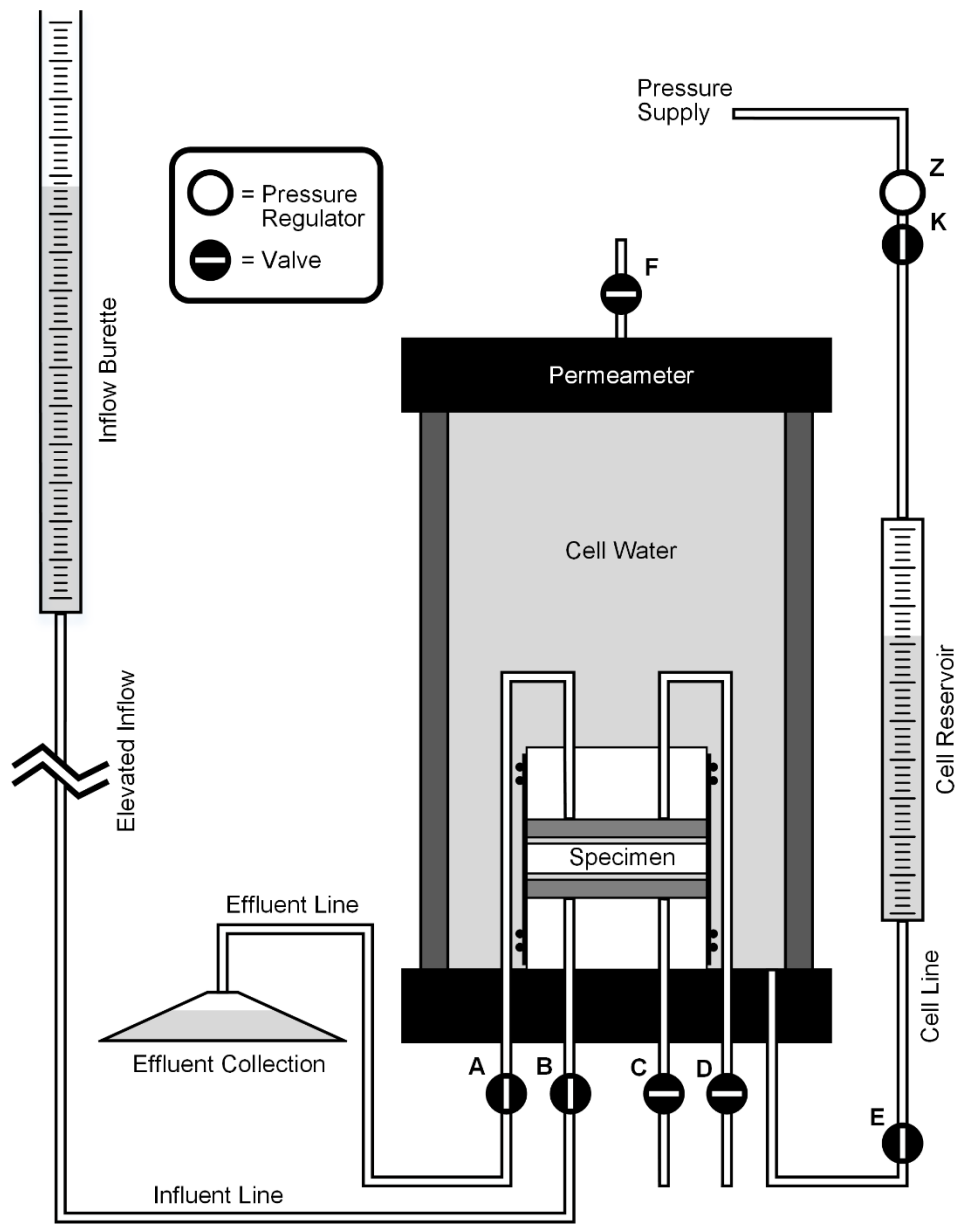


Figure 3.1. Schematic of test setup using the gravity method.

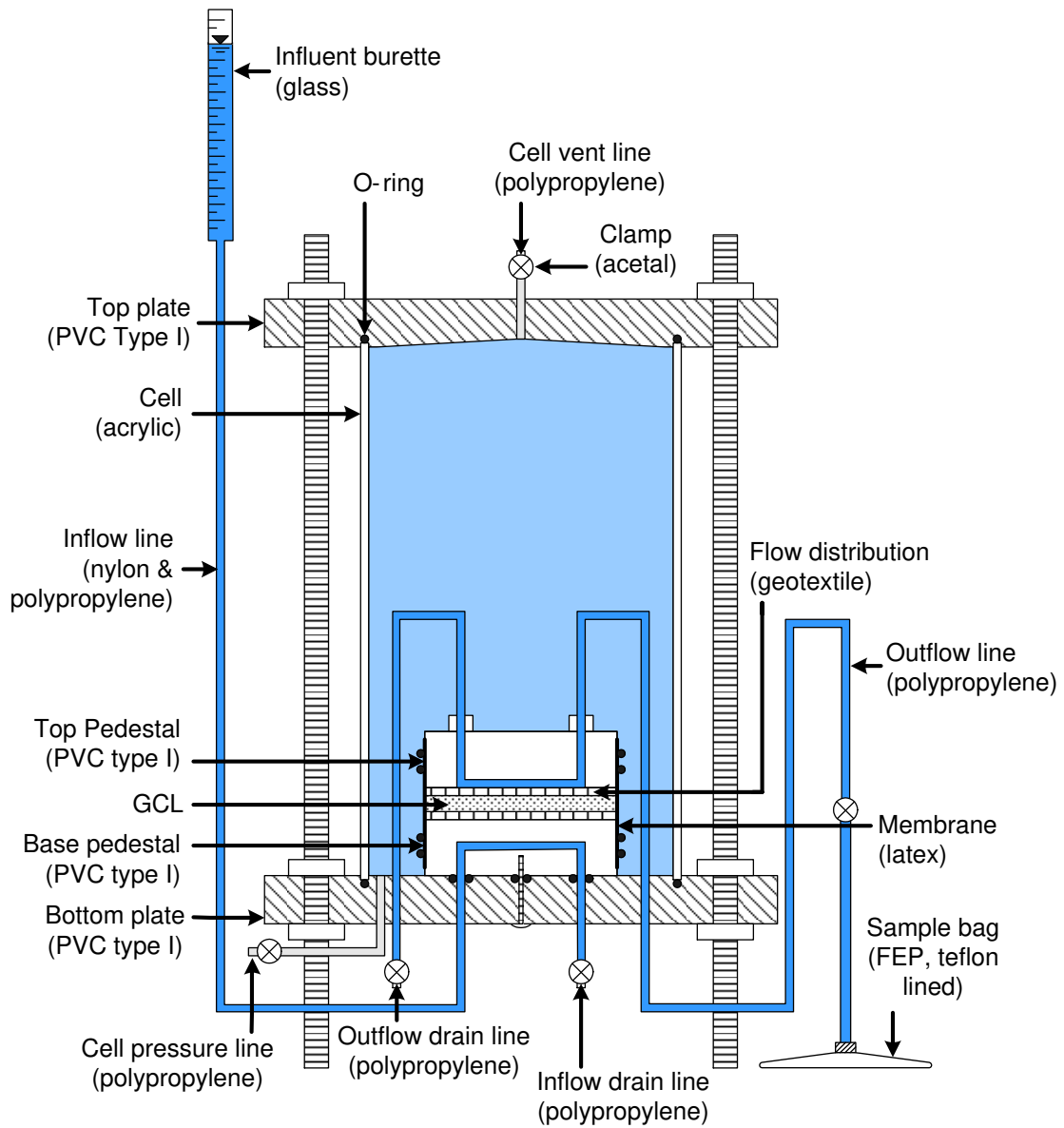


Figure 3.2. Schematic of mine-waste-leachate resistant flexile wall permeameter setup.

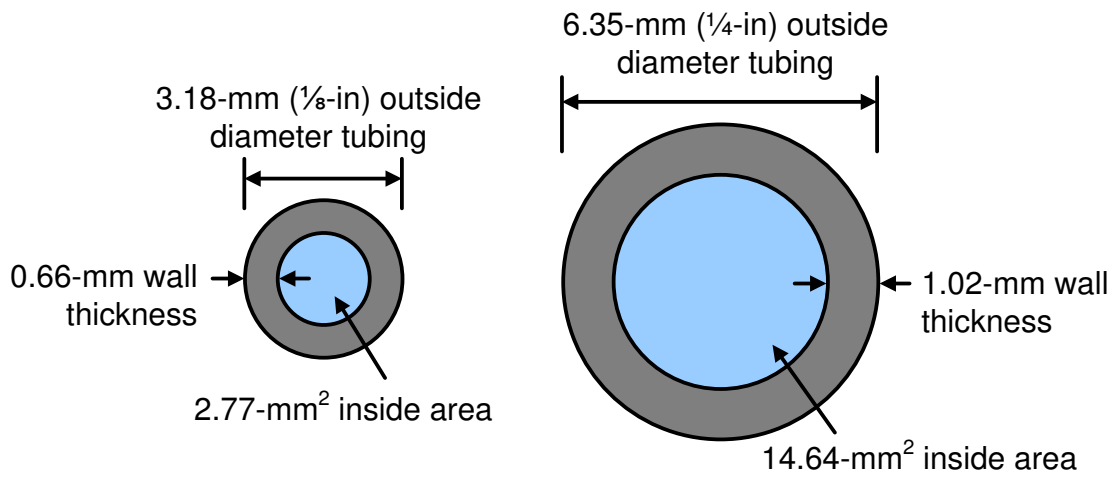


Figure 3.3. Cross-section schematic comparison of 3.18-mm (1/8-in) and 6.35-mm (1/4-in) tubing sizes.

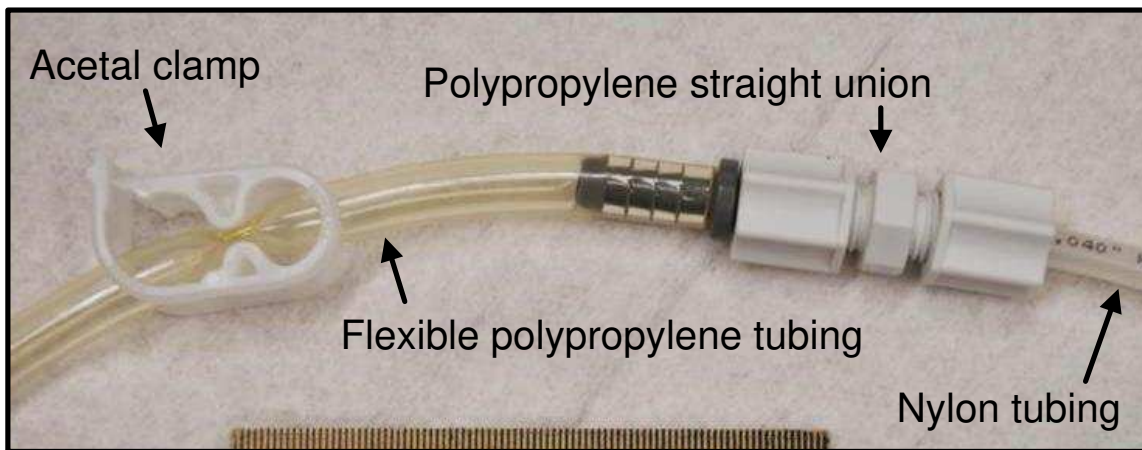


Figure 3.4. Photograph of external acetal tubing clamps used on flexible polypropylene tubing in lieu of metal valves. Scale in mm.



Figure 3.5. Photographs of (a) assembled mine-waste-leachate resistant permeameter assembly using gravity head method and (b) permeameter closeup.

Table 3.3. Testing program and results for empty permeameter flowrates

Permeameter Type	Test Series ^(a)	Flow Distribution	Flowrate (mL/s) ^(b)	Equivalent k (m/s) ^(c)
MW Permeameter ^(d)	1	None	7.6 (SD=0.10, n=3)	2.0×10^{-6}
	2	None	7.5 (SD=0.17, n=3)	2.0×10^{-6}
	3	None	8.7 (SD=0.10, n=3)	2.3×10^{-6}
	Mean		7.9 (SD=0.67, n=3)	2.1×10^{-6}
	4	Fiberglass	7.4 (SD=0.15, n=3)	2.0×10^{-6}
	5	Geotextile	7.0 (SD=0.09, n=3)	1.9×10^{-6}
Standard Permeameter ^(e)	6	Porous Stone	8.5 (SD=0.13, n=3)	2.3×10^{-6}
	7	None	0.92 (SD=0.005, n=3)	5.6×10^{-7}
	8	None	1.1 (SD=0.003, n=3)	6.4×10^{-7}
	9	None	1.1 (SD=0.02, n=3)	6.4×10^{-7}
	Mean		1.0 (SD=0.09, n=3)	6.1×10^{-7}
	10	Fiberglass	0.85 (SD=0.02, n=3)	5.1×10^{-7}

MW permeameter = mine-waste-resistant permeameter.

^(a) For the given flow distribution used, different test series represent separate permeameters

^(b) Determined from measurements made in accordance with the procedures of the gravity method

^(c) Determined using Equation 2.5 from measurements made in accordance with the procedures of the gravity method assuming a 7.0-mm thick (typical) GCL

^(d) 6-in diameter

^(e) 4-in diameter

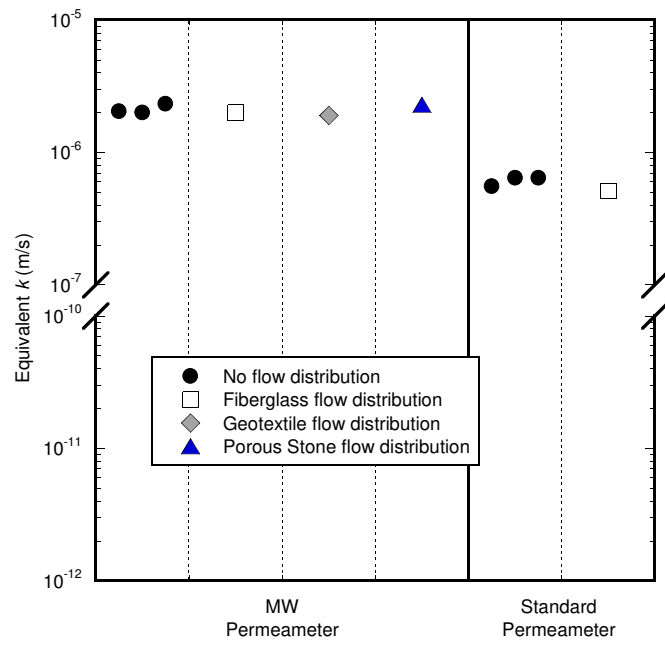


Figure 3.6. Equivalent k (m/s) through empty permeameters. MW permeameter = mine-waste-resistant permeameter.

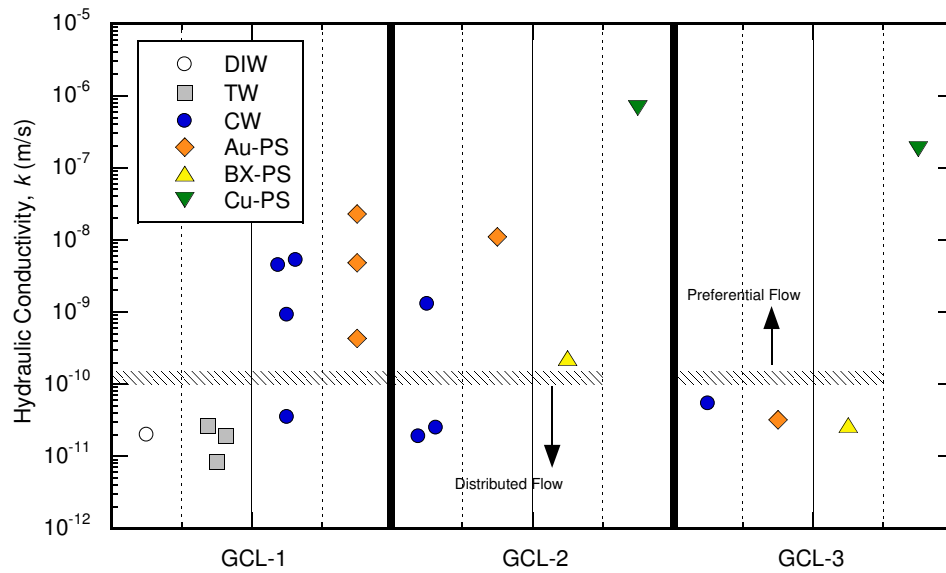


Figure 3.7. Determined hydraulic conductivity, k , for GCL-1, GCL-2, and GCL-3, permeated with deionized water (DW), tap water (TW), conservative water (CW), synthetic gold mining process solution (Au-PS), synthetic bauxite mining process solution (BX-PS), and synthetic copper mining process solution Cu-PS.

Table 3.4. Results of hydraulic conductivity tests

Test Series	Test	Material	Permeant	Final Degree of Saturation	Elapsed Time (days)		Pore Volumes of Flow, PVF		Hydraulic Conductivity, <i>k</i> (m/s)	
					Hydraulic ^(b)	Chemical ^(c)	Hydraulic ^(b)	Chemical ^(c)	Hydraulic ^(b)	Chemical ^(c)
2	2a	GCL-1	CW	91	0.18	nr	4.2	nr	4.5×10 ⁻⁹	nr
	2b	GCL-1	CW	87	0.13	nr	2.6	nr	5.3×10 ⁻⁹	nr
	2c	GCL-1	CW	104	2.9	nr	6.0	nr	9.2×10 ⁻¹⁰	nr
	2d ^(d)	GCL-1	CW	tbd	39	182	tbd	tbd	1.8×10 ⁻¹¹	3.5×10 ⁻¹¹
4	4a	GCL-1	Au-PS	93	1.4	nr	10.7	nr	4.8×10 ⁻⁹	nr
	4b	GCL-1	Au-PS	83	0.040	nr	4.2	nr	2.3×10 ⁻⁸	nr
	4c	GCL-1	Au-PS	98	1.6	nr	2.4	nr	4.3×10 ⁻¹⁰	nr
21	21a	GCL-1	DW	91	27	nr	1.5	nr	2.0×10 ⁻¹¹	nr
22	22a	GCL-1	TW	97	42	nr	10.8	nr	2.6×10 ⁻¹¹	nr
	22b	GCL-1	TW	108	38	nr	15.7	nr	1.9×10 ⁻¹¹	nr
	22c	GCL-1	TW	104	41	nr	5.7	nr	8.3×10 ⁻¹²	nr
17	17a ^(d)	GCL-3	CW	tbd	38	158	tbd	tbd	2.3×10 ⁻¹¹	5.4×10 ⁻¹¹
23	23a	GCL-3	Au-PS	95	41	nr	5.3	9.9	2.5×10 ⁻¹¹	3.2×10 ⁻¹¹
24	24a	GCL-3	BX-PS	103	45	132	5.3	10.7	5.0×10 ⁻¹¹	2.7×10 ⁻¹¹
25	25a	GCL-3	Cu-PS	72	0.0061	0.015	3.4	11.2	1.8×10 ⁻⁷	1.8×10 ⁻⁷
11	11a ^(d)	GCL-2	CW	tbd	0.22	17	tbd	tbd	8.7×10 ⁻⁹	1.9×10 ⁻¹¹
	11b	GCL-2	CW	104	18	nr	3.9	nr	2.5×10 ⁻¹¹	nr
	11c	GCL-2	CW	97	0.79	nr	2.9	nr	1.3×10 ⁻⁹	nr
26	26a	GCL-2	Au-PS	89	0.25	0.37	3.1	6.1	6.9×10 ⁻⁹	1.1×10 ⁻⁸
27	27a	GCL-2	BX-PS	90	0.13	7.0	2.5	8.5	7.6×10 ⁻⁹	2.3×10 ⁻¹⁰
28	28a	GCL-2	Cu-PS	87	0.0007	0.0057	2.1	14.9	6.4×10 ⁻⁷	6.7×10 ⁻⁷
30 ^(a)	30a ^(d)	GCL-1	CW	tbd	1.5	8.5	tbd	tbd	1.1×10 ⁻⁹	6.8×10 ⁻⁹

All test permeated using the gravity method

^(a) Higher effective stress test. 93.2 kPa versus 27.6 kPa.

^(b) Values when meeting hydraulic termination criteria

^(c) Values when meeting chemical termination criteria

^(d) Ongoing tests. Values in in the "chemical" column are current values.

DW = Deionized water

TW = Tap water

CW = Synthetic conservative water

Au-PS = Synthetic gold mining process solution

BX-PS = Synthetic bauxite mining process solution

Cu-PS = Synthetic copper mining process solution

tbd = To be determined

nr = Not reported

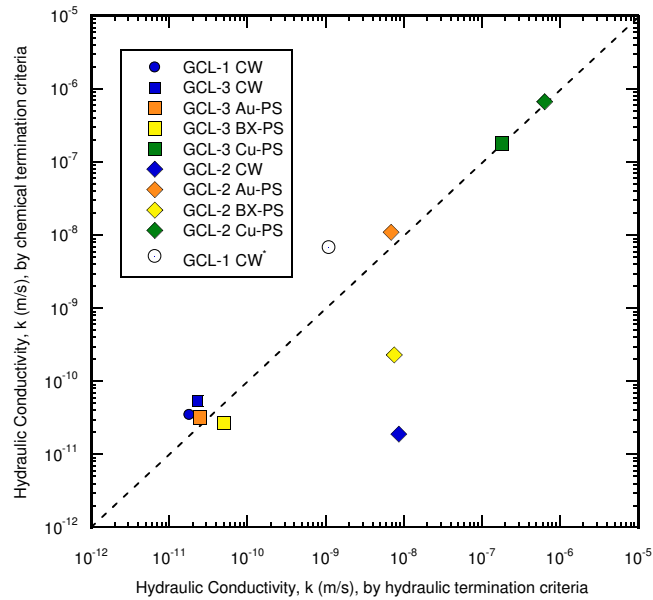


Figure 3.8. Hydraulic conductivity, k , by chemical termination criteria (hydraulic and chemical equilibrium), versus k by hydraulic termination criteria (hydraulic equilibrium) for GCL-1, GCL-2, and GCL-3 permeated with conservative water (CW), synthetic gold mining process solution (Au-PS), synthetic bauxite mining process solution (BX-PS), and synthetic copper mining process solution (Cu-PS).

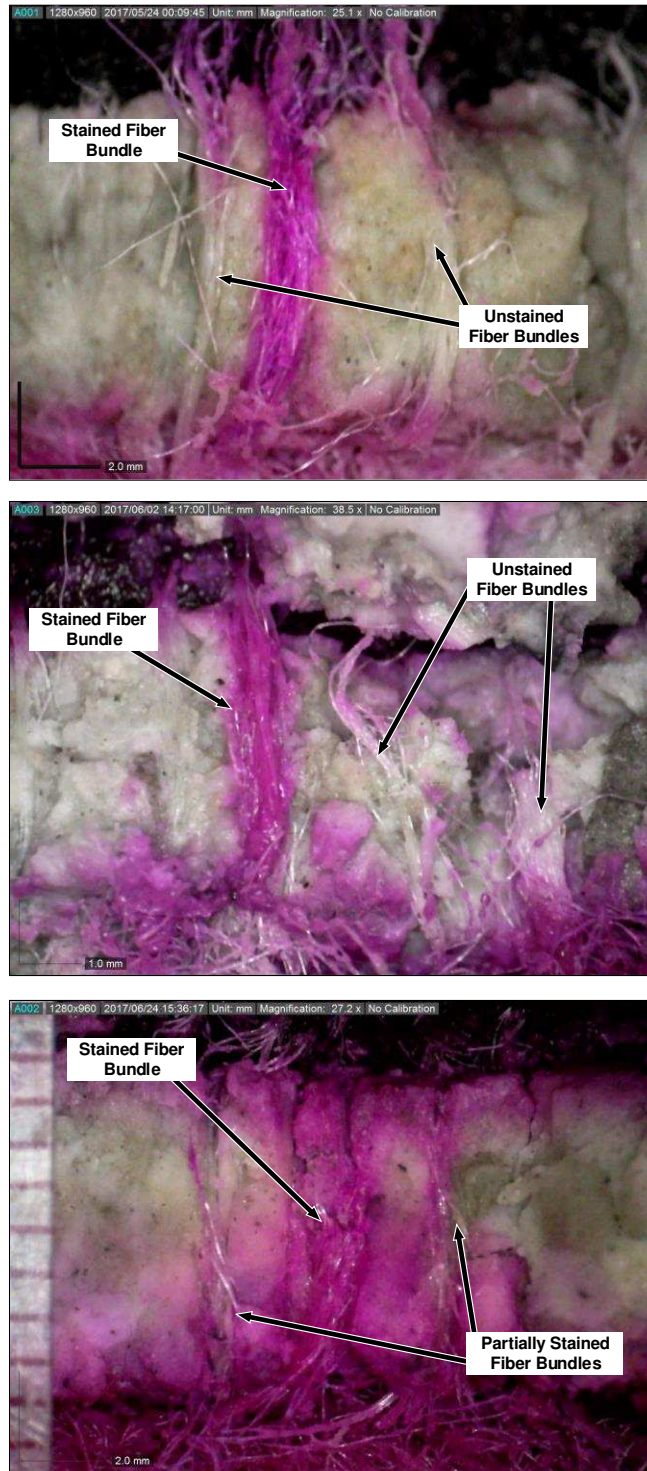


Figure 3.9. (a) Dyed specimen permeated with conservative water.(b) Dyed specimen permeated with synthetic gold mining process solution. (c) Dyed specimen permeated with synthetic bauxite mining process solution.



Figure 3.10. (a) Bentonite removed from GCL-2 permeated with synthetic copper mining process solution (Cu-PS). (b) GCL-2 cross-section permeated with Cu-PS.

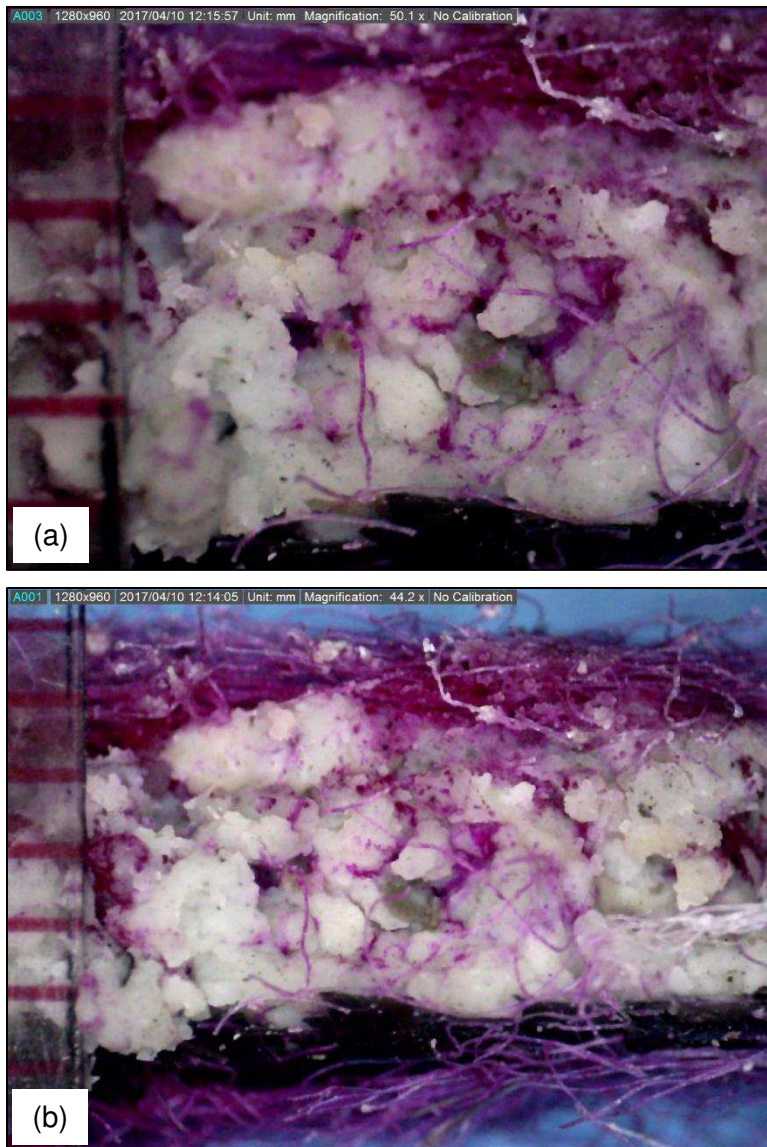


Figure 3.11. (a), (b) Dyed cross-section of GCL-2 permeated with synthetic copper mining process solution.

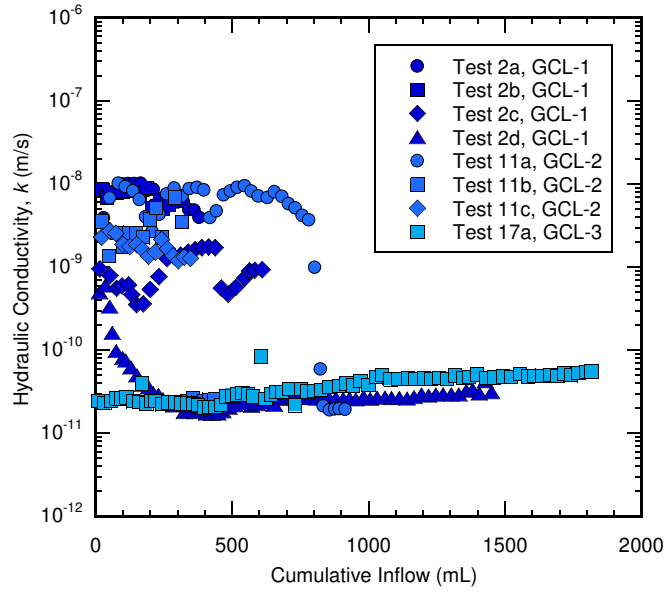


Figure 3.12. Hydraulic conductivity, k , versus cumulative inflow for specimens permeated with conservative water.

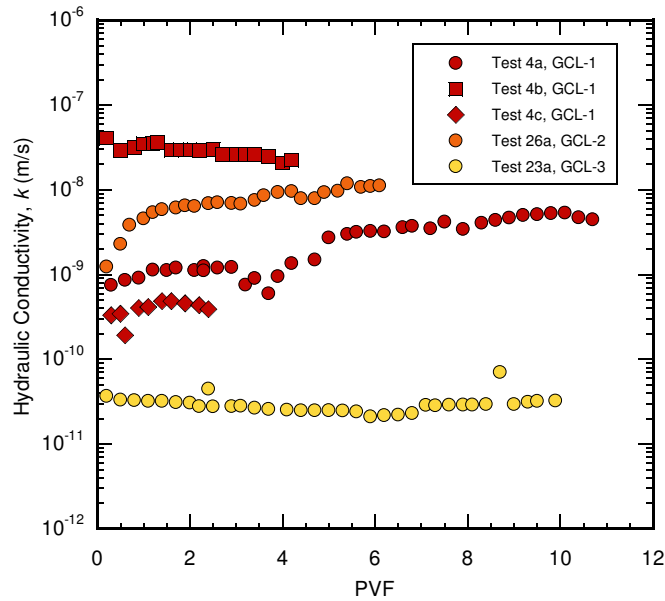


Figure 3.13. Hydraulic conductivity, k , versus pore volumes of flow (PVF) for specimens permeated with synthetic gold mining process solution.

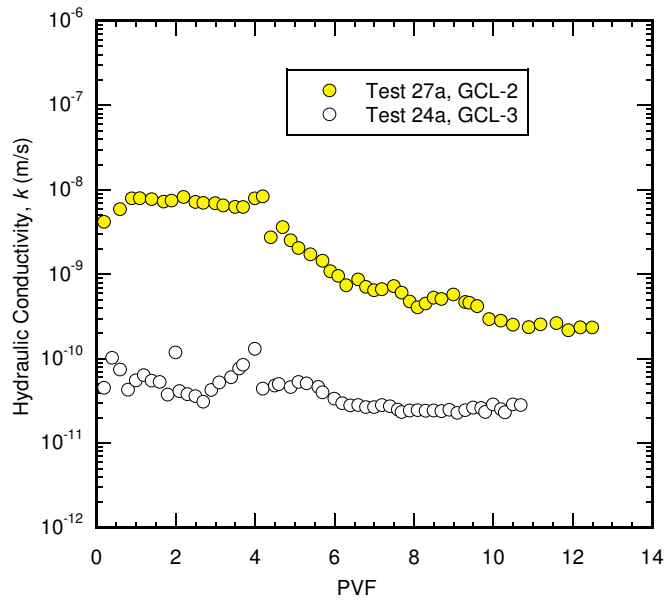


Figure 3.14. Hydraulic conductivity, k , versus pore volumes of flow (PVF) for specimens permeated with synthetic bauxite mining process solution.

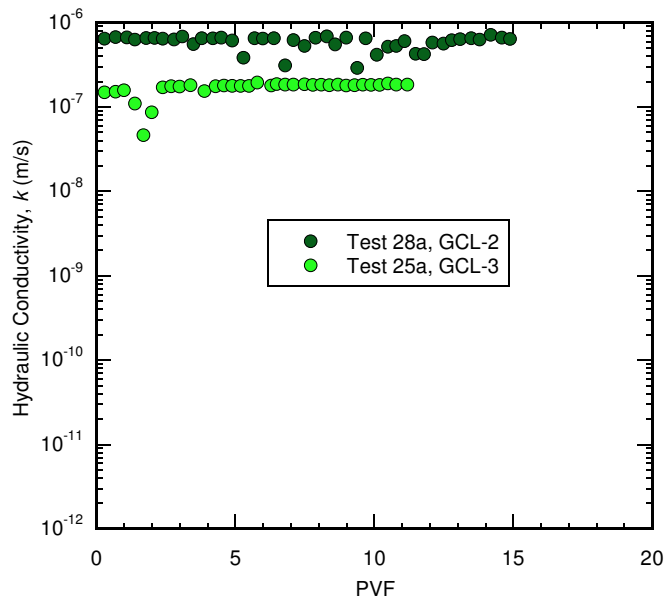


Figure 3.15. Hydraulic conductivity, k , versus pore volumes of flow (PVF) for specimens hydrated with synthetic copper mining process solution.

REFERENCES

- ASTM D1193-06, Reapproved 2011, *Standard Specification for Reagent Water*, ASTM International, West Conshohocken, PA, www.astm.org
- ASTM D2216-10, *Standard Test Methods for Laboratory Determination of Water (Moisture) Content of Soil and Rock Mass*, ASTM International, West Conshohocken, PA, www.astm.org
- ASTM D5084-16a, 2016, *Standard Test Methods for Measurement of Hydraulic Conductivity of Saturated Porous Materials Using a Flexible Wall Permeameter*, ASTM International, West Conshohocken, PA, www.astm.org
- ASTM D6766-12, 2012, *Standard Test Method for Evaluation of Hydraulic Properties of Geosynthetic Clay Liners Permeated with Potentially Incompatible Aqueous Solutions*, ASTM International, West Conshohocken, PA, www.astm.org
- ASTM D5890-11, 2011, *Stand Test Method for Swell Index of Clay Mineral Component of Geosynthetic Clay Liners*, ASTM International, West Conshohocken, PA, www.astm.org
- ASTM D5891/D5891M-02, Reapproved 2016, *Standard Test Method for Fluid Loss of Clay Component of Geosynthetic Clay Liners*, ASTM International, West Conshohocken, PA, www.astm.org
- ASTM D4318-10, 2010, *Standard Test Methods for Liquid Limit, Plastic Limit, and Plasticity Index of Soils*, ASTM International, West Conshohocken, PA, www.astm.org
- ASTM D4767-11, 2011, *Standard Test Methods for Consolidated Undrained Triaxial Compression Test for Cohesive Soils*, ASTM International, West Conshohocken, PA, www.astm.org
- Benson, C. and Meer, S. 2009. Relative abundance of monovalent and divalent cations and the impact of desiccation on geosynthetic clay liners. *J. Geotech. Geoenviron. Eng.*, 133(5), 814-827.

- Benson, C. and Meer, S. 2009. Relative abundance of monovalent and divalent cations and the impact of desiccation on geosynthetic clay liners. *J. Geotech. Geoenviron. Eng.*, 133(5), 814-827.
- Benson, C., Oren, A., and Gates, W. 2010. Hydraulic conductivity of two geosynthetic clay liners permeated with a hyperalkaline solution. *Geotext. and Geomembranes*, 28, 2016-218.
- Bergaya, F., Lagaly, G. 2013. *Handbook of Clay Science*, Volume 5, 2nd Edition. Elsevier Ltd., Amsterdam, The Netherlands.
- Bohnhoff, G., Shackelford, C. 2014 Hydraulic Conductivity of Polymerized Bentonite-Amended Backfills. *J. Geotech. Geoenviron. Eng.*, 140
- Bouazza, A. 2010. Geosynthetics lining in mining applications. Proceedings of Sixth International Conference on Environmental Geotechnics, International Society for Soil Mechanics and Geotechnical Engineers, New Delhi, India, Nov. 8-12, 2010, 221-259.
- Bradshaw, S. and Benson, C. 2014. Effect of municipal solid waste leachate on hydraulic conductivity and exchange complex of geosynthetic clay liners. *J. Geotech. and Geoenviron Eng.*, 140(4), 04013038.
- Chapuis, R.P., *Compacted Clay: Difficulties Obtaining Good Laboratory Permeability Tests. Geotechnical Testing Journal.*
- Di Emidio, G., Van Impe, W., Mazzieri, F. 2010. A polymer enhanced clay for impermeable geosynthetic clay liners. Proceedings of Sixth International Conference on Environmental Geotechnics, International Society for Soil Mechanics and Geotechnical Engineers, New Delhi, India, 963-967.
- Gates, W. and Bouazza, A. 2010. Bentonite transformations in strongly alkaline solutions. *Geotext. Geomembranes*, 28(2), 219-225.
- Ghazi Zadeh, S., Bareither, C.A., Scalia, J., Shackelford, C.D. (2017). Synthetic Solutions for Evaluating GCLs in Mining Applications, *Journal Geotechnical and Geoenvironmental Engineering, In Review.*

- Guyonnet, D., Cazaux, D., Vigier-Gailhanou, H., and Chevrier, B. 2009. Effect of cation exchange on hydraulic conductivity in a sand-bentonite-polymer-mixture. Proceedings, Sardinia 2009, 12th International Waste Management and Landfill Symposium, Environmental Sanitary Engineering Centre (CISA), Cagliari, Italy.
- Guyonnet, D. Gaucher, E. Gaboriau, H. Pons, C. Clinard, C. Norotte, V. and Didier, G. (2005). Geosynthetic clay liner interaction with leachate: correlation between permeability, microstructure, and surface chemistry. *Journal of Geotechnical and Geoenvironmental Engineering*. 131(6): 740-749.
- Jo, H. Katsumi, T. Benson, C. and Edil, T. (2001). Hydraulic conductivity and swelling of nonprehydrated GCLs permeated with single-species salt solutions. *Journal of Geotechnical and Geoenvironmental Engineering*, 127(7): 557-567.
- Jo, H., Benson, C. and Edil, T. 2004. Hydraulic conductivity and cation exchange in nonprehydrated and prehydrated bentonite permeated with weak inorganic salt solutions. *Clay. Clay Miner.*, 52(6), 661-679.
- Jo, H., Benson, C., Shackelford, C., Lee, J., and Edil, T. 2005. Long-term hydraulic conductivity of a geosynthetic clay liner permeated with inorganic salt solutions. *J. Geotech. Geoenviron. Eng.*, 131(4), 405-417.
- Jozefaciuk, G., and Matyka-Sarzynska, D. 2006. Effect of acid treatment and alkali treatment on nanopore properties of selected minerals. *Clay. Clay Miner.*, 54(2), 220–229.
- Katsumi, T., Ishimori, Ho, Onikata, M., and Fukagawa, R. 2008. Long-term barrier performance of modified bentonite materials against sodium and calcium permeant solutions. *Geotext. and Geomembr.*, 26(1), 14-30.
- Kolstad, D., Benson, C., and Edil, T., 2004, "Hydraulic Conductivity and Swell of Nonprehydrated Geosynthetic Clay Liners Permeated with Multispecies Inorganic Solutions," *Journal of Geotechnical and Geoenvironmental Engineering*, Vol. 130, No. 12, pp. 1236-1249.

- Lake, C., Rowe, R., 2000. Swelling characteristics of needlepunched, thermally treated geosynthetic clay liners. *Geotextiles and Geomembranes*. 18, 77-101.
- Lee, J. and Shackelford, C. 2005b. Impact of bentonite quality on hydraulic conductivity of geosynthetic clay liners. *J. Geotech. Geoenviron. Eng.*, 131(1), 64-77.
- Lee, J. Shackelford, C. 2005a. Concentration dependency of the prehydration effect for a geosynthetic clay liner, *Soils and Foundations (Japanese Geotechnical Society)*, 45(4): 27-41.
- Lu, N. and Likos, W. 2004. *Unsaturated Soil Mechanics*. John Wiley and Son, Inc. Hoboken, NJ.
- McBride M. 1994. *Environmental Chemistry of Soils*. Oxford University Press, New York.
- Meer, S. and Benson, C. 2007. Hydraulic conductivity of geosynthetic clay liners exhumed from landfill final covers. *J. of Geotech. and Geoenviron. Engr.*, 133(5), 550-563.
- Mesri, G. and Olson, R. 1971. Mechanisms controlling the permeability of clays. *Clay. Clay Miner.*, 19, 151-158.
- Mitchell, J. and Soga K. 2005. *Fundamentals of Soil Behavior*, 3rd Ed., John Wiley and Sons, Inc., New York, 437.
- Norrish, K., and Quirk, J. 1954. Crystalline swelling of montmorillonite, use of electrolytes to control swelling. *Nature*, 173, 255-257
- Petrov, R., and Rowe, R. 1997. Geosynthetic clay liner GCL chemical compatibility by hydraulic conductivity testing and factors impacting its performance. *Can. Geotech. J.*, 34(6), 863–885.
- Rowe, R., Brachman, R., Hosney, M., Take, W., Arnepalli, D., 2016, "Insight into hydraulic conductivity testing of GCLs exhumed after 5 and 7 years in a cover," *Canadian Geotechnical Journal*.
- Scalia, J., and Benson, C. (2010a). "Effect of permeant water on the hydraulic conductivity of exhumed geosynthetic clay liners." *Geotech. Testing J.*, 33(1), 1-11.

- Scalia, J., and Benson, C. (2010b). "Preferential flow in geosynthetic clay liners exhumed from final covers with composite barriers." *Can. Geotech. J.*, 47 1101-1111.
- Scalia, J., and Benson, C. H. 2011. Hydraulic conductivity of geosynthetic clay liners exhumed from landfill final covers with composite barriers. *J. Geotech. Geoenviron. Eng.*, 137(1), 1-13.
- Scalia, J., Benson, C., Bohnhoff, G., Edil, T., and Shackelford, C. 2014. Long-term hydraulic conductivity of a bentonite-polymer composite permeated with aggressive inorganic solutions. *J. Geotech. and Geoenviron. Eng.*, 04013025-1-13.
- Shackelford, C., Benson, C., Katsumi, T., Edil, T., and Lin, L. 2000. Evaluating the hydraulic conductivity of GCLs permeated with non-standard liquids. *Geotextiles. and Geomembranes*, 18(2-3), 133-161.
- Shackelford, C., Sevick, G., Eykholt G. 2010. Hydraulic conductivity of geosynthetic clay liners to tailings impoundment solutions. *Geotextiles and Geomembranes*. 28, 149-162.
- Sposito, G. 1984. *The Surface Chemistry of Soils*. Oxford University Press, New York.
- Tian, K., Benson, C., and Likos, W. 2016. Hydraulic conductivity of geosynthetic clay liners to low-level radioactive waste leachate. *J. Geotech. and Geoenviron. Eng.*, 142(8), 04016037
- Trauger R. and Darlington J. 2000. Next-generation geosynthetic clay liners for improved durability and performance. TR-220, Colloid Environmental Technologies Company, Arlington Heights, IL, 2-14.

APPENDIX A

Hydrating and permeating liquid chemistries

Table A.1. Synthetic conservative water target ion concentrations

Chemical Parameter	Target concentration (g/L)
Ca ²⁺	0.077
Cl ⁻	0.15
Na ⁺	0.0061

Table A.2. Synthetic gold mining process solution target ion concentrations

Chemical Parameter	Target concentration (g/L)
Ca ²⁺	0.15
Cl ⁻	0.45
K ⁺	0.017
Mg ²⁺	0.031
Na ⁺	0.53
NO ₃ ⁻	0.012
SO ₄ ²⁻	0.99

Table A.3. Synthetic bauxite mining process solution target ion concentrations

Chemical Parameter	Target concentration (g/L)
Ca ²⁺	0.094
Mg ²⁺	0.012
Na ⁺	1.01
OH ⁻	0.34
SO ₄ ²⁻	1.43

Table A.4. Synthetic copper mining process solution target ion concentrations

Chemical Parameter	Target concentration (g/L)
Al ³⁺	2.036
Ca ²⁺	0.588
Cu ²⁺	1.3
H ⁺	0.378
Mg ²⁺	5.1
Mn ²⁺	1.948
Na ⁺	3.355
K ⁺	0.789
Cl ⁻	17.906
PO ₄ ³⁻	2.298
SO ₄ ²⁻	34.279

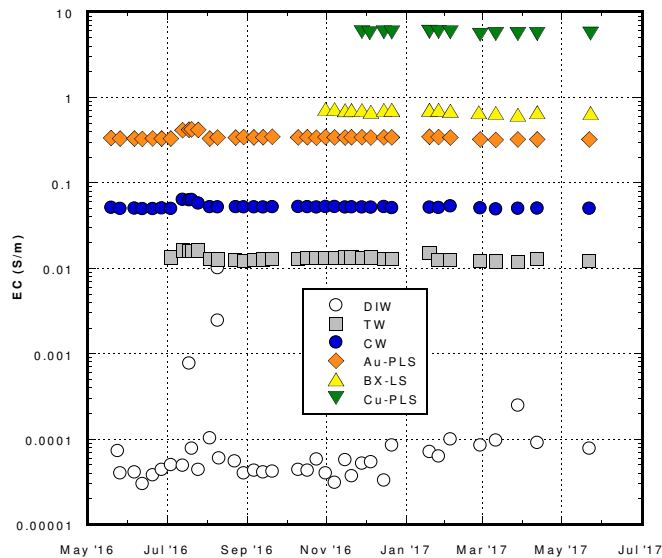


Figure A.1. EC (S/m) data of hydrating and permeating liquids plotted from May 2016 to July 2017. Note: The average EC (S/m) values presented in Table 2.1 and Table 3.1 for the DIW, TW, CW, and Au-PLS exclude measurements taken between July 13, 2017 and July 25, 2017, because the data appears to show a calibration error in the conductivity meter.

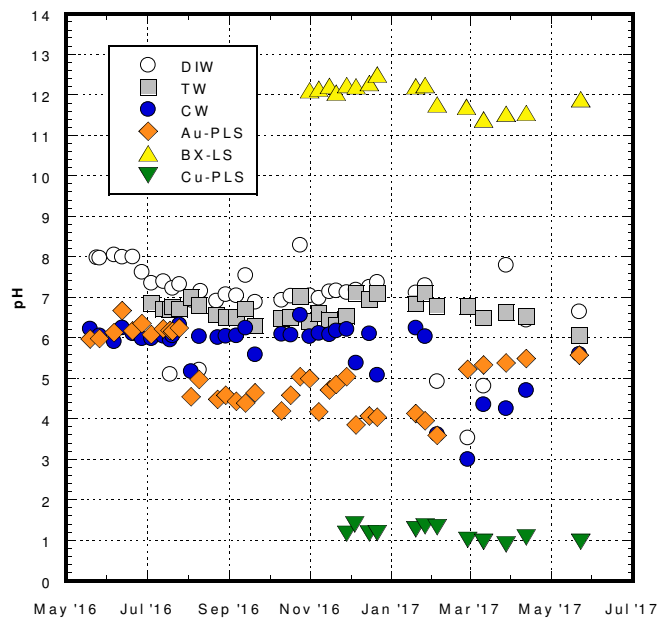


Figure A.2. pH data of hydrating and permeating liquids plotted from May 2016 to July 2017

Table A.5. Deionized water EC and pH data

Date	EC ($\mu\text{S/cm}$)	EC (S/m)	pH
5/24/2016	0.730	7.30E-05	7.98
5/26/2016	0.400	4.00E-05	7.97
6/6/2016	0.410	4.10E-05	8.05
6/12/2016	0.300	3.00E-05	7.99
6/20/2016	0.380	3.80E-05	8.00
6/27/2016	0.440	4.40E-05	7.62
7/4/2016	0.500	5.00E-05	7.35
7/13/2016	0.490	4.90E-05	7.39
7/18/2016	7.72	7.72E-04	5.10
7/20/2016	0.780	7.80E-05	7.22
7/25/2016	0.440	4.40E-05	7.32
8/3/2016	1.03	1.03E-04	6.93
8/9/2016	101	1.01E-02	5.21
8/9/2016	24.5	2.45E-03	6.90
8/10/2016	0.600	6.00E-05	7.15
8/22/2016	0.550	5.50E-05	6.91
8/29/2016	0.400	4.00E-05	7.07
9/6/2016	0.430	4.30E-05	7.04
9/13/2016	0.410	4.10E-05	7.54
9/20/2016	0.420	4.20E-05	6.88
10/10/2016	0.440	4.40E-05	6.93
10/17/2016	0.430	4.30E-05	7.03
10/24/2016	0.580	5.80E-05	8.29
10/31/2016	0.400	4.00E-05	7.04
11/7/2016	0.310	3.10E-05	6.98
11/15/2016	0.570	5.70E-05	7.14
11/20/2016	0.370	3.70E-05	7.16
11/28/2016	0.520	5.20E-05	7.12
12/5/2016	0.540	5.40E-05	7.18
12/15/2016	0.330	3.30E-05	7.25
12/21/2016	0.850	8.50E-05	7.37
1/19/2017	0.710	7.10E-05	7.11
1/26/2017	0.630	6.30E-05	7.29
2/4/2017	1.00	1.00E-04	4.92
2/27/2017	0.850	8.50E-05	3.53
3/11/2017	0.970	9.70E-05	4.81
3/28/2017	2.48	2.48E-04	7.79
4/12/2017	0.910	9.10E-05	6.44
5/22/2017	0.78	7.80E-05	6.64

Table A.6. Tap water EC and pH data

Date	EC ($\mu\text{S/cm}$)	EC (S/m)	pH
7/4/2016	134	1.34E-02	6.85
7/13/2016	162	1.62E-02	6.71
7/18/2016	160	1.60E-02	6.69
7/20/2016	158	1.58E-02	6.76
7/25/2016	162	1.62E-02	6.71
8/3/2016	128	1.28E-02	6.99
8/9/2016	127	1.27E-02	6.80
8/22/2016	125	1.25E-02	6.56
8/29/2016	122	1.22E-02	6.50
9/6/2016	126	1.26E-02	6.50
9/13/2016	127	1.27E-02	6.71
9/20/2016	130	1.30E-02	6.29
10/10/2016	128	1.28E-02	6.47
10/17/2016	131	1.31E-02	6.50
10/24/2016	131	1.31E-02	7.02
10/31/2016	131	1.31E-02	6.40
11/7/2016	132	1.32E-02	6.60
11/15/2016	134	1.34E-02	6.44
11/20/2016	134	1.34E-02	6.31
11/28/2016	133	1.33E-02	6.54
12/5/2016	134	1.34E-02	7.10
12/15/2016	129	1.29E-02	6.94
12/21/2016	129	1.29E-02	7.09
1/19/2017	153	1.53E-02	6.84
1/26/2017	125	1.25E-02	7.10
2/4/2017	125	1.25E-02	6.78
2/27/2017	122	1.22E-02	6.77
3/11/2017	120	1.20E-02	6.49
3/28/2017	119	1.19E-02	6.63
4/12/2017	128	1.28E-02	6.53
5/22/2017	123	1.23E-02	6.05

Table A.7. CW EC and pH data

Date	EC ($\mu\text{S/cm}$)	EC (S/m)	pH
5/19/2016	514	5.14E-02	6.22
5/26/2016	500	5.00E-02	6.05
6/6/2016	503	5.03E-02	5.91
6/12/2016	497	4.97E-02	6.25
6/20/2016	497	4.97E-02	6.10
6/27/2016	506	5.06E-02	5.98
7/4/2016	499	4.99E-02	5.98
7/13/2016	637	6.37E-02	6.04
7/18/2016	630	6.30E-02	5.95
7/20/2016	636	6.36E-02	6.05
7/25/2016	579	5.79E-02	6.32
8/3/2016	523	5.23E-02	5.17
8/9/2016	521	5.21E-02	6.03
8/23/2016	524	5.24E-02	6.01
8/29/2016	522	5.22E-02	6.04
9/6/2016	522	5.22E-02	6.05
9/13/2016	519	5.19E-02	6.24
9/20/2016	523	5.23E-02	5.58
10/10/2016	527	5.27E-02	6.09
10/17/2016	523	5.23E-02	6.07
10/24/2016	518	5.18E-02	6.56
10/31/2016	525	5.25E-02	6.03
11/7/2016	528	5.28E-02	6.11
11/15/2016	518	5.18E-02	6.08
11/20/2016	521	5.21E-02	6.17
11/28/2016	519	5.19E-02	6.21
12/5/2016	516	5.16E-02	5.38
12/15/2016	525	5.25E-02	6.10
12/21/2016	510	5.10E-02	5.08
1/19/2017	516	5.16E-02	6.24
1/26/2017	513	5.13E-02	6.03
2/4/2017	535	5.35E-02	3.61
2/27/2017	508	5.08E-02	3.00
3/11/2017	495	4.95E-02	4.35
3/28/2017	502	5.02E-02	4.25
4/12/2017	504	5.04E-02	4.70
5/22/2017	501	5.01E-02	5.59

Table A.8. Au-PLS EC and pH data

Date	EC (mS/cm)	EC (S/m)	pH
5/19/2016	3.35	0.335	5.97
5/26/2016	3.31	0.331	5.98
6/6/2016	3.31	0.331	6.13
6/12/2016	3.27	0.327	6.67
6/20/2016	3.32	0.332	6.17
6/27/2016	3.31	0.331	6.35
7/4/2016	3.31	0.331	6.08
7/13/2016	4.15	0.415	6.22
7/18/2016	4.19	0.419	6.18
7/20/2016	4.23	0.423	6.16
7/25/2016	4.18	0.418	6.24
8/3/2016	3.31	0.331	4.54
8/9/2016	3.40	0.340	4.97
8/23/2016	3.39	0.339	4.48
8/29/2016	3.44	0.344	4.58
9/6/2016	3.42	0.342	4.43
9/13/2016	3.43	0.343	4.39
9/20/2016	3.46	0.346	4.64
10/10/2016	3.42	0.342	4.19
10/17/2016	3.43	0.343	4.58
10/24/2016	3.38	0.338	5.04
10/31/2016	3.44	0.344	4.99
11/7/2016	3.41	0.341	4.17
11/15/2016	3.40	0.340	4.71
11/20/2016	3.43	0.343	4.85
11/28/2016	3.43	0.343	5.04
12/5/2016	3.40	0.340	3.85
12/15/2016	3.42	0.342	4.07
12/21/2016	3.41	0.341	4.04
1/19/2017	3.46	0.346	4.13
1/26/2017	3.44	0.344	3.95
2/4/2017	3.40	0.340	3.59
2/27/2017	3.23	0.323	5.22
3/11/2017	3.19	0.319	5.33
3/28/2017	3.22	0.322	5.38
4/12/2017	3.22	0.322	5.49
5/22/2017	3.22	0.322	5.57

Table A.9. BX-LS EC and pH data

Date	EC (mS/cm)	EC (S/m)	pH
10/31/2016	7.34	0.734	12.1
11/7/2016	7.31	0.731	12.2
11/15/2016	7.09	0.709	12.2
11/20/2016	7.13	0.713	12.1
11/28/2016	7.14	0.714	12.2
12/5/2016	6.82	0.682	12.2
12/15/2016	7.17	0.717	12.3
12/21/2016	7.20	0.720	12.5
1/19/2017	7.20	0.720	12.2
1/26/2017	7.20	0.720	12.2
2/4/2017	6.99	0.699	11.8
2/26/2017	6.71	0.671	11.7
3/11/2017	6.60	0.660	11.4
3/28/2017	6.30	0.630	11.5
4/12/2017	6.71	0.671	11.6
5/23/2017	6.58	0.658	11.89

Table A.10. Cu-LS EC and pH data

Date	EC (mS/cm)	EC (S/m)	pH
11/28/2016	58.4	5.84	1.16
12/4/2016	56.6	5.66	1.39
12/15/2016	58.0	5.80	1.17
12/21/2016	57.8	5.78	1.18
1/19/2017	58.7	5.87	1.27
1/26/2017	58.5	5.85	1.34
2/4/2017	57.9	5.79	1.32
2/27/2017	54.4	5.44	1.01
3/11/2017	55.2	5.52	0.96
3/28/2017	55.2	5.52	0.90
4/12/2017	55.6	5.56	1.07
5/23/2017	55.8	5.58	0.96

APPENDIX B

GCL properties

B.1 Methods for determining GCL properties

The mass per area of the bentonite, cover textiles, and carrier textiles were determined by carefully separating the cover and carrier textiles with a scalpel followed by removing and collecting all bentonite from ten, 76.2 mm by 76.2 mm (3 in by 3 in) specimens per GCL. The weights of the separated bentonite, cover textile and carrier textile for each specimen were recorded.

Fiber bundle characterization was conducted on ten, 76.2 mm by 76.2 mm (3 in by 3 in) specimens per GCL. To determine the number of fiber bundles per area the following laboratory procedure was used (note: the procedure used required to individuals, person A and person B, working together):

Testing Procedure

1. Person A obtain specimen #1
2. Person A locate one of the two edges that is in the **machine** direction (each specimen has four edges, two in the machine direction, two in the cross-machine direction)
3. Person A count the number of fiber bundles along the identified edge moving from left to right. Only bundles within 5-mm of the plane edge are counted, viz. the number of fiber bundles in a 76.2 mm (3 in) by 5 mm (3/16 in) area on the given edge of the specimen are counted. This is the most likely source of error in this procedure, as judgement is required in identifying and distinguishing fiber bundles. Using a pen, pencil, or other small tool is advised to assist with counting.
4. Person A record the counted number of bundles noting the corresponding specimen number

5. Person A locate the second edge in the given direction and repeat steps 3 and 4 with this edge.
6. Person A pass specimen #1 to person B.
7. Person B repeat steps 2 through 5 with specimen #1.
8. Repeat steps 1 through 7 with specimens #2 through #10. There are now four recorded measurements for the number of fiber bundles per 76.2 mm (3 in) in the given direction for each specimen
9. Person A obtain specimen #1 again
10. Person A locate one of the two edges that is in the **cross-machine** direction (each specimen has four edges, two in the machine direction, two in the cross-machine direction)
11. Repeat steps 3 through 8.

Analysis

12. For each specimen, average the four recorded measurements in the **machine** direction. Save this value, noting the corresponding specimen number and convert the value from the number of fiber bundles per 76.2 mm (3 in) to the number of fiber bundles per 1 m.
13. For each specimen average the four recorded measurements in the **cross-machine** direction. Save this value noting the corresponding specimen number and convert the value from the number of fiber bundles per 76.2 mm (3 in) to the number of fiber bundles per 1 m.
14. For each specimen multiply the number of fiber bundles per 1 m in the **machine** direction by the number of fiber bundles per 1 m in the **cross-machine** direction to obtain the number of fiber bundles per m².
15. Using the ten values of fiber bundles per m², calculate and report the average number of fiber bundles per area and the standard deviation.

To determine the fiber bundle size and the number of monofilament fibers per fiber bundle the following procedure was used (note: the procedure used required two individuals, person A and person B, working together):

Testing Procedure

1. Locate one of the edges in the **machine** direction on specimen #1
2. Randomly select an intact fiber bundle
3. View the selected fiber bundle under a digital stereoscopic microscope (Dino-Lite Capture 2.0) without disturbing the fiber bundle
4. Using the “Line” tool on the digital imaging software provided with the Dino-Lite Capture 2.0, draw the approximate width of the fiber bundle (refer to Figure 2.4a for an exemplar photograph).
5. Take a photograph
6. Record the distance displayed by the drawn line as the thickness of the fiber bundle
7. Place a thin rigid object underneath the fiber bundle (small allen wrenches were used in this study)
8. Using a second thin rigid object, spread out the monofilament fibers as much as possible without breaking the fibers or pulling the fibers from the carrier textiles. Refer to Figure 2.4b for an exemplar photograph.
9. Optional: use a colored marker to color the fiber and make the individual monofilament fibers easier to differentiate
10. Take a photograph
11. Person A and person B both count the number of monofilament fibers in the fiber bundle, independently

12. Person A and person B compare numbers. If the values differ by $> 5\%$, return to step 10.
If the values differ by $< 5\%$, record the average of the two values to obtain a value for the number of monofilament fiber bundles in the fiber bundle.
13. Locate one of the edges in the **cross-machine** direction on specimen #1
14. Repeat steps 2 through 12
15. Repeat steps 1 through 14 for specimens #2 through #10 for a total of 20 individual fiber bundles analyzed. A complete set of images of the fiber bundles analyzed in this study are provided in Sections B.2-B.4.

Analysis

16. Calculate and report an average and standard deviation for the 20 measurements of fiber bundle size.
17. Calculate and report an average and standard deviation for the 20 measurements of the number of monofilament fiber bundles for fiber bundle.

Lastly, the percent area of the GCL initially occupied by fiber bundles was estimated. The average fiber bundle size was used as the diameter of a representative fiber bundle, i.e. the bundle was assumed to be, on average, circular. The area of the average bundle was then multiplied by the average number of fiber bundles per m^2 to obtain the percent area covered by fiber bundles.

B.2 Determination of needle-punched fiber bundle properties for GCL-1

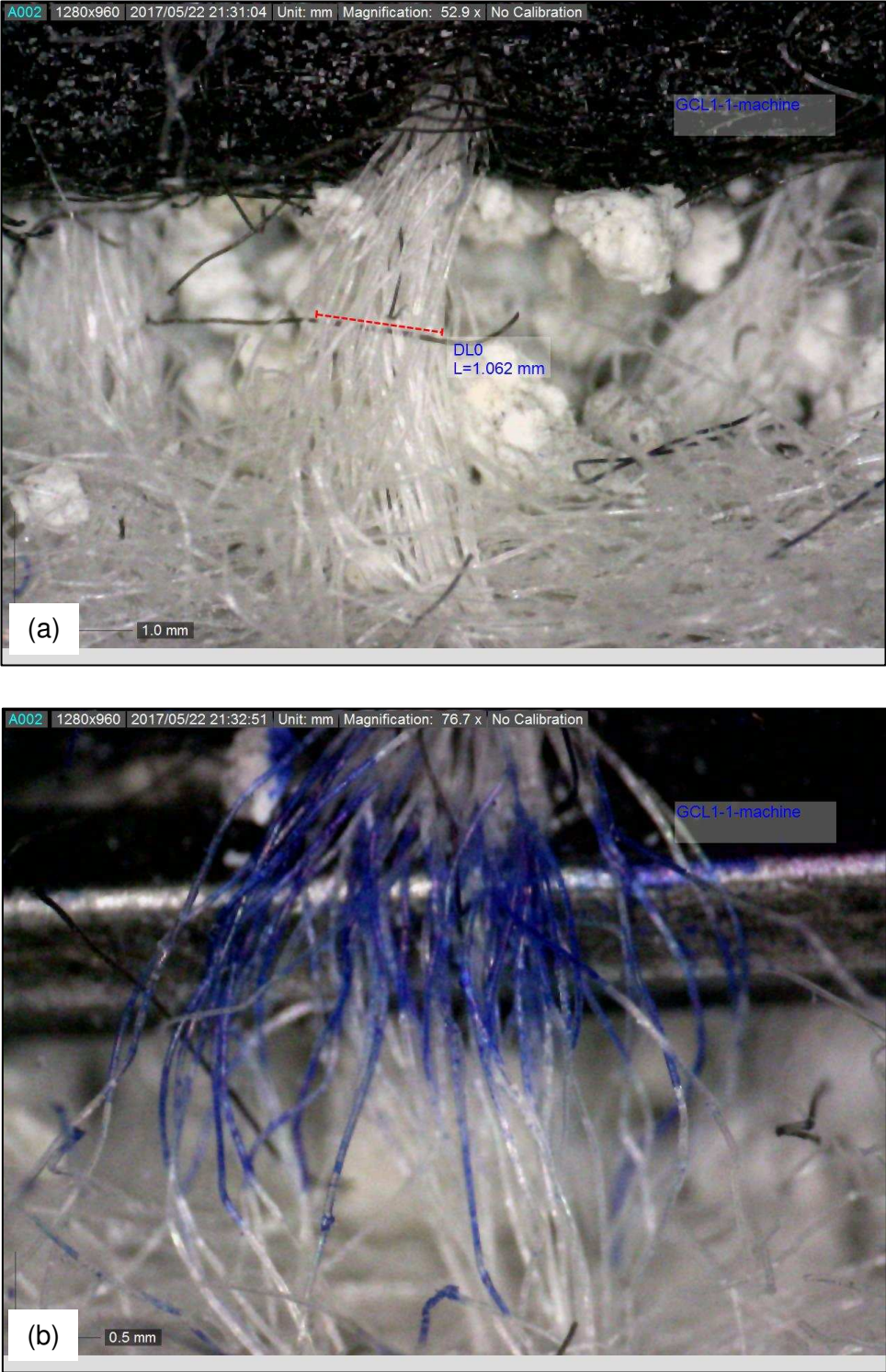


Figure B.1. Fiber bundle sample GCL1-1-MACHINE. (a) Determination of the fiber bundle thickness. (b) Determination of the number of monofilament fibers per fiber bundle.

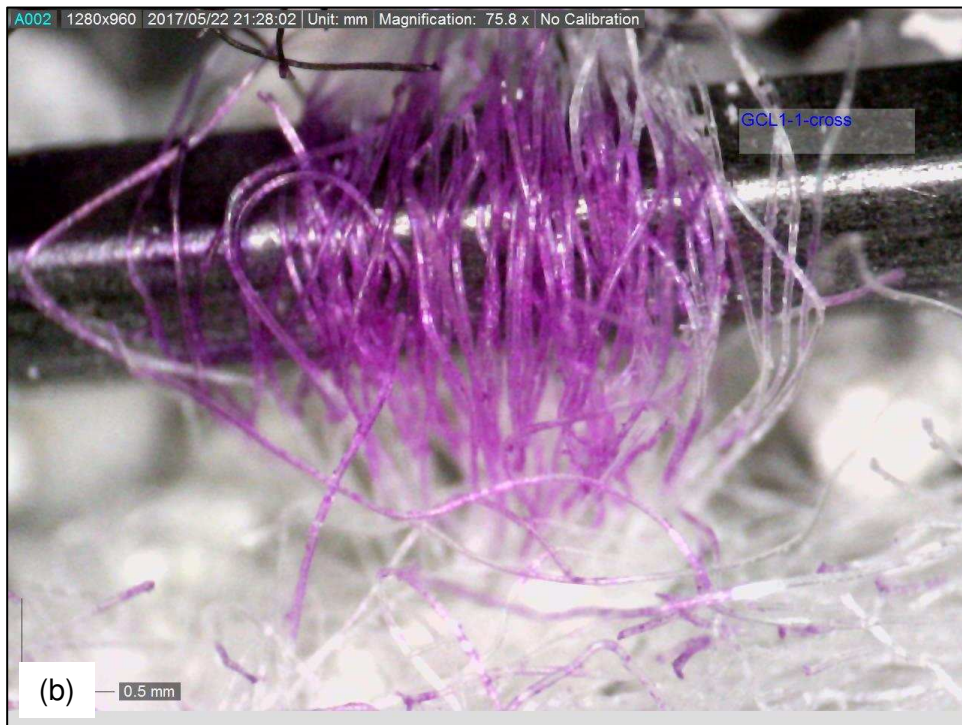
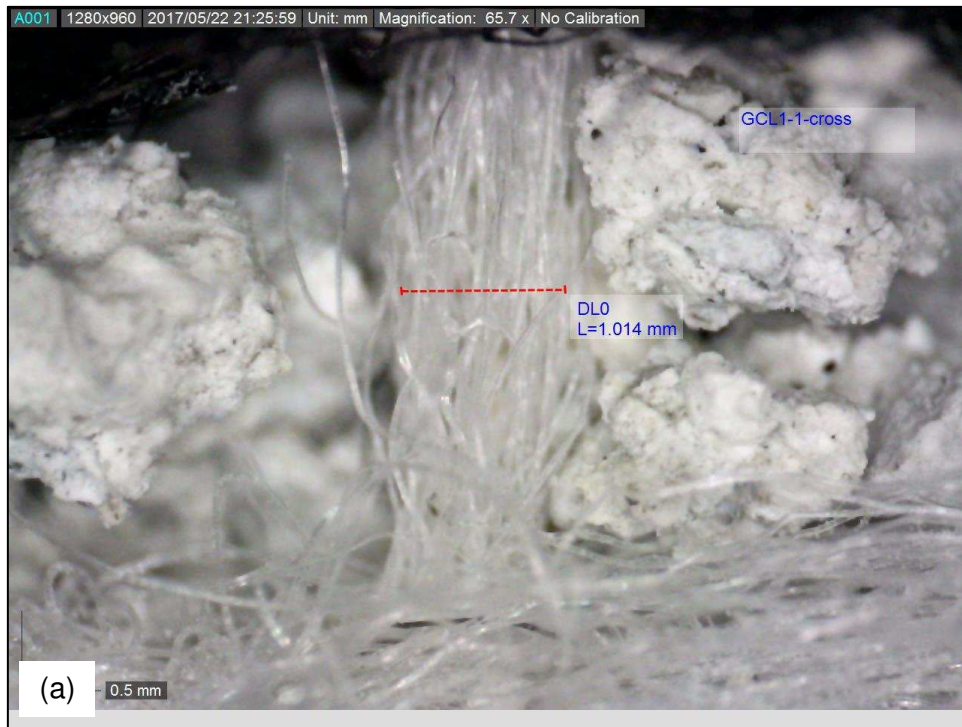


Figure B.2. Fiber bundle sample GCL1-1-CROSS. (a) Determination of the fiber bundle thickness. (b) Determination of the number of monofilament fibers per fiber bundle.

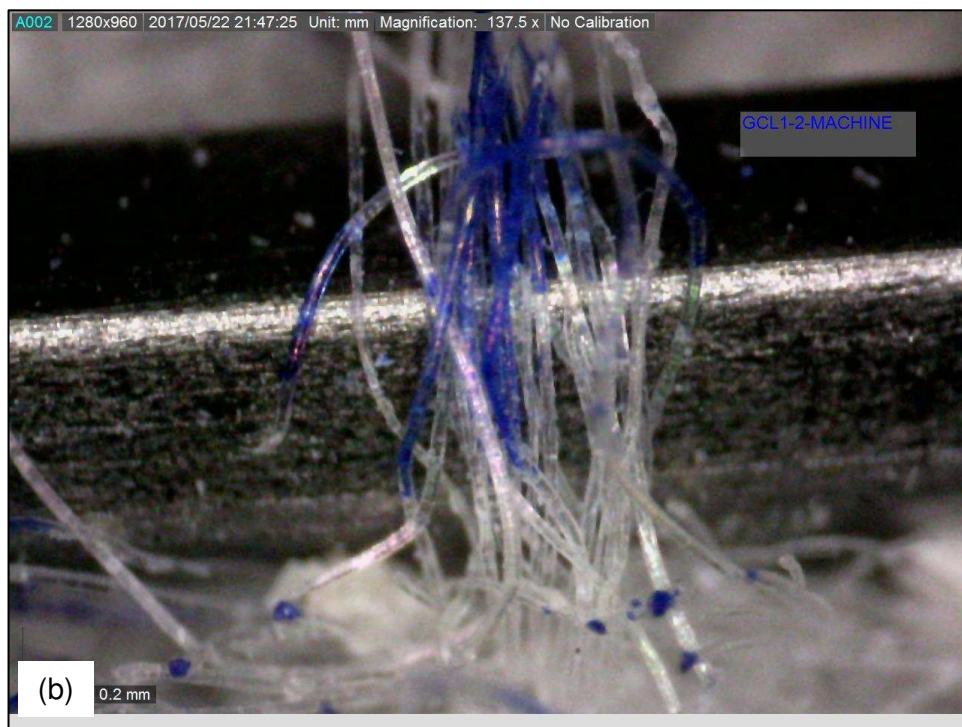


Figure B.3. Fiber bundle sample GCL1-2-MACHINE. (a) Determination of the fiber bundle thickness. (b) Determination of the number of monofilament fibers per fiber bundle.

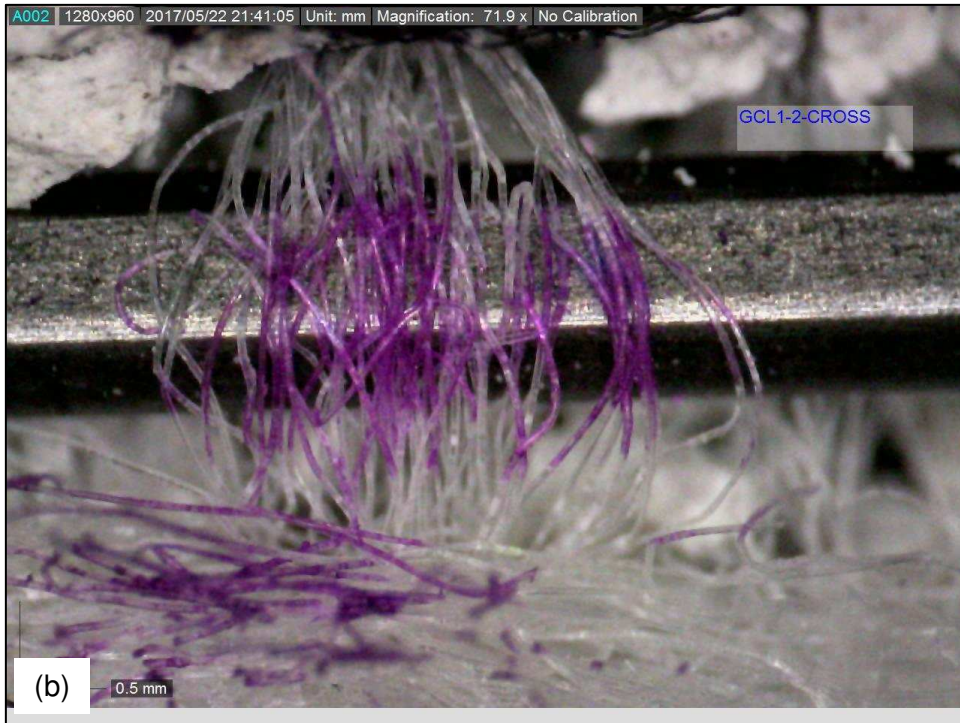
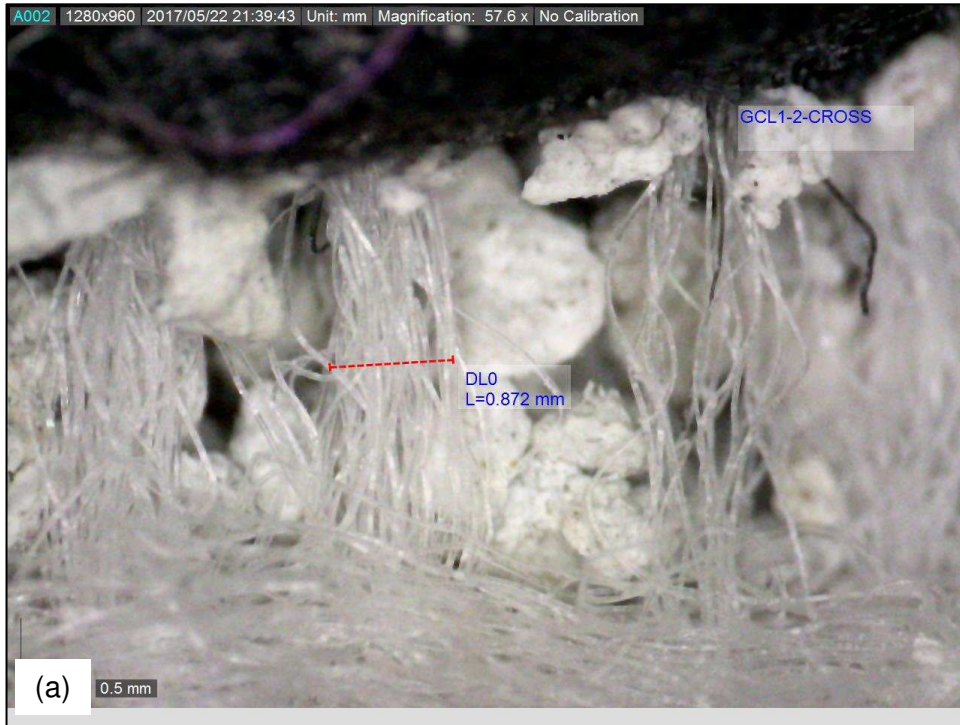


Figure B.4. Fiber bundle sample GCL1-2-CROSS. (a) Determination of the fiber bundle thickness. (b) Determination of the number of monofilament fibers per fiber bundle.

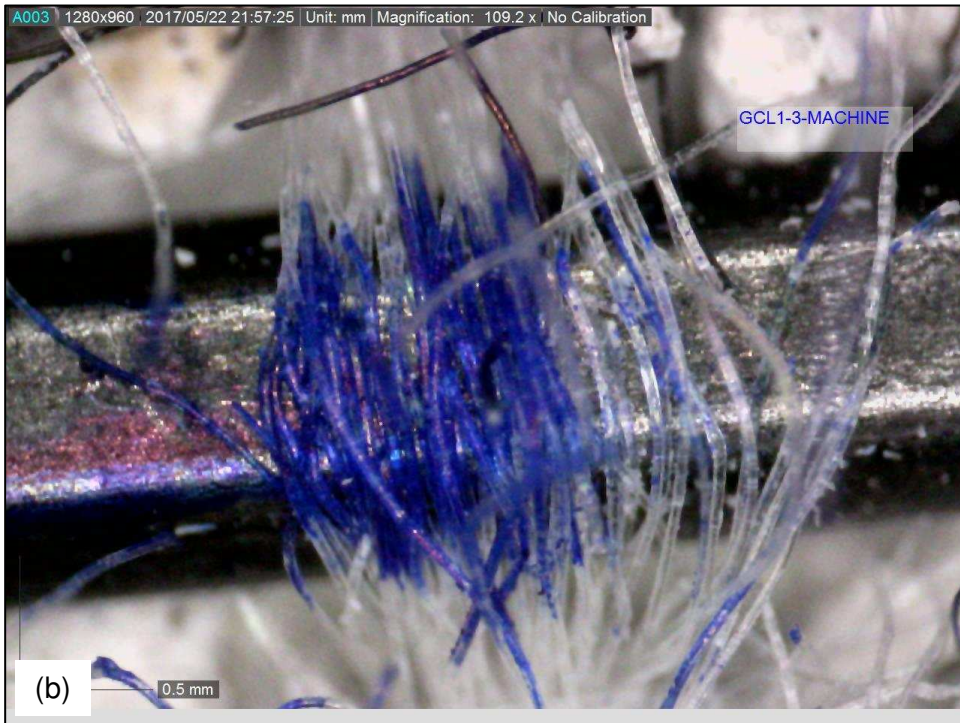


Figure B.5. Fiber bundle sample GCL1-3-MACHINE. (a) Determination of the fiber bundle thickness. (b) Determination of the number of monofilament fibers per fiber bundle.

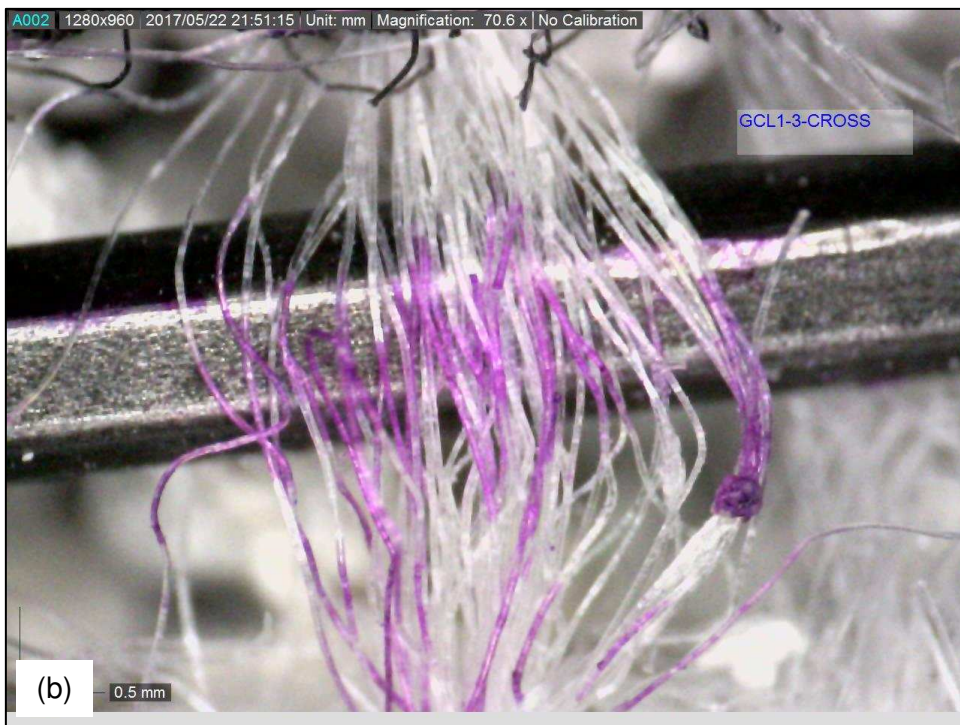
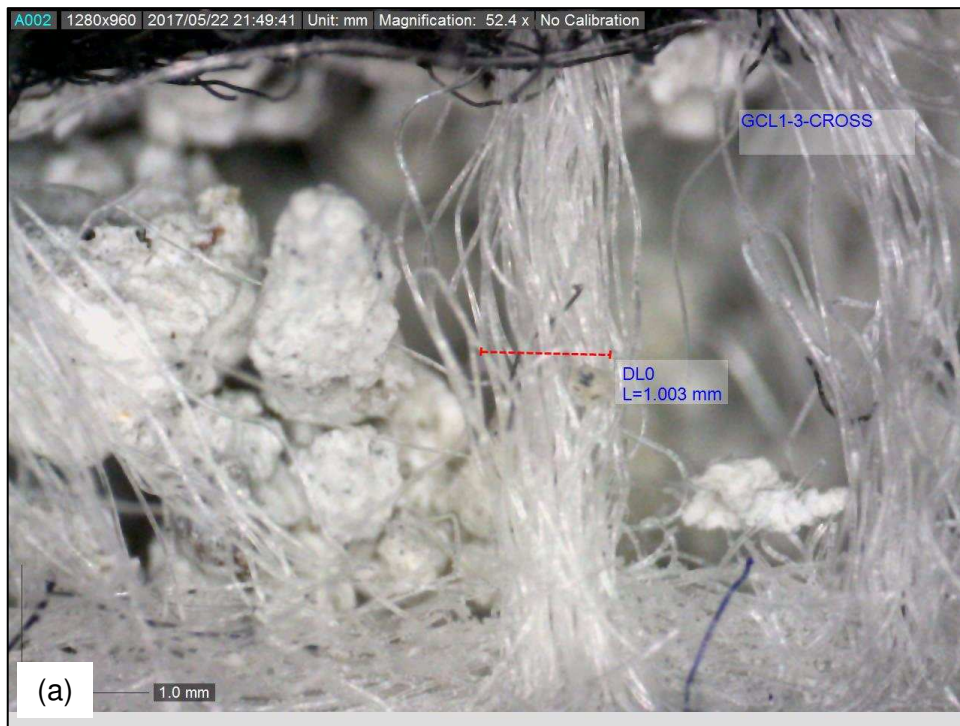


Figure B.6. Fiber bundle sample GCL1-3-CROSS. (a) Determination of the fiber bundle thickness. (b) Determination of the number of monofilament fibers per fiber bundle.

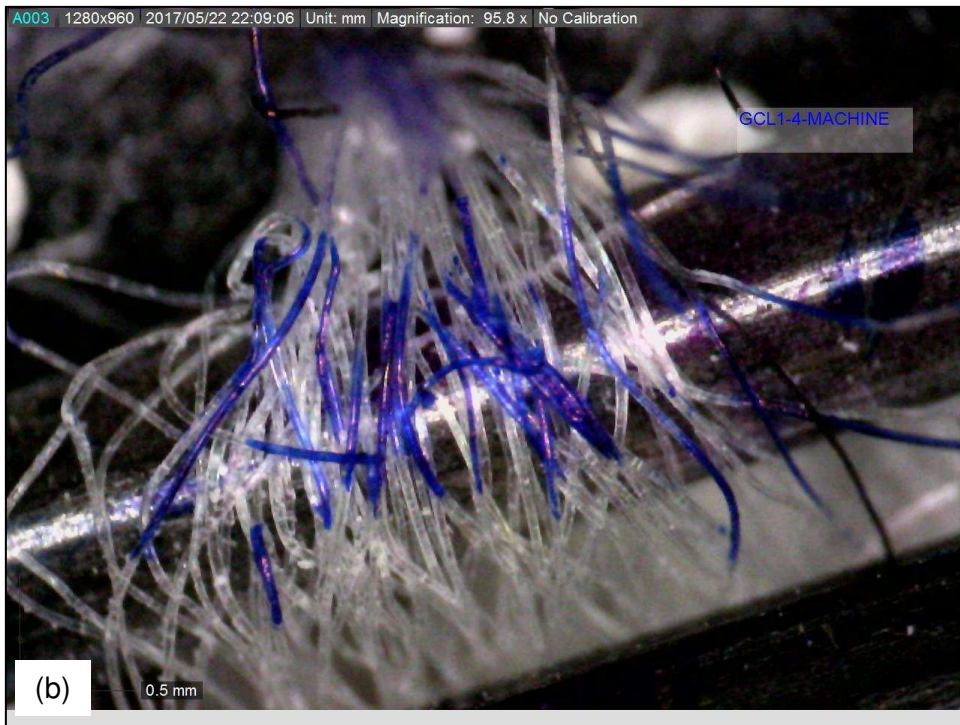


Figure B.7. Fiber bundle sample GCL1-4-MACHINE. (a) Determination of the fiber bundle thickness. (b) Determination of the number of monofilament fibers per fiber bundle.

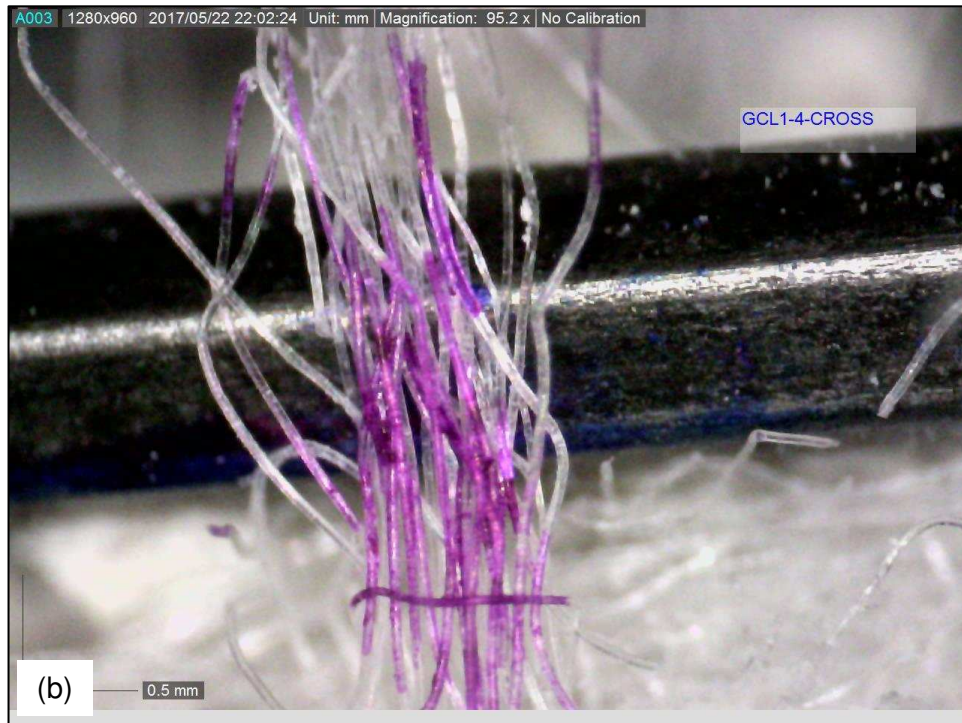
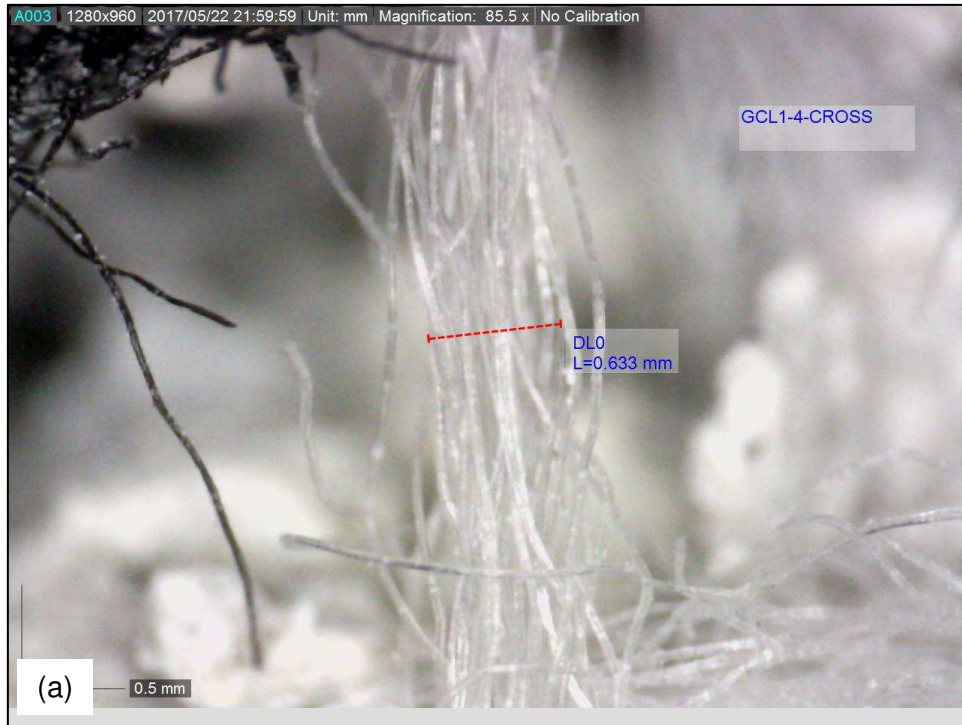


Figure B.8. Fiber bundle sample GCL1-4-CROSS. (a) Determination of the fiber bundle thickness. (b) Determination of the number of monofilament fibers per fiber bundle.

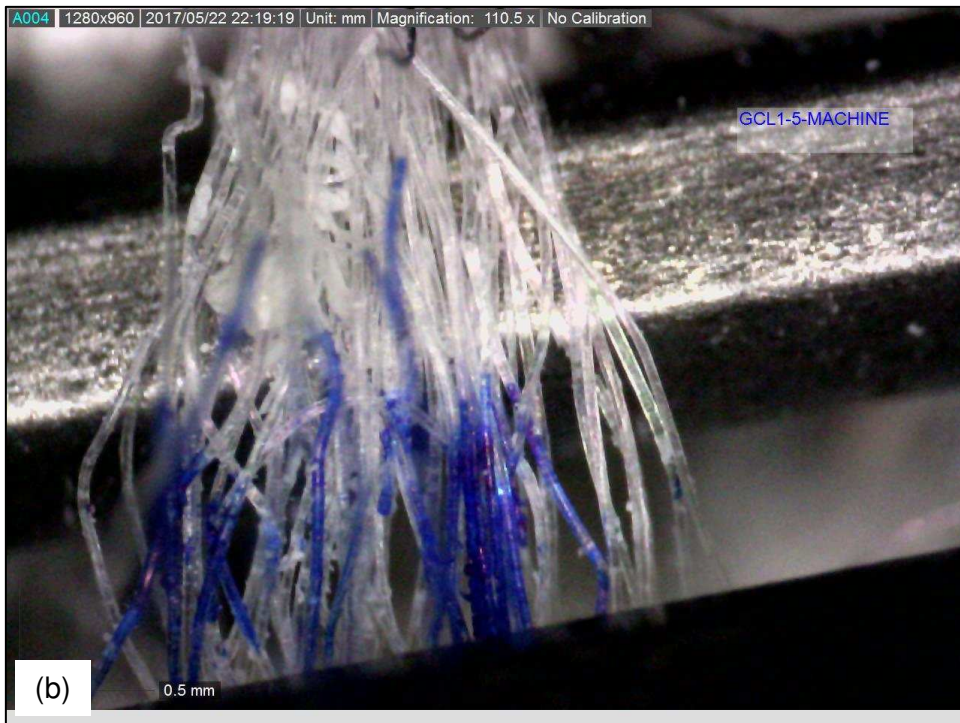
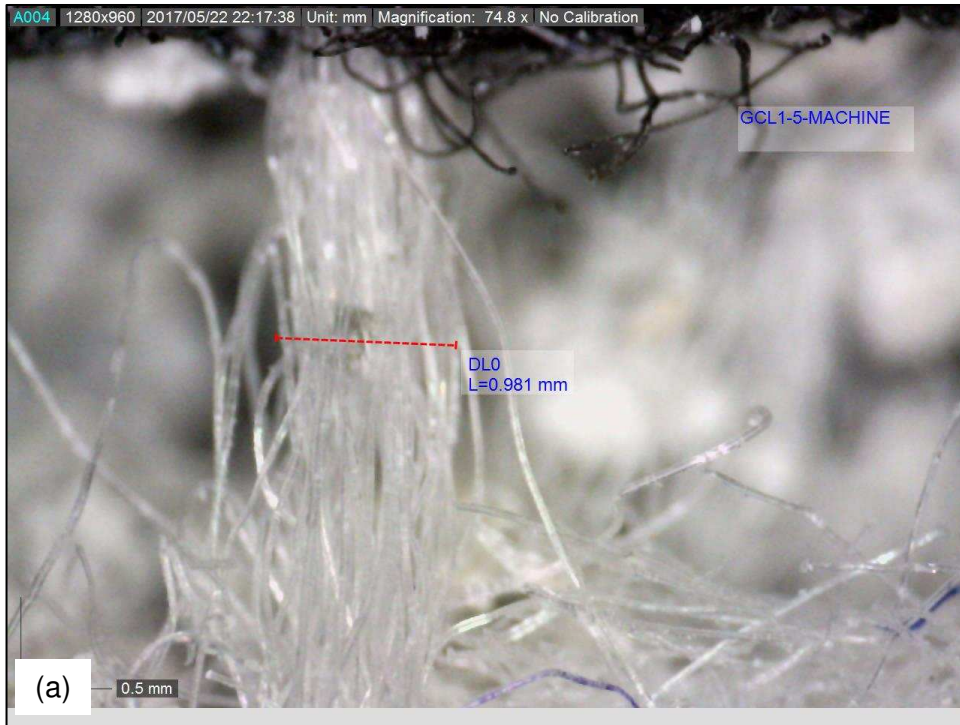


Figure B.9. Fiber bundle sample GCL1-5-MACHINE. (a) Determination of the fiber bundle thickness. (b) Determination of the number of monofilament fibers per fiber bundle.

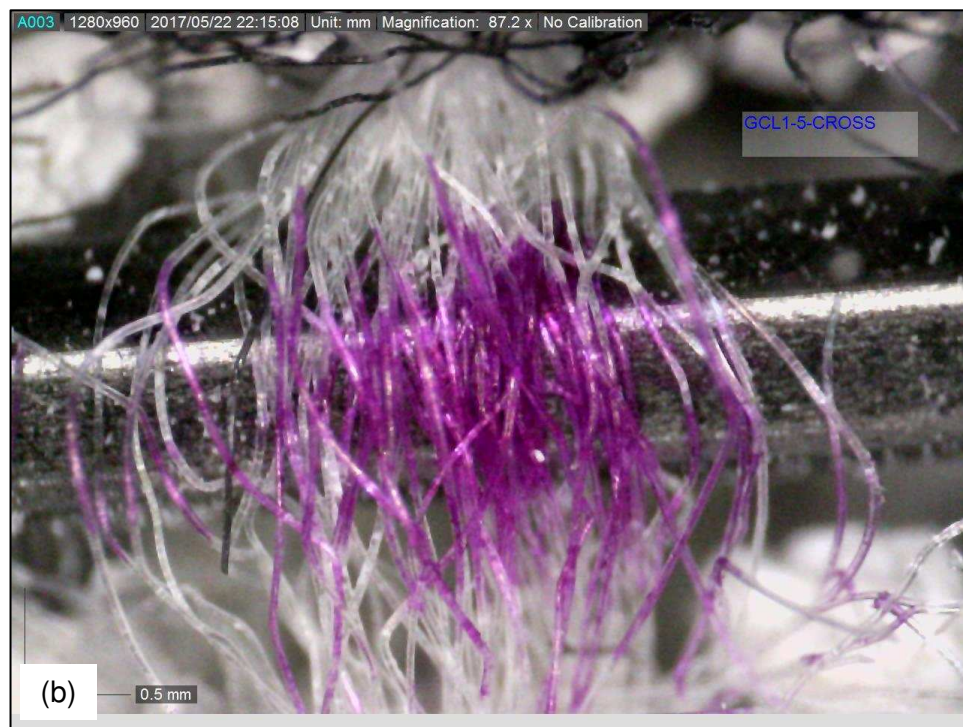


Figure B.10. Fiber bundle sample GCL1-5-CROSS. (a) Determination of the fiber bundle thickness. (b) Determination of the number of monofilament fibers per fiber bundle.

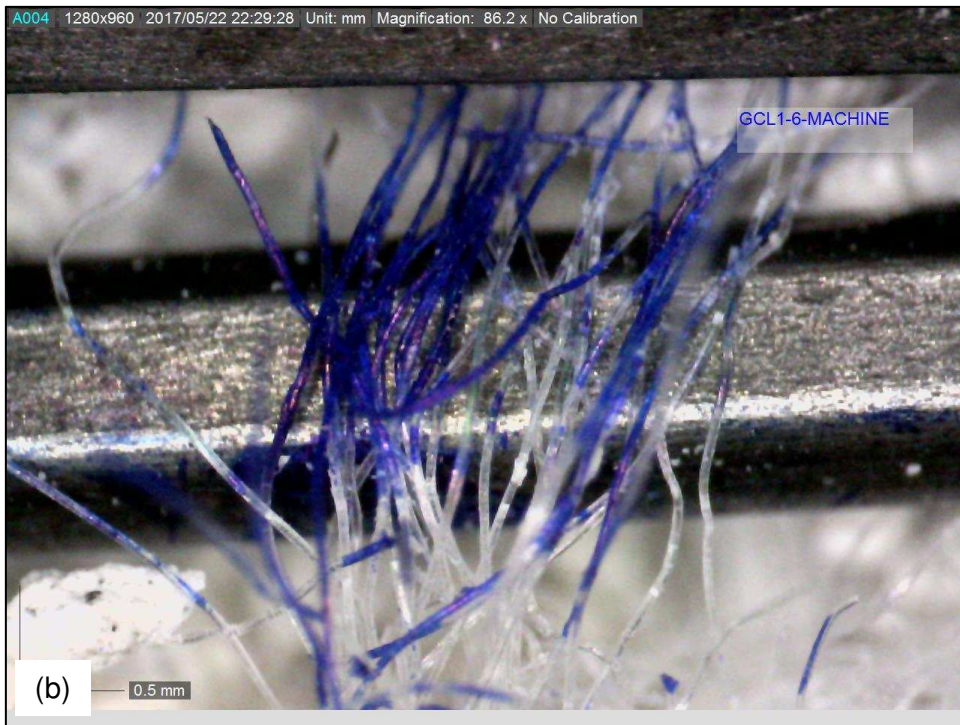
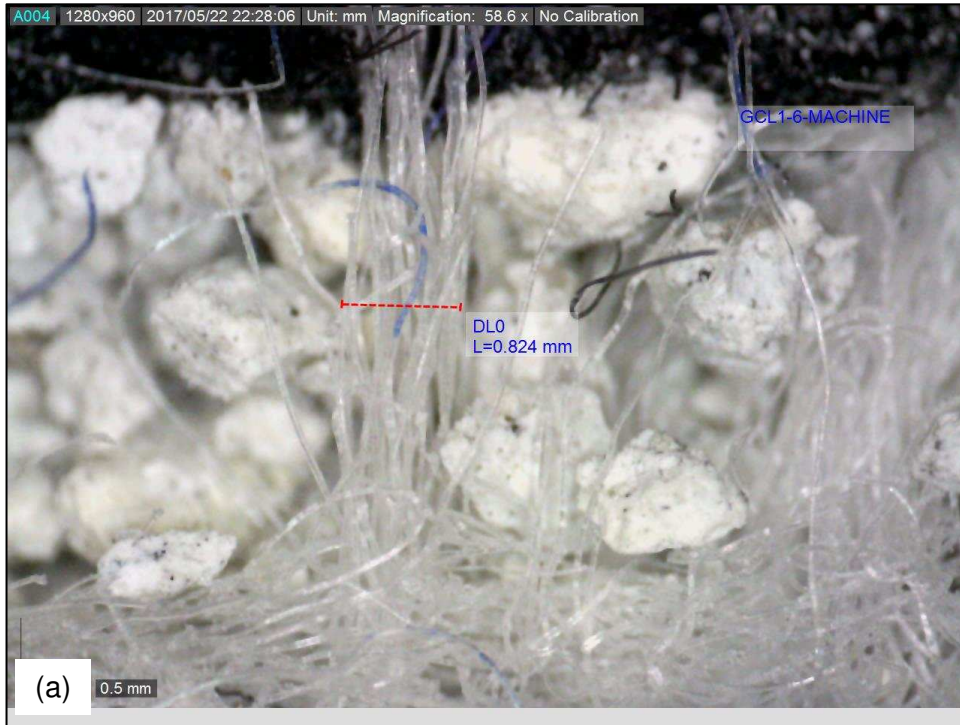


Figure B.11. Fiber bundle sample GCL1-6-MACHINE. (a) Determination of the fiber bundle thickness. (b) Determination of the number of monofilament fibers per fiber bundle.

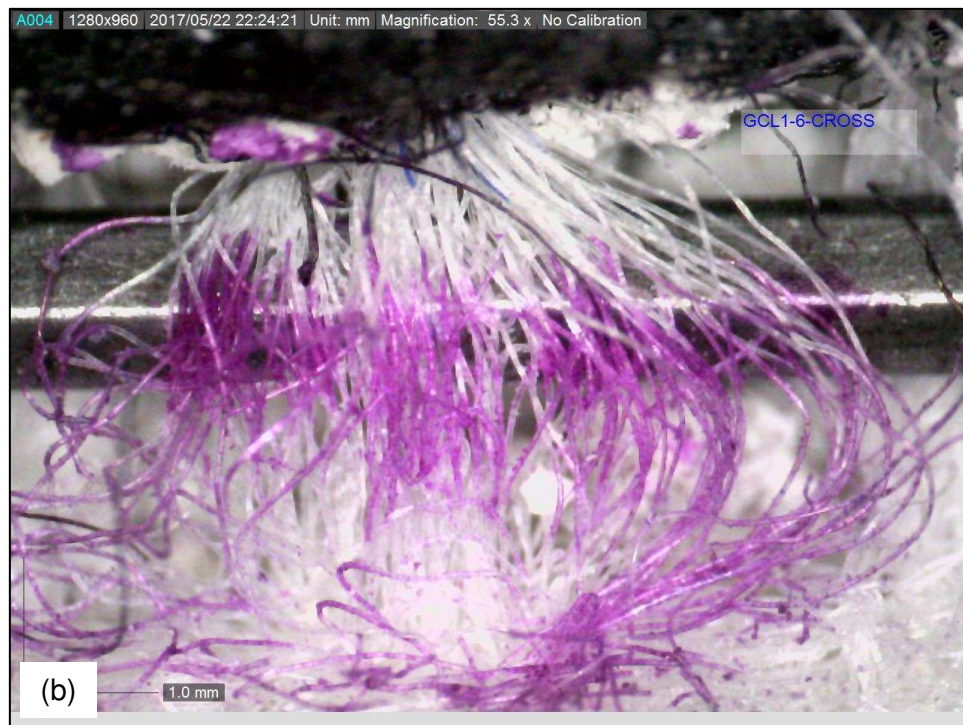
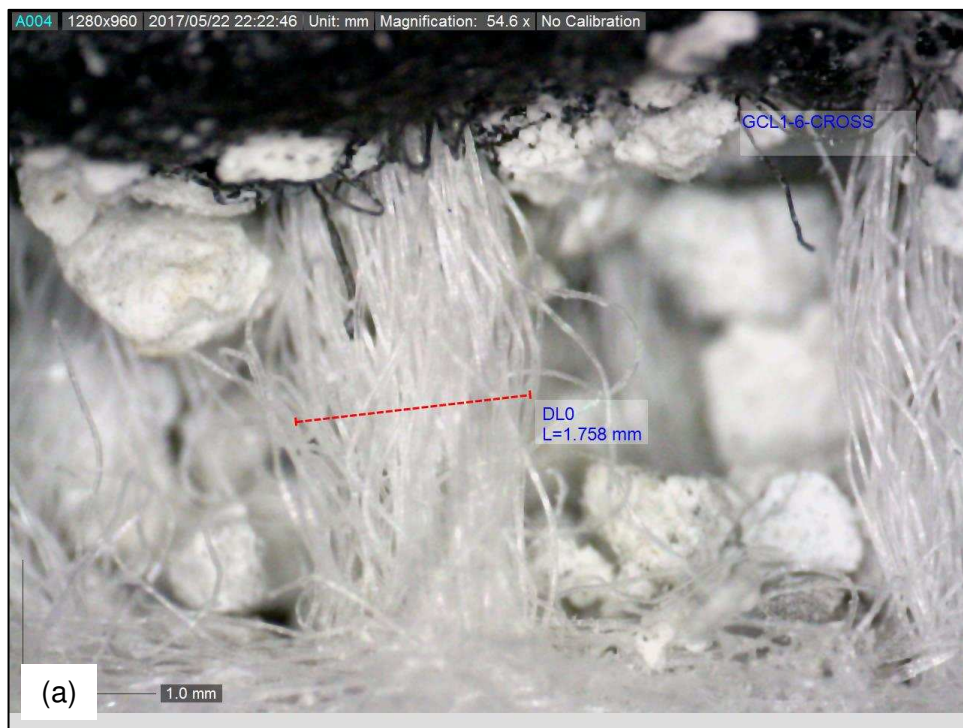


Figure B.12. Fiber bundle sample GCL1-6-CROSS. (a) Determination of the fiber bundle thickness. (b) Determination of the number of monofilament fibers per fiber bundle.

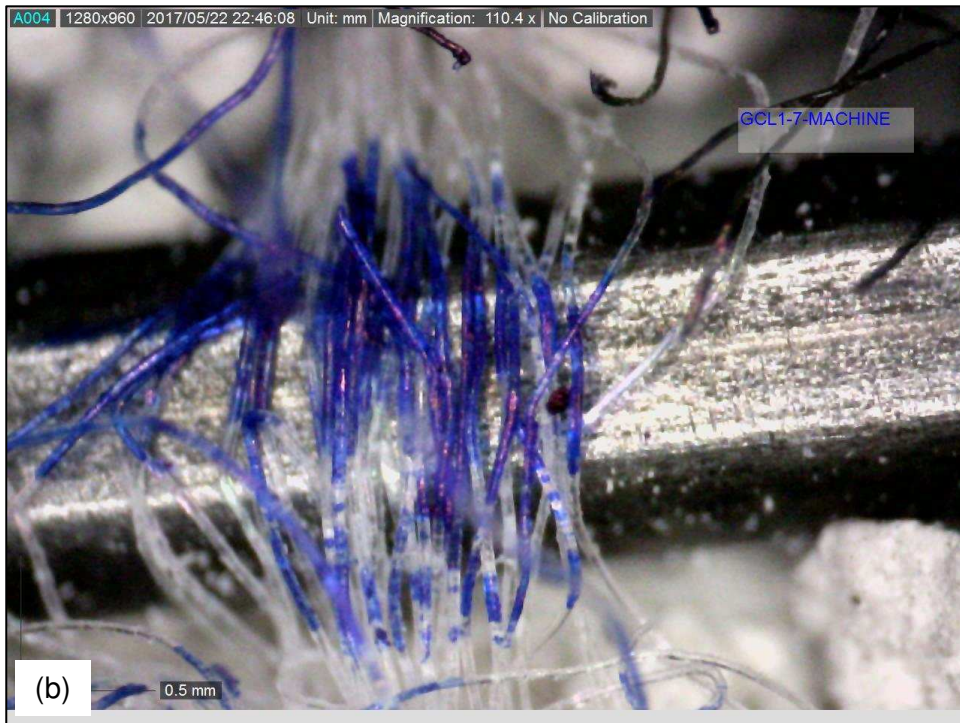
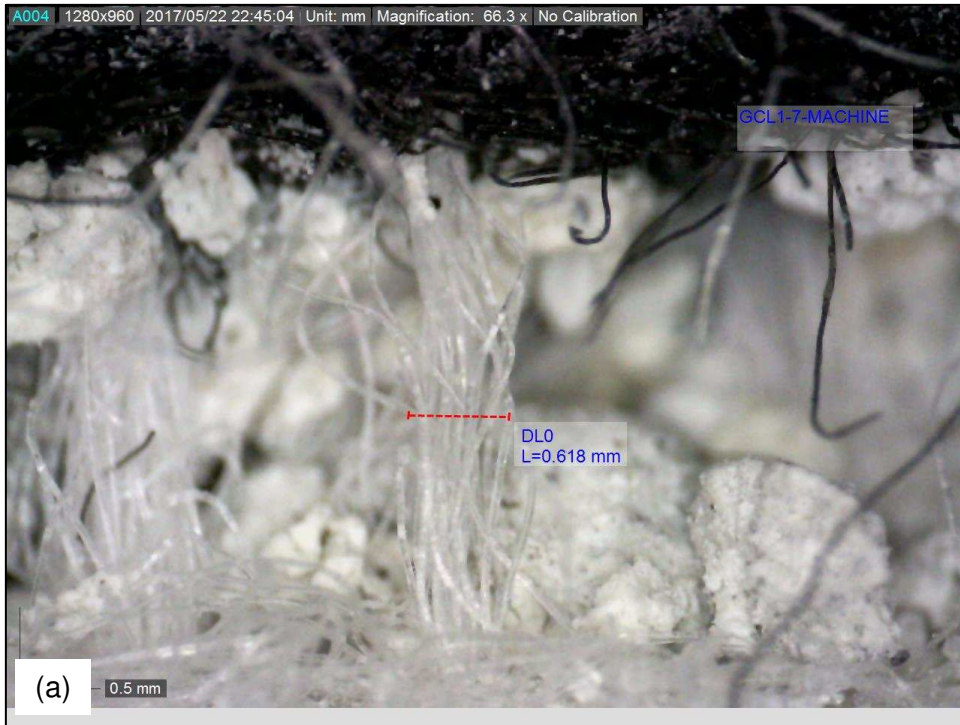


Figure B.13. Fiber bundle sample GCL1-7-MACHINE. (a) Determination of the fiber bundle thickness. (b) Determination of the number of monofilament fibers per fiber bundle.

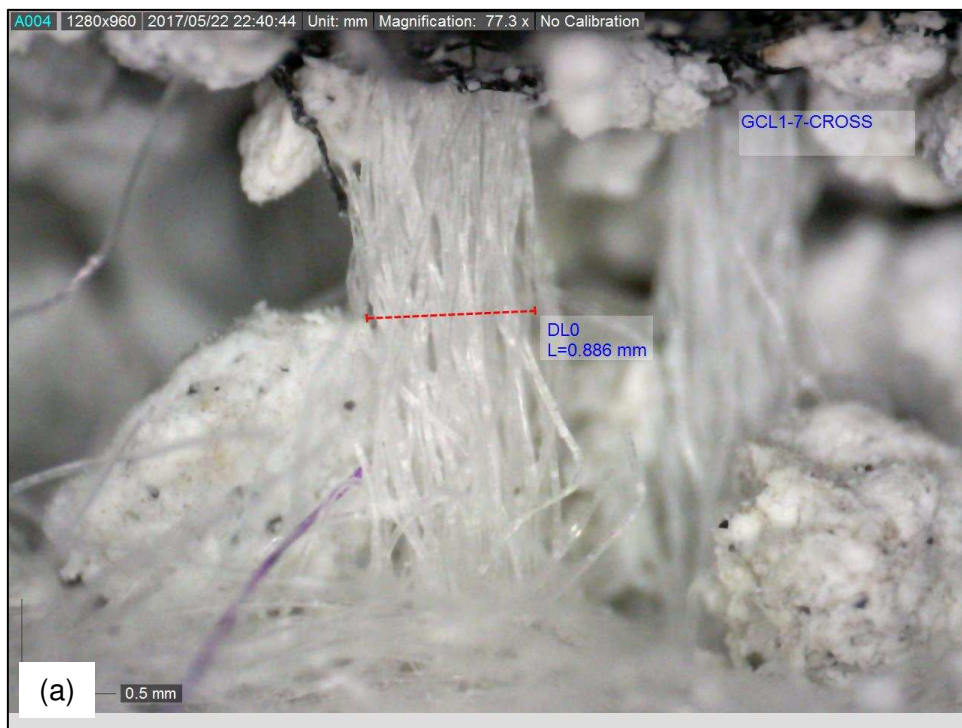


Figure B.14. Fiber bundle sample GCL1-7-CROSS. (a) Determination of the fiber bundle thickness. (b) Determination of the number of monofilament fibers per fiber bundle.

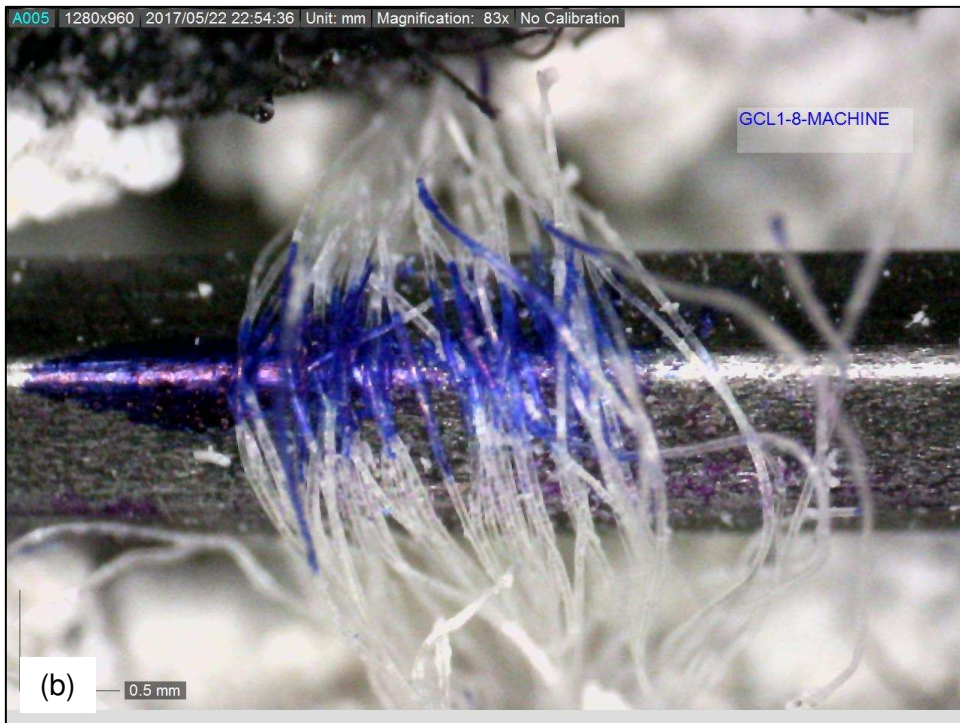
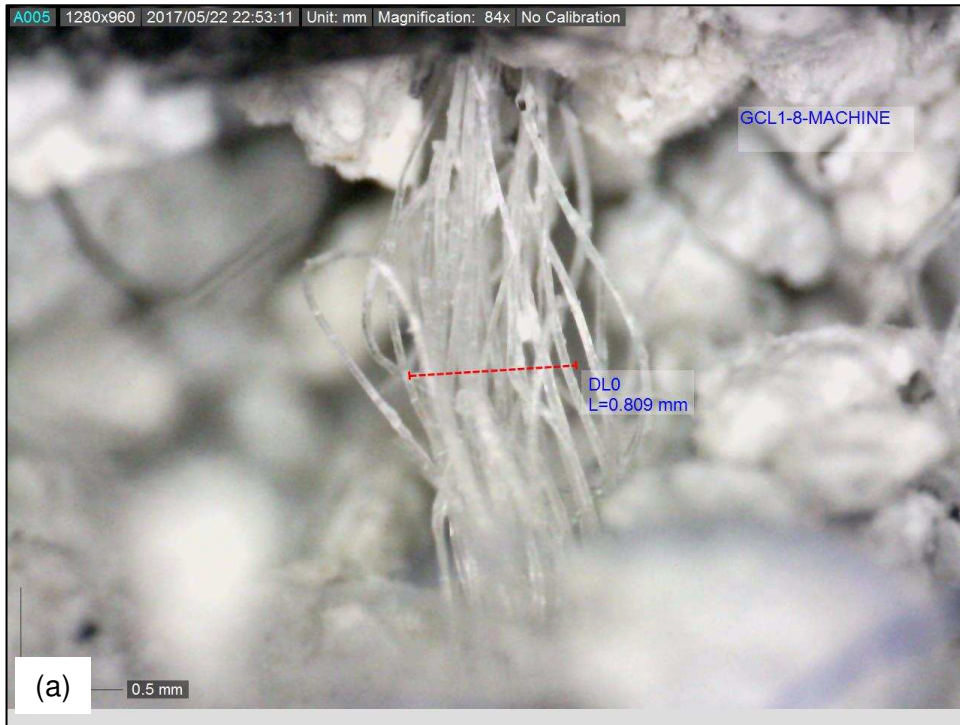


Figure B.15. Fiber bundle sample GCL1-8-MACHINE. (a) Determination of the fiber bundle thickness. (b) Determination of the number of monofilament fibers per fiber bundle.

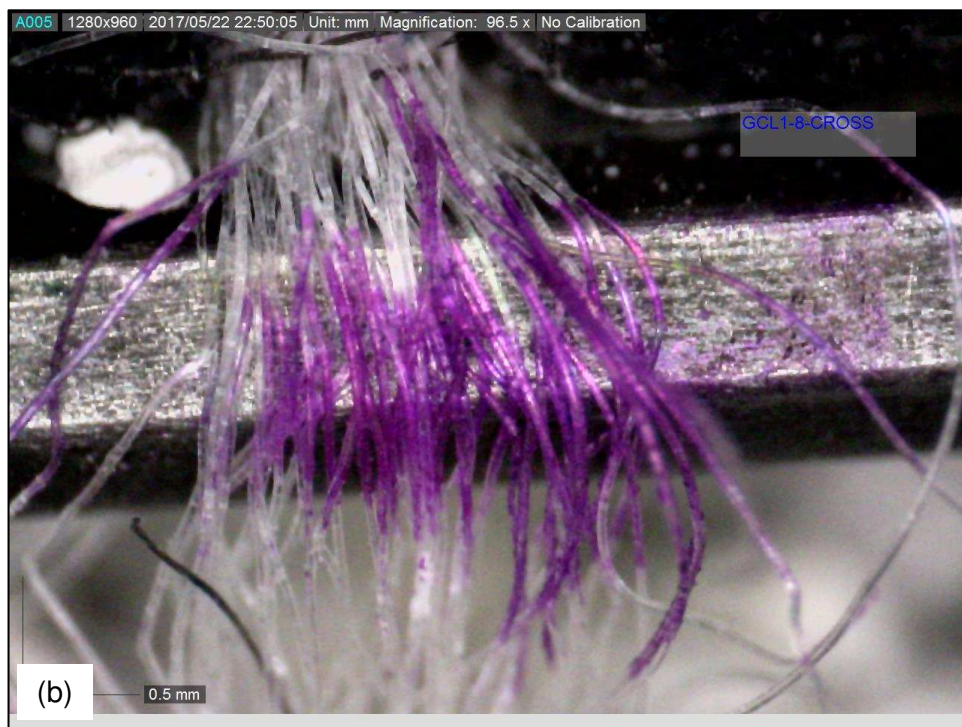
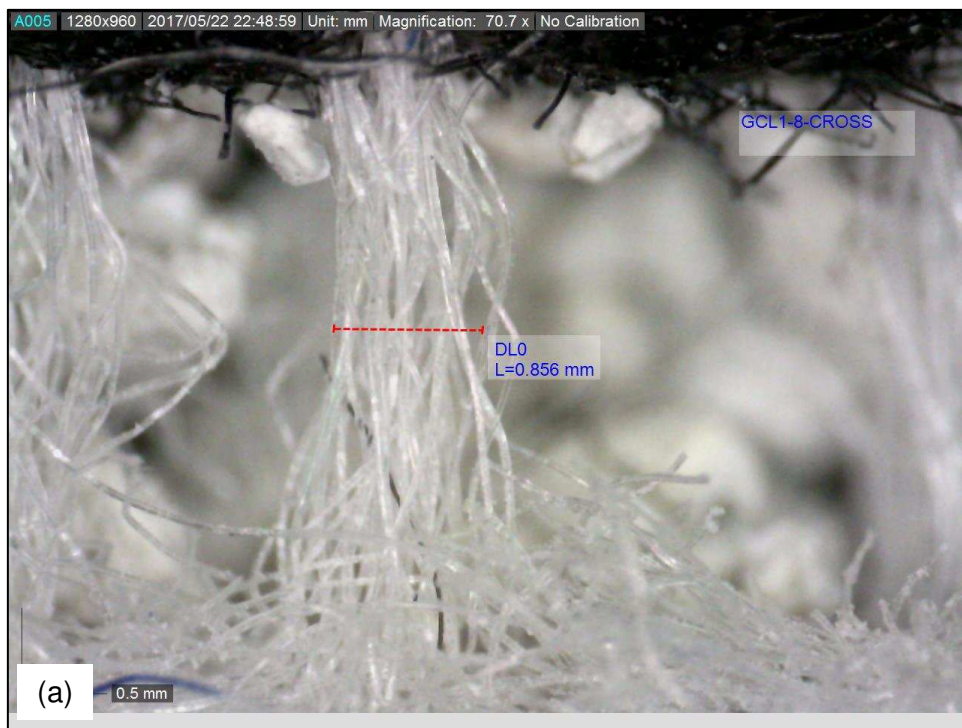


Figure B.16. Fiber bundle sample GCL1-8-CROSS. (a) Determination of the fiber bundle thickness. (b) Determination of the number of monofilament fibers per fiber bundle.

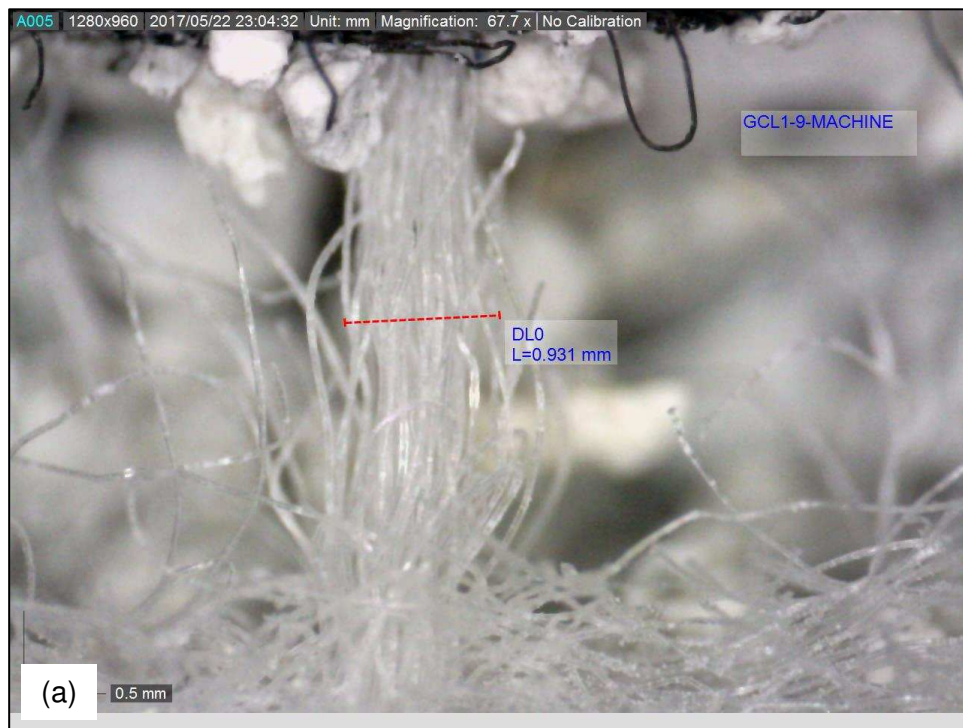


Figure B.17. Fiber bundle sample GCL1-9-MACHINE. (a) Determination of the fiber bundle thickness. (b) Determination of the number of monofilament fibers per fiber bundle.

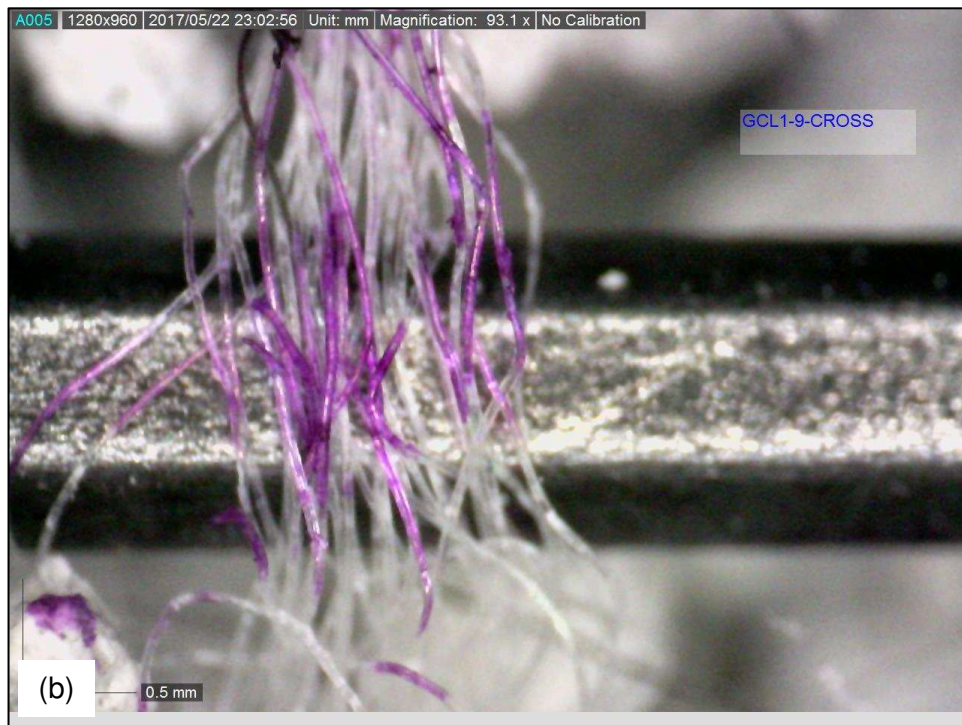
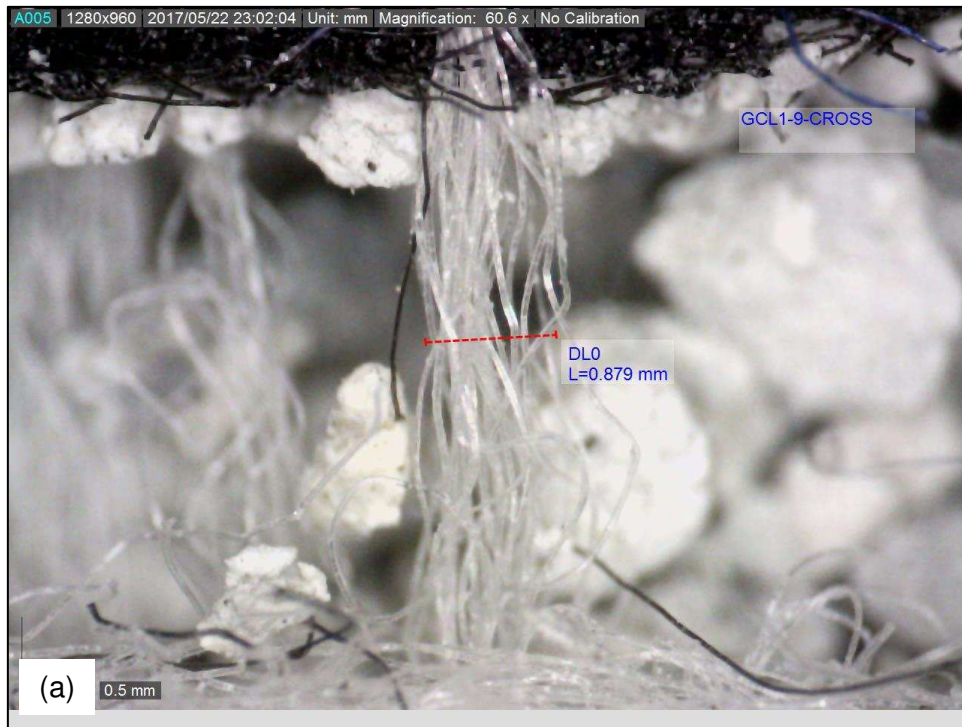


Figure B.18. Fiber bundle sample GCL1-9-CROSS. (a) Determination of the fiber bundle thickness. (b) Determination of the number of monofilament fibers per fiber bundle.

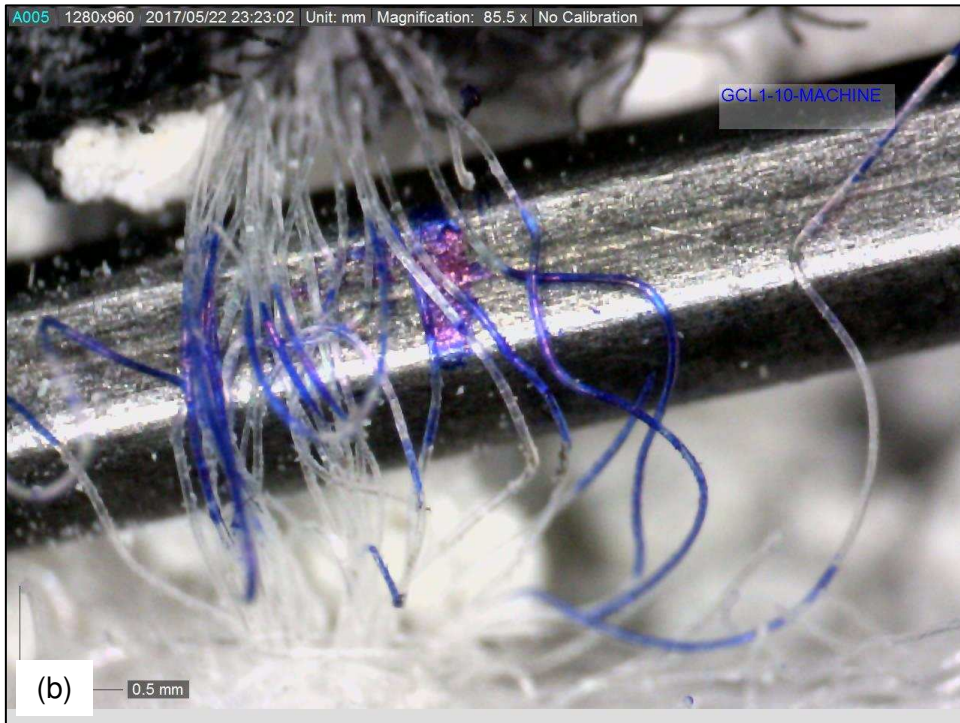
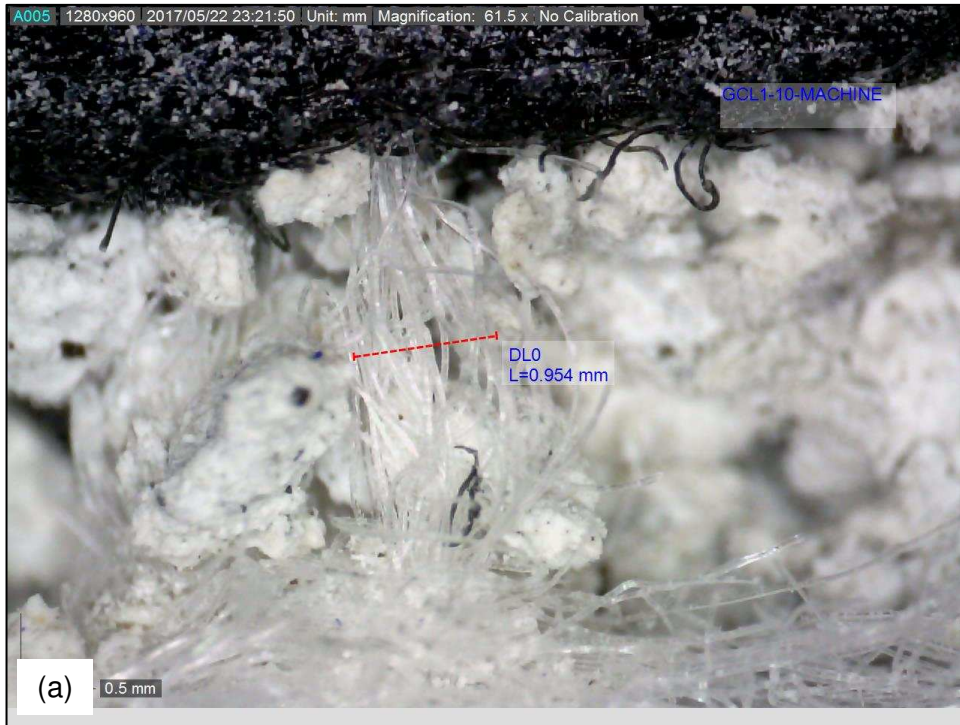


Figure B.19. Fiber bundle sample GCL1-10-MACHINE. (a) Determination of the fiber bundle thickness. (b) Determination of the number of monofilament fibers per fiber bundle.



Figure B.20. Fiber bundle sample GCL1-10-CROSS. (a) Determination of the fiber bundle thickness. (b) Determination of the number of monofilament fibers per fiber bundle.

B. 3 Determination of needle-punched fiber bundle properties for GCL-2

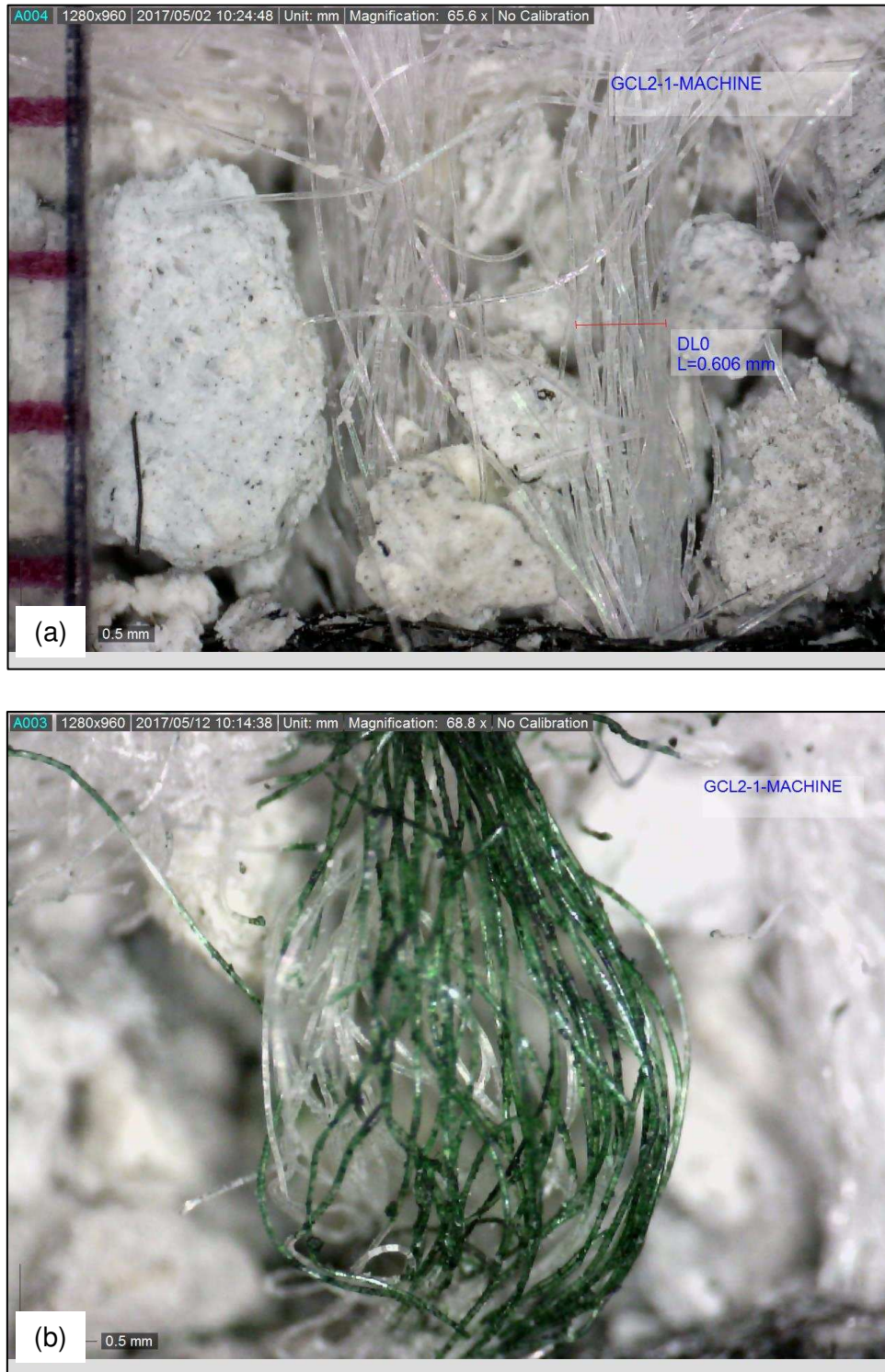


Figure B.21. Fiber bundle sample GCL2-1-MACHINE. (a) Determination of the fiber bundle thickness. (b) Determination of the number of monofilament fibers per fiber bundle.

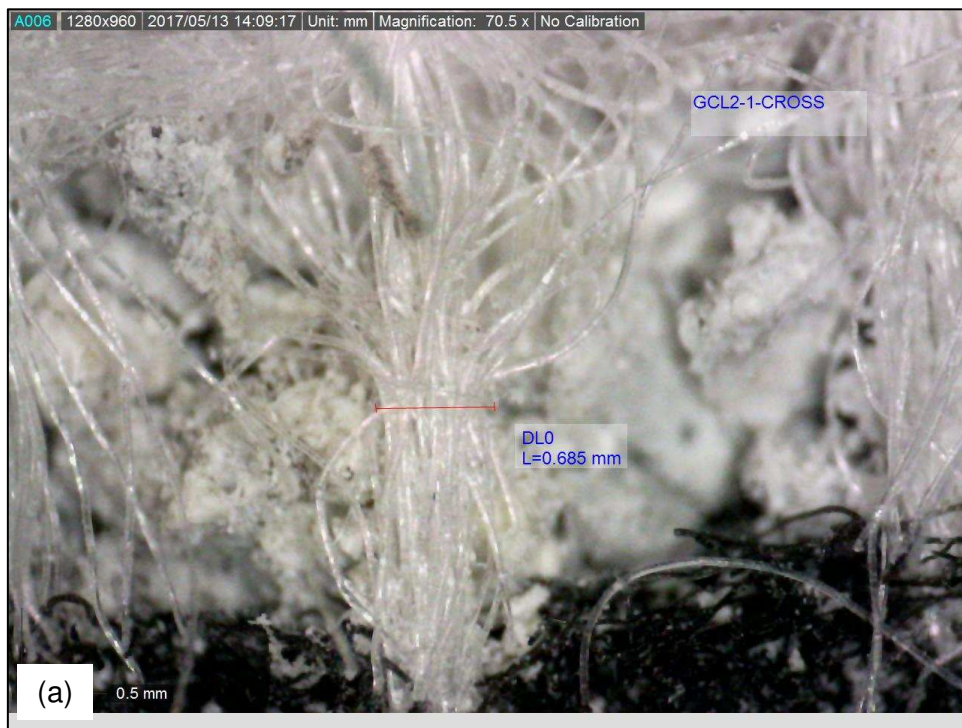


Figure B.22. Fiber bundle sample GCL2-1-CROSS. (a) Determination of the fiber bundle thickness. (b) Determination of the number of monofilament fibers per fiber bundle.

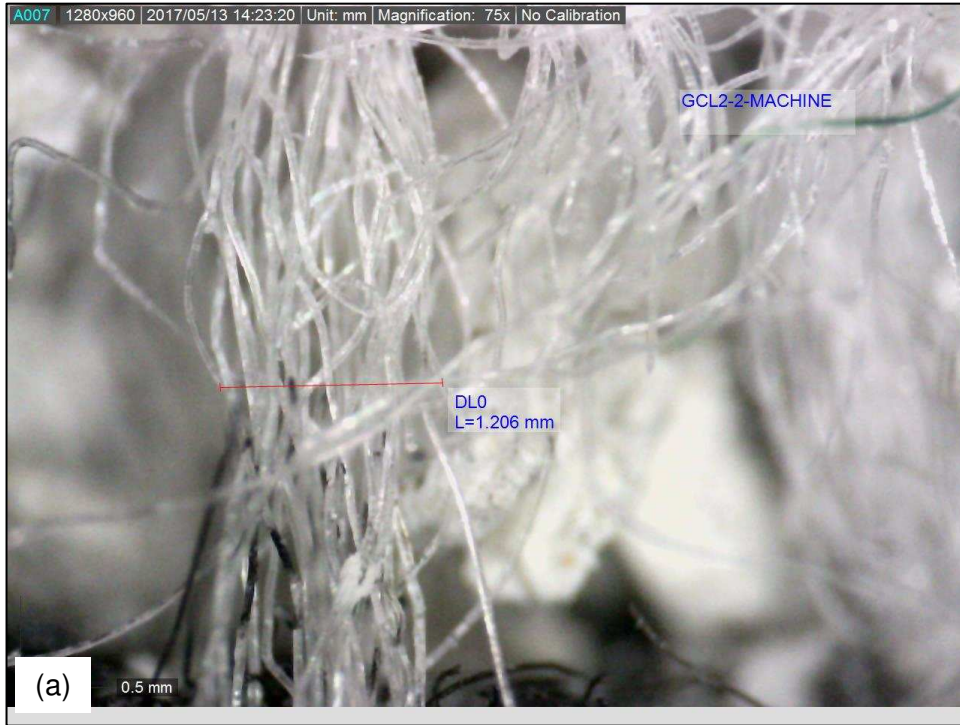


Figure B.23. Fiber bundle sample GCL2-2-MACHINE. (a) Determination of the fiber bundle thickness. (b) Determination of the number of monofilament fibers per fiber bundle.

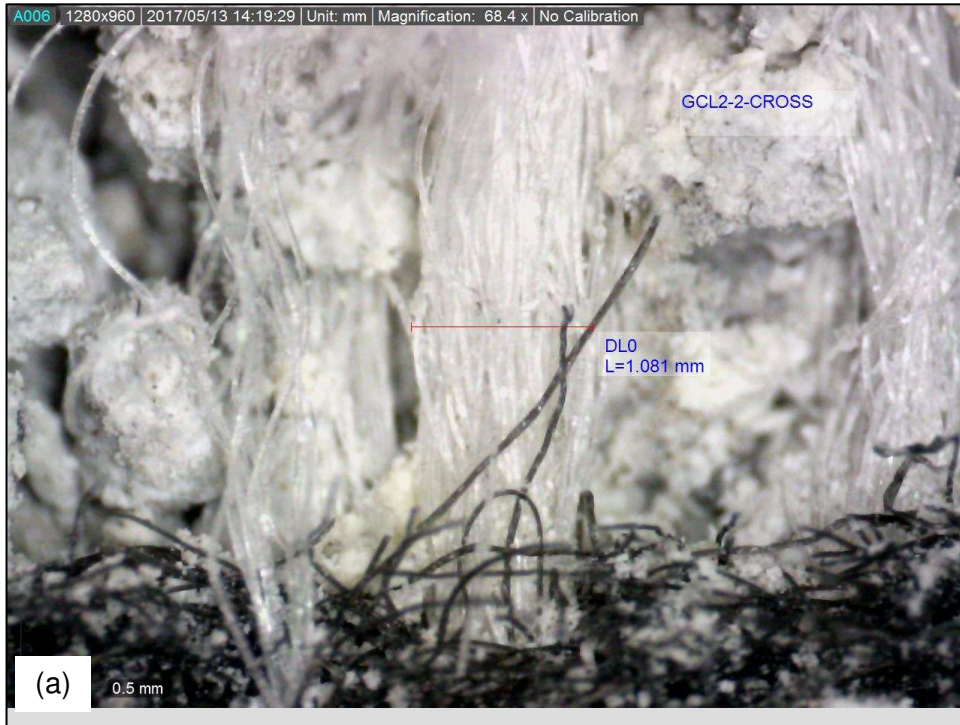


Figure B.24. Fiber bundle sample GCL2-2-CROSS. (a) Determination of the fiber bundle thickness. (b) Determination of the number of monofilament fibers per fiber bundle.



Figure B.25. Fiber bundle sample GCL2-3-MACHINE. (a) Determination of the fiber bundle thickness. (b) Determination of the number of monofilament fibers per fiber bundle.

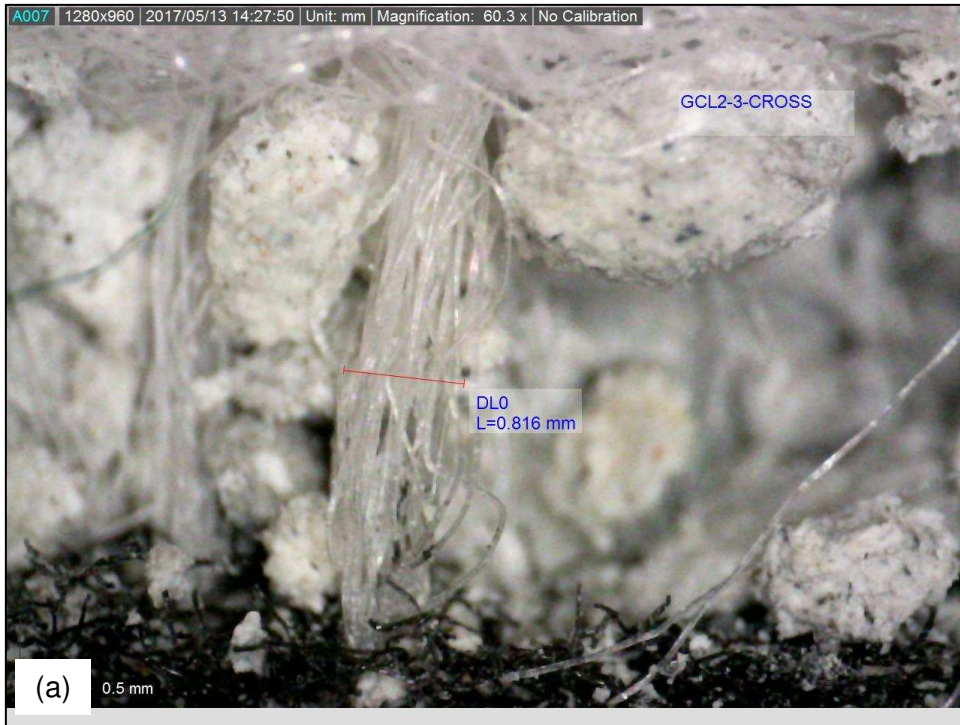


Figure B.26. Fiber bundle sample GCL2-3-CROSS. (a) Determination of the fiber bundle thickness. (b) Determination of the number of monofilament fibers per fiber bundle.

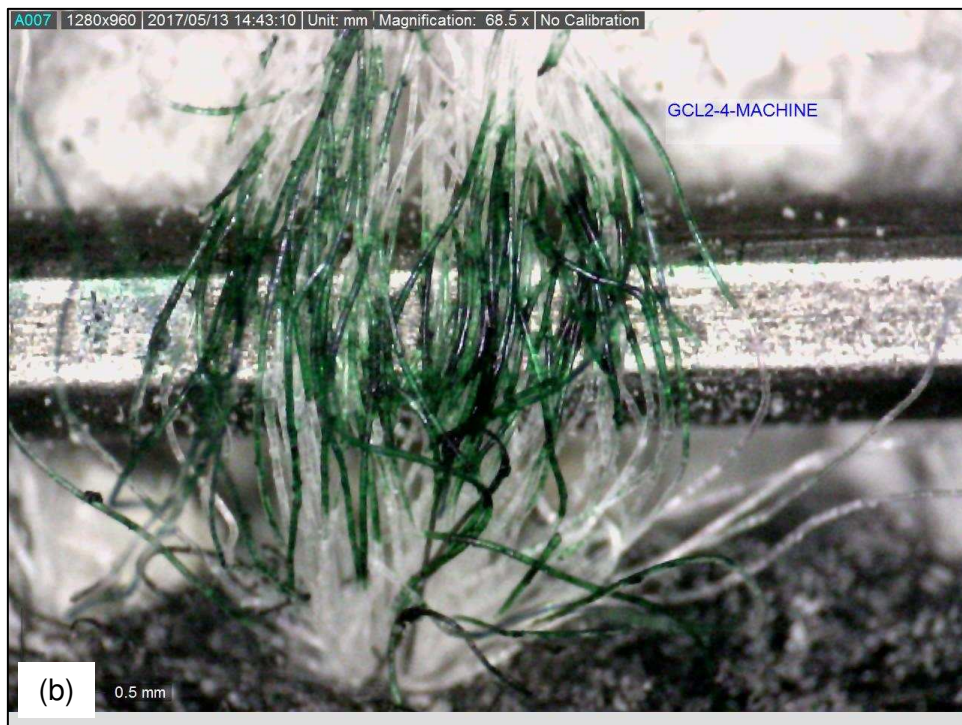


Figure B.27. Fiber bundle sample GCL2-4-MACHINE. (a) Determination of the fiber bundle thickness. (b) Determination of the number of monofilament fibers per fiber bundle.

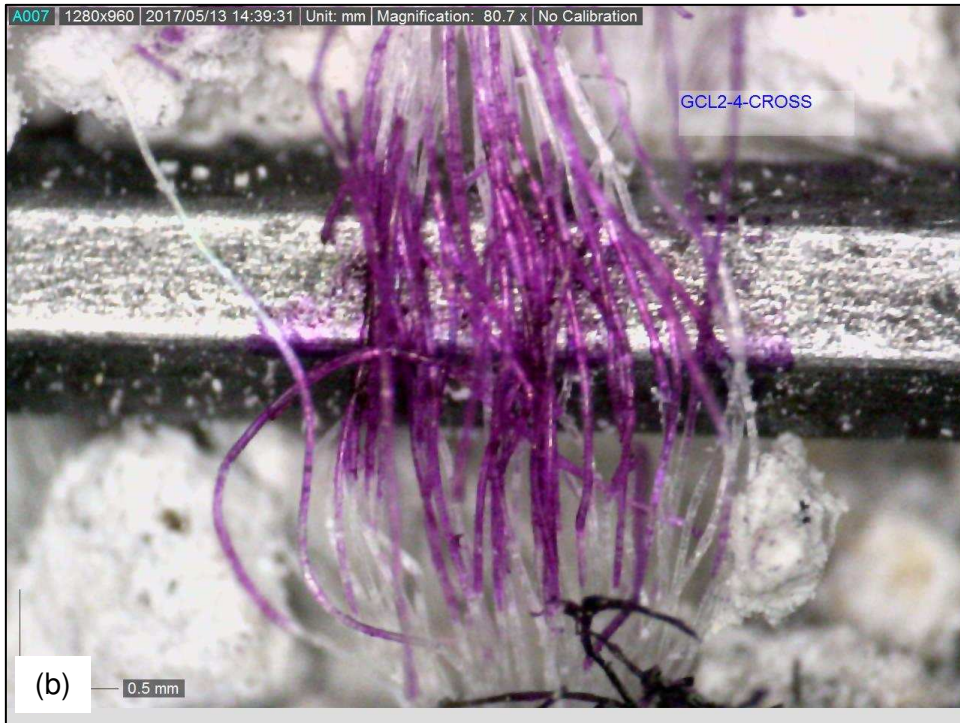


Figure B.28. Fiber bundle sample GCL2-4-CROSS. (a) Determination of the fiber bundle thickness. (b) Determination of the number of monofilament fibers per fiber bundle.



Figure B.29. Fiber bundle sample GCL2-5-MACHINE. (a) Determination of the fiber bundle thickness. (b) Determination of the number of monofilament fibers per fiber bundle.

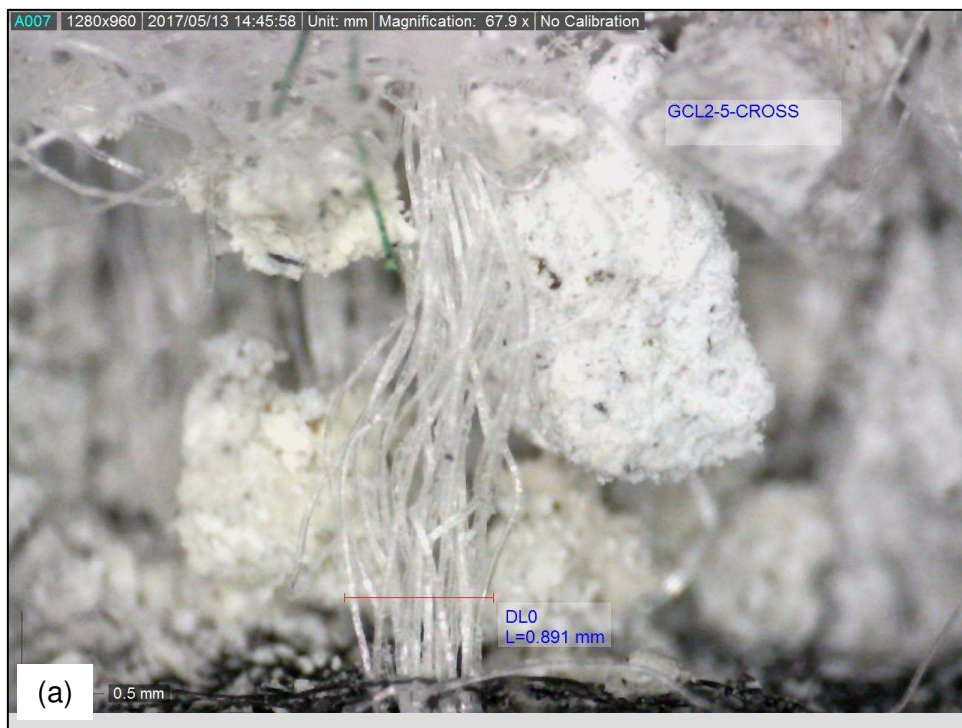


Figure B.30. Fiber bundle sample GCL2-5-CROSS. (a) Determination of the fiber bundle thickness. (b) Determination of the number of monofilament fibers per fiber bundle.

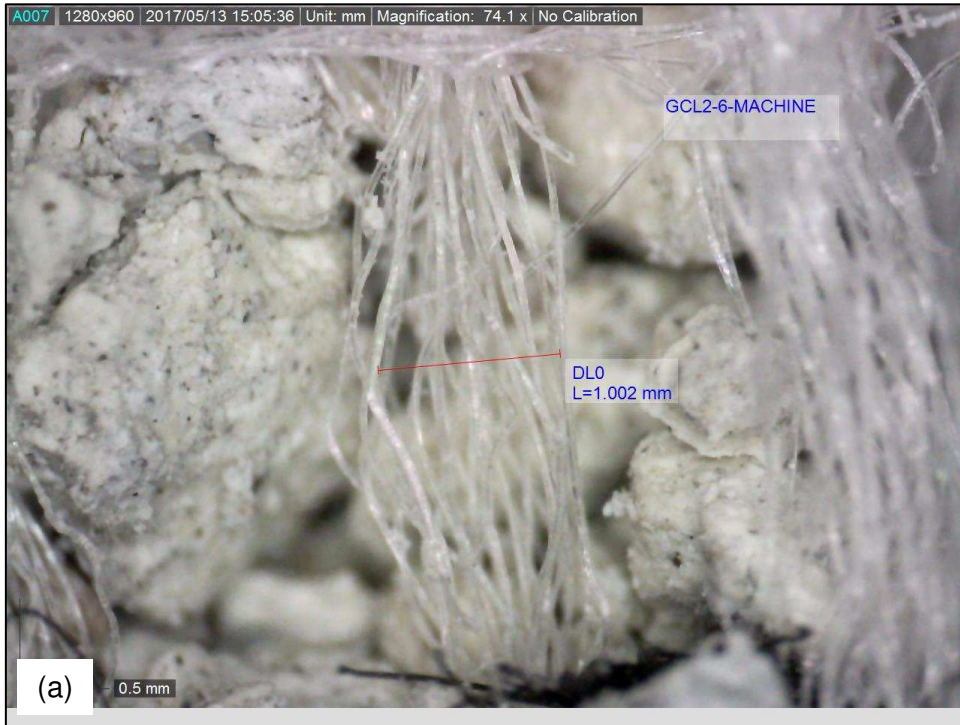


Figure B.31. Fiber bundle sample GCL2-6-MACHINE. (a) Determination of the fiber bundle thickness. (b) Determination of the number of monofilament fibers per fiber bundle.

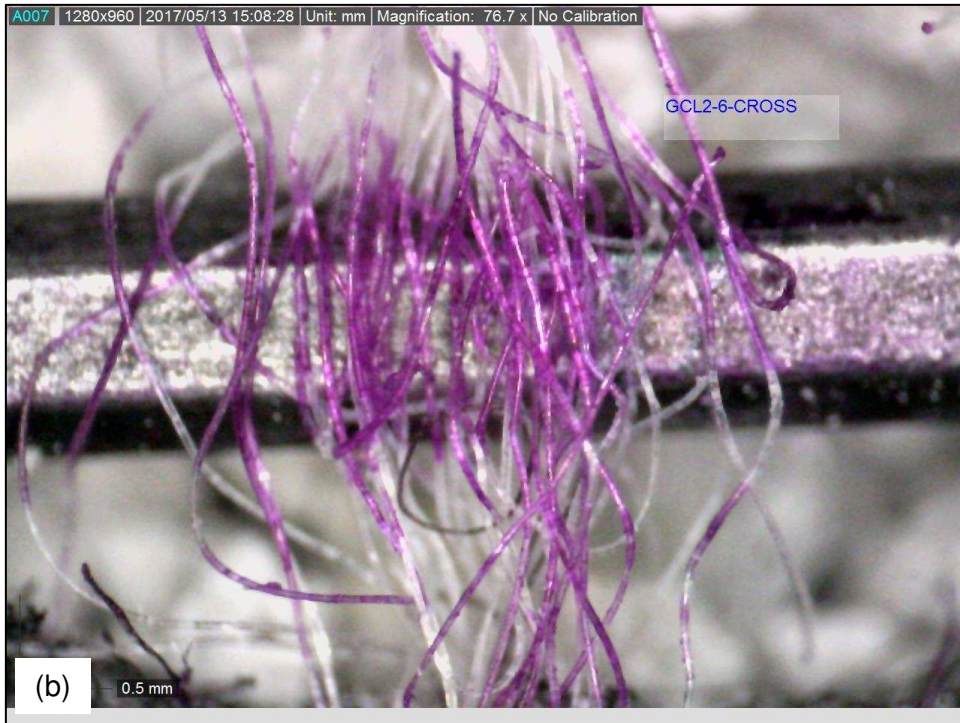


Figure B.32. Fiber bundle sample GCL2-6-CROSS. (a) Determination of the fiber bundle thickness. (b) Determination of the number of monofilament fibers per fiber bundle.

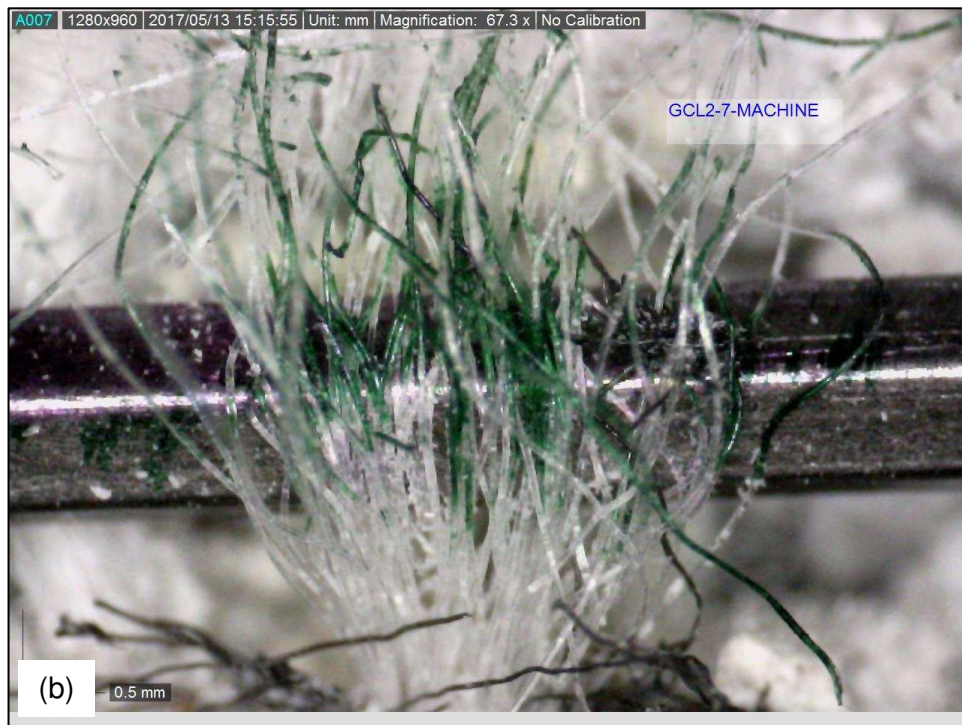
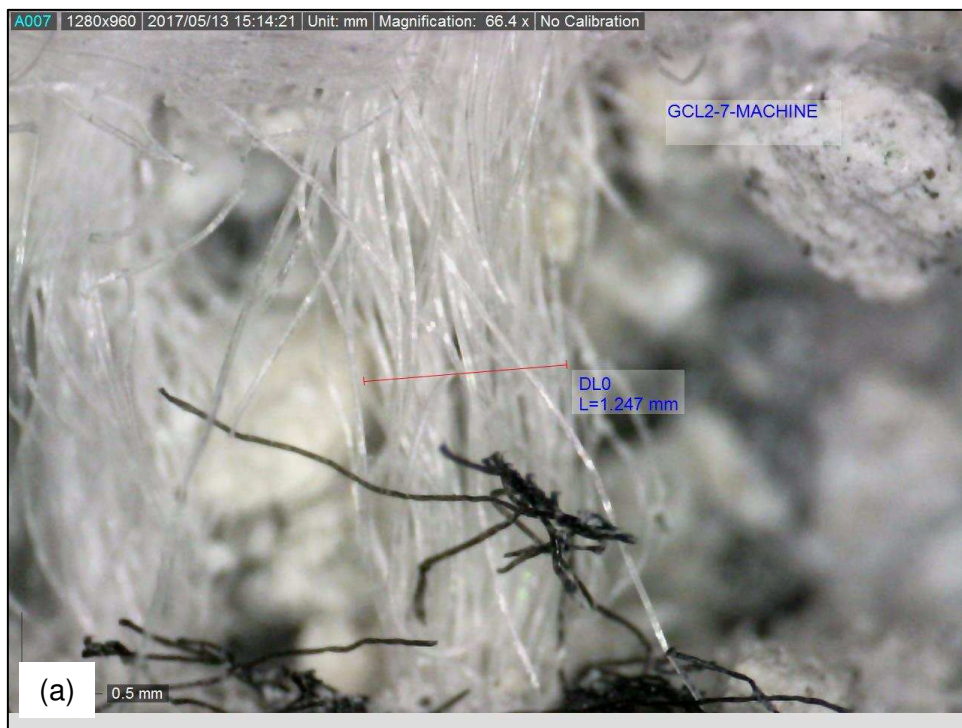


Figure B.33. Fiber bundle sample GCL2-7-MACHINE. (a) Determination of the fiber bundle thickness. (b) Determination of the number of monofilament fibers per fiber bundle.

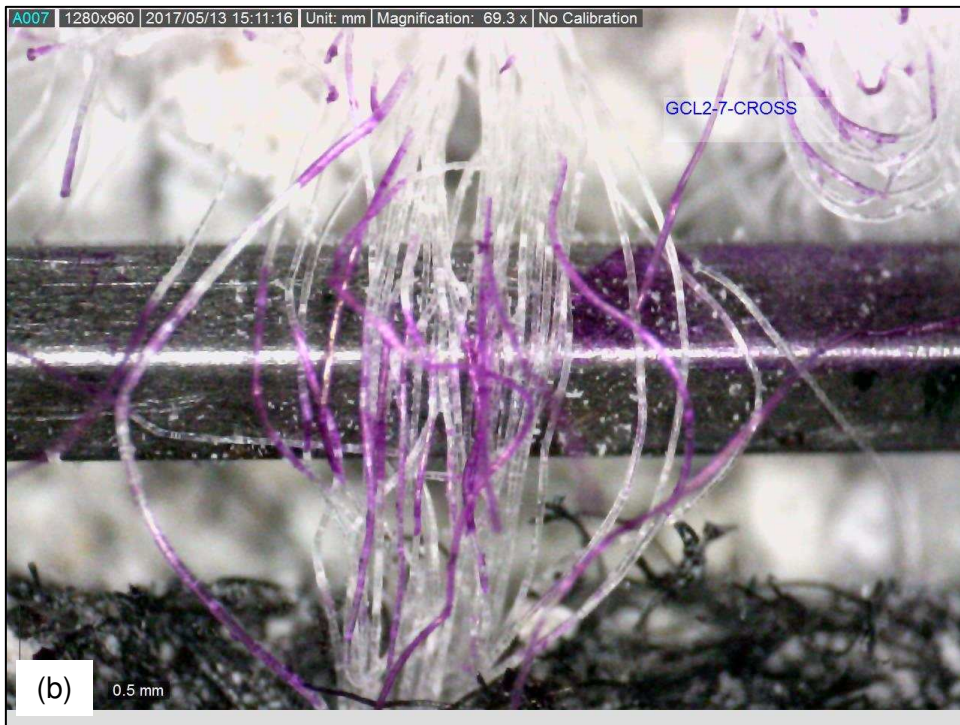


Figure B.34. Fiber bundle sample GCL2-7-CROSS. (a) Determination of the fiber bundle thickness. (b) Determination of the number of monofilament fibers per fiber bundle.



Figure B.35. Fiber bundle sample GCL2-8-MACHINE. (a) Determination of the fiber bundle thickness. (b) Determination of the number of monofilament fibers per fiber bundle.

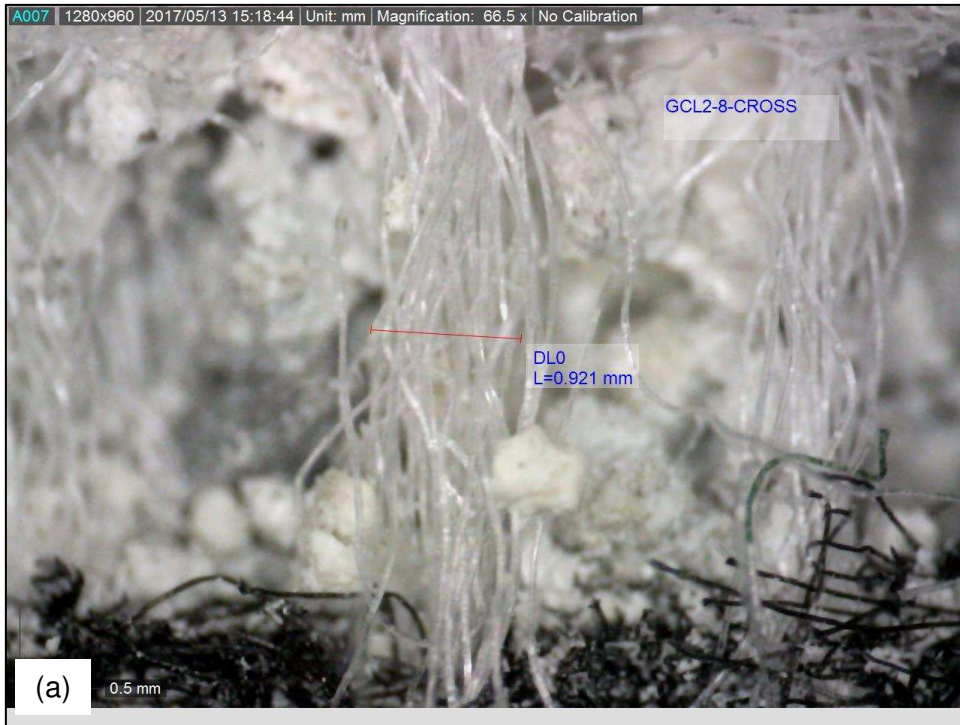


Figure B.36. Fiber bundle sample GCL2-8-CROSS. (a) Determination of the fiber bundle thickness. (b) Determination of the number of monofilament fibers per fiber bundle.

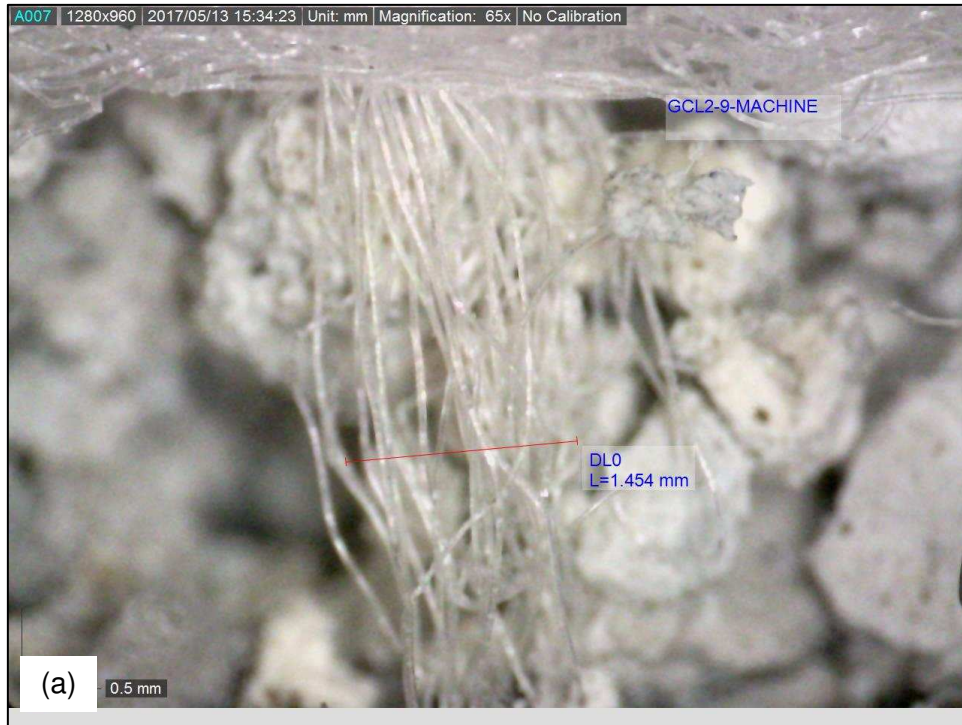


Figure B.37. Fiber bundle sample GCL2-9-MACHINE. (a) Determination of the fiber bundle thickness. (b) Determination of the number of monofilament fibers per fiber bundle.

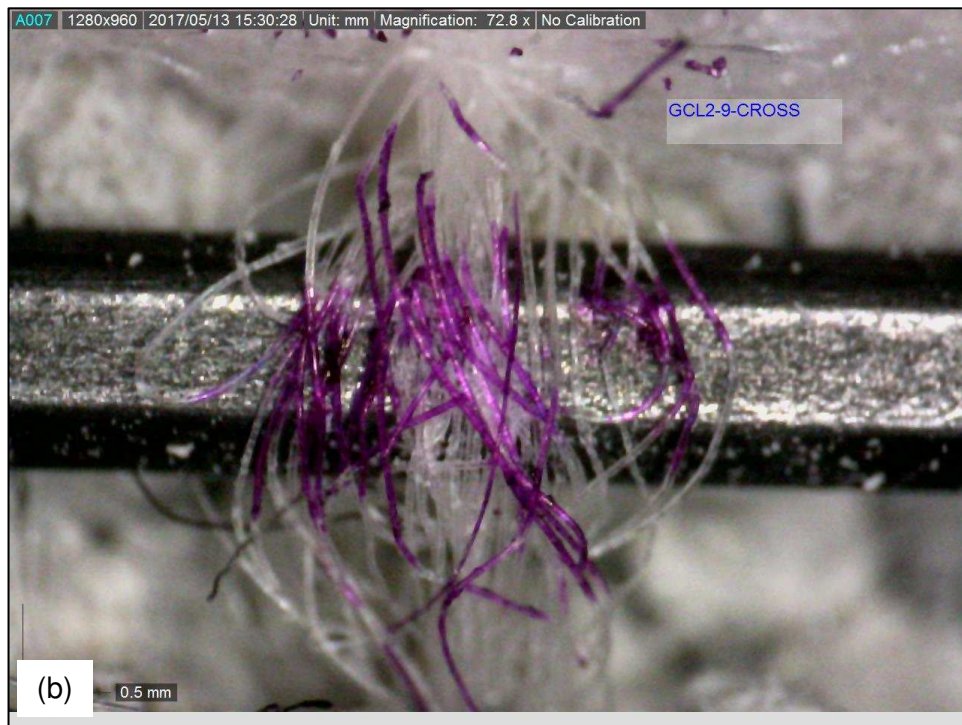
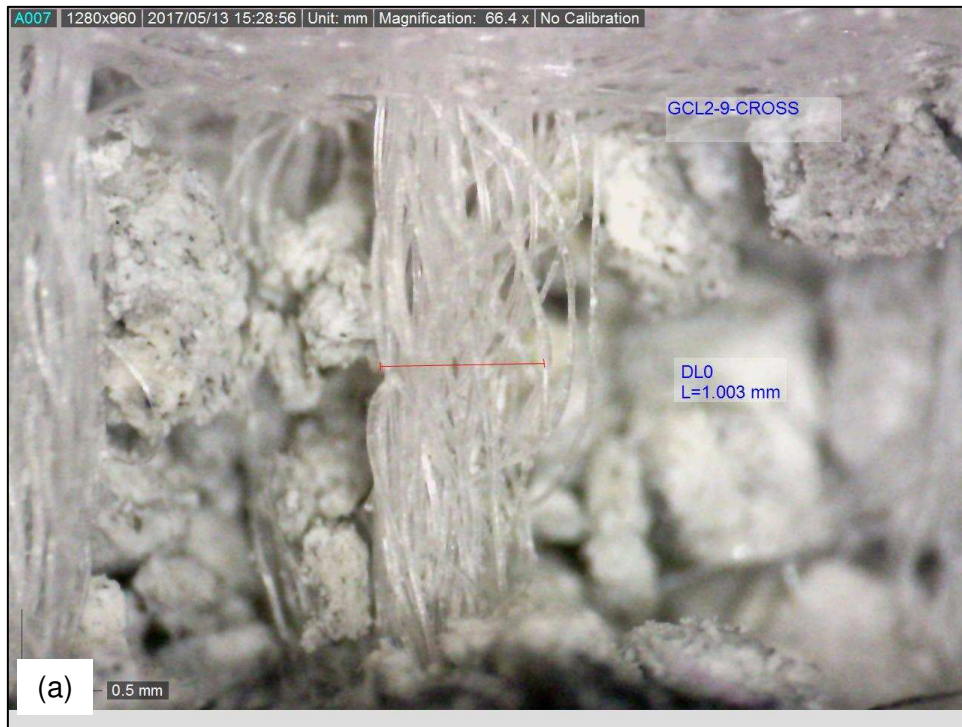


Figure B.38. Fiber bundle sample GCL2-9-CROSS. (a) Determination of the fiber bundle thickness. (b) Determination of the number of monofilament fibers per fiber bundle.

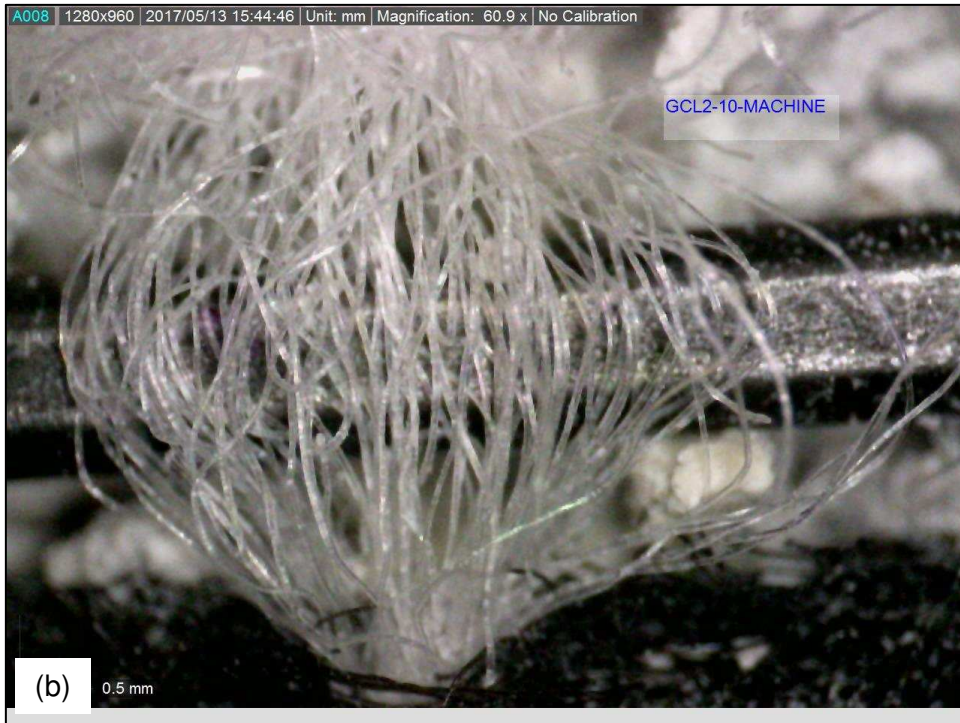
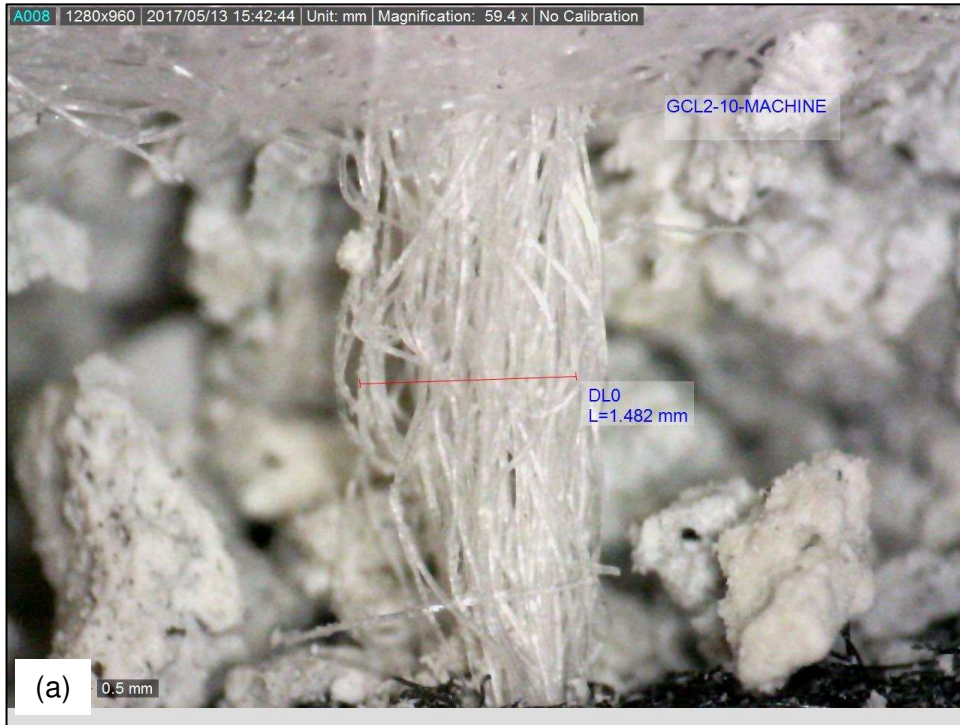


Figure B.39. Fiber bundle sample GCL2-10-MACHINE. (a) Determination of the fiber bundle thickness. (b) Determination of the number of monofilament fibers per fiber bundle.



Figure B.40. Fiber bundle sample GCL2-10-CROSS. (a) Determination of the fiber bundle thickness. (b) Determination of the number of monofilament fibers per fiber bundle.

B.1 Determination of needle-punched fiber bundle properties for GCL-3

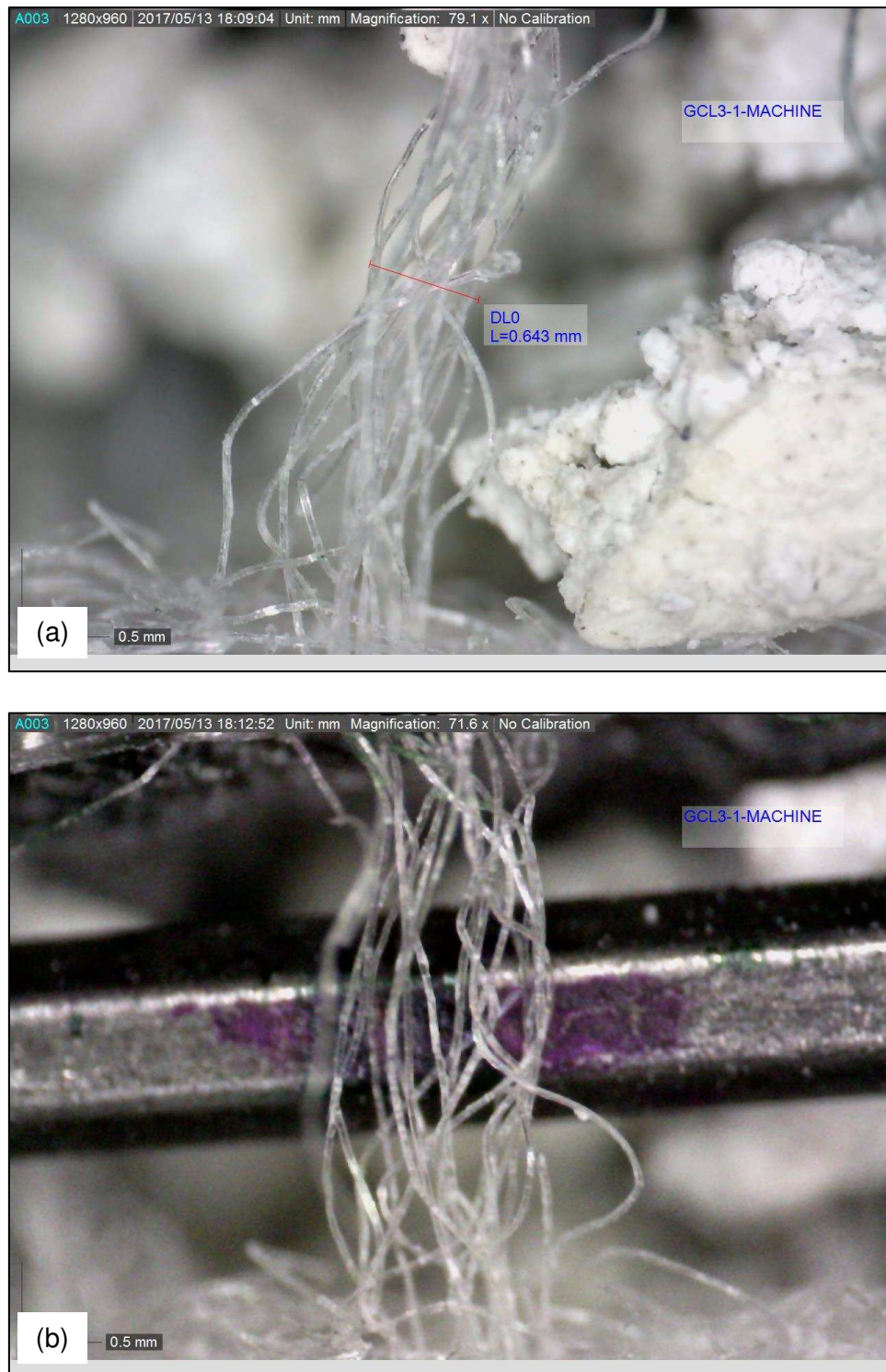


Figure B.41. Fiber bundle sample GCL3-1-MACHINE. (a) Determination of the fiber bundle thickness. (b) Determination of the number of monofilament fibers per fiber bundle.

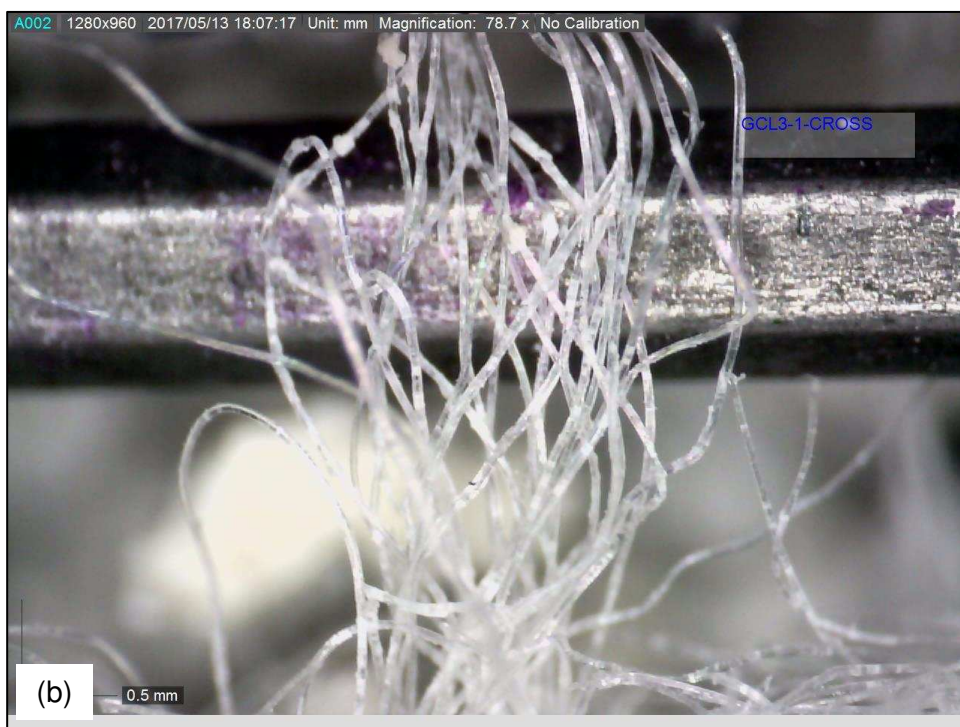


Figure B.42. Fiber bundle sample GCL3-1-CROSS. (a) Determination of the fiber bundle thickness. (b) Determination of the number of monofilament fibers per fiber bundle.

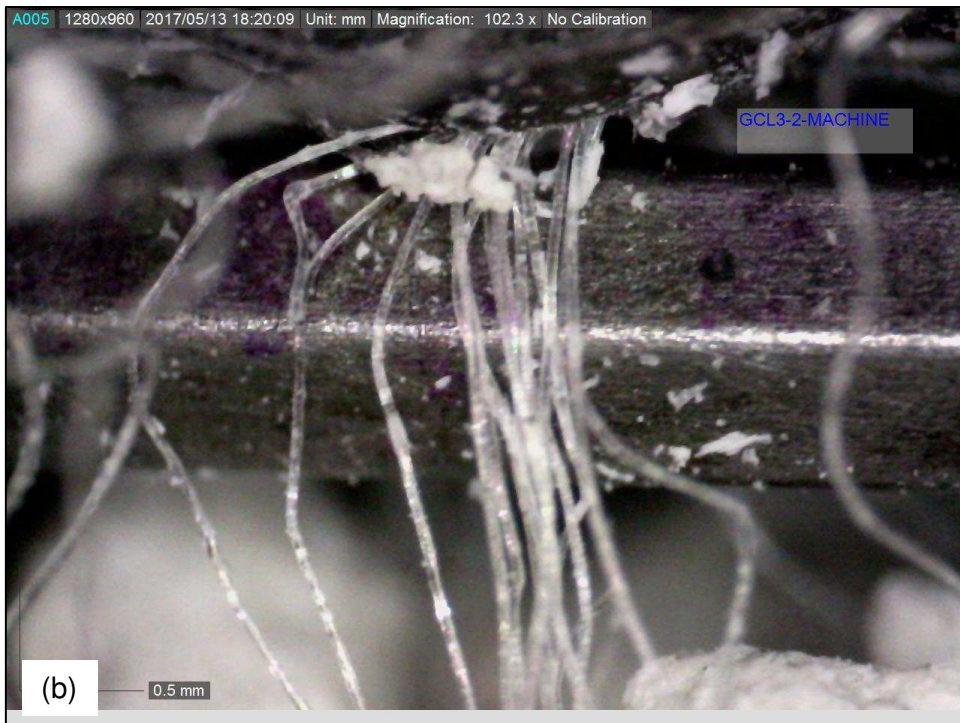


Figure B.43. Fiber bundle sample GCL3-2-MACHINE. (a) Determination of the fiber bundle thickness. (b) Determination of the number of monofilament fibers per fiber bundle.

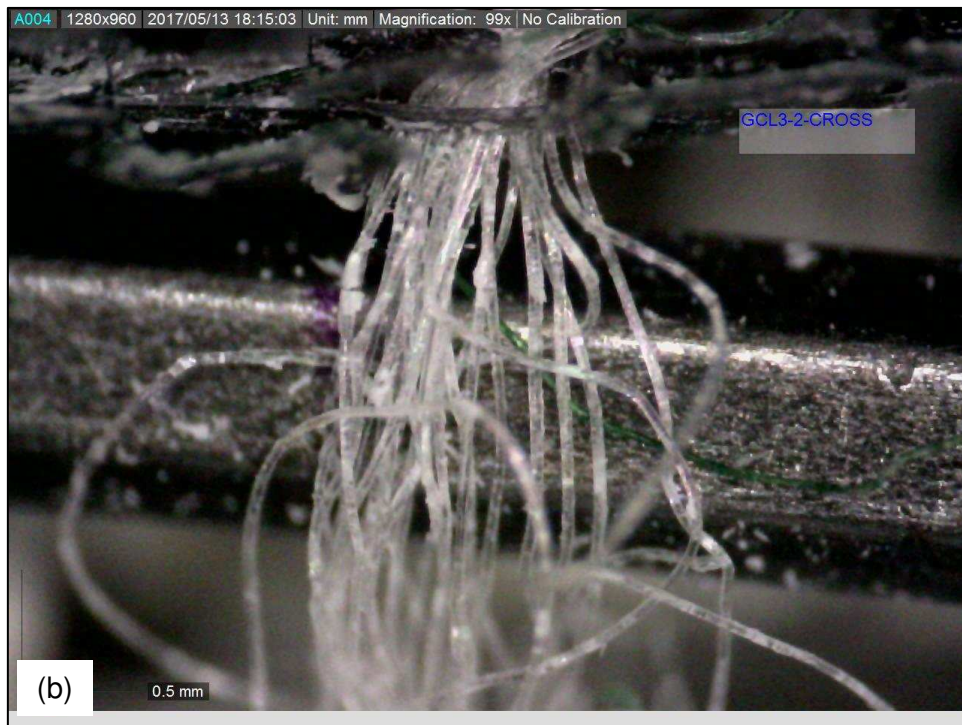


Figure B.44. Fiber bundle sample GCL3-2-CROSS. (a) Determination of the fiber bundle thickness. (b) Determination of the number of monofilament fibers per fiber bundle.



Figure B.45. Fiber bundle sample GCL3-3-MACHINE. (a) Determination of the fiber bundle thickness. (b) Determination of the number of monofilament fibers per fiber bundle.

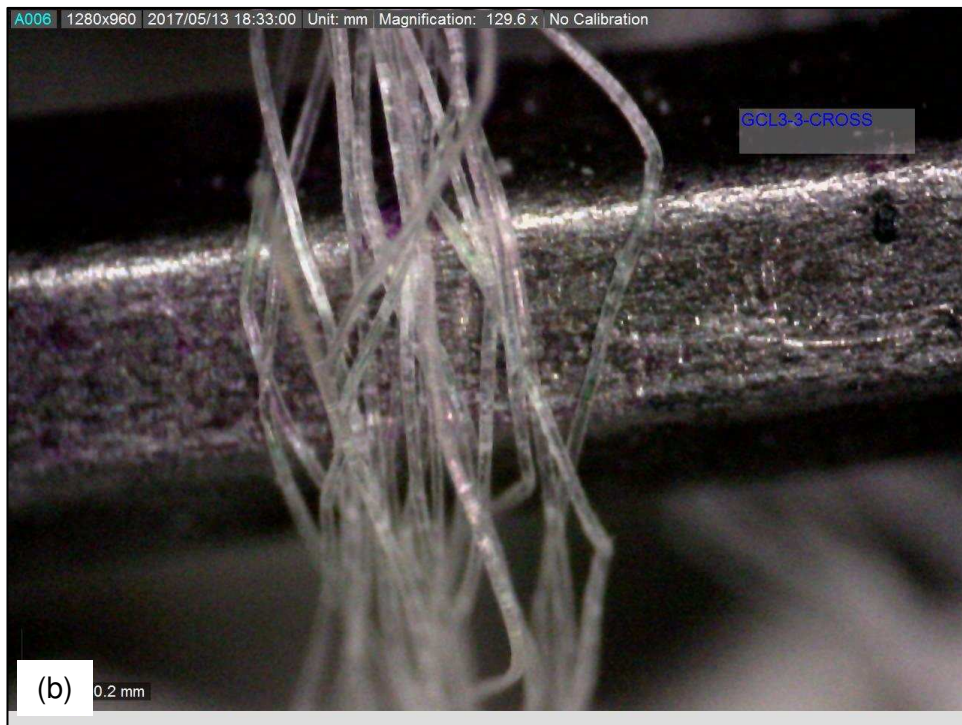


Figure B.46. Fiber bundle sample GCL3-3-CROSS. (a) Determination of the fiber bundle thickness. (b) Determination of the number of monofilament fibers per fiber bundle.

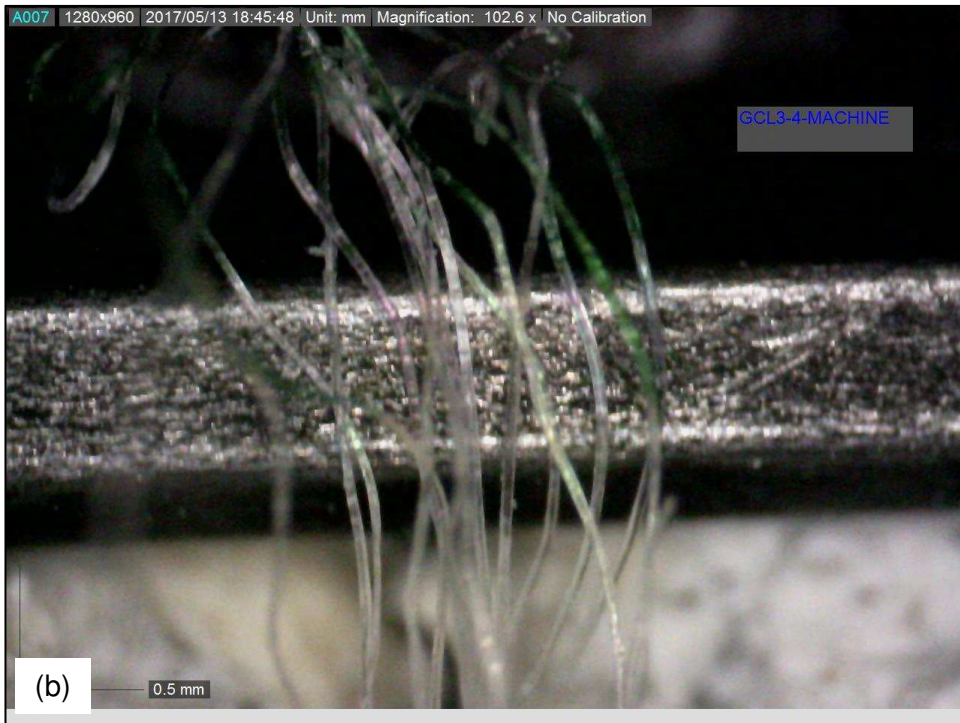
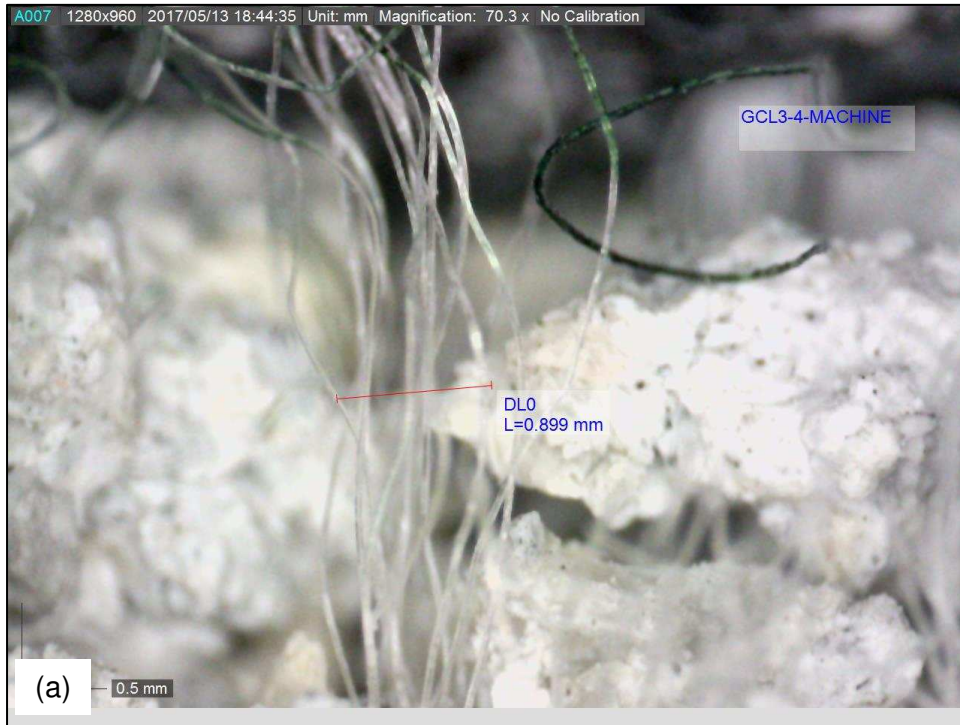


Figure B.47. Fiber bundle sample GCL3-4-MACHINE. (a) Determination of the fiber bundle thickness. (b) Determination of the number of monofilament fibers per fiber bundle.

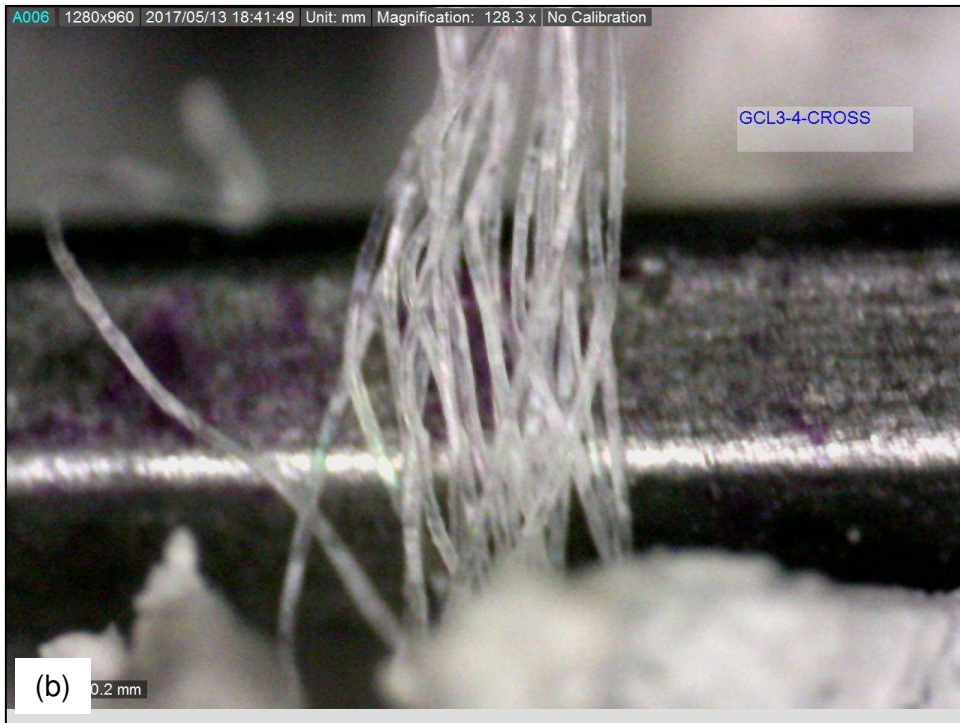


Figure B.48. Fiber bundle sample GCL3-4-CROSS. (a) Determination of the fiber bundle thickness. (b) Determination of the number of monofilament fibers per fiber bundle.

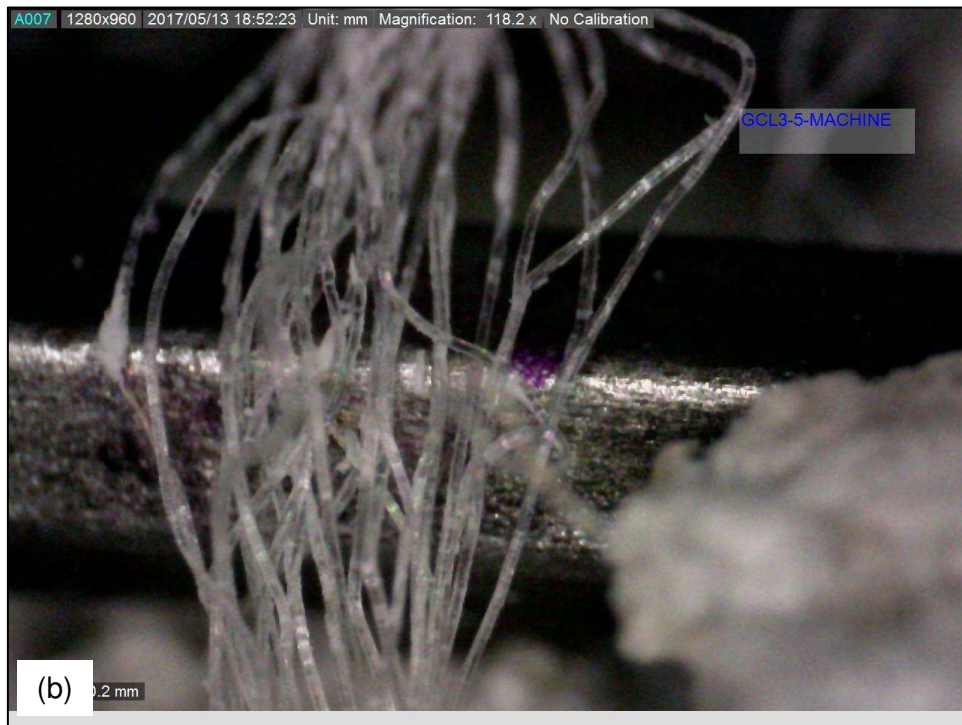
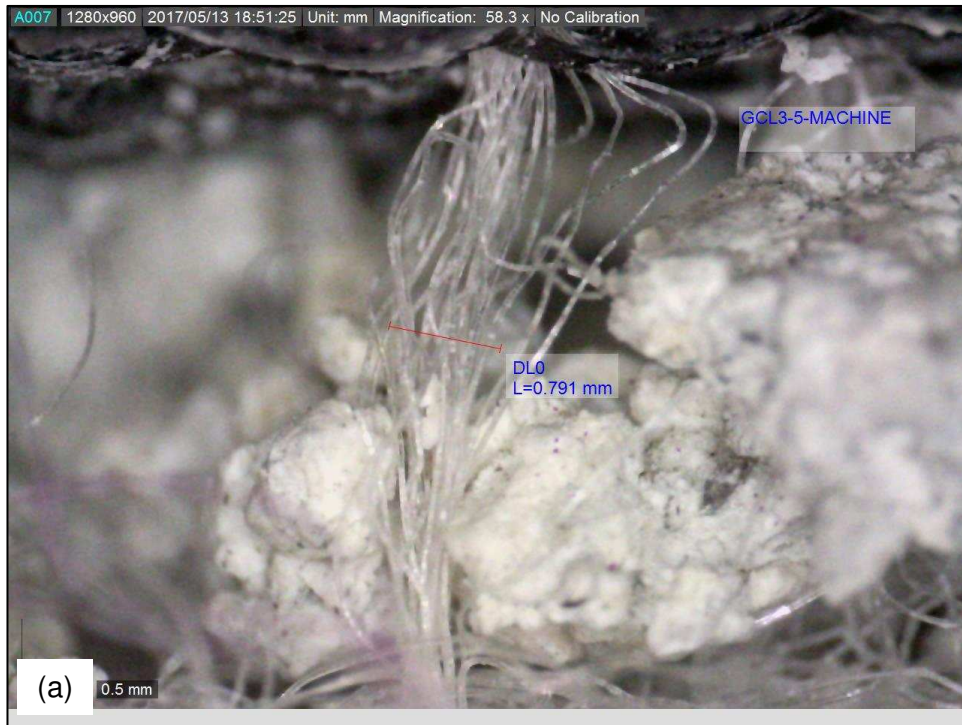


Figure B.49. Fiber bundle sample GCL3-5-MACHINE. (a) Determination of the fiber bundle thickness. (b) Determination of the number of monofilament fibers per fiber bundle.

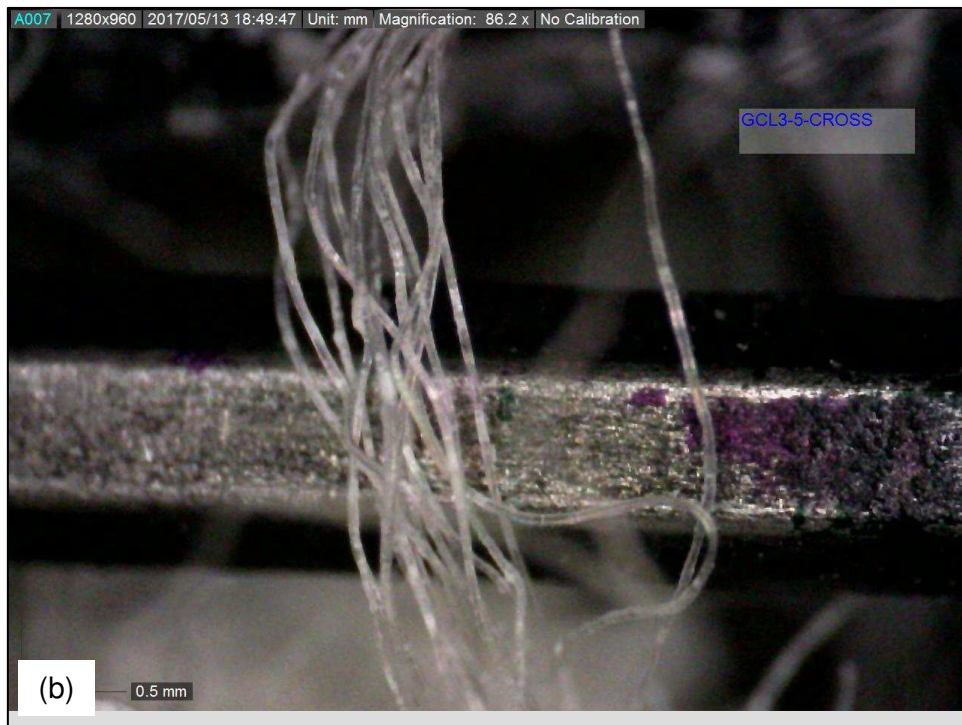


Figure B.50. Fiber bundle sample GCL3-5-CROSS. (a) Determination of the fiber bundle thickness. (b) Determination of the number of monofilament fibers per fiber bundle.

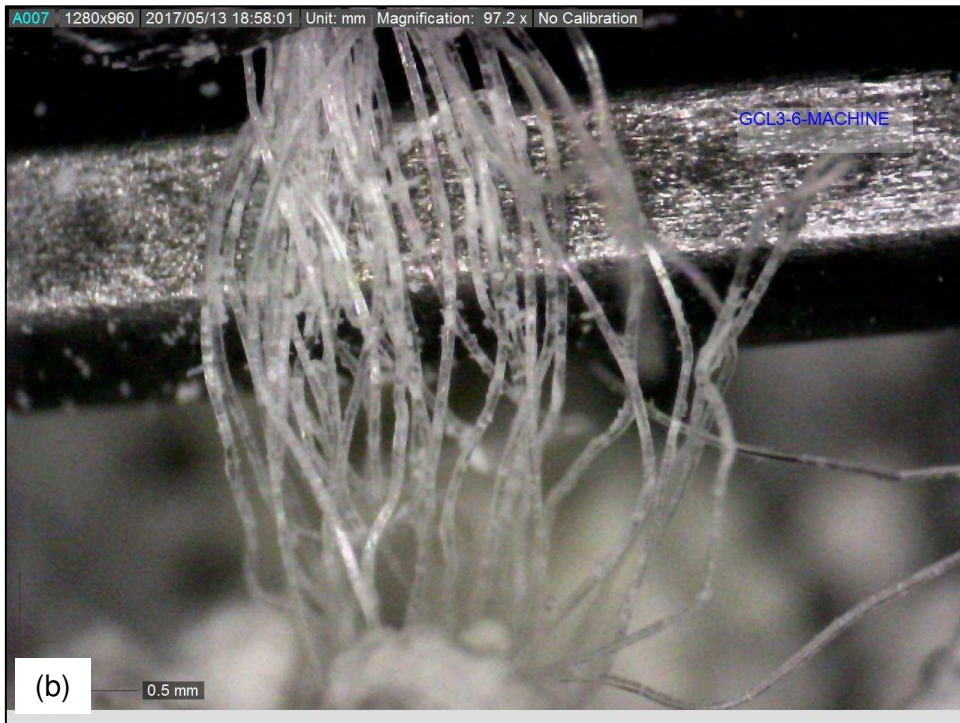


Figure B.51. Fiber bundle sample GCL3-6-MACHINE. (a) Determination of the fiber bundle thickness. (b) Determination of the number of monofilament fibers per fiber bundle.

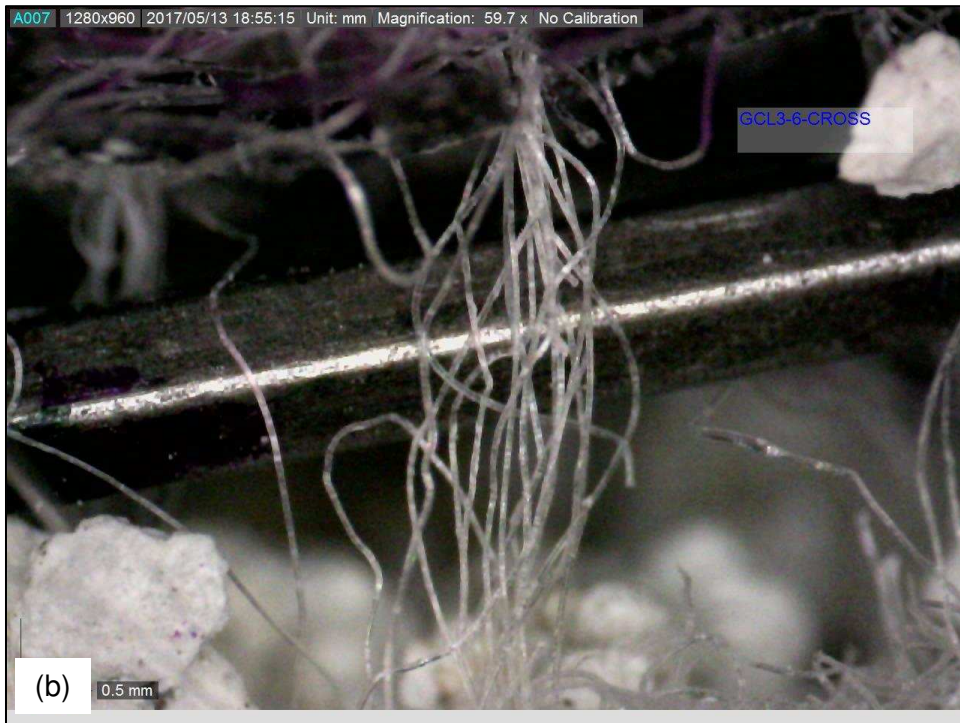
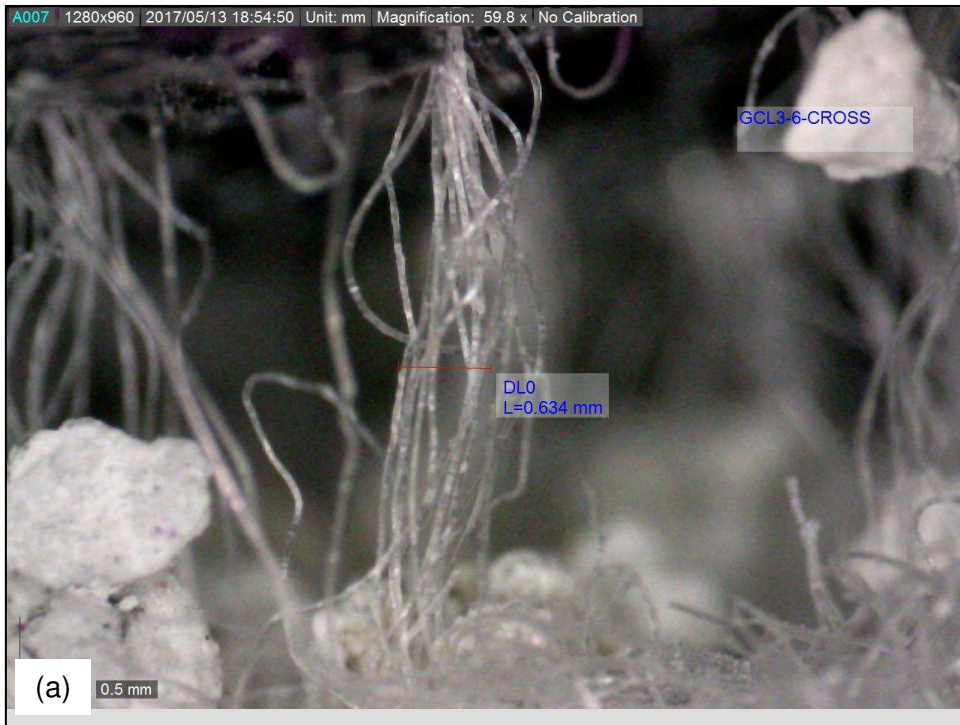


Figure B.52. Fiber bundle sample GCL3-6-CROSS. (a) Determination of the fiber bundle thickness. (b) Determination of the number of monofilament fibers per fiber bundle.

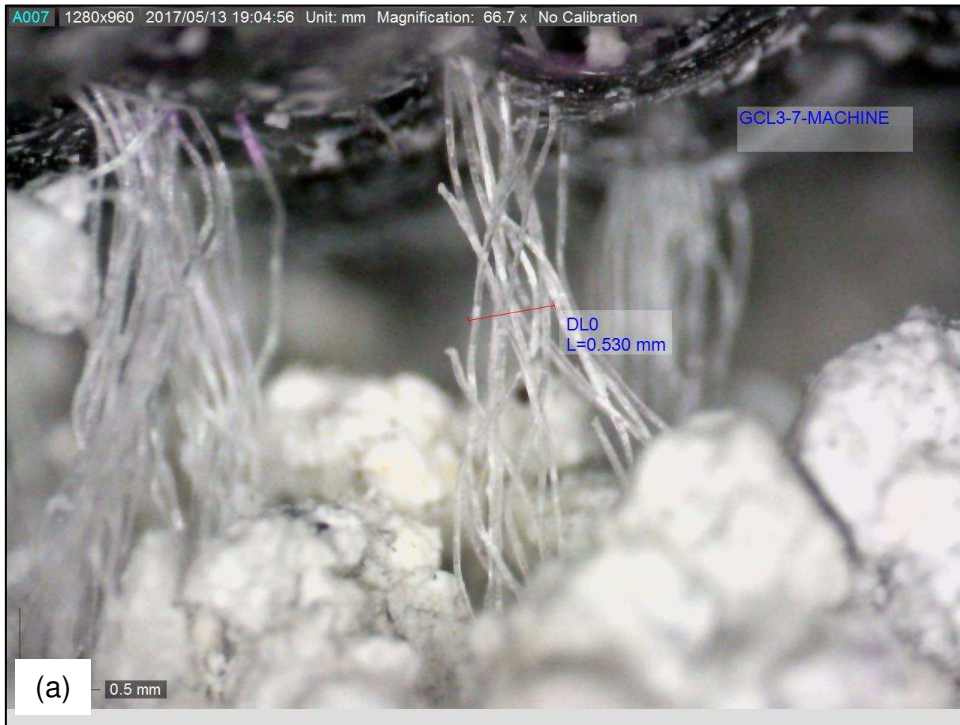


Figure B.53. Fiber bundle sample GCL3-7-MACHINE. (a) Determination of the fiber bundle thickness. (b) Determination of the number of monofilament fibers per fiber bundle.

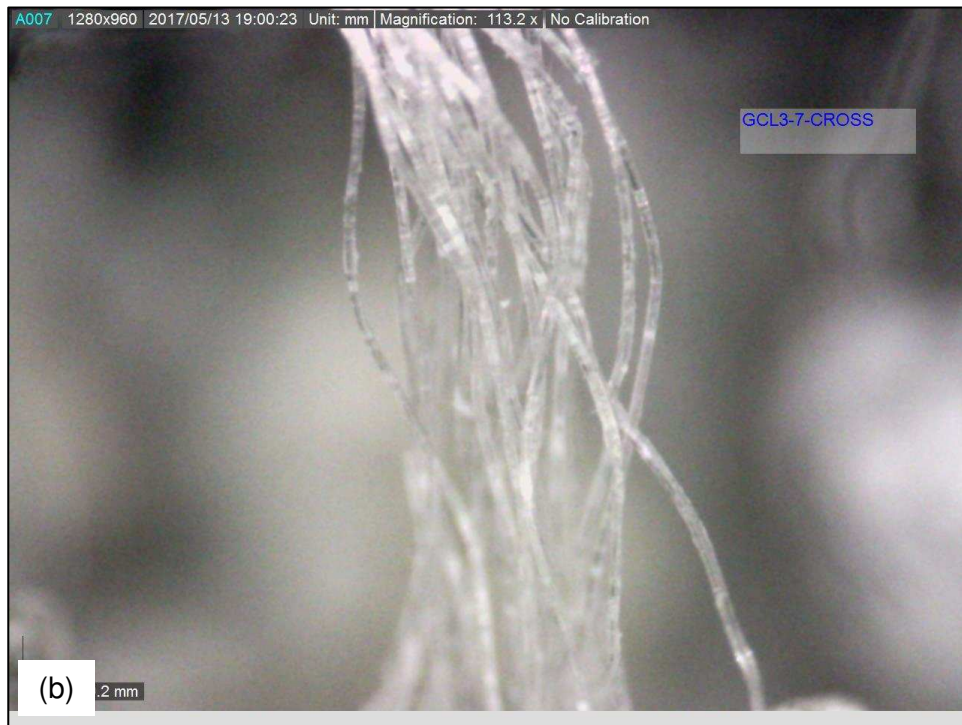
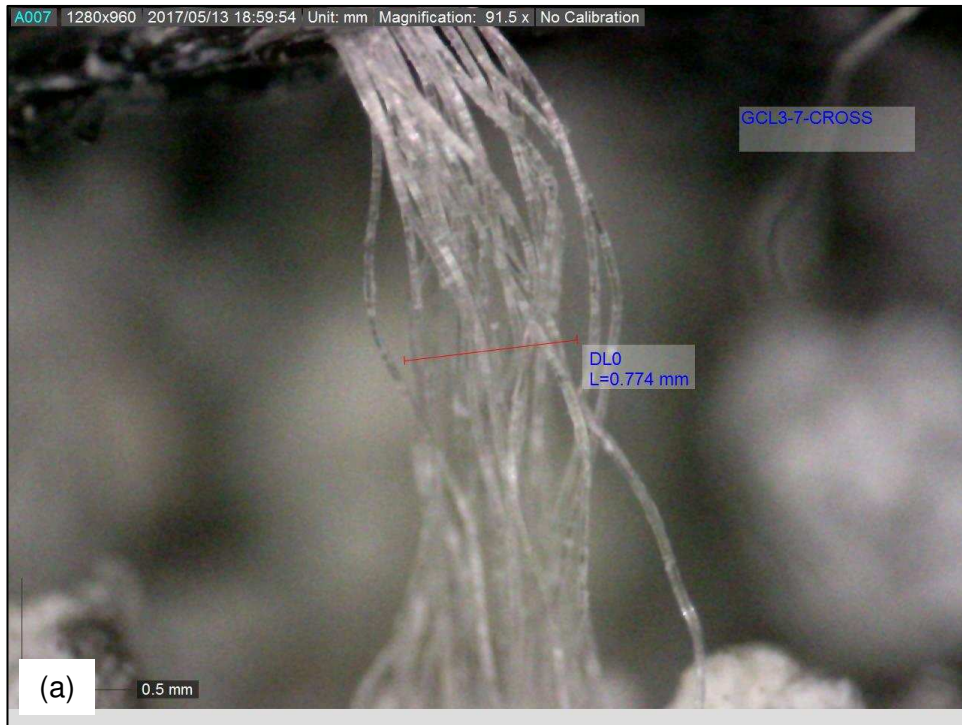


Figure B.54. Fiber bundle sample GCL3-7-CROSS. (a) Determination of the fiber bundle thickness. (b) Determination of the number of monofilament fibers per fiber bundle.

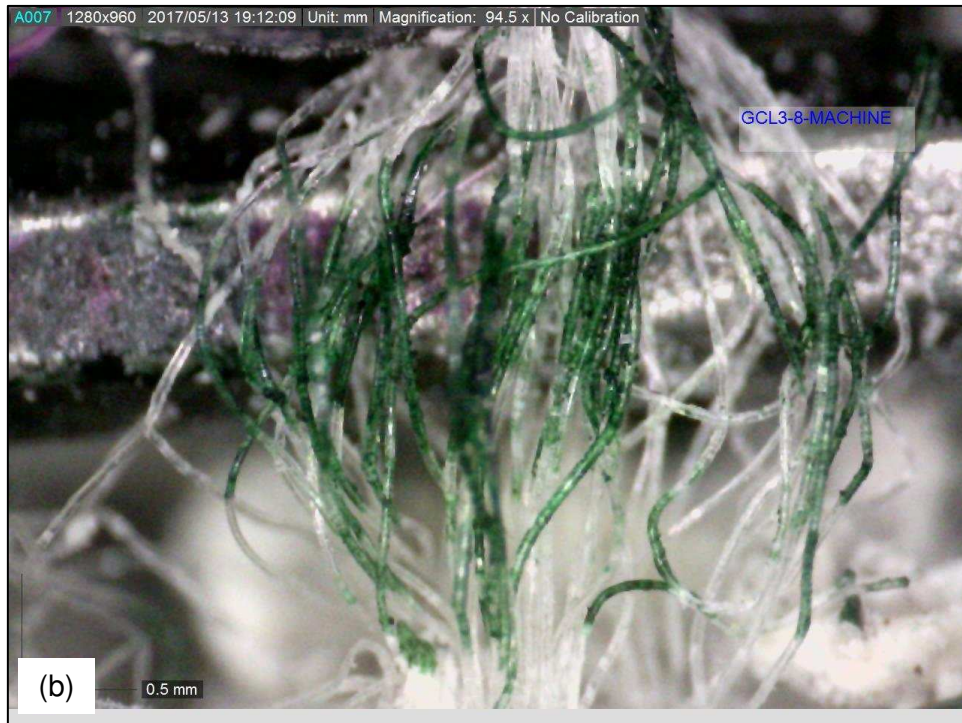
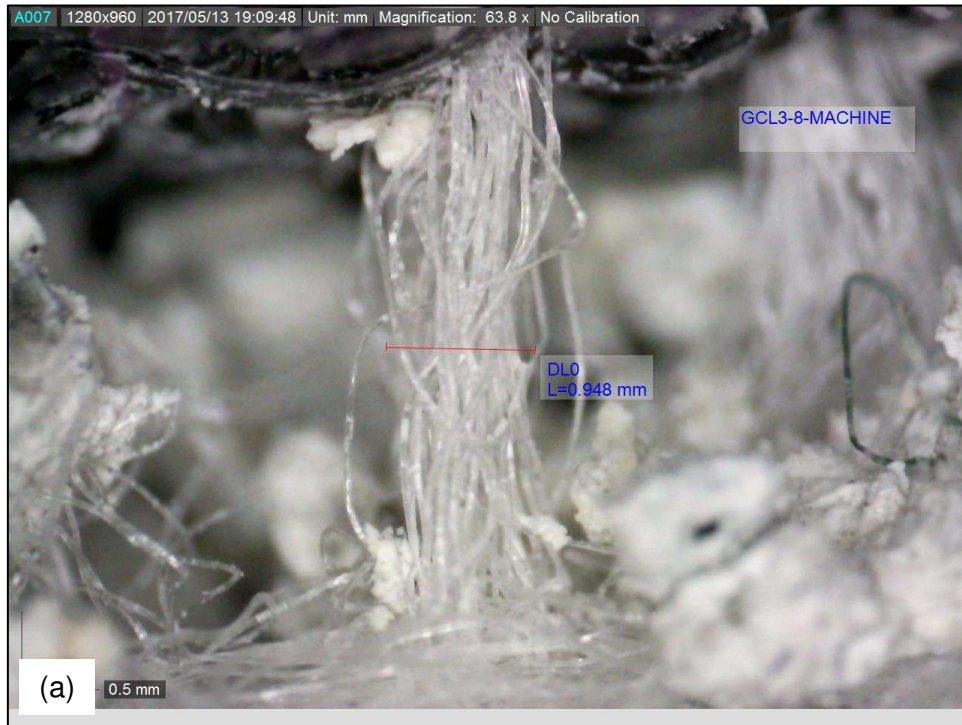


Figure B.55. Fiber bundle sample GCL3-8-MACHINE. (a) Determination of the fiber bundle thickness. (b) Determination of the number of monofilament fibers per fiber bundle.



Figure B.56. Fiber bundle sample GCL3-8-CROSS. (a) Determination of the fiber bundle thickness. (b) Determination of the number of monofilament fibers per fiber bundle.

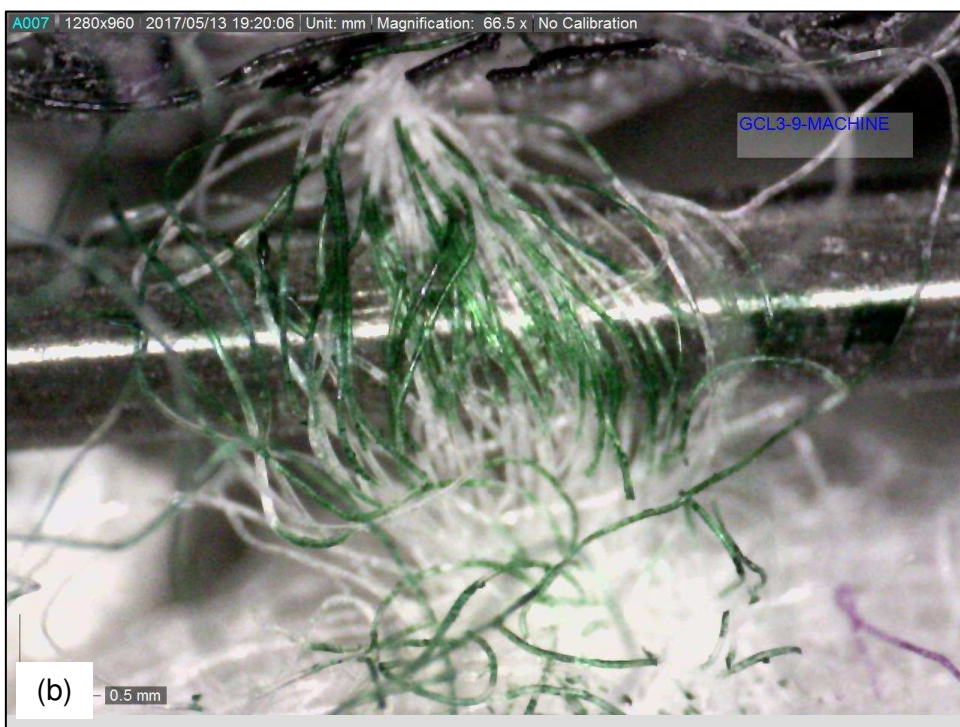
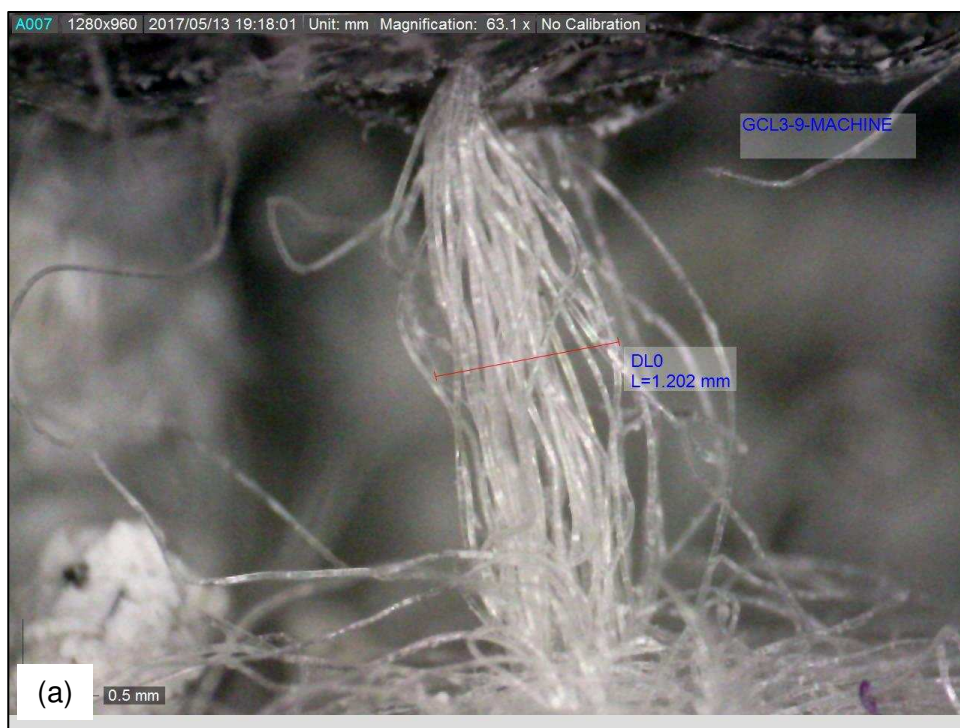


Figure B.57. Fiber bundle sample GCL3-9-MACHINE. (a) Determination of the fiber bundle thickness. (b) Determination of the number of monofilament fibers per fiber bundle.

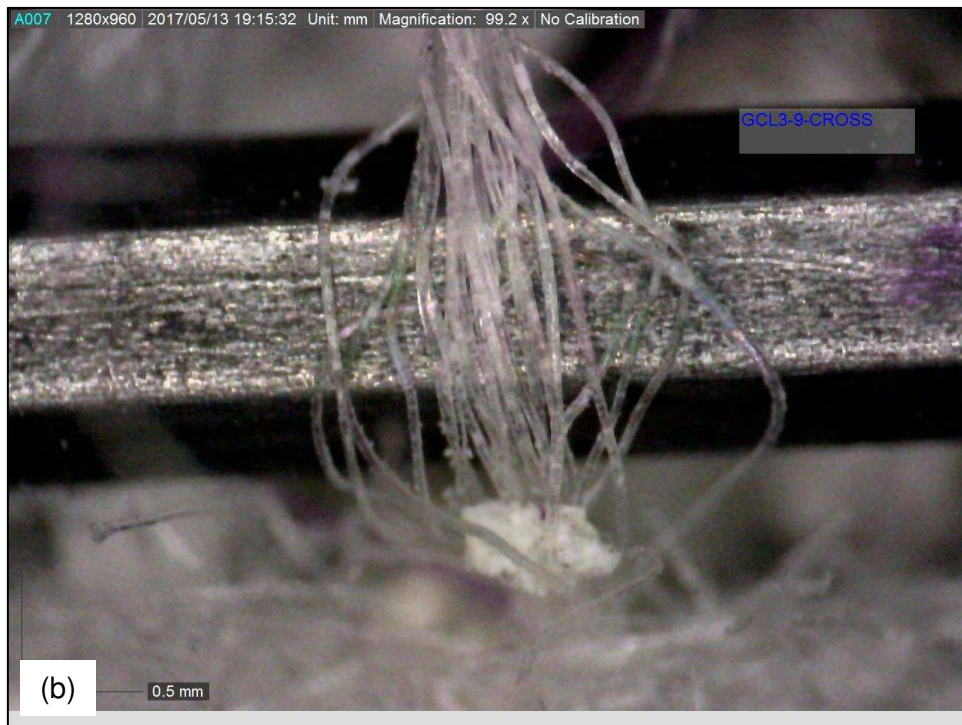


Figure B.58. Fiber bundle sample GCL3-9-CROSS. (a) Determination of the fiber bundle thickness. (b) Determination of the number of monofilament fibers per fiber bundle.

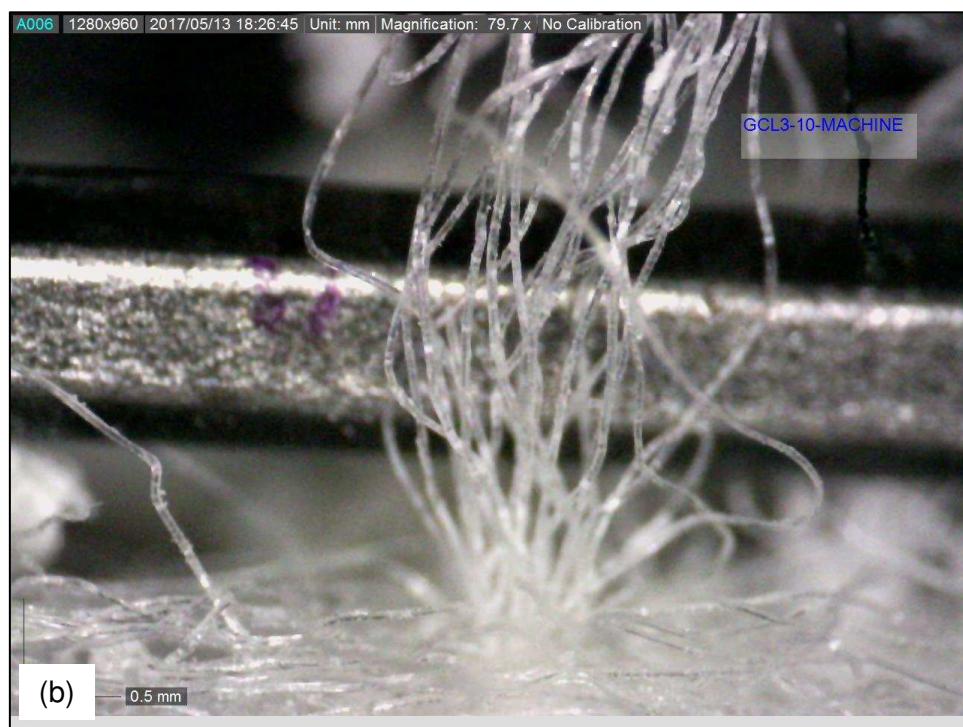
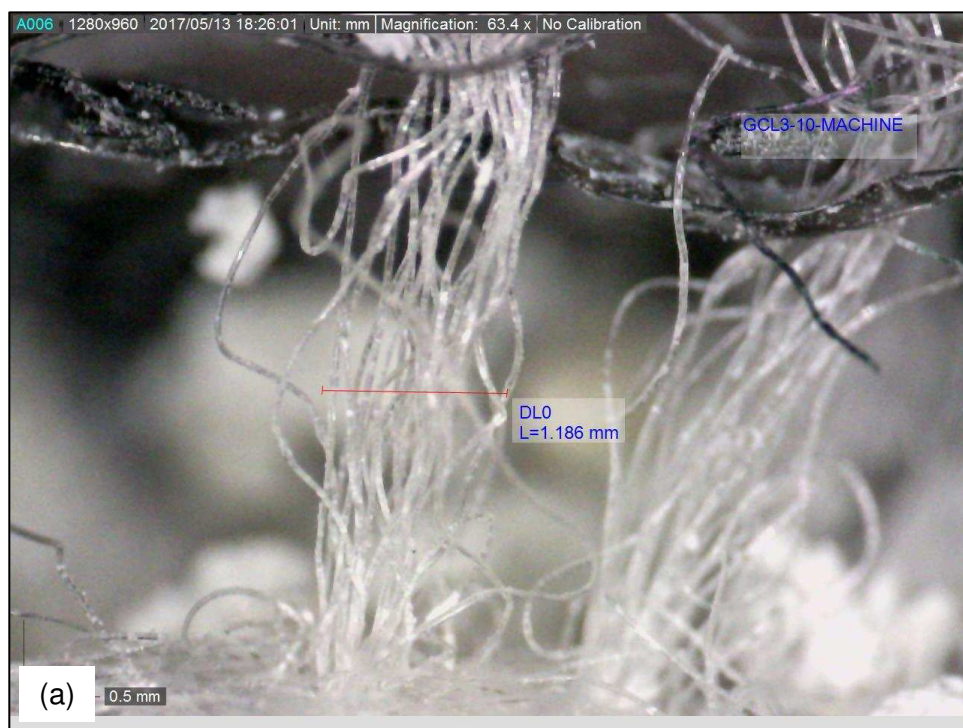


Figure B.59. Fiber bundle sample GCL3-10-MACHINE. (a) Determination of the fiber bundle thickness. (b) Determination of the number of monofilament fibers per fiber bundle.

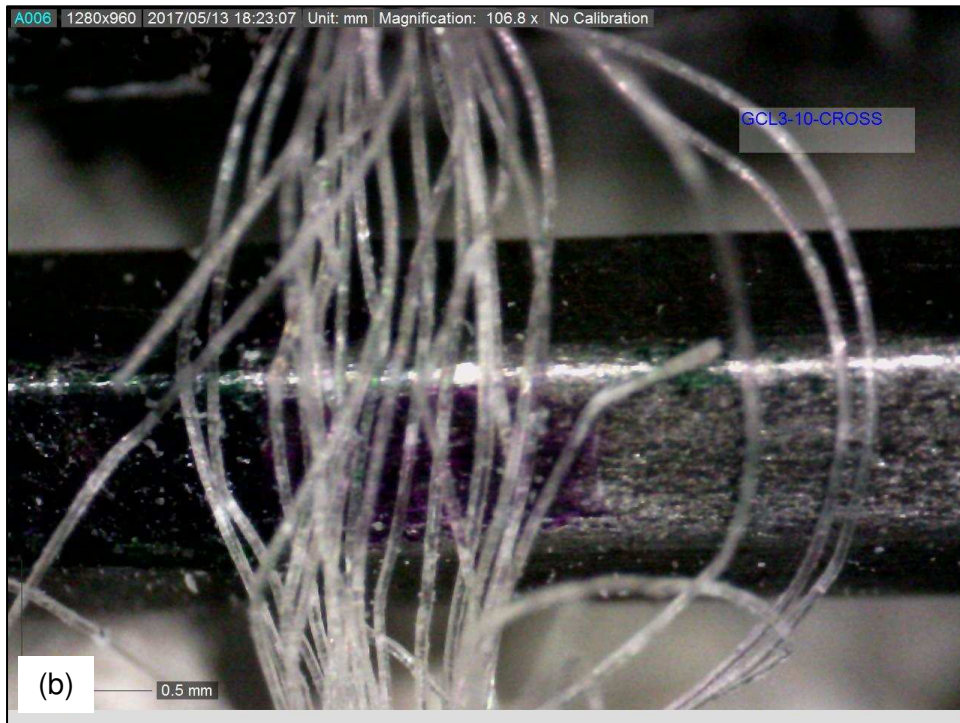


Figure B.60. Fiber bundle sample GCL3-10-CROSS. (a) Determination of the fiber bundle thickness. (b) Determination of the number of monofilament fibers per fiber bundle.

B.5 Data analysis plots

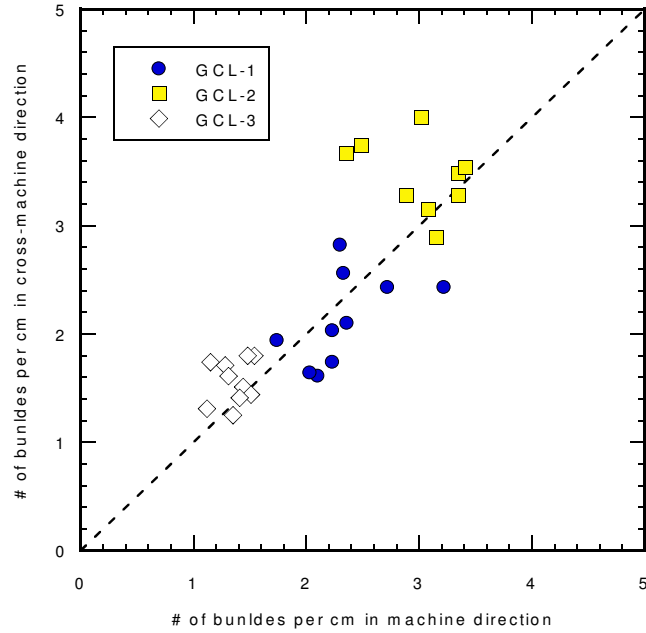


Figure B.61. Number of fiber bundles per cm counted in the machine direction versus the number of fiber bundles per cm counted in the cross machine direction.

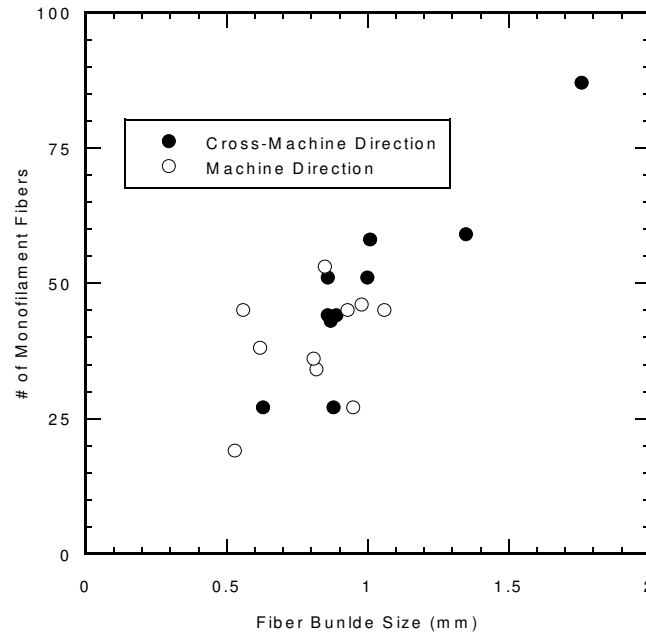


Figure B.62. Fiber bundle size (mm) versus the number of monofilament fibers per fiber bundle for GCL-1

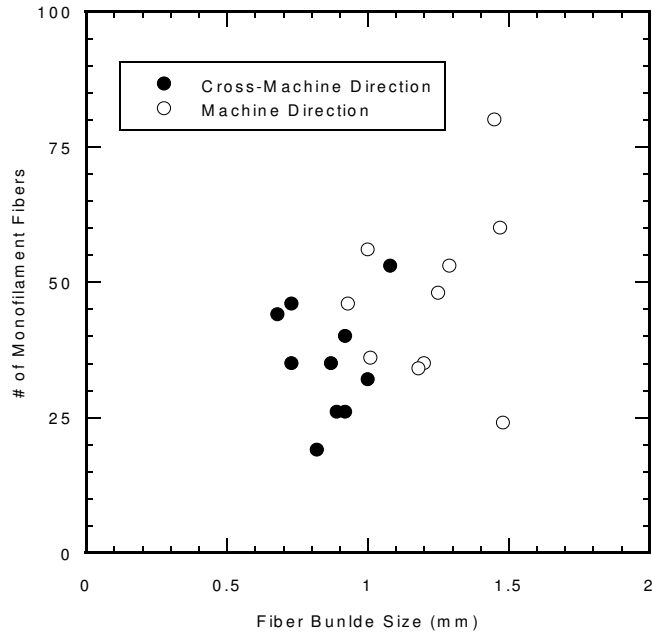


Figure B.63. Fiber bundle size (mm) versus the number of monofilament fibers per fiber bundle for GCL-2

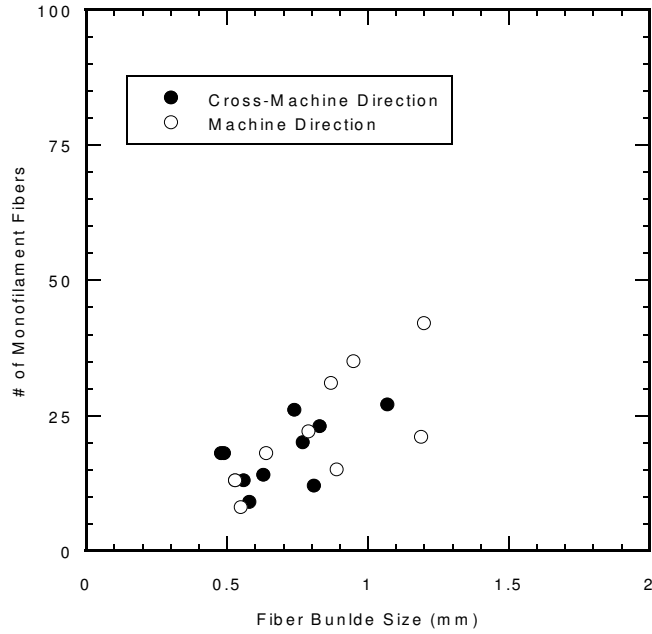


Figure B.64. Fiber bundle size (mm) versus the number of monofilament fibers per fiber bundle for GCL-3

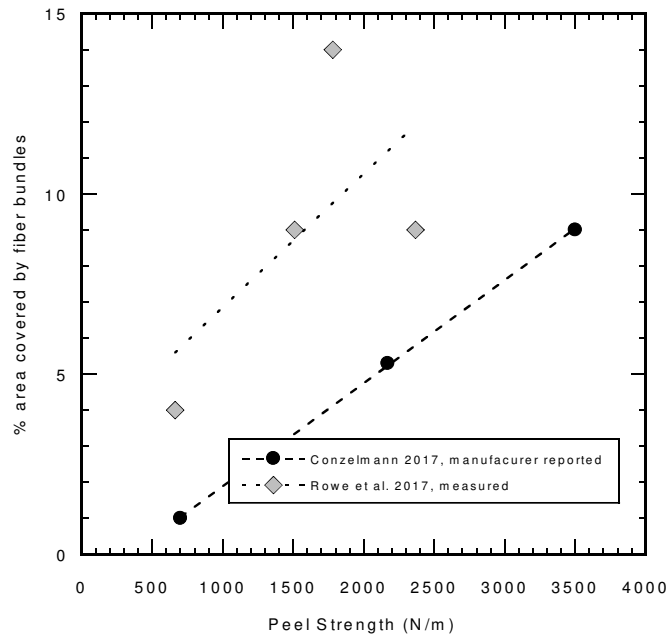


Figure B.65. Comparison of percent area of GCL covered by fiber bundles to data in Rowe et al. 2017. Note that the peel strength for this study is manufacturer reported while Rowe et al. 2017 uses measured peel strength

APPENDIX C

Burette Stand Calibration

The burette stands used for hydraulic conductivity testing by the gravity method are made of wood and consist of towers with numbered pinholes, and frames that are attached to the towers through any one of the pinholes. Each stand contains two towers and two frames. The frames hold the burettes and each have the capacity for eight burettes. Figure C.6 shows an image of one of the stands used. The stands were designed and built by CSU undergraduate research assistant Justin Thompson.

The equation presented below can be used to calculate the head loss across the specimen based on the liquid level in the burette:

$$\Delta h = R(50 - w) + a + b(N-1) - c - x + y \quad (C.1)$$

where Δh is the head loss across the specimen in cm, R is the ratio of distance in cm to one mL mark on the burette, w is the liquid level in the burette recorded in mL, a , b , and c are calibration numbers for the burette stand used (provided in Table C.1), N is the pinhole number where the burette frame is placed on the tower for a given test (Figure C.1,C.2), x is the distance from the floor to the permeameter outlet for a given test (Figure C.4), and y is the distance from the burette frame base to the 50 mL mark on the burette for a given test (Figure C.5).

For tests where unmarked glass tubes with attached markings are used in place of manufactured burettes with mL marks, R would become 1, the inverse slope correction of multiplying R by $(50 - w)$ could be negated by placing the cm markings in such a way that there is an increase in value with increasing elevation, (the manufactured glass burettes decrease in mL markings with increasing elevation), and thus Equation C.1 could simplify to:

$$\Delta h = w + a + b(N-1) - c - x + y \quad (\text{C.2})$$

where all of the variables are the same except for w which would now be recorded in cm instead of mL. Variables a , b , c , x , and y all also have units of cm and would need to be corrected if alternative units for w are desired.

Table C.1. Burette frame calibration

Stand	a	b	c
#1	50.1	5.0	31.1
#2	46.9	5.0	31.1
#3	46.9	5.0	31.1
#4	47.1	5.0	31.1

a = distance from floor to first pinhole measured in cm (Figure C.1)

b = distance between pinholes measured in cm (Figure C.2)

c = distance from the location of the pin on the frame to the frame base measured in cm (Figure C.3)

Values presented represent an average of four measurements



Figure C.1. Measurement of variable a , the distance from floor to the first pinhole measured in cm.

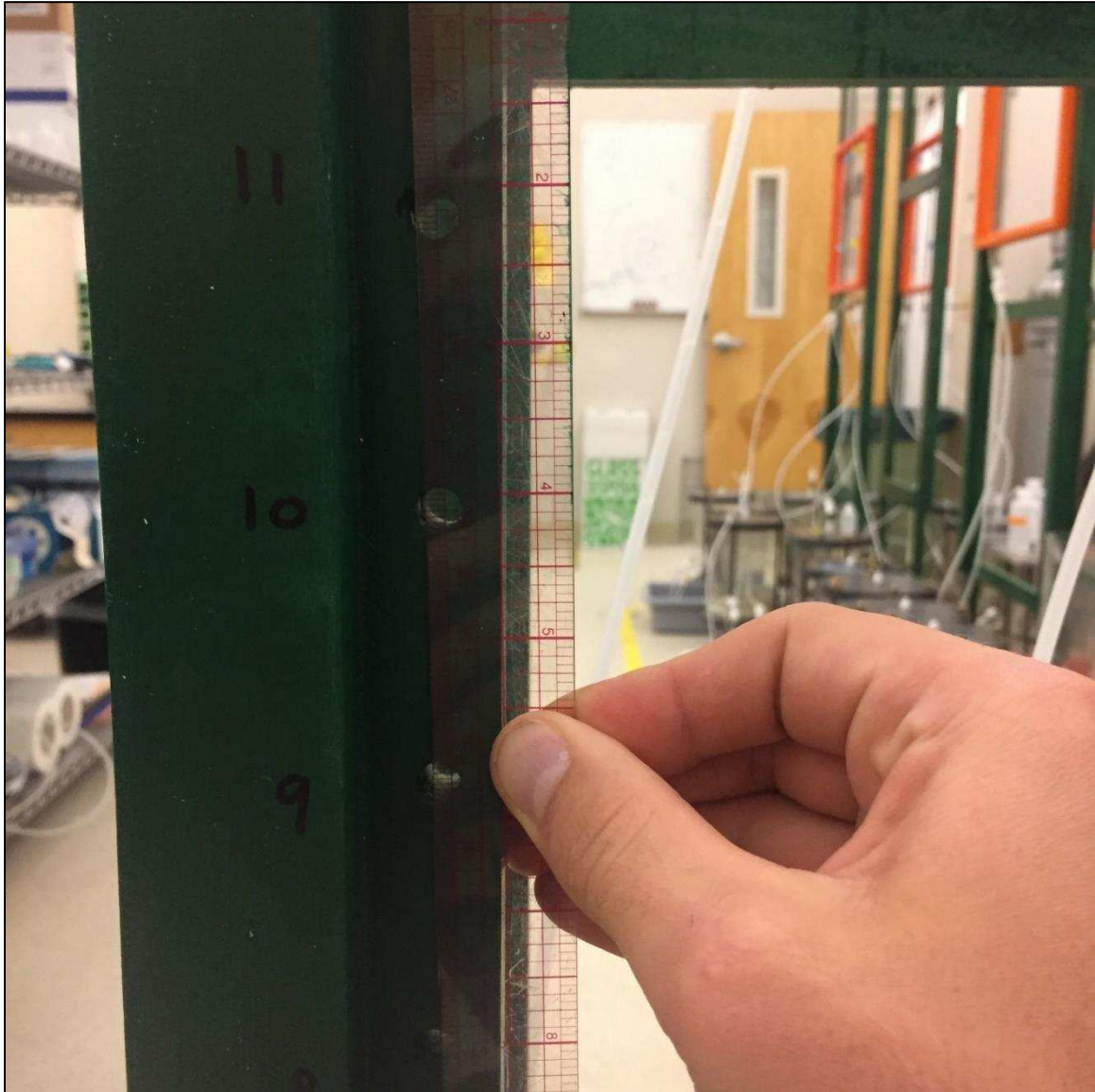


Figure C.2 Measurement of variable b , the distance between pinholes measured in cm.

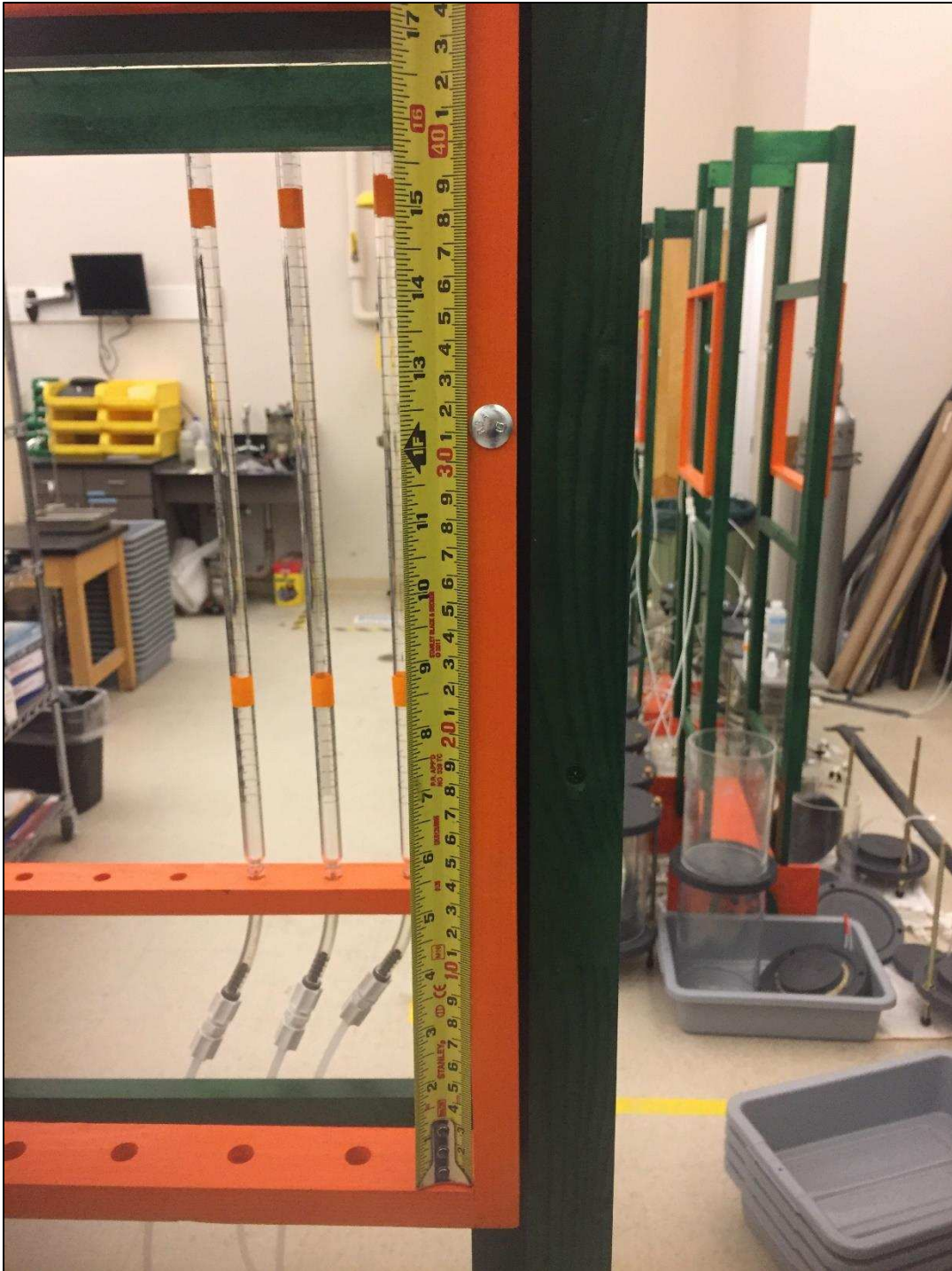


Figure C.3. Measurement of variable c , the distance from the location of the pin on the frame to the frame base measured in cm.

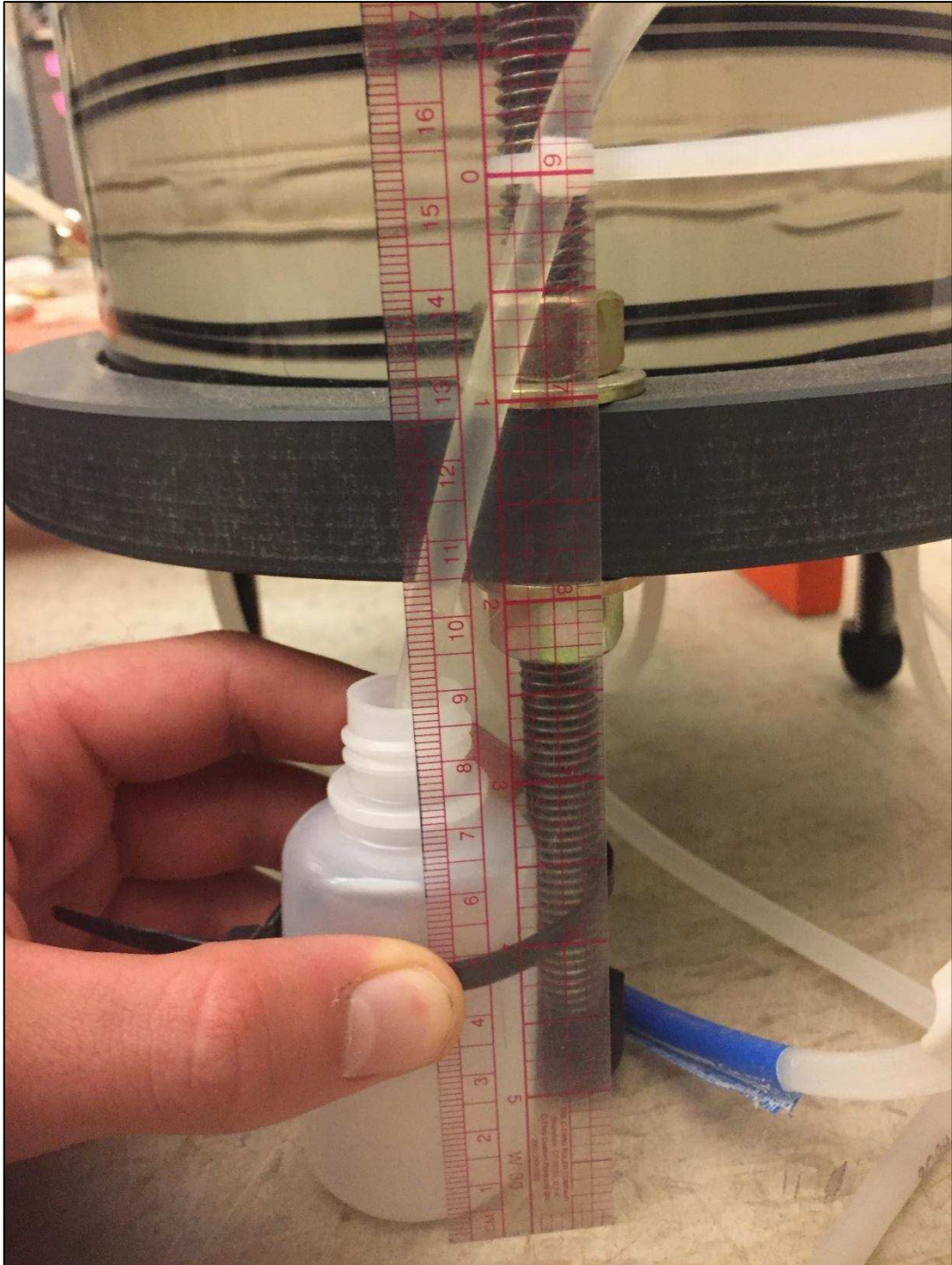


Figure C.4. Measurement of variable x , the distance from the floor to the permeameter outlet for a given test.

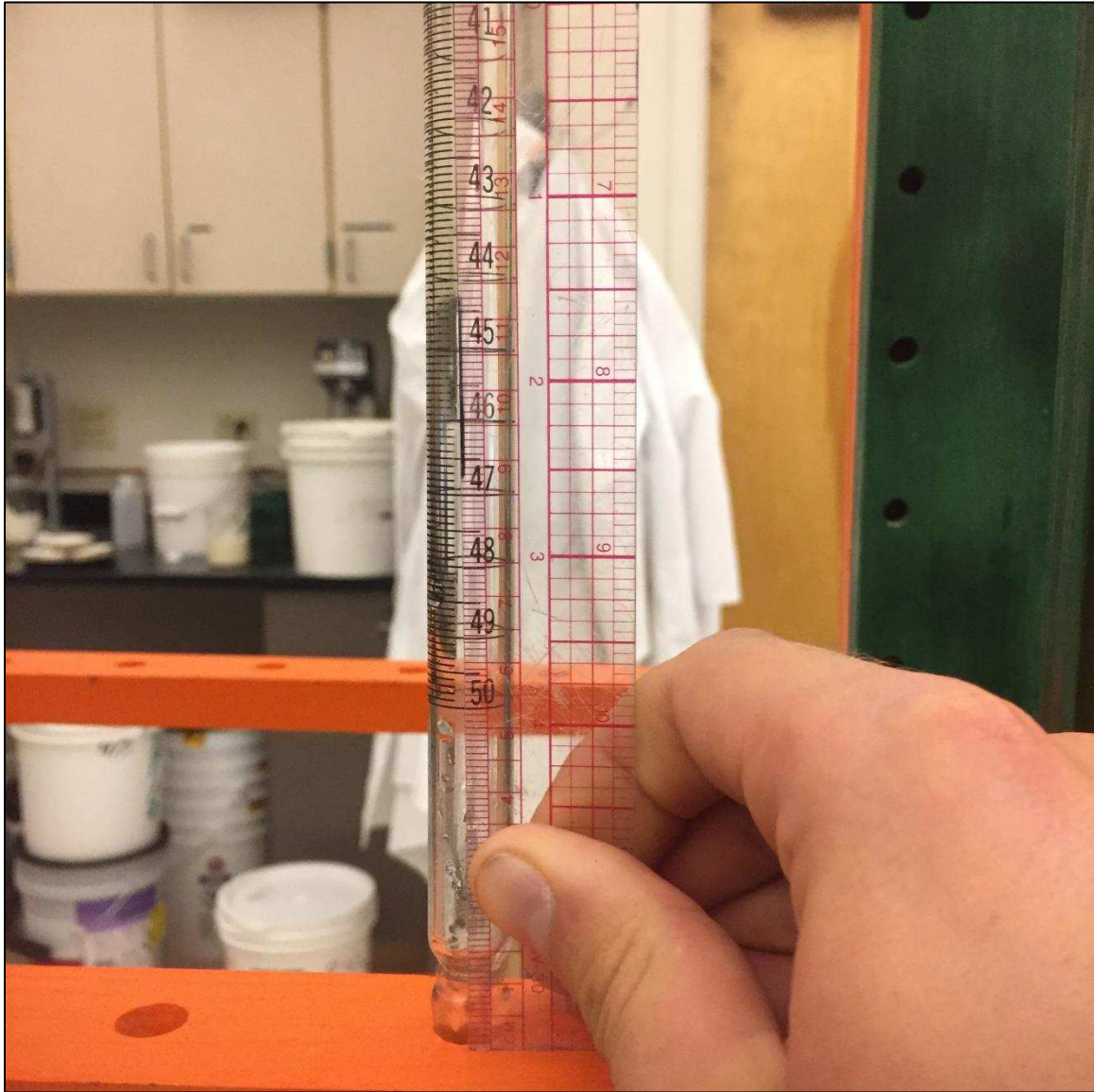


Figure C.5. Measurement of variable y , the distance from the burette frame base to the 50 mL mark on the burette for a given test.



Figure C.6. Burette Stand. The towers are painted green while the frames are painted orange. The base that holds up the towers is also painted orange.

APPENDIX D
Data Summary Tables

Table D.1. Summary of hydraulic and chemical properties of tests conducted in Chapter 2

Test Series	Test Number	Material	Method	Test Liquid	Test ID	Elapsed Time (days)	Pore Volumes of Flow, PVF	Pore Volumes of Flow, PVF ^(g)	EC Ratio, EC _{out} /EC _{in}	pH Ratio, pH _{out} /pH _{in}	Hydraulic Conductivity, k (m/s)	Hydraulic Conductivity, k (m/s) ^(g)
1	1a ^(b)	GCL-1	S-Method	CW	DN12-S-L1	81	13.4	15.4	2.37	1.20	6.7E-11	5.9E-11
	1b ^(b)	GCL-1	S-Method	CW	DN12-S-L2	57	4.7	5.4	6.84	1.28	2.5E-11	2.2E-11
	1c ^(a)	GCL-1	S-Method	CW	DN12-S-L3	88	tbid	tbid	3.03	1.11	3.4E-11	tbid
2	2a ^(b)	GCL-1	G-Method	CW	DN12-L1	0.18	3.6	4.2	N/A	N/A	5.3E-09	4.5E-09
	2b ^(b)	GCL-1	G-Method	CW	DN12-L2	0.13	2.3	2.6	N/A	N/A	6.1E-09	5.3E-09
	2c	GCL-1	G-Method	CW	DN12-L3	2.9	5.4	6.0	2.92	1.31	1.0E-09	9.2E-10
	2d ^(a)	GCL-1	G-Method	CW	DN12-L4	39	tbid	tbid	4.88	1.52	1.8E-11	tbid
3	3a	GCL-1	S-Method	Au-PS	DN12-S-G1	45	1.7	1.9	2.77	1.48	1.5E-11	1.3E-11
	3b	GCL-1	S-Method	Au-PS	DN12-S-G2	84	8.5	10.5	1.36	1.40	3.5E-11	2.9E-11
	3c ^(a)	GCL-1	S-Method	Au-PS	DN12-S-G3	15	7.3	8.6	1.27	1.48	4.4E-11	3.8E-11
4	4a	GCL-1	G-Method	Au-PS	DN12-G1	1.4	9.0	10.7	1.07	1.33	5.7E-09	4.8E-09
	4b ^(b)	GCL-1	G-Method	Au-PS	DN12-G2	0.040	3.6	4.2	N/A	N/A	2.6E-08	2.3E-08
	4c	GCL-1	G-Method	Au-PS	DN12-G2	1.6	2.0	2.4	1.66	1.62	4.9E-10	4.3E-10
5	5a ^(a)	GCL-1	S-M1	CW	DN12-S-L4	53	5.1	6.1	4.56	1.37	3.6E-11	3.1E-11
6	6a ^(a)	GCL-1	S-M2	CW	DN12-S-L5	58	4.5	4.8	4.09	1.29	2.9E-11	2.5E-11
7	7a	GCL-1	S-M3	CW	DN12-S-L6	62	5.1	5.9	4.54	1.23	3.8E-11	3.4E-11
8	8a	GCL-1	S-M4	CW	DN12-S-L8	61	4.4	4.9	6.36	1.21	2.5E-11	2.2E-11
	8b	GCL-1	S-M4	CW	DN12-S-L9	56	3.5	4.0	10.34	1.37	2.7E-11	2.3E-11
	9a	GCL-1	S-M5	CW	DN12-S-L10	47	3.1	3.7	8.90	1.44	2.3E-11	1.9E-11
10	10a ^(a)	GCL-2	S-Method	CW	DN9-S-L2	82	tbid	tbid	4.61	1.21	2.0E-11	tbid
	10b	GCL-2	S-Method	CW	DN9-S-L3	25	4.4	5.1	2.28	1.24	3.3E-11	2.9E-11
	10c	GCL-2	S-Method	CW	DN9-S-L4	18	6.1	6.9	2.07	1.28	3.3E-11	3.0E-11
11	11a ^(a)	GCL-2	G-Method	CW	DN9-L1	0.22	tbid	tbid	2.85	1.10	8.7E-09	tbid
	11b	GCL-2	G-Method	CW	DN9-L2	18	3.3	3.9	2.71	1.37	2.9E-11	2.5E-11
	11c	GCL-2	G-Method	CW	DN9-L3	0.79	2.5	2.9	2.29	1.55	1.5E-09	1.3E-09
12	12a	GCL-2	S-M6	CW	DN9-S-L5	38	7.0	8.9	3.32	1.27	2.6E-11	2.1E-11
	12b	GCL-2	S-M6	CW	DN9-S-L6	18	3.1	3.6	5.26	1.34	3.0E-11	2.6E-11
	12c	GCL-2	S-M6	CW	DN9-S-L7	16	17.1	20.2	1.44	1.26	3.7E-11	3.1E-11
13	13a	GCL-2	S-M7	CW	DN9-S-L8	32	2.9	3.4	5.28	1.28	3.2E-11	2.7E-11
	13b	GCL-2	S-M7	CW	DN9-S-L9	34	tbid	tbid	tbid	tbid	6.0E-11	tbid
	13c	GCL-2	S-M7	CW	DN9-S-L10	49	tbid	tbid	tbid	tbid	1.8E-10	tbid
14	14a ^(a)	GCL-1 ^(h)	S-Method	CW	DN15-S-L1	86	tbid	tbid	2.44	1.10	4.0E-11	tbid
15	15a ^(a)	GCL-1 ^(h)	G-Method	CW	DN15-L1	31	tbid	tbid	3.83	1.31	4.4E-11	tbid
16	16a ^(a)	GCL-3	S-Method	CW	R200-S-L1	88	tbid	tbid	4.70	1.25	2.0E-11	tbid
17	17a ^(a)	GCL-3	G-Method	CW	R200-L1	38	tbid	tbid	3.28	1.54	2.3E-11	tbid
18	18a	GB	S-Method	CW	B-S-L3	72	6.7	-	10.1	1.38	1.7E-11	-
19	19a	GB	G-Method	CW	B-L1	54	7.1	-	5.8	1.35	1.4E-11	-
20	20a	GCL-1	S-Method	DW	DN12-S-D1	69	5.6	6.4	599	1.03	3.0E-11	2.6E-11
21	21a	GCL-1	G-Method	DW	DN12-D1	27	1.3	1.5	1143	1.78	2.3E-11	2.0E-11

All values reported based on hydraulic termination criteria of ASTM D6766-12

GB = Granular Bentonite

S-Method = Standard method

G-Method = Gravity method

CW = Conservative water

Au-PS = Synthetic mining process solution

DW = Deionized water

S-M1 = Modified S-Method with 1 hr between backpressure increments

S-M2 = Modified S-Method with 4 hr between backpressure increments

S-M3 = Modified S-Method with 4 hr between 35 kPa (5 psi) backpressure increments

S-M4 = Modified S-Method with 5 psi backpressure increments

S-M5 = Modified S-Method with 1 day between 35 kPa (5 psi) backpressure increments

S-M6 = Modified S-Method where hydration is completed under elevated pressure, i.e. no backpressure steps are used.

S-M7 = Modified S-Method where phase one is equivalent G-Method and phase two is S-Method.

^(a) Long term tests running to chemical equilibrium that have not been terminated. Data provided in the "Chemical" column represents the current value of the progression of the test not the terminated value.

^(b) Average textile thicknesses and water contents used.

^(c) Average bentonite water content, and average textile thicknesses and water contents used.

^(d) Average bentonite and textile water contents used.

^(e) Meeting hydraulic equilibrium termination criteria (ASTM 5084)

^(f) Meeting chemical equilibrium termination criteria (ASTM 6766)

^(g) Values after applying the correction that takes into account the textile weights and thicknesses.

^(h) Higher peel strength version of GCL-1, 2710 N/m (15 ppi) compared to 2170 N/m (12 ppi)

nr = values not reported

tbid = to be determined

Table D.2. Summary of physical properties of tests conducted in Chapter 2

Test Series	Test Number	Material	Method	Test Liquid	Test ID	Final Degree of Saturation	Final Degree of Saturation ^(a)	Water Content	Porosity	Porosity ^(a)	Void Ratio	Void Ratio ^(a)	Dry Density (Mg/m ³)	Dry Density (Mg/m ³) ^(a)	Avg. Hydraulic Gradient	Avg. Hydraulic Gradient ^(a)	Avg. Effective Stress (kPa)	Specimen Thickness (mm)		Textile Thickness (mm)		Textile Water Content	
																		Total	Bentonite	Cover Textile	Carrier Textile	Cover Textile	White Textile
1	1a ^(b)	GCL-1	S-Method	CW	DN12-S-L1	88%	89%	103%	0.76	0.76	3.12	3.09	0.65	0.65	174	200	26.1	8.32	7.24	0.43	0.65	167%	160%
	1b ^(b)	GCL-1	S-Method	CW	DN12-S-L2	94%	95%	113%	0.76	0.76	3.22	3.18	0.63	0.64	167	190	26.4	8.82	7.74	0.43	0.65	167%	160%
	1c ^(b)	GCL-1	S-Method	CW	DN12-S-L3	tdb	tdb	tdb	tdb	tdb	tdb	tdb	tdb	tdb	tdb	tdb	tdb	tdb	tdb	tdb	tdb	tdb	tdb
2	2a ^(b)	GCL-1	G-Method	CW	DN12-L1	90%	91%	103%	0.75	0.75	3.06	3.03	0.66	0.66	179	207	27.6	7.86	6.78	0.43	0.65	167%	160%
	2b ^(b)	GCL-1	G-Method	CW	DN12-L2	87%	87%	110%	0.77	0.77	3.39	3.38	0.61	0.61	169	194	27.5	8.41	7.33	0.43	0.65	167%	160%
	2c	GCL-1	G-Method	CW	DN12-L3	105%	104%	109%	0.74	0.74	2.77	2.79	0.71	0.70	162	181	27.6	8.65	7.74	0.33	0.58	149%	185%
	2d ^(b)	GCL-1	G-Method	CW	DN12-L4	tdb	tdb	tdb	tdb	tdb	tdb	tdb	tdb	tdb	tdb	tdb	tdb	tdb	tdb	tdb	tdb	tdb	tdb
3	3a	GCL-1	S-Method	Au-PS	DN12-S-G1	83%	85%	87%	0.74	0.73	2.80	2.74	0.70	0.71	165	187	26.4	9.21	8.13	0.48	0.80	127%	156%
	3b	GCL-1	S-Method	Au-PS	DN12-S-G2	89%	96%	91%	0.73	0.72	2.74	2.53	0.71	0.76	213	257	26.4	6.85	5.67	0.47	0.71	147%	105%
	3c ^(b)	GCL-1	S-Method	Au-PS	DN12-S-G3	87%	89%	89%	0.73	0.73	2.73	2.68	0.72	0.72	214	252	26.3	7.20	6.12	0.43	0.65	167%	160%
4	4a	GCL-1	G-Method	Au-PS	DN12-G1	91%	93%	88%	0.72	0.72	2.58	2.53	0.74	0.76	196	231	27.5	7.24	6.14	0.41	0.69	146%	197%
	4b ^(b)	GCL-1	G-Method	Au-PS	DN12-G2	83%	83%	93%	0.75	0.75	2.98	2.97	0.67	0.67	185	215	27.5	7.72	6.65	0.43	0.65	167%	160%
	4c	GCL-1	G-Method	Au-PS	DN12-G2	92%	98%	90%	0.72	0.71	2.63	2.47	0.73	0.77	181	210	27.4	7.97	6.88	0.42	0.67	93%	112%
5	5a ^(b)	GCL-1	S-M1	CW	DN12-S-L4	92%	95%	109%	0.76	0.75	3.18	3.07	0.64	0.66	175	206	26.0	8.05	6.84	0.51	0.71	167%	160%
	6a ^(b)	GCL-1	S-M2	CW	DN12-S-L5	90%	92%	109%	0.76	0.76	3.24	3.18	0.63	0.64	171	197	26.4	8.70	7.55	0.47	0.68	167%	160%
7	7a	GCL-1	S-M3	CW	DN12-S-L6	102%	103%	119%	0.76	0.76	3.12	3.10	0.65	0.65	148	169	26.1	9.04	7.92	0.50	0.62	203%	186%
8	8a	GCL-1	S-M4	CW	DN12-S-L8	98%	96%	104%	0.74	0.74	2.81	2.87	0.70	0.69	149	165	26.2	9.48	8.54	0.42	0.53	207%	188%
	8b	GCL-1	S-M4	CW	DN12-S-L9	99%	98%	110%	0.75	0.75	2.97	3.02	0.67	0.66	163	187	26.5	8.78	7.68	0.41	0.70	222%	231%
9	9a	GCL-1	S-M5	CW	DN12-S-L10	95%	97%	106%	0.75	0.75	2.97	2.93	0.67	0.68	193	226	26.5	7.58	6.47	0.51	0.60	186%	171%
10	10a ^(a)	GCL-2	S-Method	CW	DN9-S-L2	tdb	tdb	tdb	tdb	tdb	tdb	tdb	tdb	tdb	tdb	tdb	tdb	tdb	tdb	tdb	tdb	tdb	tdb
	10b	GCL-2	S-Method	CW	DN9-S-L3	108%	109%	143%	0.78	0.78	3.54	3.52	0.59	0.59	157	180	26.1	10.05	8.77	0.69	0.59	205%	195%
	10c	GCL-2	S-Method	CW	DN9-S-L4	112%	111%	146%	0.78	0.78	3.48	3.51	0.60	0.59	162	183	26.1	9.87	8.72	0.61	0.54	215%	179%
11	11a ^(a)	GCL-2	G-Method	CW	DN9-L1	tdb	tdb	tdb	tdb	tdb	tdb	tdb	tdb	tdb	tdb	tdb	tdb	tdb	tdb	tdb	tdb	tdb	tdb
	11b	GCL-2	G-Method	CW	DN9-L2	99%	104%	135%	0.78	0.78	3.64	3.45	0.58	0.60	149	174	27.6	9.47	8.13	0.74	0.60	144%	113%
	11c	GCL-2	G-Method	CW	DN9-L3	91%	97%	131%	0.79	0.78	3.83	3.60	0.55	0.58	145	168	27.6	9.71	8.41	0.74	0.56	103%	72%
12	12a	GCL-2	S-M6	CW	DN9-S-L5	91%	91%	115%	0.77	0.75	3.38	3.04	0.61	0.66	157	195	26.3	8.83	7.15	0.82	0.87	133%	149%
	12b	GCL-2	S-M6	CW	DN9-S-L6	104%	106%	130%	0.77	0.77	3.36	3.27	0.61	0.63	173	204	26.2	9.16	7.77	0.68	0.71	196%	194%
	12c	GCL-2	S-M6	CW	DN9-S-L7	104%	107%	138%	0.78	0.77	3.54	3.44	0.59	0.60	155	182	26.1	9.46	8.07	0.71	0.68	193%	176%
	13	13a	GCL-2	S-M7	CW	DN9-S-L8	91%	95%	124%	0.78	0.78	3.62	3.48	0.58	0.60	148	173	26.2	9.70	8.29	0.71	0.70	177%
13	13b	GCL-2	S-M7	CW	DN9-S-L9	tdb	tdb	tdb	tdb	tdb	tdb	tdb	tdb	tdb	tdb	tdb	tdb	tdb	tdb	tdb	tdb	tdb	tdb
	13c	GCL-2	S-M7	CW	DN9-S-L10	tdb	tdb	tdb	tdb	tdb	tdb	tdb	tdb	tdb	tdb	tdb	tdb	tdb	tdb	tdb	tdb	tdb	tdb
14	14a ^(a)	GCL-1 ^(b)	S-Method	CW	DN15-S-L1	tdb	tdb	tdb	tdb	tdb	tdb	tdb	tdb	tdb	tdb	tdb	tdb	tdb	tdb	tdb	tdb	tdb	tdb
15	15a ^(a)	GCL-1 ^(b)	G-Method	CW	DN15-L1	tdb	tdb	tdb	tdb	tdb	tdb	tdb	tdb	tdb	tdb	tdb	tdb	tdb	tdb	tdb	tdb	tdb	tdb
16	16a ^(a)	GCL-3	S-Method	CW	R200-S-L1	tdb	tdb	tdb	tdb	tdb	tdb	tdb	tdb	tdb	tdb	tdb	tdb	tdb	tdb	tdb	tdb	tdb	tdb
17	17a ^(a)	GCL-3	G-Method	CW	R200-L1	tdb	tdb	tdb	tdb	tdb	tdb	tdb	tdb	tdb	tdb	tdb	tdb	tdb	tdb	tdb	tdb	tdb	tdb
18	18a	GB	S-Method	CW	B-S-L3	106%	-	114%	0.74	-	2.86	-	0.69	-	231	-	26.5	6.03	6.03	-	-	-	-
19	19a	GB	G-Method	CW	B-L1	96%	-	100%	0.73	-	2.76	-	0.71	-	237	-	27.5	5.98	5.98	-	-	-	-
20	20a	GCL-1	S-Method	DW	DN12-S-D1	103%	102%	116%	0.75	0.75	3.01	3.02	0.67	0.66	180	209	26.3	8.18	7.04	0.41	0.73	250%	192%
21	21a	GCL-1	G-Method	DW	DN12-D1	93%	91%	108%	0.76	0.76	3.11	3.16	0.65	0.64	164	182	27.4	8.86	7.97	0.30	0.59	172%	138%

^(a) Long term tests running to chemical equilibrium that have not been terminated. Data provided in the "Chemical" column of a given parameter represents the current value of the progression of the test not the terminated value.

^(b) Average textile thicknesses and water contents used.

^(c) Average bentonite water content, and average textile thicknesses and water contents used.

^(d) Average bentonite and textile water contents used.

^(e) Values after applying the correction that takes into account the textile weights and thicknesses.

^(f) Higher peel strength version of GCL-1, 2710 N/m (15 ppi) compared to 2170 N/m (12 ppi)

GB = Granular Bentonite

S-Method = Standard method

G-Method = Gravity method

CW = Conservative water

Au-PS = Synthetic mining process solution

DW = Deionized water

S-M1 = Modified S-Method with 1 hr between backpressure increments

S-M2 = Modified S-Method with 4 hr between backpressure increments

S-M3 = Modified S-Method with 4 hr between 35 kPa (5 psi) backpressure increments

S-M4 = Modified S-Method with 5 psi backpressure increments

S-M5 = Modified S-Method with 1 day between 35 kPa (5 psi) backpressure increments

S-M6 = Modified S-Method where hydration is completed under elevated pressure, i.e. no backpressure steps are used.

S-M7 = Modified S-Method where phase one is equivalent G-Method and phase two is S-Method.

nr = values not reported

tdb = to be determined

Table D.3. Summary of hydraulic and chemical properties of tests conducted in Chapter 3

Test Series	Test Number	Material	Test Liquid	Test ID	Elapsed Time (days)		Pore Volumes of Flow, PVF		Pore Volumes of Flow, PVF ^(g)		EC Ratio, EC _{out} /EC _{in}		pH Ratio, pH _{out} /pH _{in}		Hydraulic Conductivity, k (m/s)		Hydraulic Conductivity, k (m/s) ^(g)	
					Hydraulic ^(e)	Chemical ^(f)	Hydraulic ^(e)	Chemical ^(f)	Hydraulic ^(e)	Chemical ^(f)	Hydraulic ^(e)	Chemical ^(f)	Hydraulic ^(e)	Chemical ^(f)	Hydraulic ^(e)	Chemical ^(f)	Hydraulic ^(e)	Chemical ^(f)
2 ^(c)	2a ^(b)	GCL-1	CW	DN12-L1	0.18	nr	3.6	nr	4.2	nr	nr	nr	nr	nr	5.3E-09	nr	4.5E-09	nr
	2b ^(b)	GCL-1	CW	DN12-L2	0.13	nr	2.3	nr	2.6	nr	nr	nr	nr	nr	6.1E-09	nr	5.3E-09	nr
	2c	GCL-1	CW	DN12-L3	2.9	nr	5.4	nr	6.0	nr	2.92	nr	1.31	nr	1.0E-09	nr	9.2E-10	nr
	2d ^(a)	GCL-1	CW	DN12-L4	39	182	tbid	tbid	tbid	tbid	4.88	2.43	1.52	1.16	1.8E-11	3.5E-11	tbid	tbid
4 ^(f)	4a	GCL-1	Au-PS	DN12-G1	1.4	nr	9.0	nr	10.7	nr	1.07	nr	1.33	nr	5.7E-09	nr	4.8E-09	nr
	4b ^(b)	GCL-1	Au-PS	DN12-G2	0.040	nr	3.6	nr	4.2	nr	N/A	nr	nr	nr	2.6E-08	nr	2.3E-08	nr
	4c	GCL-1	Au-PS	DN12-G3	1.6	nr	2.0	nr	2.4	nr	1.66	nr	1.62	nr	4.9E-10	nr	4.3E-10	nr
21 ⁽ⁱ⁾	21a	GCL-1	DW	DN12-D1	27	nr	1.3	nr	1.5	nr	1143	nr	1.78	nr	2.3E-11	nr	2.0E-11	nr
22	22a ^(b)	GCL-1	TW	Test #1	42	nr	9.5	nr	10.8	nr	nr	nr	nr	nr	2.9E-11	nr	2.6E-11	nr
	22b ^(b)	GCL-1	TW	Test #2	38	nr	13.7	nr	15.7	nr	nr	nr	nr	nr	2.1E-11	nr	1.9E-11	nr
	22c ^(b)	GCL-1	TW	Test #3	41	nr	4.9	nr	5.7	nr	nr	nr	nr	nr	9.5E-12	nr	8.3E-12	nr
17 ^(f)	17a ^(e)	GCL-3	CW	R200-L1	38	158	tbid	tbid	tbid	tbid	3.28	1.78	1.54	1.13	2.3E-11	5.4E-11	tbid	tbid
23	23a	GCL-3	Au-PS	R200-G1	41	nr	4.8	8.9	5.3	9.9	1.18	1.08	1.67	1.59	2.7E-11	3.5E-11	2.5E-11	3.2E-11
24	24a	GCL-3	BX-PS	R200-B1	45	132	5.1	10.1	5.3	10.7	0.52	0.48	0.77	0.73	5.3E-11	2.8E-11	5.0E-11	2.7E-11
25	25a	GCL-3	Cu-PS	R200-C1	0.0061	0.015	3.1	10.4	3.4	11.2	0.88	0.91	0.96	0.87	1.9E-07	2.0E-07	1.8E-07	1.8E-07
11 ⁽ⁱ⁾	11a ^(a)	GCL-2	CW	DN9-L1	0.22	17	tbid	tbid	tbid	tbid	2.85	1.94	1.10	1.33	8.7E-09	1.9E-11	tbid	tbid
	11b	GCL-2	CW	DN9-L2	18	nr	3.3	nr	3.9	nr	2.71	nr	1.37	nr	2.9E-11	nr	2.5E-11	nr
	11c	GCL-2	CW	DN9-L3	0.79	nr	2.5	nr	2.9	nr	2.29	nr	1.55	nr	1.5E-09	nr	1.3E-09	nr
26	26a	GCL-2	Au-PS	DN9-G1	0.25	0.37	2.5	5.0	3.1	6.1	1.23	1.04	1.22	1.26	8.4E-09	1.3E-08	6.9E-09	1.1E-08
27	27a	GCL-2	BX-PS	DN9-B1	0.13	7.0	2.0	6.8	2.5	8.5	0.66	0.69	0.59	0.98	9.2E-09	2.8E-10	7.6E-09	2.3E-10
28	28a	GCL-2	Cu-PS	DN9-C1	0.00069	0.0057	1.6	11.1	2.1	14.9	0.78	0.90	1.21	1.08	8.1E-07	8.4E-07	6.4E-07	6.7E-07
15 ^(f)	15a ^(e)	GCL-1 ^(h)	CW	DN15-L1	31	164	tbid	tbid	tbid	tbid	3.83	1.36	1.31	1.22	4.4E-11	2.6E-11	tbid	tbid
29	29a	GCL-1 ^(h)	Au-PS	DN15-G1	33	94	3.3	7.7	3.8	8.8	1.24	1.08	1.29	1.34	4.1E-11	4.2E-11	3.6E-11	3.7E-11
30	30a ^(a)	GCL-1	CW	DN12-L6	1.5	8.5	tbid	tbid	tbid	tbid	2.64	1.52	1.39	0.96	1.1E-09	6.8E-09	tbid	tbid

All tests performed using the gravity method

DW = Deionized water

TW = Tap water

CW = Conservative ater

Au-PS = Synthetic gold mining process solution

BX-PS = Synthetic bauxite mining process solution

Cu-PS = Synthetic copper mining process solution

^(a) Long term tests running to chemical equilibrium that have not bet been terminated. Data provided in the "Chemical" column of a given paramter represents the current value of the progression of the test not the terminated value.

^(b) Average textile thicknesses and water contents used

^(e) Meeting hydraulic equilibrium termination criteria of ASTM D6766-12

^(f) Meeting chemical equilibrium termination criteria of ASTM D6766-12

^(g) Values after applying the correction that takes into account the textile weights and thicknesses.

^(h) Higher peel strength version of GCL-1, 2710 N/m (15 ppi) compared to 2170 N/m (12 ppi)

⁽ⁱ⁾ Included in both Chapter 1 and Chapter 2

nr = values not reported

tbid = to be determined

Table D.4. Summary of physical properties of tests conducted in Chapter 3

Test Series	Test Number	Material	Test Liquid	Test ID	Final Degree of Saturation	Final Degree of Saturation ^(a)	Water Content	Porosity	Porosity ^(a)	Void Ratio	Void Ratio ^(a)	Dry Density (Mg/m ³)	Dry Density (Mg/m ³) ^(a)	Avg. Hydraulic Gradient	Avg. Hydraulic Gradient ^(a)	Avg. Effective Stress (kPa)	Specimen Thickness (mm)		Textile Thickness (mm)		Textile Water Content		
																	Total	Bentonite	Cover Textile	Carrier Textile	Cover Textile	White Textile	
2 ^(b)	2a ^(b)	GCL-1	CW	DN12-L1	90%	91%	103%	0.75	0.75	3.06	3.03	0.66	0.66	179	207	27.6	7.86	6.78	0.43	0.65	167%	160%	
	2b ^(b)	GCL-1	CW	DN12-L2	87%	87%	110%	0.77	0.77	3.39	3.38	0.61	0.61	169	194	27.5	8.41	7.33	0.43	0.65	167%	160%	
	2c	GCL-1	CW	DN12-L3	105%	104%	109%	0.74	0.74	2.77	2.79	0.71	0.70	162	181	27.6	8.65	7.74	0.33	0.58	149%	185%	
	2d ^(a)	GCL-1	CW	DN12-L4	tbd	tbd	tbd	tbd	tbd	tbd	tbd	tbd	tbd	tbd	tbd	tbd	tbd	tbd	tbd	tbd	tbd	tbd	tbd
4 ^(b)	4a	GCL-1	Au-PS	DN12-G1	91%	93%	88%	0.72	0.72	2.58	2.53	0.74	0.76	196	231	27.5	7.24	6.14	0.41	0.69	146%	197%	
	4b ^(b)	GCL-1	Au-PS	DN12-G2	83%	83%	93%	0.75	0.75	2.98	2.97	0.67	0.67	185	215	27.5	7.72	6.65	0.43	0.65	167%	160%	
	4c	GCL-1	Au-PS	DN12-G3	92%	98%	90%	0.72	0.71	2.63	2.47	0.73	0.77	181	210	27.4	7.97	6.88	0.42	0.67	93%	112%	
21 ^(b)	21a	GCL-1	DW	DN12-D1	93%	91%	108%	0.76	0.76	3.11	3.16	0.65	0.64	164	182	27.4	8.86	7.97	0.30	0.59	172%	138%	
	22a ^(b)	GCL-1	TW	Test #1	97%	97%	130%	0.78	0.78	3.59	3.56	0.58	0.59	226	256	20.3	9.04	7.96	0.43	0.65	167%	160%	
22 ^(b)	22b ^(b)	GCL-1	TW	Test #2	106%	108%	126%	0.76	0.76	3.18	3.11	0.64	0.65	232	265	20.3	8.77	7.70	0.43	0.65	167%	160%	
	22c ^(b)	GCL-1	TW	Test #3	102%	104%	123%	0.76	0.76	3.22	3.15	0.63	0.64	254	293	20.3	8.03	6.95	0.43	0.65	167%	160%	
17 ^(b)	17a ^(a)	GCL-3	CW	R200-L1	tbd	tbd	tbd	tbd	tbd	tbd	tbd	tbd	tbd	tbd	tbd	tbd	tbd	tbd	tbd	tbd	tbd	tbd	tbd
23	23a	GCL-3	Au-PS	R200-G1	90%	95%	109%	0.76	0.75	3.25	3.08	0.63	0.65	219	238	27.5	6.45	5.92	0.27	0.25	78%	26%	
24	24a	GCL-3	BX-PS	R200-B1	105%	103%	138%	0.78	0.78	3.50	3.58	0.59	0.58	161	170	27.5	8.77	8.30	0.28	0.19	258%	249%	
25	25a	GCL-3	Cu-PS	R200-C1	77%	72%	70%	0.71	0.72	2.42	2.57	0.78	0.75	220	240	27.5	6.43	5.88	0.30	0.25	37%	611%	
11 ^(b)	11a ^(a)	GCL-2	CW	DN9-L1	tbd	tbd	tbd	tbd	tbd	tbd	tbd	tbd	tbd	tbd	tbd	tbd	tbd	tbd	tbd	tbd	tbd	tbd	tbd
	11b	GCL-2	CW	DN9-L2	99%	104%	135%	0.78	0.78	3.64	3.45	0.58	0.60	149	174	27.6	9.47	8.13	0.74	0.60	144%	113%	
	11c	GCL-2	CW	DN9-L3	91%	97%	131%	0.79	0.78	3.83	3.60	0.55	0.58	145	168	27.6	9.71	8.41	0.74	0.56	103%	72%	
26	26a	GCL-2	Au-PS	DN9-G1	81%	89%	92%	0.75	0.73	3.02	2.76	0.66	0.71	155	186	27.6	9.10	7.53	0.92	0.66	126%	129%	
27	27a	GCL-2	BX-PS	DN9-B1	80%	90%	101%	0.77	0.75	3.36	2.97	0.61	0.67	155	189	27.6	9.06	7.45	0.91	0.70	90%	76%	
28	28a	GCL-2	Cu-PS	DN9-C1	71%	87%	61%	0.70	0.65	2.29	1.87	0.81	0.93	176	222	27.7	7.90	6.27	0.83	0.80	49%	75%	
15 ^(b)	15a ^(a)	GCL-1 ^(a)	CW	DN15-L1	tbd	tbd	tbd	tbd	tbd	tbd	tbd	tbd	tbd	tbd	tbd	tbd	tbd	tbd	tbd	tbd	tbd	tbd	tbd
29	29a	GCL-1 ^(a)	Au-PS	DN15-G1	93%	98%	128%	0.79	0.78	3.67	3.48	0.57	0.60	156	177	27.5	9.14	8.07	0.40	0.67	100%	65%	
30	30a ^(a)	GCL-1	CW	DN12-L6	tbd	tbd	tbd	tbd	tbd	tbd	tbd	tbd	tbd	tbd	tbd	93.2	tbd	tbd	tbd	tbd	tbd	tbd	tbd

All test performed using the gravity method

DW = Deionized water

TW = Tap water

CW = Conservative ater

Au-PS = Synthetic gold mining process solution

BX-PS = Synthetic bauxite mining process solution

Cu-PS = Synthetic copper mining process solution

^(a) Long term tests running to chemical equilibrium that have not been terminated. Data provided in the "Chemical" column of a given paramter represents the current value of the progression of the test not the terminated value.

^(b) Average textile thicknesses and water contents used

^(c) Values after applying the correction that takes into account the textile weights and thicknesses.

^(d) Higher peel strength version of GCL-1, 2710 N/m (15 ppi) compared to 2170 N/m (12 ppi)

^(e) Included in both Chapter 1 and Chapter 2

nr = values not reported

tbd = to be determined

APPENDIX E

Additional Plots

E.1 HYDRAULIC CONDUCTIVITY VERSUS ELAPSED TIME AND PORE VOLUMES OF FLOW

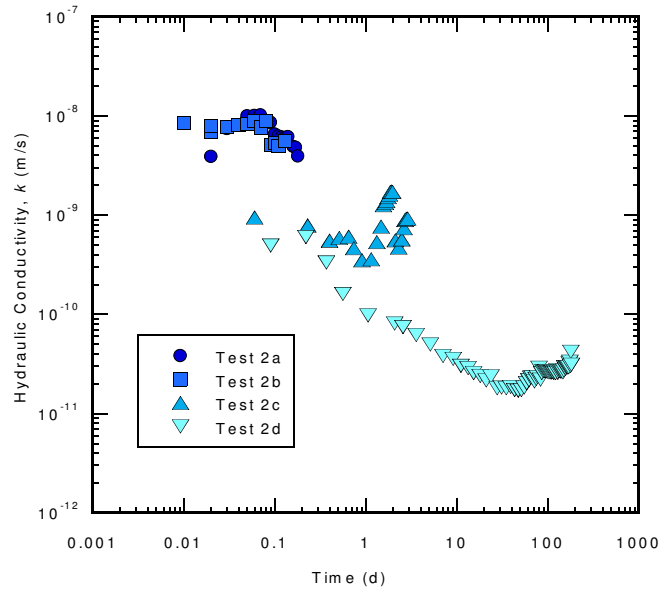


Figure E.1. Hydraulic conductivity, k , versus log time for test series 2, GCL-1 permeated with conservative water.

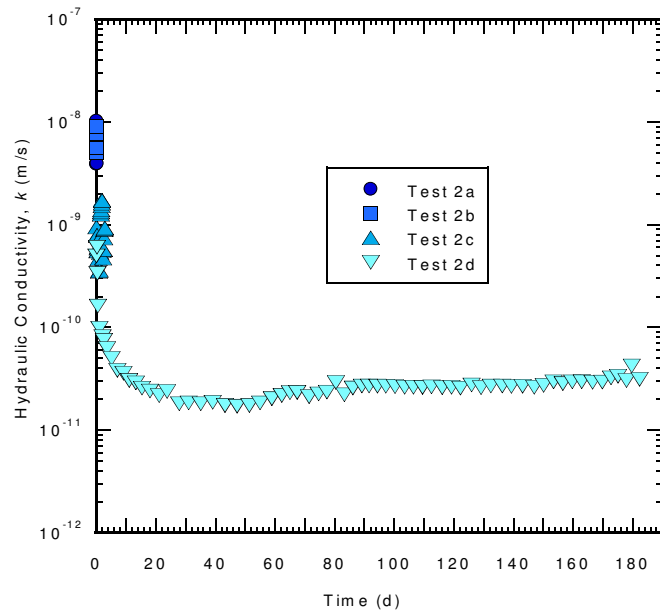


Figure E.2. Hydraulic conductivity, k , versus time for test series 2, GCL-1 permeated with conservative water.

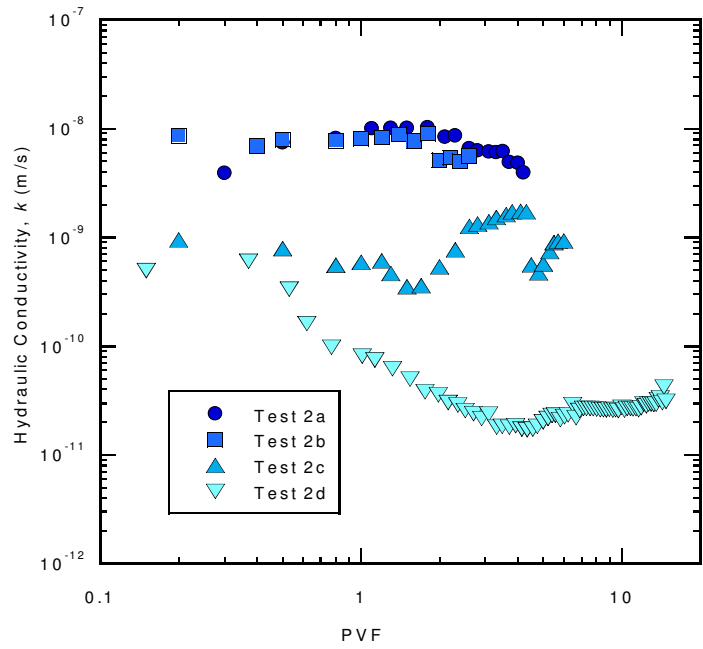


Figure E.3. Hydraulic conductivity, k , versus log pore volumes of flow (PVF) for test series 2, GCL-1 permeated with conservative water.

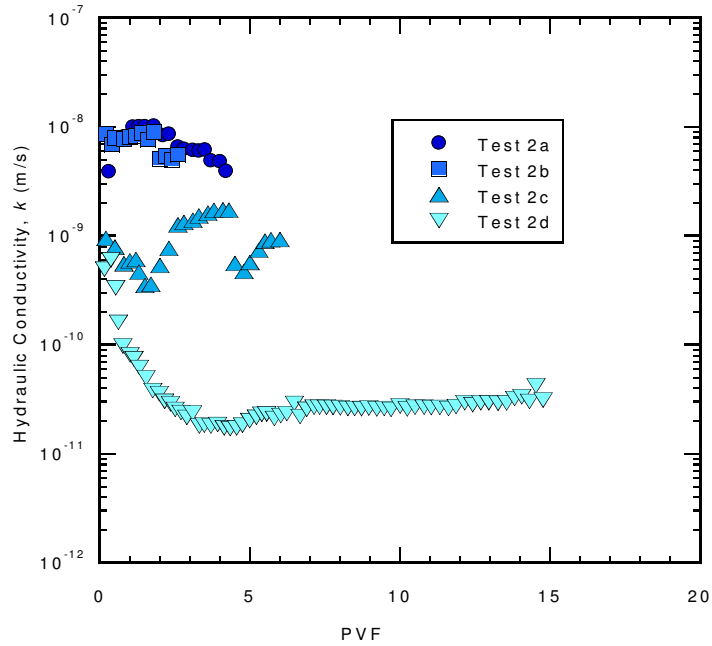


Figure E.4. Hydraulic conductivity, k , versus pore volumes of flow (PVF) for test series 2, GCL-1 permeated with conservative water.

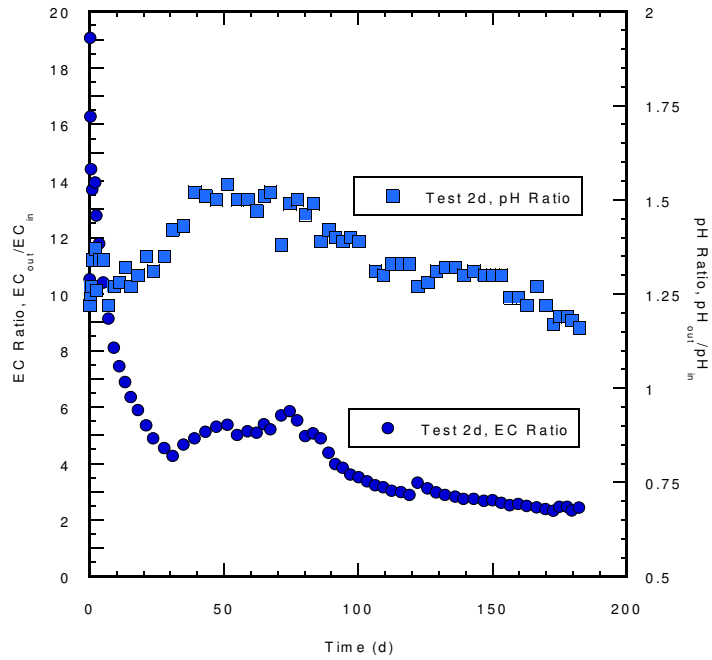


Figure E.5. EC Ratio and pH Ratio versus time for Test 2d, GCL-1 permeated with conservative water.

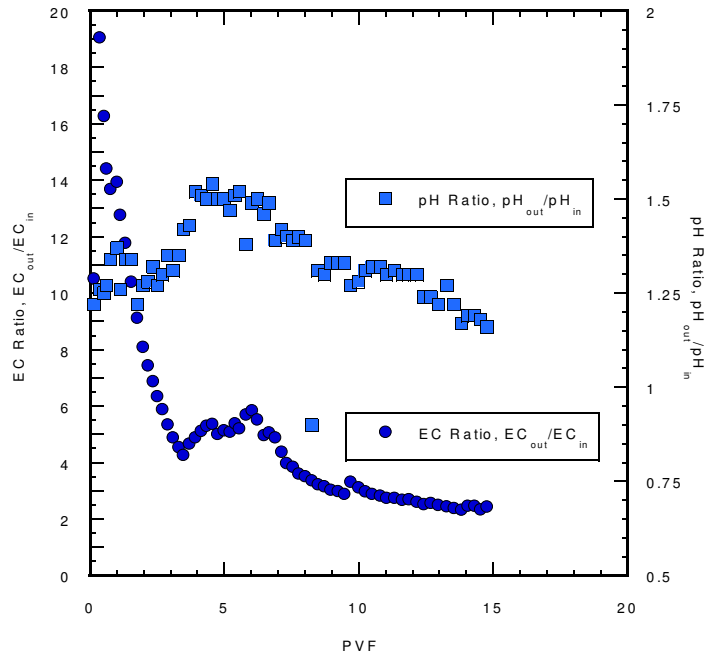


Figure E.6. EC Ratio and pH Ratio versus pore volumes of flow (PVF) for Test 2d, GCL-1 permeated with conservative water.

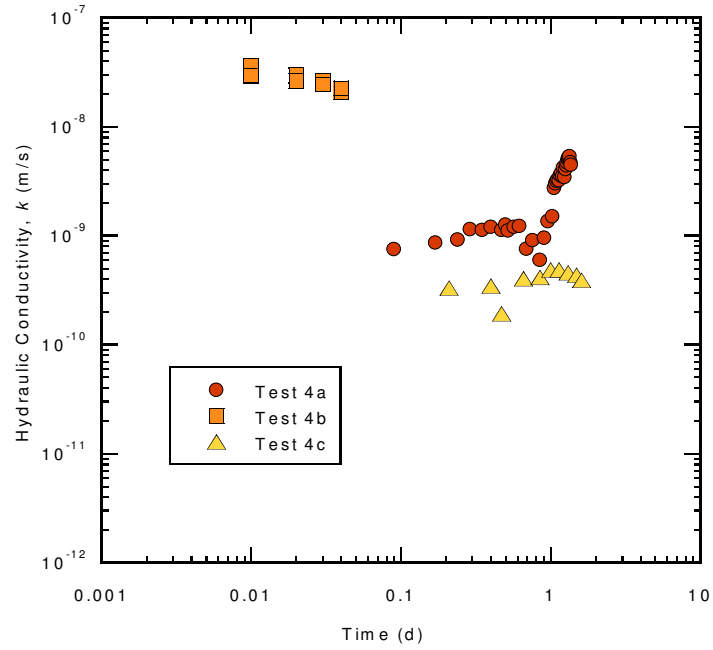


Figure E.7. Hydraulic conductivity, k , versus log time for test series 4, GCL-1 permeated with synthetic gold mining process solution.

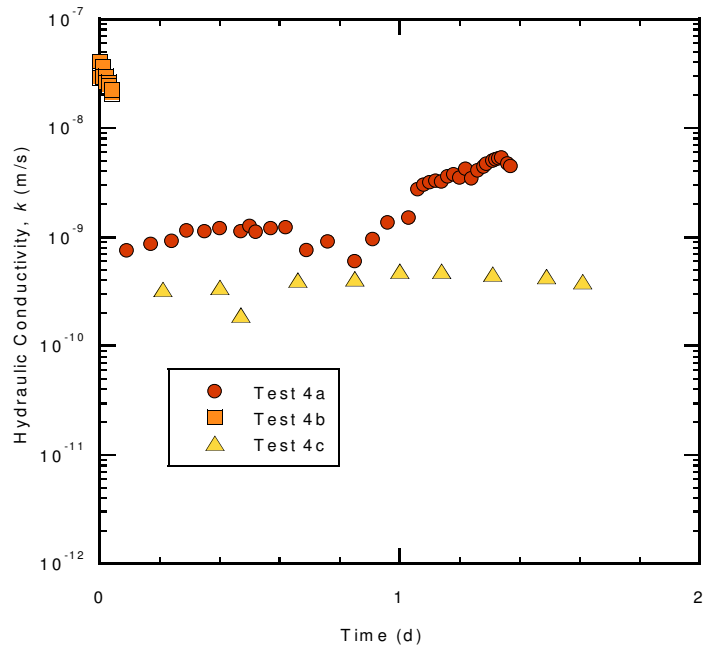


Figure E.8. Hydraulic conductivity, k , versus time for test series 4, GCL-1 permeated with synthetic gold mining process solution.

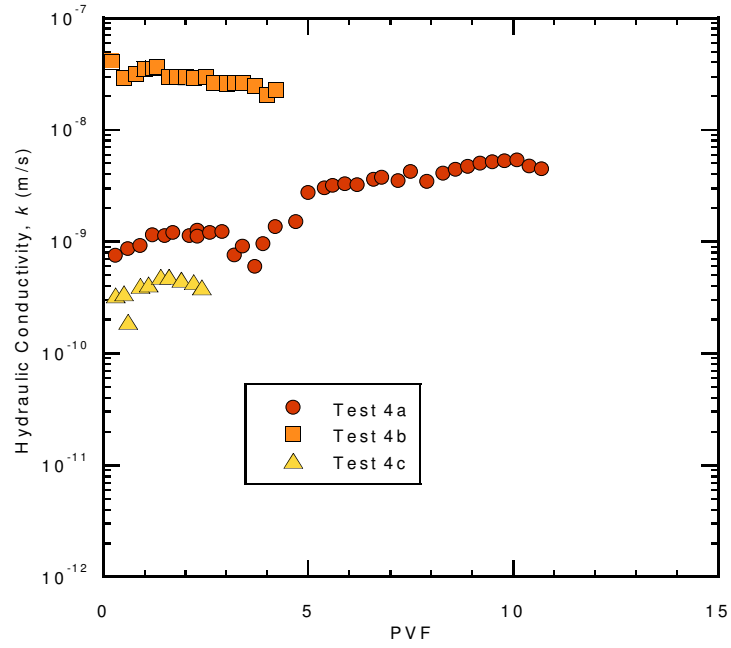


Figure E.9. Hydraulic conductivity, k , versus pore volumes of flow (PVF) for test series 4, GCL-1 permeated with synthetic gold mining process solution.

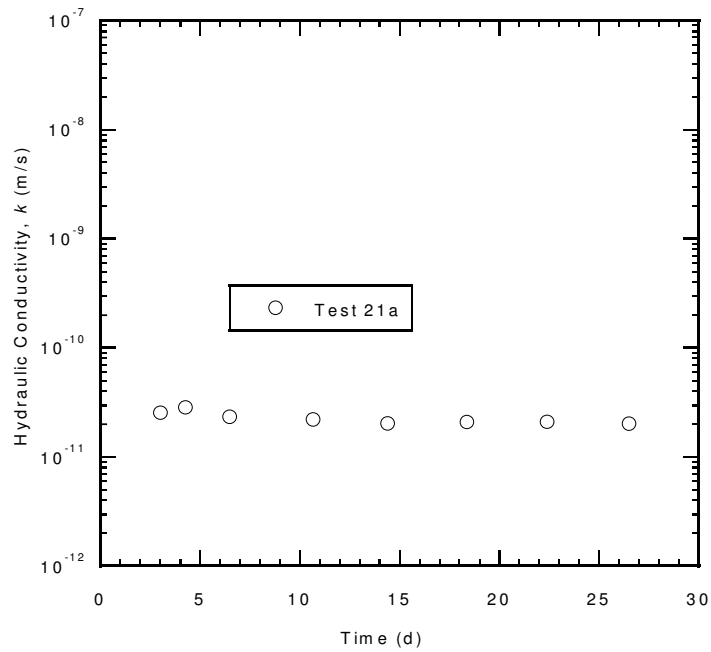


Figure E.10. Hydraulic conductivity, k , versus time for test series 21, GCL-1 permeated with deionized water.

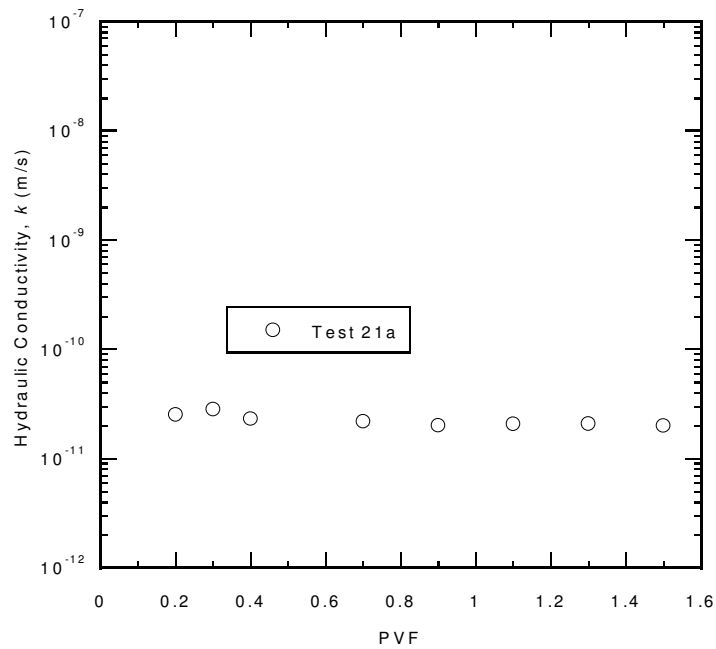


Figure E.11. Hydraulic conductivity, k , versus pore volumes of flow (PVF) for test series 21, GCL-1 permeated with deionized water.

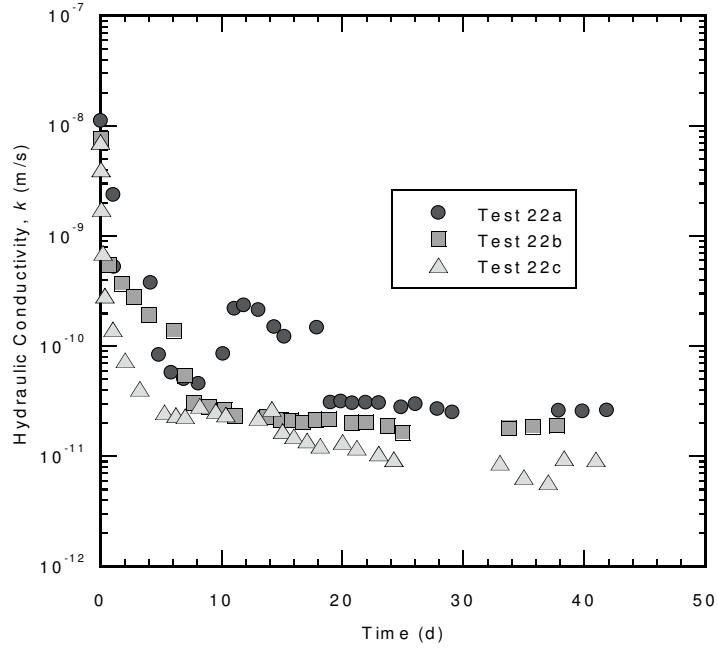


Figure E.12. Hydraulic conductivity, k , versus time for test series 22, GCL-1 permeated with tap water.

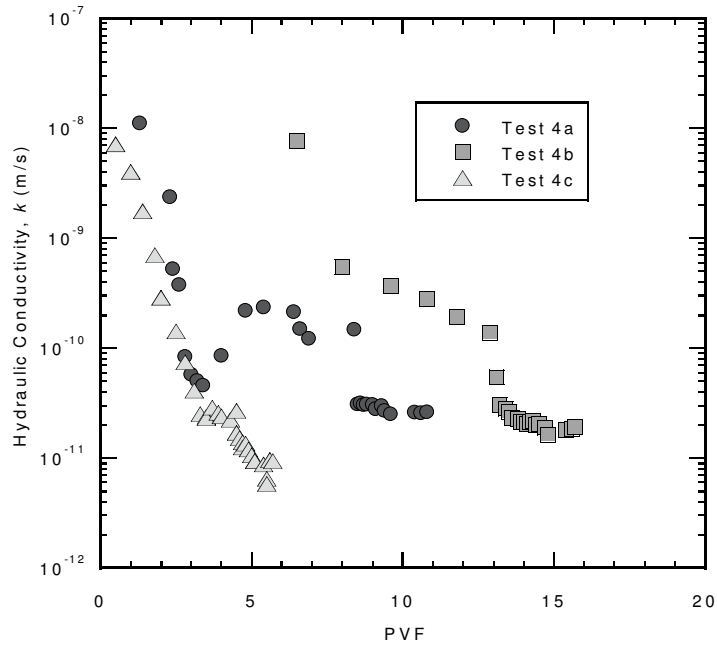


Figure E.13. Hydraulic conductivity, k , versus pore volumes of flow (PVF) for test series 22, GCL-1 permeated with tap water.

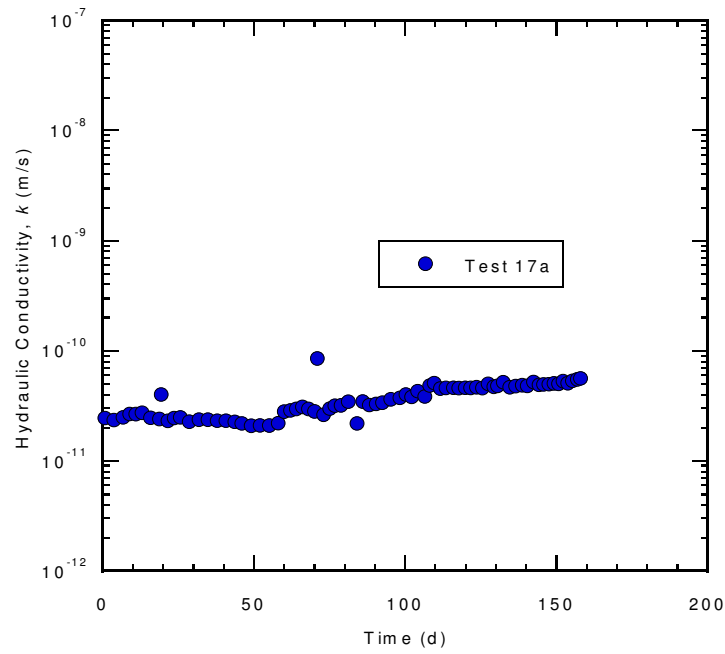


Figure E.14. Hydraulic conductivity, k , versus time for test series 17, GCL-3 permeated with conservative water.

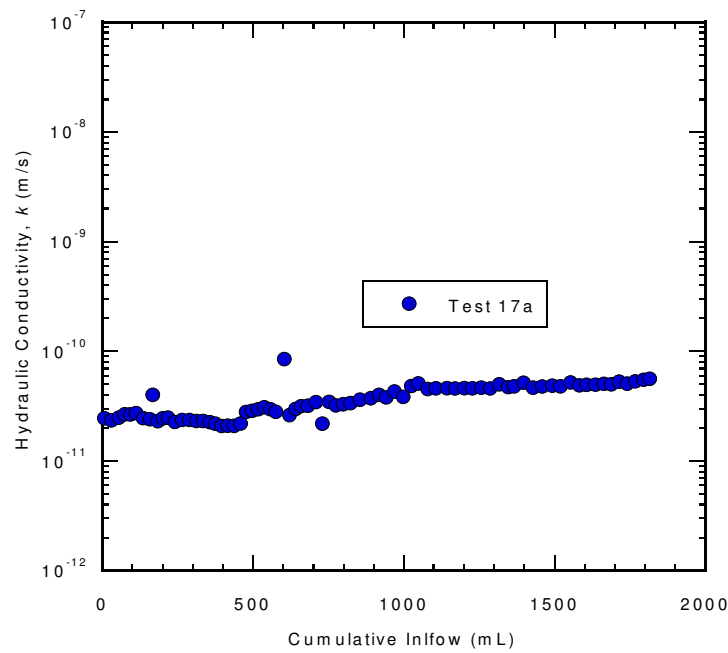


Figure E.15. Hydraulic conductivity, k , versus cumulative inflow (mL) for test series 17, GCL-3 permeated with conservative water.

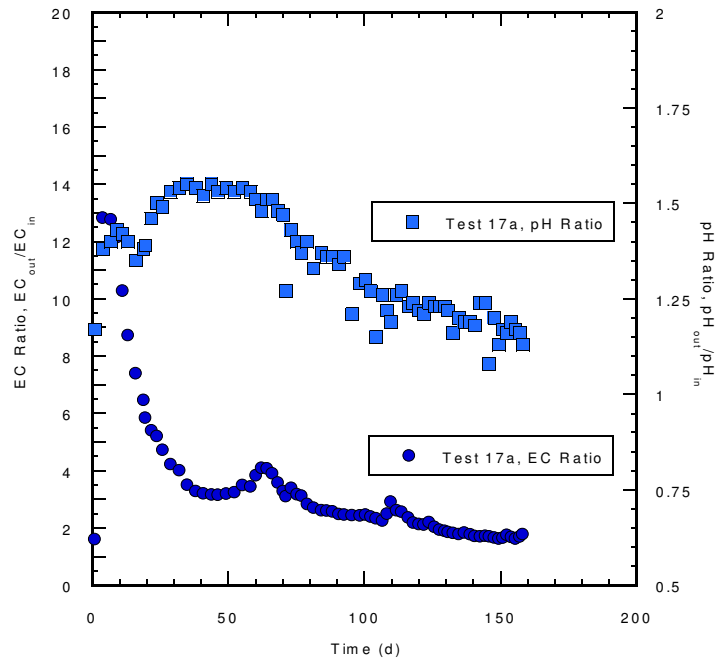


Figure E.16. EC Ratio and pH Ratio versus time for Test 17a, GCL-3 permeated with conservative water.

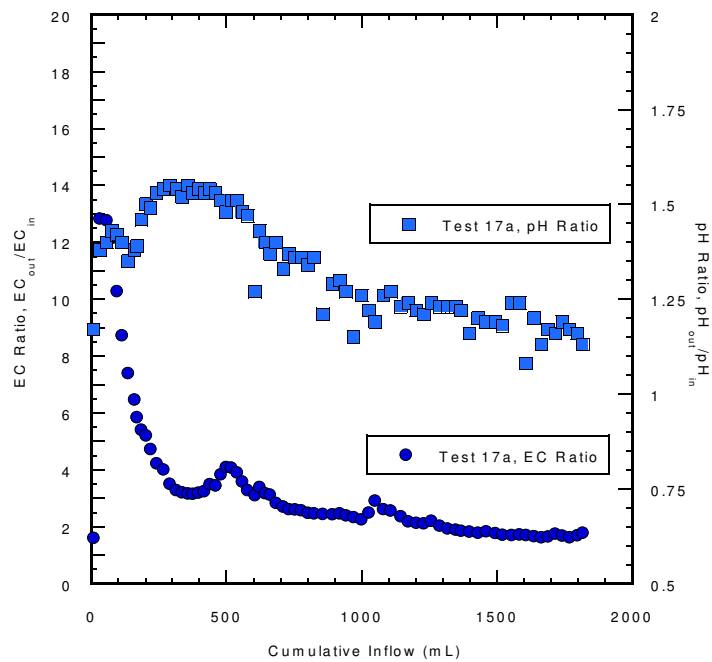


Figure E.17. EC Ratio and pH Ratio versus cumulative inflow for Test 17a, GCL-3 permeated with conservative water.

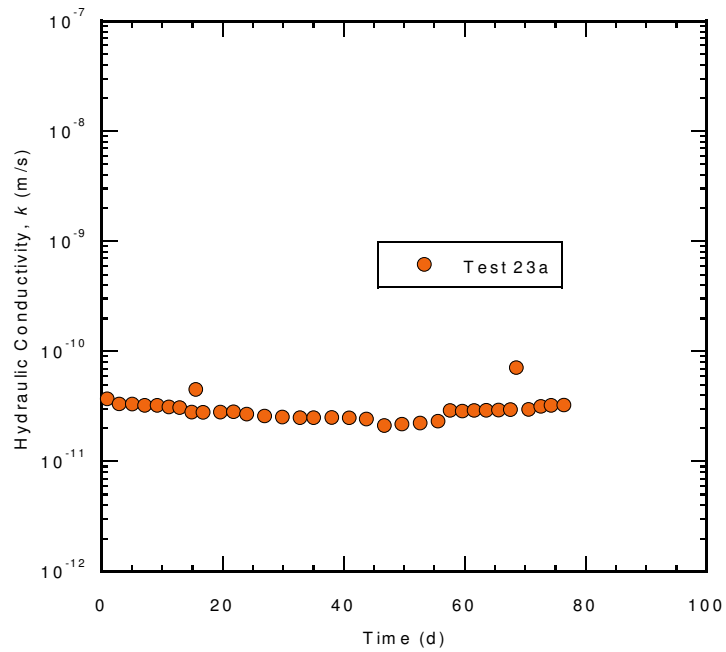


Figure E.18. Hydraulic conductivity, k , versus time for test series 23, GCL-3 permeated with synthetic gold mining process solution.

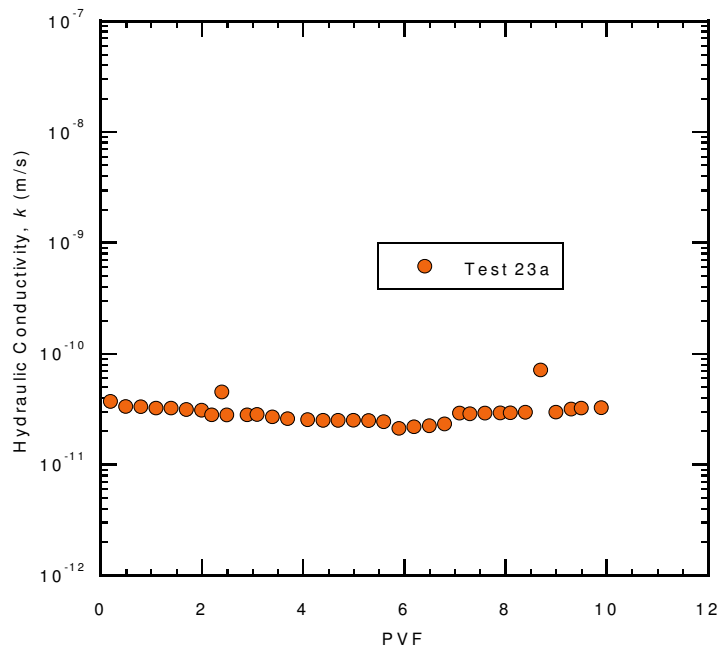


Figure E.19. Hydraulic conductivity, k , versus pore volumes of flow (PVF) for test series 23, GCL-3 permeated with synthetic gold mining process solution.

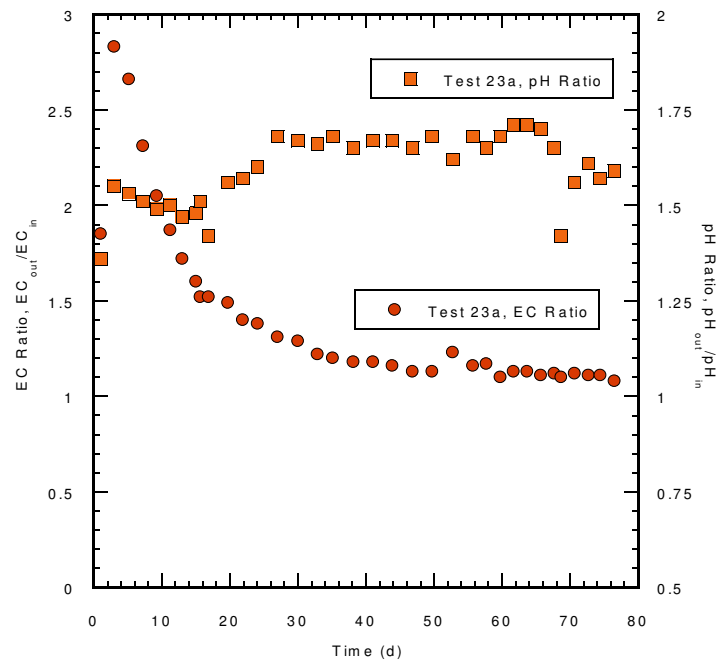


Figure E.20. EC Ratio and pH Ratio versus cumulative inflow (mL) for Test 23a, GCL-3 permeated with synthetic gold mining process solution.

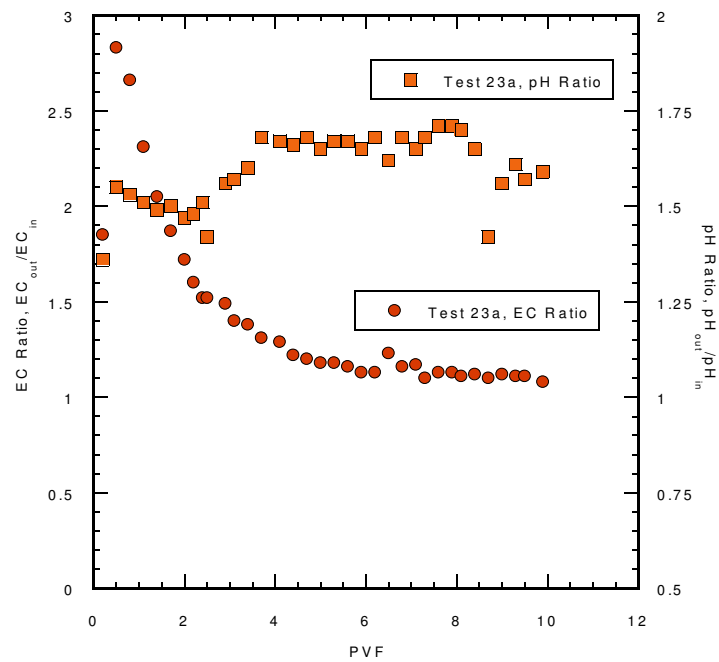


Figure E.21. EC Ratio and pH Ratio versus pore volumes of flow (PVF) for Test 23a, GCL-3 permeated with synthetic gold mining process solution.

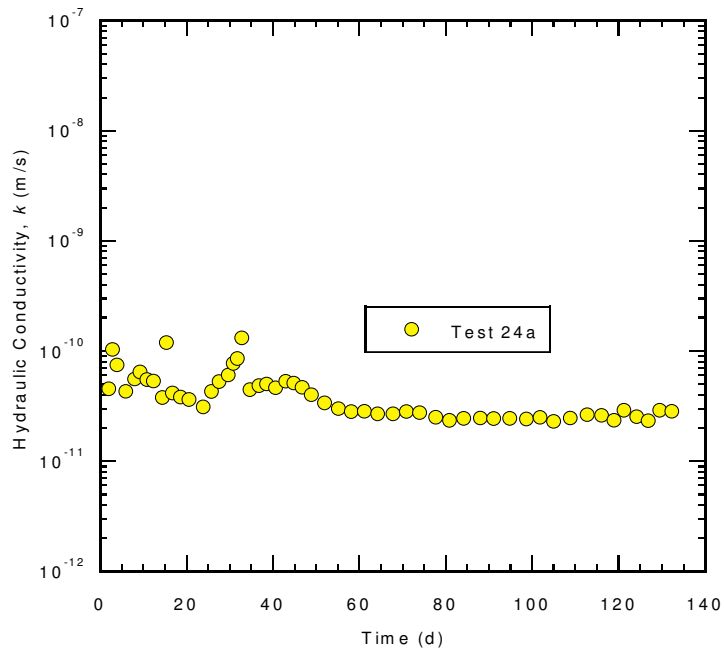


Figure E.22. Hydraulic conductivity, k , versus time for test series 24, GCL-3 permeated with synthetic bauxite mining process solution.

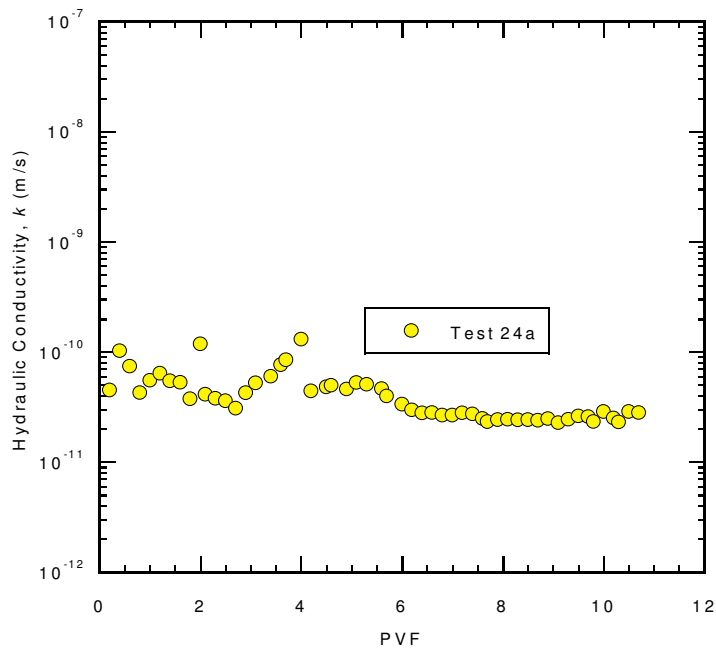


Figure E.23. Hydraulic conductivity, k , versus pore volumes of flow (PVF) for test series 24, GCL-3 permeated with synthetic bauxite mining process solution.

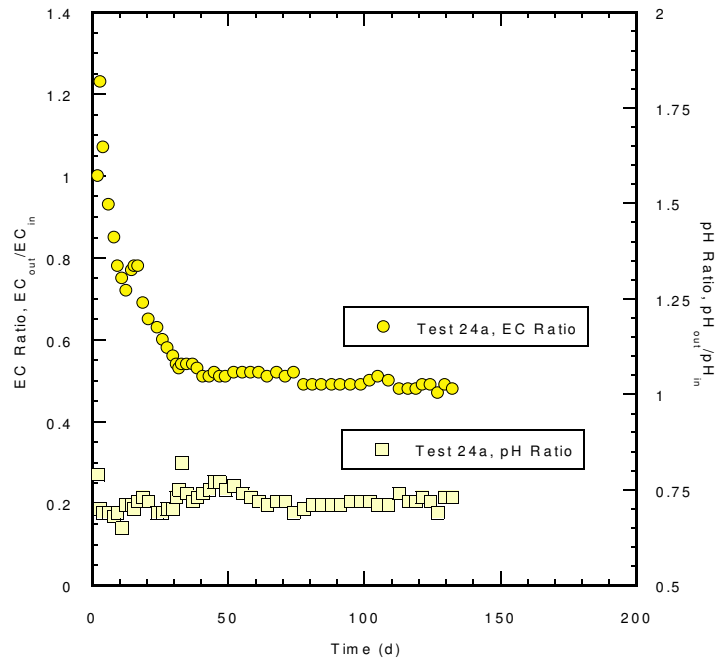


Figure E.24. EC Ratio and pH Ratio versus time for Test 24a, GCL-3 permeated with synthetic bauxite mining process solution.

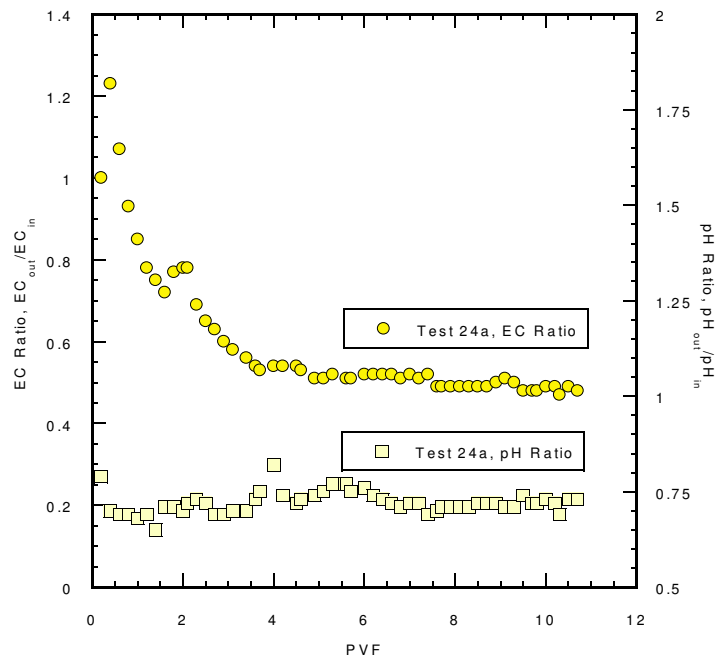


Figure E.25. EC Ratio and pH Ratio versus pore volumes of flow (PVF) for Test 24a, GCL-3 permeated with synthetic bauxite mining process solution.

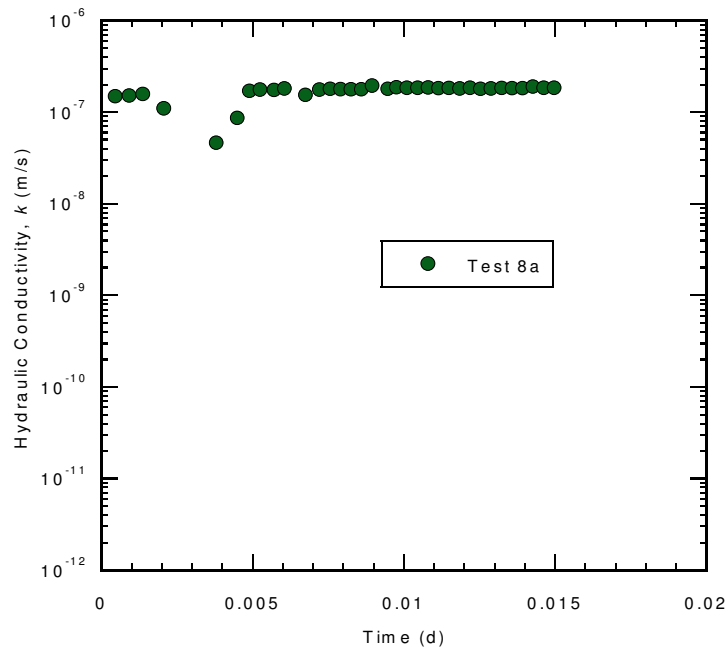


Figure E.26. Hydraulic conductivity, k , versus time for test series 25, GCL-3 permeated with synthetic copper mining process solution.

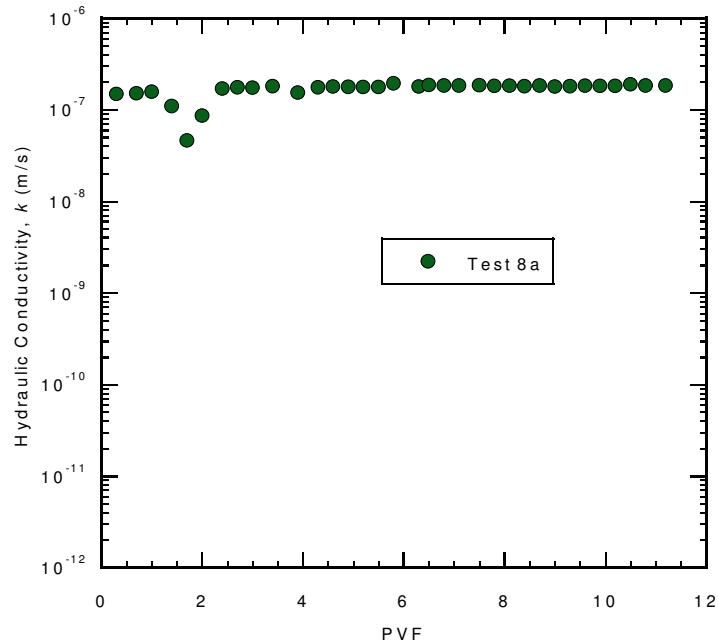


Figure E.27. Hydraulic conductivity, k , versus pore volumes of flow (PVF) for test series 25, GCL-3 permeated with synthetic copper mining process solution.

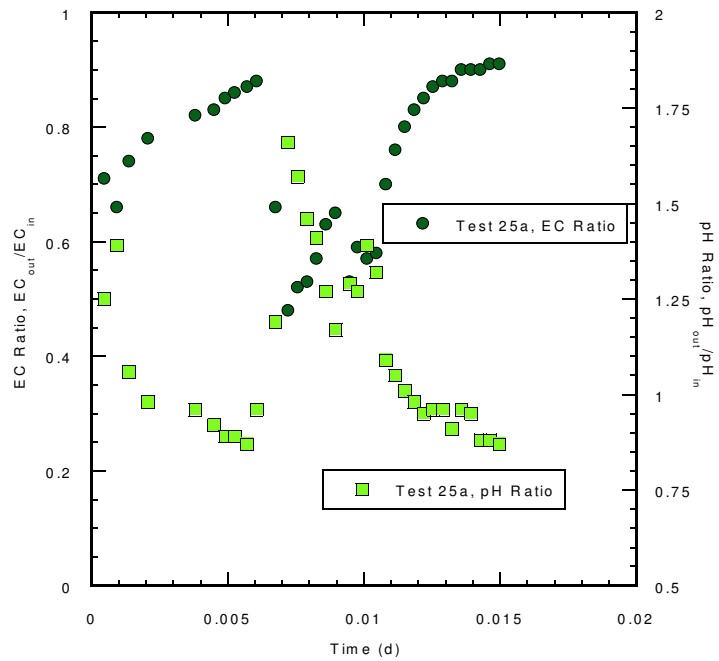


Figure E.28. EC Ratio and pH Ratio versus log time for Test 25a, GCL-3 permeated with synthetic copper mining process solution.

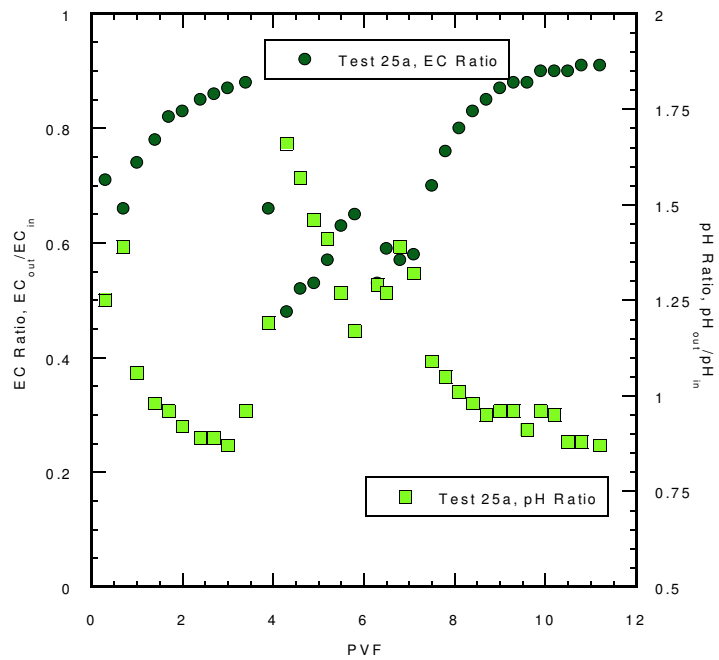


Figure E.29. EC Ratio and pH Ratio versus pore volumes of flow (PVF) for Test 25a, GCL-3 permeated with copper bauxite mining process solution.

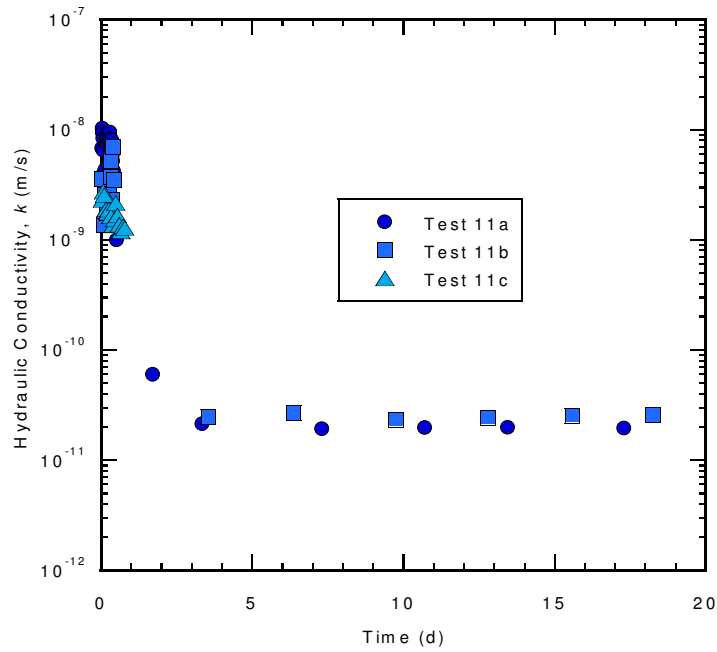


Figure E.30. Hydraulic conductivity, k , versus time for test series 11, GCL-2 permeated with conservative water.

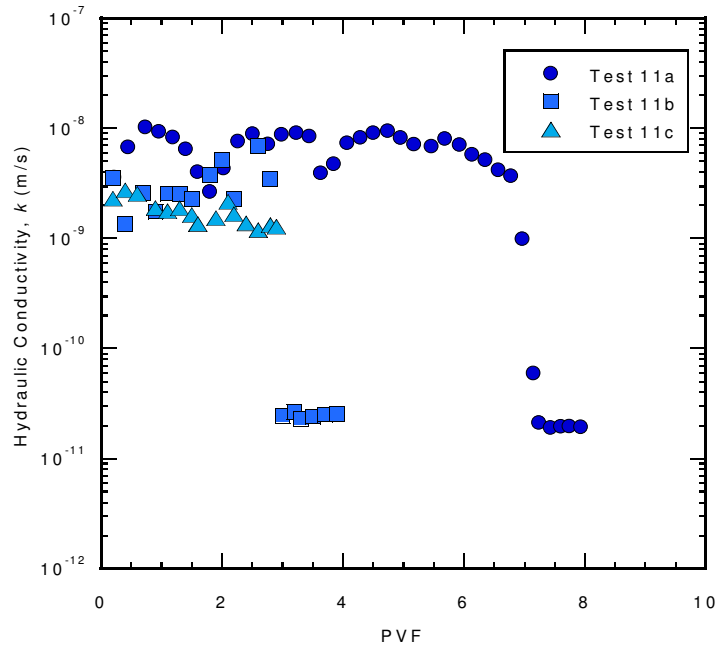


Figure E.31. Hydraulic conductivity, k , versus pore volumes of flow (PVF) for test series 11, GCL-2 permeated with conservative water.

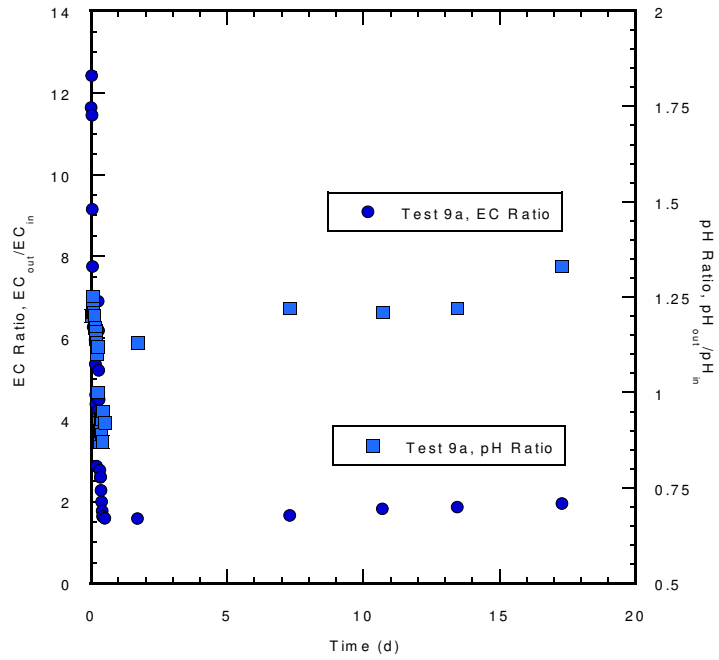


Figure E.32. EC Ratio and pH Ratio versus time for Test 11a, GCL-2 permeated with conservative water.

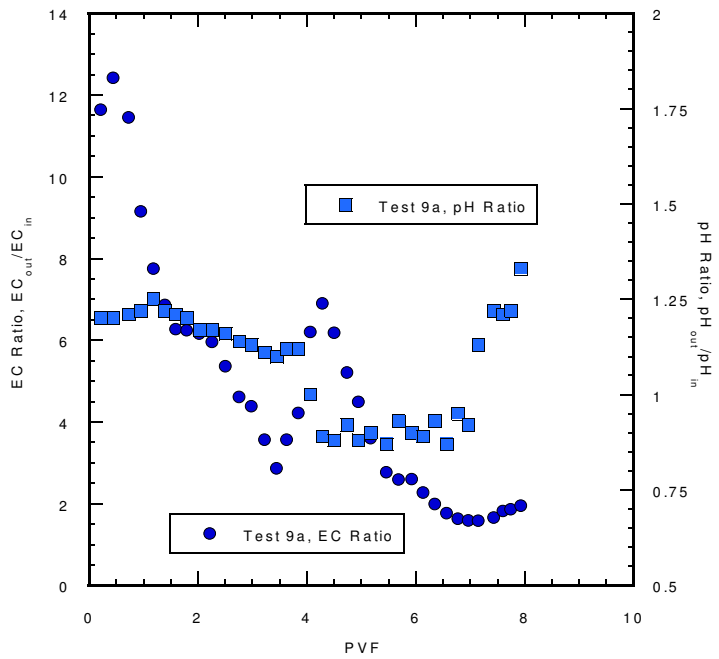


Figure E.33. EC Ratio and pH Ratio versus pore volumes of flow (PVF) for Test 11a, GCL-2 permeated with conservative water.

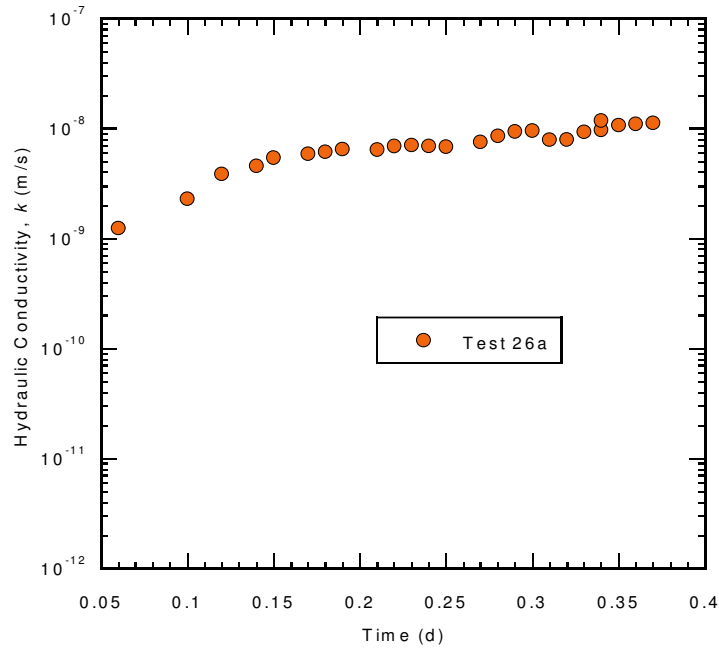


Figure E.34. Hydraulic conductivity, k , versus time for test series 26, GCL-2 permeated with synthetic gold mining process solution.

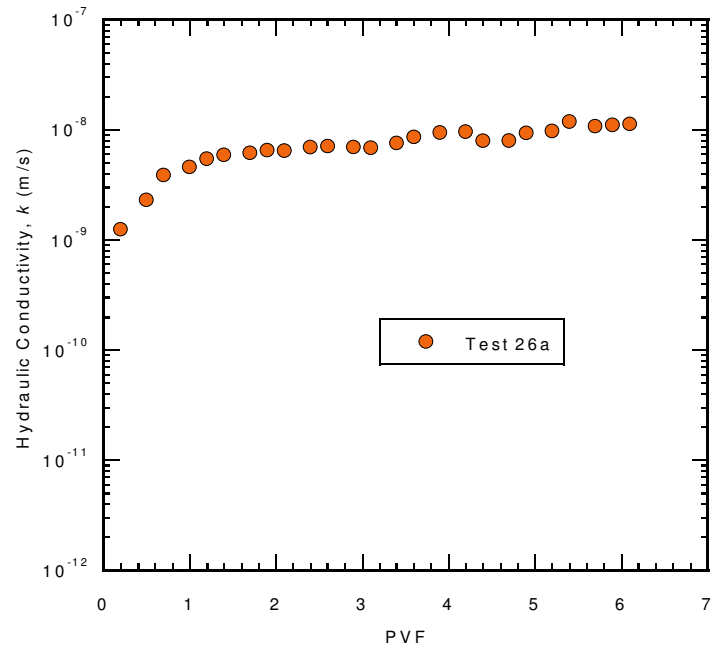


Figure E.35. Hydraulic conductivity, k , versus pore volumes of flow (PVF) for test series 26, GCL-2 permeated with synthetic gold mining process solution.

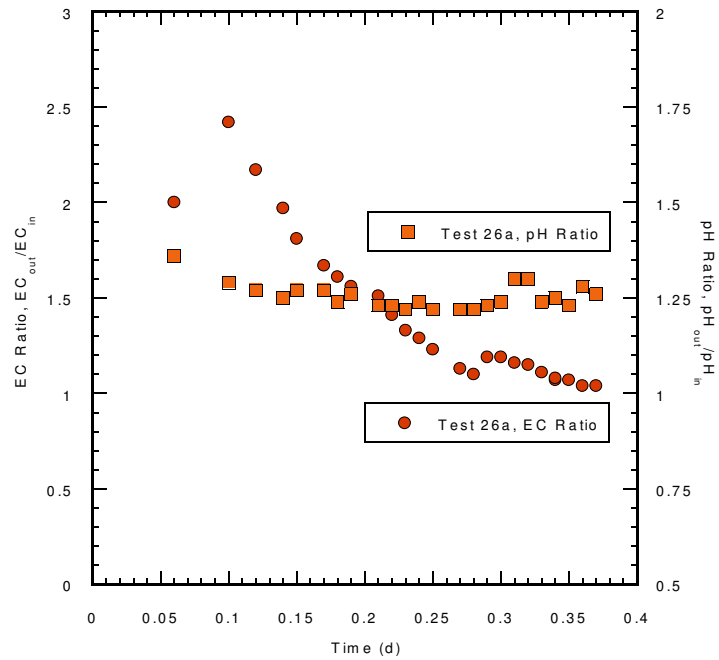


Figure E.36. EC Ratio and pH Ratio versus time for Test 26a, GCL-2 permeated with synthetic gold mining process solution.

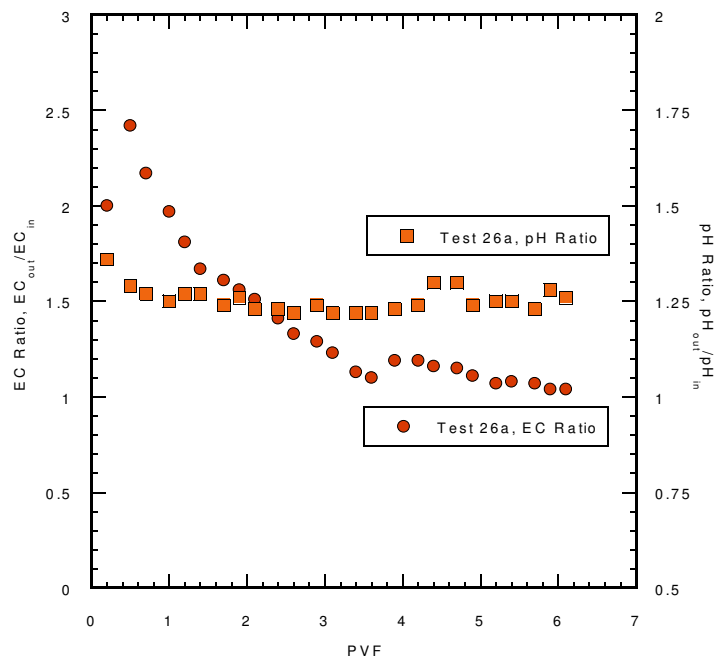


Figure E.37. EC Ratio and pH Ratio versus pore volumes of flow (PVF) for Test 26a, GCL-2 permeated with synthetic gold mining process solution.

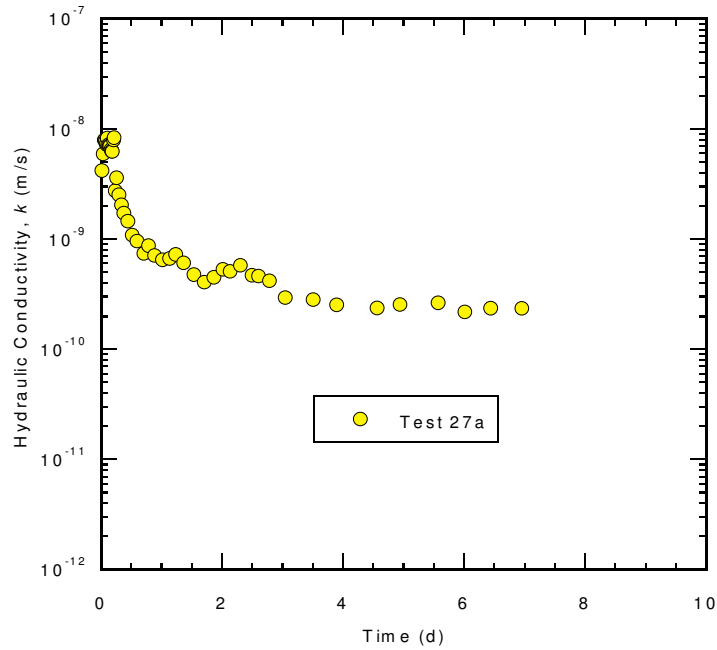


Figure E.38. Hydraulic conductivity, k , versus time for test series 27, GCL-2 permeated with synthetic bauxite mining process solution.

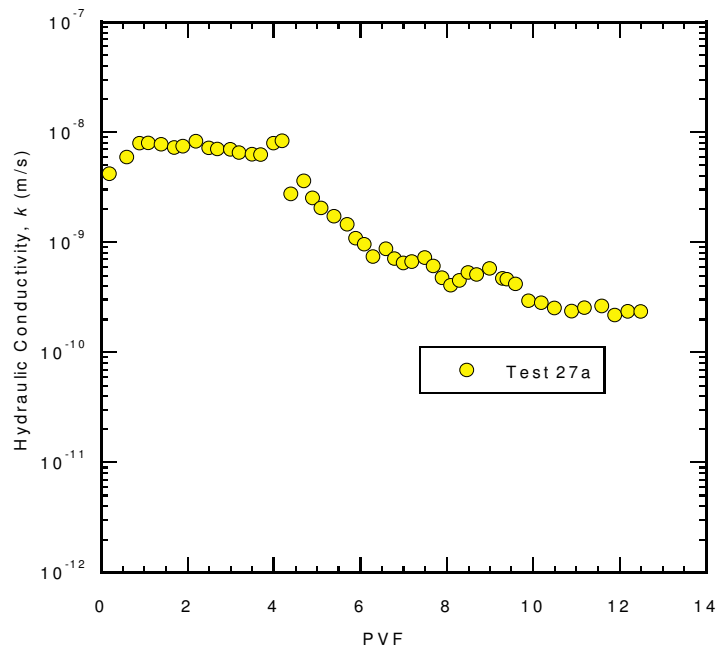


Figure E.39. Hydraulic conductivity, k , versus pore volumes of flow (PVF) for test series 27, GCL-2 permeated with synthetic bauxite mining process solution.

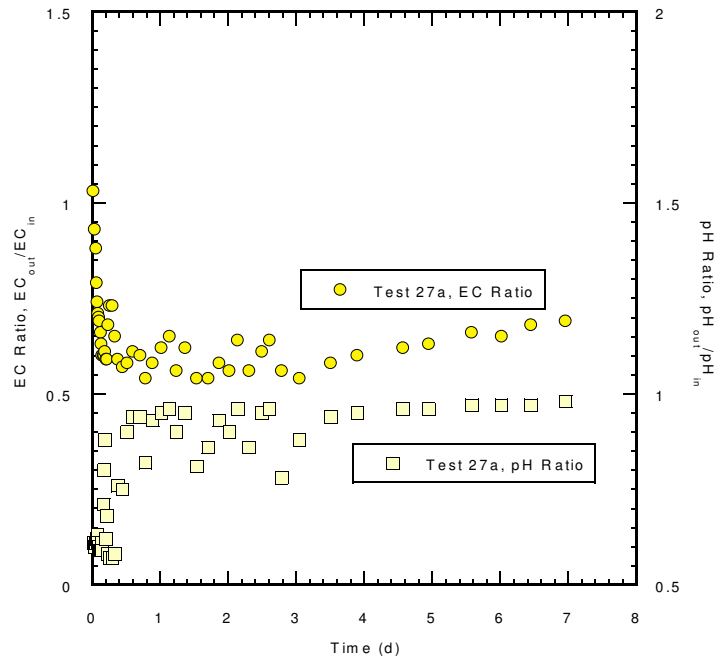


Figure E.40. EC Ratio and pH Ratio versus time for Test 27a, GCL-2 permeated with synthetic bauxite mining process solution.

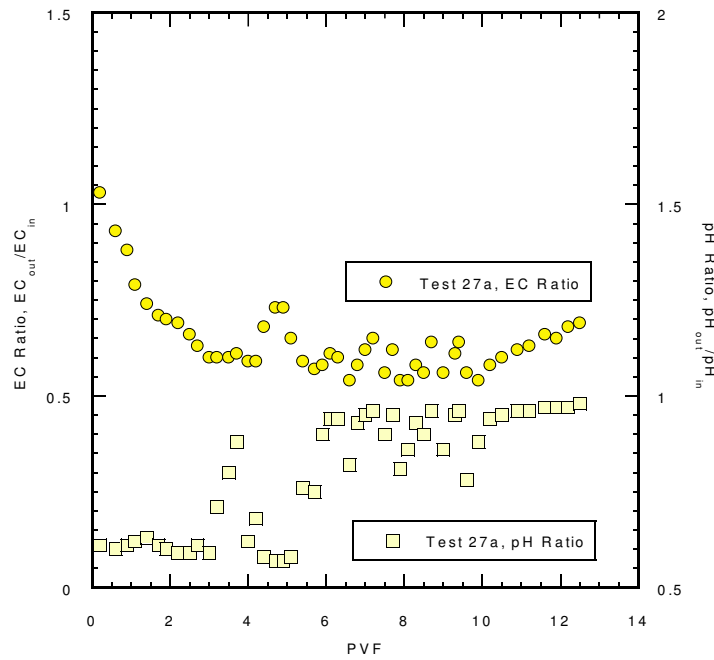


Figure E.41. EC Ratio and pH Ratio versus pore volumes of flow (PVF) for Test 27a, GCL-2 permeated with synthetic bauxite mining process solution.

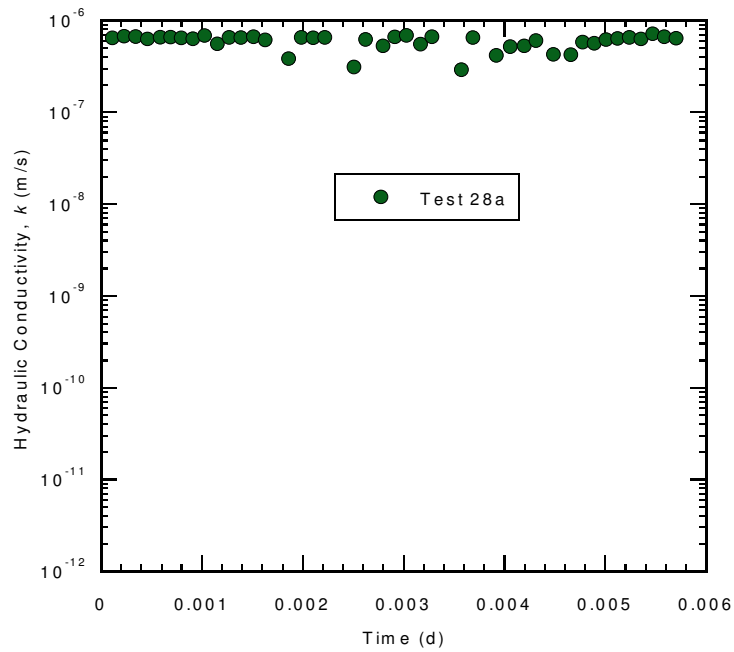


Figure E.42. Hydraulic conductivity, k , versus time for test series 28, GCL-2 permeated with synthetic copper mining process solution.

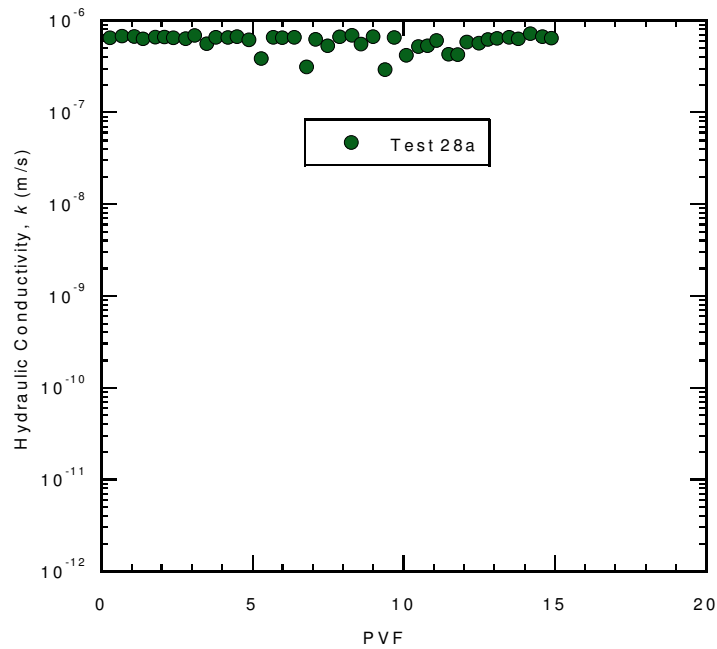


Figure E.43. Hydraulic conductivity, k , versus pore volumes of flow (PVF) for test series 28, GCL-2 permeated with synthetic copper mining process solution.

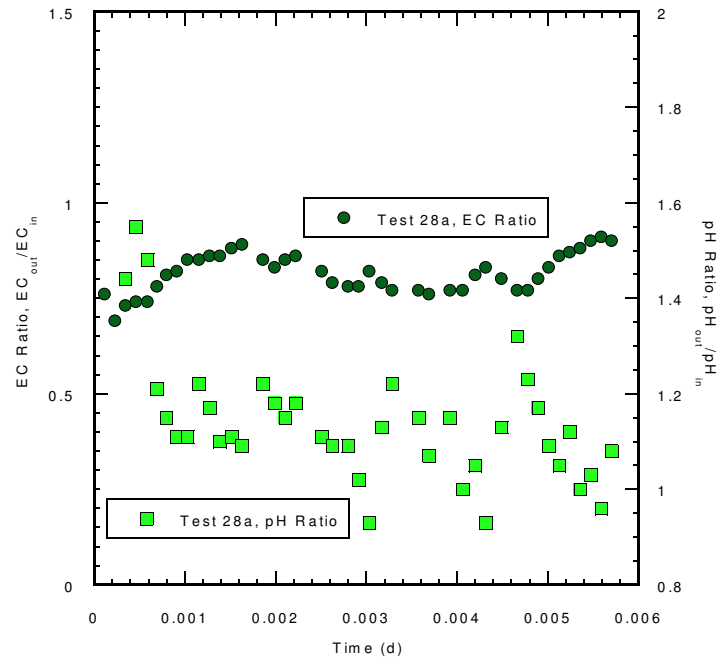


Figure E.44. EC Ratio and pH Ratio versus time for Test 28a, GCL-2 permeated with synthetic copper mining process solution.

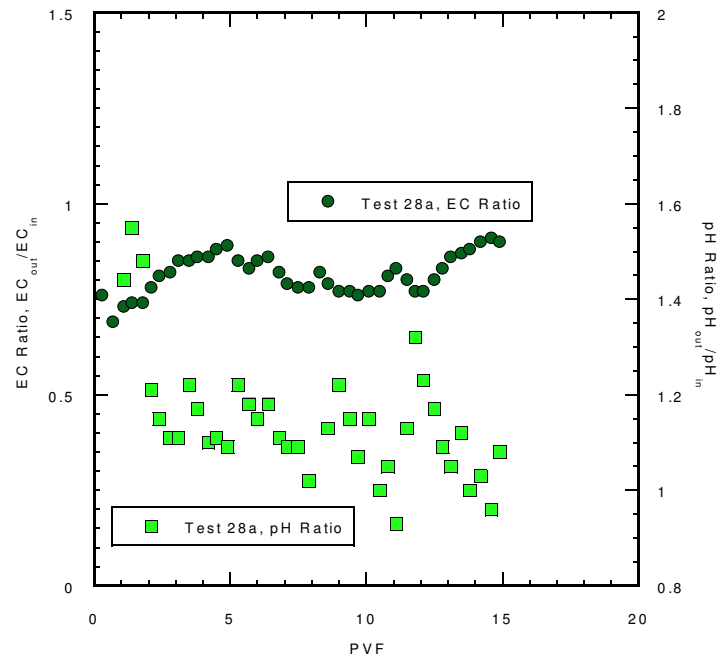


Figure E.45. EC Ratio and pH Ratio versus pore volumes of flow (PVF) for Test 28a, GCL-2 permeated with synthetic copper mining process solution.

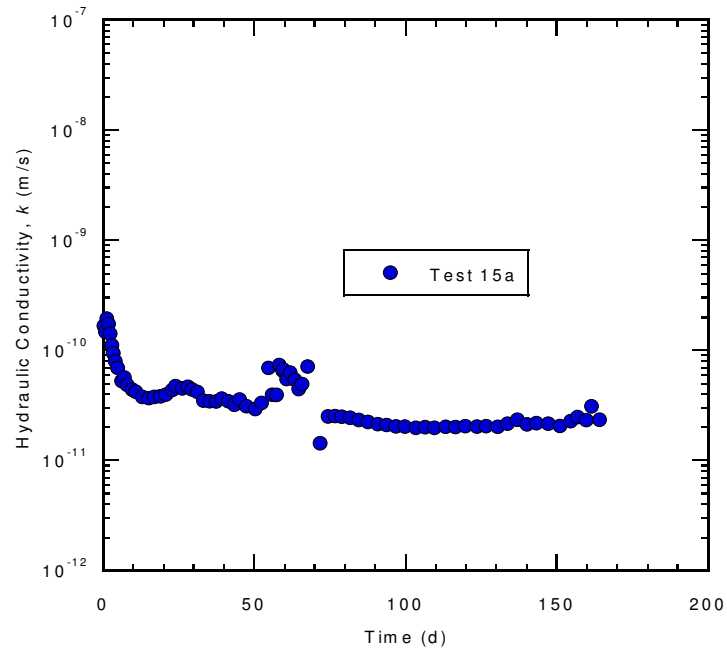


Figure E.46. Hydraulic conductivity, k , versus time for test series 15, GCL-1 (2710 N/m) permeated with conservative water.

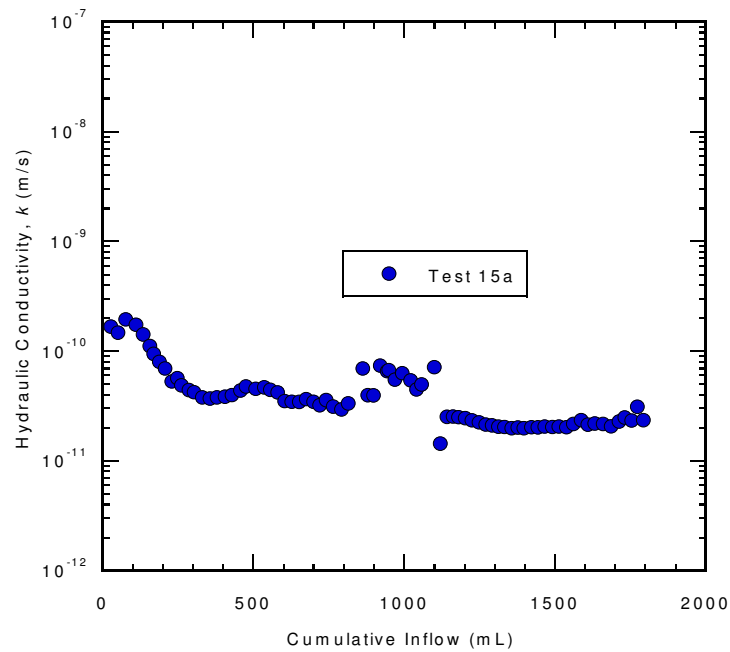


Figure E.47. Hydraulic conductivity, k , versus cumulative inflow (mL) for test series 15, GCL-1 (2710 N/m) permeated with conservative water.

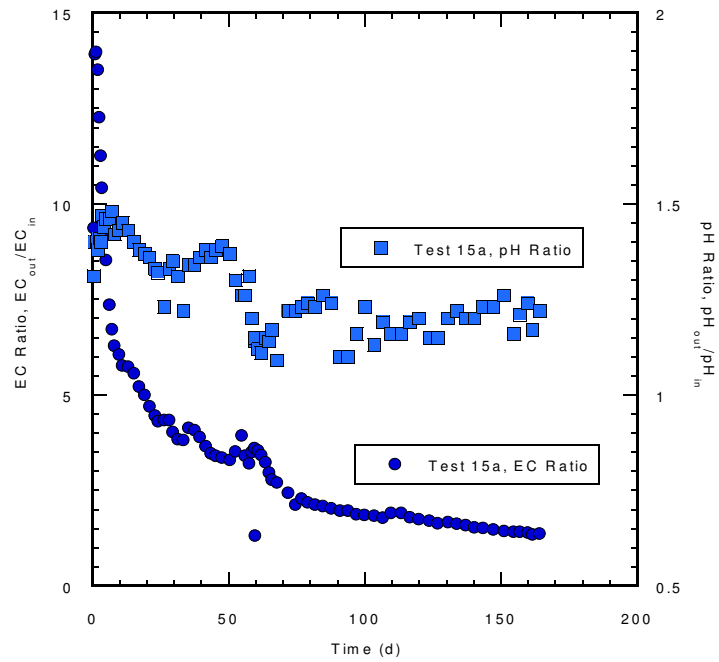


Figure E.48. EC Ratio and pH Ratio versus time for Test 15a, GCL-1 (2710 N/m) permeated with conservative water.

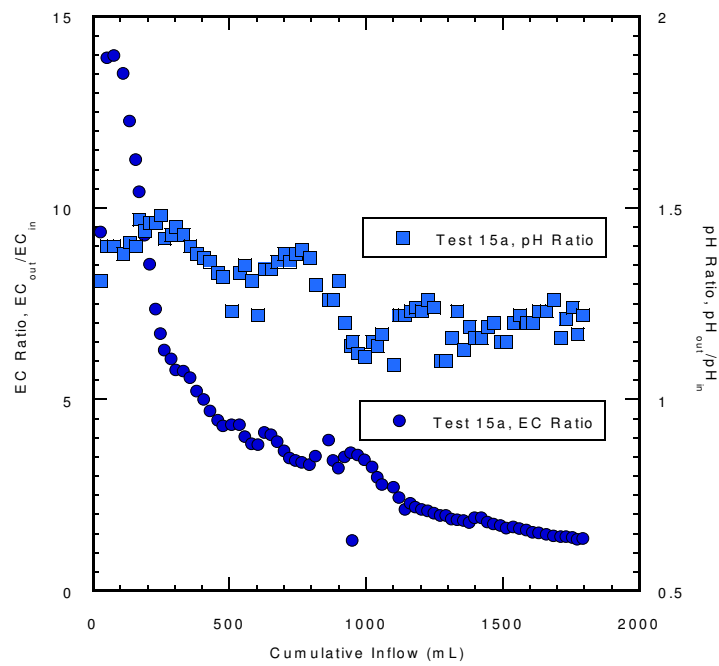


Figure E.49. EC Ratio and pH Ratio versus cumulative inflow (mL) for Test 15a, GCL-1 (2710 N/m) permeated with conservative water.

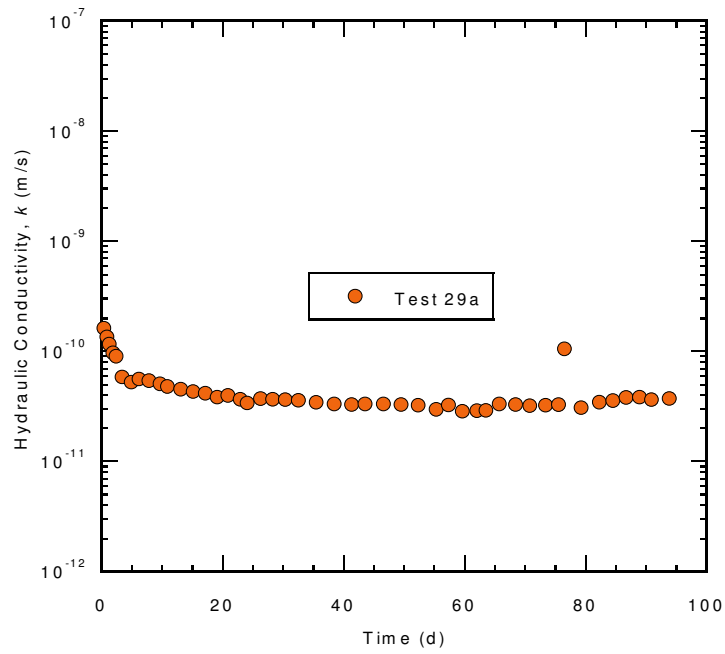


Figure E.50. Hydraulic conductivity, k , versus time for test series 29, GCL-1 (2710 N/m) permeated with synthetic gold mining process solution.

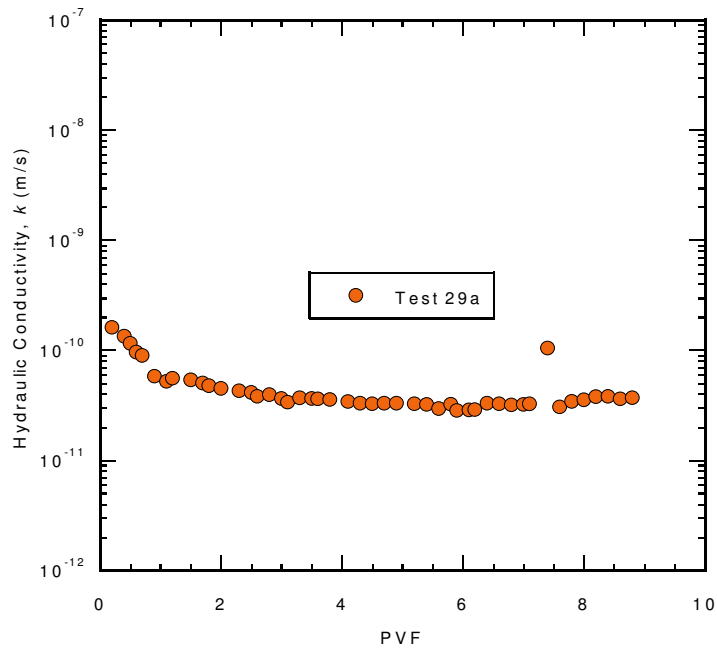


Figure E.51. Hydraulic conductivity, k , versus pore volumes of flow (PVF) for test series 29, GCL-1 (2710 N/m) permeated with synthetic gold mining process solution.

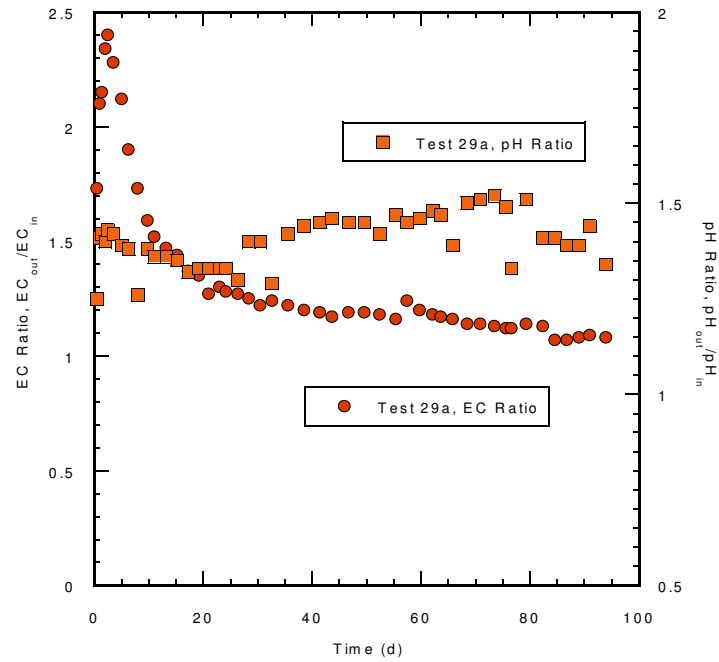


Figure E.52. EC Ratio and pH Ratio versus time for Test 29a, GCL-1 (2710 N/m) permeated with synthetic gold mining process solution.

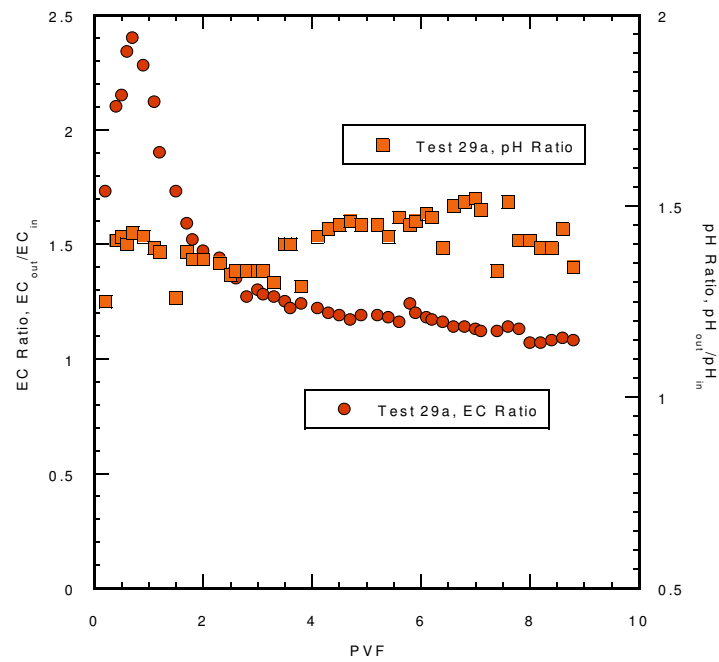


Figure E.53. EC Ratio and pH Ratio versus pore volumes of flow (PVF) for Test 29a, GCL-1 (2710 N/m) permeated with synthetic gold mining process solution.

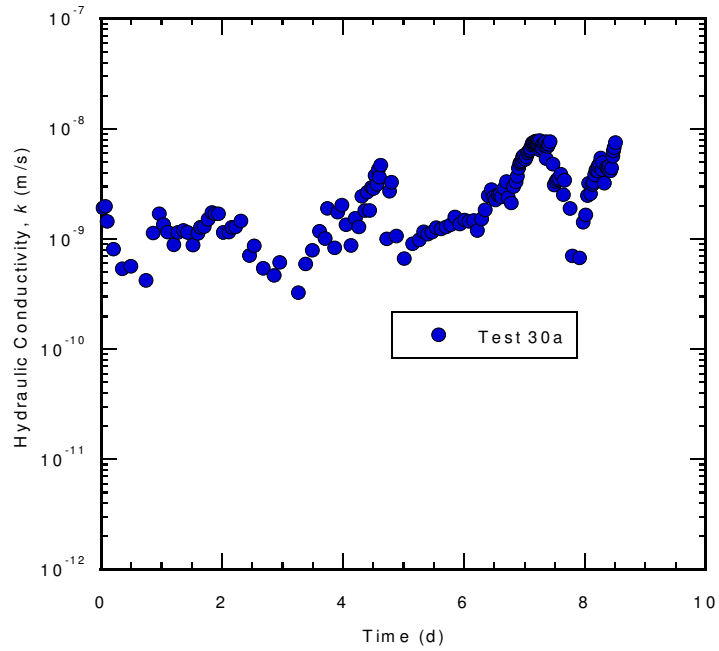


Figure E.54. Hydraulic conductivity, k , versus time for test series 30, GCL-1 permeated with conservative water.

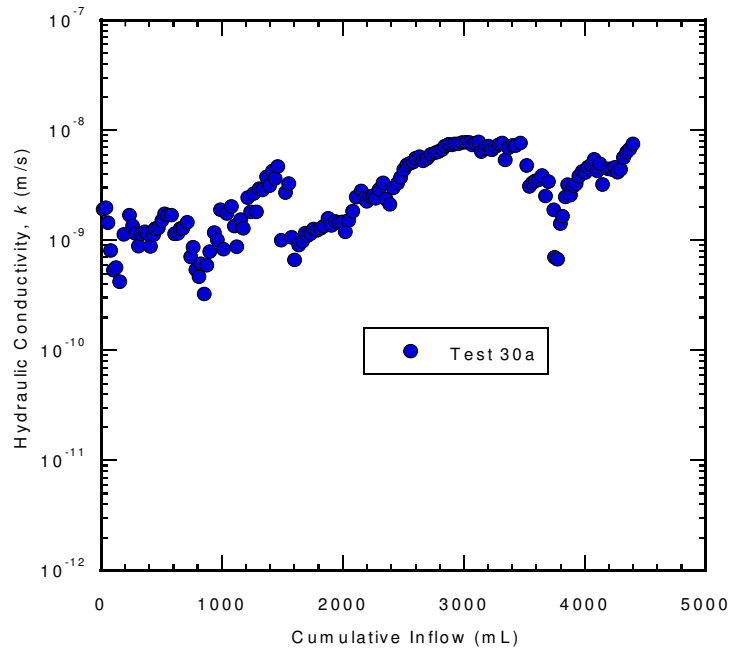


Figure E.55. Hydraulic conductivity, k , versus cumulative inflow for test series 30, GCL-1 permeated with conservative water.

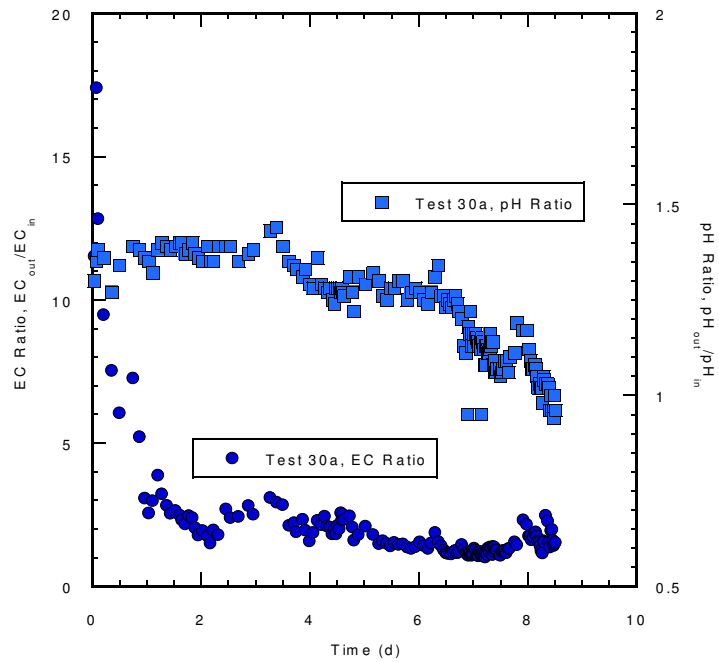


Figure E.56. EC Ratio and pH Ratio versus time for Test 30a, GCL-1 permeated with conservative water.

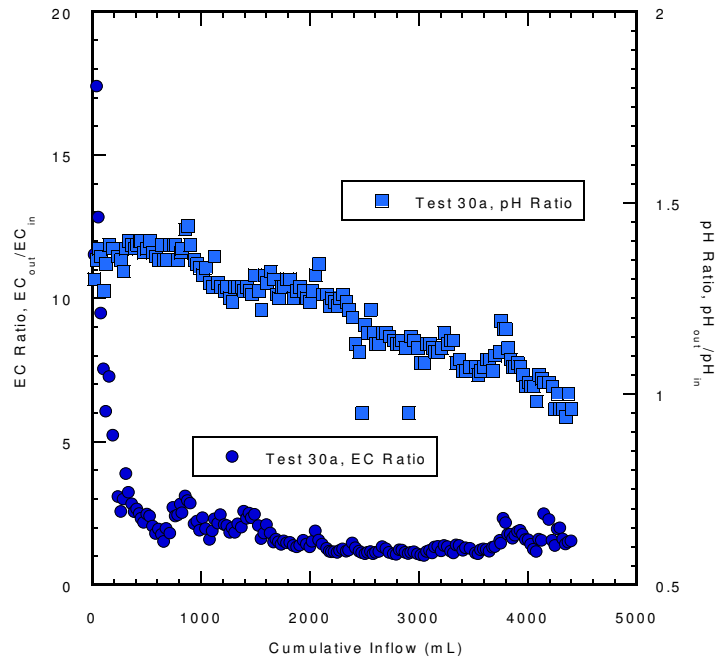


Figure E.57. EC Ratio and pH Ratio versus cumulative inflow (mL) for Test 30a, GCL-1 permeated with conservative water.

E.2 COMPARISON PLOTS BASED ON GCL TYPE

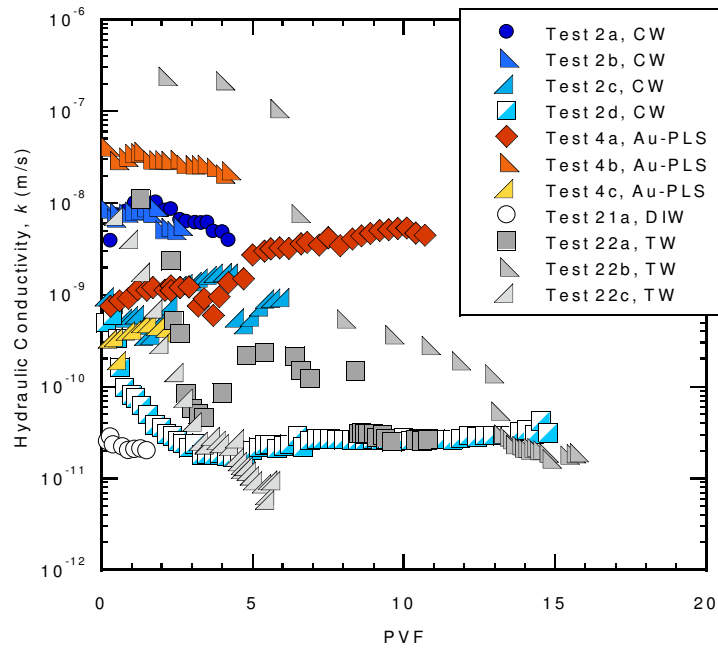


Figure E.58. Hydraulic conductivity, k , versus pore volumes of flow (PVF) for GCL-1

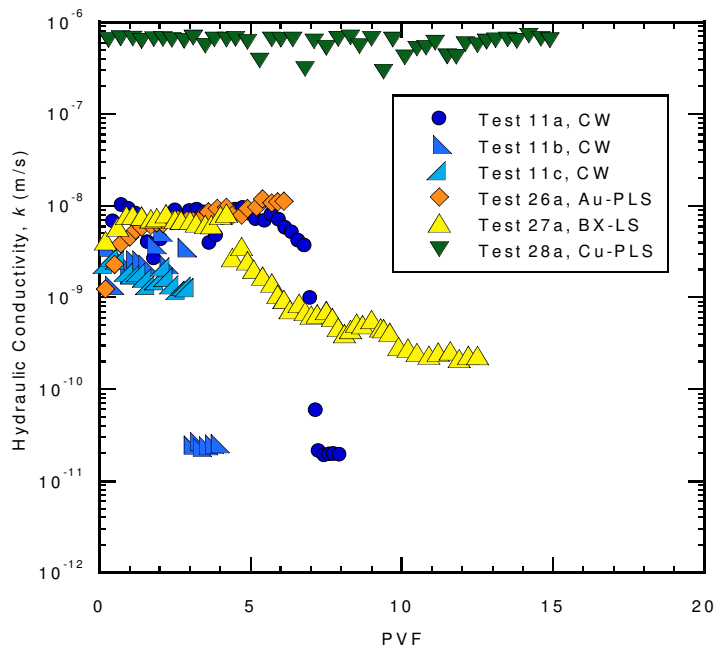


Figure E.59. Hydraulic conductivity, k , versus pore volumes of flow (PVF) for GCL-2

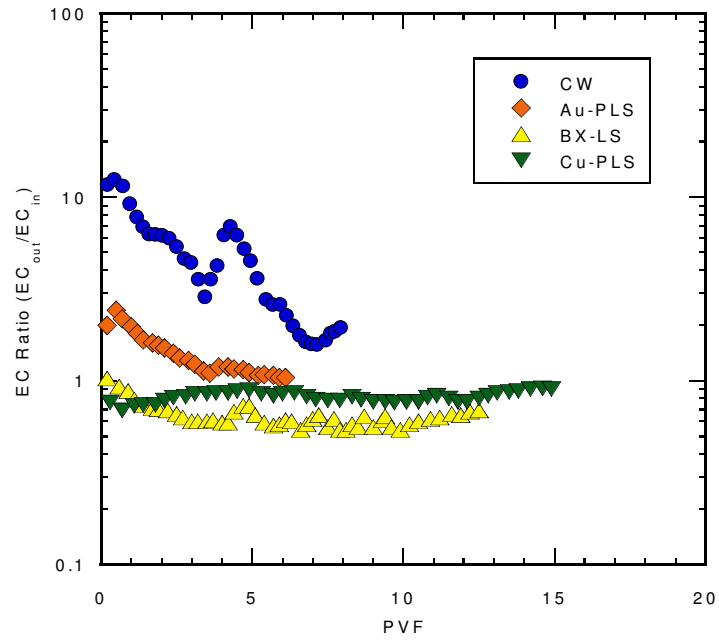


Figure E.60. EC Ratio versus pore volumes of flow (PVF) for GCL-2.

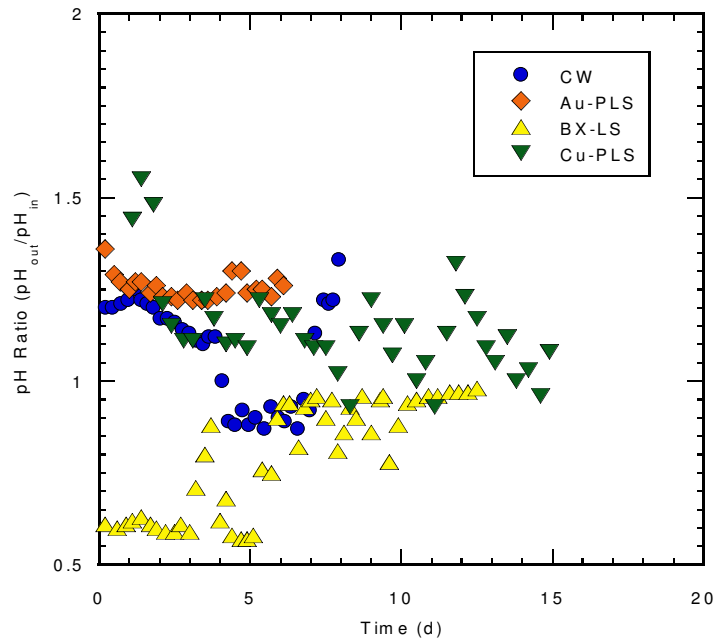


Figure E.61 pH Ratio versus pore volumes of flow (PVF) for GCL-2.

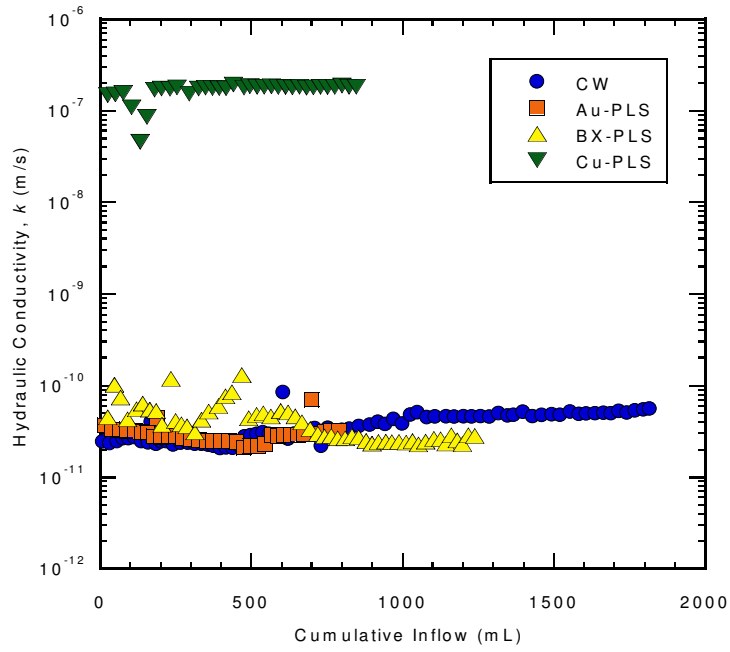


Figure E.62. Hydraulic conductivity, k , versus cumulative inflow for GCL-3

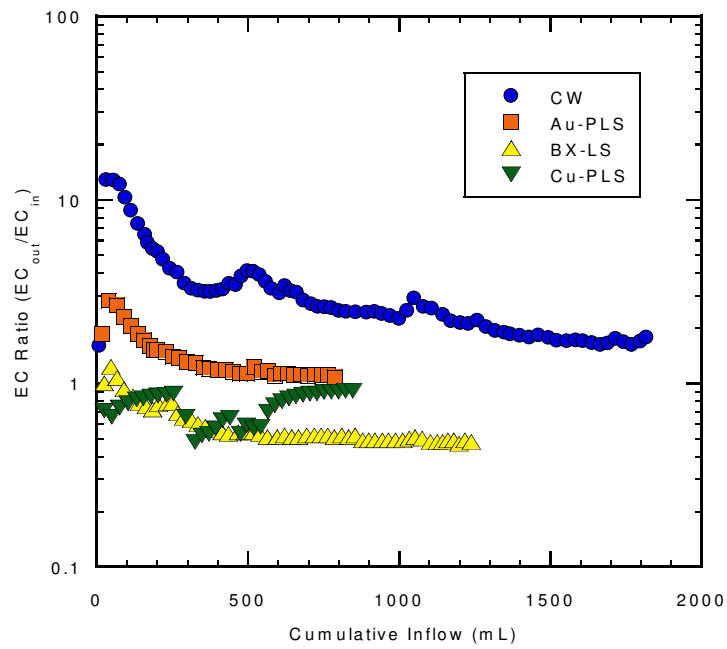


Figure E.63 EC ratio versus cumulative inflow for GCL-3

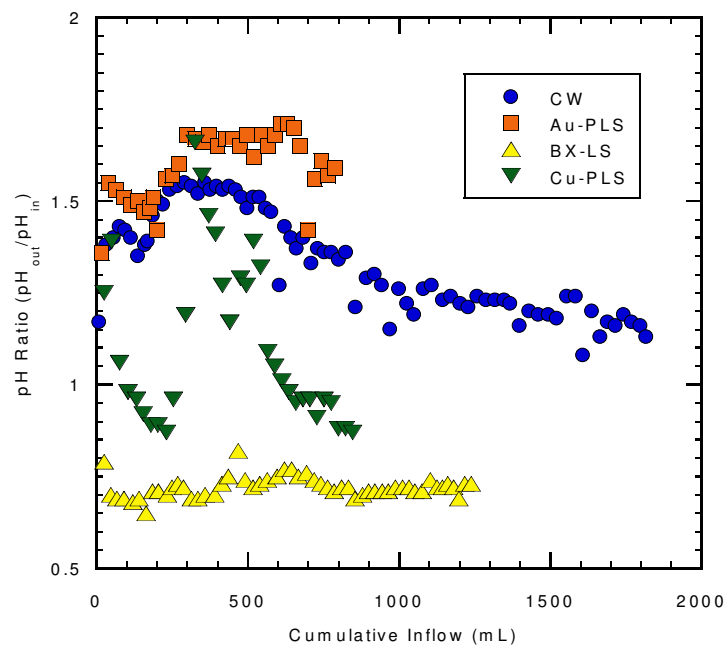


Figure E.64. pH ratio versus cumulative inflow for GCL-3

E.3 COMPARISON BASED ON PERMEANT LIQUID

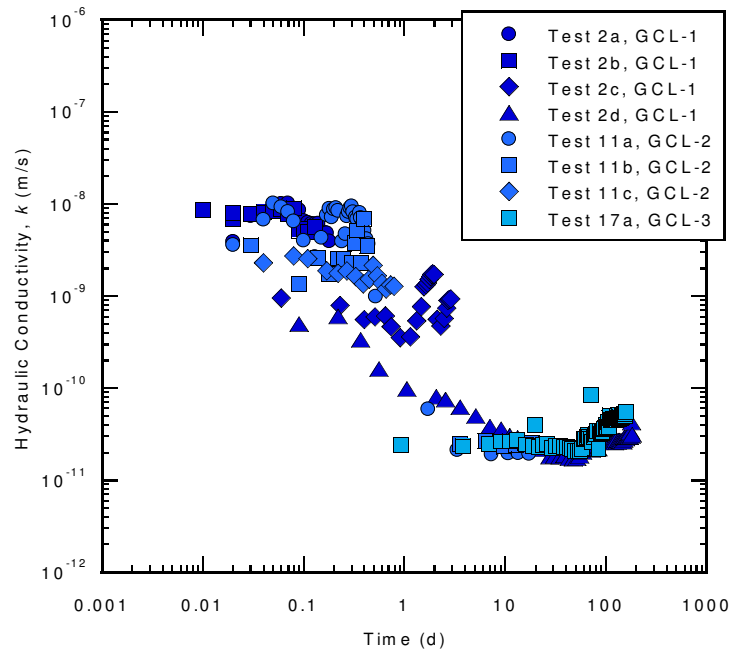


Figure E.65. Hydraulic conductivity, k , versus log time for specimens permeated with conservative water.

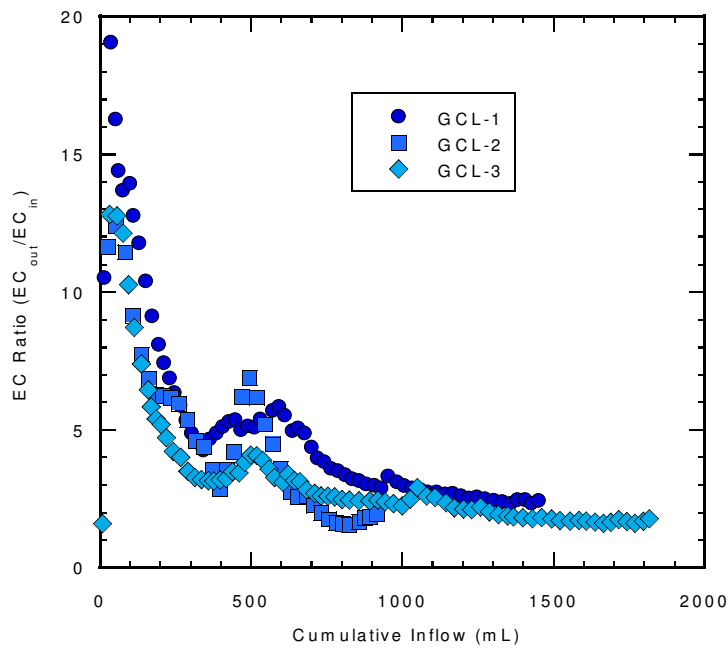


Figure E.66. EC Ratio versus cumulative inflow for specimens permeated with conservative water

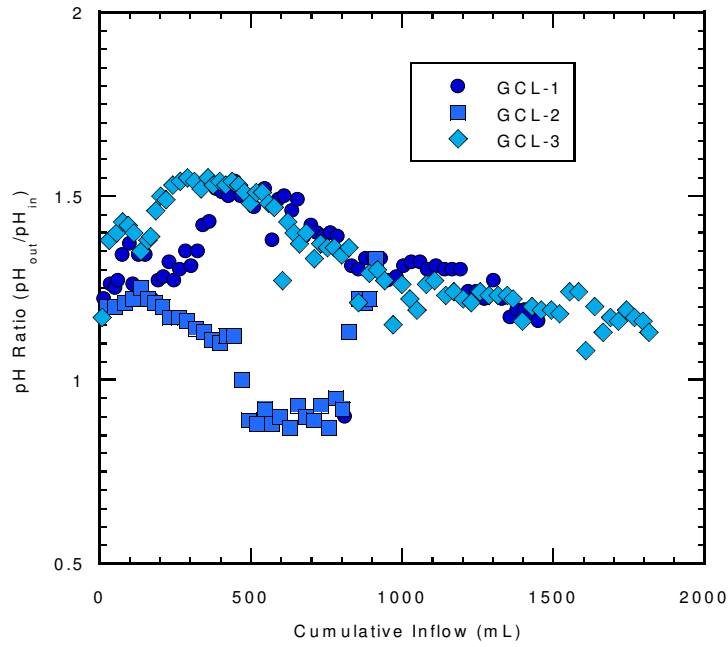


Figure E.67. pH Ratio versus cumulative inflow for specimens permeated with conservative water

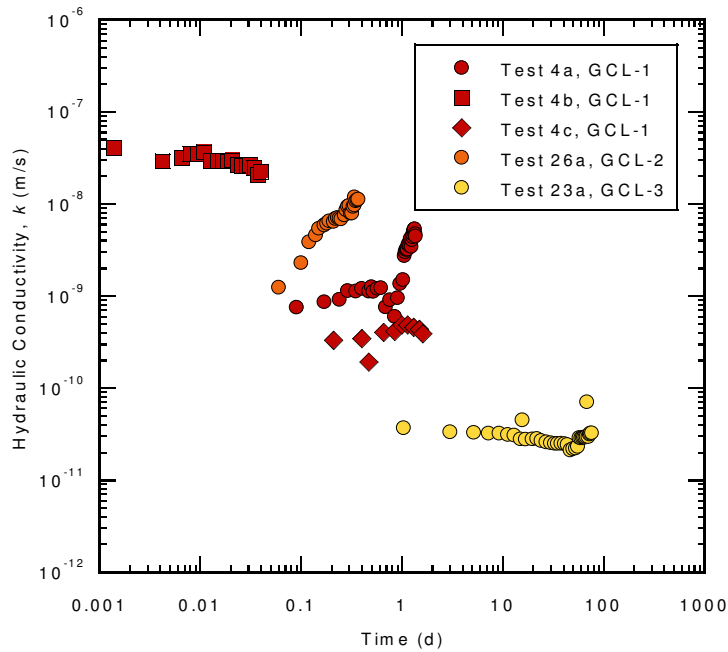


Figure E.68. Hydraulic conductivity, k , versus log time for specimens permeated with synthetic gold mining process solution.

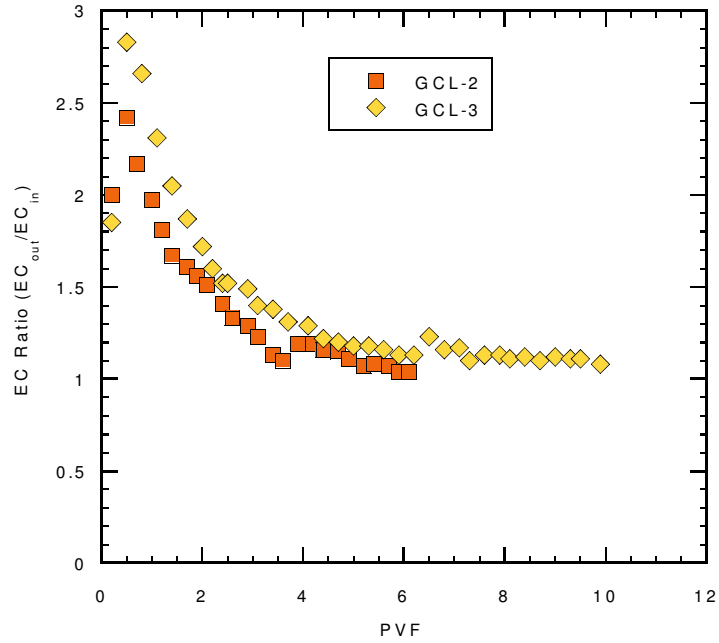


Figure E.69. Hydraulic conductivity, k , versus pore volumes of flow (PVF) for specimens permeated with synthetic gold mining process solution.

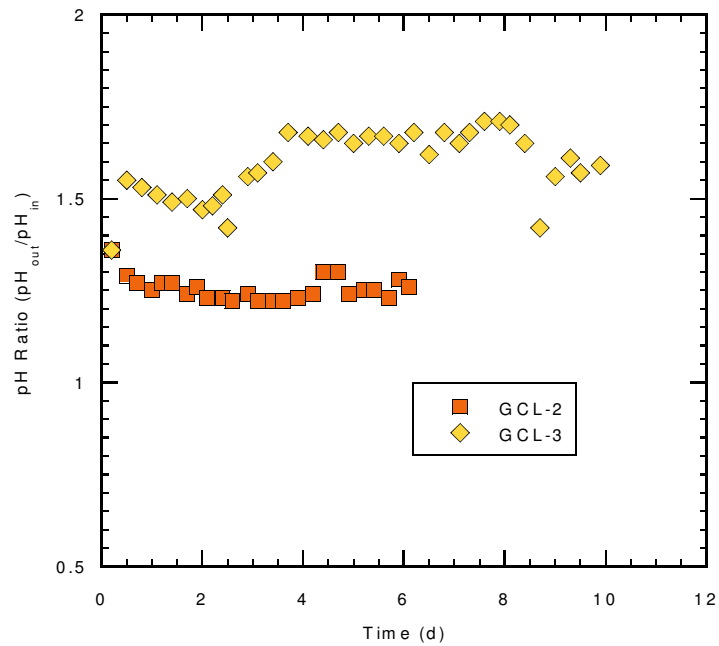


Figure E.70. pH Ratio versus time for specimens permeated with synthetic gold mining process solution.

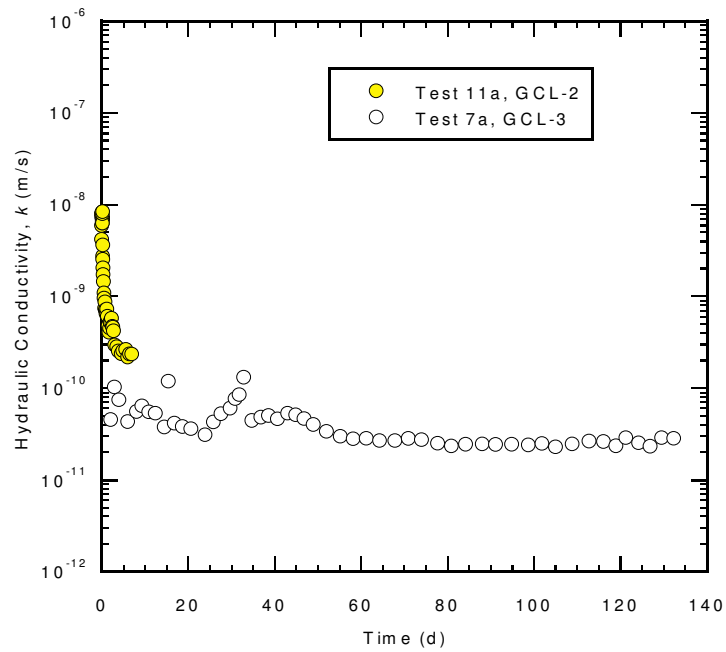


Figure E.71. Hydraulic conductivity, k , versus time for specimens permeated with synthetic bauxite mining process solution.

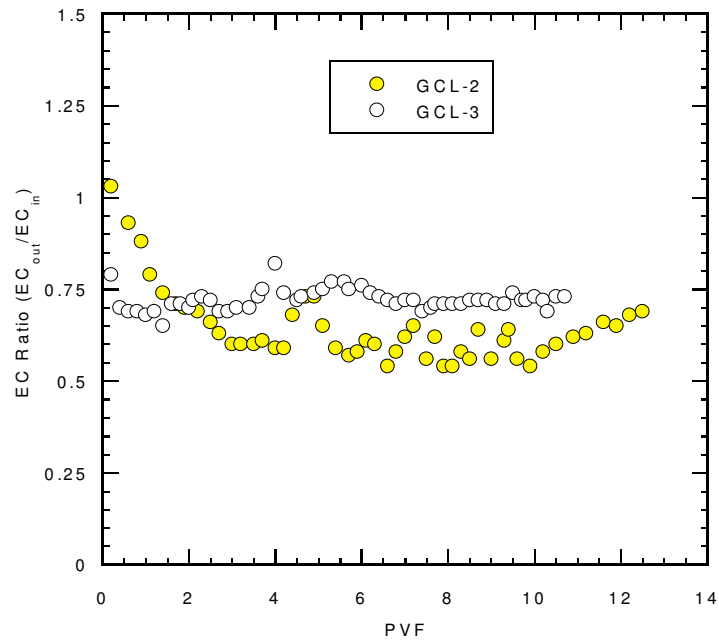


Figure E.72. EC Ratio versus pore volumes of flow (PVF) for specimens permeated with synthetic bauxite mining process solution.

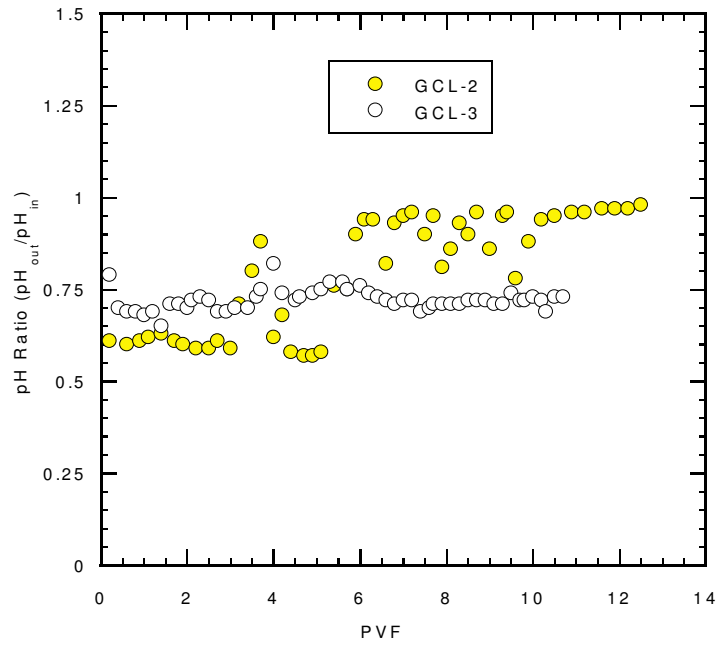


Figure E.73. pH ratio versus pore volume of flow (PVF) for specimens permeated with synthetic bauxite mining process solution.

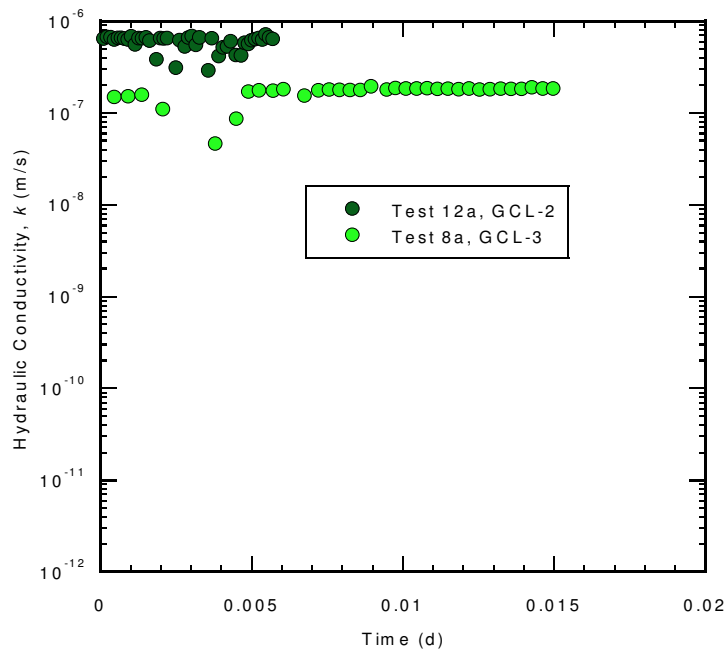


Figure E.74. Hydraulic conductivity, k , versus log time for specimens permeated with synthetic copper mining process solution.

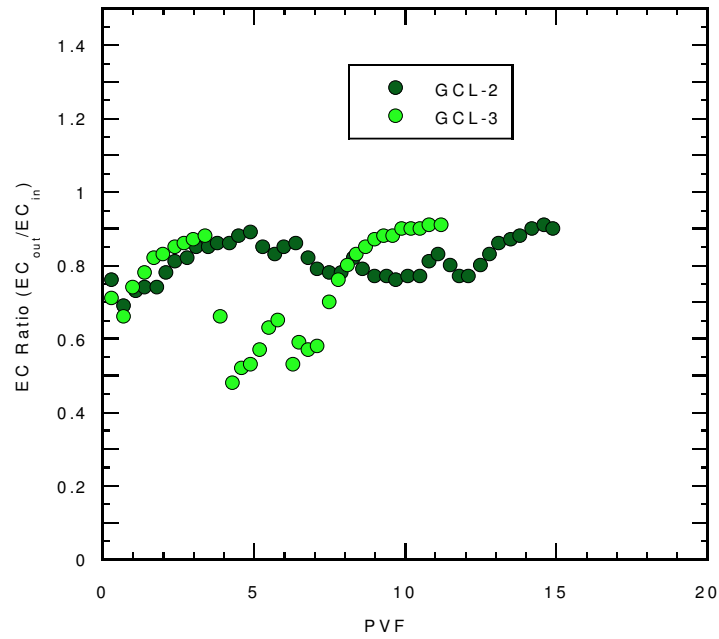


Figure E.75. EC Ratio versus pore volumes of flow (PVF) for specimens permeated with synthetic copper mining process solution.

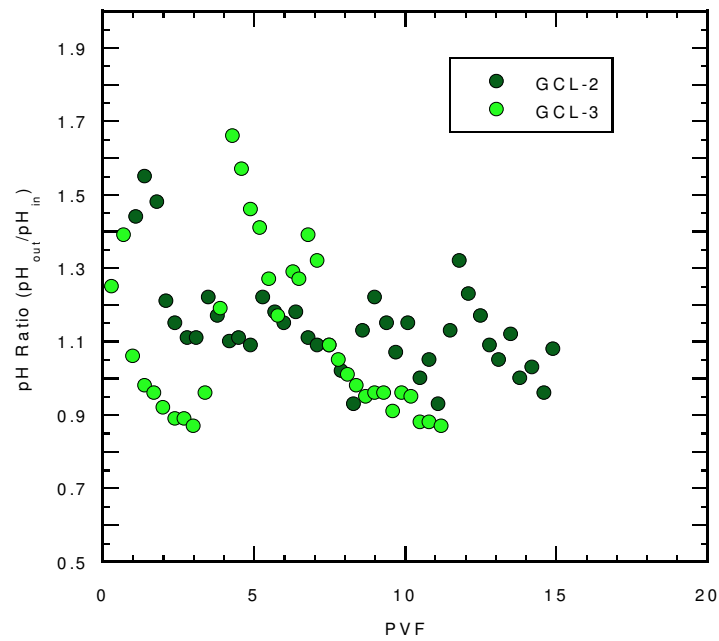


Figure E.76. pH Ratio versus pore volumes of flow (PVF) for specimens permeated with synthetic copper mining process solution.

E.4 COMPARISON OF HYDRAULIC CONDUCTIVITY TO FIBER BUNDLE PROPERTIES

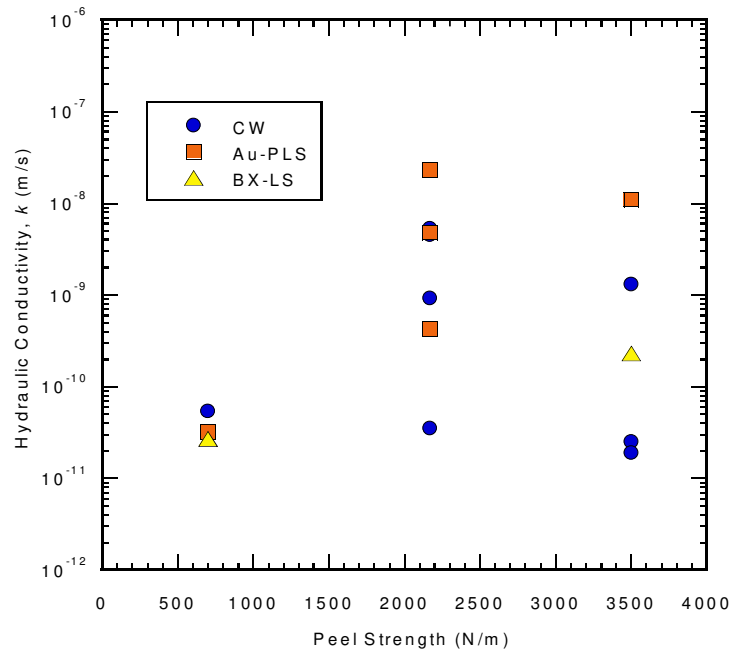


Figure E.77. Hydraulic conductivity, k , versus manufacturer reported average peel strength.

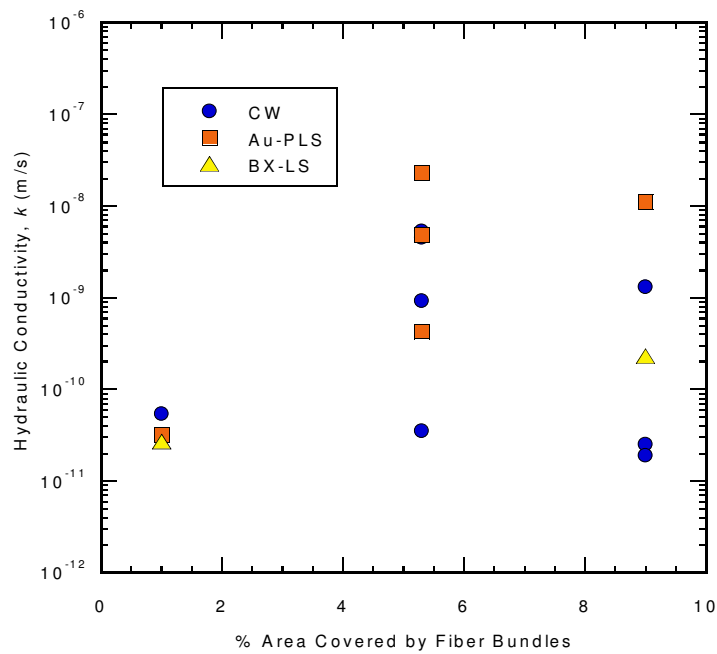


Figure E.78. Hydraulic conductivity, k , versus estimated percent area covered by fiber bundles.

APPENDIX F

Additional photographs

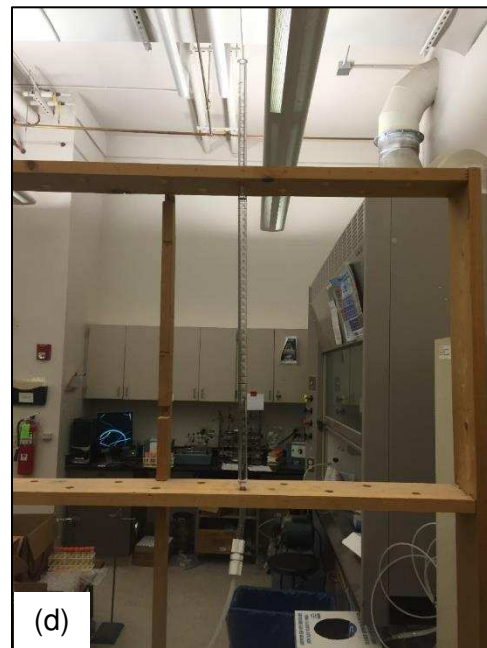
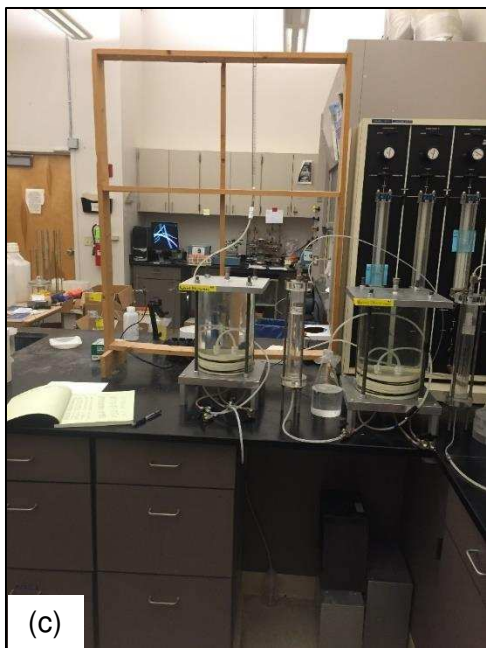
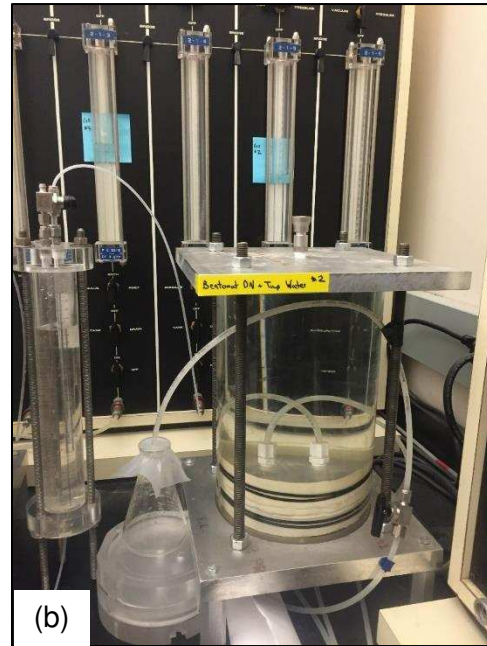
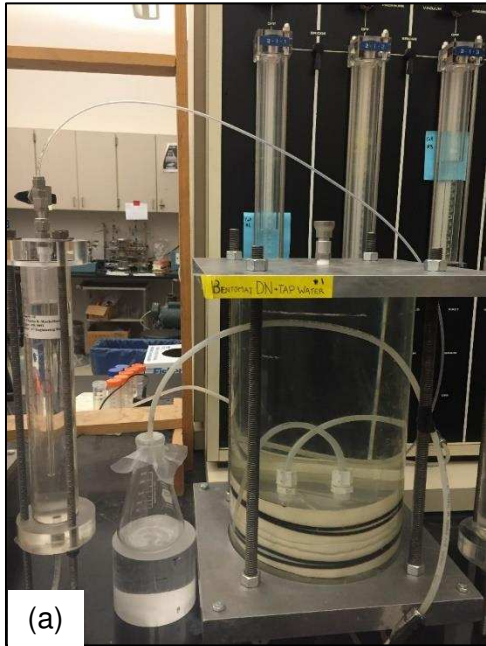


Figure F.1. Experimental setup of Test Series 22, GCL-1 permeated with tap water. (a) Permeameter. (b) Permeameter. (c) Full set up. (d) Old burette stand.

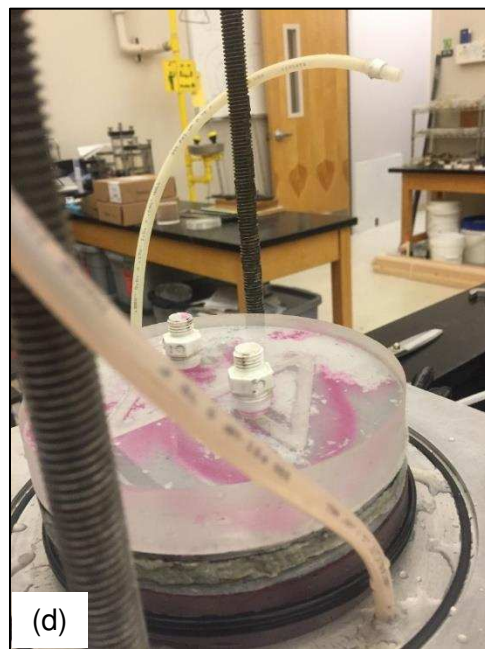
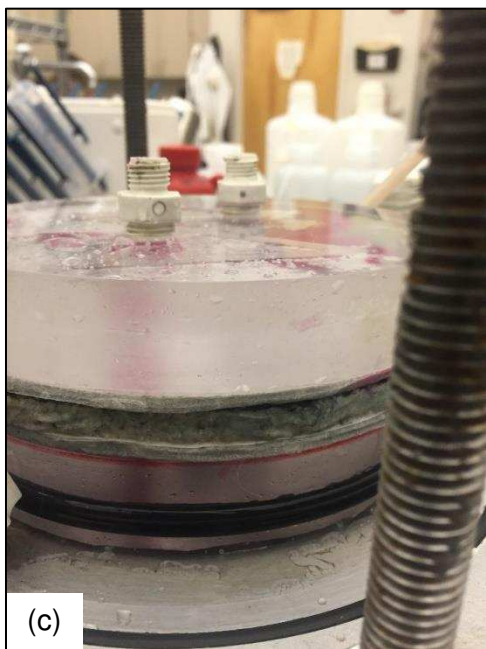
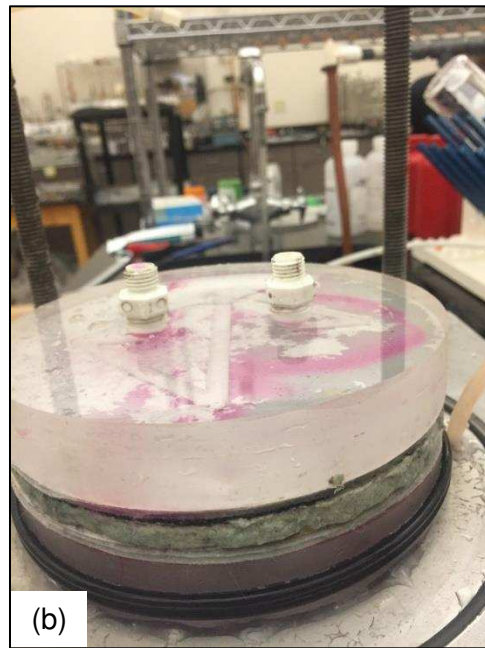
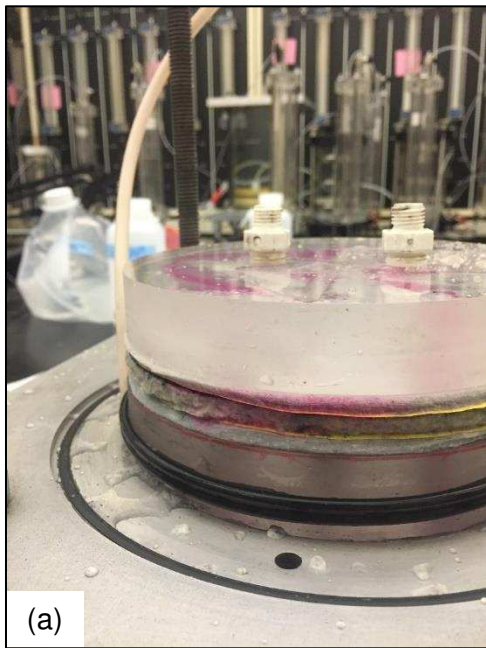


Figure F.2. (a), (b), (c), (d) Dyed disassembly of Test 4a.

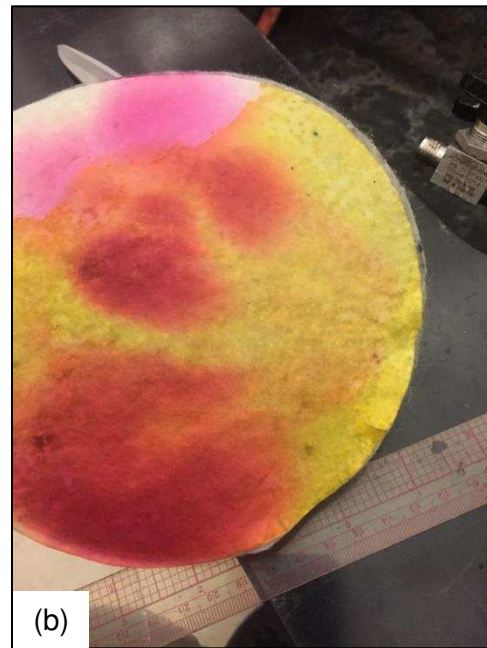


Figure F.3. Test 4a dyed disassembly, (a) top view of effluent geotextile, (b) bottom view of effluent filter paper, (c) bottom view of influent geotextile, (d) view of influent side of GCL.

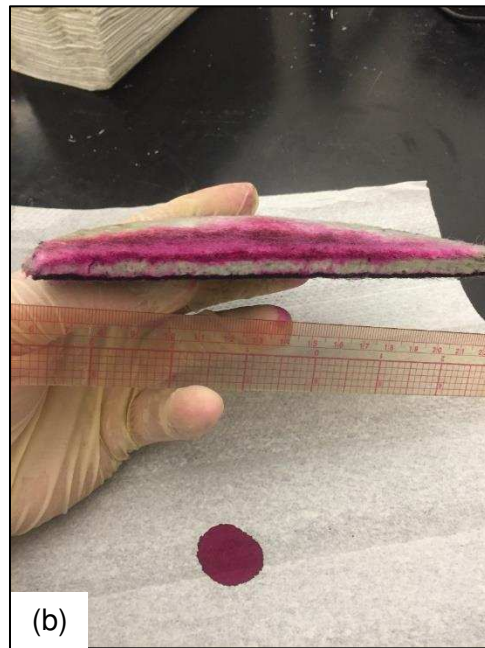


Figure F.4. Test 4a dyed disassembly, (a) view of influent side of GCL, (b) GCL cross section, (c) GCL cross section, (d) GCL cross section.



Figure F.5. Test 4a dyed disassembly, (a) GCL cross section, (b) GCL cross section, (c) GCL cross section, view of fiber bundles, (d) GCL cross section, view of fiber bundles.



Figure F.6. Test 4a dyed disassembly, (a), (b), (c), (d) GCL cross section, view of fiber bundles.

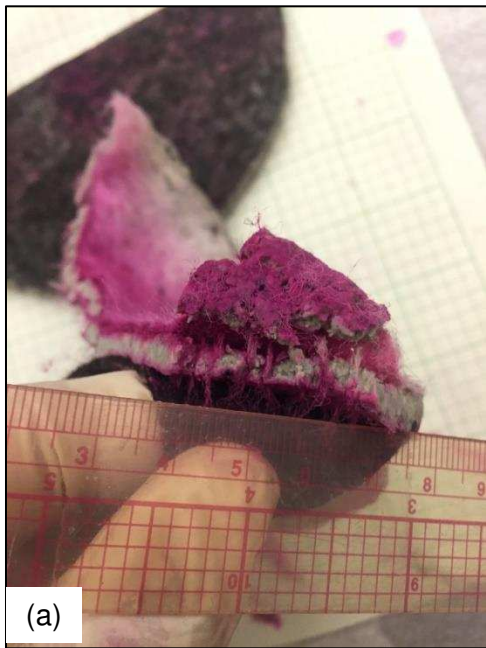


Figure F.7. Test 4a dyed disassembly, (a), (b), (c), (d) GCL cross section, view of fiber bundles.



Figure F.8. Test 4a dyed disassembly. GCL cross section, view of fiber bundles.

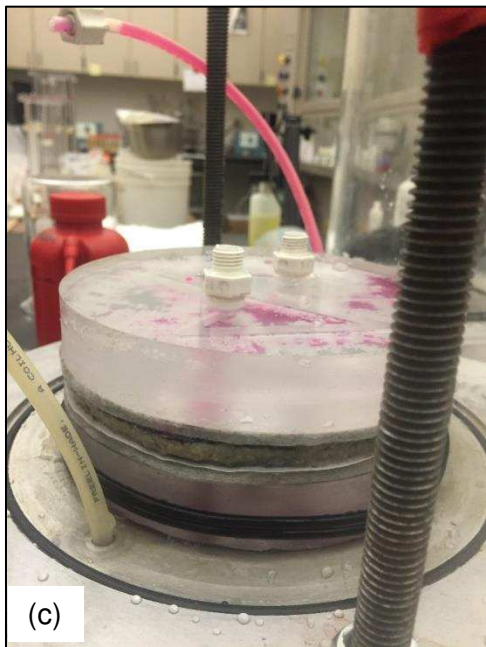


Figure F.9. (a), (b), (c), (d) Test 4b dyed disassembly.



Figure F.10. (a), (b), (c), (d) Test 4b dyed disassembly.

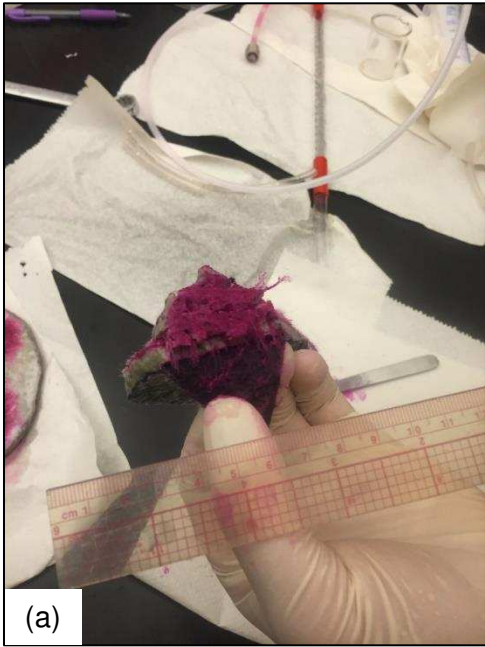


Figure F.11. (a), (b), (c), (d) Test 4b dyed disassembly.

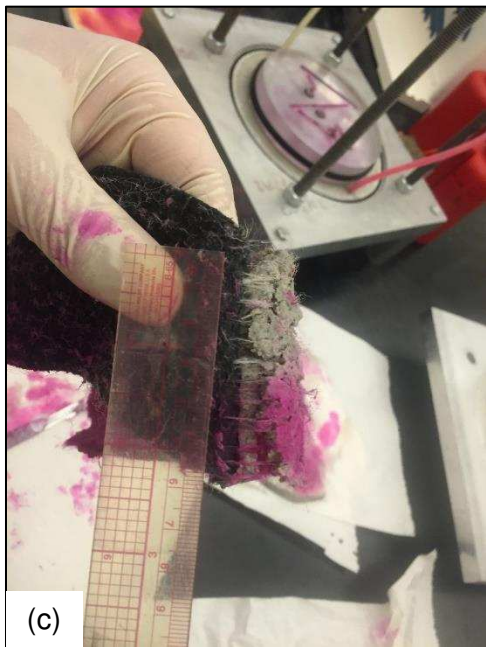


Figure F.12. (a), (b), (c), (d) Test 4b dyed disassembly.



Figure F.13. (a), (b), (c) Test 4b dyed disassembly.

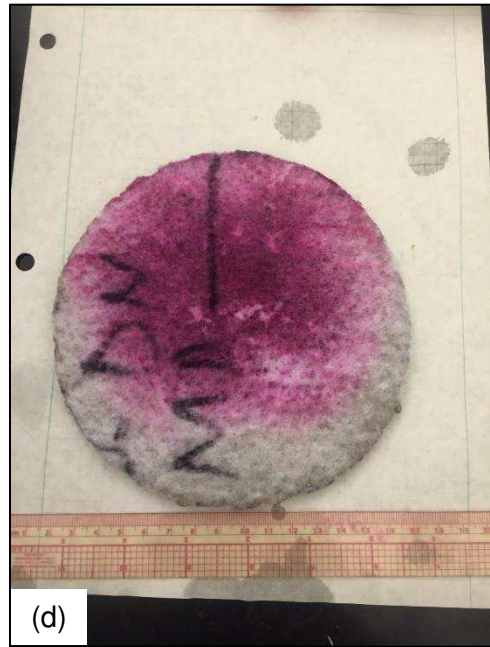


Figure F.14. (a), (b), (c), (d) Test 4c dyed disassembly.

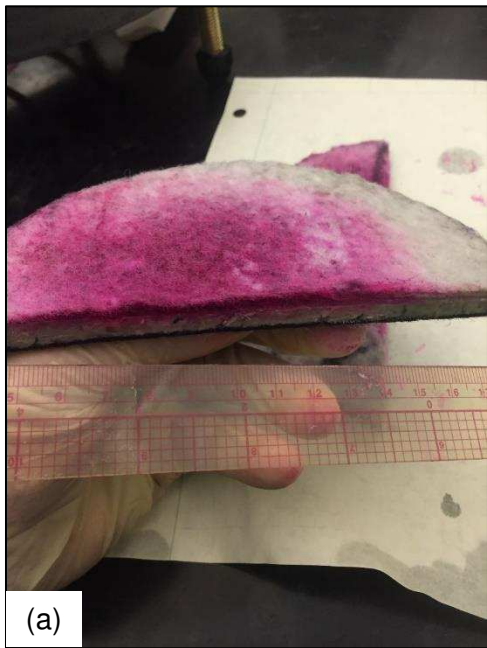


Figure F.15. (a), (b), (c), (d) Test 4c dyed disassembly.

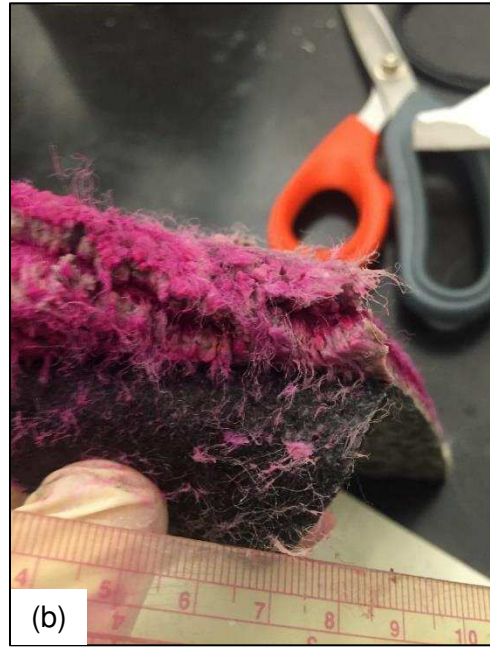


Figure F.16. (a), (b), (c), (d) Test 4c dyed disassembly.



Figure F.17. (a), (b), (c), Test 4c dyed disassembly.

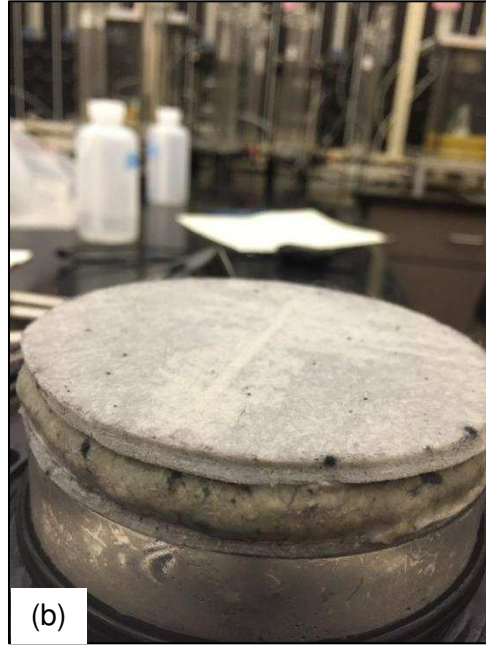


Figure F.18. (a), (b), (c), (d) Test 1a disassembly.

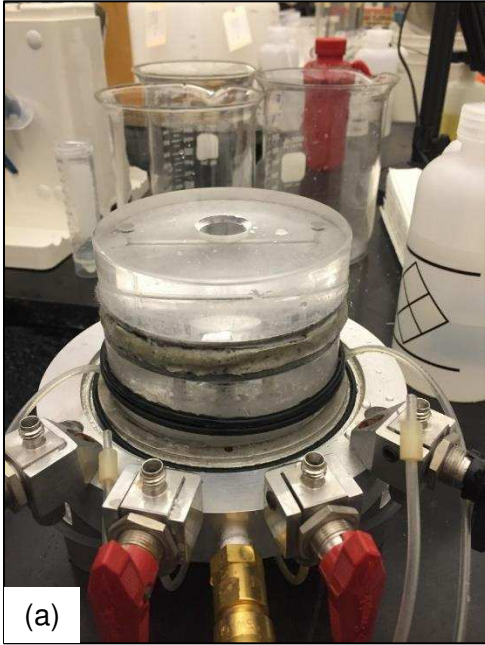


Figure F.19. (a), (b), (c), (d) Test 1b disassembly.



Figure F.20. (a), (b) Test 1b disassembly.

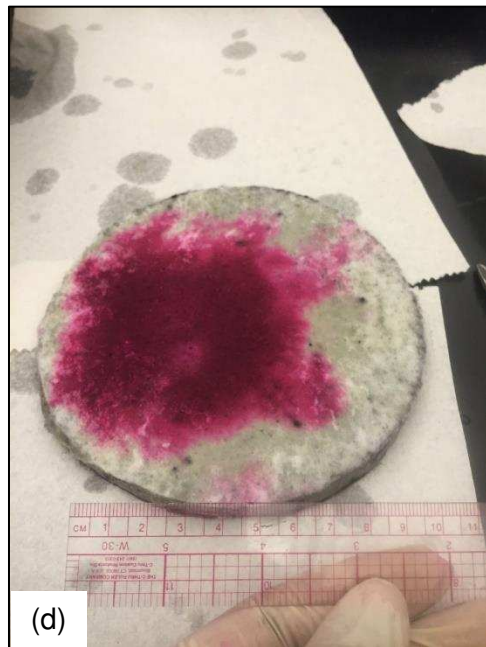
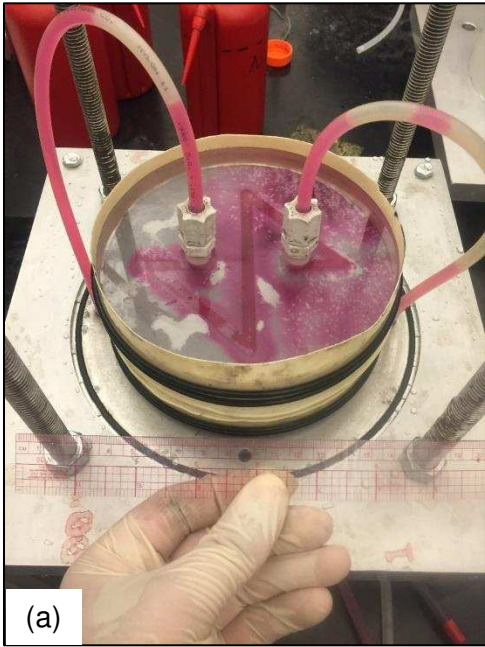


Figure F.21. (a), (b), (c), (d) Test 2a dyed disassembly.



Figure F.22. (a), (b), (c), (d) Test 2a dyed disassembly.



Figure F.23. (a), (b), (c), (d) Test 2a dyed disassembly.



Figure F.24. (a), (b), (c), (d) Test 2a dyed disassembly.



Figure F.25. (a), (b), (c), (d) Test 2a dyed disassembly.



Figure F.26. (a), (b), (c) Test 2a dyed disassembly.

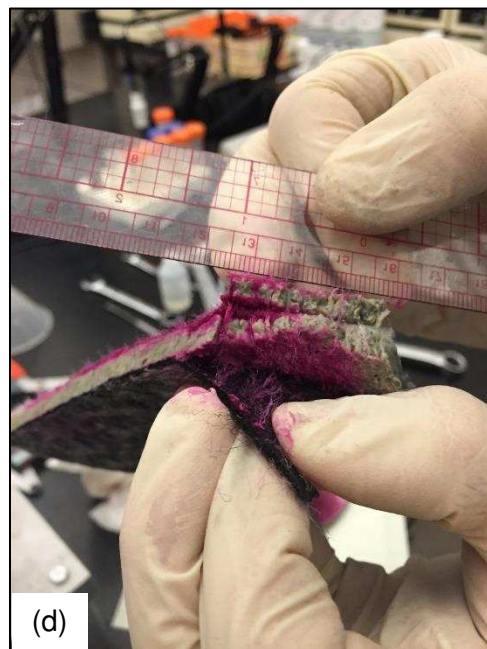
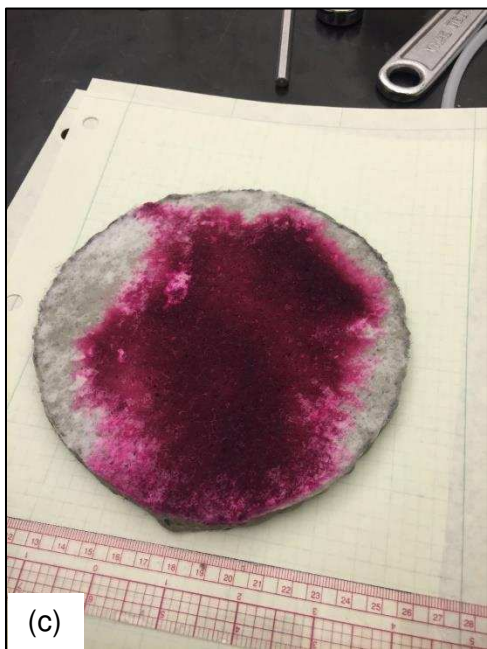
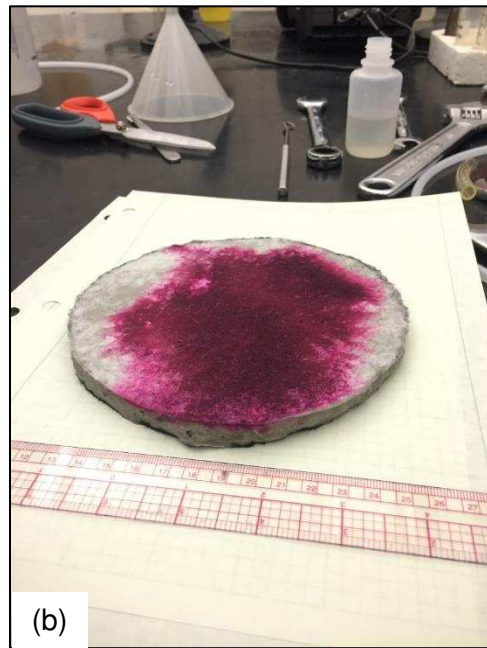
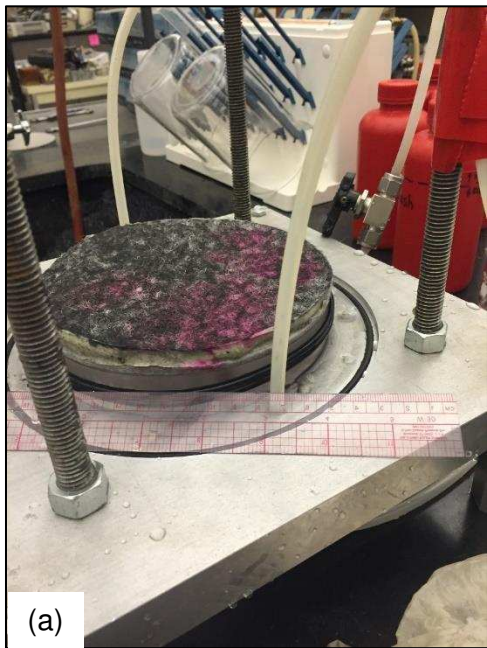


Figure F.27. (a), (b), (c), (d) Test 2b dyed disassembly.



Figure F.28. (a), (b), (c), (d) Test 2b dyed disassembly.

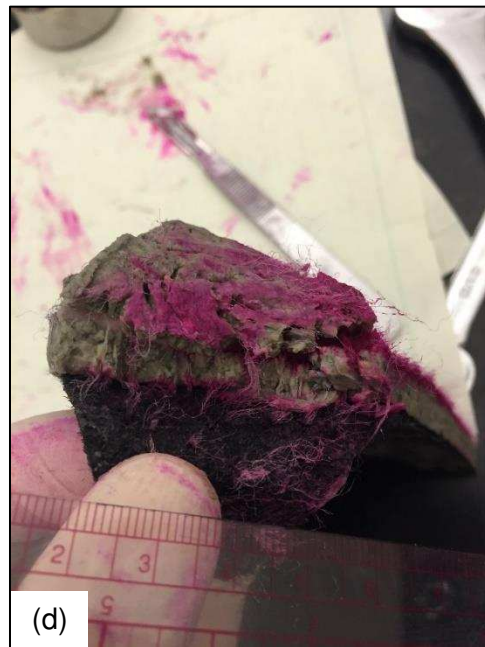
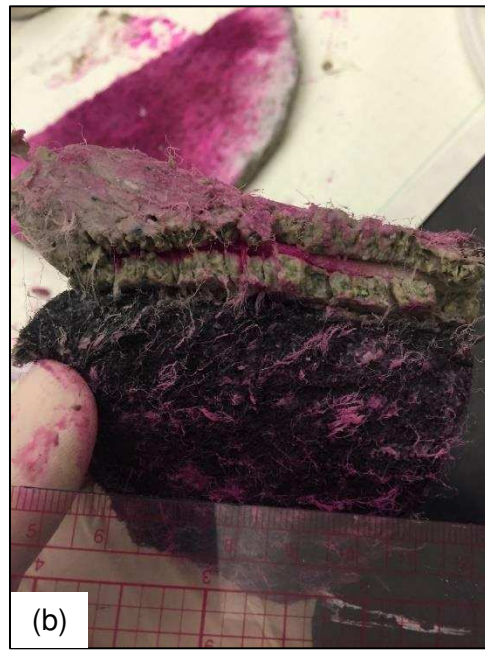


Figure F.29. (a), (b), (c), (d) Test 2b dyed disassembly.

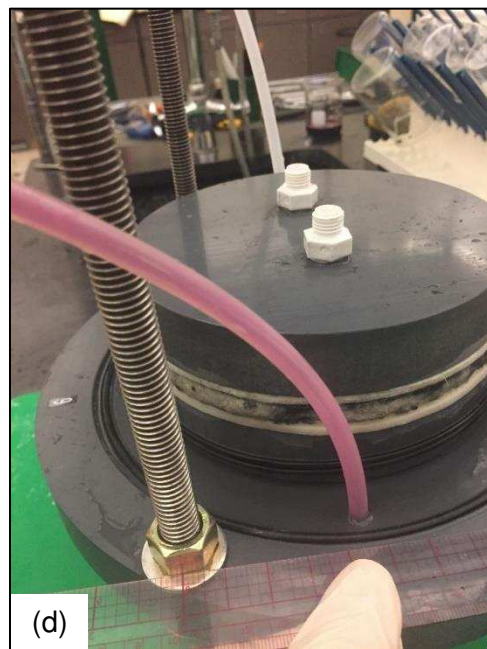
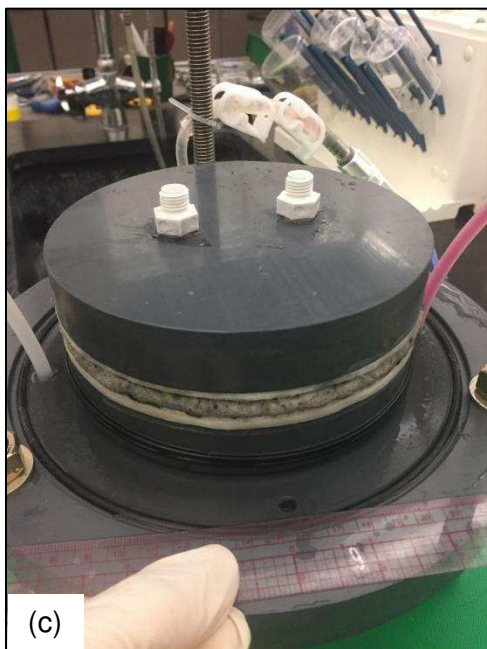
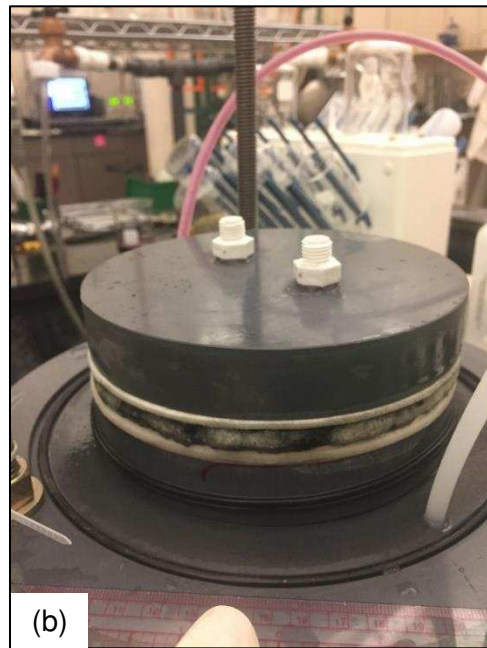


Figure F.30. (a), (b), (c), (d) Test 27a dyed disassembly.

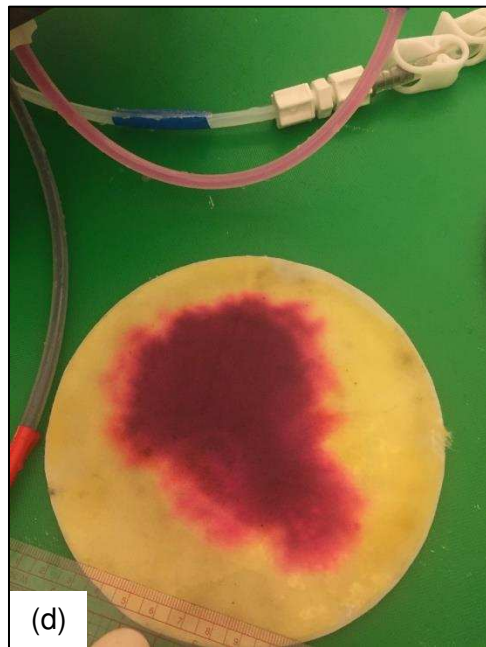
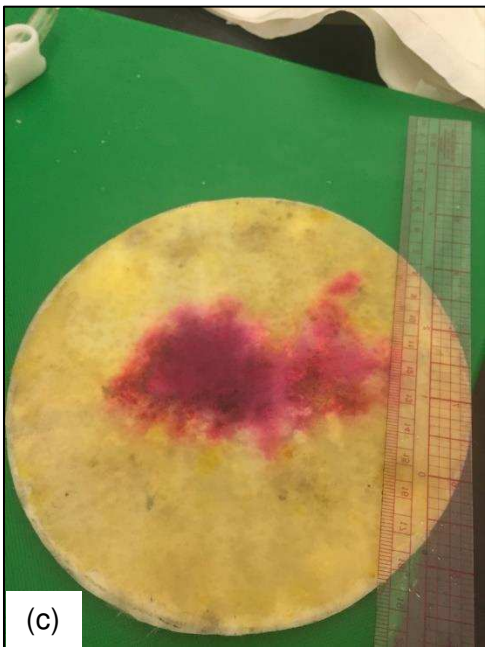
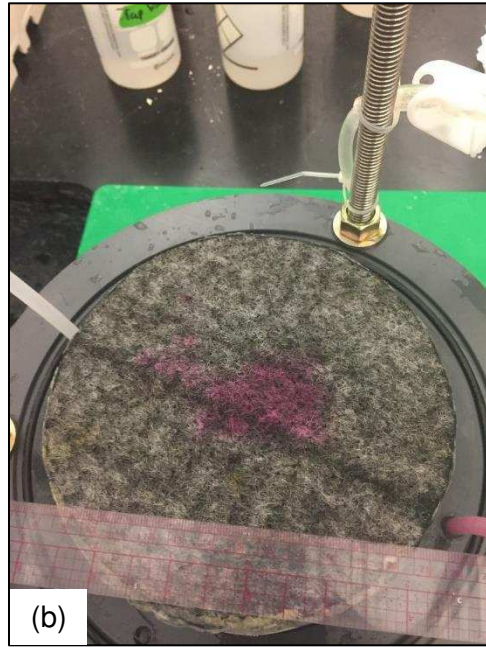
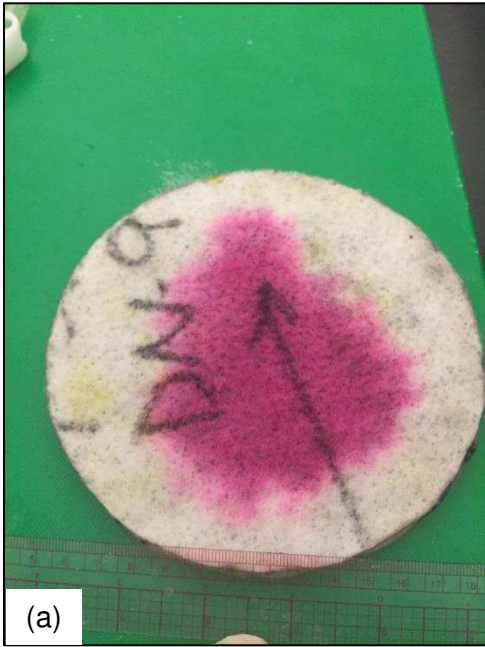


Figure F.31. (a), (b), (c), (d) Test 27a dyed disassembly.



(a)



(b)



(c)



(d)

Figure F.32. (a), (b), (c), (d) Test 27a dyed disassembly.

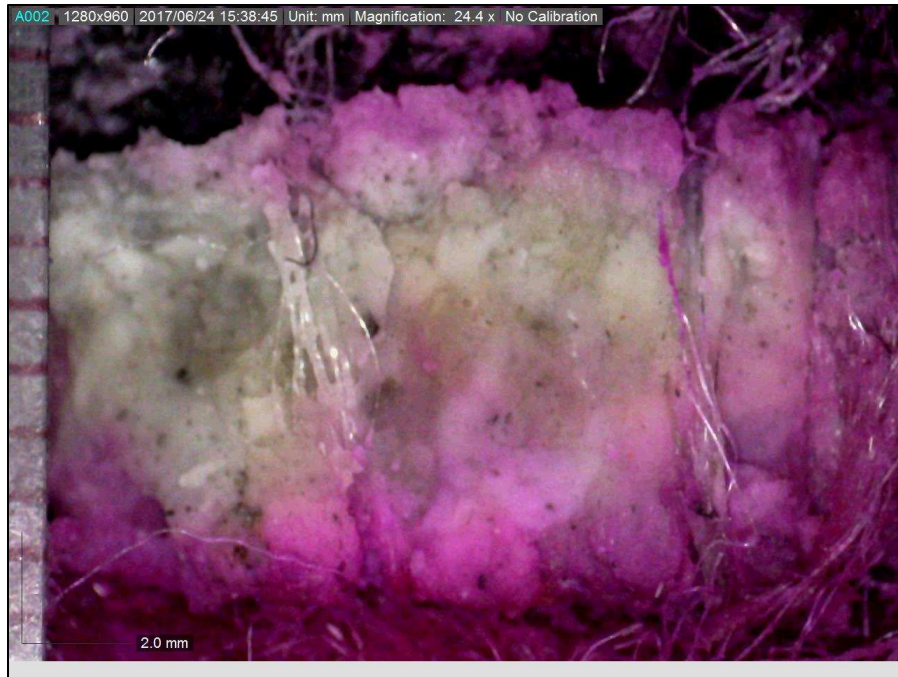


Figure F.33. Test 27a, DN9-B1. Snapped cross section. Unstained fiber bundles (portion of stained fiber bundle visible on right).

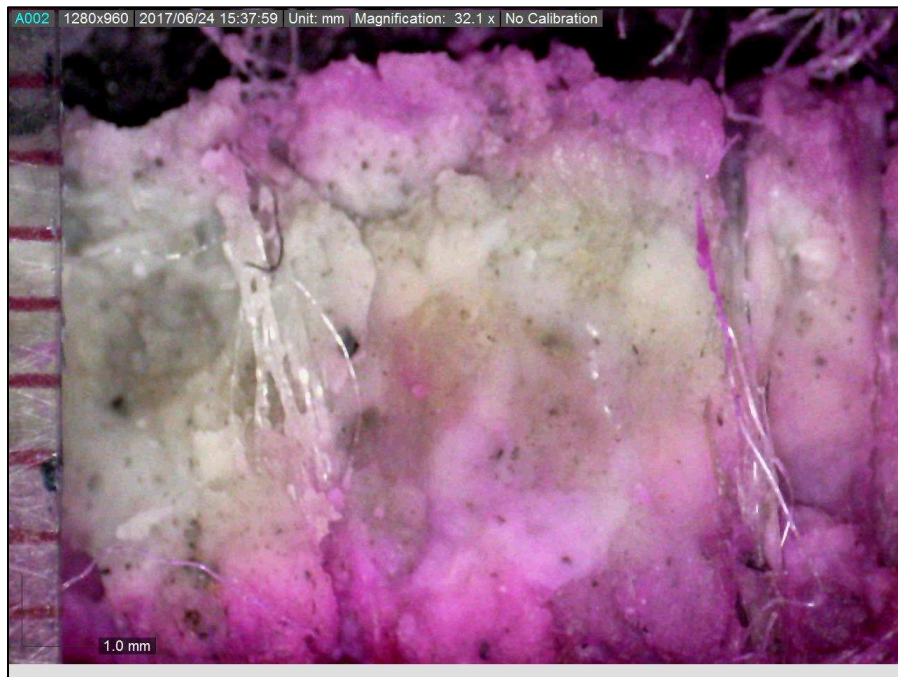


Figure F.34. Test 27a, DN9-B1. Unstained fiber bundles, zoomed in.

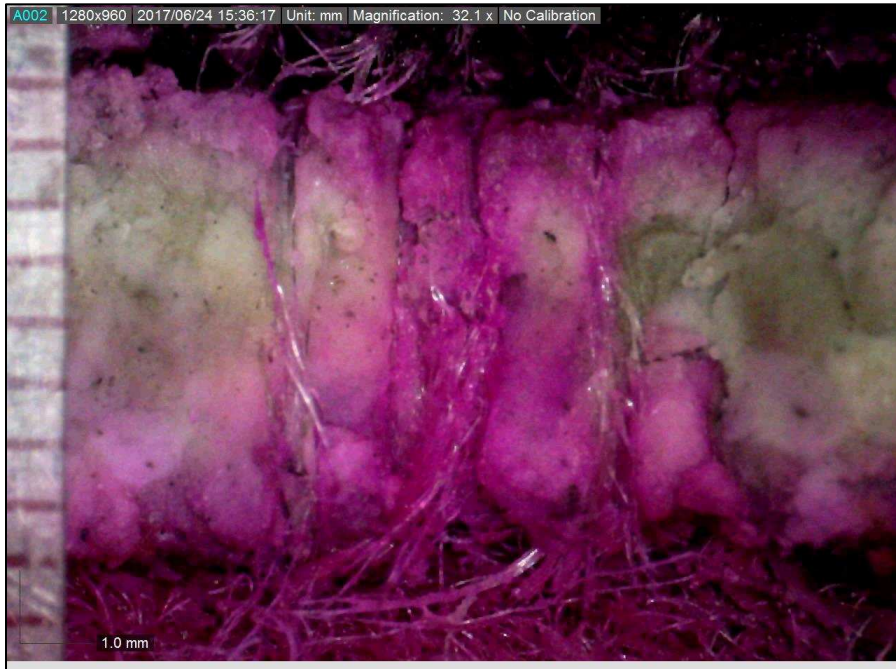


Figure F.35. Test 27a, DN9-B1. Stained fiber bundle demonstrating preferential flow.



Figure F.36. Test 27a, DN9-B1. Stained fiber bundle demonstrating preferential flow, zoomed in.



Figure F.37. Test 27a, DN9-B1. Snapped cross section. Similar staining of fiber bundle and clay portion, demonstrating possible less preferential flow in this portion of the GCL.

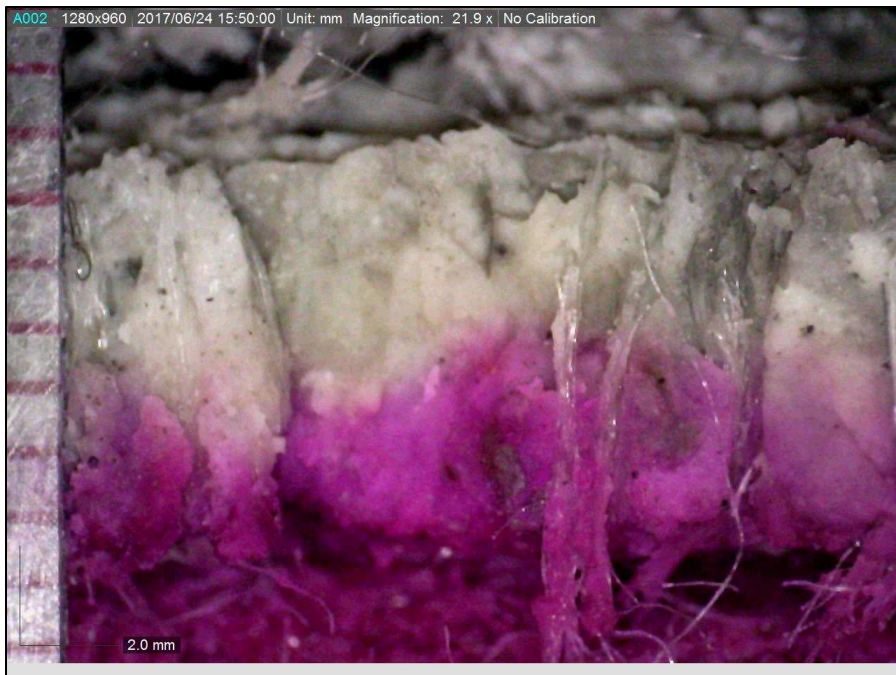


Figure F.38. Test 27a, DN9-B1. Snapped cross section. Similar staining of fiber bundle and clay portion, demonstrating possible less preferential flow in this portion of the GCL. Zoomed in.



Figure F.39. Test 27a, DN9-B1. Cut cross-section

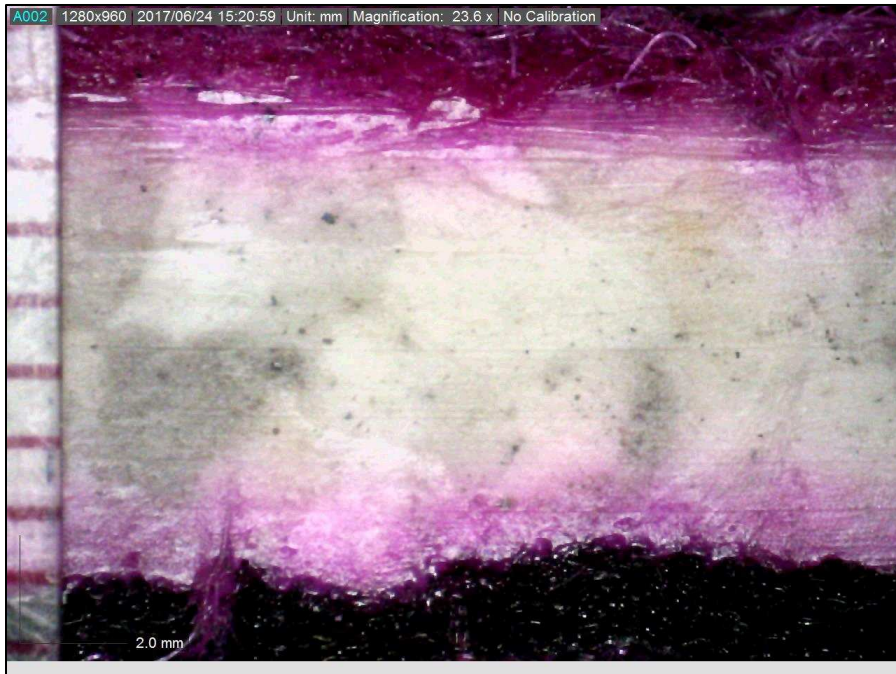


Figure F.40. Test 27a, DN9-B1. Cut cross-section, zoomed in.

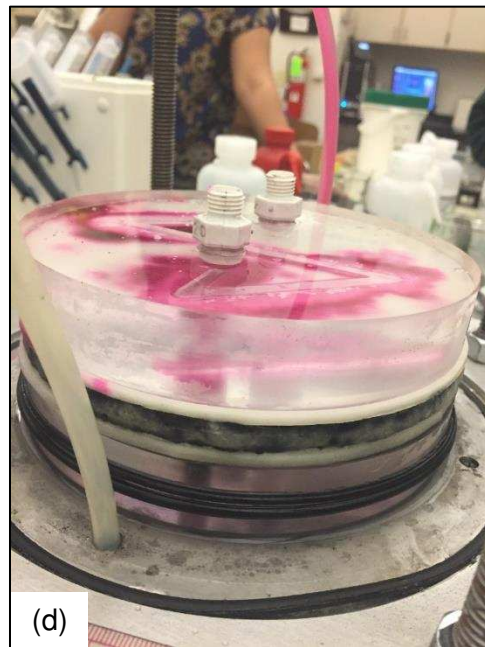
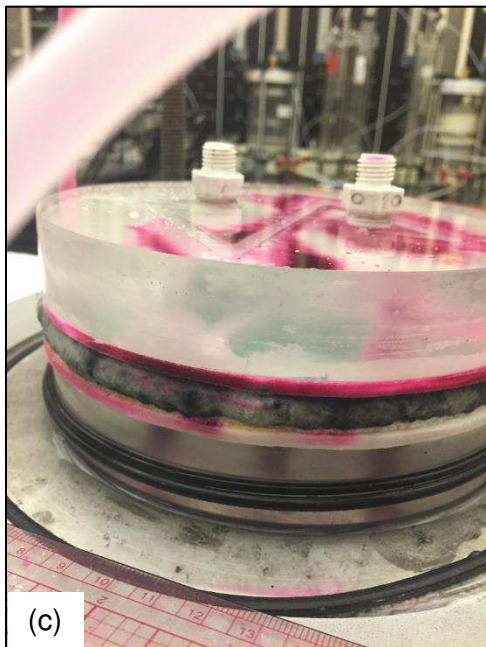


Figure F.41. (a), (b), (c), (d) Test 26a dyed disassembly.

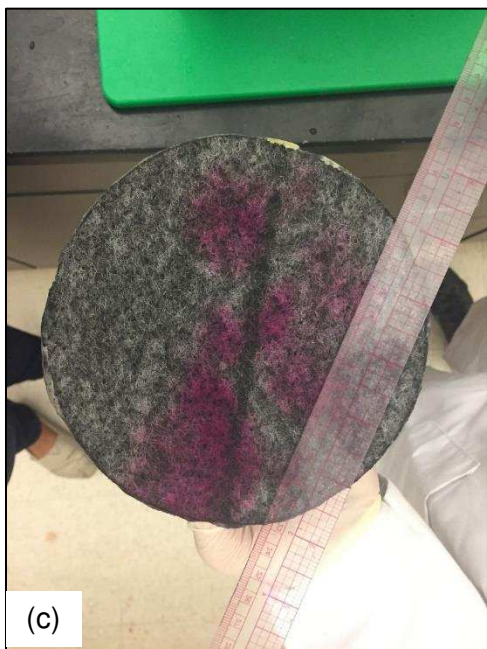


Figure F.42. (a), (b), (c), (d) Test 26a dyed disassembly.

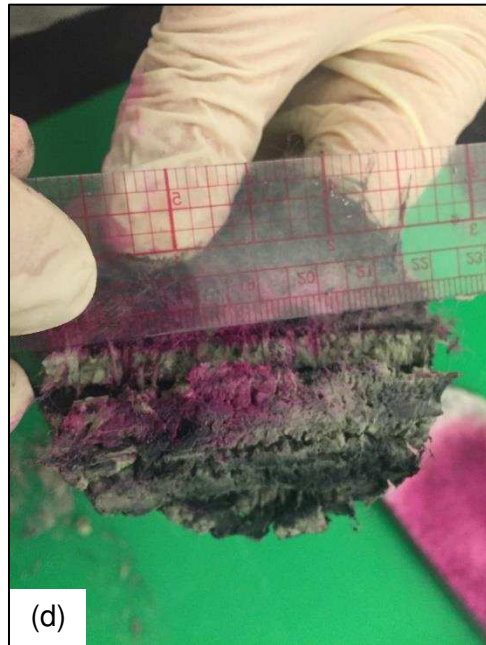
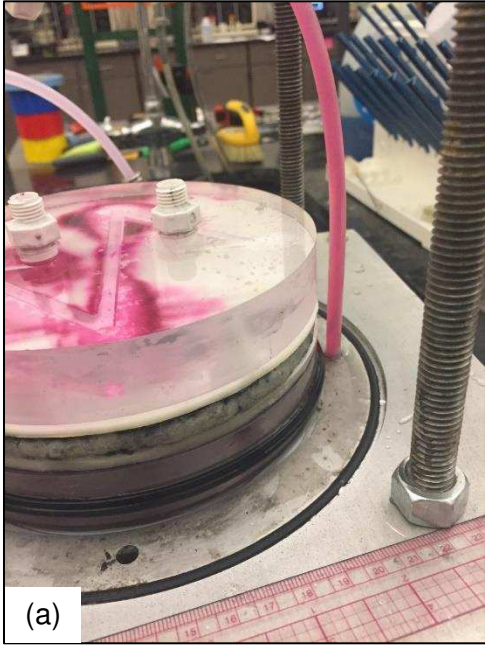


Figure F.43. (a), (b), (c), (d) Test 26a dyed disassembly.



Figure F.44. (a), (b), (c), (d) Test 26a dyed disassembly.

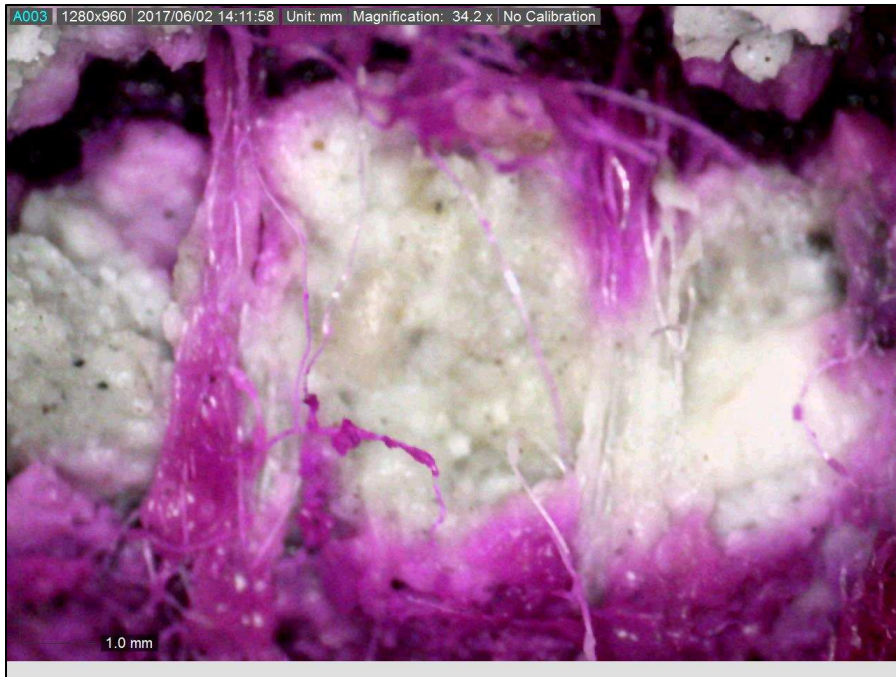


Figure F.45. Test 26a, DN9-G1. Snapped cross-section. Stained fiber bundle (left) and partially stained fiber bundle (right).



Figure F.46. Test 26a, DN9-G1. Snapped cross-section. Adjacent stained fiber bundles.



Figure F.47. Test 26a, DN9-G1. Snapped cross-section. Stained fiber bundle (middle) and unstained fiber bundles (left and right).



Figure F.48. Test 26a, DN9-G1. Snapped cross-section. Stained fiber bundle (middle) and unstained fiber bundles (left and right). Zoomed in.

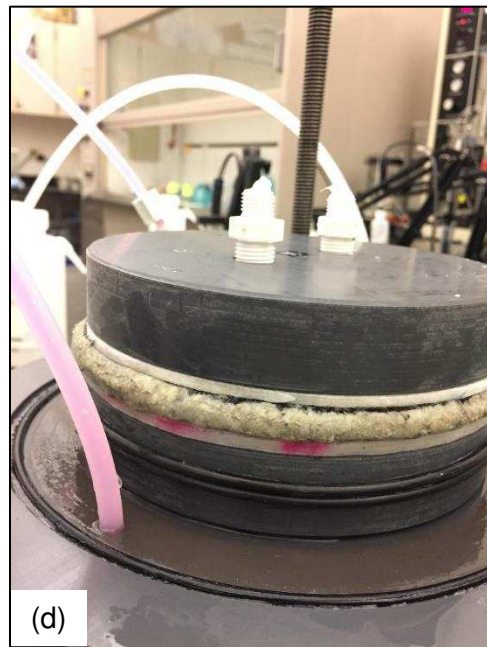
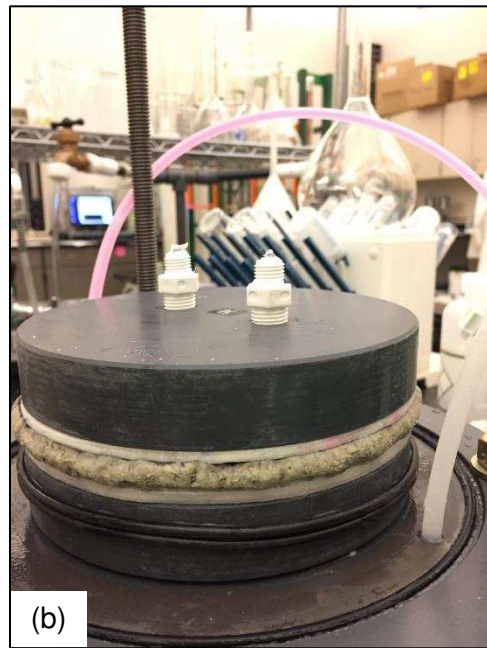


Figure F.49. (a), (b), (c), (d) Test 11c dyed disassembly.

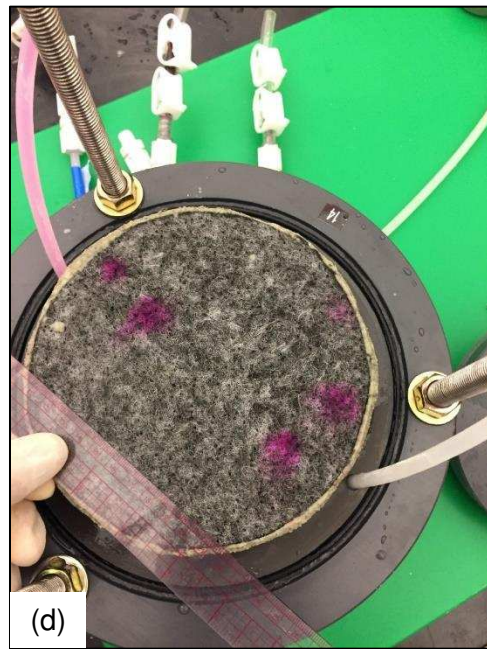


Figure F.50. (a), (b), (c), (d) Test 11c dyed disassembly.

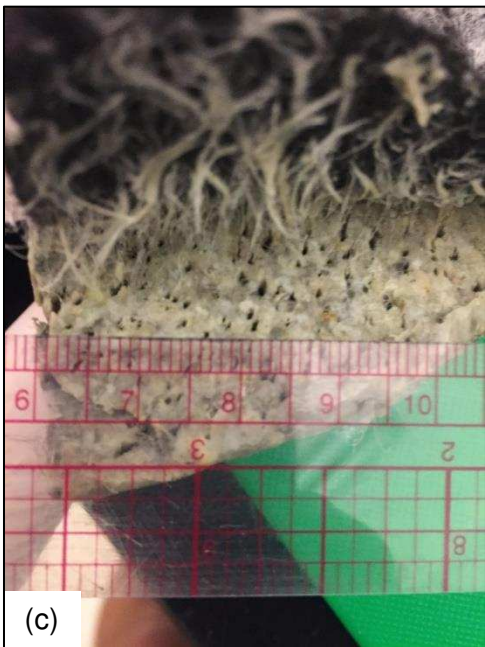


Figure F.51. (a), (b), (c), (d) Test 11c dyed disassembly.



Figure F.52. (a), (b) Test 11c dyed disassembly.

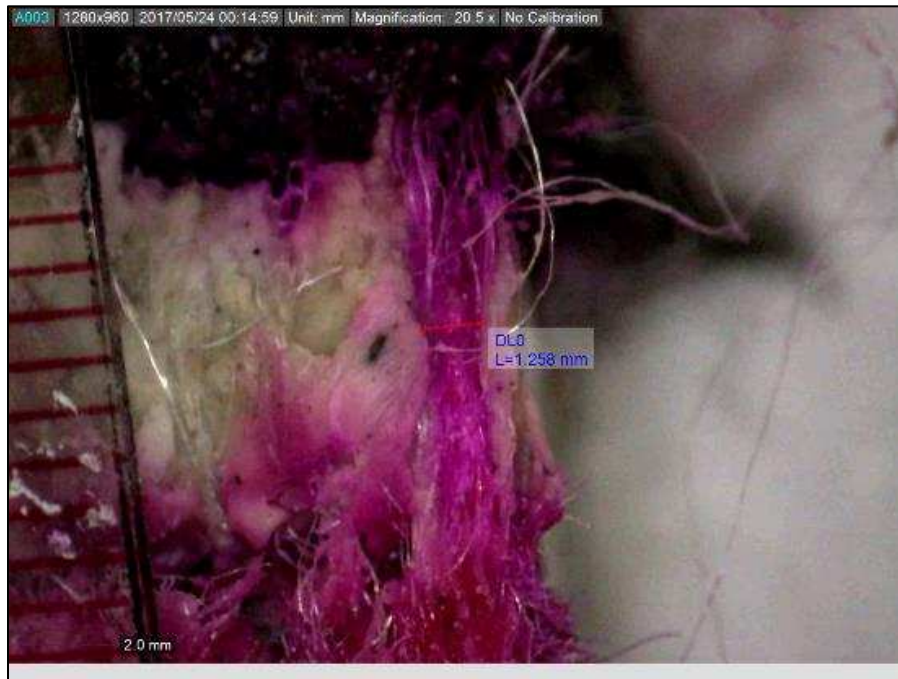


Figure F.53. Test 11c, DN9-L3. Snapped cross-section. Stained fiber bundle.

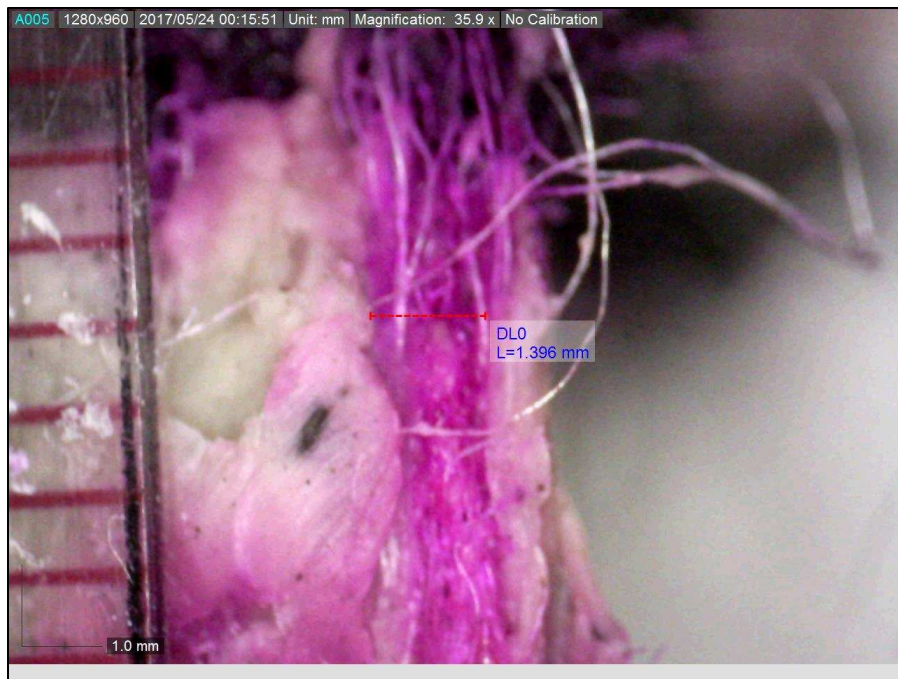


Figure F.54. Test 11c, DN9-L3. Snapped cross-section. Stained fiber bundle. Zoomed in

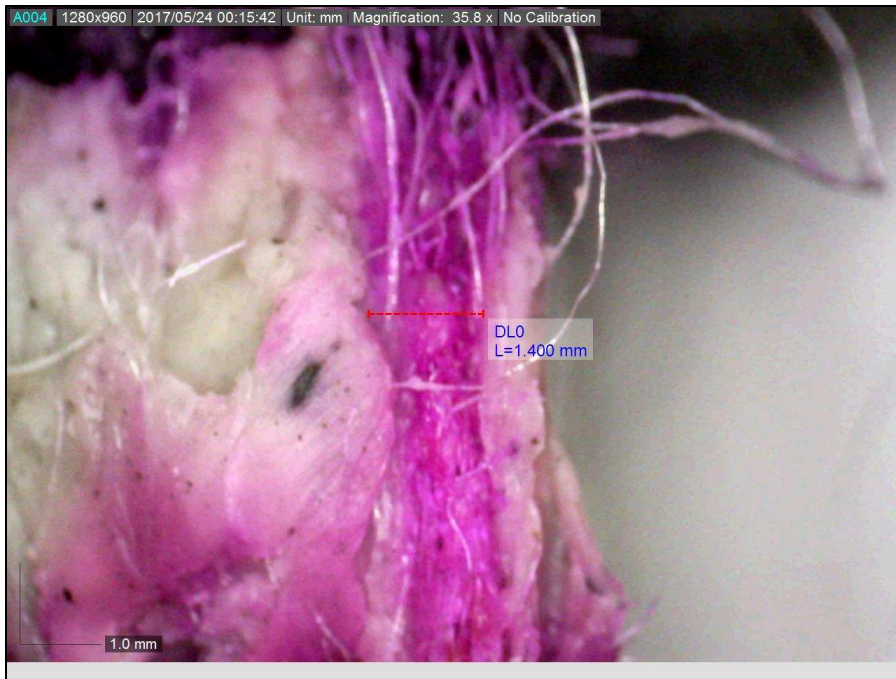


Figure F.55. Test 11c, DN9-L3. Snapped cross-section. Stained fiber bundle. Zoomed in



Figure F.56. Test 11c, DN9-L3. Snapped cross-section. Stained fiber bundle (middle). Unstained fiber bundles (left and right).

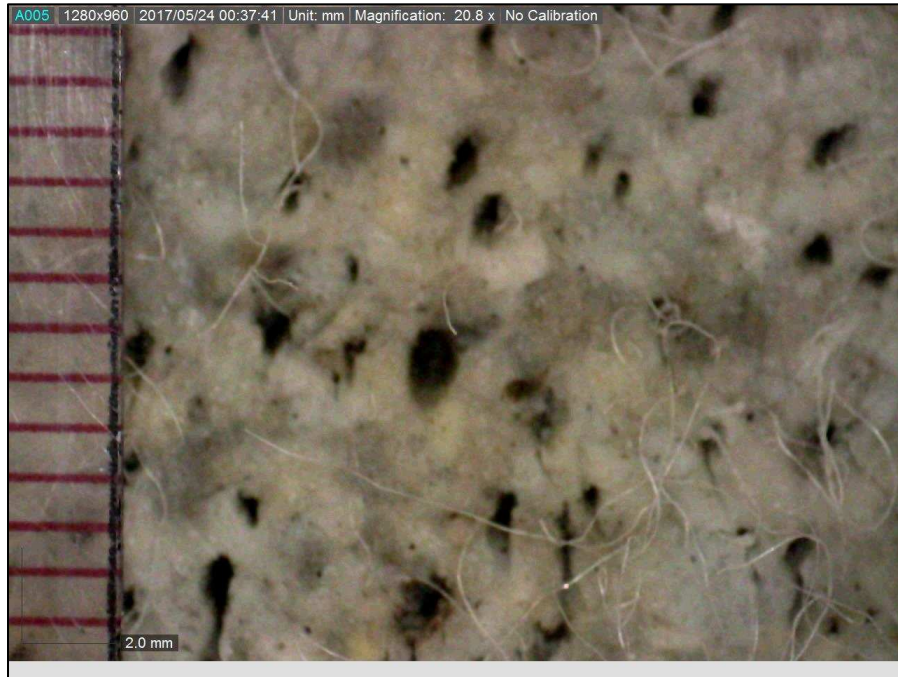


Figure F.57. Test 11c, DN9-L3. Top view of bentonite after textiles were removed and bundles were pulled from the bentonite.

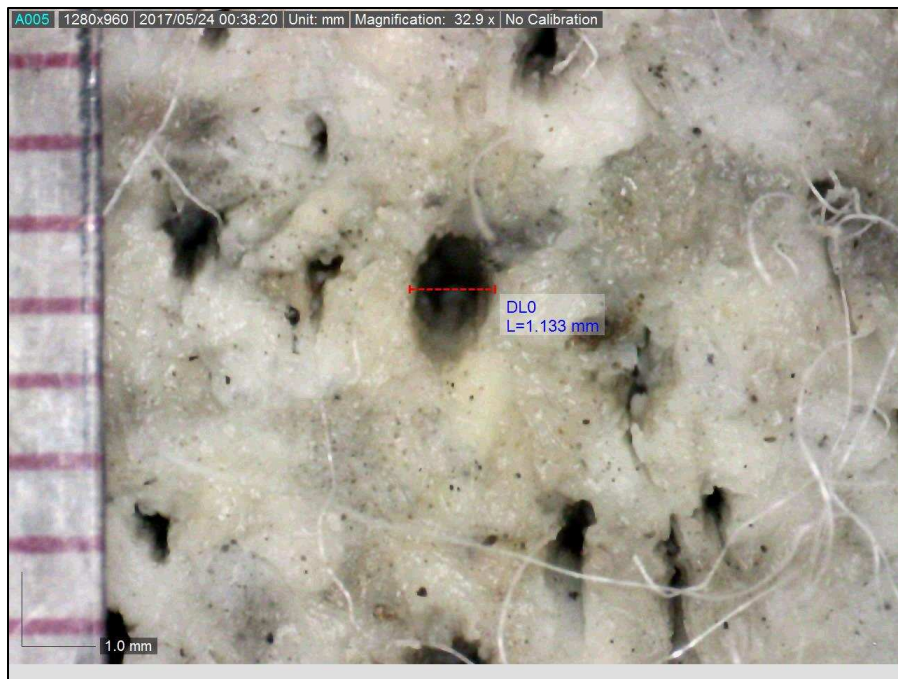


Figure F.58. Test 11c, DN9-L3. Top view of bentonite after textiles were removed and bundles were pulled from the bentonite. Zoomed in.

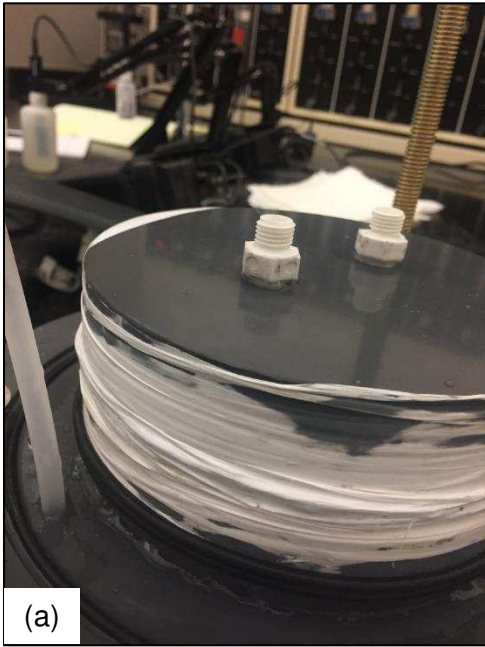


Figure F.59. (a), (b), (c), (d) Test 28a disassembly.

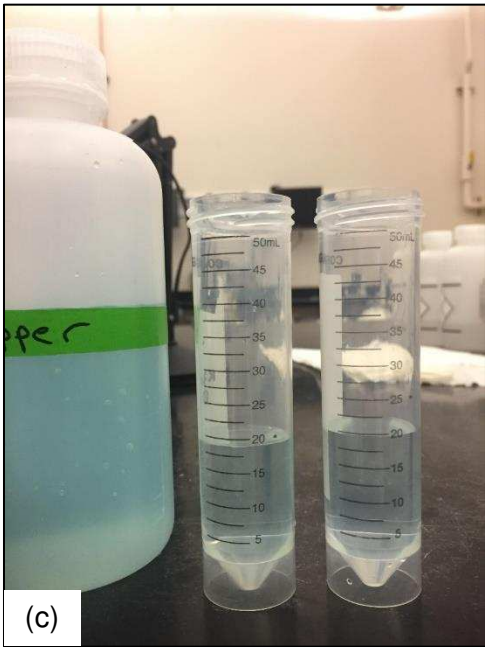


Figure F.60. (a), (b) Test 28a disassembly. (c) Visual comparison of effluent versus influent.

DN9-C1:

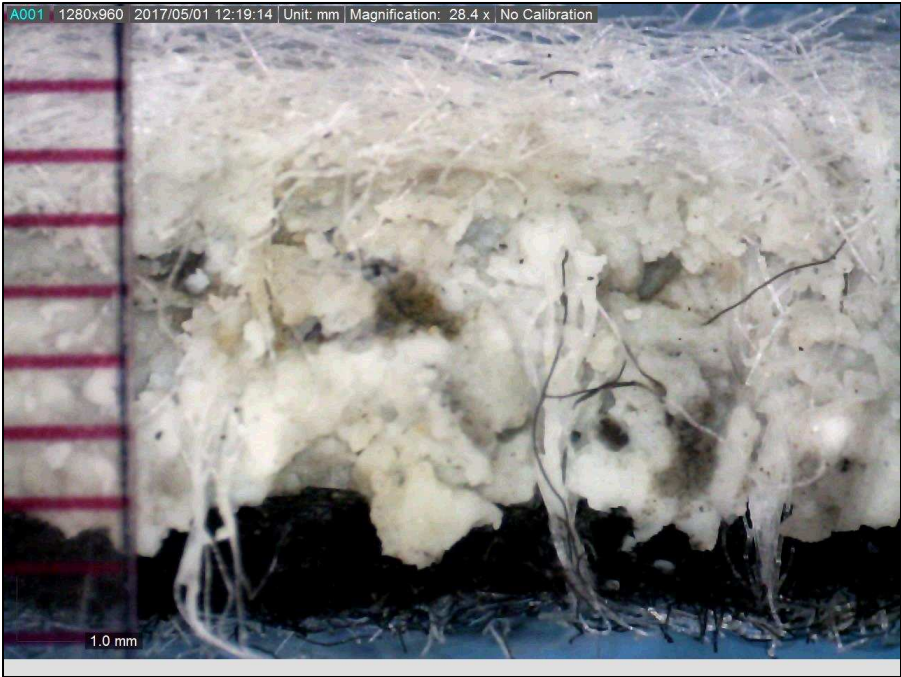


Figure F.61. Test 28a, DN9-C1. Snapped cross-section.



Figure F.62. Test 28a, DN9-C1. Snapped cross-section.



Figure F.63. Test 28a, DN9-C1. Snapped cross-section.



Figure F.64. Test 28a, DN9-C1. Snapped cross-section.

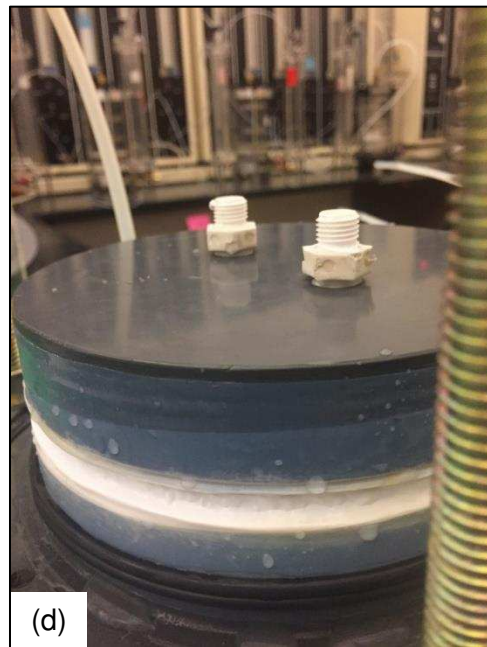
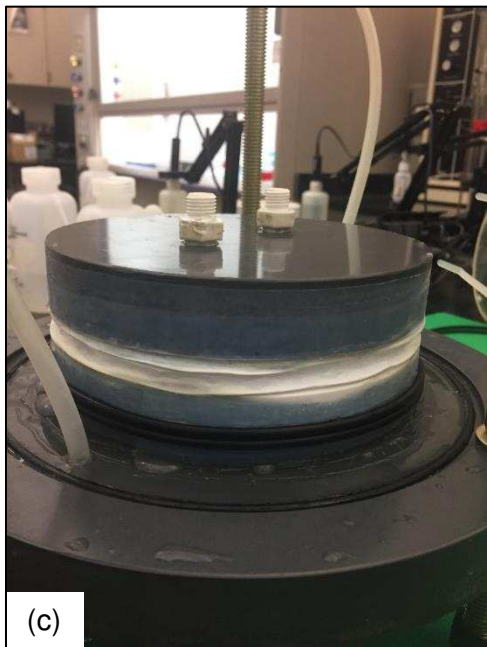
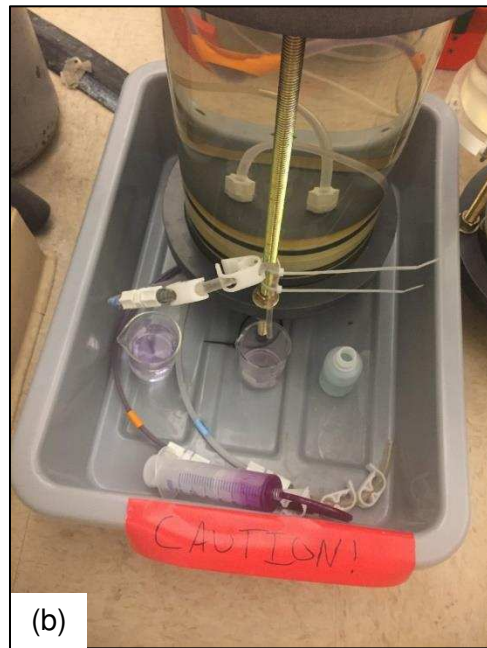


Figure F.65. (a), (b), (c), (d) Test 25a dyed disassembly.

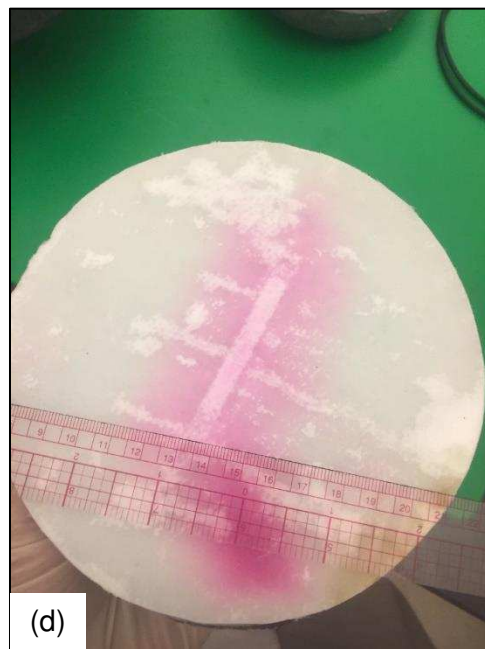
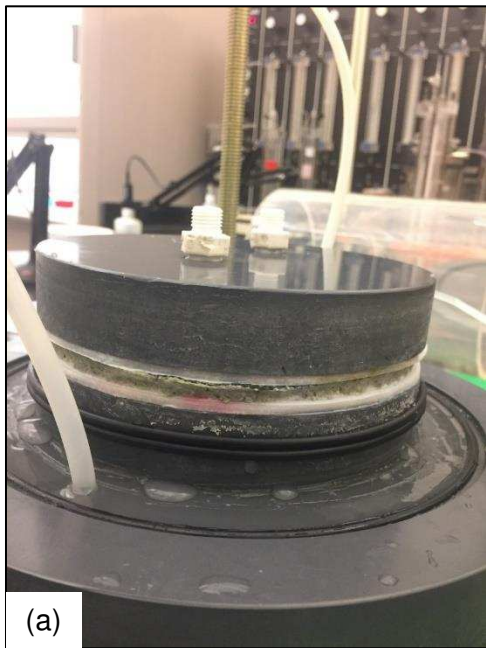


Figure F.66. (a), (b), (c), (d) Test 25a dyed disassembly.

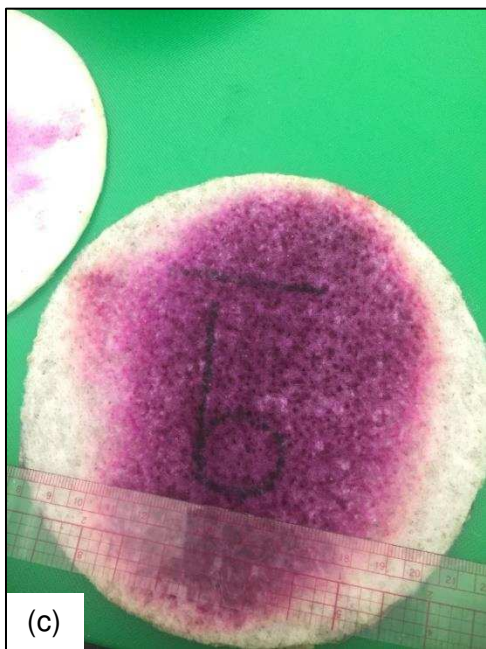
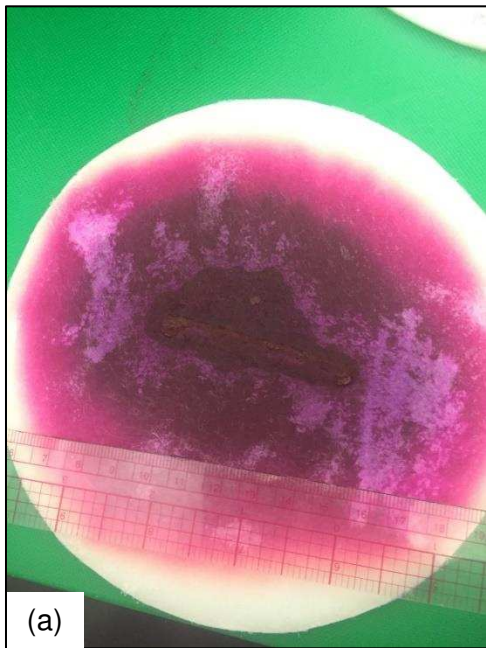


Figure F.67. (a), (b), (c), (d) Test 25a dyed disassembly.



Figure F.68. (a), (b), (c), (d) Test 25a dyed disassembly.

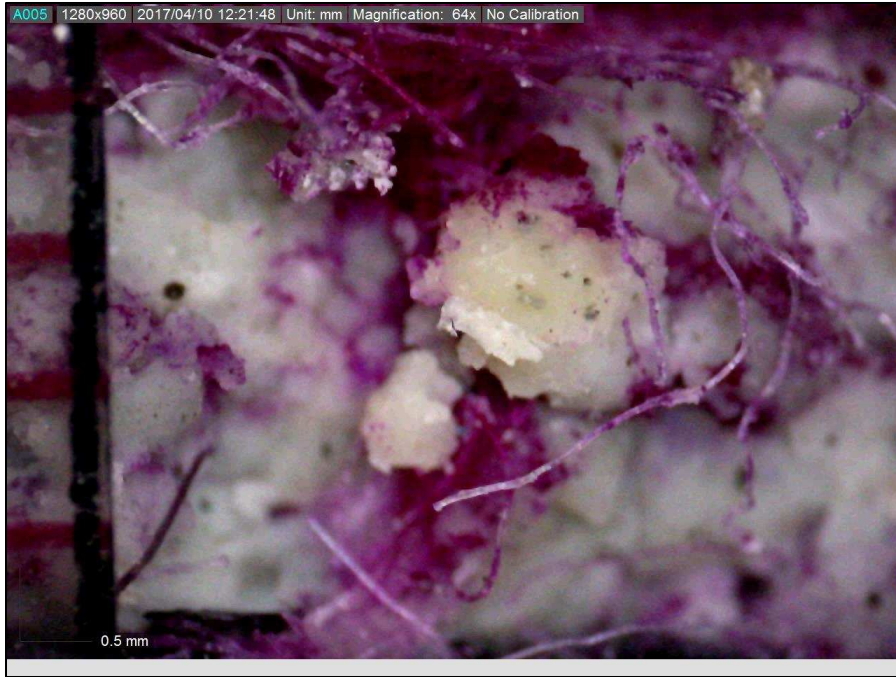


Figure F.69. Test 25a dyed disassembly cross-section

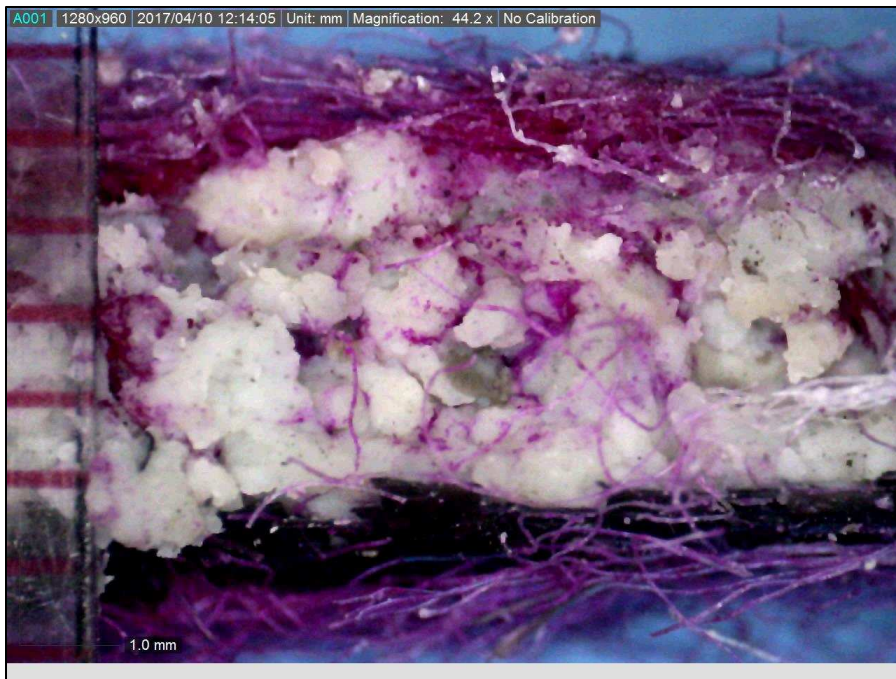


Figure F.70. Test 25a dyed disassembly cross-section

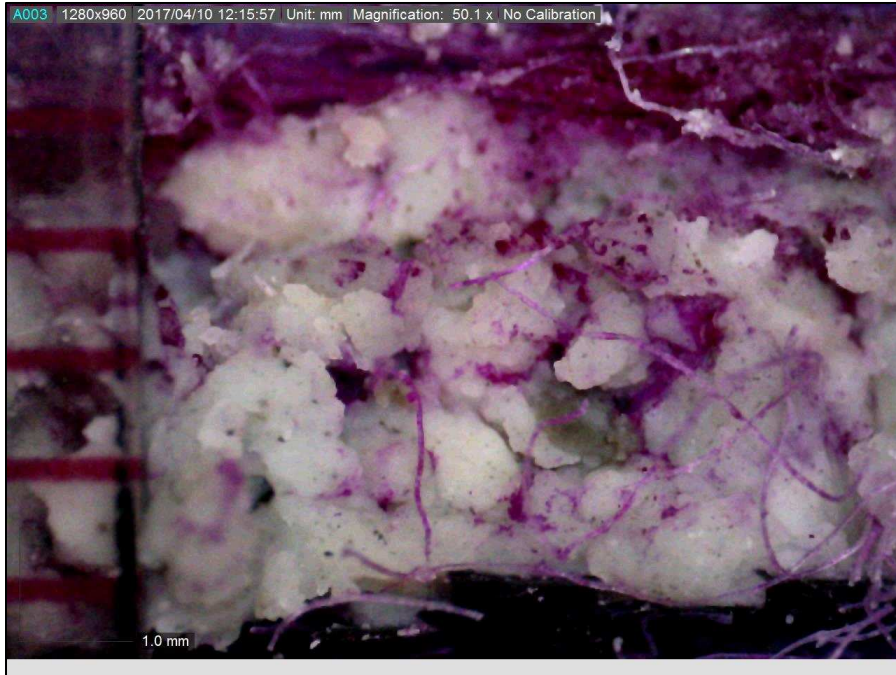


Figure F.71. Test 25a dyed disassembly cross-section

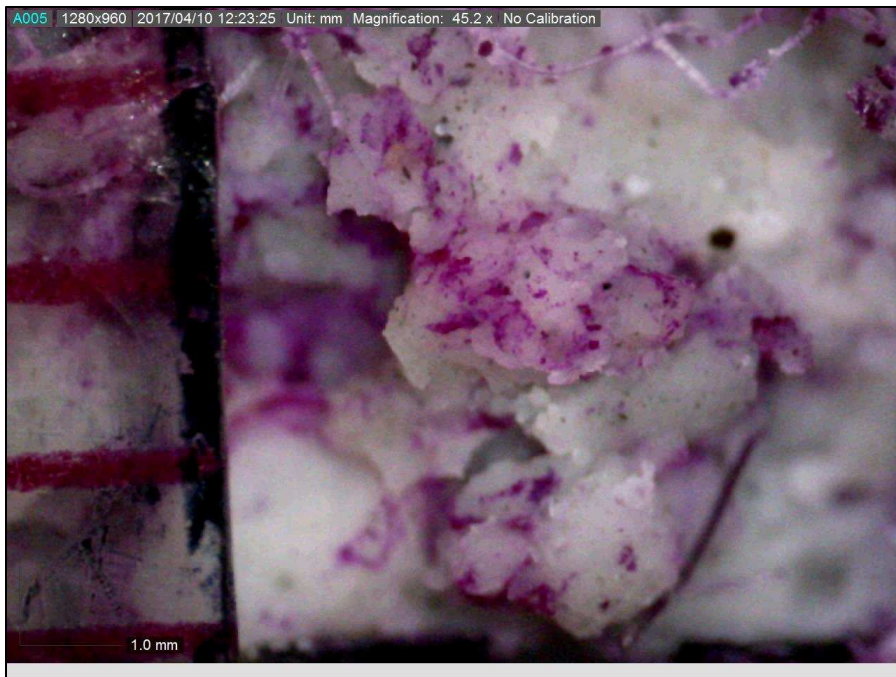


Figure F.72. Test 25a dyed disassembly cross-section



Figure F.73. Test 25a dyed disassembly cross-section

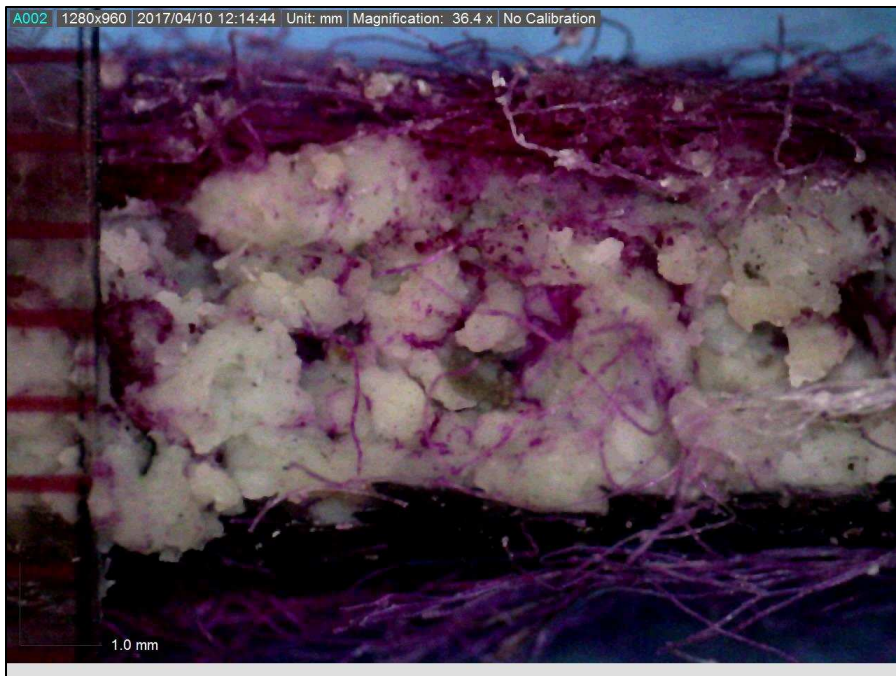


Figure F.74. Test 25a dyed disassembly cross-section

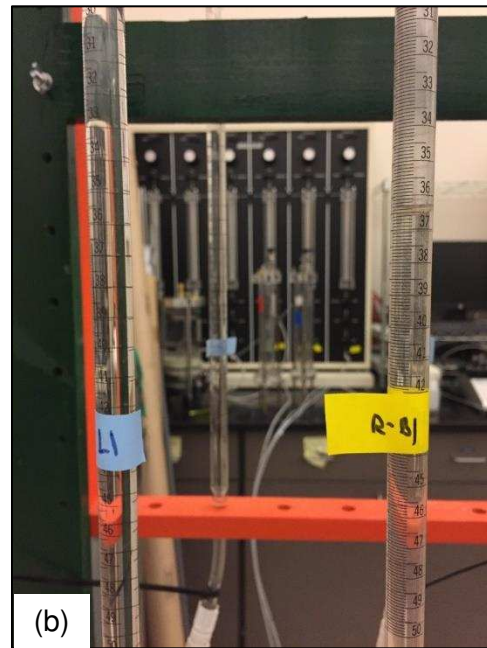
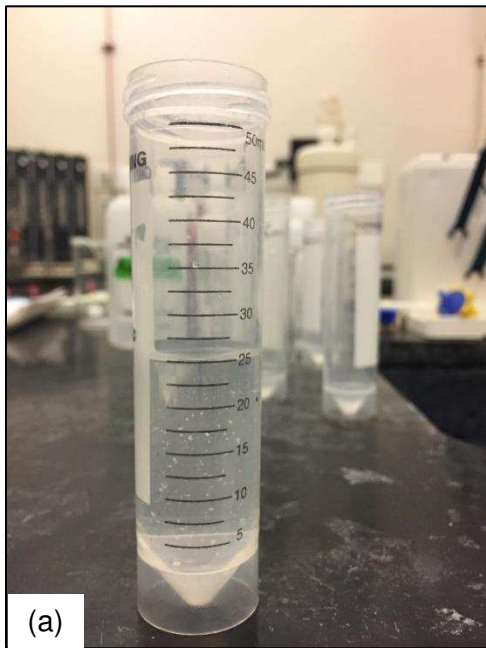


Figure F.75. (a), (b), (c) Test 24a disassembly.



Figure F.76. Test 24a disassembly cross-section



Figure F.77. Test 24a disassembly cross-section



Figure F.78. Test 24a disassembly cross-section



Figure F.79. Test 24a disassembly cross-section



Figure F.80. Test 24a disassembly cross-section



Figure F.81. Test 24a disassembly cross-section



Figure F.82. Test 24a disassembly cross-section



Figure F.83. Test 24a disassembly cross-section



Figure F.84. Test 24a disassembly cross-section



Figure F.85. Test 24a disassembly cross-section

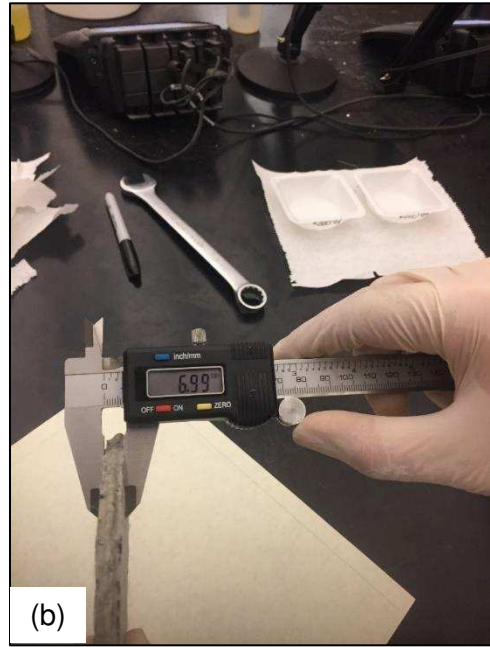


Figure F.86. (a), (b), (c), (d) Photographs of textile correction method.

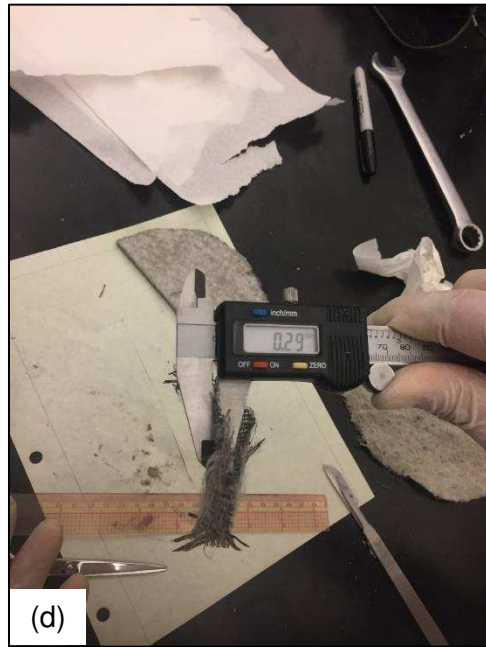


Figure F.87. (a), (b), (c), (d) Photographs of textile correction method.



Figure F.88. (a), (b), (c), (d) Photographs of textile correction method.

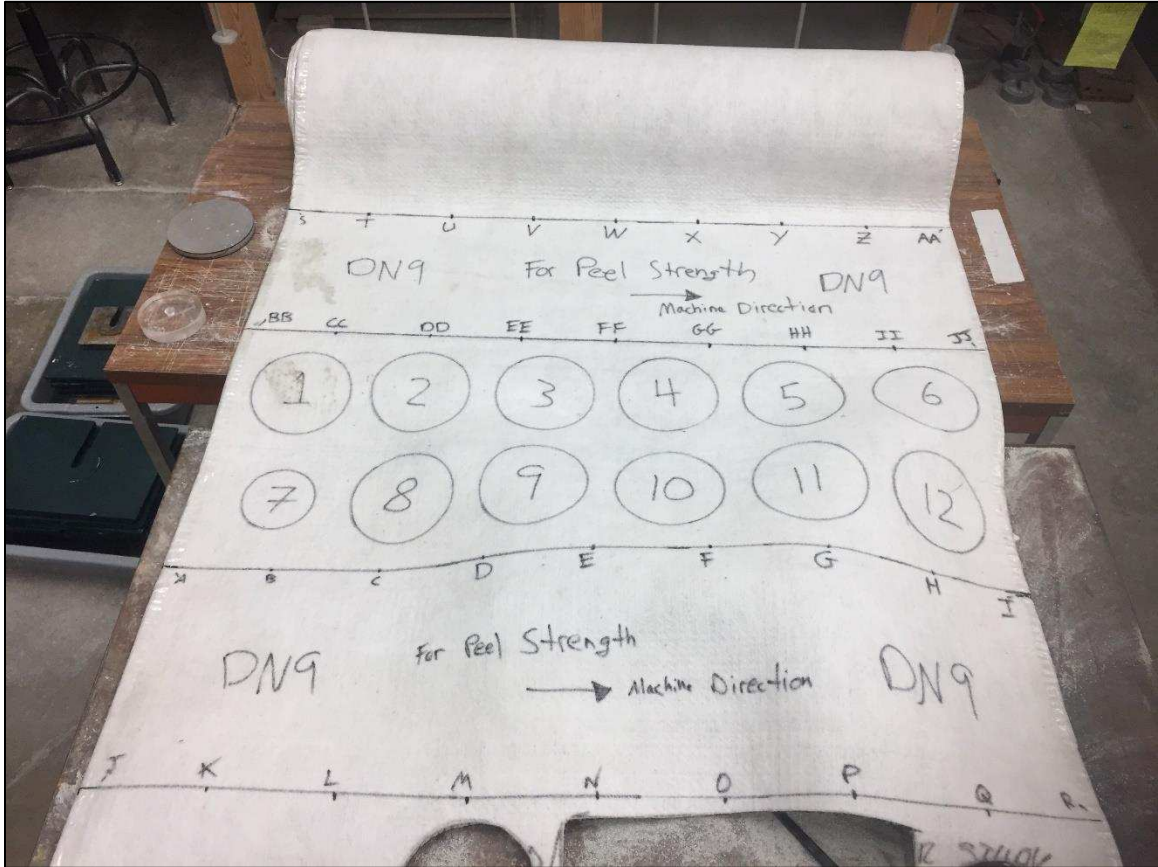


Figure F.89. Methodology for cutting specimens from GCL-2 roll #1

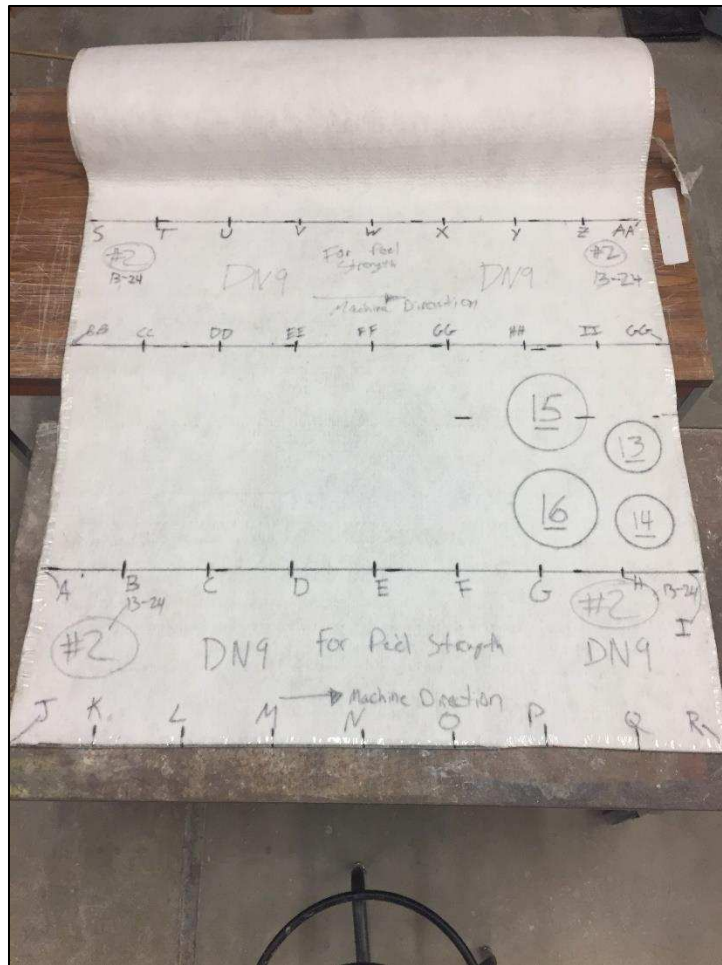


Figure F.90. Methodology for cutting specimens from GCL-2 roll #2.

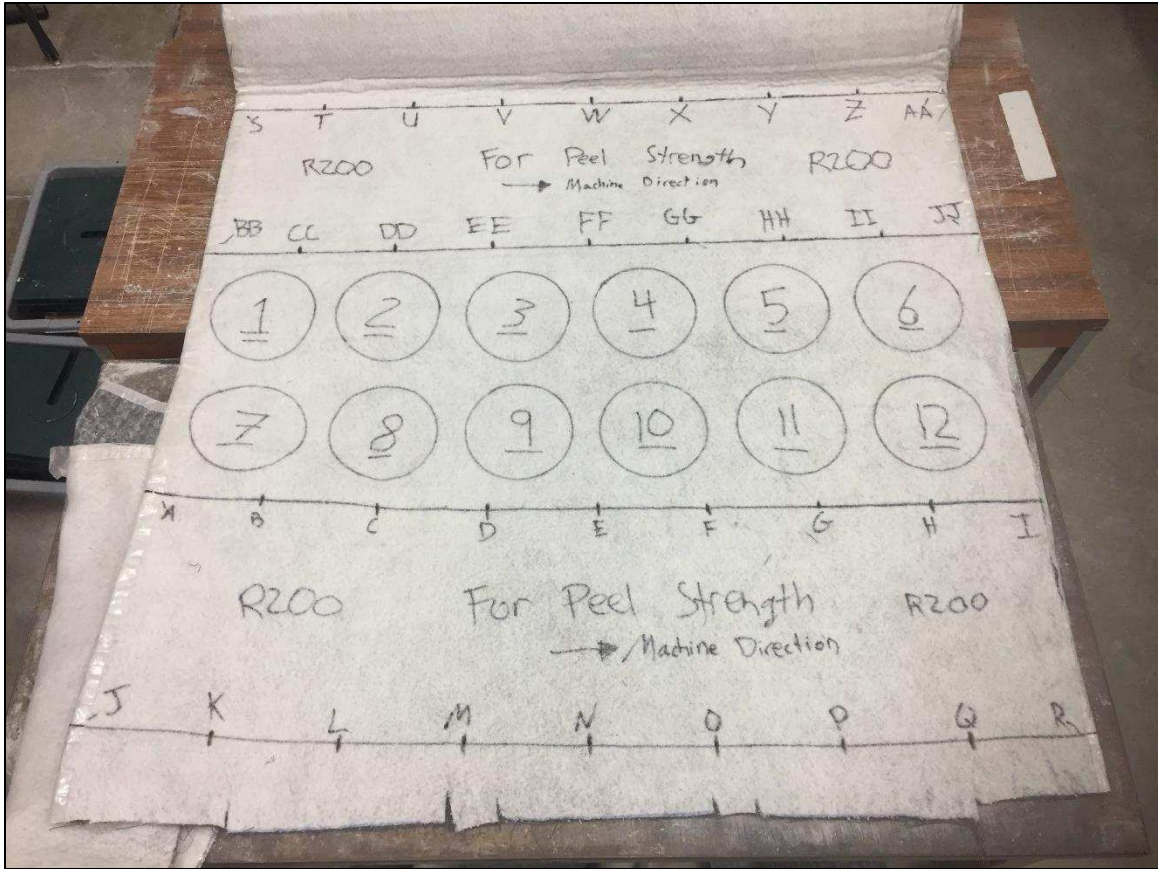



Figure F.91. Methodology for cutting specimens from GCL-3 roll.

APPENDIX G

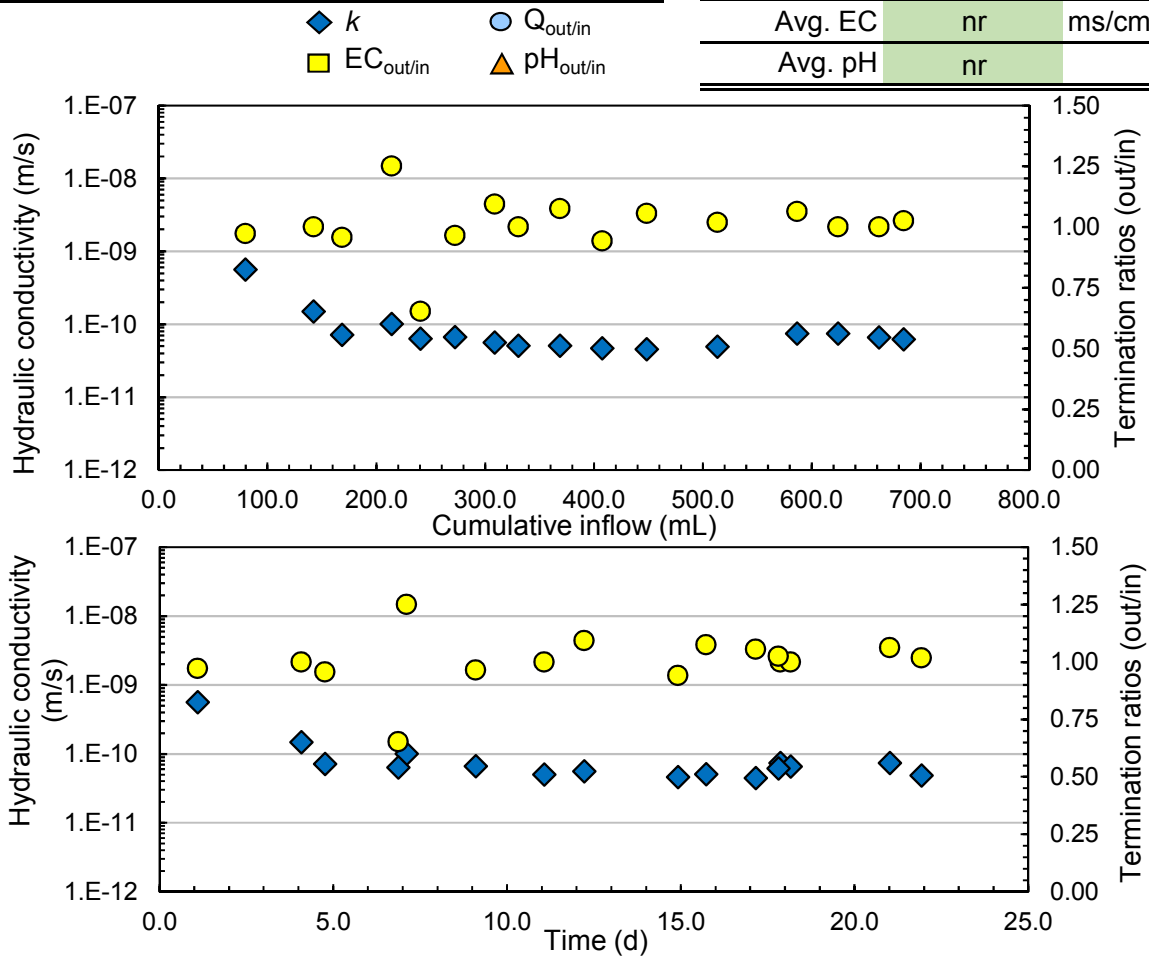
Test Summary Sheets

Hydraulic Conductivity—Standard Method


Test ID	1a	Test start date	2016/04/04	
GCL type	DN (12 ppi)	Notes 		
Student	Conzelmann, Joel			
Permeant liquid	CW			
Prehydrated (Y/N)	N			
Specimen diameter	10.2			cm
	4.0			in
Avg. effective stress	27.4			kPa
	4.0			psi

Terminated test results

k [D5084]	6.73E-11	m/s	k [D6766]	nr	m/s
PVF [D5084]	13.2		PVF [D6766]	nr	
time [D5084]	17.81	d	time [D6766]	nr	d
			Avg. EC	nr	ms/cm
			Avg. pH	nr	

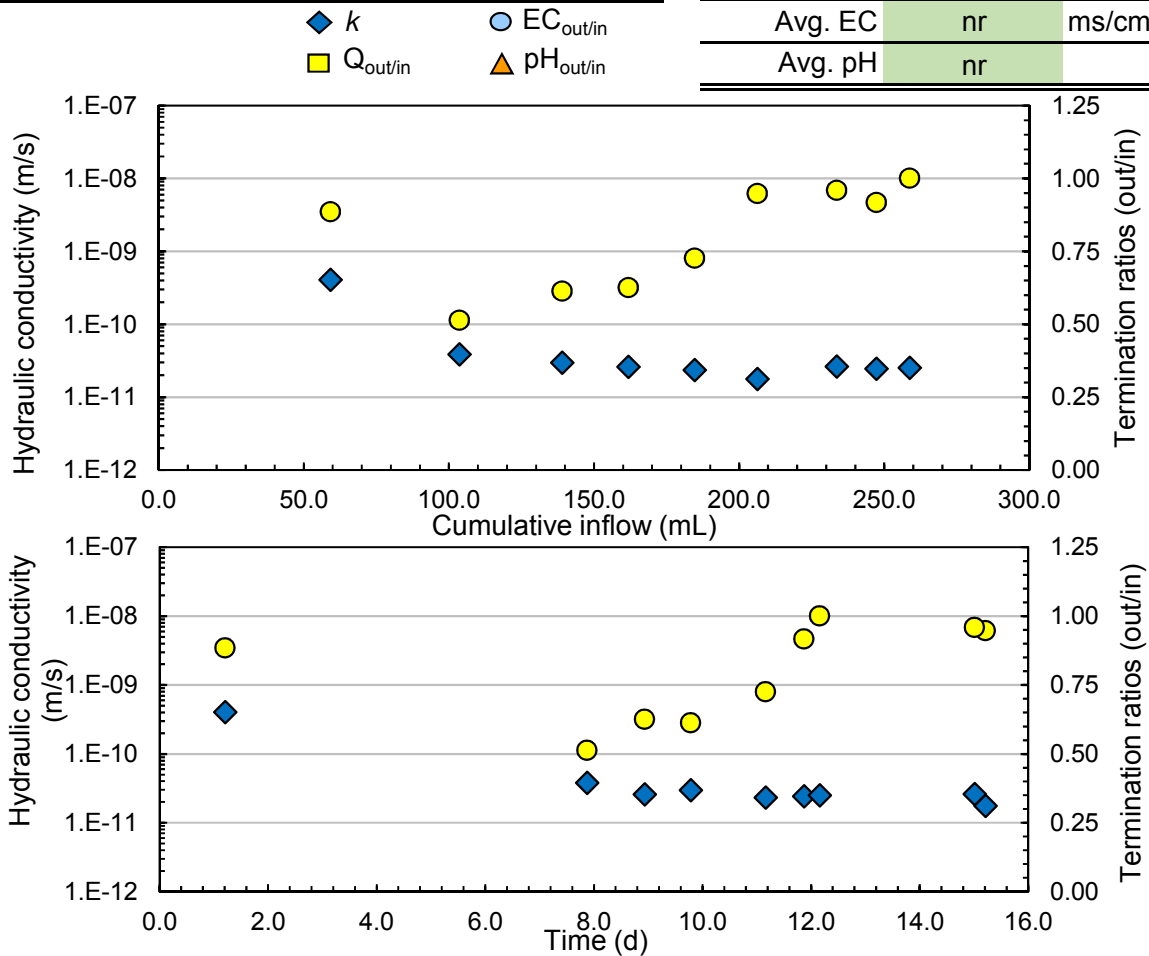


Hydraulic Conductivity—Standard Method


Test ID	1b	Test start date	2016/04/25
GCL type	DN (12 ppi)	Notes 	
Student	Conzelmann, Joel		
Permeant liquid	CW		
Prehydrated (Y/N)	N		
Specimen diameter	10.2 cm		
	4.0 in		
Avg. effective stress	26.4 kPa		
	3.8 psi		

Terminated test results

k [D5084]	2.52E-11	m/s	k [D6766]	nr	m/s
PVF [D5084]	4.7		PVF [D6766]	nr	
time [D5084]	12.16	d	time [D6766]	nr	d
			Avg. EC	nr	ms/cm
			Avg. pH	nr	

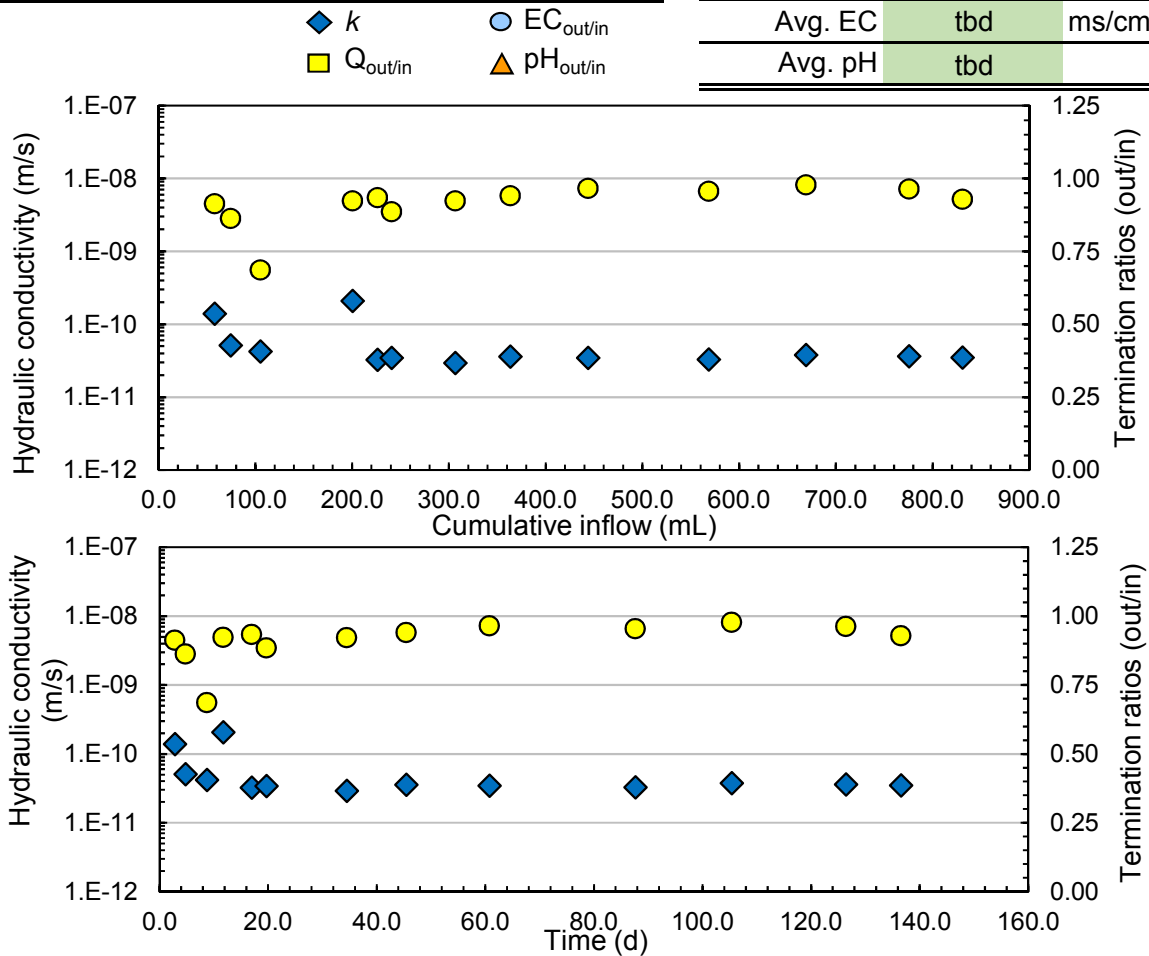


Hydraulic Conductivity—Standard Method


Test ID	1c	Test start date	2016/04/04	
GCL type	DN (12 ppi)	Notes 		
Student	Conzelmann, Joel			
Permeant liquid	CW			
Prehydrated (Y/N)	N			
Specimen diameter	10.2			cm
	4.0			in
Avg. effective stress	tbd			kPa
	tbd			psi

Terminated test results

<i>k</i> [D5084]	3.43E-11	m/s	<i>k</i> [D6766]	tbd	m/s
PVF [D5084]	tbd		PVF [D6766]	tbd	
time [D5084]	87.61	d	time [D6766]	tbd	d
			Avg. EC	tbd	ms/cm
			Avg. pH	tbd	

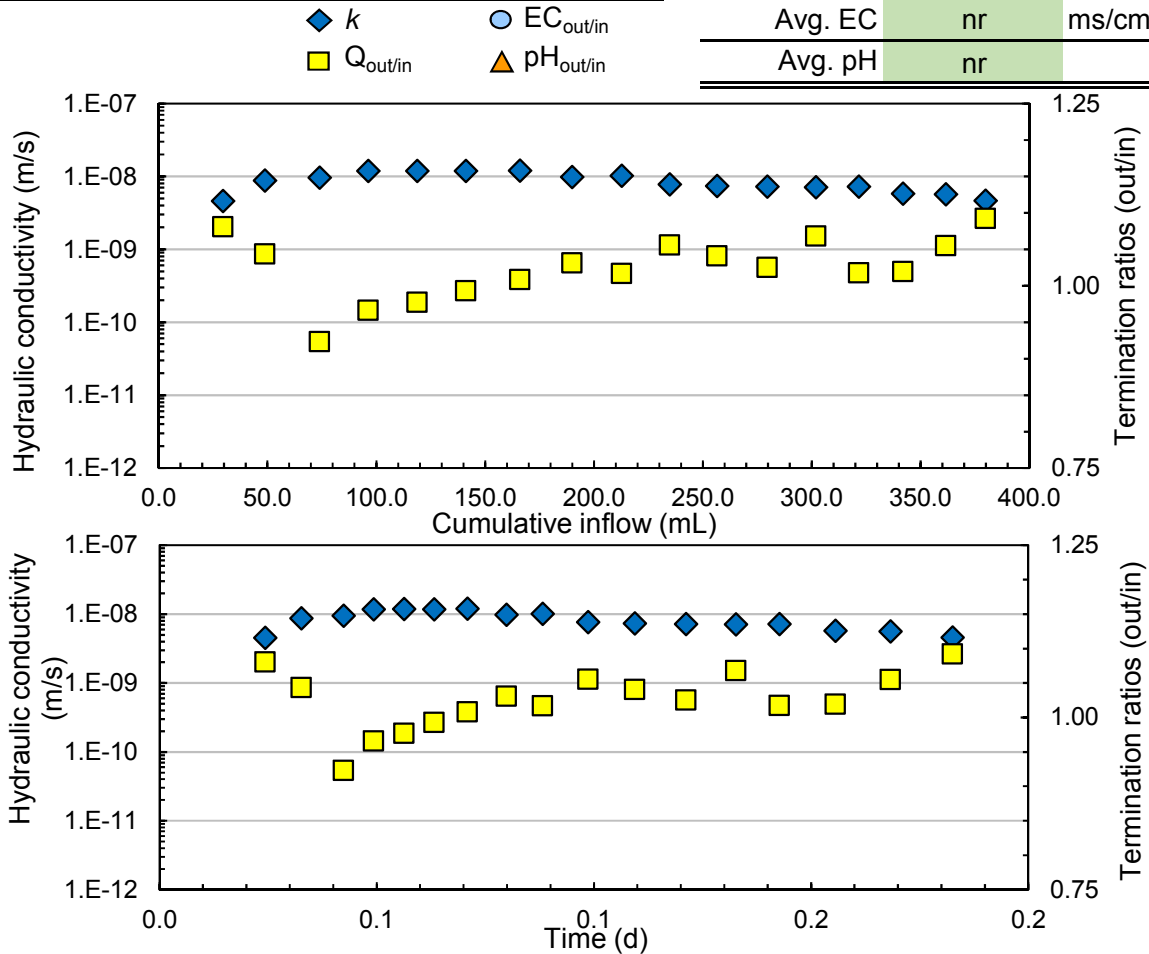


Hydraulic Conductivity—Gravity Method


Test ID	2a	Test start date	2016/05/05	
GCL type	DN (12 ppi)	Notes 		
Student	Conzelmann, Joel			
Permeant liquid	CW			
Prehydrated (Y/N)	N			
Specimen diameter	15.1			cm
	5.9			in
Avg. effective stress	27.7			kPa
	4.0			psi

Terminated test results

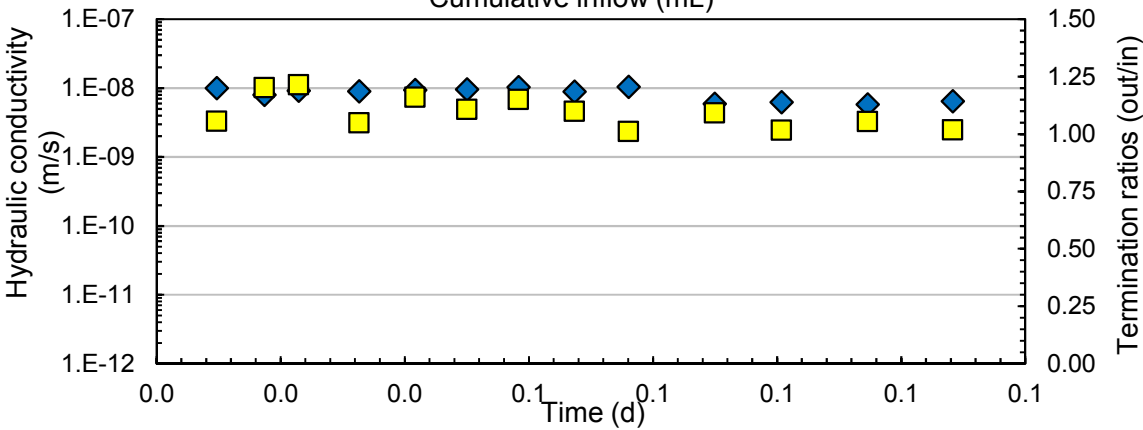
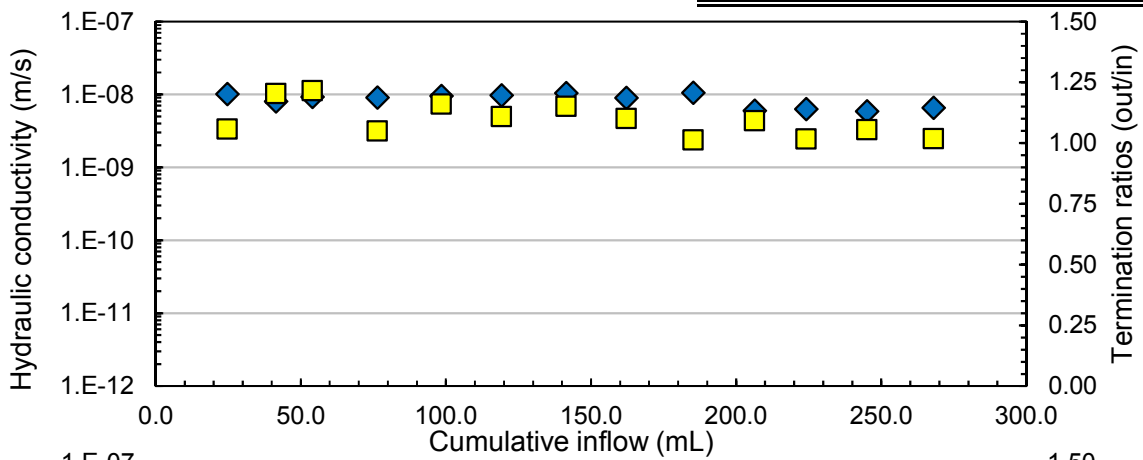
k [D5084]	5.35E-09	m/s	k [D6766]	nr	m/s
PVF [D5084]	3.5		PVF [D6766]	nr	
time [D5084]	0.18	d	time [D6766]	nr	d
			Avg. EC	nr	ms/cm
			Avg. pH	nr	




Hydraulic Conductivity—Gravity Method

Test ID	2b	Test start date	2016/05/05	
GCL type	DN (12 ppi)	Notes 		
Student	Conzelmann, Joel			
Permeant liquid	CW			
Prehydrated (Y/N)	N			
Specimen diameter	15.1			cm
	5.9			in
Avg. effective stress	27.6			kPa
	4.0			psi

Terminated test results			
k [D5084]	6.20E-09	m/s	
PVF [D5084]	2.3		
time [D5084]	0.13	d	
◆ k ○ EC _{out/in} ■ Q _{out/in} ▲ pH _{out/in}			
k [D6766]	nr	m/s	
PVF [D6766]	nr		
time [D6766]	nr	d	
Avg. EC	nr	ms/cm	
Avg. pH	nr		

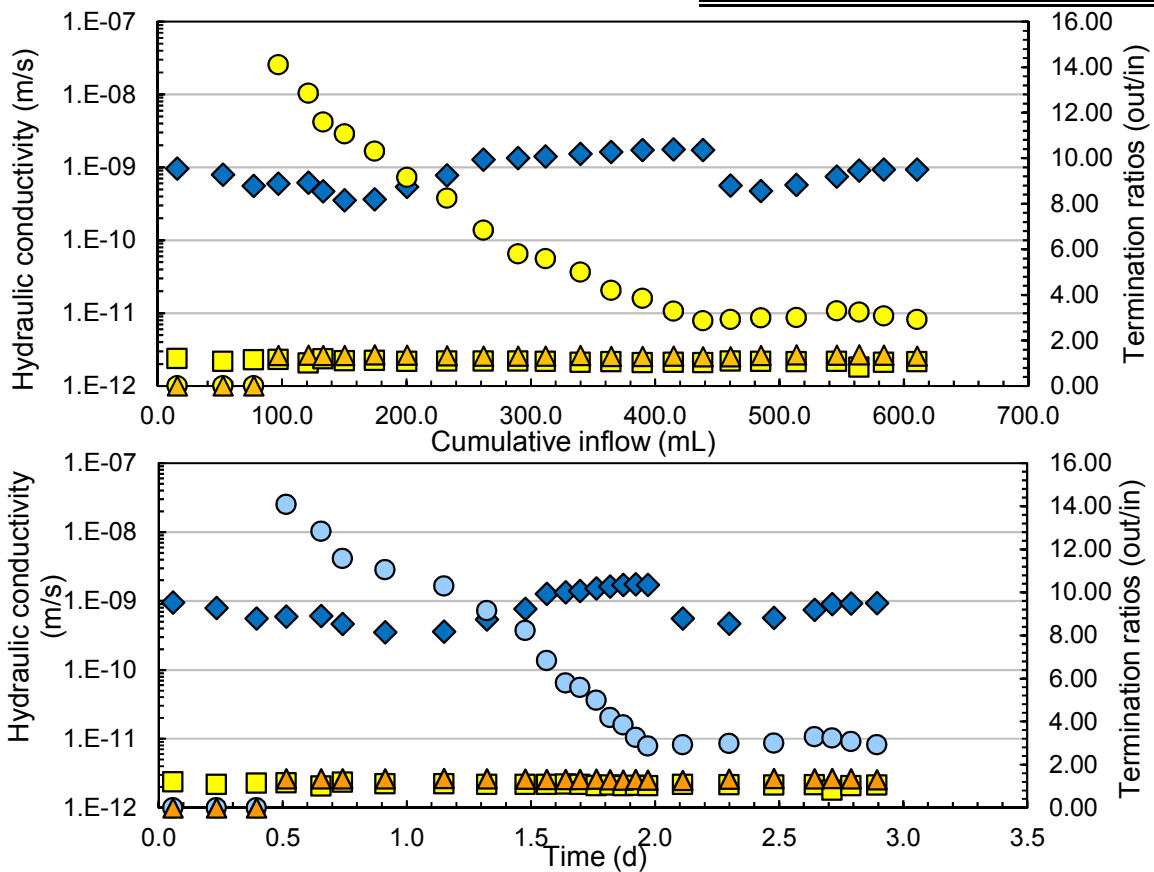


Hydraulic Conductivity—Gravity Method


Test ID	2c	Test start date	2016/08/02	
GCL type	DN (12 ppi)	Notes		
Student	Conzelmann, Joel			
Permeant liquid	CW			
Prehydrated (Y/N)	N			
Specimen diameter	15.1			cm
	5.9			in
Avg. effective stress	27.7			kPa
	4.0			psi

Terminated test results

k [D5084]	9.20E-10	m/s	k [D6766]	nr	m/s
PVF [D5084]	6.0		PVF [D6766]	nr	
time [D5084]	2.89	d	time [D6766]	nr	d
			Avg. EC	nr	ms/cm
			Avg. pH	nr	



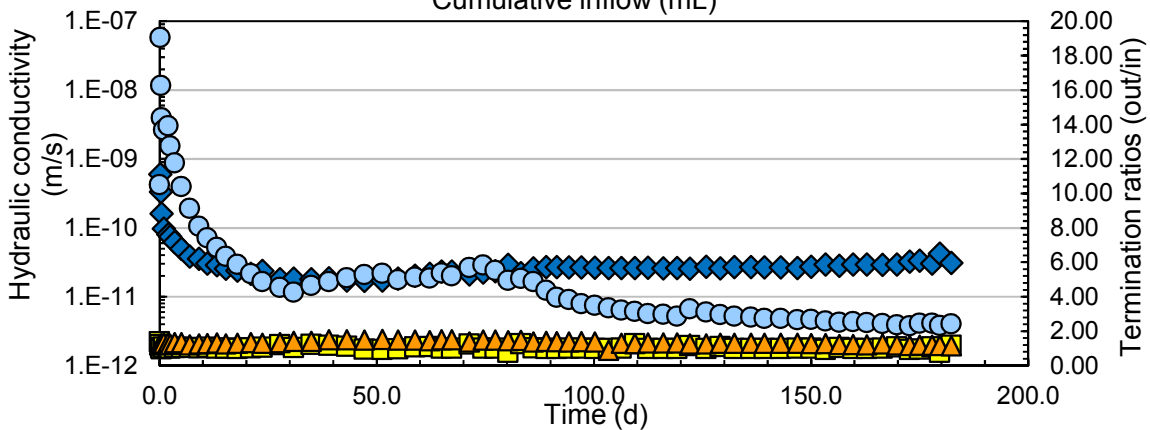
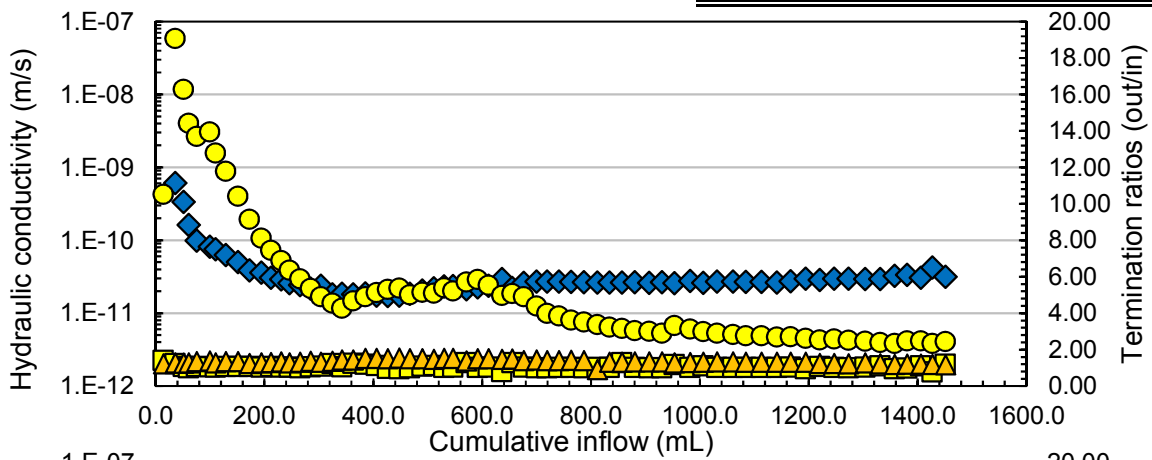
Hydraulic Conductivity—Gravity Method

Test ID	2d	Test start date	2016/10/16	
GCL type	DN (12 ppi)	Notes 		
Student	Conzelmann, Joel			
Permeant liquid	CW			
Prehydrated (Y/N)	N			
Specimen diameter	15.1			cm
	5.9			in
Avg. effective stress	27.6			kPa
	4.0			psi


Terminated test results

k [D5084]	1.83E-11	m/s	k [D6766]	tbd	m/s
PVF [D5084]	tbd		PVF [D6766]	tbd	
time [D5084]	39.0	d	time [D6766]	tbd	d
			Avg. EC	tbd	ms/cm
			Avg. pH	tbd	

- ◆ k ● $EC_{out/in}$
- $Q_{out/in}$ ▲ $pH_{out/in}$



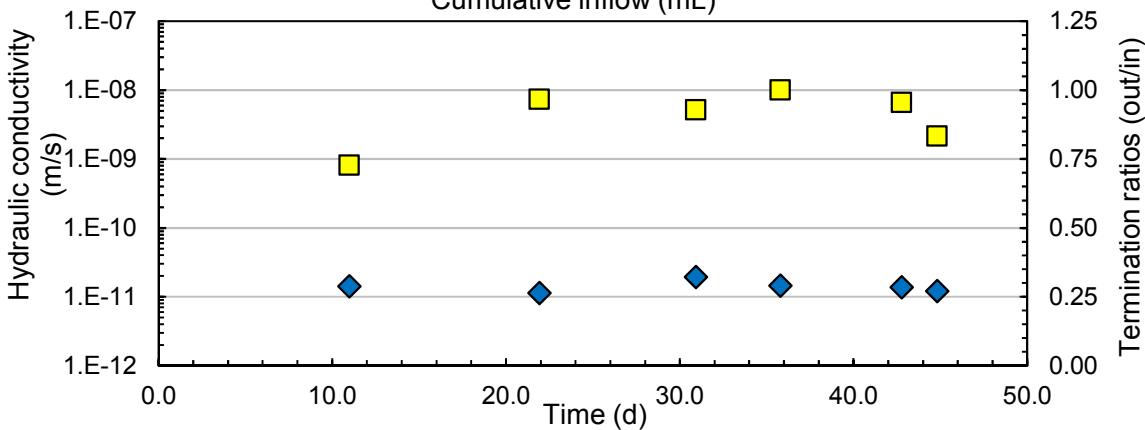
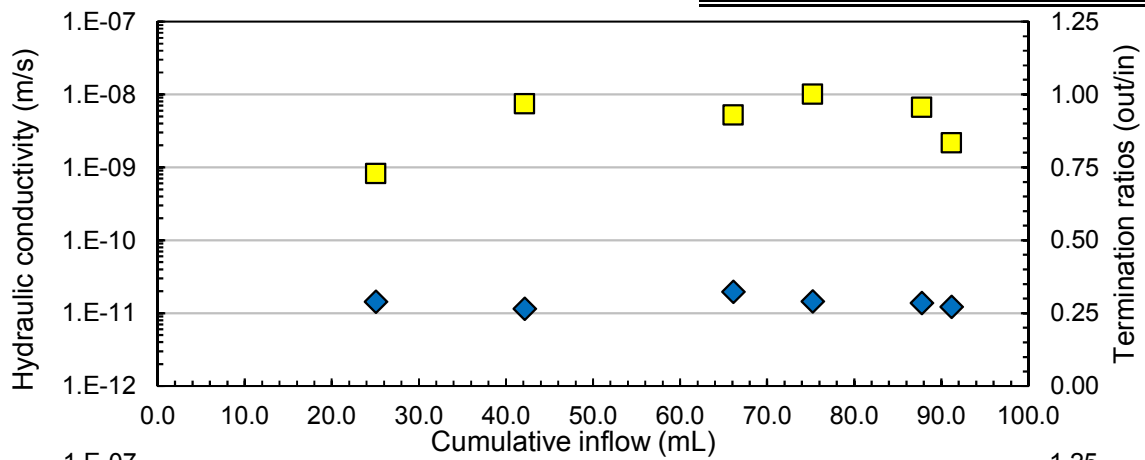
Hydraulic Conductivity—Standard Method

Test ID	3a	Test start date	2016/05/13	
GCL type	DN (12 ppi)	Notes 		
Student	Conzelmann, Joel			
Permeant liquid	Au-PS			
Prehydrated (Y/N)	N			
Specimen diameter	10.2			cm
	4.0			in
Avg. effective stress	26.4			kPa
	3.8			psi

Terminated test results

k [D5084]	1.35E-11	m/s	k [D6766]	nr	m/s
PVF [D5084]	1.9		PVF [D6766]	nr	
time [D5084]	44.81	d	time [D6766]	nr	d
			Avg. EC	nr	ms/cm
			Avg. pH	nr	

- ◆ k ● $EC_{out/in}$
- $Q_{out/in}$ ▲ $pH_{out/in}$

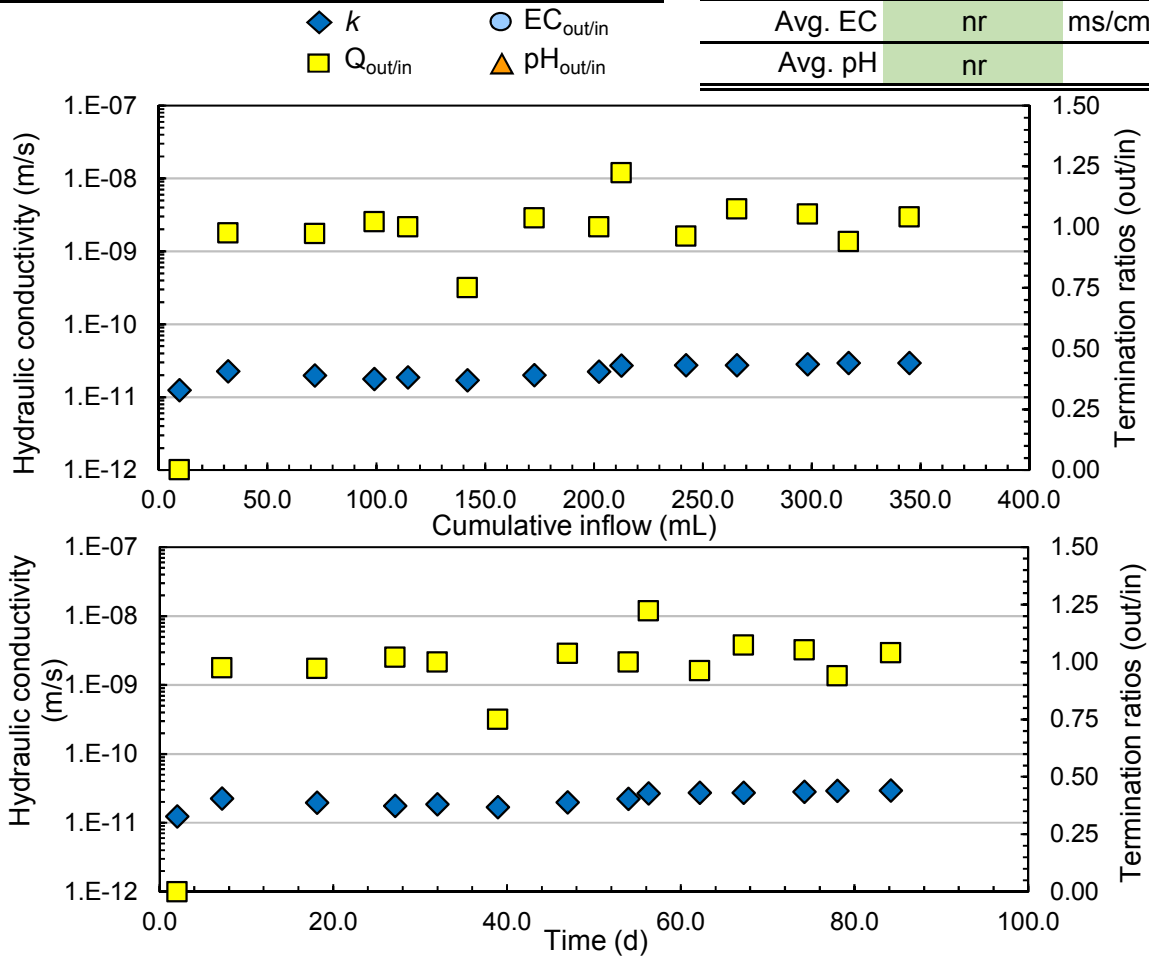


Hydraulic Conductivity—Standard Method


Test ID	3b	Test start date	2016/05/19	
GCL type	DN (12 ppi)	<div style="text-align: left; padding-bottom: 10px;">Notes</div>		
Student	Conzelmann, Joel			
Permeant liquid	Au-PS			
Prehydrated (Y/N)	N			
Specimen diameter	10.2			cm
	4.0			in
Avg. effective stress	26.4			kPa
	3.8			psi

Terminated test results

k [D5084]	2.90E-11	m/s	k [D6766]	nr	m/s
PVF [D5084]	10.5		PVF [D6766]	nr	
time [D5084]	84.15	d	time [D6766]	nr	d
			Avg. EC	nr	ms/cm
			Avg. pH	nr	

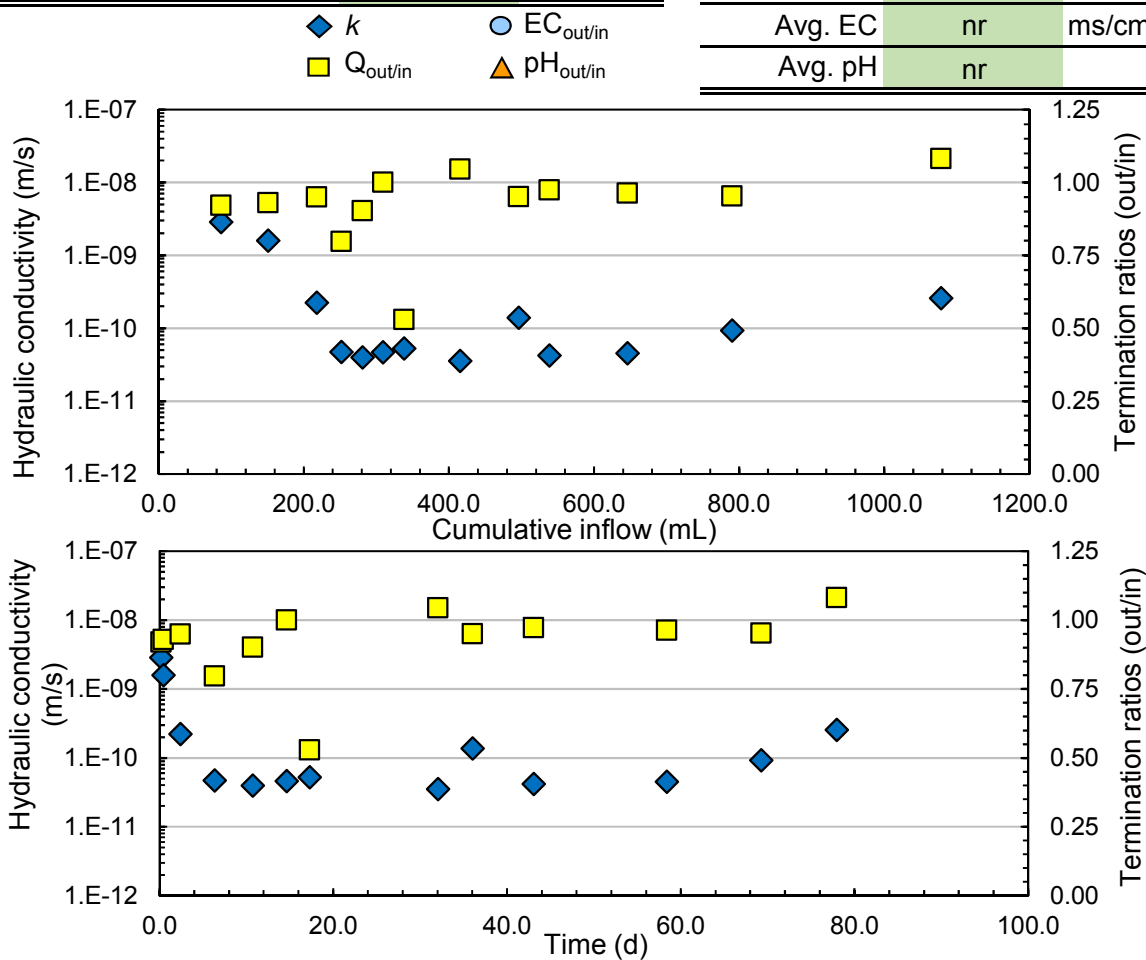


Hydraulic Conductivity—Standard Method

Test ID	3c	Test start date	2016/12/14	
GCL type	DN (12 ppi)	Notes 		
Student	Conzelmann, Joel			
Permeant liquid	Au-PS			
Prehydrated (Y/N)	N			
Specimen diameter	10.2			cm
	4.0			in
Avg. effective stress	26.4			kPa
	3.8			psi

Terminated test results

k [D5084]	4.45E-11	m/s	k [D6766]	nr	m/s
PVF [D5084]	7.1		PVF [D6766]	nr	
time [D5084]	14.63	d	time [D6766]	nr	d
			Avg. EC	nr	ms/cm
			Avg. pH	nr	

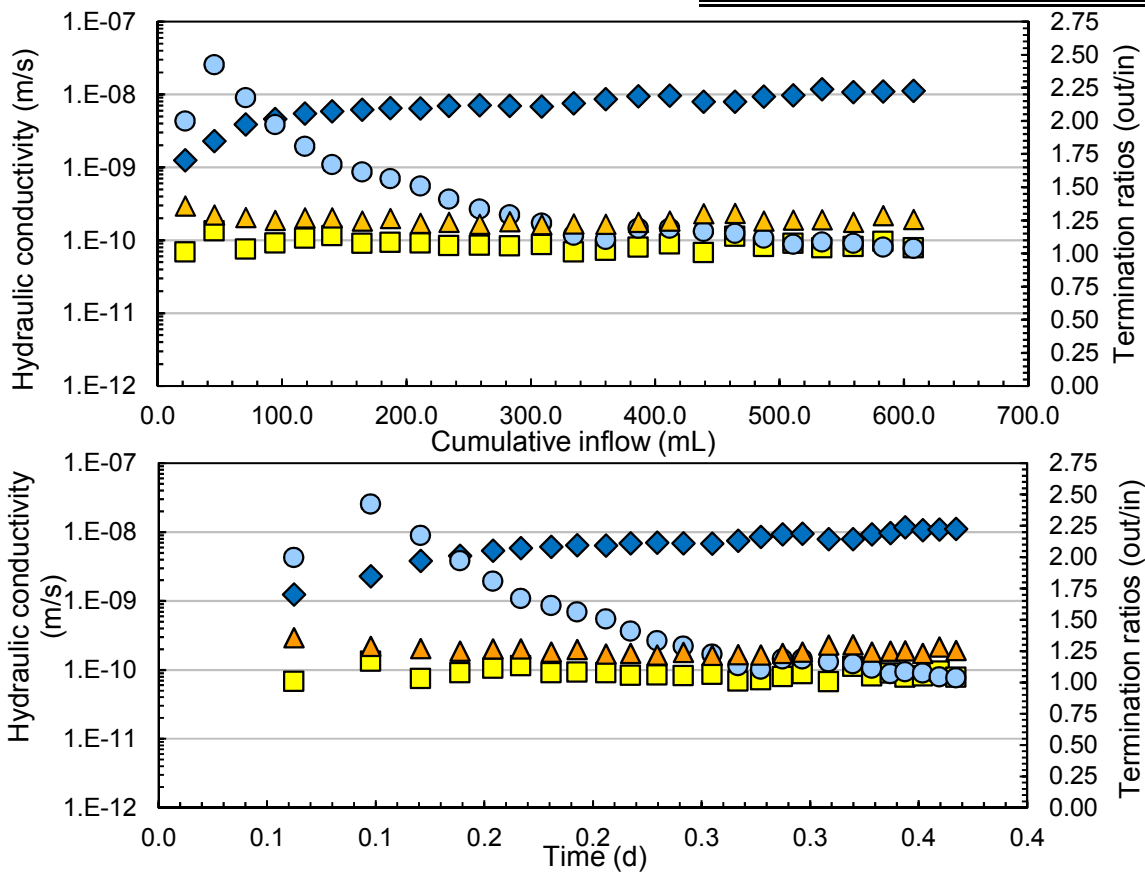


Hydraulic Conductivity—Gravity Method


Test ID	4a, DN9-G1	Test start date	2017/02/17
GCL type	DN (12 ppi)	<div style="display: flex; align-items: center; justify-content: center;"> <div style="margin-right: 20px;">Notes</div> </div>	
Student	Conzelmann, Joel		
Permeant liquid	Au-PLS		
Prehydrated (Y/N)	N		
Specimen diameter	15.1 cm		
	5.9 in		
Avg. effective stress	27.6 kPa		
	4.0 psi		

Terminated test results

k [D5084]	6.93E-09	m/s
PVF [D5084]	3.1	
time [D5084]	0.25	d
k [D6766]	1.10E-08	m/s
PVF [D6766]	6.1	
time [D6766]	0.37	d
Avg. EC	3.53	ms/cm
Avg. pH	6.40	

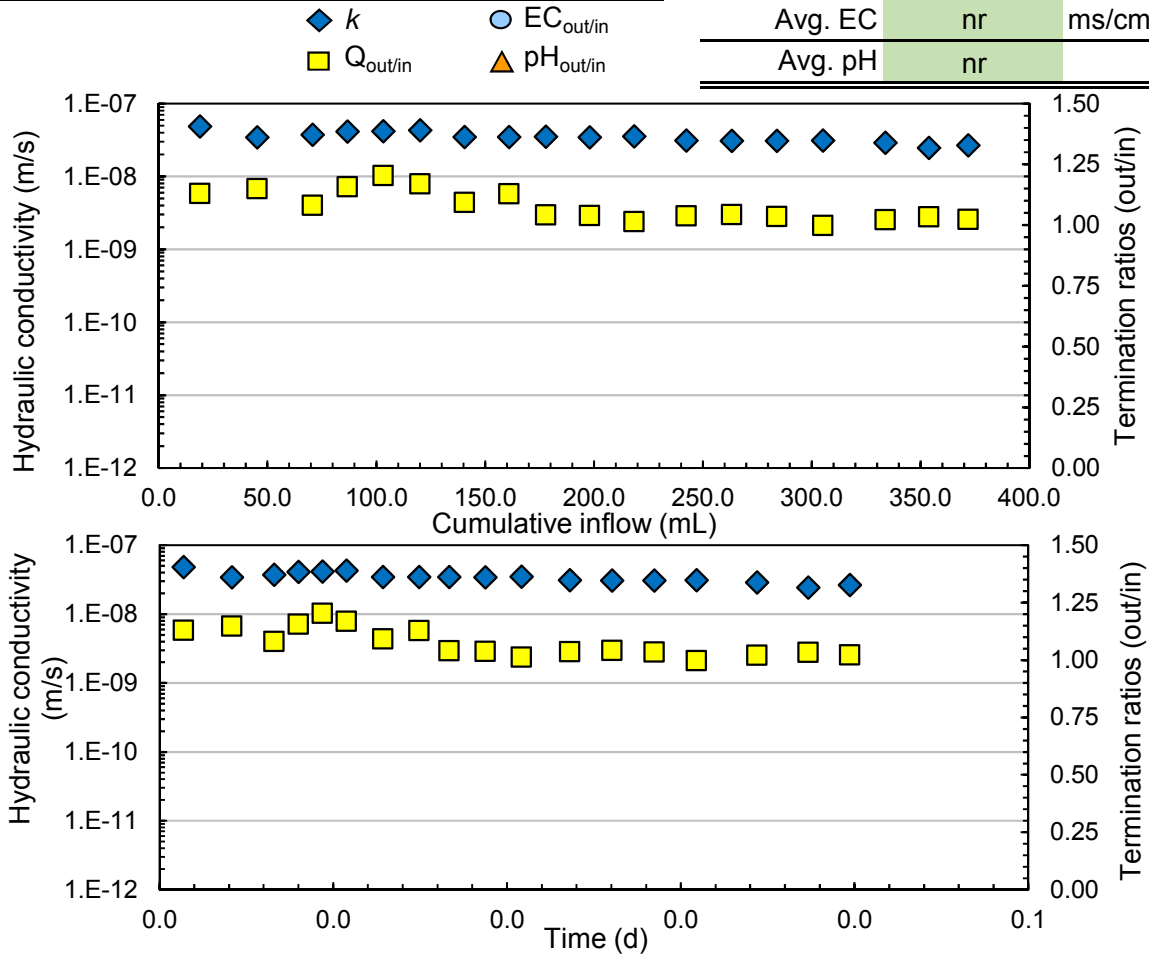


Hydraulic Conductivity—Gravity Method


Test ID	4b	Test start date	2016/05/05	
GCL type	DN (12 ppi)	<div style="text-align: left; margin-bottom: 10px;">Notes</div> 		
Student	Conzelmann, Joel			
Permeant liquid	Au-PLS			
Prehydrated (Y/N)	N			
Specimen diameter	15.1			cm
	5.9			in
Avg. effective stress	27.6			kPa
	4.0			psi

Terminated test results

k [D5084]	2.67E-08	m/s	k [D6766]	nr	m/s
PVF [D5084]	3.5		PVF [D6766]	nr	
time [D5084]	0.04	d	time [D6766]	nr	d
			Avg. EC	nr	ms/cm
			Avg. pH	nr	

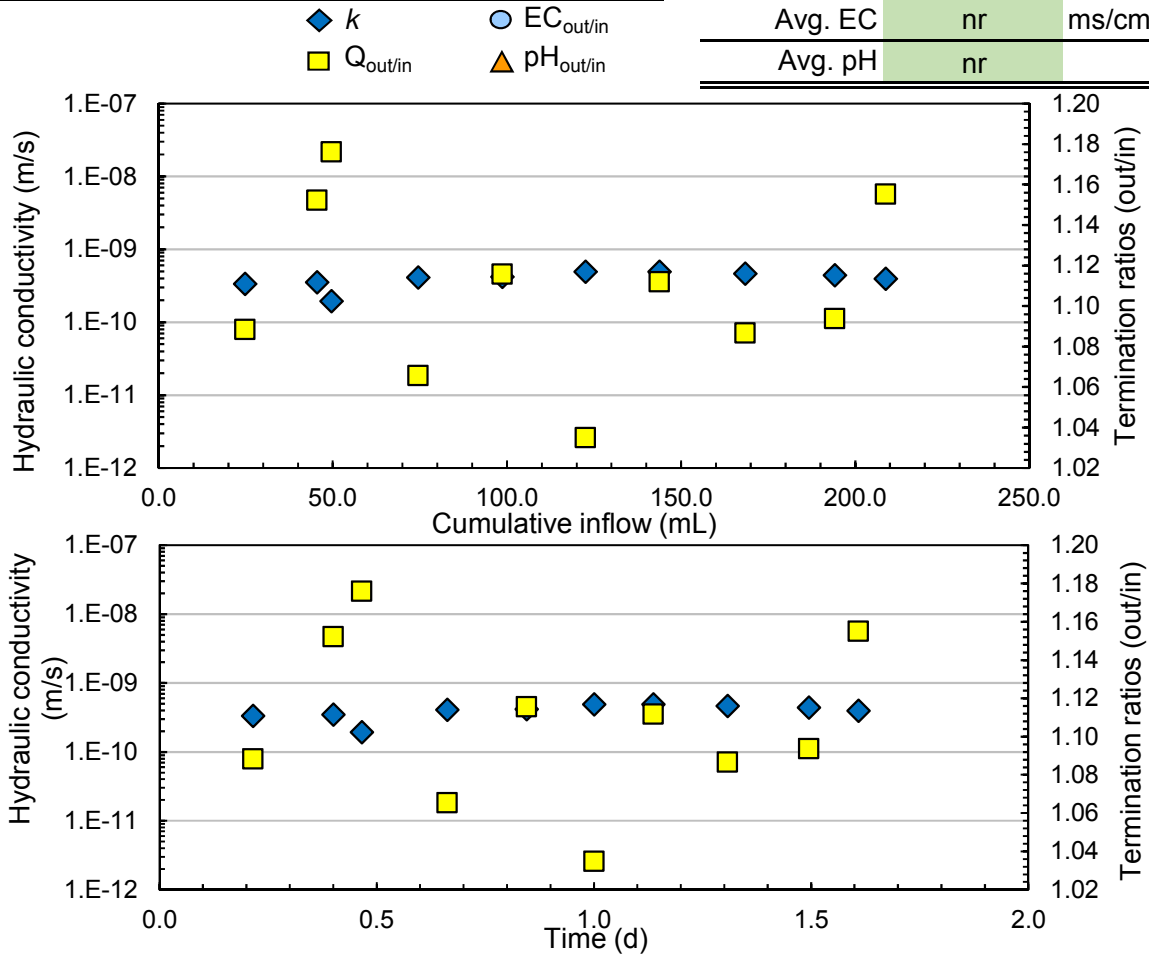


Hydraulic Conductivity—Gravity Method

Test ID	4c	Test start date	2016/06/08
GCL type	DN (12 ppi)	Notes 	
Student	Conzelmann, Joel		
Permeant liquid	Au-PLS		
Prehydrated (Y/N)	N		
Specimen diameter	15.1 cm		
	5.9 in		
Avg. effective stress	27.4 kPa		
	4.0 psi		

Terminated test results

k [D5084]	4.33E-10	m/s	k [D6766]	nr	m/s
PVF [D5084]	2.4		PVF [D6766]	nr	
time [D5084]	1.61	d	time [D6766]	nr	d
			Avg. EC	nr	ms/cm
			Avg. pH	nr	

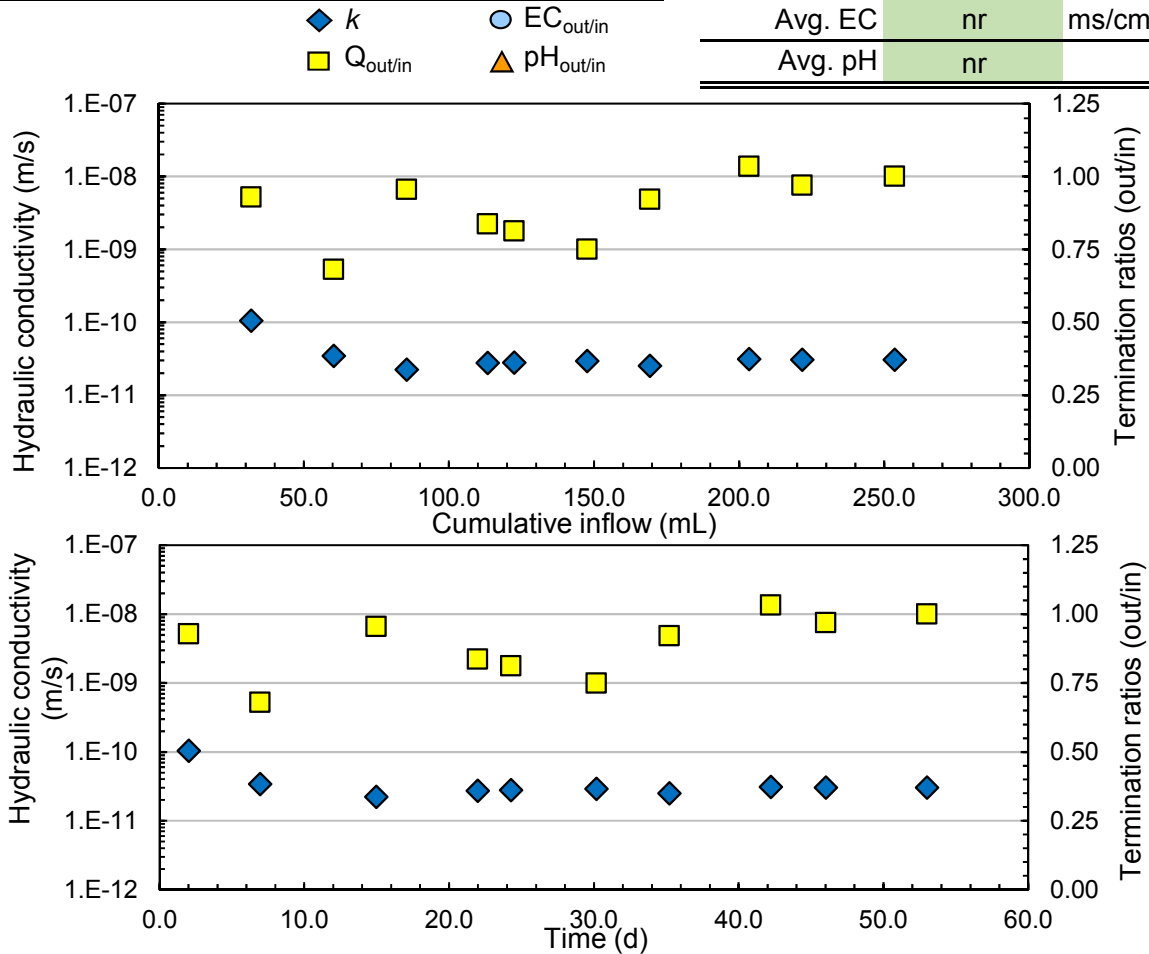


Hydraulic Conductivity—Standard Method

Test ID	5a	Test start date	2016/06/15	
GCL type	DN (12 ppi)	Notes Modified, SM-1 		
Student	Conzelmann, Joel			
Permeant liquid	CW			
Prehydrated (Y/N)	N			
Specimen diameter	10.2			cm
	4.0			in
Avg. effective stress	26.4			kPa
	3.8			psi

Terminated test results

k [D5084]	3.08E-11	m/s	k [D6766]	nr	m/s
PVF [D5084]	6.1		PVF [D6766]	nr	
time [D5084]	53.00	d	time [D6766]	nr	d
			Avg. EC	nr	ms/cm
			Avg. pH	nr	

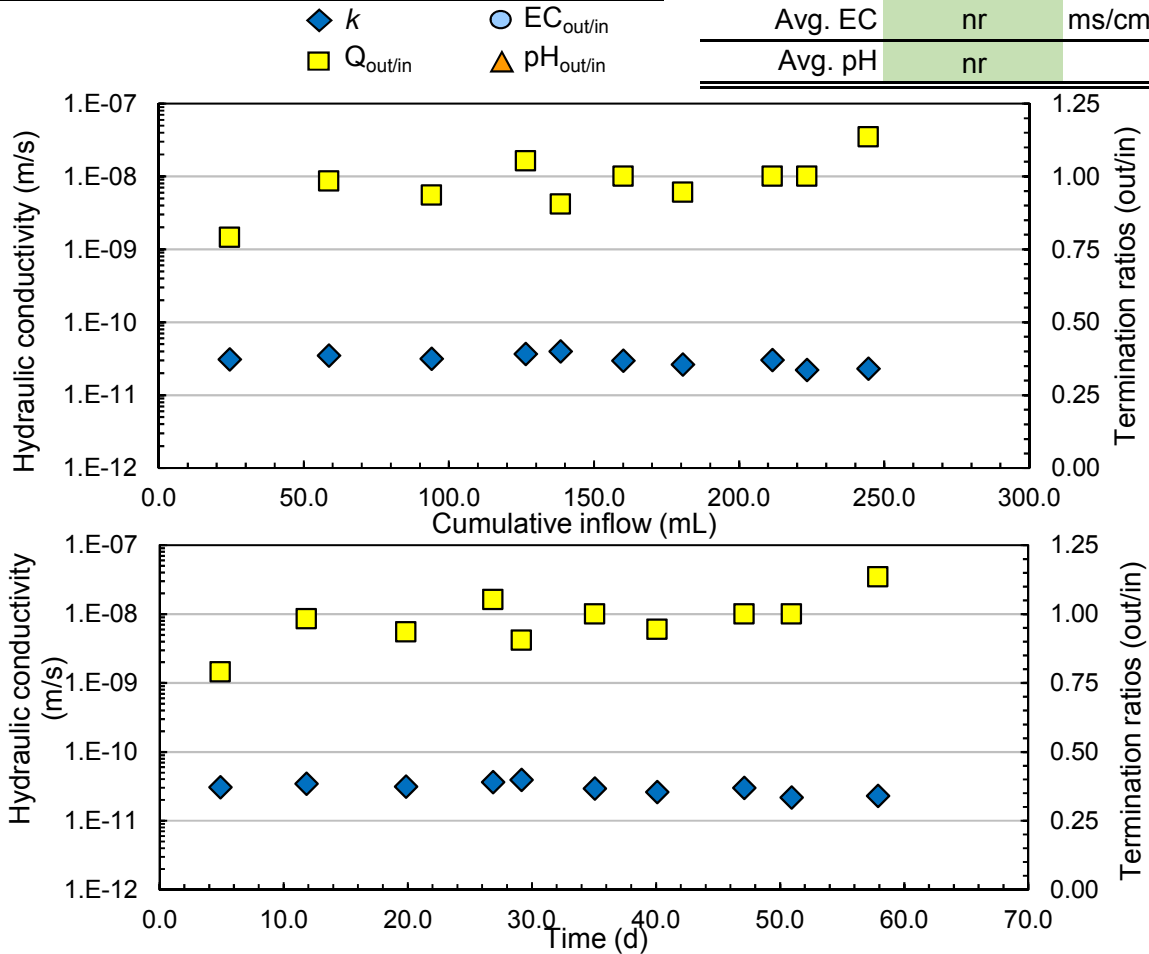


Hydraulic Conductivity—Standard Method

Test ID	6a	Test start date	2016/06/15	
GCL type	DN (12 ppi)	Notes Modified, S-M2 		
Student	Conzelmann, Joel			
Permeant liquid	CW			
Prehydrated (Y/N)	N			
Specimen diameter	10.2			cm
	4.0			in
Avg. effective stress	26.4			kPa
	3.8			psi

Terminated test results

k [D5084]	2.50E-11	m/s	k [D6766]	nr	m/s
PVF [D5084]	5.2		PVF [D6766]	nr	
time [D5084]	57.89	d	time [D6766]	nr	d
			Avg. EC	nr	ms/cm
			Avg. pH	nr	

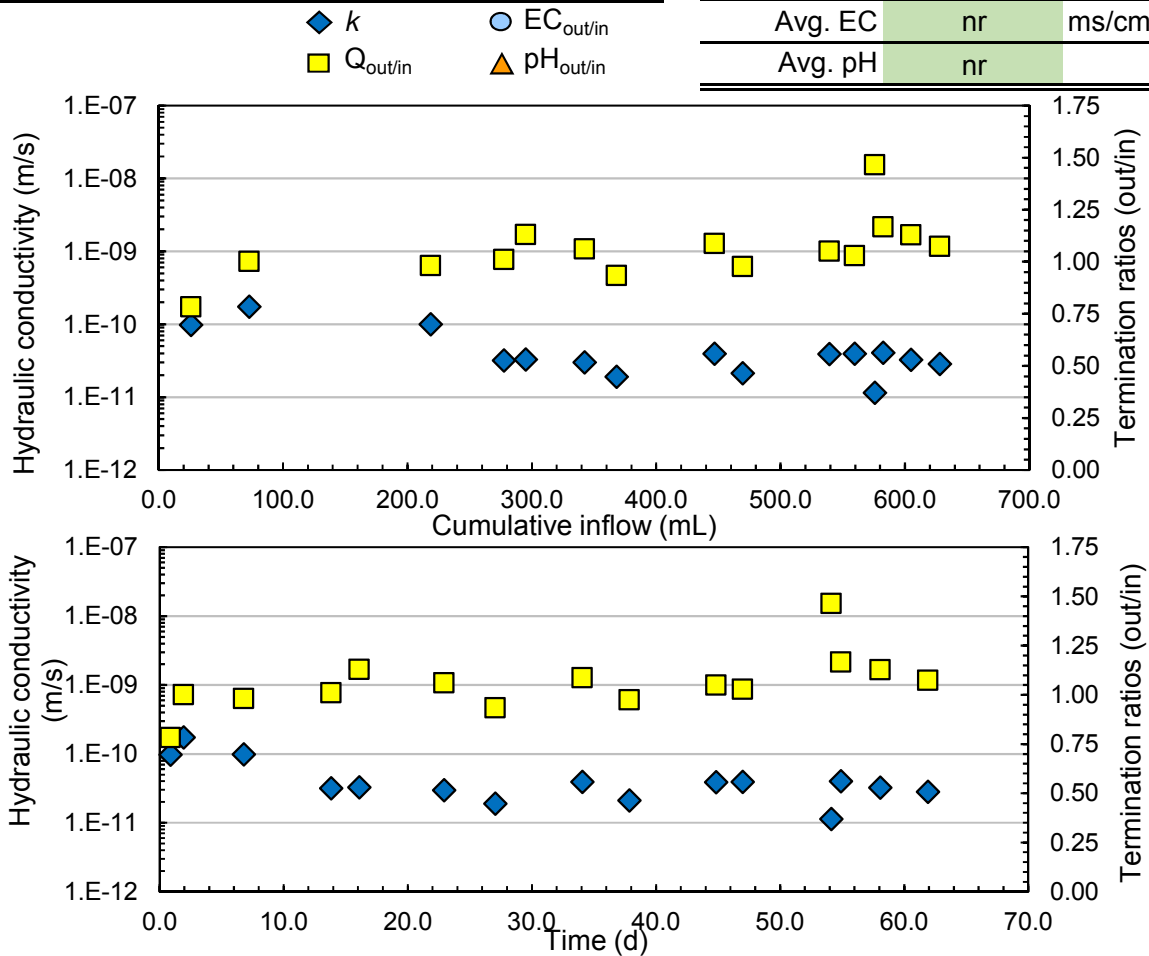


Hydraulic Conductivity—Standard Method


Test ID	7a	Test start date	2016/06/22	
GCL type	DN (12 ppi)	Notes Modified, S-M3 		
Student	Conzelmann, Joel			
Permeant liquid	CW			
Prehydrated (Y/N)	N			
Specimen diameter	15.1			cm
	5.9			in
Avg. effective stress	26.4			kPa
	3.8			psi

Terminated test results

k [D5084]	3.37E-11	m/s	k [D6766]	nr	m/s
PVF [D5084]	5.9		PVF [D6766]	nr	
time [D5084]	61.90	d	time [D6766]	nr	d
			Avg. EC	nr	ms/cm
			Avg. pH	nr	

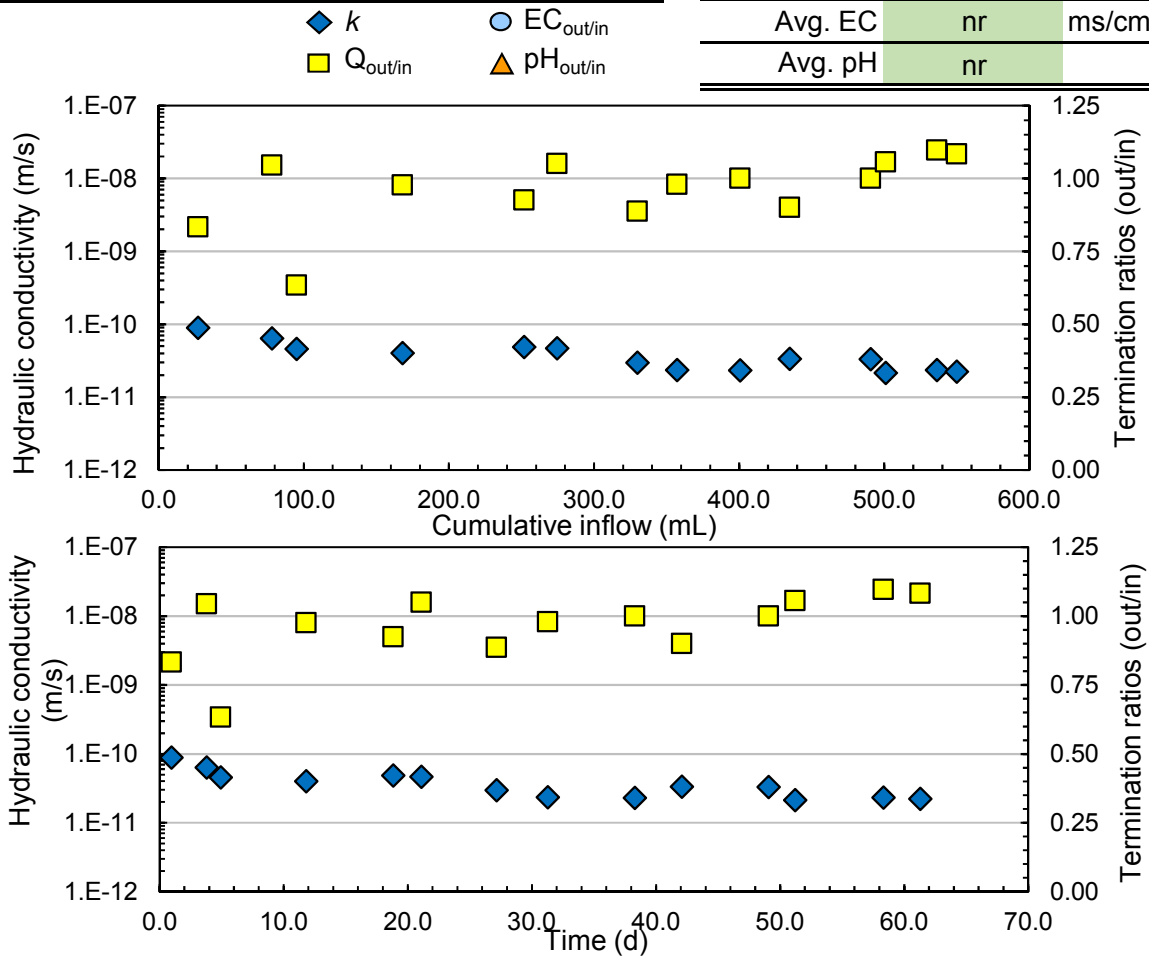


Hydraulic Conductivity—Standard Method

Test ID	8a	Test start date	2016/06/21	
GCL type	DN (12 ppi)	Notes Modified, S-M4 		
Student	Conzelmann, Joel			
Permeant liquid	CW			
Prehydrated (Y/N)	N			
Specimen diameter	15.1			cm
	5.9			in
Avg. effective stress	26.4			kPa
	3.8			psi

Terminated test results

k [D5084]	2.24E-11	m/s	k [D6766]	nr	m/s
PVF [D5084]	4.9		PVF [D6766]	nr	
time [D5084]	61.27	d	time [D6766]	nr	d
			Avg. EC	nr	ms/cm
			Avg. pH	nr	

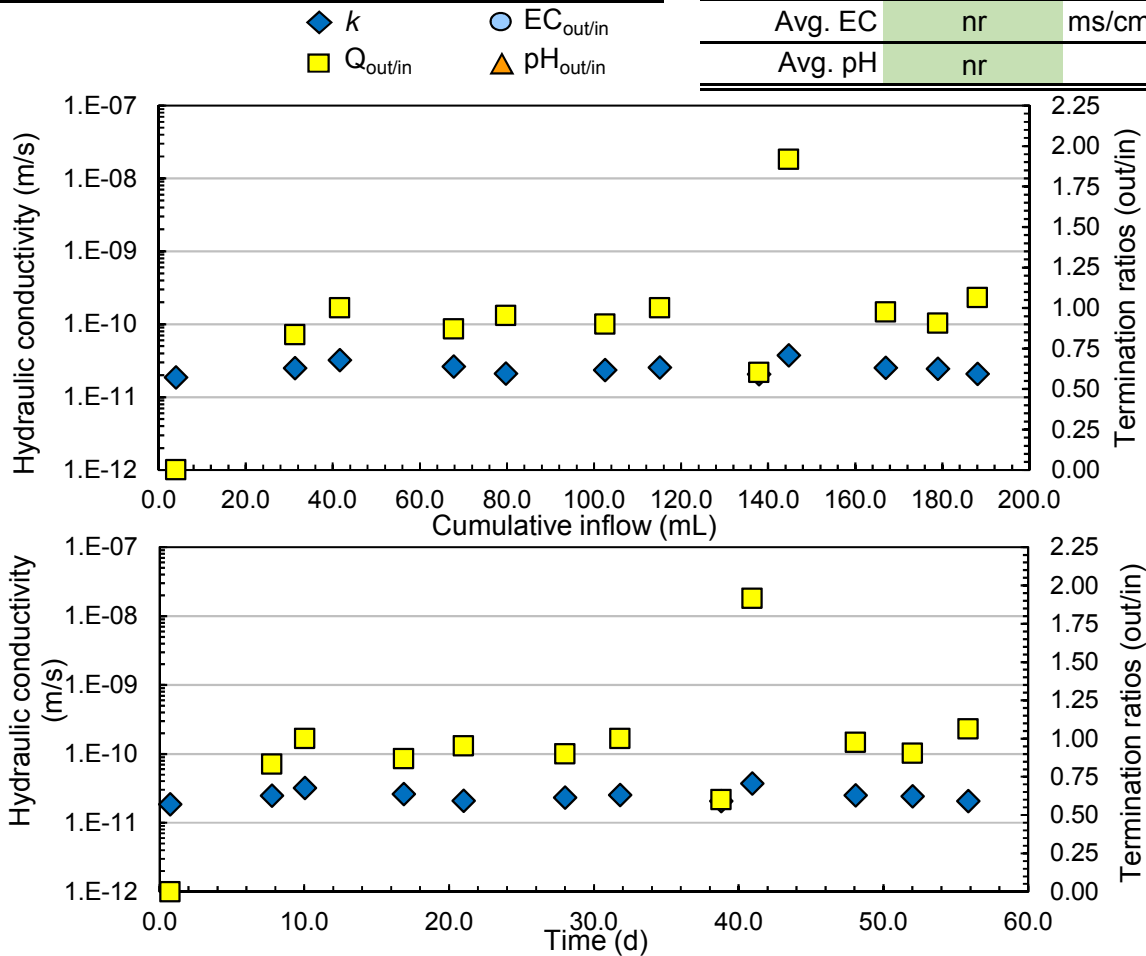


Hydraulic Conductivity—Standard Method

Test ID	8b	Test start date	2016/07/01	
GCL type	DN (12 ppi)	Notes Modified, S-M4 		
Student	Conzelmann, Joel			
Permeant liquid	CW			
Prehydrated (Y/N)	N			
Specimen diameter	10.2			cm
	4.0			in
Avg. effective stress	26.4			kPa
	3.8			psi

Terminated test results

k [D5084]	2.34E-11	m/s	k [D6766]	nr	m/s
PVF [D5084]	4.0		PVF [D6766]	nr	
time [D5084]	55.84	d	time [D6766]	nr	d
			Avg. EC	nr	ms/cm
			Avg. pH	nr	

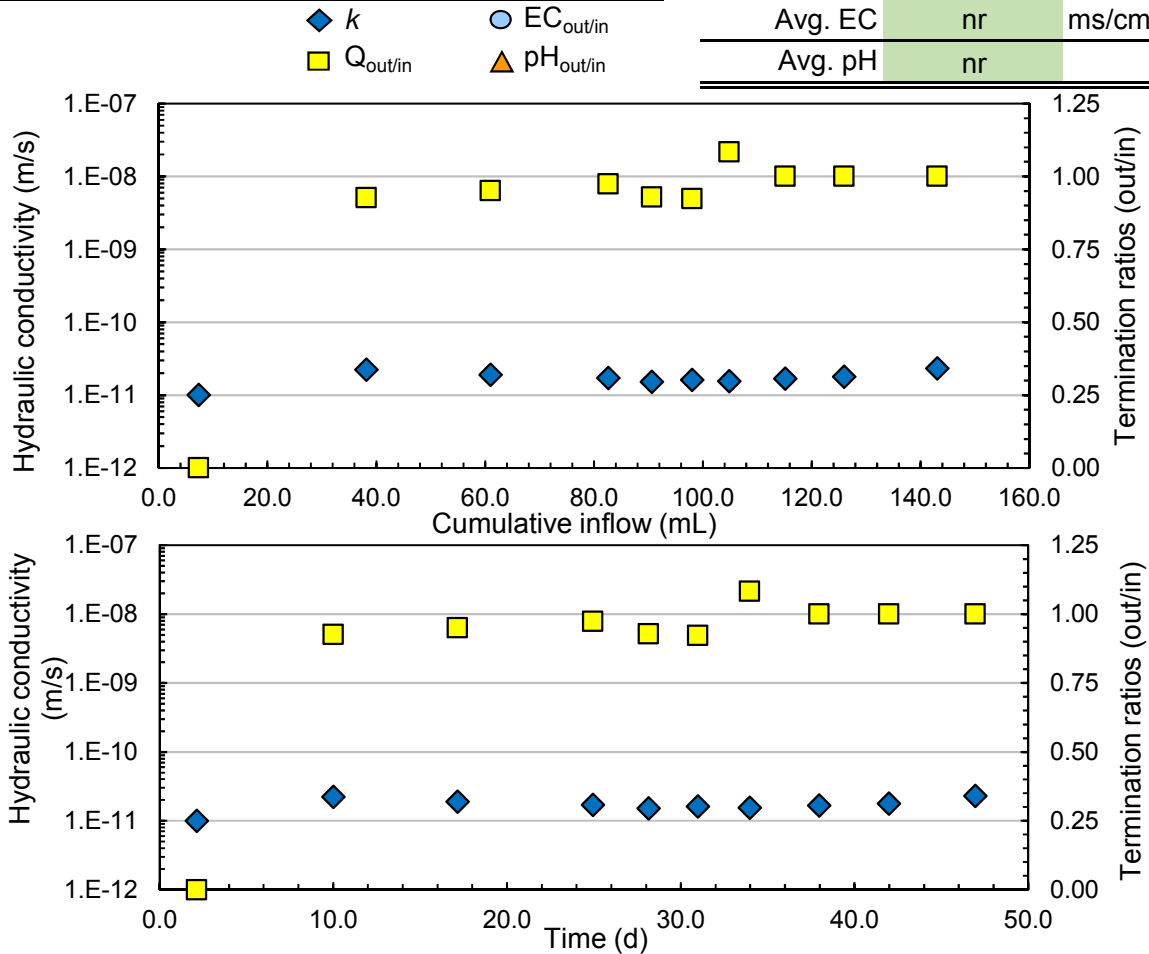


Hydraulic Conductivity—Standard Method

Test ID	9a	Test start date	2016/08/12	
GCL type	DN (12 ppi)	Notes Modified, S-M5 		
Student	Conzelmann, Joel			
Permeant liquid	CW			
Prehydrated (Y/N)	N			
Specimen diameter	10.2			cm
	4.0			in
Avg. effective stress	26.4			kPa
	3.8			psi

Terminated test results

k [D5084]	1.93E-11	m/s	k [D6766]	nr	m/s
PVF [D5084]	3.7		PVF [D6766]	nr	
time [D5084]	46.94	d	time [D6766]	nr	d
			Avg. EC	nr	ms/cm
			Avg. pH	nr	

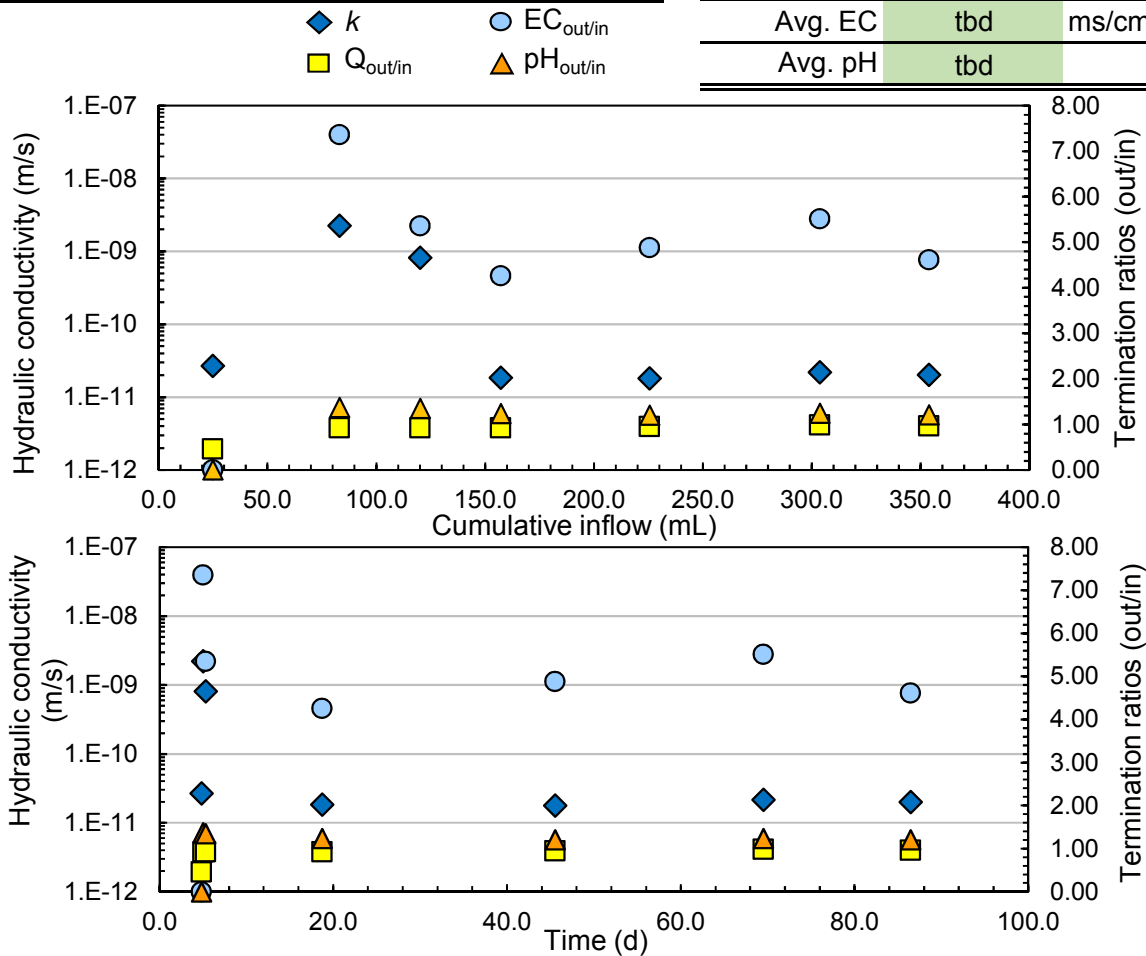


Hydraulic Conductivity—Standard Method


Test ID	10a	Test start date	2017/02/08	
GCL type	DN9	<div style="display: flex; align-items: center; justify-content: center;"> <div style="margin-right: 20px;">Notes</div> </div>		
Student	Conzelmann, Joel			
Permeant liquid	CW			
Prehydrated (Y/N)	N			
Specimen diameter	10.2			cm
	4.0			in
Avg. effective stress	26.4			kPa
	3.8			psi

Terminated test results

k [D5084]	2.00E-11	m/s	k [D6766]	tbd	m/s
PVF [D5084]	tbd		PVF [D6766]	tbd	
time [D5084]	86.45	d	time [D6766]	tbd	d
			Avg. EC	tbd	ms/cm
			Avg. pH	tbd	

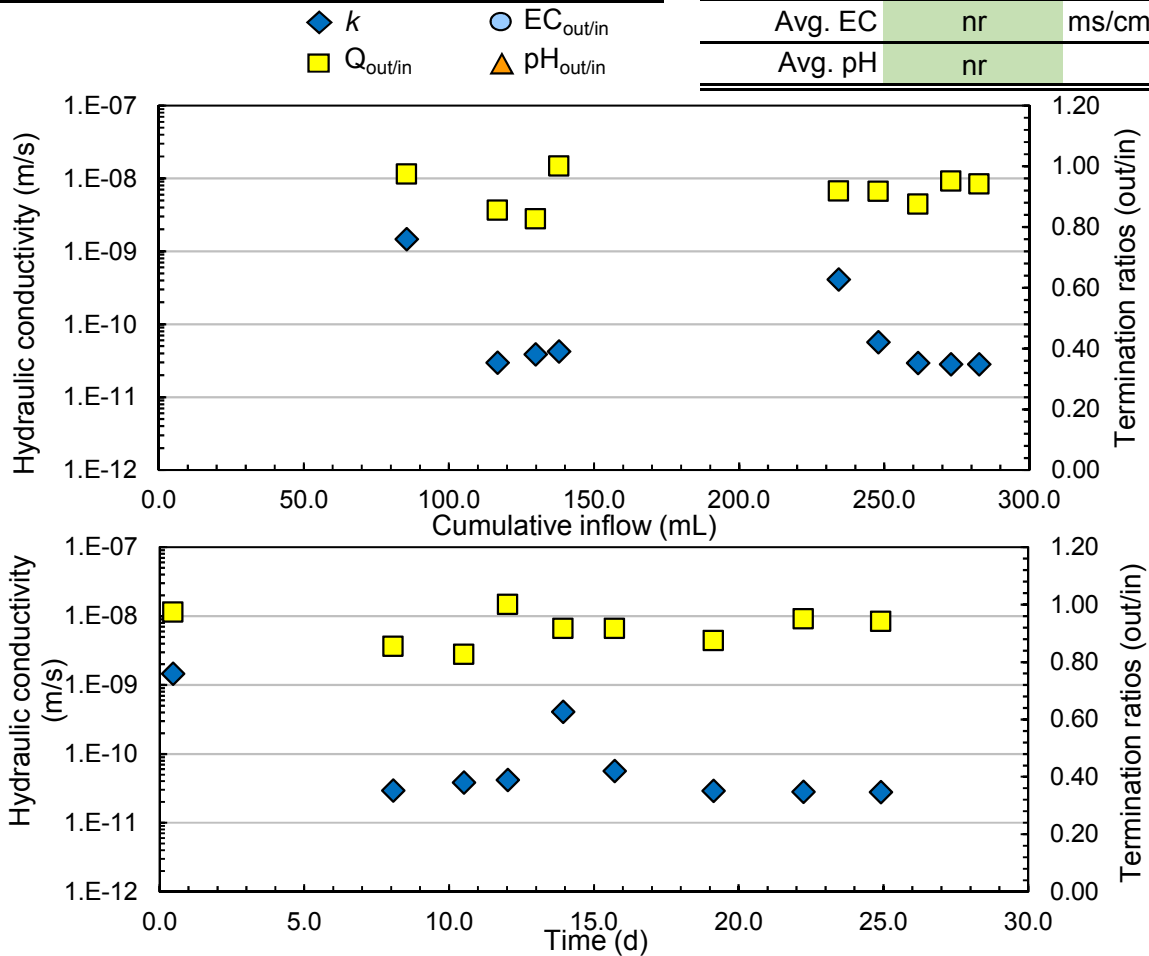


Hydraulic Conductivity—Standard Method


Test ID	10b	Test start date	2017/05/13	
GCL type	DN9	Notes 		
Student	Conzelmann, Joel			
Permeant liquid	CW			
Prehydrated (Y/N)	N			
Specimen diameter	10.2			cm
	4.0			in
Avg. effective stress	26.4			kPa
	3.8			psi

Terminated test results

<i>k</i> [D5084]	2.86E-11	m/s	<i>k</i> [D6766]	nr	m/s
PVF [D5084]	5.1		PVF [D6766]	nr	
time [D5084]	24.90	d	time [D6766]	nr	d
			Avg. EC	nr	ms/cm
			Avg. pH	nr	

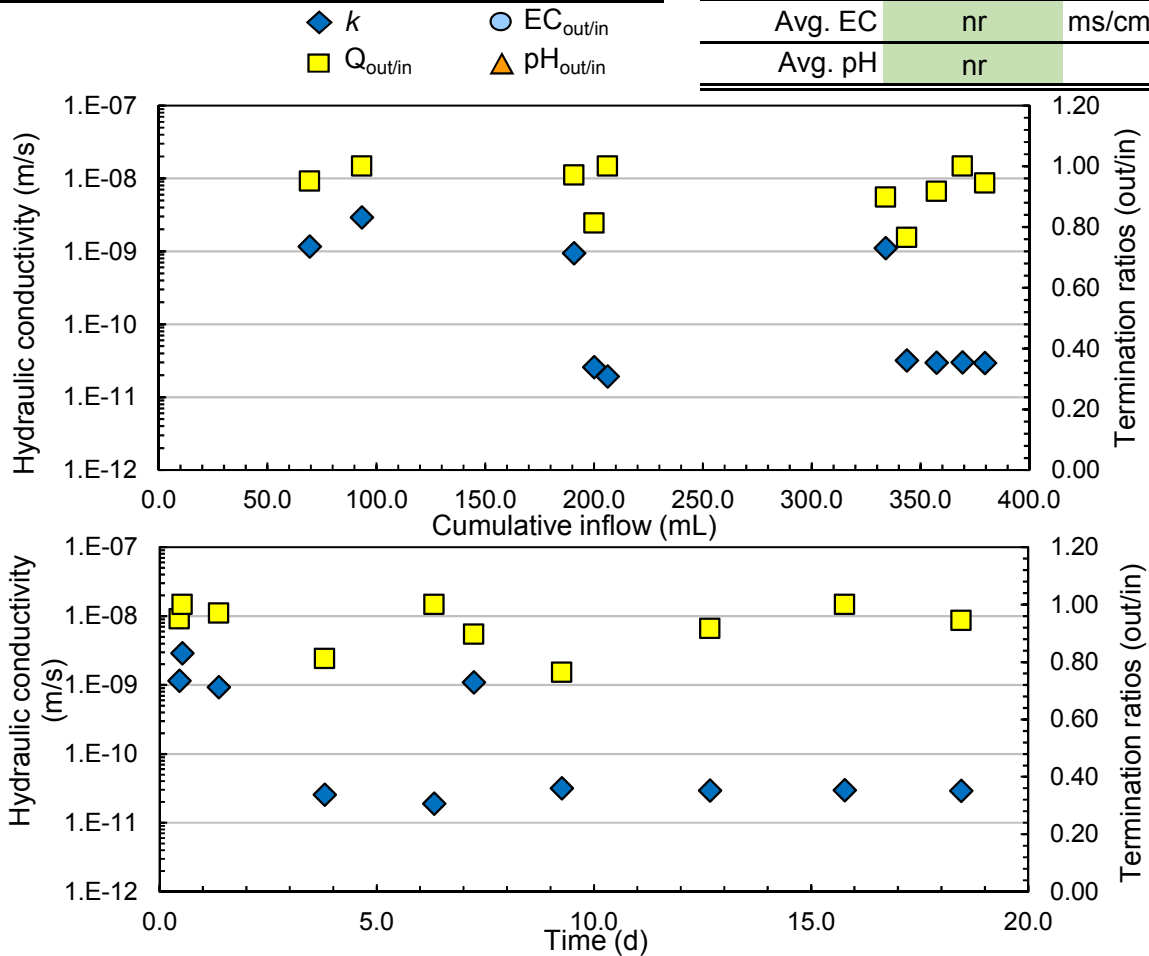


Hydraulic Conductivity—Standard Method


Test ID	10c	Test start date	2017/05/13	
GCL type	DN9	<div style="text-align: left;">Notes</div> 		
Student	Conzelmann, Joel			
Permeant liquid	CW			
Prehydrated (Y/N)	N			
Specimen diameter	10.2			cm
	4.0			in
Avg. effective stress	26.4			kPa
	3.8			psi

Terminated test results

k [D5084]	2.96E-11	m/s	k [D6766]	nr	m/s
PVF [D5084]	6.9		PVF [D6766]	nr	
time [D5084]	18.45	d	time [D6766]	nr	d
			Avg. EC	nr	ms/cm
			Avg. pH	nr	

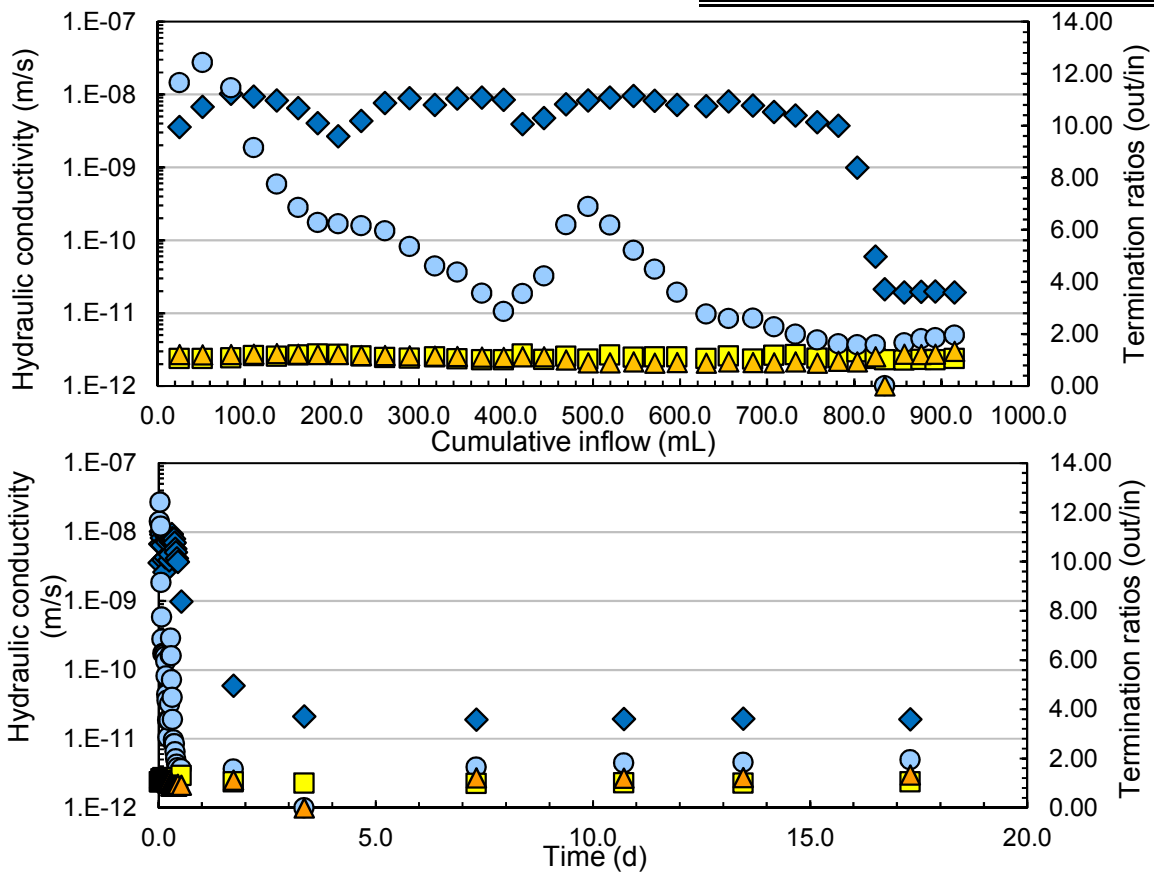


Hydraulic Conductivity—Gravity Method

Test ID	11a	Test start date	2017/02/16	
GCL type	DN9	Notes		
Student	Conzelmann, Joel			
Permeant liquid	CW			
Prehydrated (Y/N)	N			
Specimen diameter	15.1			cm
	5.9			in
Avg. effective stress	27.6			kPa
	4.0			psi

Terminated test results

k [D5084]	8.74E-09	m/s	k [D6766]	tbd	m/s
PVF [D5084]	tbd		PVF [D6766]	tbd	
time [D5084]	0.22	d	time [D6766]	tbd	d
			Avg. EC	tbd	ms/cm
			Avg. pH	tbd	

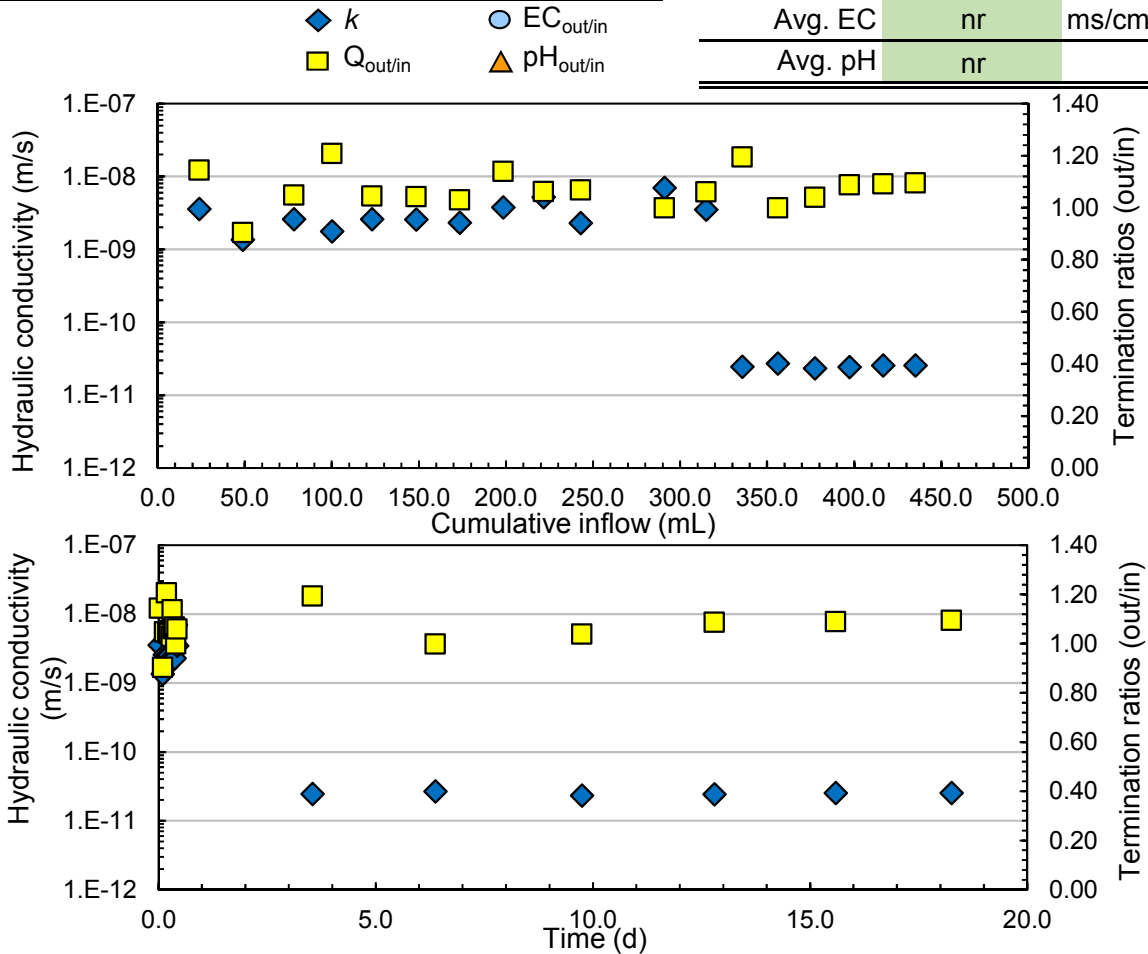


Hydraulic Conductivity—Gravity Method


Test ID	11b	Test start date	2017/05/20	
GCL type	DN9	<div style="display: flex; align-items: center; justify-content: center;"> <div style="margin-right: 20px;">Notes</div> </div>		
Student	Conzelmann, Joel			
Permeant liquid	CW			
Prehydrated (Y/N)	N			
Specimen diameter	15.1			cm
	5.9			in
Avg. effective stress	27.6			kPa
	4.0			psi

Terminated test results

k [D5084]	2.50E-11	m/s	k [D6766]	nr	m/s
PVF [D5084]	3.9		PVF [D6766]	nr	
time [D5084]	18.25	d	time [D6766]	nr	d
			Avg. EC	nr	ms/cm
			Avg. pH	nr	

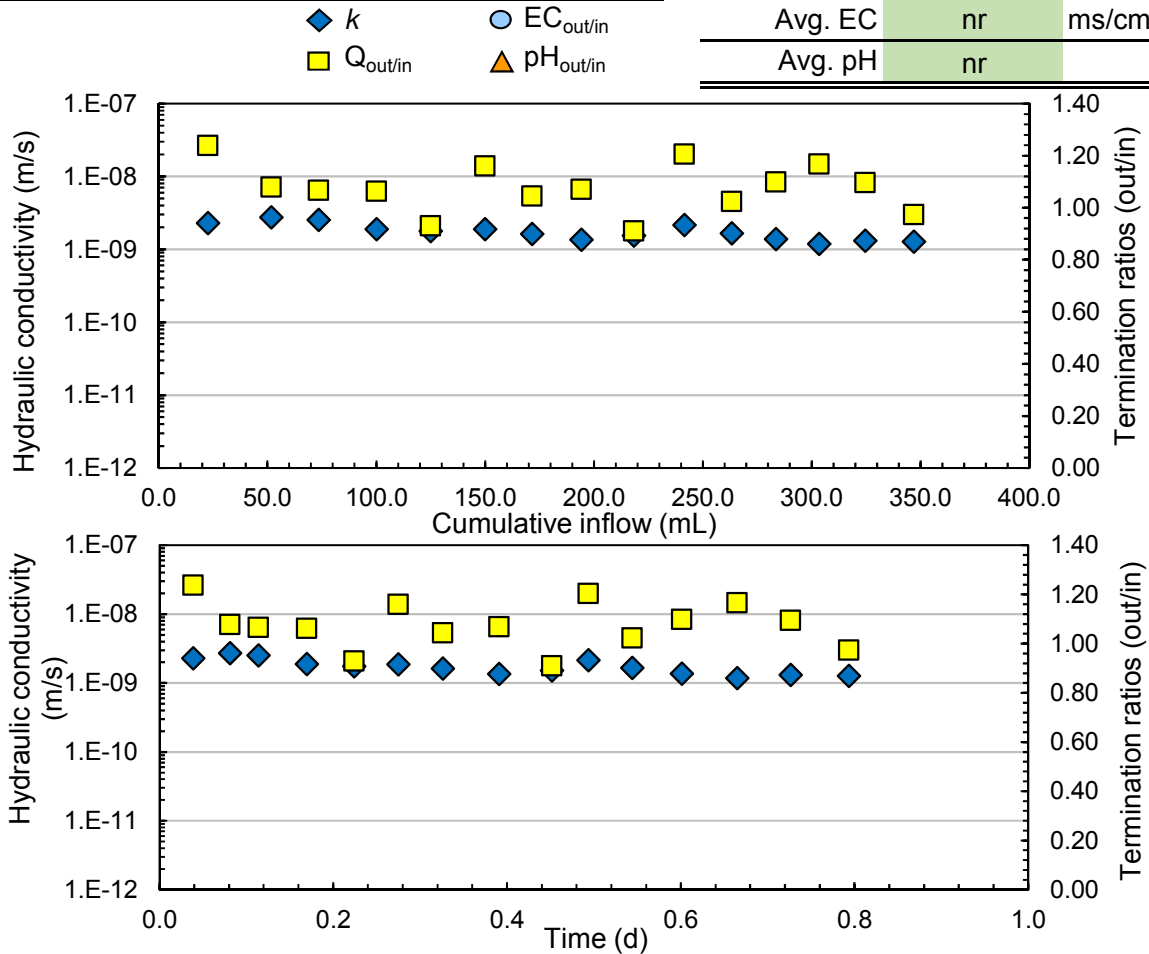


Hydraulic Conductivity—Gravity Method


Test ID	11c	Test start date	2017/05/20	
GCL type	DN9	<div style="text-align: left;">Notes</div> 		
Student	Conzelmann, Joel			
Permeant liquid	CW			
Prehydrated (Y/N)	N			
Specimen diameter	15.1			cm
	5.9			in
Avg. effective stress	27.6			kPa
	4.0			psi

Terminated test results

k [D5084]	1.26E-09	m/s	k [D6766]	nr	m/s
PVF [D5084]	2.9		PVF [D6766]	nr	
time [D5084]	0.79	d	time [D6766]	nr	d
			Avg. EC	nr	ms/cm
			Avg. pH	nr	

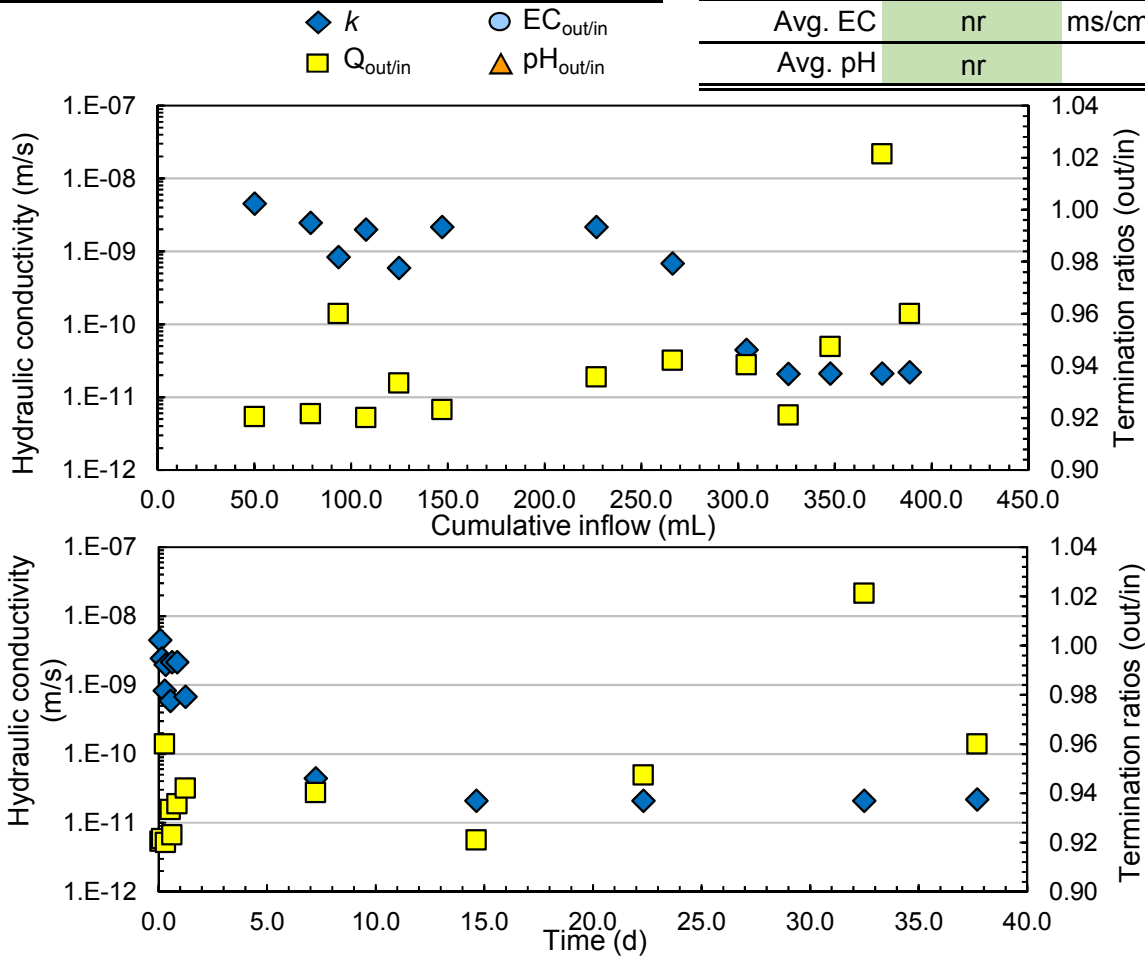


Hydraulic Conductivity—Standard Method


Test ID	12a	Test start date	2017/03/31	
GCL type	DN9	Notes Modified, S-M6 		
Student	Conzelmann, Joel			
Permeant liquid	CW			
Prehydrated (Y/N)	N			
Specimen diameter	10.2			cm
	4.0			in
Avg. effective stress	26.4			kPa
	3.8			psi

Terminated test results

<i>k</i> [D5084]	2.12E-11	m/s	<i>k</i> [D6766]	nr	m/s
PVF [D5084]	8.9		PVF [D6766]	nr	
time [D5084]	37.68	d	time [D6766]	nr	d
			Avg. EC	nr	ms/cm
			Avg. pH	nr	

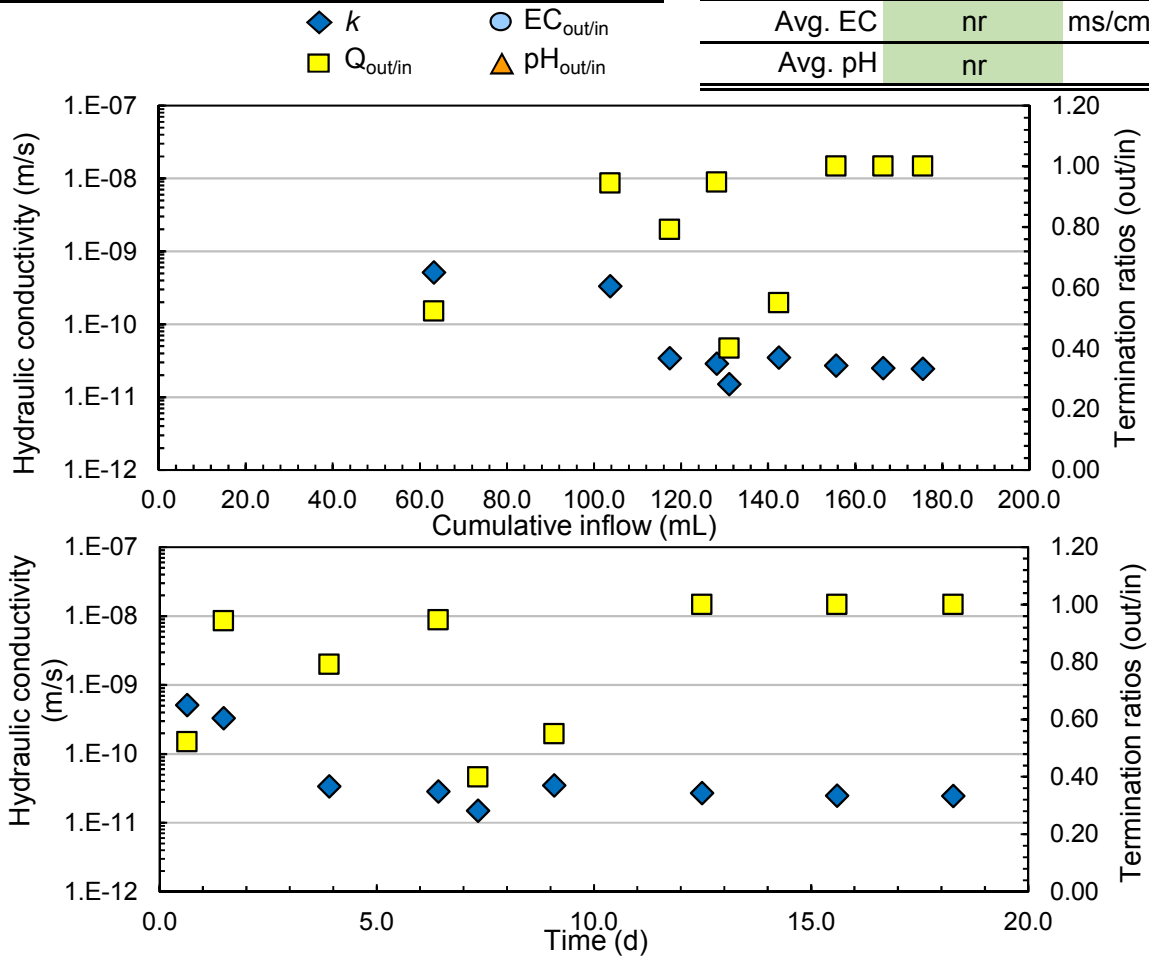


Hydraulic Conductivity—Standard Method


Test ID	12b	Test start date	2017/05/13	
GCL type	DN9	Notes Modified, S-M6 		
Student	Conzelmann, Joel			
Permeant liquid	CW			
Prehydrated (Y/N)	N			
Specimen diameter	10.2			cm
	4.0			in
Avg. effective stress	26.4			kPa
	3.8			psi

Terminated test results

k [D5084]	2.54E-11	m/s	k [D6766]	nr	m/s
PVF [D5084]	3.6		PVF [D6766]	nr	
time [D5084]	18.27	d	time [D6766]	nr	d
			Avg. EC	nr	ms/cm
			Avg. pH	nr	

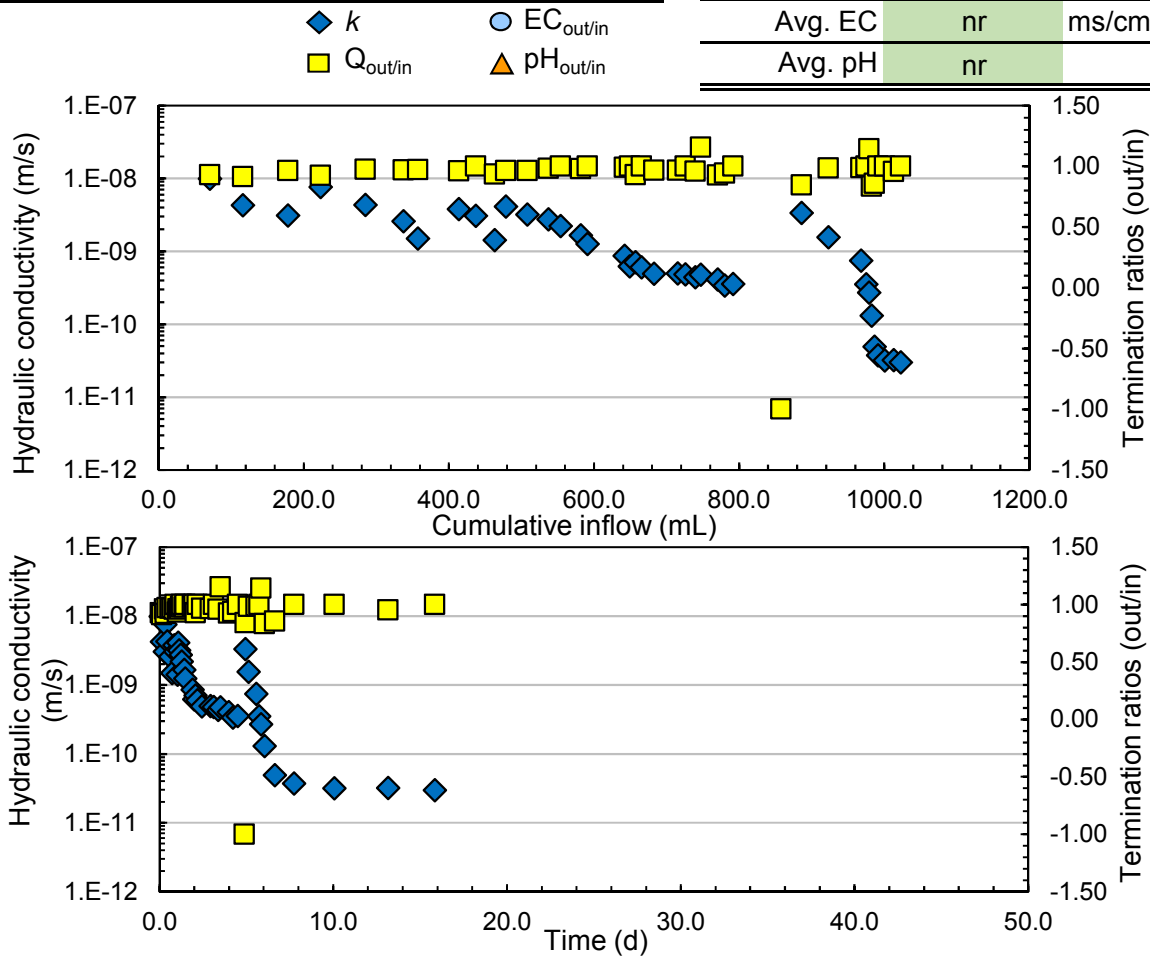


Hydraulic Conductivity—Standard Method


Test ID	12c	Test start date	2017/05/13	
GCL type	DN9	Notes Modified, S-M6 		
Student	Conzelmann, Joel			
Permeant liquid	CW			
Prehydrated (Y/N)	N			
Specimen diameter	10.2			cm
	4.0			in
Avg. effective stress	26.4			kPa
	3.8			psi

Terminated test results

k [D5084]	3.13E-11	m/s	k [D6766]	nr	m/s
PVF [D5084]	20.2		PVF [D6766]	nr	
time [D5084]	15.83	d	time [D6766]	nr	d
			Avg. EC	nr	ms/cm
			Avg. pH	nr	

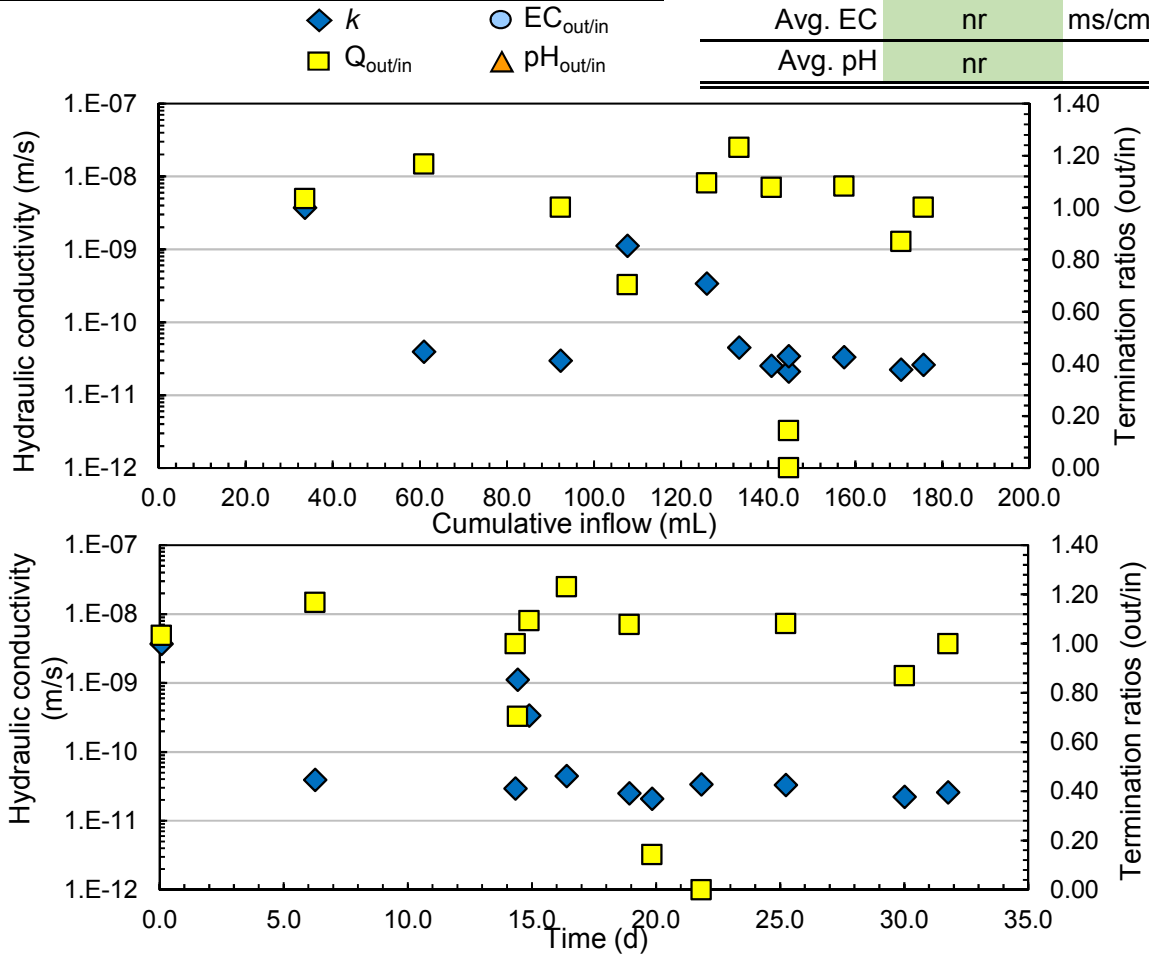


Hydraulic Conductivity—Standard Method


Test ID	13a	Test start date	2017/04/26	
GCL type	DN9	Notes Modified, S-M7 		
Student	Conzelmann, Joel			
Permeant liquid	CW			
Prehydrated (Y/N)	N			
Specimen diameter	10.2			cm
	4.0			in
Avg. effective stress	26.4			kPa
	3.8			psi

Terminated test results

k [D5084]	2.71E-11	m/s	k [D6766]	nr	m/s
PVF [D5084]	3.4		PVF [D6766]	nr	
time [D5084]	31.76	d	time [D6766]	nr	d
			Avg. EC	nr	ms/cm
			Avg. pH	nr	

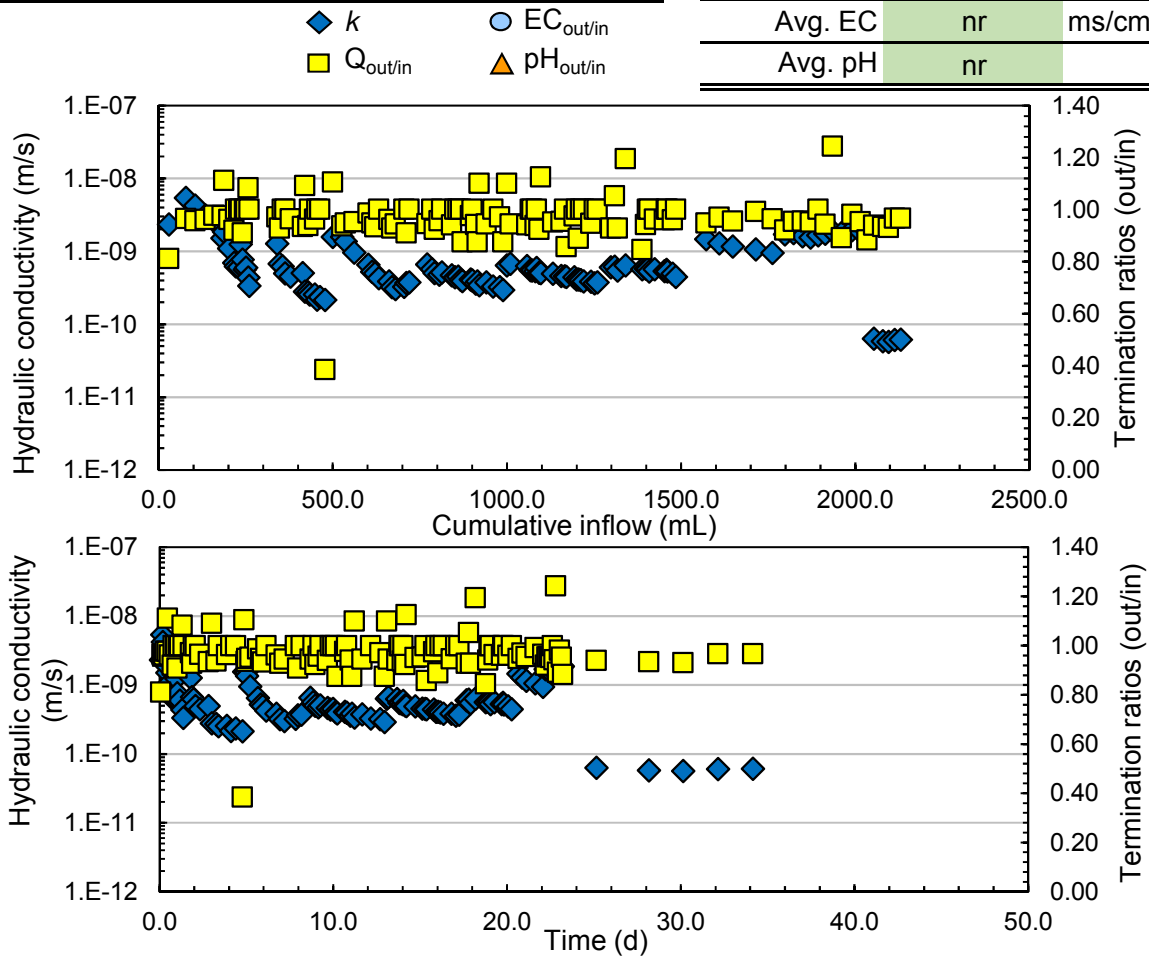


Hydraulic Conductivity—Standard Method

Test ID	13b	Test start date	2017/05/13
GCL type	DN9	Notes Modified, S-M7 	
Student	Conzelmann, Joel		
Permeant liquid	CW		
Prehydrated (Y/N)	N		
Specimen diameter	10.2 cm 4.0 in		
Avg. effective stress	26.4 kPa 3.8 psi		

Terminated test results

k [D5084]	tbd	m/s	k [D6766]	nr	m/s
PVF [D5084]	tbd		PVF [D6766]	nr	
time [D5084]	tbd	d	time [D6766]	nr	d
			Avg. EC	nr	ms/cm
			Avg. pH	nr	

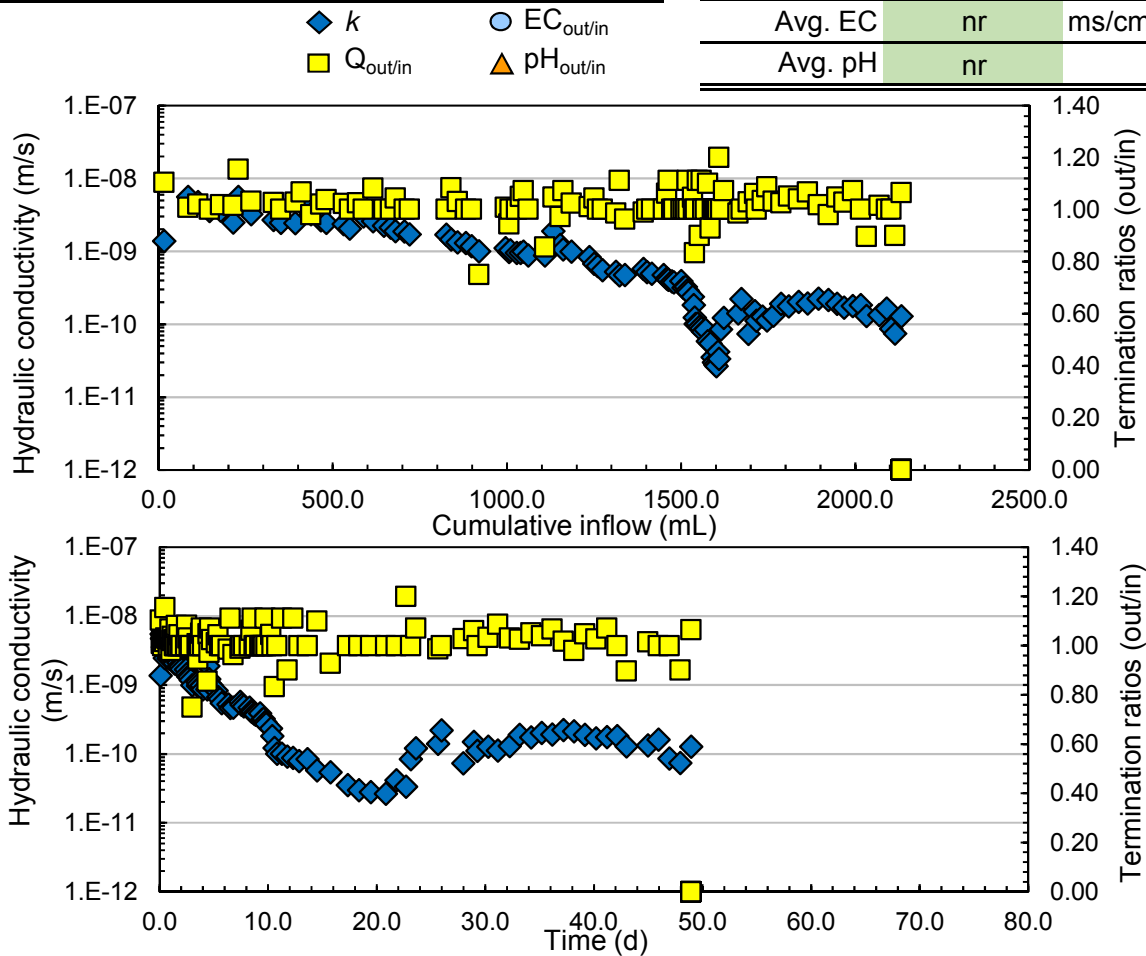


Hydraulic Conductivity—Standard Method

Test ID	13c	Test start date	2017/05/13
GCL type	DN9	Notes Modified, S-M7 	
Student	Conzelmann, Joel		
Permeant liquid	CW		
Prehydrated (Y/N)	N		
Specimen diameter	10.2 cm 4.0 in		
Avg. effective stress	26.4 kPa 3.8 psi		

Terminated test results

k [D5084]	tbd	m/s	k [D6766]	nr	m/s
PVF [D5084]	tbd		PVF [D6766]	nr	
time [D5084]	tbd	d	time [D6766]	nr	d
			Avg. EC	nr	ms/cm
			Avg. pH	nr	

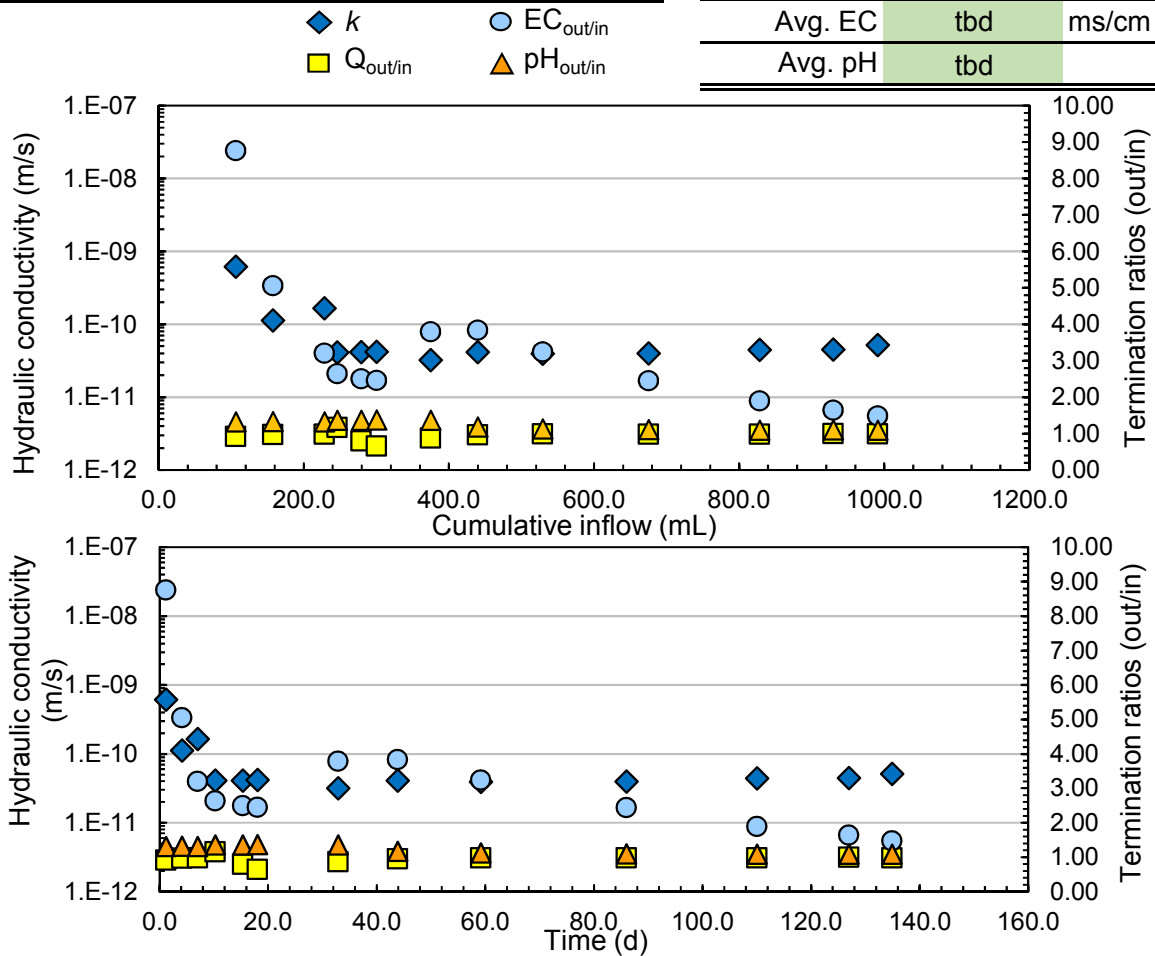


Hydraulic Conductivity—Standard Method

Test ID	14a	Test start date	2016/12/15	
GCL type	DN (15 ppi)	Notes DN (15 ppi) 		
Student	Conzelmann, Joel			
Permeant liquid	CW			
Prehydrated (Y/N)	N			
Specimen diameter	10.2			cm
	4.0			in
Avg. effective stress	26.4			kPa
	3.8			psi

Terminated test results

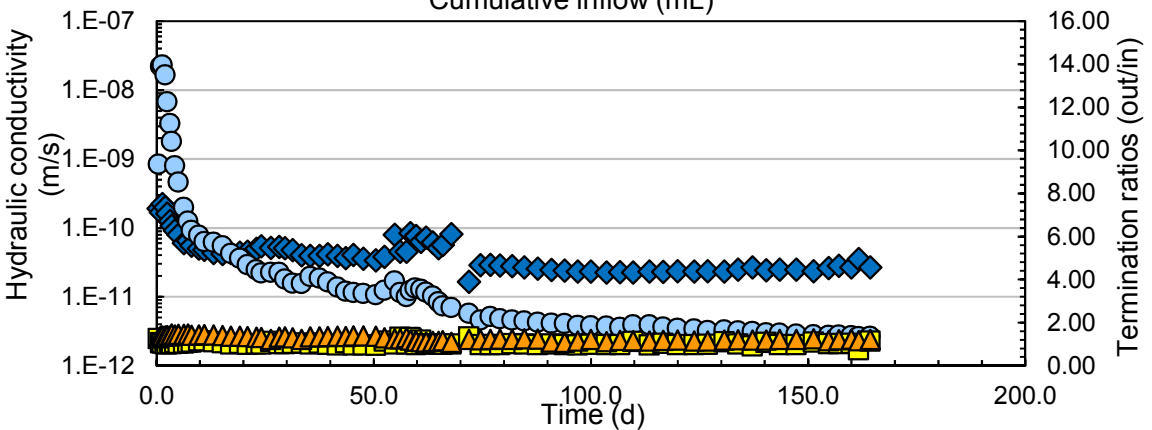
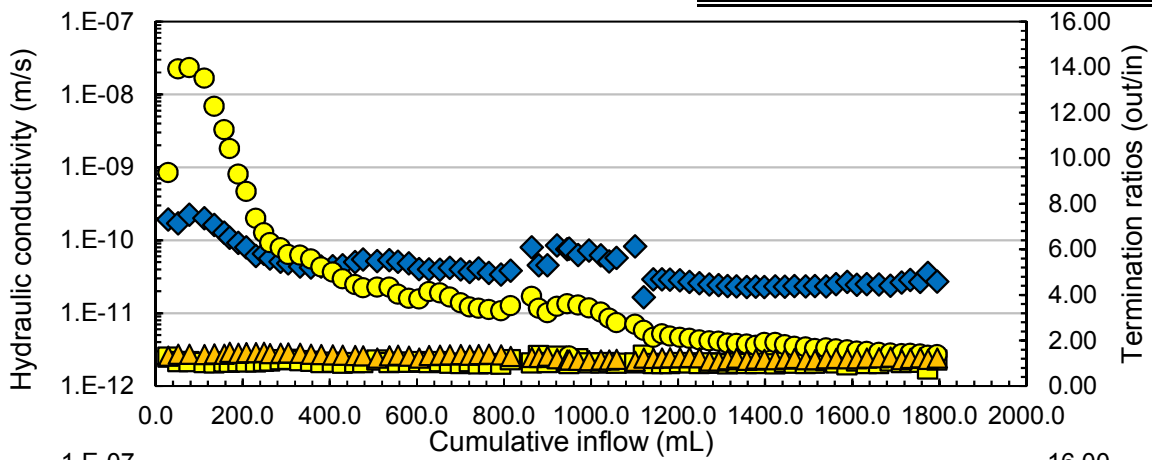
k [D5084]	4.00E-11	m/s	k [D6766]	tbd	m/s
PVF [D5084]	tbd		PVF [D6766]	tbd	
time [D5084]	85.98	d	time [D6766]	tbd	d
			Avg. EC	tbd	ms/cm
			Avg. pH	tbd	




Hydraulic Conductivity—Gravity Method

Test ID	15a	Test start date	2016/09/21
GCL type	DN (15 ppi)	Notes DN (15 ppi) 	
Student	Conzelmann, Joel		
Permeant liquid	CW		
Prehydrated (Y/N)	N		
Specimen diameter	15.1 cm		
	5.9 in		
Avg. effective stress	27.6 kPa		
	4.0 psi		

Terminated test results			
k [D5084]	4.37E-11	m/s	
PVF [D5084]	tbd		
time [D5084]	31.34	d	
◆ k ● EC _{out/in} ■ Q _{out/in} ▲ pH _{out/in}			
k [D6766]	tbd	m/s	
PVF [D6766]	tbd		
time [D6766]	tbd	d	
Avg. EC	tbd	ms/cm	
Avg. pH	tbd		

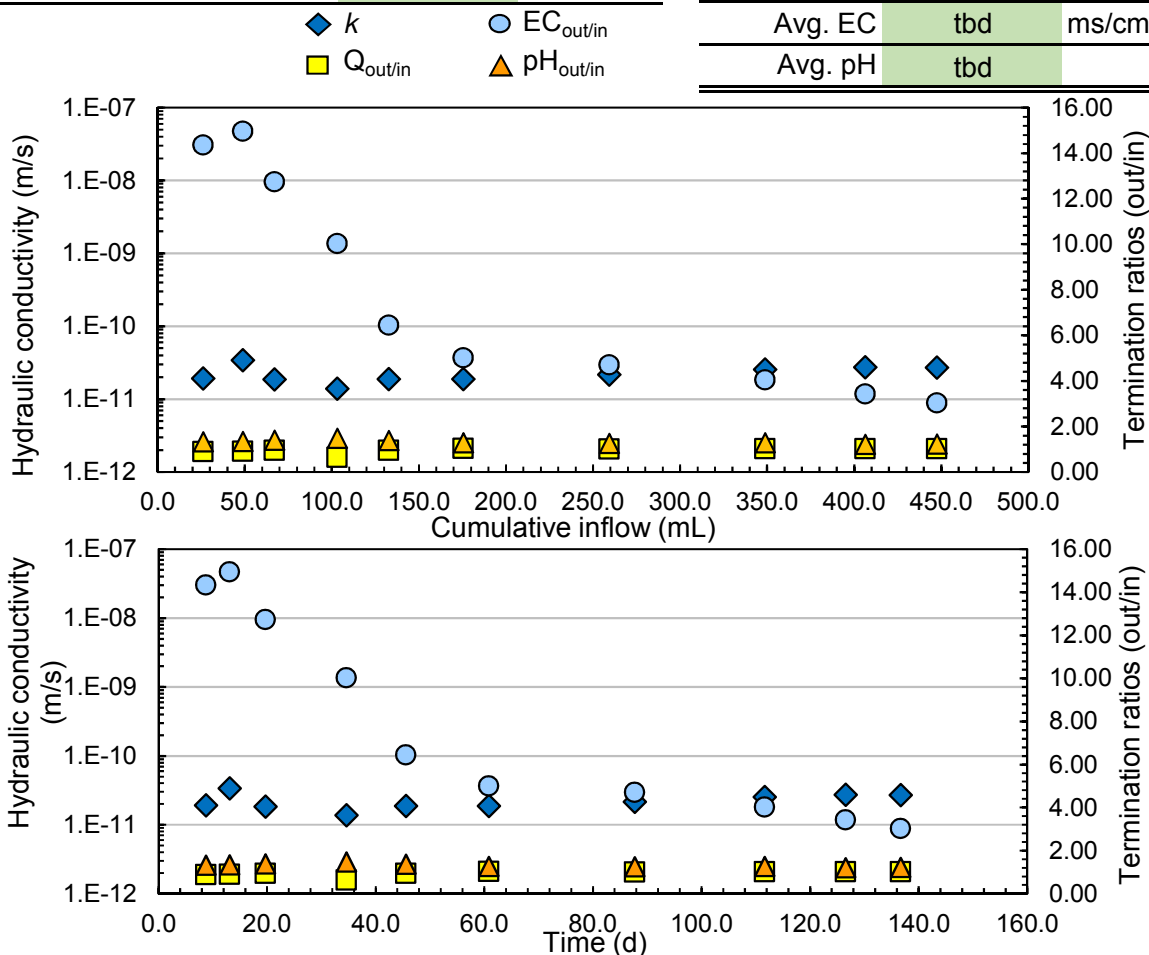


Hydraulic Conductivity—Standard Method


Test ID	16a	Test start date	2016/12/15	
GCL type	200R	Notes 		
Student	Conzelmann, Joel			
Permeant liquid	CW			
Prehydrated (Y/N)	N			
Specimen diameter	10.2			cm
	4.0			in
Avg. effective stress	26.4			kPa
	3.8			psi

Terminated test results

<i>k</i> [D5084]	1.98E-11	m/s	<i>k</i> [D6766]	tbd	m/s
PVF [D5084]	tbd		PVF [D6766]	tbd	
time [D5084]	87.7	d	time [D6766]	tbd	d
			Avg. EC	tbd	ms/cm
			Avg. pH	tbd	

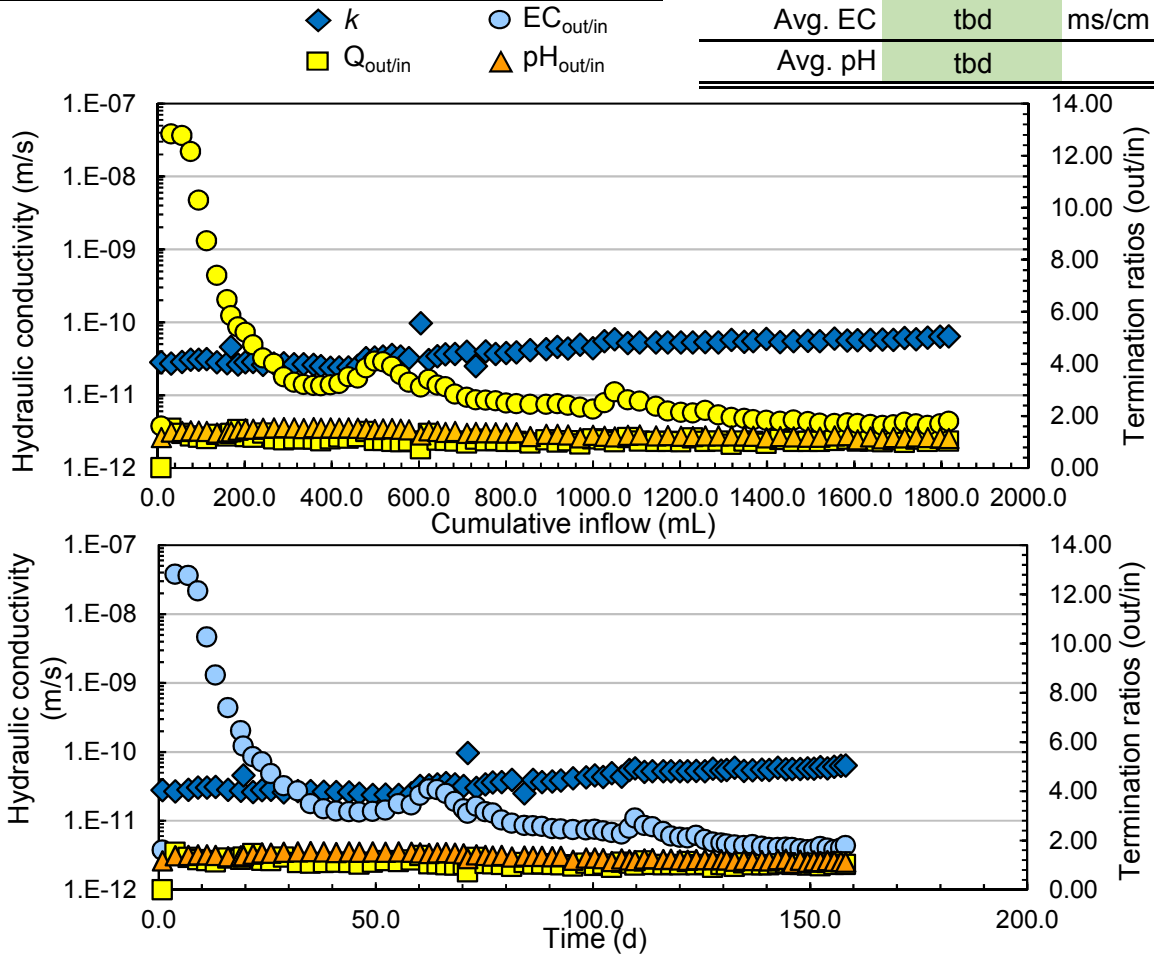


Hydraulic Conductivity—Gravity Method

Test ID	17a	Test start date	2016/10/18	
GCL type	200R	Notes 		
Student	Conzelmann, Joel			
Permeant liquid	CW			
Prehydrated (Y/N)	N			
Specimen diameter	15.1			cm
	5.9			in
Avg. effective stress	27.6			kPa
	4.0			psi

Terminated test results

<i>k</i> [D5084]	2.33E-11	m/s	<i>k</i> [D6766]	tbd	m/s
PVF [D5084]	tbd		PVF [D6766]	tbd	
time [D5084]	38.02	d	time [D6766]	tbd	d
			Avg. EC	tbd	ms/cm
			Avg. pH	tbd	

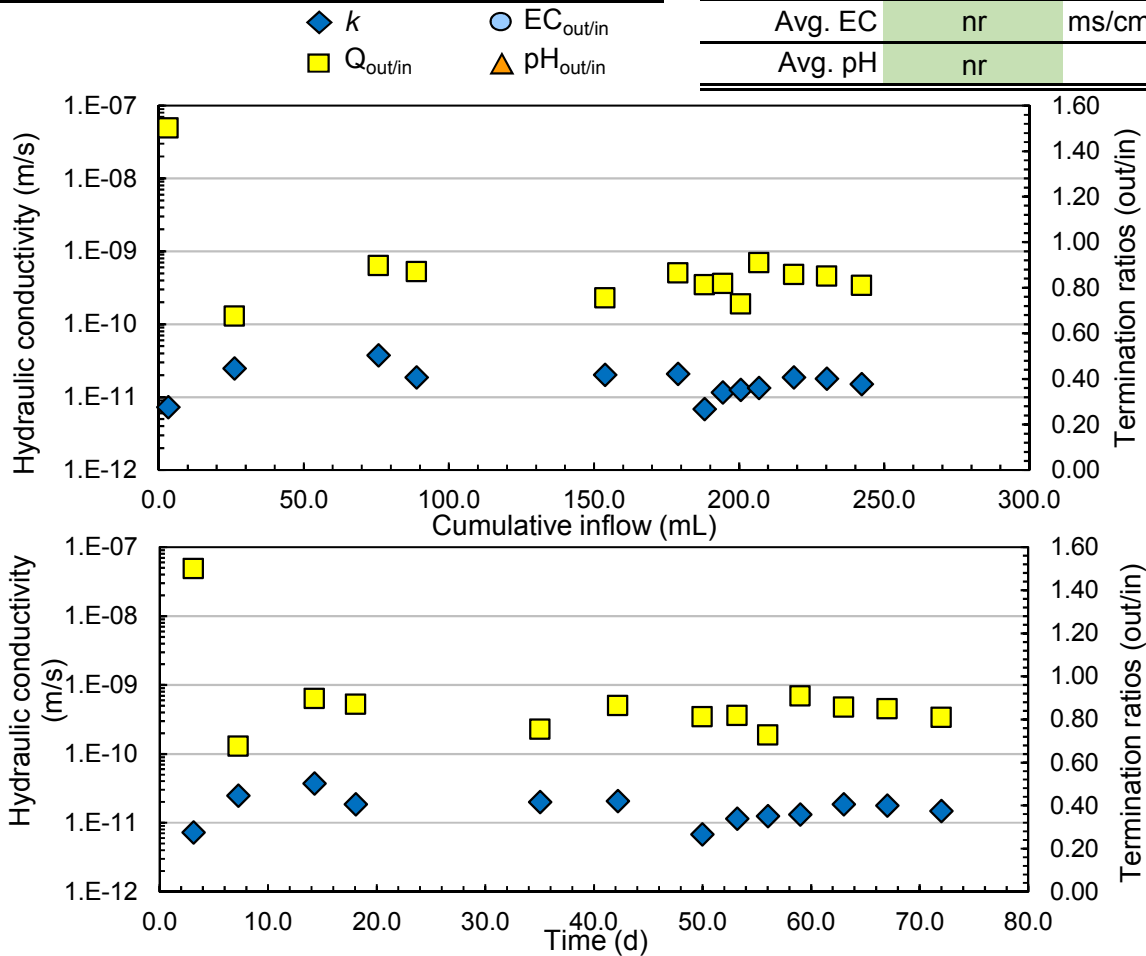


Hydraulic Conductivity—Standard Method

Test ID	18a	Test start date	2016/07/15	
GCL type	GB	<div style="text-align: left; padding-bottom: 10px;">Notes</div>		
Student	Conzelmann, Joel			
Permeant liquid	CW			
Prehydrated (Y/N)	N			
Specimen diameter	10.2			cm
	4.0			in
Avg. effective stress	26.4			kPa
	3.8			psi

Terminated test results

k [D5084]	1.71E-11	m/s	k [D6766]	nr	m/s
PVF [D5084]	6.7		PVF [D6766]	nr	
time [D5084]	71.99	d	time [D6766]	nr	d
			Avg. EC	nr	ms/cm
			Avg. pH	nr	

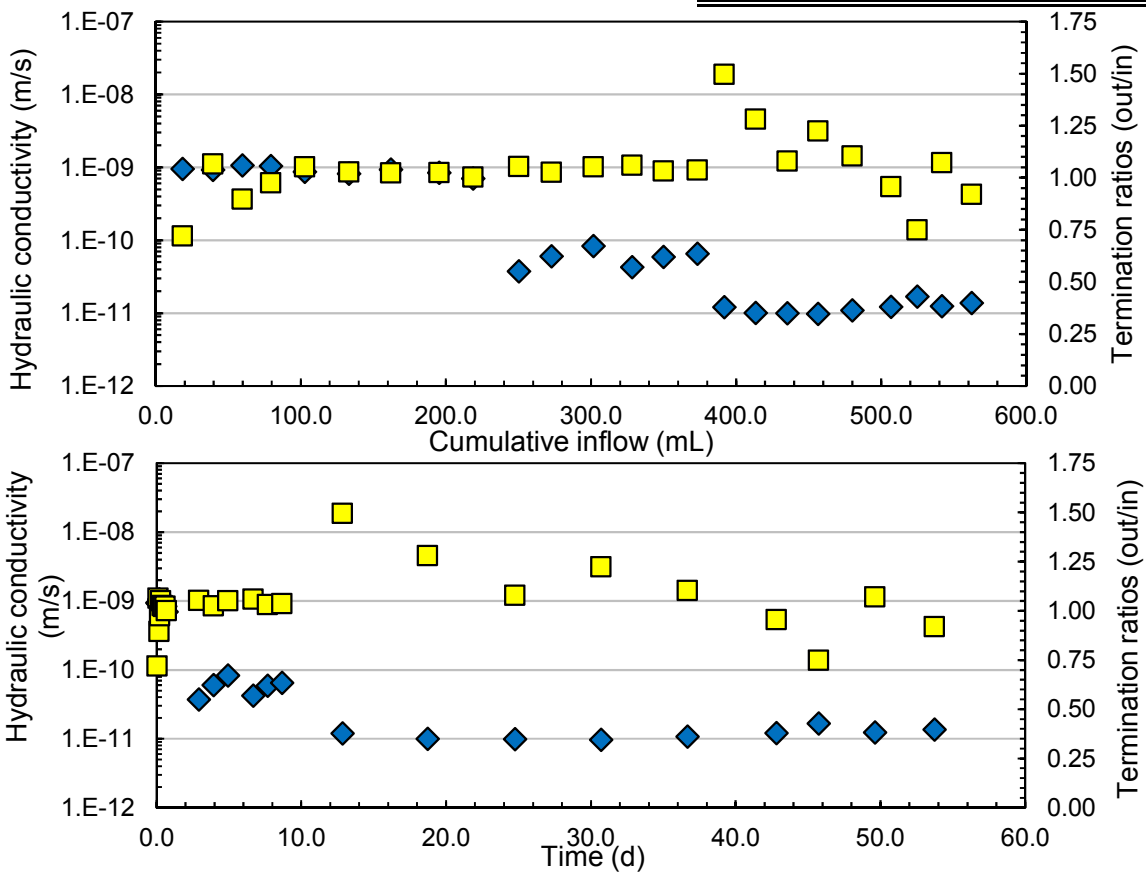


Hydraulic Conductivity—Gravity Method

Test ID	19a	Test start date	2016/05/25	
GCL type	GB	<div style="display: flex; align-items: center; justify-content: center;"> <div style="margin-right: 20px;">Notes</div> </div>		
Student	Conzelmann, Joel			
Permeant liquid	CW			
Prehydrated (Y/N)	N			
Specimen diameter	15.1			cm
	5.9			in
Avg. effective stress	27.6			kPa
	4.0			psi

Terminated test results

k [D5084]	1.43E-11	m/s	k [D6766]	nr	m/s
PVF [D5084]	7.1		PVF [D6766]	nr	
time [D5084]	53.73	d	time [D6766]	nr	d
			Avg. EC	nr	ms/cm
			Avg. pH	nr	

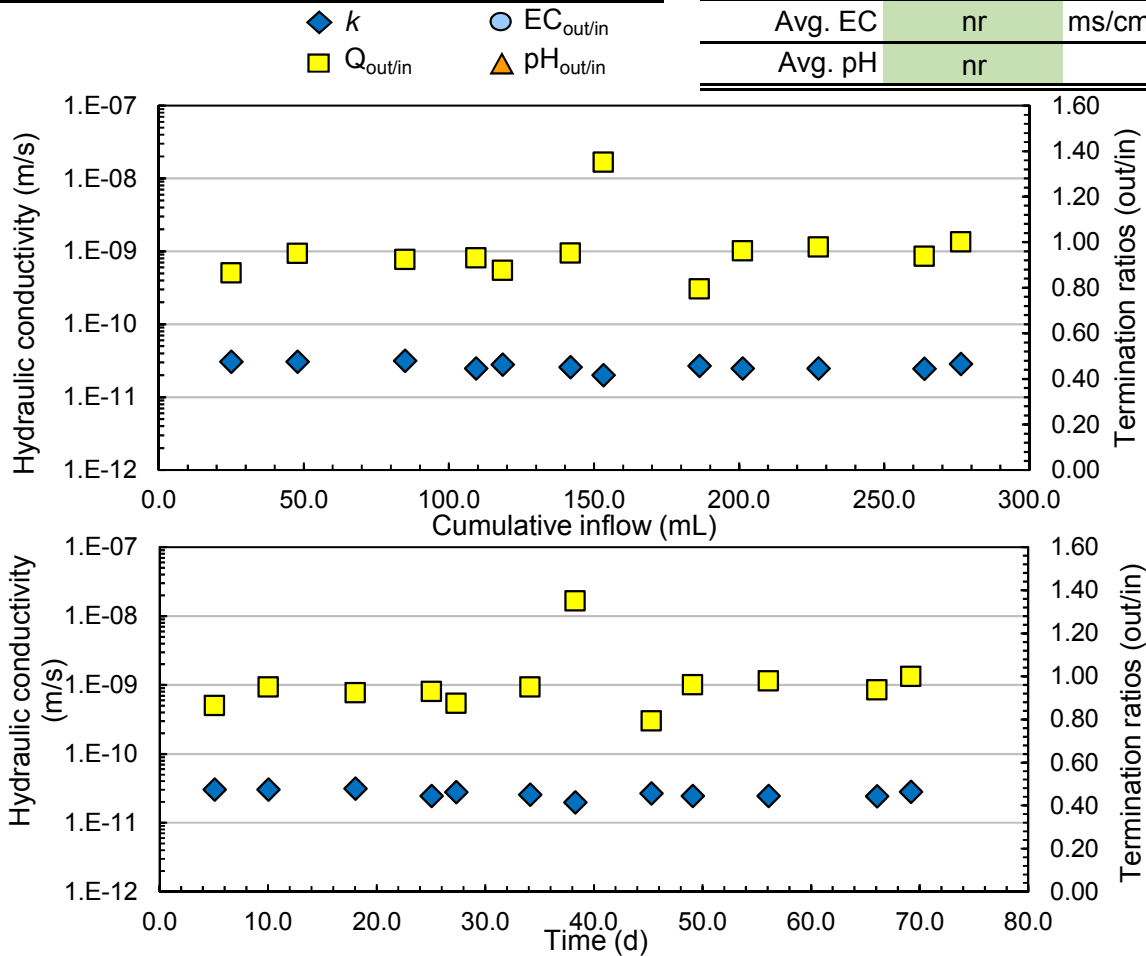


Hydraulic Conductivity—Standard Method

Test ID	20a	Test start date	2016/06/14	
GCL type	DN (12 ppi)	<div style="display: flex; align-items: center; justify-content: center;"> <div style="margin-right: 20px;">Notes</div> </div>		
Student	Conzelmann, Joel			
Permeant liquid	DW			
Prehydrated (Y/N)	N			
Specimen diameter	10.2			cm
	4.0			in
Avg. effective stress	26.4			kPa
	3.8			psi

Terminated test results

k [D5084]	2.58E-11	m/s	k [D6766]	nr	m/s
PVF [D5084]	6.4		PVF [D6766]	nr	
time [D5084]	69.19	d	time [D6766]	nr	d
			Avg. EC	nr	ms/cm
			Avg. pH	nr	

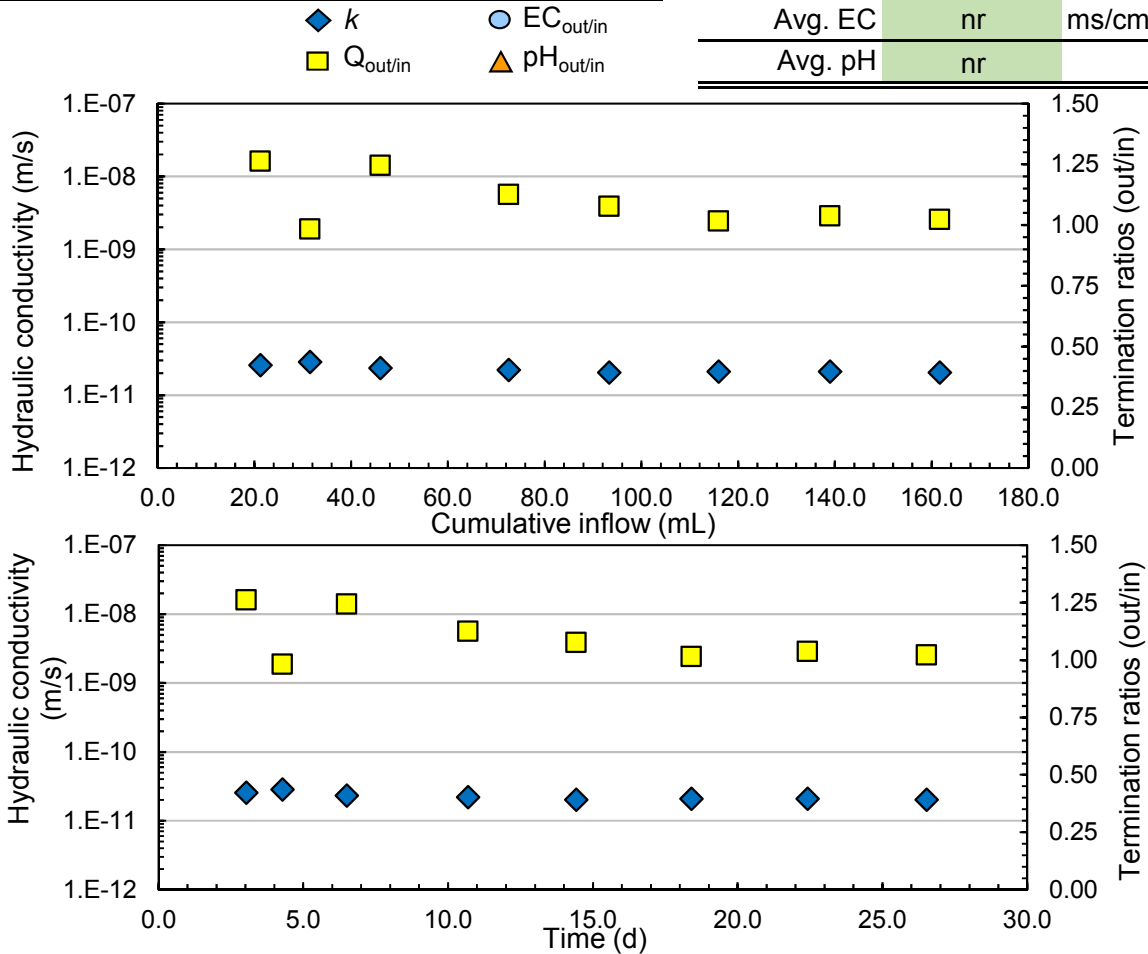


Hydraulic Conductivity—Gravity Method

Test ID	21a	Test start date	2016/05/23	
GCL type	DN (12 ppi)	<div style="text-align: left; margin-bottom: 10px;">Notes</div>		
Student	Conzelmann, Joel			
Permeant liquid	DW			
Prehydrated (Y/N)	N			
Specimen diameter	15.1			cm
	5.9			in
Avg. effective stress	27.5			kPa
	4.0			psi

Terminated test results

k [D5084]	2.07E-11	m/s	k [D6766]	nr	m/s
PVF [D5084]	1.5		PVF [D6766]	nr	
time [D5084]	26.52	d	time [D6766]	nr	d
			Avg. EC	nr	ms/cm
			Avg. pH	nr	

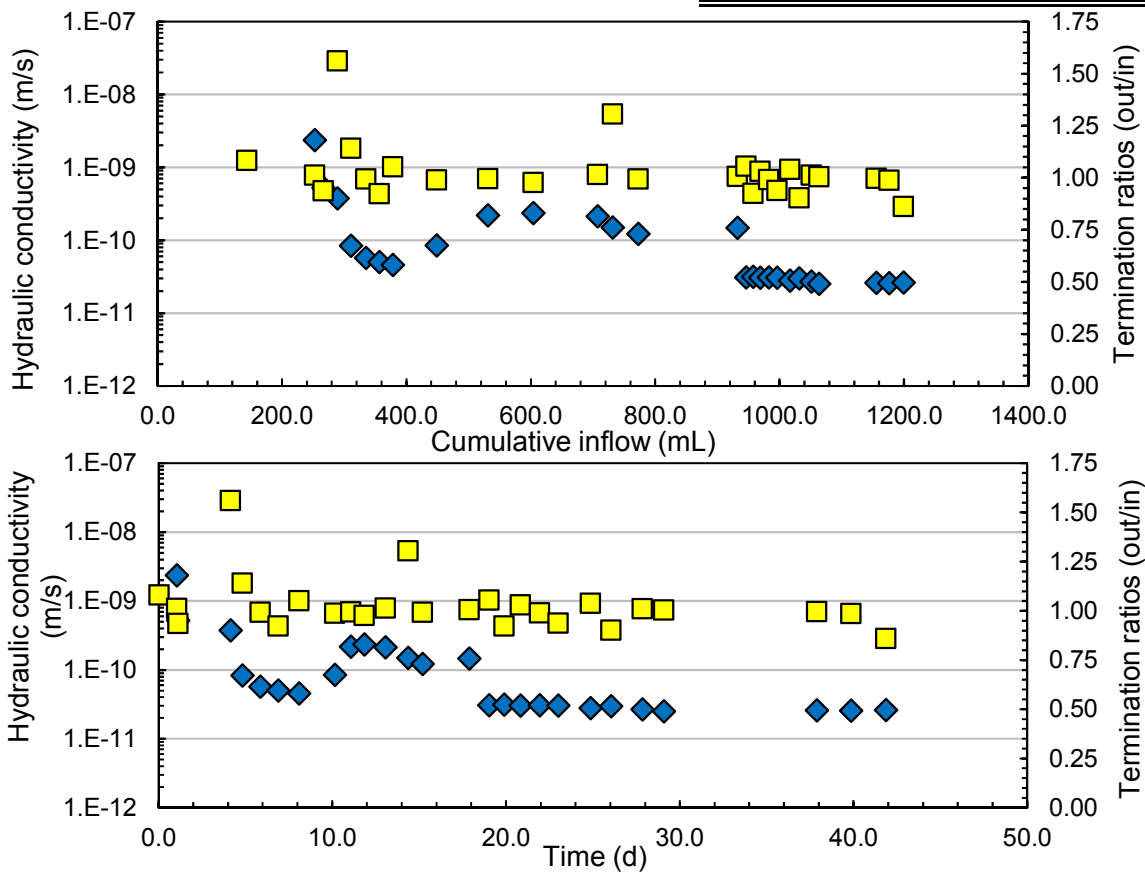


Hydraulic Conductivity—Gravity Method


Test ID	22a	Test start date	2016/01/14	
GCL type	DN (12 ppi)	<div style="display: flex; align-items: center; justify-content: center;"> <div style="margin-right: 20px;">Notes</div> </div>		
Student	Conzelmann, Joel			
Permeant liquid	TW			
Prehydrated (Y/N)	N			
Specimen diameter	15.1			cm
	5.9			in
Avg. effective stress	26.1			kPa
	3.8			psi

Terminated test results

k [D5084]	2.59E-11	m/s
PVF [D5084]	8.3	
time [D5084]	41.86	d
<div style="display: flex; justify-content: space-around; font-size: small;"> ◆ k ● EC_{out/in} </div> <div style="display: flex; justify-content: space-around; font-size: small;"> ■ Q_{out/in} ▲ pH_{out/in} </div>		
k [D6766]	nr	m/s
PVF [D6766]	nr	
time [D6766]	nr	d
Avg. EC	nr	ms/cm
Avg. pH	nr	

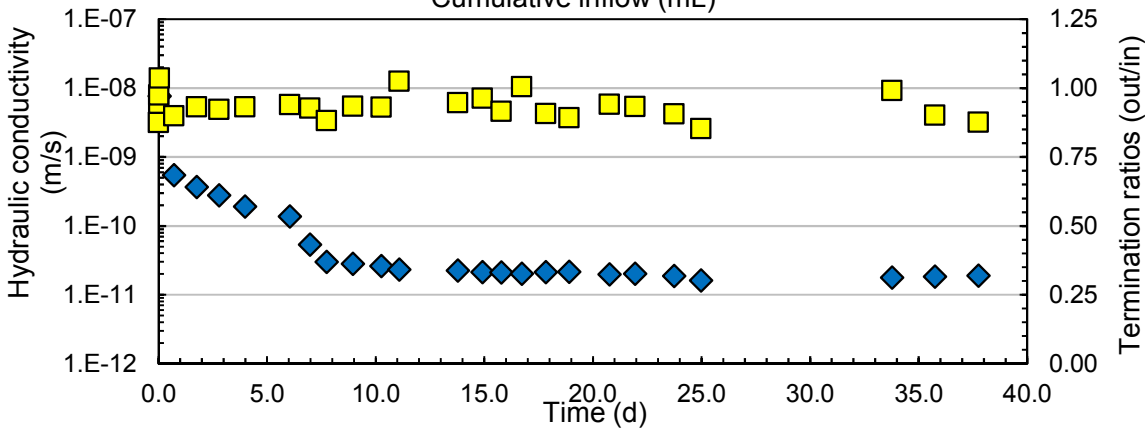
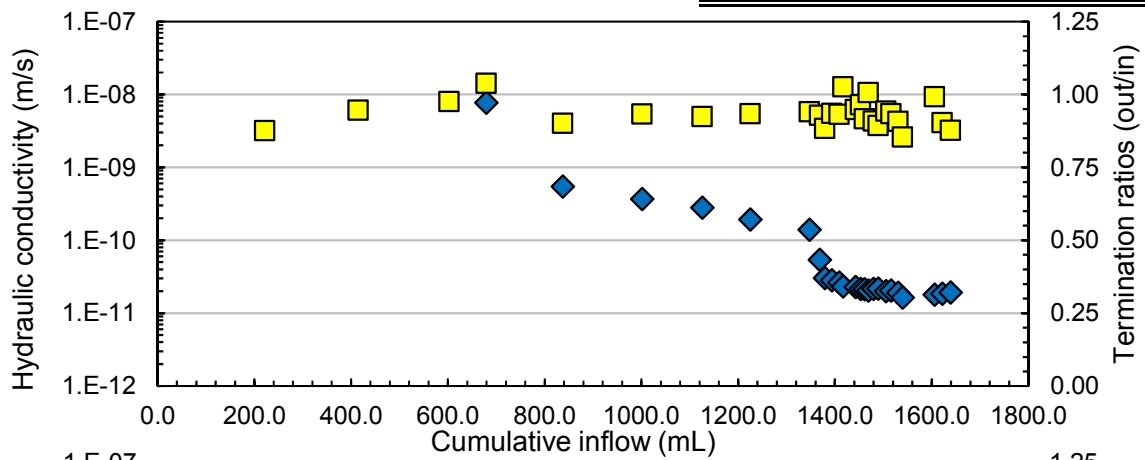
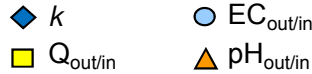


Hydraulic Conductivity—Gravity Method

Test ID	22b	Test start date	2016/01/18	
GCL type	DN (12 ppi)	Notes 		
Student	Conzelmann, Joel			
Permeant liquid	TW			
Prehydrated (Y/N)	N			
Specimen diameter	15.1			cm
	5.9			in
Avg. effective stress	26.1			kPa
	3.8			psi

Terminated test results

k [D5084]	1.85E-11	m/s	k [D6766]	nr	m/s
PVF [D5084]	12.7		PVF [D6766]	nr	
time [D5084]	37.75	d	time [D6766]	nr	d
			Avg. EC	nr	ms/cm
			Avg. pH	nr	

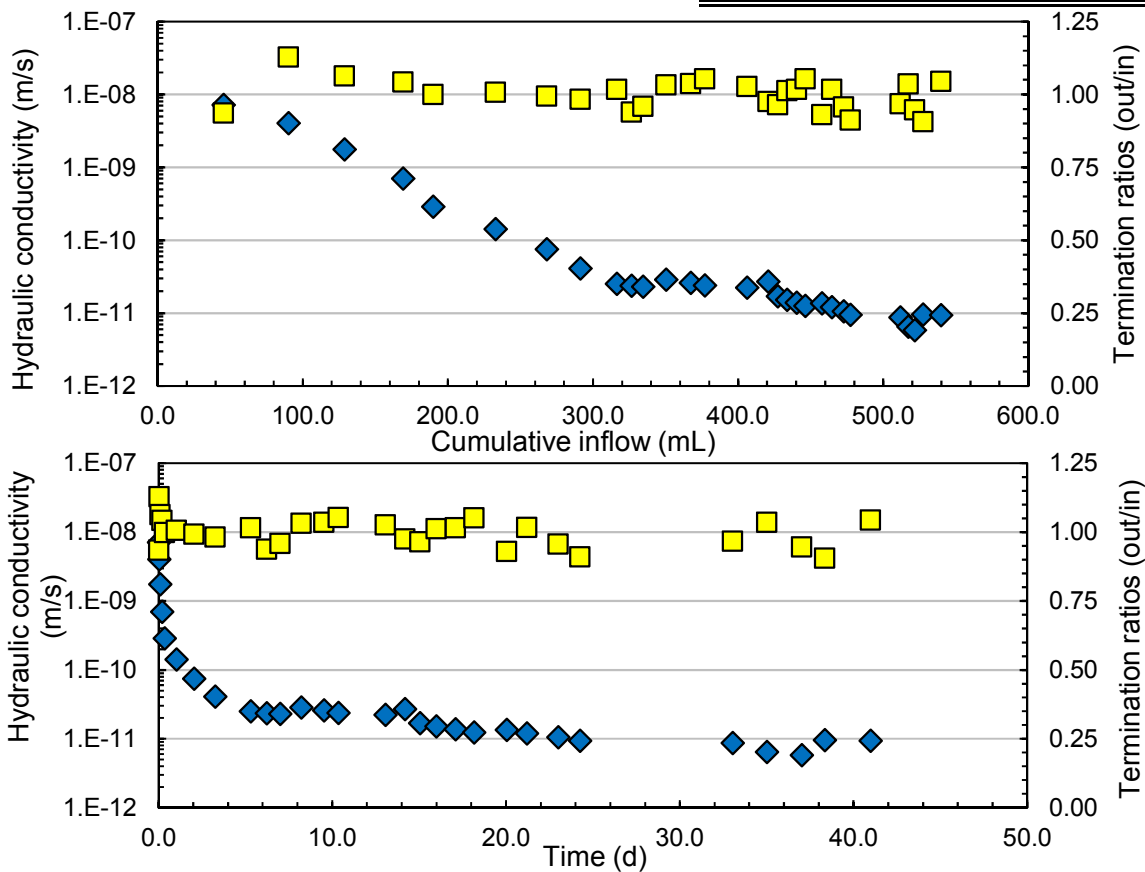


Hydraulic Conductivity—Gravity Method


Test ID	22c	Test start date	2016/01/19	
GCL type	DN (12 ppi)	<div style="text-align: left; margin-bottom: 10px;">Notes</div>		
Student	Conzelmann, Joel			
Permeant liquid	TW			
Prehydrated (Y/N)	N			
Specimen diameter	15.1			cm
	5.9			in
Avg. effective stress	26.1			kPa
	3.8			psi

Terminated test results

k [D5084]	8.26E-12	m/s	k [D6766]	nr	m/s
PVF [D5084]	4.9		PVF [D6766]	nr	
time [D5084]	40.97	d	time [D6766]	nr	d
			Avg. EC	nr	ms/cm
			Avg. pH	nr	

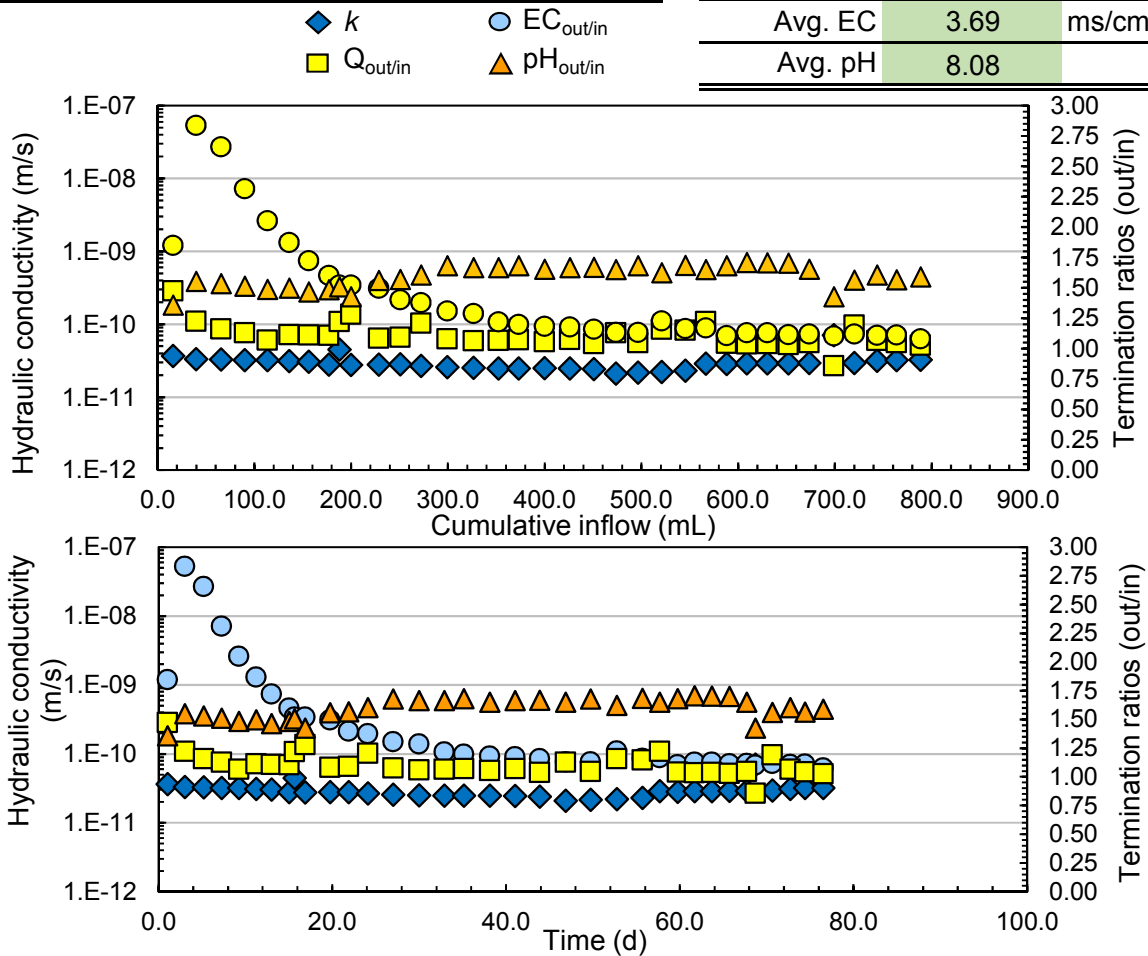


Hydraulic Conductivity—Gravity Method

Test ID	23a	Test start date	2016/10/21	
GCL type	200R	<div style="text-align: left;">Notes</div> 		
Student	Conzelmann, Joel			
Permeant liquid	Au-PLS			
Prehydrated (Y/N)	N			
Specimen diameter	15.1			cm
	5.9			in
Avg. effective stress	27.6			kPa
	4.0			psi

Terminated test results

k [D5084]	2.48E-11	m/s	k [D6766]	3.19E-11	m/s
PVF [D5084]	5.3		PVF [D6766]	9.9	
time [D5084]	41.04	d	time [D6766]	76.50	d
			Avg. EC	3.69	ms/cm
			Avg. pH	8.08	

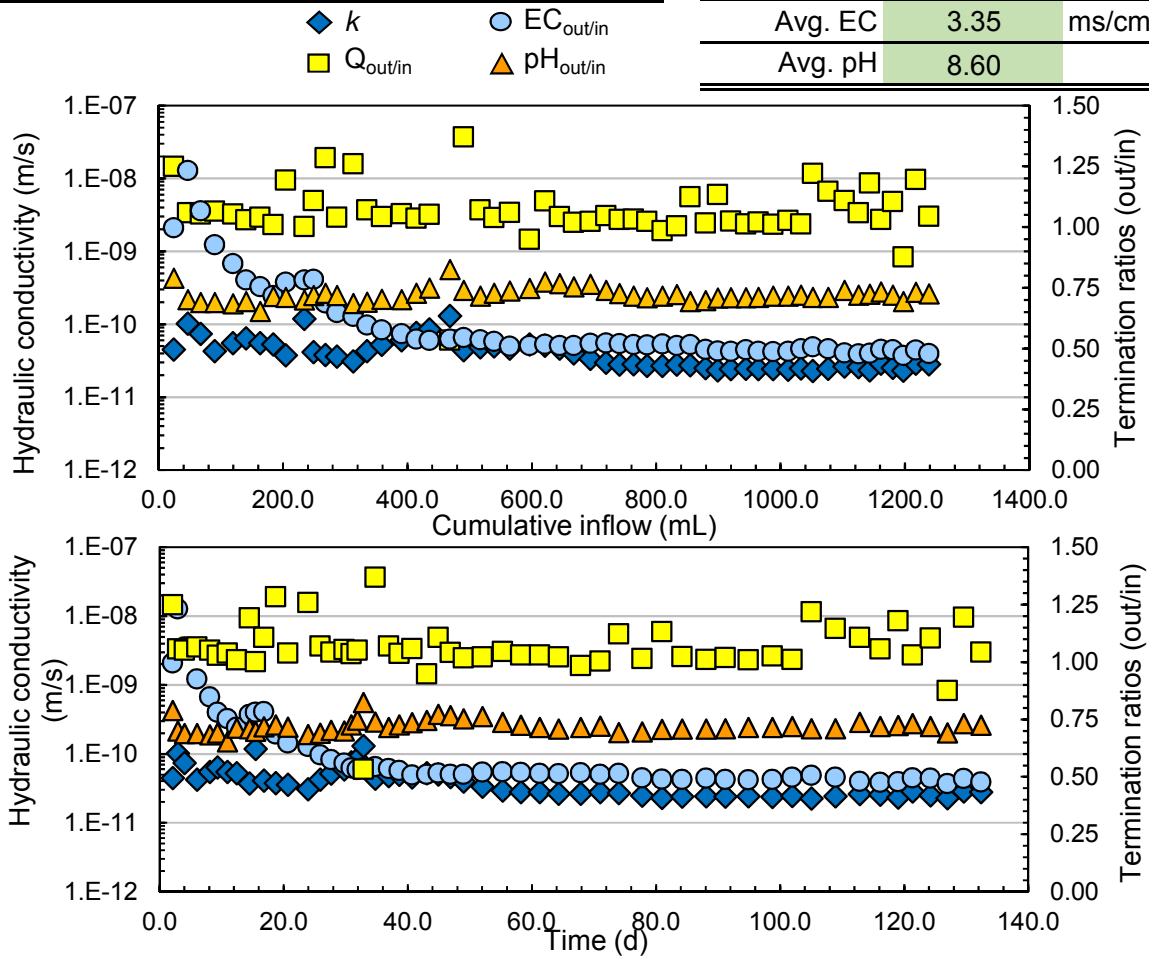


Hydraulic Conductivity—Gravity Method


Test ID	24a	Test start date	2016/12/02	
GCL type	200R	<div style="display: flex; align-items: center; justify-content: center;"> <div style="margin-right: 20px;">Notes</div> </div>		
Student	Conzelmann, Joel			
Permeant liquid	BX-PS			
Prehydrated (Y/N)	N			
Specimen diameter	15.1			cm
	5.9			in
Avg. effective stress	27.5			kPa
	4.0			psi

Terminated test results

k [D5084]	4.97E-11	m/s	k [D6766]	2.65E-11	m/s
PVF [D5084]	5.3		PVF [D6766]	10.7	
time [D5084]	44.90	d	time [D6766]	132.36	d
			Avg. EC	3.35	ms/cm
			Avg. pH	8.60	

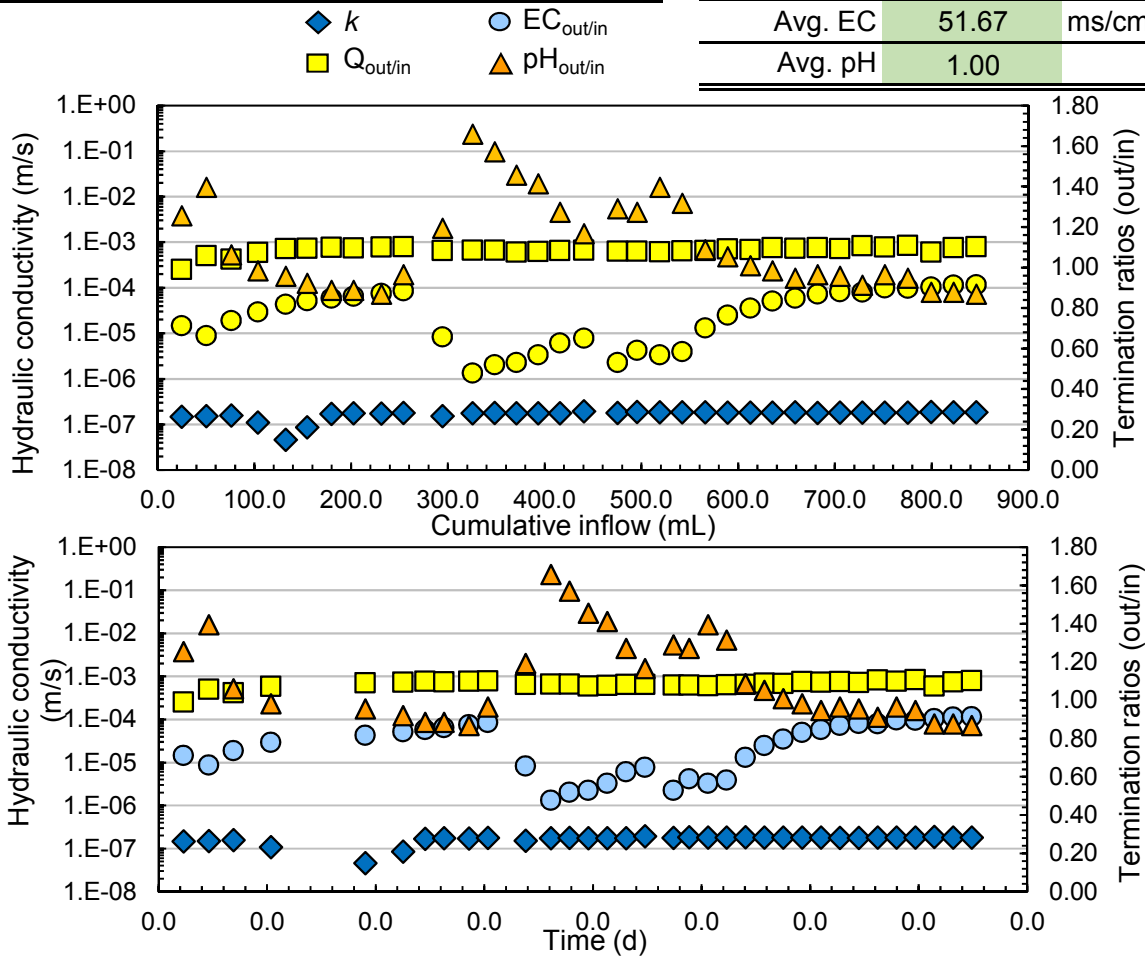


Hydraulic Conductivity—Gravity Method

Test ID	25a	Test start date	2017/03/07	
GCL type	200R	Notes		
Student	Conzelmann, Joel			
Permeant liquid	Cu-PS			
Prehydrated (Y/N)	N			
Specimen diameter	15.1			cm
	5.9			in
Avg. effective stress	27.6			kPa
	4.0			psi

Terminated test results

k [D5084]	1.76E-07	m/s	k [D6766]	1.85E-07	m/s
PVF [D5084]	3.4		PVF [D6766]	11.2	
time [D5084]	0.01	d	time [D6766]	0.01	d
			Avg. EC	51.67	ms/cm
			Avg. pH	1.00	

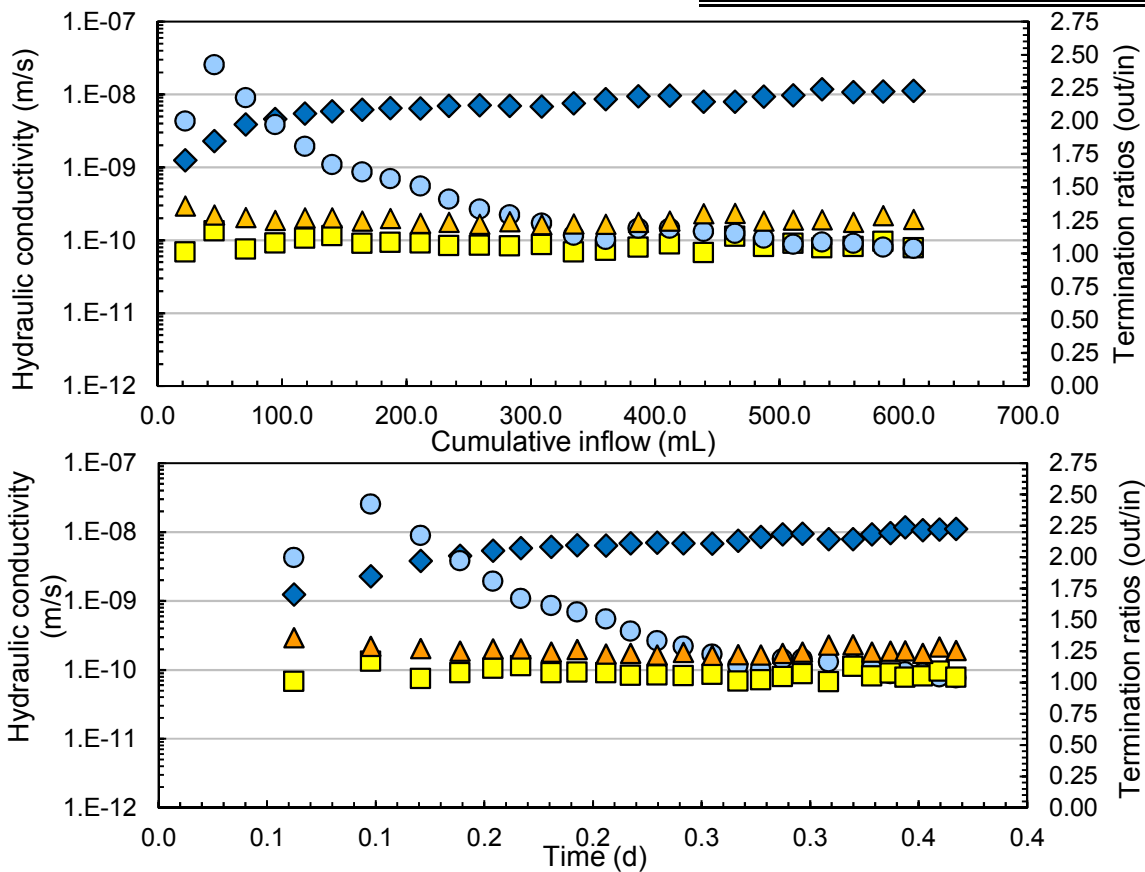


Hydraulic Conductivity—Gravity Method


Test ID	26a	Test start date	2017/02/17	
GCL type	DN9	<div style="display: flex; align-items: center; justify-content: center;"> <div style="margin-right: 20px;">Notes</div> </div>		
Student	Conzelmann, Joel			
Permeant liquid	Au-PLS			
Prehydrated (Y/N)	N			
Specimen diameter	15.1			cm
	5.9			in
Avg. effective stress	27.6			kPa
	4.0			psi

Terminated test results

k [D5084]	6.93E-09	m/s	k [D6766]	1.10E-08	m/s
PVF [D5084]	3.1		PVF [D6766]	6.1	
time [D5084]	0.25	d	time [D6766]	0.37	d
			Avg. EC	3.53	ms/cm
			Avg. pH	6.40	

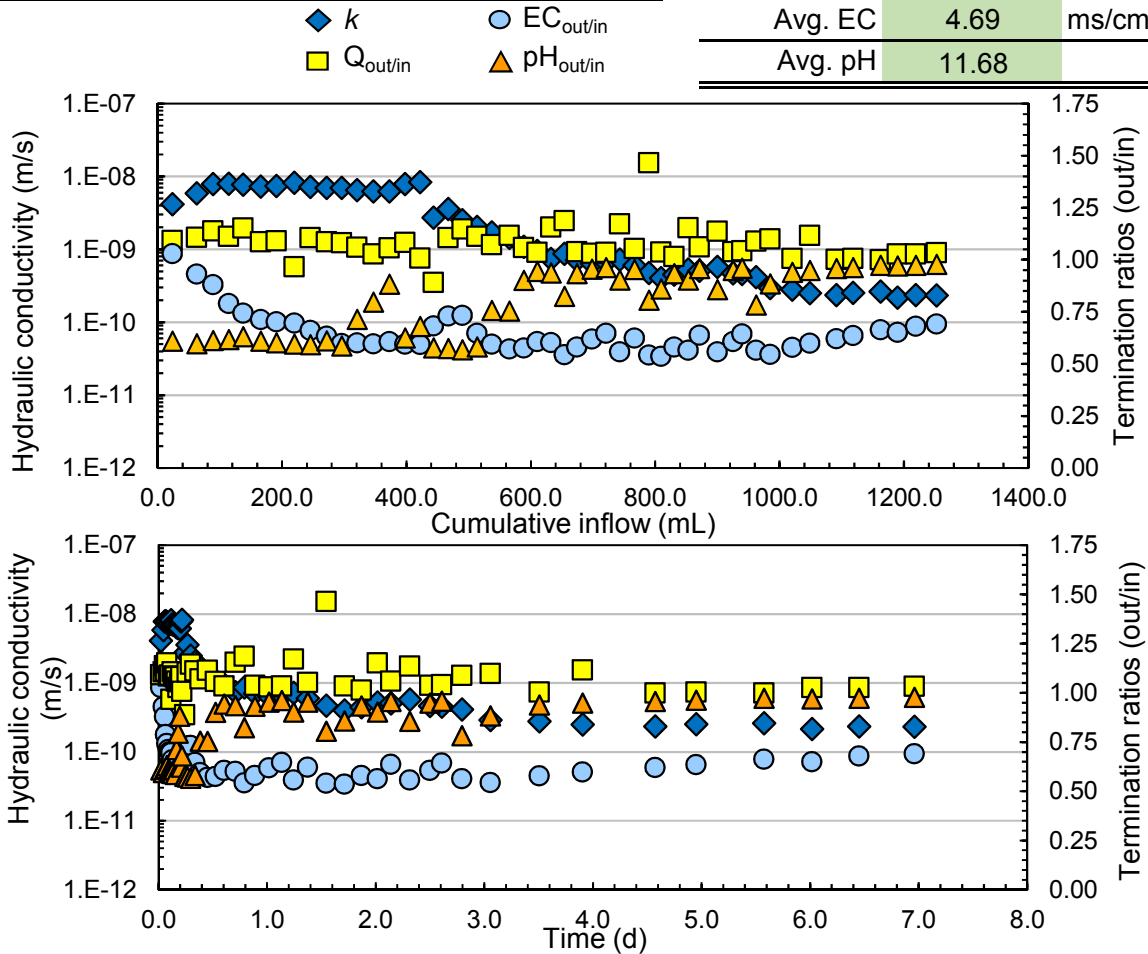


Hydraulic Conductivity—Gravity Method


Test ID	27a	Test start date	2017/02/16	
GCL type	DN9	Notes		
Student	Conzelmann, Joel			
Permeant liquid	BX-PS			
Prehydrated (Y/N)	N			
Specimen diameter	15.1			cm
	5.9			in
Avg. effective stress	27.6			kPa
	4.0			psi

Terminated test results

k [D5084]	7.57E-09	m/s	k [D6766]	2.28E-10	m/s
PVF [D5084]	2.5		PVF [D6766]	12.5	
time [D5084]	0.13	d	time [D6766]	6.96	d
			Avg. EC	4.69	ms/cm
			Avg. pH	11.68	

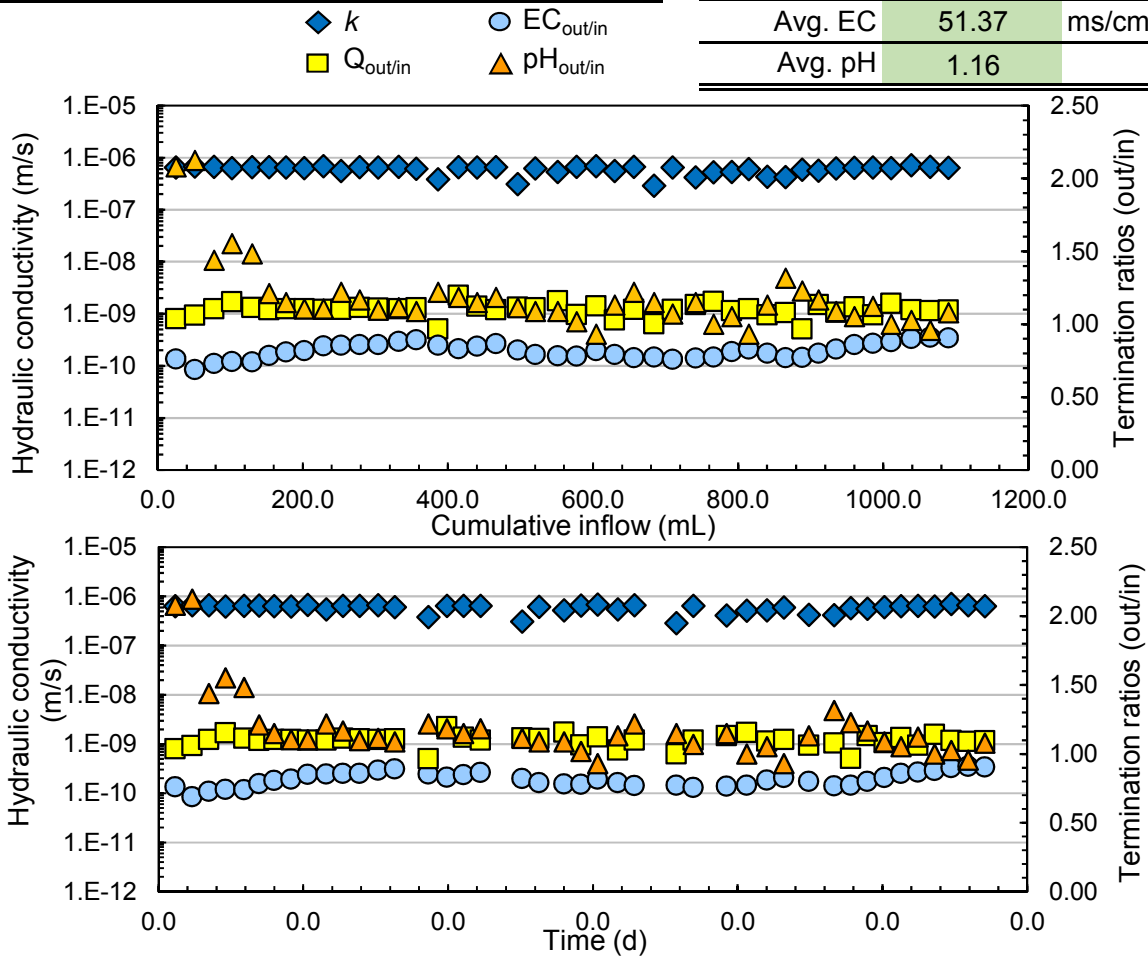


Hydraulic Conductivity—Gravity Method


Test ID	28a	Test start date	2017/02/16	
GCL type	DN9			
Student	Conzelmann, Joel			
Permeant liquid	Cu-PS			
Prehydrated (Y/N)	N			
Specimen diameter	15.1			cm
	5.9			in
Avg. effective stress	27.7			kPa
	4.0			psi

Terminated test results

<i>k</i> [D5084]	6.43E-07	m/s	<i>k</i> [D6766]	6.69E-07	m/s
PVF [D5084]	2.1		PVF [D6766]	0.0	
time [D5084]	0.001	d	time [D6766]	0.01	d
			Avg. EC	51.37	ms/cm
			Avg. pH	1.16	

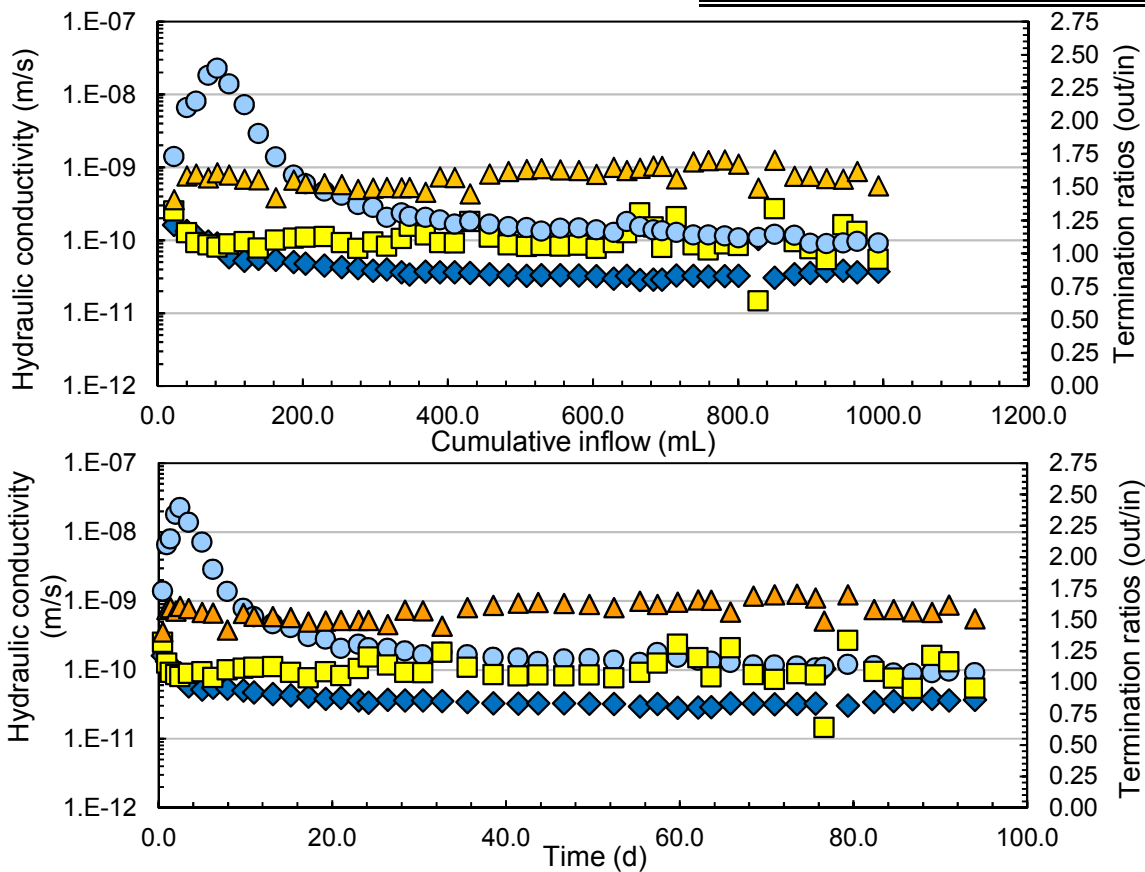


Hydraulic Conductivity—Gravity Method

Test ID	29a	Test start date	2016/09/22	
GCL type	DN (15 ppi)	Notes 		
Student	Conzelmann, Joel			
Permeant liquid	Au-PLS			
Prehydrated (Y/N)	N			
Specimen diameter	15.1			cm
	5.9			in
Avg. effective stress	27.5			kPa
	4.0			psi

Terminated test results

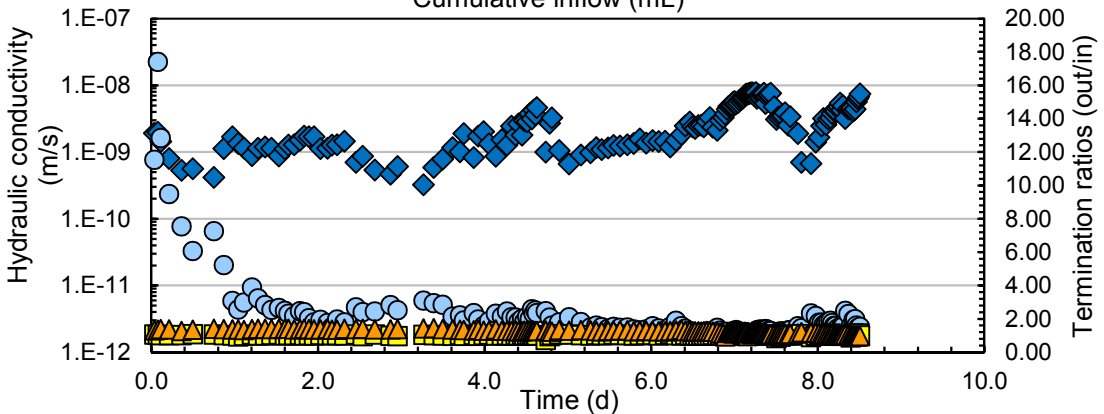
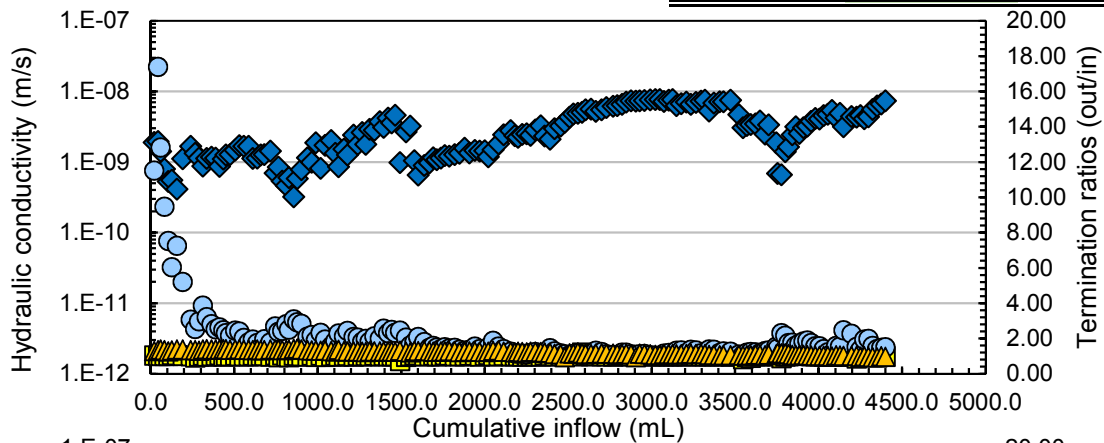
k [D5084]	3.60E-11	m/s	k [D6766]	3.70E-11	m/s
PVF [D5084]	3.8		PVF [D6766]	8.8	
time [D5084]	32.62	d	time [D6766]	93.95	d
			Avg. EC	3.63	ms/cm
			Avg. pH	7.95	



Hydraulic Conductivity—Gravity Method

Test ID	30a	Test start date	2016/11/08
GCL type	DN (12 ppi)	Notes Higher effective stress 	
Student	Conzelmann, Joel		
Permeant liquid	CW		
Prehydrated (Y/N)	N		
Specimen diameter	15.1	cm	
	5.9	in	
Avg. effective stress	93.2	kPa	
	13.5	psi	

Terminated test results			
k [D5084]	1.06E-09	m/s	
PVF [D5084]	tbd		
time [D5084]	1.53	d	
<div style="display: flex; justify-content: space-around; font-size: small;"> ◆ k ○ EC_{out/in} </div> <div style="display: flex; justify-content: space-around; font-size: small;"> ■ Q_{out/in} ▲ pH_{out/in} </div>			
k [D6766]	tbd	m/s	
PVF [D6766]	tbd		
time [D6766]	tbd	d	
Avg. EC	tbd	ms/cm	
Avg. pH	tbd		



APPENDIX H

Procedural Analysis Between the Standard Method and Gravity Method

Table H.1 Standard Method

Event	Time of event	Cell Pressure_Panel (psi)	Cell Pressure_Specimen (psi)	Inflow Pressure_Panel (psi)	Outflow Pressure_Panel (psi)	Inflow Pressure_Specimen (psi)	Outflow Pressure_specimen (psi)	Inflow effective stress (psi)	Outflow effective Stress (psi)	Average Effective Stress (psi)	Hydration State	Comments	
Fill cell w/ water	?			n/a	n/a	0	0	?	?	?	Dry Granules (exterior hydrated)	Inflow and outflow valves closed	
Flushing Lines													
Connect cell to panel		15	15	10	0	0	0	15	15	15	Dry Granules (exterior hydrated)	Inflow and outflow valves closed	
Open 1st inflow valve to panel	-5 seconds	15	15	10	0	10	10	5	5	5	Granules begin hydrating	1 inflow valve closed, outflow valves closed	
Open 2nd inflow valve to atm	-30 seconds - 1 min	15	15	10	0	10	10	5	5	5	Granules begin hydrating	flushing inflow lines	
Close 2nd inflow valve		15	15	10	0	10	10	5	5	5	Granules begin hydrating	finish flushing inflow lines	
Open 1st outflow valve to atm	30 second - 1 min	15	15	10	0	10	0	5	15	10	Granules hydrating	flushing outflow lines	
Close 1st outflow valve	5 seconds	15	15	10	0	10	10	5	5	5	Granules hydrating	flushing outflow lines	
Open 2nd outflow valve to atm in interface device	30 second - 5 min	15	15	10	0	10	0	5	15	10	Granules hydrating	flushing outflow lines	
Close 2nd outflow valve	1 min	15	15	10	0	10	10	5	5	5	Granules hydrating	Done flushing all drainage lines	
Backpressure Saturation													
Bridge inflow and outflow on panel	1 min	15	15	10	10	10	10	5	5	5	Granules hydrating	All valves still closed	
Open inflow valve to panel	1 s	15	15	10	10	10	10	5	5	5	Granules hydrating		
Open outflow valve to panel	1 s	15	15	10	10	10	10	5	5	5	Granules hydrating		
Wait 1 min	1 min	15	15	10	10	10	10	5	5	5	Granules hydrating		
Close outflow valve to panel	1 s	15	15	10	10	10	10	5	5	5	Granules hydrating		
Close inflow valve to panel	1 s	15	15	10	10	10	10	5	5	5	Granules hydrating		
Close cell to panel	1 s	15	15	10	10	10	10	5	5	5	Granules hydrating		
Increase Cell pressure on panel	1 min	25	15	10	10	10	10	5	5	5	Granules hydrating		
Increase backpressure	1 min	25	15	20	20	10	10	5	5	5	Granules hydrating		
Open cell to panel	1 s	25	25	20	20	10	10	15	15	15	Granules hydrating		
Open inflow to panel	1 s	25	25	20	20	20	20	10	5	15	10	Granules hydrating	
Open outflow to panel	1 s	25	25	20	20	20	20	5	5	5	Granules hydrating		
Wait 1 min	1 min	25	25	20	20	20	20	5	5	5	Granules hydrating		
Close outflow valve to panel	1 s	25	25	20	20	20	20	5	5	5	Granules hydrating		
Close inflow valve to panel	1 s	25	25	20	20	20	20	5	5	5	Granules hydrating		
Close cell to panel	1 s	25	25	20	20	20	20	5	5	5	Granules hydrating		
Increase Cell pressure on panel	1 min	35	25	20	20	20	20	5	5	5	Granules hydrating		
Increase backpressure	1 min	35	25	30	30	20	20	5	5	5	Granules hydrating		
Open cell to panel	1 s	35	35	30	30	20	20	15	15	15	Granules hydrating		
Open inflow to panel	1 s	35	35	30	30	30	30	5	15	10	Granules hydrating		
Open outflow to panel	1 s	35	35	30	30	30	30	5	5	5	Granules hydrating		
Wait 1 min	1 min	35	35	30	30	30	30	5	5	5	Granules hydrating		
Repeat to last stage											Granules hydrating		
Wait 1 min	1 min	75	75	70	70	70	70	0	0	0	Granules hydrating		
Close outflow valve to panel	1 s	75	75	70	70	70	70	5	5	5	Granules hydrating		
Close inflow valve to panel	1 s	75	75	70	70	70	70	5	5	5	Granules hydrating		
Close cell to panel	1 s	75	75	70	70	70	70	5	5	5	Granules hydrating		
Increase Cell pressure on panel	1 min	80	75	70	70	70	70	5	5	5	Granules hydrating		
Increase backpressure	1 min	80	75	75	75	70	70	5	5	5	Granules hydrating		
Open cell to panel	1 s	80	80	75	75	75	75	10	10	10	Granules hydrating		
Open inflow to panel	1 s	80	80	75	75	75	75	5	10	7.5	Granules hydrating		
Open outflow to panel	1 s	80	80	75	75	75	75	5	5	5	Granules hydrating		
Wait 48 hr	48 h	80	80	75	75	75	75	5	5	5	Granules hydrating		
Permeation													
Close outflow valve to panel	1 s	80	80	75	75	75	75	5	5	5	Bentonite Saturated		
Close inflow valve to panel	1 s	80	80	75	75	75	75	5	5	5	Bentonite Saturated		
Close cell to panel	1 s	80	80	75	75	75	75	5	5	5	Bentonite Saturated		
Increase inflow pressure	1 min	80	80	77	75	75	75	5	5	5	Bentonite Saturated		
Open cell to panel	1 s	80	80	77	75	75	75	5	5	5	Bentonite Saturated		
Open inflow to panel	1 s	80	80	77	75	77	75	3	5	4	Bentonite Saturated		
Open outflow to panel	1 s	80	80	77	75	77	75	3	5	4	Bentonite Saturated		
Take readings	?	80	80	77	75	77	75	3	5	4	Bentonite Saturated		

Table H.2 Gravity Method

Event	Time of event	Cell Pressure_Specimen (psi)	Inflow Pressure_Specimen (psi)	Outflow Pressure_specimen (psi)	Inflow effective stress (psi)	Outflow effective Stress (psi)	Average Effective Stress (psi)	Hydration State	Comments
Fill cell w/ water		?	0	0	?	?	?	Dry Granules (exterior hydrated)	
Flushing Lines/Saturation									
Connect cell to panel	1 min	5	0	0	5	5	5	Dry Granules (exterior hydrated)	
Fill inflow pipet	30 s	5	2	2	3	3	3	Granules begin hydrating	
Open 2nd inflow valve	1-2 min	5	2	2	3	3	3	Granules hydrating	
Close 2nd inflow valve	15 s	5	2	2	3	3	3	Granules hydrating	
Open 1 outflow valve	2-3 min	5	2	0	3	5	4	Granules hydrating	
Close 1 outflow valve	5 s	5	2	2	3	3	3	Granules hydrating	
Open 2nd outflow valve	2-3 min	5	2	0	3	5	4	Granules hydrating	
Close 2nd outflow valve	5 s	5	2	2	3	3	3	Granules hydrating	
Wait 48 hrs	48 h	5	2	2	3	3	3	Granules hydrating	
					0	0	0	Granules hydrating	
Permeation									
Open outflow valve	1 s	5	2	0	3	5	4	Granules hydrating	
Wait	?	5	2	0	3	5	4	Granules hydrating	
Close outflow valve - take reading	5-15 min	5	2	2	3	3	3	Granules hydrating	